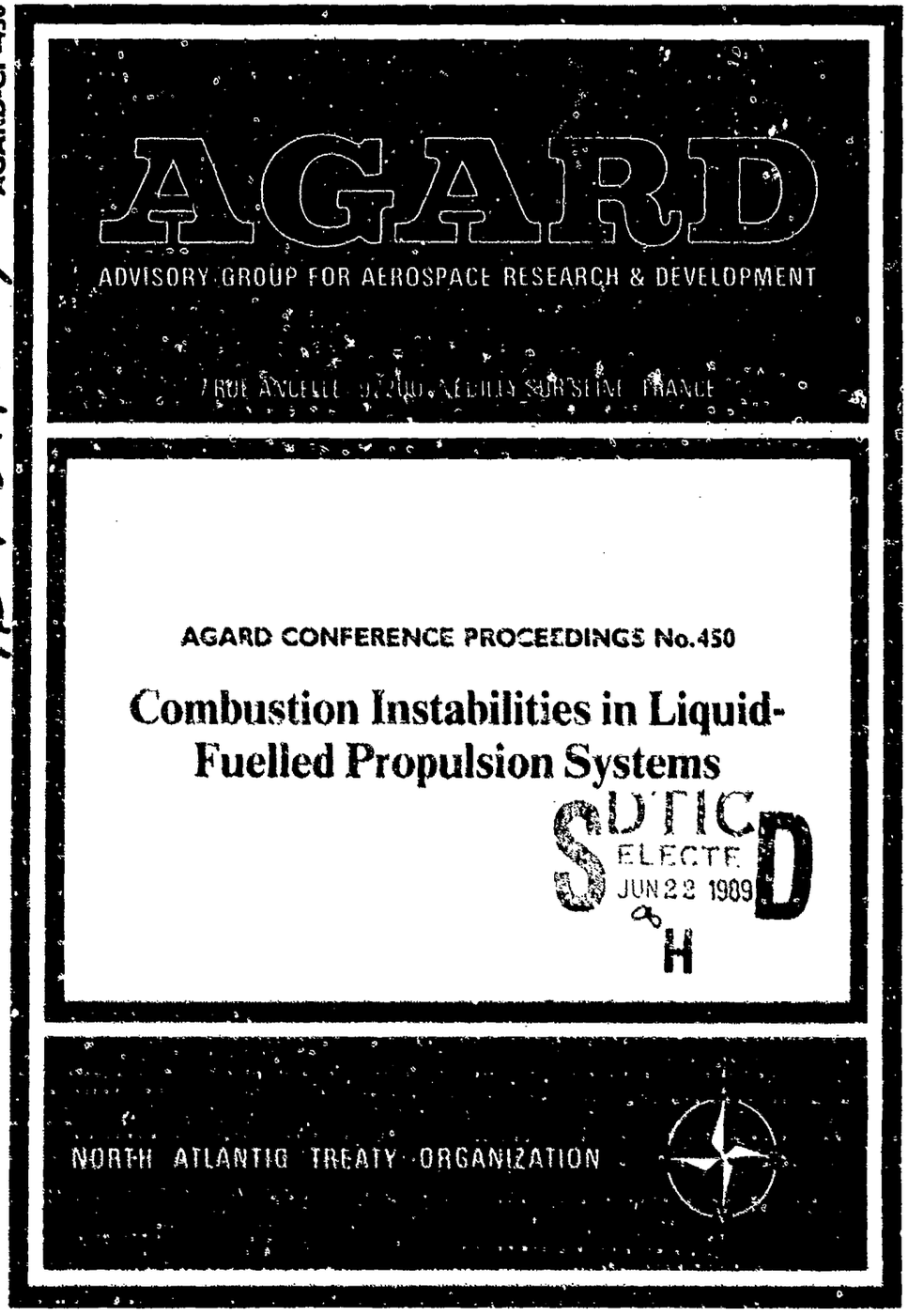
AD-A211 109

AGARD-CP-450



DISTRIBUTION AND AVAILABILITY
ON BACK COVER

DISTRIBUTION STATEMENT A
Approved for public release;
Distribution Unlimited

89 6 20 178

NORTH ATLANTIC TREATY ORGANIZATION

ADVISORY GROUP FOR AEROSPACE RESEARCH AND DEVELOPMENT

(ORGANISATION DU TRAITE DE L'ATLANTIQUE NORD)

AGARD Conference Proceedings No.450

COMBUSTION INSTABILITIES IN LIQUID-FUELLED PROPULSION SYSTEMS

Papers presented at the Propulsion and Energetics Panel 72nd *B* Specialists' Meeting,
held in Bath, United Kingdom, 6--7 October 1988.

THE MISSION OF AGARD

According to its Charter, the mission of AGARD is to bring together the leading personalities of the NATO nations in the fields of science and technology relating to aerospace for the following purposes:

- Recommending effective ways for the member nations to use their research and development capabilities for the common benefit of the NATO community;
- Providing scientific and technical advice and assistance to the Military Committee in the field of aerospace research and development (with particular regard to its military application);
- Continuously stimulating advances in the aerospace sciences relevant to strengthening the common defence posture;
- Improving the co-operation among member nations in aerospace research and development;
- Exchange of scientific and technical information;
- Providing assistance to member nations for the purpose of increasing their scientific and technical potential;
- Rendering scientific and technical assistance, as requested, to other NATO bodies and to member nations in connection with research and development problems in the aerospace field.

The highest authority within AGARD is the National Delegates Board consisting of officially appointed senior representatives from each member nation. The mission of AGARD is carried out through the Panels which are composed of experts appointed by the National Delegates, the Consultant and Exchange Programme and the Aerospace Applications Studies Programme. The results of AGARD work are reported to the member nations and the NATO Authorities through the AGARD series of publications of which this is one.

Participation in AGARD activities is by invitation only and is normally limited to citizens of the NATO nations.

The content of this publication has been reproduced
directly from material supplied by AGARD or the authors.

Published April 1989

Copyright © AGARD 1989
All Rights Reserved

ISBN 92-835-0503-4

Printed by Specialised Printing Services Limited
40 Chigwell Lane, Loughton, Essex IG10 3TZ

RECENT PUBLICATIONS OF THE PROPULSION AND ENERGETICS PANEL

Conference Proceedings

Testing and Measurement Techniques in Heat Transfer and Combustion
AGARD Conference Proceedings No.281, 55th *A* Meeting, May 1980

Centrifugal Compressors, Flow Phenomena and Performance
AGARD Conference Proceedings No.282, 56th *B* Meeting, May 1980

Turbine Engine Testing
AGARD Conference Proceedings No.293, 56th Meeting, Sep/October 1980

Helicopter Propulsion Systems
AGARD Conference Proceedings No.302, 57th Meeting, May 1981

Ramjets and Ramrockets for Military Applications
AGARD Conference Proceedings No.307, 58th Meeting, October 1981

Problems in Bearings and Lubrication
AGARD Conference Proceedings No.323, 59th Meeting, May/June 1982

Engine Handling
AGARD Conference Proceedings No.324, 60th Meeting, October 1982

Viscous Effects in Turbomachines
AGARD Conference Proceedings No.351, 61st *A* Meeting, June 1983

Auxiliary Power Systems
AGARD Conference Proceedings 352, 61st *B* Meeting, May 1983

Combustion Problems in Turbine Engines
AGARD Conference Proceedings 353, 62nd Meeting, October 1983

Hazard Studies for Solid Propellant Rocket Motors
AGARD Conference Proceedings 367, 63rd *A* Meeting, May/June 1984

Engine Cyclic Durability by Analysis and Testing
AGARD Conference Proceedings No.368, 63rd *B* Meeting, May/June 1984

Gears and Power Transmission Systems for Helicopters and Turboprops
AGARD Conference Proceedings No.369, 64th Meeting October 1984

Heat Transfer and Cooling in Gas Turbines
AGARD Conference Proceedings No.390, 65th Meeting, May 1985

Smokeless Propellants
AGARD Conference Proceedings No.391, 66th *A* Meeting, September 1985

Interior Ballistics of Guns
AGARD Conference Proceedings No.392, 66th *B* Meeting, September 1985

Advanced Instrumentation for Aero Engine Components
AGARD Conference Proceedings No.399, 67th Meeting, May 1986

Engine Response to Distorted Inflow Conditions
AGARD Conference Proceedings No.400, 68th *A* Meeting, September 1986

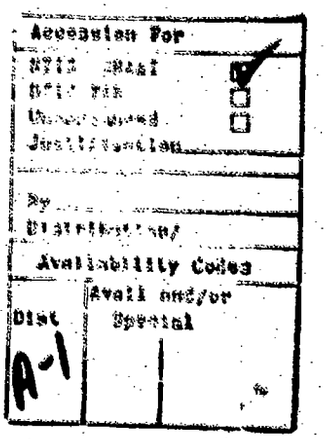
Transonic and Supersonic Phenomena in Turbomachines
AGARD Conference Proceedings No.401, 68th *B* Meeting, September 1986

Advanced Technology for Aero Engine Components
AGARD Conference Proceedings No.421, 69th Meeting, September 1987

Combustion and Fuels in Gas Turbine Engine
AGARD Conference Proceedings No.422, 70th Meeting, October 1987

Engine Condition Monitoring – Technology and Experience
AGARD Conference Proceedings No.448, 71st Meeting, May/June 1988





Working Group Reports

Aircraft Fire Safety
AGARD Advisory Report 132, Vol.1 and Vol.2. Results of WG11 (September and November 1979)

Turbulent Transport Phenomena (in English and French)
AGARD Advisory Report 150. Results of WG 09 (February 1980)

Through Flow Calculations in Axial Turbomachines
AGARD Advisory Report 175. Results of WG 12 (October 1981)

Alternative Jet Engine Fuels
AGARD Advisory Report 181. Vol.1 and Vol.2. Results of WG 13 (July 1982)

Suitable Averaging Techniques in Non-Uniform Internal Flows
AGARD Advisory Report 182 (in English and French). Results of WG 14 (June/August 1983)

Producibility and Cost Studies of Aviation Kerosines
AGARD Advisory Report 227. Results of WG 16 (June 1985)

Performance of Rocket Motors with Metallized Propellants
AGARD Advisory Report 230. Results of WG 17 (September 1986)

Lecture Series

Non-Destructive Inspection Methods for Propulsion Systems and Components
AGARD LS 103 (April 1979)

The Application of Design to Cost and Life Cycle Cost to Aircraft Engines
AGARD LS 107 (May 1980)

Microcomputer Applications in Power and Propulsion Systems
AGARD LS 113 (April 1981)

Aircraft Fire Safety
AGARD LS 123 (June 1982)

Operation and Performance Measurement of Engines in Sea Level Test Facilities
AGARD LS 132 (April 1984)

Ramjet and Ramrocket Propulsion Systems for Missiles
AGARD LS 136 (September 1984)

3-D Computation Techniques Applied to Internal Flows in Propulsion Systems
AGARD LS 140 (June 1985)

Engine Airframe Integration for Rotorcraft
AGARD LS 148 (June 1986)

Design Methods Used in Solid Rocket Motors
AGARD LS 150 (April 1987)
AGARD LS 150 (Revised) (April 1988)

Other Publications

Airbreathing Engine Test Facility Register
AGARD AG 269 (July 1981)

Rocket Altitude Test Facility Register
AGARD AG 297 (March 1987)

Manual for Aeroelasticity in Turbomachines
AGARD AG 298/1 (March 1987)
AGARD AG 298/2 (June 1988)

Application of Modified Loss and Deviation Correlations to Transonic Axial Compressors
AGARD Report 745 (November 1987)

THEME

Recent Symposia on combustion (Fall 1983 and Fall 1987) of this Panel dealt with stabilized combustion. This Specialists' Meeting was concerned with combustion instabilities and oscillations occurring in liquid-fuelled engines: i.e. gas turbine engines, ramjet engines and rockets. A better fundamental understanding is required in order to achieve further improvements in engine design, and the meeting was intended to provide a forum for discussing the state-of-the-art and for outlining a possible impact on future design. The scope of the meeting included: acoustics and flow instabilities; combustion-induced pressure oscillations; effect of geometry, equivalent ratio, etc.; ramjet specific problems; modelling; and experimental techniques and results.

***

Les Symposia organisés par le Panel sur le thème de la combustion au cours des dernières années (à l'automne 1983 et à l'automne 1987) portèrent sur la combustion stabilisée. La présente réunion de spécialistes fut consacrée aux instabilités et aux oscillations de la combustion se produisant dans les moteurs à carburants liquides, c'est à dire, les turbomoteurs, les moteurs-fusées.

Tout perfectionnement ultérieur dans le domaine de la conception des moteurs passe nécessairement par une meilleur compréhension de ces phénomènes, et la réunion a servi de forum pour une discussion de l'état de l'art et pour une évaluation de l'impact de telles considérations sur les réalisations futures.

Le programme de la réunion a compris: l'acoustique et les instabilités du flux, les oscillations de pression provoquées par la combustion, effet de géométrie, rapport équivalent etc.; problèmes spécifiques aux statoréacteurs; modélisation et les techniques expérimentales et les résultats.

PROPULSION AND ENERGETICS PANEL

Chairman: Dr W.L.MacMillan
EHF Communication Satellite
Defence Research Establishment
Ottawa, Ontario K1A 0Z4
Canada

Deputy Chairman: M. l'Ing. Princ. de l'Armement P.Ramette
Société Européenne de Propulsion
Attaché au Directeur Technique pour les
Activités Spatiales
Boite Postale 303
92156 Suresnes Cedex
France

PROGRAMME COMMITTEE

Mr L.N.Gilbert (Chairman)
Head, Technology Programs Management Office
– Code 320
Naval Weapons Center
China Lake, California 93555, US

Prof. D.Dini
Universita di Pisa
Dipartimento di Macchine
Via Diotisalvi 3
56100 Pisa, Italy

Dr D.E.Colbourne
Assistant Director, Engines 1
MOD (PE) St Giles Court
1–13 St Giles High Street
London WC2H 8LD, UK

Prof. M.N.R.Nina
CTAMFUL
Instituto Superior Tecnico
Avenida Rovisco Pais
1096 Lisboa Codex, Portugal

Dipl.-Ing. B.Crispin
Messerschmitt-Bölkow-Blohm GmbH
Unternehmensbereich Apparate Abt AE 15
Postfach 80 11 49
8000 München 80, Germany

M. l'Ing. Princ. de l'Armement P.Ramette
Société Européenne de Propulsion
Attaché au Directeur Technique pour les
Activités Spatiales
Boite Postale 303
92156 Suresnes Cedex, France

HOST NATION COORDINATOR

Dr D.E.Colbourne

PANEL EXECUTIVE

Dr E.Riester
AGARD-NATO-PEP
7 rue Ancelle
92200 Neuilly sur Seine
France

ACKNOWLEDGEMENT

The Propulsion and Energetics Panel wishes to express its thanks to the National Delegates from the United Kingdom for the invitation to hold this meeting in Bath, and for the facilities and personnel which made the meeting possible.

CONTENTS

	Page
RECENT PUBLICATIONS OF PEP	iii
THEME	v
PROPULSION AND ENERGETICS PANEL	vi
TECHNICAL EVALUATION REPORT by F.E.C.Culick	ix
	Reference
SESSION I – KEYNOTE/OVERVIEW	
COMBUSTION INSTABILITIES IN LIQUID-FUELED PROPULSION SYSTEMS – AN OVERVIEW by F.E.C.Culick	1
SESSION II – TURBINE ENGINE DEVELOPMENT EXPERIENCE	
COMBUSTOR INFLUENCE ON FIGHTER ENGINE OPERABILITY by T.L.DuBell and A.J.Cifone	2
CHARACTERISTICS OF COMBUSTION DRIVEN PRESSURE OSCILLATIONS IN ADVANCED TURBO-FAN ENGINES WITH AFTERBURNER by B.E.Henderson and J.S.Lewis	3
DYNAMIC INSTABILITY CHARACTERISTICS OF AIRCRAFT TURBINE ENGINE COMBUSTORS by M.J.Kenworthy, et al.	4
SESSION III – ROCKET AND RAMJET DEVELOPMENT EXPERIENCE	
RECHERCHE EXPERIMENTALE SUR LA STABILITE DES PETITS MOTEURS FUSEES A ERGOLS STOCKABLES par R.Foucaud et R.Lecourt	5
LOW FREQUENCY AND HIGH FREQUENCY COMBUSTION OSCILLATION PHENOMENA INSIDE A ROCKET COMBUSTION CHAMBER FED BY LIQUID OR GASEOUS PROPELLANTS by D.Preclik and P.Spagna	6
Paper 7 withdrawn	
EFFETS DES INSTABILITES DE BASSE FREQUENCE SUR LE FONCTIONNEMENT DES PRISES D'AIR DE STATOREACTEUR par C.Sans	8
RECENT DEVELOPMENTS IN RAMJET PRESSURE OSCILLATION TECHNOLOGY by P.A.Chun, J.A.Loundagin, J.A.Nabity and S.E.Ayler	9
SESSION IV – THEORETICAL MODELLING AND EXPERIMENTAL METHODS AND RESULTS	
REHEAT BUZZ – AN ACOUSTICALLY COUPLED COMBUSTION INSTABILITY by A.P.Dowling	10
ATTENUATION OF REHEAT BUZZ BY ACTIVE CONTROL by P.J.Langhorne and N.Hooper	11
NUMERICAL SIMULATIONS OF PRESSURE OSCILLATIONS IN A RAMJET COMBUSTOR by W-H.Jou and S.Menon	12
SIMULATION NUMERIQUE DU FONCTIONNEMENT INSTATIONNAIRE D'UN FOYER A ELARGISSEMENT BRUSQUE par F.Garnier, B.Labegorre, M.Serrano et A.Lavergne	13

Reference

VERY-LOW-FREQUENCY OSCILLATIONS IN LIQUID-FUELED RAMJETS
by F.H.Reardon 14

OSCILLATIONS IN NON-AXISYMMETRIC DUMP COMBUSTORS
by J.H.Whitelaw, S.Sivasegaram, K.C.Schadow and E.Gutmark 15

ACOUSTIC-VORTEX-CHEMICAL INTERACTIONS IN AN IDEALIZED RAMJET
by K.Kailasanath, J.H.Gardner, J.P.Boris and E.S.Oran 16

COMBUSTION-DRIVEN OSCILLATION IN LARGE COMBUSTION SYSTEMS FOR POWER GENERATION
by G.Benelli, V.Cossalter and G.De Michele 17

TECHNICAL EVALUATION REPORT

by

F.E.C.Culick
California Institute of Technology
201 Karman Laboratory
Mail Stop 301–46
California Institute of Technology
Pasadena, CA 91125, USA

1. SUMMARY

The 72nd (B) Propulsion and Energetics Panel Specialists' Meeting, "Combustion Instabilities in Liquid-Fuelled Propulsion Systems" was held in Bath, United Kingdom, on 6–7 October 1988. The meeting generally fulfilled its objectives of providing a forum for discussing the state-of-the-art and for assessing the impacts of current knowledge arising on future design. Recent and continuing research was reported for the three chief types of liquid-fuelled propulsion systems: gas turbines, including afterburners; liquid rockets; and ramjet engines. The papers encompassed both theoretical and experimental works treating acoustics and flow instabilities; combustion-driven pressure oscillations; modelling and numerical analyses; experimental techniques and results; and special problems relating to the various types of systems.

Although combustion instabilities have been troublesome for more than four decades, many problems remain unsolved. Recent work, particularly related to ramjets, and potential applications of liquid rocket engines in vehicles now being studied, made this meeting very timely. The presence of pressure oscillations in afterburners continues to cause concern in the development of new engines. A particularly welcome feature of the meeting was the participation by all three major engine manufacturers, General Electric, Pratt and Whitney, and Rolls Royce.

In addition to recent developments along traditional lines, one scheduled paper and an informal presentation treated the subject of active control of combustion instabilities. Only the first laboratory experiments have been carried out during the past two years or so but the results are impressive and constitute ample justification for vigorous continuing research. Successful methods of control may be important not only for applications to operational propulsion devices but also for use in conducting research experiments.

There are fundamental reasons, primarily the high densities of energy release, that combustion chambers in modern propulsion systems are susceptible to combustion instabilities. Their possible occurrence must be anticipated in any new design. As performance is pushed to higher levels, so also is the likelihood of pressure oscillations. It is therefore important to sustain continuing research on the subject and to ensure rapid flow of information to the engine designers and manufacturers. It appears reasonable that a subsequent meeting having essentially the same purposes as 72B could fruitfully be held in 3 – 4 years.

2. INTRODUCTION

Combustion instabilities in liquid rockets were first observed in the early 1940s. They were the object of much active research during the 1950s and 1960s when larger motors were developed, both for strategic systems and for the Apollo vehicle. In the late 1940s and early 1950s unacceptable high frequency instabilities were discovered in afterburners and somewhat later similar oscillations appeared in ramjet configurations.

Little research was done on instabilities in liquid rockets from the early 1970s until recently. Proposed development of new launch systems for large payloads has generated renewed interest in the subject. In contrast, instabilities in thrust augmentors have been a continuing problem since their discovery. Their presence must always be recognized in new designs, and appropriate steps taken to minimize their possible effects in operation. By far most of the work on instabilities in augmentors has been done by the engine manufacturers; development by trial and error is standard practice. Because of the proprietary nature of the work, relatively few results have been generally available.

In the late 1970s problems of lower frequency instabilities in ramjet engines motivated new research programmes in several countries. Until that time, higher frequency transverse oscillations had been the chief source of concern. The lower frequency axial or longitudinal modes interact with the inlet shock system and can have serious, even catastrophic, effects on engine performance. In response to the need to understand these instabilities, vigorous research programmes carried on during the past eight years, in many organizations, have led to new understanding of the problem. To provide a context for examining the contributions to this meeting, it is worthwhile recalling the broad technical characteristics of combustion instabilities.

Combustion chambers for propulsion systems and powerplants are never intended to exhibit pressure oscillations. Normal design considerations commonly do not include thorough considerations of truly unsteady combustion and flow. Yet unsteady motions are always present, as random motions generically called "combustion instabilities". Noisy motions cause structural vibrations over a broad frequency band, usually requiring only routine qualification of the vehicle and equipment. The amount of energy contained in the noise field is a negligibly small part of the total energy available and causes no measurable reduction in the performance of the system. Likewise, combustion instabilities even at the highest amplitudes observed consume a small fraction of the available chemical energy. The oscillations do not directly affect the steady thrust produced by the systems. Serious problems may nevertheless arise due to structural vibrations generated by oscillatory pressures within the chamber, or induced by fluctuations of the thrust. In extreme cases internal surface heat transfer rates may be amplified ten-fold or more, causing excessive erosion of chamber walls.

Special practical problems have arisen in the three classes of liquid-fuelled systems. Strong coupling between chamber pressure oscillations, low frequency structural vibrations and the propellant feed system produces the common POGO instability in large vehicles powered by liquid rockets. Axial oscillations in ramjet engines have recently become troublesome; their influence on the shock system in the inlet diffuser can produce a reduction of the inlet stability margin. Because of their light construction, thrust augmentors are susceptible to failure of flameholders or of the basic structure when combustion instabilities become severe. Many augmentors must therefore be operated with reduced performance in portions of the flight envelope.

Combustion instabilities may be regarded as the unsteady motion of a dynamic system capable of sustaining oscillations over a broad range of frequencies. The term 'combustion instability' is usefully descriptive but slightly misleading. In most instances the combustion processes themselves are stable — uncontrolled explosions or other intrinsic instabilities are not usually at work. The presence of an instability in a combustion chamber is established by observing either the gas pressure or accelerations of the enclosure. Excitation and sustenance of an oscillation occurs because of coupling between the combustion processes and the gas dynamic motions, both of which alone may be stable. If the fluctuation of energy release responding to a pressure disturbance causes a further change of pressure in phase with the initial disturbance, then the result may be an instability. Thus one may view the behaviour as that of a stable open-loop system (the gasdynamics) made unstable by a positive feedback loop, the gain being associated with the combustion processes.

Owing to the internal coupling between combustion processes and unsteady motions, an observer perceives an unstable motion as "self-excited". The amplitude of the motion grows out of the noise without the need for an external influence. Two fundamental reasons explain the prevalence of instabilities in combustion systems:

(i) an exceedingly small part of the available energy is sufficient to produce unacceptably large unsteady motions;

(ii) the processes leading to attenuate unsteady motions are weak, chiefly because combustion chambers are nearly closed.

These two characteristics are common to all combustion systems and imply that the possibility of instabilities occurring during development of a new device must be recognized and anticipated. Treating combustion instabilities is part of the necessary price to be paid for high performance chemical propulsion systems.

The fact that only a small part of the total power produced is involved suggests that the existence and severity of combustion instabilities may be sensitive to apparently minor changes in the system. That conclusion is supported by experience. Moreover, the complicated chemical and flow processes prohibit construction of a complete theory developed from first principles. It is therefore essential that theoretical work always be closely allied with experimental results. No single analysis will encompass all possible instabilities in the various practical systems. There are nevertheless many features common to the three types of combustion chambers discussed in this paper. While it is not possible to predict accurately the occurrence or details of instabilities, a framework does exist for understanding their general behaviour and for formulating statements summarizing the chief characteristics. For practical purposes, theory serves mainly to analyse, understand, and predict trends of behaviour. Experimental data are always required to deduc[illegible] quantitative results.

All combustion instabilities are unsteady motions of the compressible gases within the chamber. If the amplitude is small, the instability is closely related to classical acoustical behaviour occurring in the absence of combustion and mean flow. The geometry of the chamber is therefore a dominant influence. Corresponding to classical results, travelling and standing waves are found at frequencies approximated quite well by familiar formulas depending only on the speed of sound and the dimensions of the chamber.

Such wave motions comprise the majority of instabilities observed in the three types of systems discussed here. They are driven by the energy released by the combustion processes and influenced by the mean flow as well as by the conditions at the inlet and exhaust. Under suitable circumstances the flow of energy to the waves may so dominate the losses that nonlinear behaviour becomes significant; in extreme cases shock waves may form. Nevertheless, because the propagation speed of disturbances is a weak function of the amplitude, the frequencies don't differ greatly from classical values computed for the same geometry. Hence mere prediction of frequency is no test of a theory of combustion instability.

Owing to the presence of combustion and mean flow, other kinds of motion are possible, having frequencies below that of the fundamental wave mode. For any chamber, the lowest frequency is associated with a "bulk" mode, in which the pressure is nearly uniform throughout, but pulsating in time. The velocity fluctuation is nearly zero. This mode corresponds to the vibrations of a Helmholtz resonator obtained, for example, by blowing over the open end of a bottle. In a combustion chamber, the driving source may be directly the burning processes; or it may be due to oscillations in the supply of reactants, caused in turn by the variations of pressure in the chamber. In a liquid rocket, structural oscillations of the vehicle or the feed system may also participate, producing the POGO instability.

Motions in the range of frequencies between those of the bulk mode and the wave motions are also possible. Instabilities in this intermediate frequency range have been observed in liquid rockets for which the influence of unsteady behaviour of the propellant supply system may extend over a broad frequency range. The shift of frequency upward from the value for the bulk mode is due to the combined action of boundary conditions (including the fuel system) and the coupling between combustion processes and the gasdynamics. In afterburners, the inlet flow is not choked, so disturbances in the chamber can propagate upstream. As a result, it is possible that much of the engine may participate in the oscillation, producing frequencies quite different from those one would estimate from the geometry of the afterburner itself. This interpretation emphasizes the view that one may conveniently regard a combustion instability as an oscillation in the gasdynamic medium perturbed by other processes in the system, mainly the burning, the mean flow, and the boundary conditions.

While it is surely true that combustion is the ultimate source of the energy for the unsteady motions, and therefore in some sense the 'mechanism' for instabilities, this observation is broad and offers little help in understanding or curing the problem in practice. It is essential to identify more precisely the specific mechanism causing the particular instability at hand. In liquid-fuelled rockets the most important mechanisms are associated with the formation of liquid drops from the injected streams and vaporization. Chemical kinetics is of course fundamental to the reactive processes but generally occurs on time scales much shorter than the periods of unsteady motions. The most successful analyses of insta' ilities in liquid-fuelled rockets have been based on mechanisms involving droplet formation, vaporization and combustion.

Similar processes must take place in ramjets and afterburners but there is considerable evidence that flow separation and the formation of vortex structures may be more significant. The chief reason is due to the different geometry. Both kinds of devices are commonly designed with rearward facing steps or bluff bodies to anchor the mixing and combustion zones. The associated shear layers tend to be unstable, shedding vortices in the frequency range of acoustic modes for the chamber. Coupling with the acoustic field encourages this resonance. The vortex motions then cause periodic entrainment of unburnt reactants and, subsequently, periodic combustion. The unsteady energy release is coupled to the field, closing the feedback loop.

Whatever the mechanism, energy must be supplied to the oscillating flow field at a suitable location in space and time during a cycle of motion. If the energy addition is improperly timed, the oscillation may in fact be attenuated. This condition led early in the history of the subject to the notion of time lag as a means of interpreting the mechanism for causing instabilities. Apparently von Kármán in 1941 suggested introducing a time lag in the theoretical description as a means of explaining combustion instabilities. Whatever may have been the first proposal, it was Crocco and his co-workers and students at Princeton who developed and applied the idea during the 1950s and 1960s. It remains as the basis of one of the most or three standard methods for studying instabilities.

In practice, the $n - \tau$ model (meaning almost always the model constructed by Crocco) has been used chiefly in what might fairly be called indirect fashion. An analysis for the stability of small amplitude oscillations is carried out with the $n - \tau$ model representing the unsteady source acting as the feedback mechanism. The usual procedure is to assume that everything else is known and calculate the loss or growth τ for neutral stability (i.e. no growth or decay) of the various modes. These results can be used, for example, to correlate data and to deduce the values of n and τ associated with any various injector designs. Unless the detailed processes are analyzed, theoretical values of n and τ are not known a priori and the $n - \tau$ model cannot be used for predicting actual behaviour. Nevertheless, this approach seems to have been the most common strategy for studying instabilities in liquid-fuel rockets.

Although the $n - \tau$ model has been applied to systems other than liquid rockets -- one paper in this meeting uses this approach as a vehicle for correlating observations of instabilities in ramjet engines -- this approach is severely limited. It is important to understand how this representation of unsteady combustion fits in the general context of combustion instabilities. Thus the first paper of the meeting is an overview of the subject, and includes a description of a general framework for treating combustion instabilities in any combustion chamber. The formulation is certainly unique, but it does provide a convenient basis for assessing all possible mechanisms causing instabilities.

Not only do the mechanisms for instabilities differ among the various propulsion systems, but it is also possible that no single mechanism explains the existence of unstable motions in a given system. For example, pulsations of fuel flow and periodic combustion in large vortices together may produce an instability, or one may be clearly dominant under different operating conditions. Despite the long history of combustion instabilities in all three types of systems discussed in this meeting, much research must continue on the fundamental processes. Changes of the geometry, fuel or injection system must be expected to raise the possibility of new instabilities. There is no substitute for understanding the basic reasons for observed behaviour, with particular emphasis on the characteristics common to all combustion chambers.

Under these conditions, continuing support of research in the subject area is essential. Only with constant attention to the evolving technology is it possible to avoid the difficult and costly position of being unprepared to cope with problems arising in the development of new systems. Despite the considerable progress achieved in the past, much remains to be learned and accomplished. It seems often too easy to assume that the basic problems have been solved, or do not present any further difficulties, and, therefore, that continued support is unnecessary. The distinguished British aeronautical engineer, Sir Harold Nichols-Lowes, addressed the point well in his 22nd Wilbur Wright Memorial Lecture in 1934:

> "A successful research enables problems which once we used hopelessly complicated to be expressed so simply that we soon forget that they ever were problems. Thus the more successful a research the more difficult does it become for those who see the result to appreciate the labour which has been put into it. This perhaps is why the very people who live on the results of past research are so often the most critical of the labour and effort which, in their time, is being expended to simplify the problems of the future."

The subject of this meeting is in the first instance important because of its impact on practical propulsion systems. Therefore, however fundamental one might regard the research problems, it is essential always that the work be closely related to practical issues. The papers given in this meeting reflect that need. Six of the seventeen papers deal with work motivated directly by unsteady motions in actual systems or in development programmes. A seventh is concerned with interpretation of extensive data taken from a ramjet combustor tested in a laboratory for parametric studies. And an eighth treats results of tests using a liquid-fuelled rocket motor under development. The remaining nine papers, and an informal presentation, cover topics that are fairly classed as applied research.

Thus the substance of the meeting spanned the appropriate spectrum from research to applications. That feature is of course reflected as well in the audience, providing a good forum of exchange. In fact there are two mixing criteria that were satisfied by the meeting. First, as the above remarks emphasize, it is necessary that researchers talk with design and development groups; and, perhaps less obvious, it is beneficial that a common meeting should occur among the communities of liquid rockets, ramjets and gas turbines. Both sorts of activities have increased somewhat in the past few years; this meeting, and its published proceedings, will be a positive influence.

For purposes of the following discussion, it is convenient to classify the papers somewhat differently from the organization of the meeting agenda. This is not a perfectly definitive classification, but four groups serve well: Combustion Instabilities in Design and Development; Combustion Instabilities in Liquid Rockets; Combustion Instabilities in Ducts and Active Control and Use of Computational Fluid Dynamics.

3. EVALUATION OF PAPERS

The papers given at the meeting are listed in the table of contents (pages vi and vii). Paper [1] by Culick, titled "Combustion Instabilities in Liquid-Fueled Combustion Systems" is a lengthy survey of both experimental and theoretical work for all three types of systems: liquid rockets, thrust augmentors and ramjets. Little published work exists for instabilities in primary gas turbine combustors, and, generally, afterburners present substantially more serious problems; hence the emphasis on the latter in this review. A section of the paper also covers the important subject of passive and active control.

Control of combustion instabilities in practical propulsion systems has traditionally been accomplished by passive means. Either the design is changed in some respect — typically the injection system is modified — or passive devices are installed, usually baffles or acoustic liners. Applications to liquid rockets have been thoroughly covered in the literature; their important use in afterburners has tended to be more of a proprietary matter. Within the past two years or so, interest has rapidly grown in the prospects for using active feedback control. The available results are discussed in the review; the more significant current researches also were reported in the meeting.

This survey paper is intended partly as a general summary of combustion instabilities in liquid-fuelled systems and partly as a discussion showing those features of the problems that are common to all systems. Thus it provides a global context as well as an introduction to the papers given at the meeting.

3.1 Combustion Instabilities in Design and Development

Six papers, numbers [2], [3], [4], [17], [8] and [9] report work motivated by problems encountered either in actual full-scale systems, or in development. Also discussed in this section, paper [14] is concerned with interpretation of extensive data taken in parametric tests of a laboratory ramjet combustor. Paper number [6] could also be placed in this class but will be discussed in the following section.

Papers [2], [3] and [4] were well-received contributions from the major engine manufacturers. The first, reporting work by a group at Pratt and Whitney, West Palm Beach is concerned with a problem of transient coupling between the main gas turbine combustor and the compressor. The term 'operability' in the title "Combustor Influence on Fighter Engine Operability" refers to the necessity to avoid extinction of combustion if successful recovery from compressor stall is to be effected. While this is not a problem considered traditionally as a form of combustion instability, the designer and development engineer must increasingly attend to all aspects of transient behaviour together. Whatever the origins, fluctuations of pressure or airflow imposed externally are potentially causes of instabilities.

During extreme manoeuvres, for example, distortion of the inlet flow may cause compressor stall. While the fuel flow to the combustor remains stable, the stalled compresor causes the airflow to the combustor to oscillate, becoming reversed in part of the cycle. Engine recovery is impossible if combustion ceases. This problem is being investigated by Pratt and Whitney in a transient test facility funded by the US Navy. The apparatus provides means of investigating the stability of a combustion chamber, and its injection system, when subjected to realistic transient inputs, but without the need to operate an entire engine. In their paper, Duffell and Cifone describe some recent results, emphasizing the importance of this relatively little-known problem.

In paper [3], "Characteristics of Combustion Driven Pressure Oscillations in Advanced Turbo-Fan Engines with Afterburner", Henderson and Lewis of Rolls-Royce describe their use of experimental and theoretical methods to "ensure unrestricted operation of the afterburner system throughout the required operating range" of an advanced turbo-fan engine. Fuel/air ratio is the primary variable controlling afterburner "buzz", low-frequency longitudinal instabilities in the range 50–200 Hz. (These low frequencies are sometimes also called "rumble".) Screech instabilities involve transverse modes in the frequency range 500–5000 Hz. The dominant factors causing screech seem to be the bypass fuel/air ratio and temperature

Henderson and Lewis give an excellent description of the problems of screech and buzz, including some data and a summary of their approach to achieving successful operation of the afterburner. This is probably the best published paper this writer has seen on the subject. It serves equally as an informative introduction to the problems of screech and buzz, and as a good summary of successful strategies for solution.

Kenworthy et al describe recent General Electric work in paper [4], "Dynamic Instability Characteristics of Aircraft Turbine Combustors". Surprisingly, there is little open literature dealing with this subject — even less than has been published on instabilities in afterburners. Thus this paper is a useful contribution because it covers recent work and because the material elaborates a relatively unfamiliar problem.

The paper covers both experimental work and analysis used to interpret the data. It is an interesting aspect of the work that the data have been taken in a sector combustor rig, in this case using a sector of a CF6-80A combustor. With this configuration, only longitudinal modes can be studied unless special measures are taken to fit the symmetry of transverse modes — and then limitations must always remain. The analysis used had been previously worked out and is described only briefly in this paper. Insufficient information is given to comment on the substance or validity of the analysis. Broadly the model used is familiar: acoustic modes are driven by unsteady heat release. Thus the first matter is to construct a relation connecting flutuations of heat release to other characteristics of the system. The details of the model are not given, but it appears that a representation using a time lag is used, with combustion assumed to occur at a thin axial location (approximately a flame front). Approximations to the boundary conditions presented by the compressor exhaust and turbine inlet are important pieces of the computations.

Eventually distributions of amplitudes and phases of oscillations are calculated and show quite good agreement with measurements. Some of the data were used to set values of the boundary conditions giving best fit of the analytical results. Those values were then used in subsequent predictions. Evidently the dependence of the predicted results on fuel/air ratio was accommodated by changes in the time lag. The results obtained so far are indeed encouraging; future work will involve tests with sectors of combustor designs for other engines.

Two papers dealt with system problems in ramjet engines. Paper number [8], "Effets des Instabilités du Basse Frequence sur le Fonctionnement des Prises d'Air de Statoréacteur", by Sons et al ONERA reported some interesting experiments on the dynamics of an inlet. Following earlier tests of a two-dimensional inlet, extensive tests have been done with a circular inlet/diffuser operated supersonic in a wind tunnel. Oscillations representing unsteady motions in a combustion chamber were imposed with a rotating device placed at the downstream end. The frequency could be varied up to 200 Hertz.

The distribution of unsteady pressure was measured with twelve transducers, some of which were placed to detect the location of the inlet shock. Even with oscillations having maximum amplitude as large as 20% of the mean pressure, inlet buzz was not induced. This successful operation is attributed to the favourable influence of internal boundary layer bleed, a result consistent with the experience of others. The paper contains considerable data for the operation of the inlet and constitutes a useful contribution to the literature on inlet dynamics.

A major problem in the design of ramjet engines is achieving good matching of the dynamic characteristics of the supersonic inlet/diffuser and the combustor. This matter has been studied experimentally at the US Naval Weapons Center for a system using an eight-inch diameter coaxial dump combustor; some results are reported in paper number [9] by Chun et al, "Recent Developments in Ramjet Pressure Oscillation Technology". The purpose of the work has been mainly to establish characterizations of the stability of a ramjet combustor by using steady-state and dynamic measurements. For practical design purposes it is particularly important to determine the dependence of frequencies and amplitudes of oscillations on fuel/air ratio, inlet temperature and type of fuel for a given injection system and geometry.

This paper is a summary of experimental results, with descriptions of the techniques used. No analysis has been applied to interpret the possible mechanisms. An interesting aspect is that anticipated low-frequency modes did not appear. The observed oscillations, in the neighbourhood of 1.7 KHz, 3.5 KHz and 5.4 KHz (mainly) are evidently transverse modes, but no analysis is given to identify which ones were excited. It would be particularly useful to determine what modifications of the injection system are required to produce longitudinal modes.

More than seven years ago, a lengthy series of tests was carried out at the Aero Propulsion Laboratory, Air Force Wright Aeronautical Laboratories, to determine the influences of geometrical and operating parameters on the instabilities in a coaxial ramjet combustor. With paper [14], "Very-Low-Frequency Oscillations in Liquid-Fueled Ramjets", Reardon has summarized his efforts to correlate the data and discover what mechanisms may be responsible. He confined his attention to oscillations in which the combustion chamber vibrated in a bulk mode: the pressure is then nearly uniform in the chamber and pulsates in time.

In addition to correlating the data acquired in more than 200 tests, Reardon has attempted to construct analytical models of various processes, to assess which were more significant in causing the instabilities. Based on his experience with liquid rockets, he adopted the time-lag model to represent the combustion processes. He assumed that the sensitive time lag was dominated by the chemical reaction time and that combustion occurred in a thin flame front located at an axial position chosen to give best predictions of steady-state behaviour. The usual formula for the time-lag model of unsteady combustion was then combined with representations of other processes in the linearized equation for conservation of energy. That provided a form used for a stability analysis based on Nyquist's method.

Owing to the many approximations in the modelling, Reardon's conclusions should be regarded with kindly scepticism (as he is aware). He finds that oscillating fuel and air supply rates are the primary excitation, in the sense that those contributions alone predicted instabilities in nearly 70% of the observed cases. Inclusion of vortex shedding and convective waves did not

significantly improve the predictions. This global conclusion is chiefly a consequence of using the time-lag model, a choice that has not been shown to be a good one for ramjet engines. Nevertheless, the work discussed in this paper constitutes the most ambitious effort to bring order to the most comprehensive parametric test data available for ramjet engines.

Paper number [17], "Combustion-Driven Oscillations in Large Combustion Systems for Power Generation", by Benelli, Cossalter and DeMichele, working at the Italian Thermal and Nuclear Energy Research Centre, may seem at first out of place in a meeting devoted to propulsion systems. In fact the work demonstrates one of the major points of the first paper of this meeting, that combustion instabilities in all types of chambers may be handled within a common framework. The strategies followed to understand and cure undesired oscillations in a stationary power plant are fundamentally the same as those applied to a propulsion system.

The practical problem was that the power plant in question could not be operated at full power, owing to the excitation of pressure oscillations. Eventually the level of oscillations was reduced sufficiently so that the air flow, and therefore the power, could be brought to full design values. To achieve that result, a finite element analysis of the chamber was carried out to determine the natural mode shapes, frequencies, and damping (which was dominated by the action of the exhaust duct). Good agreement between measured and predicted frequencies was found. Moreover, also in accord with test results, the calculations showed that the 5th and 8th modes were unstable.

Then the strategy was to modify the injectors in order to affect the distribution of combustion and therefore the coupling between heat release and the acoustic waves. This was carried out successfully in accordance with Rayleigh's criterion, described in paper [1] of the meeting. The report of this work is a well-written instructive account of the application of basic principles to an important practical problem. It can profitably be read by anyone concerned with combustion instabilities.

3.2 Liquid Rockets

Two papers, numbers [5] and [6], were concerned with combustion instabilities in liquid rockets. The first, "Recherche Expérimentale sur la Stabilité des Petits Moteurs Fusées à Ergols Stockables", by Foucaud and Lecourt reports experimental results of a programme intended to determine the sensitivity of the injection zone to acoustic disturbances. This is a fundamental problem directly related to the unsteady heat release in the chamber.

The experiments were done with a device adapted from an apparatus used first many years ago by Nadaud and Kuentzmann at ONERA to investigate the sensitivity of solid propellants. The essential idea is to expose the propellant, or in the present case individual injector elements, to a controllable acoustic disturbance. This is an effective tactic, because the experimenter does not have to cope with the difficulties accompanying self-excited oscillations. Moreover, it is relatively easy and inexpensive to test the behaviour of different types of injectors and fuels. Some results have been obtained as part of a comprehensive programme for investigating combustion instabilities in large rocket motors. Thus the data will be compared with analysis of the formation of sprays and eventually will be incorporated in calculations of stability.

Preclik and Spagna have reported some results of tests with a full-scale motor in paper number [6], "Low Frequency and High Frequency Combustion Chambers Fed by Liquid or Gaseous Propellants". They have used Crocco's time lag model of the unsteady combustion processes combined with approximate representations of the impedances of the injector and nozzle to correlate their data. All tests were run in the HM-7 combustion chamber developed for the third stage of the ARIANE vehicle. The propellants were hydrogen and oxygen, injected as either liquids or gases. Normally, the concentric tube injector is intended to supply liquid oxygen and gaseous hydrogen to the combustion chamber.

Instabilities were observed only during the transient starting and stopping periods. Low frequency oscillations, in the range of a few hundred Hertz, were found always to involve oscillations in the liquid oxygen supply system, although during shut-down the nitrogen purge system also participated.

High frequency oscillations were observed during start-up only if the temperature of the injected fuel was below a critical value dependent on the injector configuration; the temperature was above the thermodynamic critical value so the hydrogen was gaseous. Thus coupling between the hydrogen supply system and the combustion chamber is essential. Evidently under those conditions, the oxygen entered as a gas. However, high frequency oscillations were also found in some cases when the propellant feed systems were not participating in the motions.

The authors provide approximate interpretations of their observations. On that basis, they offer possible means of controlling the instabilities in the system they studied. Mainly they note that to eliminate the action of the supply system, the impedance of the injector should be increased, by itself or in the feedlines. According to their analysis, shorter time lags should promote stability, achieved by modifications to the injector design.

3.3 Combustion Instabilities in Space Ducts and Active Control

For more than five years a research programme at Cambridge University has been directed to the problem of combustion instabilities in afterburners. Rolls Royce have provided funding for the work and are to be commended for such an admirable continuing commitment. It is rare indeed that a private company has the vision and resolve to sustain such a programme in a university. Papers [10] and [11] report recent progress in that work.

In paper [10], "Reheat Buzz — An Acoustically Coupled Combustion Instability", Dowling provides a simplified version of a previous analysis of the linear unstable motions in the apparatus used for the Cambridge experimental work. The one-dimensional conservation equations for unsteady motions are solved with boundary conditions representing a choked inlet and either a subsonic or choked exhaust nozzle. Experimental data were used for the unsteady heat release, inferred from observations of light emission by C_2 radicals. The results show good agreement with observations of the frequency and spacial structure of the oscillations. Moreover, the effects of changes in fuel/air ratio, inlet temperature, total flow rate and length of duct are faithfully described

Active control of combustion instabilities in liquid rockets was first proposed by Tsien in 1953. The method has never been used in practice, primarily, it seems, because adequate sensors and instrumentation have not been available. Recent developments in solid state devices and microprocessors have changed the situation dramatically. Beginning in 1983, the Cambridge group have been investigating several possible methods of active control of the instabilities in their test rig analysed by Dowling in paper [10]. The most recent efforts involving active control of the fuel supply, seem definitely to point in the direction of possible application to full-scale devices. The subject is still in very early stages of research but its promise is illustrated by the results reported by Langhorne and Hooper in paper [11], "Attenuation of Reheat Buzz by Active Control".

The basic idea is to measure some variable characterizing an observed instability and use this feedback signal to control the fuel supply and, ultimately, the unsteady energy release. Owing to peculiarities of the configuration, a secondary controlled source of fuel/air mixture was used in the Cambridge rig. With only 3% more fuel added, the amplitude of the peak oscillation was more than halved while the total acoustic energy in the frequency range 0—400 Hz was reduced to 18% of its uncontrolled value. Moreover, the controller allowed operation to higher fuel/air ratios because the flame stability limit was extended.

The prospective development of active control, also discussed by Candel in an informal presentation describing work at Ecole Central in Paris, was perhaps the most dramatic and tantalizing subject addressed at the meeting. It will be a considerable time before practical applications can be realized — and it is surely not yet obvious that they ever will be. But the ability to control unsteady motions in laboratory experiments will definitely become a widely used method for research on combustion systems.

Paper number [15], "Oscillations in Non-Axisymmetric Dump Combustors" described work at the Imperial College of Science and Technology (Whitelaw and Sivasegaram) and at the US Naval Weapons Center (Schadow and Gutmark). The main thrust of the experimental efforts has been passive control of the coupling between large-scale vortex structures and acoustic modes. Test results have been obtained for a range of burner geometries; the chief variables were length/diameter and shape of cross-section. Special advantage is taken of the shape by modifying the location of fuel injection.

Probably the most significant global conclusion is that the tendency to instabilities is discouraged if fuel is injected in such a fashion as to avoid combustion within large shed vortices. This result was first demonstrated experimentally by Schadow and his co-workers. It is clearly an important matter for engine designers, already providing qualitative guidelines in respect to important influences of geometry. Observations have been made over broad ranges of operating conditions as well as geometrical variables. It is clear that significant effects have been identified in the laboratory. Enough has done to merit incorporating the ideas in design and development tests of full-scale engines.

3.4 Use of Computational Fluid Dynamics

While computational fluid dynamics has become an integral part of the design process for external aircraft and missile dynamics, its use for internal flows has been developing much less rapidly. No doubt this situation is due partly to the importance of viscous effects to internal flows, and the fact that in many problems — notably flows in combustors — the difficulties of turbulence modelling must be faced squarely. Thus for practical purposes, evolutionary design by trial and error has been an acceptable procedure. Computational methods apparently have yet to offer substantial advantages of cost, despite continual progress in analysis of flows in compressors, turbines and combustion chambers.

Only in the past 5—7 years has CFD been applied to ramjet combustors and liquid rockets, chiefly in connection with combustion instabilities; the use of comprehensive analysis for ramjets and rockets has not been motivated by problems of design for higher performance. Papers [12] and [16] summarize progress in two US efforts devoted to computations of unsteady flows and ramjet combustors; paper [13] is a report of work at DERA, covering the initial results obtained with adaptation of a code developed elsewhere, originally for analysis of flows in diesel engines.

Paper [12], "Numerical Simulation of Pressure Oscillations" by Jou and Menon of Flow Research, Inc., treats "large eddy simulations of compressible cold flow in a ramjet combustor configuration". Their computations are based on the compressible Navier-Stokes equations for axisymmetric flow; thus laminar viscous effects are included, but turbulent modelling is not. The geometry studied is exactly that used in laboratory tests at the Naval Weapons Center. Extensive data have established the importance of vortex shedding and coupling with the acoustical motions as a dominant mechanism for excitation of acoustic modes. This process can drive acoustic modes in cold flow; combustion in a reacting flow tends to cause higher amplitudes. Thus the restriction of these computations to cold flow necessarily excludes some important details but the results capture much of the basic behaviour.

An important, and highly commendable, feature of this work is that the authors attempt to treat their numerical results much as one would process experimental data. They perform spectral analysis and, more difficult, attempt to identify and distinguish the vorticity and acoustic fluctuations. The latter is accomplished by computing the instantaneous dilation field that serves as the source of the acoustic motions.

The computations of the large-scale structures compare well with experimental data taken elsewhere for flow past a backward facing step. These vortices not only radiate (weakly) acoustic waves that ultimately interfere constructively to form classical acoustic wave modes, but are also responsible for exciting coupled vorticity/acoustic modes. When vorticity impinges on the nozzle, pressure disturbances are created that propagate upstream, are reflected from the upstream end of the chamber, and again ultimately interfere to form a steady mode of oscillation. However, in this case the frequencies of the possible modes are significantly different from the classical values. The authors have constructed a simple model of thse coupled modes, giving a method for estimating the frequencies.

Jou and Menon have only commented on their intentions to include combustion processes. Kailasanath et al in paper [16], "Acoustic-Vortex-Chemical Interactions in an Idealized Ramjet" discuss their results for both non-reacting and reactive flows obtained at the Naval Research Laboratory. They solve the equations for compressible unsteady flow in an axisymmetric configuration intended to mimic that used in the tests at the Naval Weapons Center. However, the nozzle is represented by an axisymmetric array of small orifices. Viscous stresses are not accounted for, and no artificial viscosity is introduced. Residual numerical diffusion is present at scales of the order of the grid size; those short wavelength artifacts are rapidly damped but apparently act to initiate the unsteady vortex motions. The numerical computations are directed to the interactions between the vortex structures and the acoustic modes, which are largely inviscid processes.

Here too the authors carry out spectral analysis of their results, as well as providing pictures of the flow showing the behaviour at successive instants of time. The results seem to compare favourably with those of Jou and Menon, although careful comparison is not possible because the two works have not solved exactly the same problems. Perhaps the more interesting part of the work by Kailasanath et al is their effort to include combustion processes. They simplify the reaction scheme for a premixed hydrogen/air mixture by using a two-step model. Experimental data are used to estimate the induction time separating the two steps, energy release taking place in the second. The authors recognized that the model is crude -- a necessary restriction to save computing costs -- so their results concentrate mainly on the qualitative effects of energy release.

They find that the vortex motions cause significant spatial and temporal variations in the energy release. Application of Rayleigh's criterion shows that unsteady combustion drives the waves in the region 3--4.5 diameters downstream of the inlet plane. Large energy release tends to destroy many of the features of the vortex field existing in cold flow; vortex merging is prevented and the flow is dominated by a single large vortex. There seems as yet to be no experimental results available to confirm or deny this observation.

The last paper [13], "Simulation Numérique du Fonctionnement Instationnaire d'un Foyer à l'Elargissement Brusque" by Garnier et al also treats a dump combustor. The significant difference is that injection of liquid fuel is treated explicitly. A computer code, KIVA, obtained from the Los Alamos National Laboratory has been adapted for this work. Evidently the chief modifications were required to account for inflow and exhaust of propellants and combustion products. The computations become elaborate because the gas and liquid phases must be distinguished and in addition turbulence modelling and a realistic representation of chemical reactions are included. Unlike most other works dealing with two phase flow, calculations of the two phases are treated together in a three-step scheme described briefly in the paper.

Results are given for a configuration quite similar to that used in the two papers discussed above. Liquid fuel is assumed injected both in the inlet duct just upstream of the dump plane, and at the face of the dump plane itself. Only initial results are given, showing unsteady development of the flow at various instants of time. Qualitatively, at least, the flow appears to be realistic.

The paper is a good summary of the method and contains a comprehensive list of references. It is the first report of what appears to be a promising and fruitful approach to numerical analysis of unsteady flows in liquid-fuelled combustors.

4. CONCLUSIONS

The papers presented at this meeting reflect well recent work and the present status of combustion instabilities in liquid-fuelled propulsion systems. With a nearly even split of coverage between developmental and research problems, the proceedings should serve as a good introduction to the subject.

It seems that the most obvious deficiency in the meeting was a failure to include papers dealing with the production, vaporisation and combustion of sprays. Much has been accomplished in recent years on the subject of the steady behaviour of sprays. Less is understood of the unsteady combustion, but certainly enough to have justified at least one paper. Both theoretical and experimental results should be attended to in any future meeting on combustion instabilities. A related problem, which is especially significant for design and development, is that of the distribution of fuels and fuel/oxidizer ratio over the inlet plane to the combustor. This boundary condition apparently has considerable -- sometimes crucial -- influence on combustion instabilities. Unfortunately, little is known of the distributions actually occurring in practice.

Applications of computational fluid dynamics and the use of active control are the most promising new subjects covered in the meeting. The papers given reported work from the groups most active in those areas.

The Programme Committee is to be congratulated for organizing a successful meeting that succeeded in covering the subject of combustion instabilities in topical fashion.

5. RECOMMENDATIONS

Although combustion instabilities will likely always remain unwanted in propulsion systems, their continued existence can be guaranteed for reasons discussed briefly in the introduction. Large amplitude oscillations can be very expensive to treat when they arise late in a development programme. Thus it is necessary that research and engine designers maintain continuing exchange of their experiences and progress.

An AGARD Specialists' Meeting is a particularly good medium for such exchange of information. No other organization provides the opportunity for bringing together international experts in a relatively narrow field for two days' intensive discussion.

It is therefore entirely appropriate that the subject of combustion instabilities be included, say, every 3—4 years in the schedule of PEP meetings. Some benefit may be gained by covering instabilities in solid-fuelled as well as liquid-fuelled systems in a single meeting. There are in fact many common problems. The opportunity to compare progress in, for example, the use of computational fluid dynamics would benefit both communities.

COMBUSTION INSTABILITIES IN LIQUID-FUELED PROPULSION SYSTEMS – AN OVERVIEW

by

F.E.C.Culick
201 Karman Laboratory
Mail Stop 301–46
California Institute of Technology
Pasadena, CA 91125, USA

Abstract

Combustion of reactants in a confined volume favors excitation of unsteady motions over a broad range of frequencies. A relatively small conversion of the energy released will produce both random fluctuations or noise, and, under many circumstances, organized oscillations generically called combustion instabilities. Owing to the high energy densities and low losses in combustion chambers designed for propulsion systems, the likelihood of combustion instabilities is high. The accompanying heat transfer to exposed surfaces, and structural vibrations are often unacceptable, causing failure in extreme cases. This paper is a brief review of combustion instabilities in liquid-fueled propulsion systems—rockets, ramjets, and thrust augmentors—with emphasis on work accomplished during the past decade. To provide a common framework for discussing the wide range of works, a theory of two-phase flow is reviewed as the basis for an approximate analysis of combustion instabilities. The analysis is directed primarily to treatment of linear stability; it is sufficiently general to accommodate all processes occurring in actual systems. A new result has been obtained for an extended form of Rayleigh's criterion and its relation to the growth constant for unstable waves. The chief mechanisms for combustion instabilities in liquid-fueled systems are reviewed, followed by a summary of the common methods of analysis and applications to the three classes of propulsion systems. Control of instabilities by passive and active means is examined briefly.

Table of Contents

1. **Introduction** 2

2. **Some General Features of Combustion Instabilities and the Theoretical Foundations** 4
   2.1. Conservation Equations 5
   2.2. Formulation of an Approximate Analysis 8
   2.3. The Problem of Linear Stability 12
   2.4. Evaluating the Linear Contributions to the Frequency shift and growth constant 14
   2.5. Rayleigh's Criterion 16
   2.6. The Connection Between Rayleigh's Criterion and the Growth Constant 18

3. **Mechanisms of Combustion Instabilities** 19
   3.1. Interpretation with a Time Lag 19
   3.2. Atomization, Droplet Vaporization and Burning 21
   3.3. Convective Waves 23
   3.4. Vortex Shedding and Combustion 26

4. **Methods of Analysis** 30
   4.1. Numerical Analysis and Simulation of Combustion Instabilities 30
   4.2. Analyses Based on the Time Lag Model 32
   4.3. Use of Green's Function to Compute Linear Stability 35
   4.4. Application of Galerkin's Method 36

5. **Remarks on Instabilities in the Three Types of Systems** 37
   5.1. Combustion Instabilities in Liquid Rockets 37
      5.1.1. POGO Instabilities 38
   5.2. Combustion Instabilities in Thrust Augmentors 39
   5.3. Combustion Instabilities in Ramjet Engines 42
      5.3.1 Unsteady Behavior of the Inlet/Diffuser 43
      5.3.2 Vortex Shedding and Combustion Instabilities 44
      5.3.3 Mode Shapes: Experimental and Calculated 45
      5.3.4 Numerical Analysis of Flows in Ramjet Combustors 46
      5.3.5 Convective Waves of Entropy and Vorticity 48
      5.3.6 The Time Lag Model Applied to Combustion Instabilities in Ramjet Engines 49

6. **Passive and Active Control of Combustion Instabilities** 49
   6.1 Passive Control Devices 50
   6.2 Active Control of Combustion Instabilities 54

7. **Concluding Remarks** 58

References 59

1. INTRODUCTION

Chemical propulsion systems depend fundamentally on the conversion of energy stored in molecular bonds to mechanical energy of a vehicle. The first stage of that process is combustion of fuel and oxidizer. Burning takes place at relatively high pressure in a vessel open only to admit reactants and to exhaust the hot products. Liquid-fueled rockets, ramjets and thrust augmentors (afterburners) are intended to operate under conditions that vary little during the time required for a disturbance to propagate across the combustion chamber. Normal design considerations for such systems commonly do not include thorough consideration of truly unsteady combustion and flow.

Yet unsteady motions are always present, as random fluctuations or noise, and often as organized vibratory motions generically termed "combustion instabilities". Noisy motions cause structural vibrations over a broad frequency band, usually requiring only routine qualification of the vehicle and equipment. The amount of energy contained in the noise field is a negligibly small part of the total energy available and causes no measurable reduction in the performance of the machine.

Likewise, combustion instabilities even at the highest amplitudes observed consume a small fraction of the available chemical energy. The oscillations do not directly affect the steady thrust produced by the systems. Serious problems may nevertheless arise due to structural vibrations generated by oscillatory pressures within the chamber, or induced by fluctuations of the thrust. In extreme cases internal surface heat transfer rates may be amplified ten-fold or more, causing excessive erosion of chamber walls.

Special practical problems have arisen in the three classes of liquid-fueled systems. Strong coupling between chamber pressure oscillations, low frequency structural vibrations and the propellant feed system produces the common POGO instability in liquid rockets. Axial oscillations in ramjet engines have recently become troublesome; their influence on the shock system in the inlet diffuser can produce a reduction of the inlet stability margin. Because of their light construction, thrust augmentors are susceptible to failure of flameholders or of the basic structure when combustion instabilities become severe. Many augmentors must therefore be operated with reduced performance in portions of the flight envelope.

Combustion instabilities may be regarded as the unsteady motions of a dynamical system capable of sustaining oscillations over a broad range of frequencies. The term 'combustion instability' is usefully descriptive but slightly misleading. In most instances the combustion processes themselves are stable - uncontrolled explosions or other intrinsic instabilities are not usually at work. The presence of an instability in a combustion chamber is established by observing either the gas pressure or accelerations of the enclosure. Excitation and sustenance of an oscillation occurs because of coupling between the combustion processes and the gas dynamical motions, both of which alone may be stable. If the fluctuation of energy release responding to a pressure disturbance causes a further change of pressure in phase with the initial disturbance, then the result may be an instability. Thus one may view the behavior as that of a stable open-loop system (the gasdynamics) made unstable by a positive feedback loop, the gain being associated with the combustion processes.

Owing to the internal coupling between combustion processes and unsteady motions, an observer perceives an unstable motion as "self-excited". The amplitude of the motion grows out of the noise without the need for an external influence. Two fundamental reasons explain the prevalence of instabilities in combustion systems:

i.) an exceedingly small part of the available energy is sufficient to produce unacceptably large unsteady motions;

ii.) the processes tending to attenuate unsteady motions are weak, chiefly because combustion chambers are nearly closed.

These two characteristics are common to all combustion systems and imply that the possibility of instabilities occurring during development of a new device must be recognized and anticipated. Treating combustion instabilities is part of the necessary price to be paid for high performance chemical propulsion systems.

The fact that only a small part of the total power produced is involved suggests that the existence and severity of combustion instabilities may be sensitive to apparently minor changes in the system. That conclusion is supported by experience. Moreover, the complicated chemical and flow processes prohibit construction of a complete theory developed from first principles. It is therefore essential that theoretical work always be closely allied with experimental results. No single analysis will encompass all possible instabilities in the various practical systems. There are nevertheless many features common to the three types of combustion chambers discussed in this paper. While it is not possible to predict accurately the occurrence or details of instabilities, a framework does exist for understanding their general behavior and for formulating statements summarizing the chief characteristics. For practical purposes, theory serves mainly to analyze, understand, and predict trends of behavior. Experimental data are always required to deduce quantitative results.

All combustion instabilities are unsteady motions of the compressible gases within the chamber. If the amplitude is small, the instability is closely related to classical acoustical behavior occurring in the absence of combustion and mean flow. The geometry of the chamber is therefore a dominant influence. Corresponding to classical results, traveling and standing waves are found at frequencies approximated quite well by familiar formulas depending only on the speed of sound and the dimensions of the chamber.

Such wave motions comprise the majority of instabilities observed in the three types of systems discussed here. They are driven by the energy released by the combustion processes and influenced by the mean flow as well as by the conditions at the inlet and exhaust. Under suitable circumstances the flow of energy to the waves may so dominate the losses that nonlinear behavior becomes significant; in extreme cases shock waves may form.

Nevertheless, because the propagation speed of disturbances is a weak function of the amplitude, the frequencies don't differ greatly from classical values computed for the same geometry. Hence mere prediction of frequency is no test of a theory of combustion instability.

Owing to the presence of combustion and mean flow, other kinds of motion are possible, having frequencies below that of the fundamental wave mode. For any chamber, the lowest frequency is associated with a "bulk" mode, in which the pressure is nearly uniform throughout, but pulsating in time. The velocity fluctuation is nearly zero. This mode corresponds to the vibrations of a Helmholtz resonator obtained, for example, by blowing over the open end of a bottle. In a combustion chamber, the driving source may be directly the burning processes: or it may be due to oscillations in the supply of reactants, caused in turn by the variations of pressure in the chamber. In a liquid rocket, structural oscillations of the vehicle or the feed system may also participate, producing the POGO instability.

Motions in the range of frequencies between those of the bulk mode and the wave motions are also possible. Instabilities in this intermediate frequency range have been observed in liquid rockets for which the influence of unsteady behavior of the propellant supply system may extend over a broad frequency range. The shift of frequency upward from the value for the bulk mode is due to the combined action of boundary conditions (including the fuel system) and the coupling between combustion processes and the gasdynamics. In afterburners, the inlet flow is not choked, so disturbances in the chamber can propagate upstream. As a result, it is possible that much of the engine may participate in oscillation, producing frequencies quite different from those one would estimate from the geometry of the afterburner itself. This interpretation emphasizes the view that one may conveniently regard a combustion instability as an oscillation in the gasdynamic medium perturbed by other processes in the system, mainly the burning, the mean flow, and the boundary conditions. General features of the possible oscillations and formulation of the theoretical framework are discussed further in Section 2, partly as a means of classifying observed instabilities. A new result given in Section 2.5 is a form of Rayleigh's criterion accounting for all linear processes. That leads naturally to direct connection with the growth constant, Section 2.6. Thus two general ways of assessing unstable behavior are shown to be equivalent.

Section 2 contains lengthy, though abbreviated, calculations included here chiefly for two reasons. First, it is important to realize that combustion instabilities in all liquid-fueled systems can be accommodated within a common theoretical framework. The analysis given here certainly is not unique, but it is a convenient form encompassing at least the essential ideas of most previous works. The second reason is that the calculations produce several general results that we use in later discussions of specific problems. However, it is unnecessary to know the details of the analysis to understand the applications of the results in the remainder of the paper.

While it is surely true that combustion is the ultimate source of the energy for the unsteady motions, and therefore in some sense the 'mechanism'for instabilities, this observation is broad and offers little help in understanding or curing the problem in practice. It is essential to identify more precisely the specific mechanism causing the particular instability at hand. In liquid-fueled rockets the most important mechanisms are associated with the formation of liquid drops (or droplets, since they are quite small!) from the injected streams and vaporization. Chemical kinetics is of course fundamental to the reactive processes but generally occur on time scales much shorter than the periods of unsteady motions. The most successful analyses of instabilities in liquid-fueled rockets have been based on mechanisms involving droplet formation, vaporization and combustion.

Similar processes must take place in ramjets and afterburners but there is considerable evidence that flow separation and the formation of vortex structures may be more significant. The chief reason is due to the different geometry. Both kinds of devices are commonly designed with rearward facing steps or bluff bodies to anchor the mixing and combustion zones. The associated shear layers tend to be unstable, shedding vortices in the frequency range of acoustic modes, for the chamber. Coupling with the acoustic field encourages this resonance. The vortex motions then cause periodic entrainment of unburnt reactants and, subsequently, periodic combustion. The unsteady energy release is coupled to the field, closing the feedback loop.

Whatever the mechanism, energy must be supplied to the oscillating flow field at a suitable location in space and time during a cycle of motion. If the energy addition is improperly timed, the oscillation may in fact be attenuated. This condition led early in the history of the subject to the notion of time lag as a means of interpreting the mechanisms for causing instabilities. Apparently von Karman in 1941 suggested introducing a time lag in the theoretical description as a means of explaining combustion instabilities. Whatever may have been the first proposal, it was Crocco and his co-workers and students at Princeton who developed and applied the idea during the 1950's and 1960's. It remains as the basis of one of the two or three standard methods for studying instabilities.

The time lag is usually defined as the interval from the instant at which an element of liquid reactant enters the chambers to the time at which combustion of that mass is completed. Following Crocco's early work virtually all formulations assume that the conversion processes acting during the lag period are dependent on pressure only. Some work has accounted for dependence on velocity. For the most common case, the result of reasoning in this basis produces a representation of the unsteady energy release in the chamber, a formula containing two parameters, the time lag τ and the pressure index n. Such a description is commonly referred to as the $n-\tau$ model, meaning almost always the model constructed by Crocco.

In practice, the $n-\tau$ model has been used chiefly in what might fairly be called indirect fashion. An analysis for the stability of small amplitude oscillations is carried out with the $n-\tau$ model representing the unsteady source acting as the feedback mechanism. Such an analysis produces two results: a formula for the frequencies of oscillations, and a formula for the rate at which those oscillations will grow or decay. If all input variables and parameters are known, the result can be used to predict, for a specified operating condition, whether the oscillations are stable or not. The difficulty is that the values of n and τ are not known: they are really present only as parameters characterizing the unsteady combustion processes in some global sense.

Hence the usual procedure is to assume that everything else is known and calculate the loci n versus τ for neutral stability (i.e. no growth or decay) of the various modes. Those results can be used, for example, to correlate data and to deduce the values of n and τ associated with, say, various injector designs. Unless the detailed processes are analyzed, theoretical values of n and τ are not known and the $n-\tau$ model cannot be used for predicting actual behavior. Nevertheless, this approach seems to have been the most common strategy for studying instabilities in liquid-fuel rockets.

Following a survey of various mechanisms is Section 3, we discuss the chief analytical schemes in Section 4. Theories and computational procedures for combustion instabilities may be classified in two ways: linear or nonlinear behavior and analytical or numerical. Whether or not nonlinear calculations are to be done rests in the first instance on decisions regarding the physical behavior. At least as a preliminary, a linear theory should be worked out first, but the limitations must be understood. Whatever the content of a linear theory, only two results are obtained: the frequencies of allowed oscillations in the system, and the rate at which small amplitude distrubances will grow or decay. If a disturbance is unstable in an actual system, the amplitude grows without limit unless one or more nonlinear processes act. That is a fundamental characteristic of self-excited systems. Moreover, full understanding of the response of a combustion system to finite initial disturbances can be gained only with a nonlinear theory. By far most of the theoretical work on combustion instabilities has been based on linear behavior. We do not review nonlinear theory in this paper.

Ultimately for applications in design of actual systems, there seems little doubt that elaborate numerical calculations are required. The complications presented by the gas dynamics, chemical processes and geometrical configurations block solution to the governing differential conservation equations in any but the simplest cases: nothing like closed form solutions can be expected. When the $n-\tau$ model is used, it is possible to progress further in that direction, mainly because much of the complicated physical behavior is effectively swept under the rug and presented in global approximation. When the details of, say, droplet dynamics are treated, only numerical results can be obtained.

In one form or other much of the physical behavior is common to all liquid-fueled systems. The different kinds of devices are distinguished either by geometrical configuration or by the ways in which reactants are introduced in the chamber. Thus the material covered in Sections 2-4 has a strongly unifying character; specific examples are called upon mainly to clarify ideas or to show typical results. In Section 5, special cases of combustion instabilities are discussed at some length to emphasize both the similarities and differences among the three classes of systems.

The prevalence of combustion instabilities has motivated efforts to develop "cures" or methods of limiting the amplitudes to acceptable values. It seems that all successful applications to operational systems have been based on passive devices. The use of baffles, acoustic liners or resonant cavities - occasionally all three in the same engine - has become commonplace, especially in liquid rockets. If the geometry permits installation, adding a device of this sort can be an effective strategy. There are mainly two reasons they work: 1) by shifting the frequencies of permitted oscillations out of the range where unsteady energy transfer to the modes is strongest; and 2) by direct attenuation of the motions, primarily due to the action of viscous stresses.

During the past several years, interest has grown in the possibilities for active control of combustion instabilities. The idea is not new, dating back to the late 1940's at least, but developments of lightweight fast computers and better sensors make active control an attractive alternative to passive control. Both subjects are discussed briefly in Section 6.

This cannot be a thorough review of the subject. In particular we do not explicitly treat design issues such as types of injectors, rationale for choices of particular passive damping devices and stability rating of chambers. Some aspects are quite well known from experience with liquid rockets especially but much work remains to treat satisfactorily contemporary systems operating at higher pressures with hydrocarbon fuels.

The list of references is divided for convenience into four groups dealing with rockets; ramjet engines; thrust augmentors; and passive and active control. I do not claim completeness and there is unavoidably some overlap, but each reference is entered in only one group. Also, not all references in the list are cited in the text. That is not a matter of value judgement, but follows from the need to curb the length of the text.

I am especially indebted to the following people who aided me early in this effort by providing me with lists of references, and in some cases copies of papers and reports: Professor A. Acosta, Caltech; Dr. Paul Kuentzmann, ONERA; Dr. P.V. Liang, Rockwell International, Rocketdyne Division; Professor C.E. Mitchell, Colorado State University; Dr. T.V. Nguyen, Aerojet TechSystems Company; Professor F.H. Reardon, Sacramento State University; Dr. Klaus Schadow of the Naval Weapons Center; Mr. A.A. Shabayek, Sverdrup Technology, Inc.; Professor V. Yang, Pennsylvania State University; and Professor B.T. Zinn of Georgia Tech. Mms. Jean Anderson and Pat Gladson of the Caltech Aeronautical Library have been most helpful locating references and making copies.

I have tried to give a fair coverage of the subject of combustion instabilities in liquid-fueled combustion systems based on the literature available to be me. I shall greatly appreciate receiving copies of works that I have not included in this survey.

2. SOME GENERAL FEATURES OF COMBUSTION INSTABILITIES AND THE THEORETICAL FOUNDATIONS

Probably the most important fundamental characteristic of combustion instabilities is that in first approximation they may be viewed as perturbations of classical acoustical motions. The chief perturbations are due to the combustion processes; the associated mean flow; and the boundary conditions imposed at the inlet and exhaust. It is a very robust approximation indeed. Often one may ignore apparently significant processes and still obtain remarkably good results for some of the dominant features.

For example, if the average temperature, and therefore speed of sound a of the chamber gases is known, close estimates for frequencies of allowable wave modes may often be had by simply dividing a by integral multiples of the length or diameter. Values within 10% or so of observed oscillations, and good approximations to the mode structures, can be obtained by numerical solution to the unperturbed classical acoustics problem solved for the same geometry as the combustion chamber.* That conclusion often remains valid even when subtantial amounts of a condensed phase are present in the chamber or when the mean flow field is highly non-uniform as happens when flow separation occurs. Large spatial variations of temperature can be more significant because the speed of sound then is non-uniform; even so, an averaged value may serve quite well. The approximation of classical acoustics also deteriorates if the Mach number of the average flow is larger than roughly 0.4, for then the Doppler effect and refraction may cause substantial distortions of the acoustic field.

One reason for emphasizing the surprising confidence that one may place in the classical acoustics approximation is that the idea seems to extend to many aspects of nonlinear behavior as well. For example, recent work, mainly for application to liquid-fueled ramjets and solid propellent rockets, suggests that under broad conditions the existence of limit cycles can be explained on the basis of nonlinear gasdynamics, with other processes affecting mainly details.

The emphasis on classical acoustics has been successful and will be followed throughout this work, because the main departures, while crucial in defining the real problems, are often small perturbations in some sense. The mean flow Mach number is generally not large over most of the combustion chamber. Even though the mass fraction of liquid may be substantial, the volume fraction remains small on average. As a result, the elasticity of the multi-phase mixture is dominated by the gases, while the inertia is a mass-weighted average of the gas and liquid phases. The boundary conditions provided by the propellant supply system and the exhaust nozzle may be significantly different from the condition for a rigid wall but those influences are easily accounted for by introducing appropriate impedance or admittance functions. And as we remarked in the introduction, the amount of energy possessed by the unsteady motions is a small part of the total chemical energy released and converted to average mechanical energy of the flow.

We therefore always seek a theoretical formulation that in an obvious fashion, when all perturbations vanish, reduces to a representation of classical waves in an enclosure. This strategy allows construction of a theoretical framework accommodating all types of propulsion systems.

It is of course the geometry and the perturbations that define the actual physical situations and distinguish one system from another. The geometry causes technical difficulties-solving equations in peculiarly-shaped volumes - and sets the spectrum of allowed oscillations. But geometry alone does not pose any fundamental problems, nor does it contain explanations of the instabilities. By far the greater part of research on combustion instabilities must therefore be spent on the perturbations of classical linear acoustics, especially directed to understanding the physical mechanisms responsible for the instabilities and their nonlinear behavior.

It is a consequence of this point of view that combustion instabilities in the three kinds of propulsion systems are profitably considered together. Much is to be gained by regarding individual examples as special cases of a general formulation such as that summarized in the following sections.

2.1 Conservation Equations

The state-of-the-art for experiment and analysis of combustion instabilities in liquid rockets as of (roughly) 1970 was summarized in the thorough reference volume edited by Harrje and Reardon (1972). A computer program, AUTOCOM [Reichel et al (1973, 1974)] essentially captured the main procedures commonly used at that time in the U.S. for treating combustion instabilities in liquid rockets. That program was re-written, for running on later computers, by Nickerson and Nguyen (1984a, 1984b), but the formulation and physical basis remained without change. Currently, extensive work is being carried out in the U.S. by the Aerojet Tactical Systems Co. [Fang(1984a, 1984b, 1987); Fang and Jones (1984); Muss and Pieper (1987, 1988); Nguyen (1988); Nguyen and Muss (1987); and Pieper and Fang (1986)]; and by Rockwell International [Liang et al (1986, 1987, 1988)]. Philippart (1987) and Philippart and Moser(1988) have reported some numerical results obtained with those computer programs, but without discussion of the physical basis for the formulations.

Following the failure during flight of the Viking motor, due to combustion instability (Souchier et al (1982)), a continuing research program has been in progress for seven years in France. Some of the results have been reported by Schmitt and Lourme (1982), Habiballah et al (1984, 1985, 1988) and by Lourme et al (1983, 1984, 1985, 1986).

All of those works begin with essentially the same physical basis, a compressible gaseous medium containing a liquid phase. Major differences arise in the representation of the mass and energy sources and in the analysis followed to obtain solutions. We shall discuss those matters later. Here we are concerned only with the broad character of the general formulation. In analysis of liquid rockets, particular emphasis is placed on the behavior of the liquid phase and the interactions between the liquid and gas phases, matters that are common to all liquid-fueled systems. The average flow field is relatively simple compared with the circumstances in ramjet engines and augmentors. Because the flow of oxidizing gas and flow separation are important features in those systems, analysis of combustion instabilities has additional complications. We defer discussion of those phenomena and begin here with a simplified formulation of the problem for liquid rockets; most of the results will be applicable to ramjet engines and thrust augmentors as well.

We assume that the medium in the chamber consists of reactant gases, liquid oxidizer and fuel, and gaseous products of combustion. Condensed products of combustion (e.g. soot) may also form and can be accommodated. For analysis of unsteady motions many of the details necessary to a successful description of the steady flow can

* Some care is required with the boundary condition at the exhaust plane. A poor choice may lead to unacceptable results.

be approximated or neglected. To simplify, the representation, we treat a two-phase mixture, a mass-average gas comprising all species, identified by subscript $(\ )_g$ and a single mass-averaged liquid phase identified by subscript $(\ )_l$. A proper analysis must account for the differences between fuel and oxidizer and for the broad range of sizes of liquid drops, streams or sheets. We shall not treat those matters here.

The conservation equations for three-dimensional motions are

$$\text{mass(gas)} \quad \frac{\partial \rho_g}{\partial t} + \nabla \cdot (\rho_g \vec{u}_g) = w_l \tag{2.1}$$

$$\text{mass(liquid)} \quad \frac{\partial \rho_l}{\partial t} + \nabla \cdot (\rho_l \vec{u}_l) = -w_l \tag{2.2}$$

$$\text{momentum} \quad \frac{\partial}{\partial t}(\rho_g \vec{u}_g + \rho_l \vec{u}_l) + \nabla \cdot (\rho_g \vec{u}_g \vec{u}_g + \rho_l \vec{u}_l \vec{u}_l) + \nabla p = \nabla \cdot \vec{\tau}_v \tag{2.3}$$

$$\text{energy} \quad \frac{\partial}{\partial t}(\rho_g e_{go} + \rho_l h_{lo}) + \nabla \cdot (\rho_g \vec{u}_g e_{go} + \rho_l \vec{u}_l h_{lo}) + \nabla \cdot (p \vec{u}_g) = Q + \nabla \cdot \vec{q} \tag{2.4}$$

The viscous stress tensor and heat flux vector (conduction) are represented by $\vec{\tau}_v$ and $\vec{q}$; Q is the energy released by homogeneous reactions in the gas phase (energy/sec.-vol.) and w_l is the rate of conversion, liquid to gas (mass/sec.-vol). Note that ρ_l is the liquid density, mass per unit volume of chamber, not the material density. The velocities $\vec{u}_g$, $\vec{u}_l$ are mass-averaged values.

Equations (2.1) - (2.4) form essentially the system used in early work, e.g. Crocco and Cheng (1956), Crocco (1963), and Harrje and Reardon (1972), and as the basis for most of the analysis incorporated in the computer program AUTOCOM. With the notable exception of the French work referred to above, most current work still does not account for different species explicitly in the conservation equations or for the manner in which liquid may be distributed among streams, sheets and droplet sizes. That does not mean that such complications are simply ignored. It has long been common practice to accommodate such details in analysis of the motion of the liquid and in the representations of the steady and unsteady sources of mass and energy. Thus rather fine distinctions between systems may appear in numerical results. For the purposes here a more blurred view is adequate to understand the main global behavior.

The momentum and energy equations (2.3) and (2.4) are correctly written in the first instance for the combined gas and liquid phases. Separate momentum equations are obtained by defining the force of interaction, $\vec{F}_l$, between the gas and liquid,

$$\vec{F}_l = -\rho_l \left[\frac{\partial \vec{u}_l}{\partial t} + \vec{u}_l \cdot \nabla \vec{u}_l \right] \tag{2.5}$$

and the heat added to the gas by heat transfer between the phases, vaporization, and chemical reaction,

$$Q_l = -\rho_l \left[\frac{\partial h_l}{\partial t} + \vec{u}_l \cdot \nabla h_l \right] \tag{2.6}$$

The enthalpy, h_l of the liquid includes the heat release associated with the transformation of liquid to gas. Note that $\vec{F}_l$ and Q_l are force and energy per unit volume of chamber. Thus F_l is the drag force acting on the average droplet times the number droplets per unit volume of chamber. With some rearrangement, the momentum and energy equations can be written

$$\rho_g \frac{\partial \vec{u}_g}{\partial t} + \rho_g \vec{u}_g \cdot \nabla \vec{u}_g + \nabla p = \nabla \cdot \vec{\tau}_v + \vec{F}_l - (\vec{u}_g - \vec{u}_l) w_l \tag{2.7}$$

$$\begin{aligned} \rho_g C_v \frac{\partial T_g}{\partial t} + \rho_g C_v \vec{u}_g \cdot \nabla T_g + p \nabla \cdot \vec{u}_g = {} & \zeta + Q_l + \nabla \cdot \vec{q} + \Phi \\ & + (h_{lo} - e_{vo}) w_l \\ & + \vec{u}_g \cdot (\vec{u}_g - \vec{u}_l) w_l + (\vec{u}_l - \vec{u}_g) \cdot \vec{F}_l \end{aligned} \tag{2.8}$$

where Φ is the dissipation function; its specific definition is unimportant here.

Equations (2.1), (2.7) and (2.8) are the equations of motion for the gas phase; and (2.2) (2.5) and (2.6) are those for the liquid phase. Within this formulation, equations (2.5) and (2.6) govern the motion of the "average droplet". It is difficult to use this approach in regions where the liquid is still moving as a stream or sheet; in practice, calculations are carried out only for droplet clouds. To determine the motions, one must specify $\vec{F}_l$ and Q_l. That's a fairly easy problem for slow motions of nonreactive particles; solution gives a familiar result for the attenuation of acoustic waves by gas/particle interactions [see, for example, Epstein and Carhart (1953), Temkin and Dobbins (1966); and Marble (1970); Culick (1975, 1976)].

The next more difficult problems involve droplets that are vaporizing or condensing. Beginning in the 1960's vaporization received serious attention as a possible contribution to driving instabilities, independently of combustion processes. We shall discuss the matter further in Sections 3 and 4.

If droplets are dispersed in the gas, the momentum and energy equations may be written in the more convenient form involving the mass-averaged properties of the two-phase mixture:

$$\rho\frac{\partial\vec{u}_g}{\partial t} + \rho\vec{u}_g\cdot\nabla\vec{u}_g + \nabla p = \nabla\cdot\vec{\tau}_v + \delta\vec{F}_l + \vec{u}_g\cdot\delta\vec{u}_l \tag{2.9}$$

$$\rho\vec{C}_v\left(\frac{\partial T_g}{\partial t} + \vec{u}_g\cdot\nabla T_g\right) + p\nabla\cdot\vec{u}_g = Q + \delta Q_l + \nabla\cdot\vec{q} + \Phi + (h_{lv} - h_v)w_l - \vec{u}_g\cdot\delta\vec{u}_l w_l + \delta\vec{u}_l\cdot\vec{F}_l \tag{2.10}$$

where

$$\delta\vec{F}_l = -\rho_l\left[\frac{\partial\delta\vec{u}_l}{\partial t} + \delta\vec{u}_l\cdot\nabla\delta\vec{u}_l + \delta\vec{u}_l\cdot\nabla\vec{u}_g + \vec{u}_g\cdot\nabla\delta\vec{u}_g\right] \tag{2.11}$$

$$\delta Q_l = -\rho_l\left[\frac{\partial\delta h_l}{\partial t} + \rho_l\delta\vec{u}_l\cdot\nabla\delta h_l + \delta\vec{u}_l\cdot\nabla(C_lT) + \vec{u}_g\cdot\nabla\delta h_l\right] \tag{2.12}$$

and $\delta\vec{u}_l = \vec{u}_l - \vec{u}_g$, $\delta h_l = h_l - C_lT$. The density of the mixture is

$$\rho = \rho_g + \rho_l = \rho_g(1 + C_m) \tag{2.13}$$

and $C_m = \rho_l/\rho_g$ is the mass fraction of liquid.

The mass weighted specific heats for the mixture are defined in the usual fashion [Marble(1969)]:

$$C_v = \frac{C_v + C_mC_l}{1 + C_m};\quad C_p = \frac{C_p + C_mC_l}{1 + C_m} \tag{2.14}$$

Now add $(1 + C_m)T$ times equations (2.1) and (2.2) to $1/C_v$ times equation (2.10) to find an equation for the pressure:

$$\frac{\partial p}{\partial t} + \vec{u}_g\cdot\nabla p + \gamma p\nabla\cdot\vec{u}_g = \frac{R}{C_v}\left[Q + \delta Q_l + \nabla\cdot\vec{q} + \Phi + \delta\vec{u}_l\cdot\vec{F}_l + \vec{u}_g\cdot(\vec{u}_g - \vec{u}_l)w_l + (h_{lv} - e_v)w_l - C_vT_g\nabla\cdot(\rho_l\delta\vec{u}_l)\right] \tag{2.15}$$

We assume that the perfect gas law is valid, $p = \rho_gRT_g$, where R is the gas constant for the gases only, for the mixture, $R = C_v - C_p$, $\gamma = C_p/C_v$ and

$$p = R_vT_g \tag{2.16}$$

The preceding manipulations have established the forms of the equations that account for the presence of liquid but are most appropriate for conditions when the mass fraction is nearly uniform, or C_m is approximately constant throughout the chamber. That is true in a solid propellant rocket, for which these equations were originally derived, and certainly not true in liquid-fueled systems. But even though C_m may vary significantly the mass averaged thermodynamic properties are not greatly affected. We shall use equations (2.9) - (2.16) without further elaboration of the possible inaccuracies. One important consequence is that the linearized form will give a good first approximation to the speed of sound accounting for the presence of liquid.

$$a = \sqrt{\gamma RT_g} = \left[\frac{\gamma}{1 + C_m}\frac{p}{\rho_g}\right]^{\frac{1}{2}} \tag{2.17}$$

The formula explicitly shows the characteristic retarded upon entry, that the propagation of disturbances is governed by the elasticity of the gas (the pressure), and by inertia supplied by the combined material, represented in the factor $(1 + C_m)\rho_g$.

We now have conservation equations in a form emphasizing the role that combustion instabilities are unsteady motions best regarded as perturbations of classical acoustics. The framework for study is based on the sum of the continuity equation (2.1) and (2.2), the momentum equation (2.9), and the energy equation (2.15) written with the pressure as the dependent variable

$$\frac{\partial p}{\partial t} + \vec{u}_g\cdot\nabla p = W \tag{2.18}$$

$$\rho\frac{\partial\vec{u}_g}{\partial t} + \rho\vec{u}_g\cdot\nabla\vec{u}_g = -\nabla p + \vec{F} \tag{2.19}$$

$$\frac{\partial T_g}{\partial t} + \gamma p\nabla\cdot\vec{u}_g = -\vec{u}_g\cdot\nabla p + P \tag{2.20}$$

For the conditions treated above:

$$W = -\rho\nabla\cdot\vec{u}_g = \nabla\cdot(\rho\delta\vec{u}_l) \tag{2.21}$$

$$\vec{F} = \nabla\cdot\vec{\tau}_v + \delta\vec{F}_l + \delta\vec{u}_l w_l \tag{2.22}$$

$$\mathcal{P} = \frac{\bar{R}}{\bar{C}_v}[Q + \delta Q_l + \nabla \cdot \vec{q} + \delta \vec{u}_l \cdot \vec{F}_l + \{(h_l - e) + \frac{1}{2}(\delta \vec{u}_l)^2\}w_l - \bar{C}_v T_g \cdot (\rho_l \delta \vec{u}_l)] \tag{2.23}$$

Equations (2.18)-(2.20) are suitable for two-and three- dimensional problems. There are many important cases of nearly pure axial or longitudinal motions arising in all three types of systems. A perfectly serviceable analysis may then be constructed using the one-dimensional approximation obtained by replacing $\vec{u}_g$ by u_g, the axial component of velocity; $\vec{u}_g \cdot \nabla$ by $u_g \frac{\partial}{\partial z}$ and $\nabla \cdot (\ )$ by $\frac{1}{S_c} \frac{\partial}{\partial z}(S_c\ )$ where S_c is the cross-section area. Equations (2.18)-(2.20) then become

$$\frac{\partial \rho}{\partial t} + u_g \frac{\partial \rho}{\partial z} = W_1 \tag{2.24}$$

$$\rho \frac{\partial u_g}{\partial t} + \rho u_g \frac{\partial u_g}{\partial z} = -\frac{\partial p}{\partial z} + \mathcal{F}_1 \tag{2.25}$$

$$\frac{\partial p}{\partial t} + \bar{\gamma} p \frac{1}{S_c} \frac{\partial}{\partial z}(S_c u_g) = -u_g \frac{\partial p}{\partial z} + \mathcal{P}_1 \tag{2.26}$$

where W_1, $\mathcal{F}_1$, $\mathcal{P}_1$ are (2.21)-(2.23) written for one-dimensional motions according to the rules given above.

2.2 Formulation of an Approximate Analysis

With the recent developments in high-speed computers, serious consideration must now be given to extensive numerical analysis of internal flows and combustion instabilities based on the complete equations of motion. That is a formidable task; it appears that the most extensive program of that sort is being pursued in France. Work in the U.S., including the computer program AUTOCOM [Reichel et al (1973, 1974) and the later version written by Nickerson and Nguyen (1984a, 1984b)] has been based on approximations to the equations explicitly ignoring, for example, possible influences of turbulence on the motions of liquid drops. Especially, approximations to the crucial source terms are generally based on models that are founded on heuristic reasoning. As a result, much reliance must be placed on correlations of data. It is the nature of flows in combustion chambers that, due to the complicated gasdynamics and chemistry, all theoretical work must eventually make use of experimental results.

Thus it is fundamental to the subject that an approximate analysis be carefully formulated and understood. We cannot here review all analyses that have been constructed. Rather, we shall develop a fairly general form to use as a framework for discussing particular results. To simplify the calculations at this point, we shall not display the details of the source terms W, $\vec{\mathcal{F}}$ and $\mathcal{P}$ in equations (2.18)- (2.20).

Write all dependent variables as sums of mean and fluctuating parts, $p = \bar{p} + p'$, etc. We assume that average values do not vary in time. That assumption is occasionally violated in actual systems but we shall not elaborate here.To second order in the fluctuations, equations (2.19) and (2.20) are

$$\bar{\rho}\frac{\partial \vec{u}_g'}{\partial t} + \nabla p' = -\bar{\rho}(\vec{u}_g \cdot \nabla \vec{u}_g + \vec{u}_g' \cdot \nabla \bar{u}_g') - \rho'(\vec{u}_g \cdot \nabla \vec{u}_g) - \rho' \frac{\partial \vec{u}_g'}{\partial t} + \vec{\mathcal{F}}' \tag{2.27}$$

$$\frac{\partial p'}{\partial t} + \bar{\gamma}\bar{p}\nabla \cdot \vec{u}_g' = -\vec{u}_g \cdot \nabla p' - \bar{\gamma}p'\nabla \cdot \vec{u}_g - \vec{u}_g' \cdot \nabla \bar{p}' - \bar{\gamma}p'\nabla \cdot \vec{u}_g' + \mathcal{P}' \tag{2.28}$$

The mean velocity varies in the chamber, but the average pressure is taken to be uniform. That assumption is assuming that the average Mach number is relatively small, a restriction commonly violated in practice. Large Mach numbers cause quantitative corrections but do not introduce fundamental changes of behavior. The equations can easily be extended to cover flows at high Mach numbers.

Equations (2.27) and (2.28) contain the six dependent variables ρ', p', T' and three velocity components. A complete set is obtained by including the perturbed forms of the continuity equation (2.15) and the equation of state (2.16):

$$\frac{\partial \rho'}{\partial t} = -\vec{u}_g \cdot \nabla \rho' - \vec{u}_g' \cdot \nabla \bar{\rho} + \vec{u}_g' + W' \tag{2.29}$$

$$p' = \bar{R}(\rho' \bar{T} + \bar{\rho} T') + \bar{R}(\rho' T') \tag{2.30}$$

Many works have been based on solutions to the equations as written here. But the primary sources of information about combustion instabilities are oscillations of pressure. Thus much is gained by forming a wave equation for p'. Differentiate (2.28) with respect to time and substitute (2.27) for $\partial \vec{u}_g'/\partial t$ to find

$$\nabla^2 p' - \frac{1}{\bar{a}^2}\frac{\partial^2 p'}{\partial t^2} = A \tag{2.31}$$

where $\bar{a}^2 = \bar{\gamma}\bar{R}\bar{T}$ is constant and

$$A = -\bar{\rho}\nabla \cdot (\vec{u}_g \cdot \nabla \vec{u}_g' + \vec{u}_g' \cdot \nabla \bar{u}_g') + \frac{1}{\bar{a}^2}\vec{u}_g \cdot \nabla \frac{\partial p'}{\partial t} + \frac{\bar{\gamma}}{\bar{a}^2}\frac{\partial p'}{\partial t}\nabla \cdot \vec{u}_g$$

$$= \nabla \cdot (\rho \vec{u}_g' \cdot \nabla \vec{u}_g' + \rho' \frac{\partial \vec{u}_g'}{\partial t}) + \frac{1}{\bar{a}^2}\frac{\partial}{\partial t}(\vec{u}_g' \cdot \nabla p') + \frac{\bar{\gamma}}{\bar{a}^2}\frac{\partial}{\partial t}(p'\nabla \cdot \vec{u}_g')$$

$$+\nabla\cdot\vec{\mathcal{F}}' - \frac{1}{\bar{a}^2}\frac{\partial^2 \cdot}{\partial t^2} \tag{2.32}$$

Boundary conditions set on the gradient of p' are found by taking the scalar product of the outward normal vector with equation (2.27)

$$\hat{n}\cdot\nabla p' = -f \tag{2.33}$$

with

$$\begin{aligned} f = \bar{\rho}\frac{\partial \vec{u}_g'}{\partial t}\cdot\hat{n} + \rho(\vec{u}_g\cdot\nabla\vec{u}_g' + \vec{u}_g'\nabla\vec{u}_g)\cdot\hat{n} \\ + \bar{\rho}(\vec{u}_g'\cdot\nabla\vec{u}_g')\cdot\hat{n} + \rho'\frac{\partial\vec{u}_g}{\partial t}\cdot\hat{n} - \vec{\mathcal{F}}'\cdot\hat{n} \end{aligned} \tag{2.34}$$

If all perturbations are absent, functions h and f vanish, and we recover the wave equation for the pressure in classical acoustics with the boundary condition for a rigid wall, $\hat{n}\cdot\nabla p' = 0$. We shall base our discussion on that case as the zeroth approximation. There may be circumstances when a different choice is more effective- e.g. if the average Mach number is high and the influence of the exhaust nozzle on the wave motions is substantial* - but it is good enough here to assume this limiting case. The general solution to the unperturbed problems can be written as a superposition of the normal modes $\psi_n(\vec{r})$ satisfying the equations.

$$\begin{aligned} \nabla^2\psi_n + k_n^2\psi_n = 0 \\ \hat{n}\cdot\nabla\psi_n = 0 \end{aligned} \tag{2.35}a,b$$

where k_n is the wavenumber, related to the frequency by

$$\omega_n = \bar{a}k_n \tag{2.36}$$

For three-dimensional problems, n stands for three indices.

The allowed values of the wavenumbers and the mode shapes ψ_n are determined entirely by the geometry of the chamber. These define the classical acoustic modes which, when perturbed, become the most common kind of combustion instabilities. Purely longitudinal modes are represented by

$$\begin{aligned} \psi_l(z) = \cos(k_l z) \\ k_l = l\frac{\pi}{L} \end{aligned} \tag{2.37}a,b$$

and the cyclic frequencies are integral multiples of the fundamental, $f_1 = \omega_1/2\pi = a/2h$. This is the result for a chamber closed at both ends, probably the most common case in propulsion systems.

For a cylindrical chamber of radius R, the mode shapes and natural frequencies are

$$\psi_{lmn} = \cos k_l z\ J_n(\kappa^{mn} r)\begin{Bmatrix}\cos n\theta \\ \sin n\theta\end{Bmatrix} \tag{2.38}a$$

$$k_n^2 \equiv k_{lmn}^2 = k_l^2 + \kappa_{mn}^2 \tag{2.38}b$$

and the κ_{mn} are the roots of

$$\left.\frac{dJ_n(\kappa_{mn}r)}{dr}\right|_{r=R} = 0 \tag{2.39}$$

Both (2.37)a and (2.38)a represent standing waves; representations of the corresponding traveling waves are easily constructed.

These results are the zeroth approximations to the majority of combustion instabilities observed in practical systems. Longitudinal modes generally fall in the lower frequency range below 1.5kHz and are found in all three types of engines. The geometries of ramjet engines and augmentors cause distortions of the mode shapes from the simple result (2.37)a, but the essential idea remains. We discuss in Section 5.3.3 how mode shapes and frequencies are composed for those cases.

For a cylindrical chamber, equations (2.38)a,b are usually good approximations to the high frequency instabilities having frequencies as high as 10-20 kHz and higher. Although mixed modes with $l \neq 0$ (i.e. having axial distributions) occur, more commonly found are purely tangential or azimuthal modes ($m \neq 0$, $n \neq 0$), purely radial modes ($m \neq 0$, $n = 0$); or combinations when m, n are both non-zero, broadly called transverse modes. These modes are the basis for the instabilities called 'screeching'; the most common mode has been the 'first tangential' for which the classical mode shape is $J_1(\kappa_{11}r)\sin\theta$ or $J_1(\kappa_{11}r)\cos\theta$).

Equations (2.35)a,b do not contain the important case having the lowest frequencies commonly called 'chugging', a bulk or Helmholtz mode. That corresponds to the solution $k_n = 0$, but exists only because there is either

* Two examples are the analyses and experiments for a small liquid rocket by Crocco, Grey, and Harrje (1960) and for a small laboratory ramjet combustor by Laverdant, Poinsot and Candel (1986). The results are not interpreted in the fashion suggested here because the nozzle causes a large frequency shift. A more accurate choice must be made for the zeroth order approximation ψ_n.

a perturbation in the volume or, usually, at the boundary, so $\hat{n} \cdot \nabla \psi_n \neq 0$. When found in liquid rockets, those modes have often been referred to as low frequency instabilities [e.g. Harrje and Reardon (1972)]. It may happen also, as in ramjets, that a portion of the system may oscillate in a bulk mode, while part exhibits a wave behavior - the frequency is of course the same throughout.

The main point here is that the classical unperturbed modes described by equations (2.35)a,b really are good approximations to a large proportion of observed combustion instabilities. The results (2.37)a,b and (2.38)a,b are the two most important special cases for actual systems but in general (2.35)a,b must be solved for the actual geometry. That is now a routine matter of numerical analysis and we may simply assume that for whatever system we wish to study, the natural mode shapes $\psi_n(\vec{r})$ and frequencies ω_n are known.

The practical question is: how do the processes represented by the functions h and f, equations (2.32) and (2.34), affect the mode shapes and frequencies ? In fact, the details of the mode shapes are of less interest because the changes are relatively small. Central to the problem of linear stability are the frequencies, which become complex quantitites: the imaginary part is the growth or decay rate of the corresponding mode. For nonlinear behavior the main questions concern the conditions under which periodic limit cycles exist, what the amplitudes are, and how their characteristics are influenced by linear processes. The approximate analysis we now construct is a basis for examining both linear and nonlinear behavior. The method amounts to comparing the unperturbed problem, for which h and f vanish, with the actual problem to be analyzed ($h, f \neq 0$).

Multiply equation (2.31) by ψ_n, (2.35)a by p', subtract the results, and integrate over the chamber:

$$\int [\psi_n \nabla^2 p' - p' \nabla^2 \psi_n] dV - \frac{1}{\bar{a}^2} \int \psi_n \frac{\partial^2 p'}{\partial t^2} dV - k_n^2 \int p' \psi_n dV = \int h dV$$

Apply Green's theorem to the left hand side, substitute the boundary conditions (2.33) and (2.35)b and re-arrange the terms to give

$$-\frac{1}{\bar{a}^2} \int \psi_n \frac{\partial^2 p'}{\partial t^2} dV - k_n^2 \int \psi_n p' dV = \int \psi_n h dV + \oint\!\!\!\oint \psi_n f \, dS \tag{2.40}$$

We now use a form of the method of least residuals, essentially a form of Galerkin's method. This approach was first applied to combustion instabilities in liquid rockets by Zinn and Powell (1968, 1970). Independently, essentially the same idea was worked out for solid propellant rockets by Culick (1971, 1975, 1976), the basis for the discussion here. The unsteady pressure field is expressed as a synthesis of the normal modes $\psi_m(\vec{r})$ with time-varying amplitudes $\eta_m(t)$:

$$p'(\vec{r}, t) = \bar{p} \sum \eta_m(t) \psi_m(\vec{r}) \tag{2.41}$$

Correspondingly, the velocity field is written

$$\vec{u}'(\vec{r}, t) = \sum \frac{\dot{\eta}_m}{\bar{\gamma} k_m^2} \nabla \psi_m(\vec{r}) \tag{2.42}$$

Term by term these series satisfy the perturbed problem, equations (2.31) and (2.33) with $h = f = 0$, providing the amplitudes satisfy

$$\ddot{\eta}_m + \omega_m^2 \eta_m = 0 \tag{2.43}$$

where $\omega_m^2 \equiv \bar{a}^2 k_m^2$. Thus $\eta_m \sim e^{\pm i \omega_m t}$ and we recover the correct representation of natural modes.

Obviously (2.41) and (2.42) are not exact representations of the actual fields, for the correct boundary conditions are not satisfied. Equation (2.41) gives $\hat{n} \cdot \nabla p' = 0$ because all ψ_m satisfy (2.35)b. Consequently, (2.41) and (2.42) do not accurately reproduce the spatial structure of the unsteady motions near the boundary. The errors are small if h and f are small and because of the spatial averaging, the equations found for the amplitudes $\eta_m(t)$ will provide a satisfactory basis for studying real problems.

The set of normal modes can be constructed so the $\psi_n(\vec{r})$ are orthogonal:

$$\int \psi_m \psi_n dV = E_n^2 \delta_{mn}$$
$$E_n^2 = \int \psi_n^2 dV \tag{2.44)a,b}$$

Substitute (2.41) in the left hand side of (2.40) and use the orthogonality property (2.44)a,b to find the system of equations for the amplitudes:

$$\frac{d^2 \eta_n}{dt^2} + \omega_n^2 \eta_n = F_n \tag{2.45}$$

with

$$F_n = -\frac{\bar{a}^2}{\bar{p} E_n^2} \left\{ \int h \psi_n dV + \oint\!\!\!\oint f \psi_n dS \right\} \tag{2.46}$$

The corresponding results for one-dimensional problems are

$$\frac{d^2 \eta_n}{dt^2} + \omega_n^2 \eta_n = F_n \tag{2.47}$$

$$F_l = -\frac{\bar{a}^2}{\bar{p}E_l^2}\{\int_0^L h_1\psi_l S_c dz + [f_1\psi_l S_c]_0^L\} \tag{2.45}$$

following the expansions for the acoustic field

$$p'(z,\ t) = \bar{p}\sum_{j=1}^{\infty}\eta_j(t)\psi_j(z)$$
$$u'(z,\ t) = \sum_{j=1}^{\infty}\frac{\dot{\eta}_j}{\bar{\gamma}k_j^2}\frac{d\psi_j(z)}{dz} \tag{2.49}a,b$$

Orthogonality is expressed as

$$\int_0^L \psi_j\psi_l S_c dz = E_l^2\delta_{jl}$$
$$E_l^2 = \int_0^L \psi_l^2 S_c dz \tag{2.50}a,b$$

Three points must be emphasized:

i.) Although the unsteady field has been synthesized of the mode shapes for standing waves, solutions to equations (2.45) and (2.47) may be used to represent standing waves with energy losses or gains, traveling waves, and discrete wave motions or pulses;

ii.) The forcing functions F_n and F_l are nonlinear functions of the pressure and velocity fluctuations, so (2.45) and (2.47) are sets of coupled nonlinear ordinary differential equations;

iii.) Many interesting one-dimensional problems involve piecewise representation of the acoustic field due to abruptly nonuniform distributions of cross-section area. The formulation (2.47)-(2.50) remains valid for those cases.

We should note also that the procedure beginning with spatial averaging and leading to (2.45) and (2.47) amounts to solving (2.31) and retaining the first term in a solution by iteration; that method is summarized in Section 4.3.

Solution to equations (2.45) or (2.47) requires first evaluation of the forces F_n or F_l. To do so the various sources must be represented, a subject discussed in the following section. The second order equations may then be solved numerically, a procedure followed by Zinn and Powell (1970, 1971). However, great advantage is gained in many problems by applying the method of time-averaging (or expansion in two time scales) to replace the second order system by an equivalent set of first order equations. This step greatly reduces the cost of routine calculations and also provides a more convenient basis for formal analysis of the general behavior. The following argument applies to both the three-dimensional and one- dimensional formulations.

Time averaging is an effective procedure for many practical problems, based on the observation that the oscillations commonly have amplitudes and phases varying slowly in time; their changes are small in one period of oscillation. Hence, the amplitudes $\eta_n(t)$ may be written in the form

$$\eta_n(t) = r_n(t)\sin(\omega_n t + \phi_n(t)) = A_n(t)\sin\omega_n t + B_n(t)\cos\omega_n t \tag{2.51}$$

The time varying phase $\phi_n(t)$ is observed as a frequency shift, the actual frequency for the perturbed mode being $d/dt(\omega_n t + \phi_n) = \omega_n + \psi_n$.

We shall not cover the method for constructing the equations for $\eta_n(t)$ and $\phi_n(t)$ or the $A_n(t)$ and $B_n(t)$. The method was developed by Krylov and Bogoliubov (1947) in a form directly applicable here to the case of purely longitudinal modes when the frequencies are integral multiples of the fundamental, equation (2.37)b. When the frequencies are not so related, as for the common case of transverse modes in a cylindrical chamber, some difficulties arise which have been treated approximately by Culick (1976), and by Yang and Culick (1986) for problems of combustion instabilities in ramjet engines.

Here we quote only the results obtained for longitudinal modes:

$$\frac{dA_n}{dt} = \frac{1}{2\pi}\int_0^{\tau_n} F_n\cos\omega_n t'dt'$$
$$\frac{dB_n}{dt} = -\frac{1}{2\pi}\int_0^{\tau_n} F_n\sin\omega_n t'dt' \tag{2.52}a,b$$

The interval of averaging has been taken equal to $\tau_n = 2\pi/\omega_n$: the equations for each mode are averaged over the period of that mode. During this interval, *all* amplitudes are supposed not to change significantly. That is, the A_m, B_m appearing in F_n are taken to be constant when the integrals are performed.

If the nonlinear processes are due only to second order acoustics, then F_n has the form [Culick (1976)]

$$F_n = -\sum_{i=1}^{\infty}[D_{ni}\dot{\eta}_i + E_{\eta i}\eta_i] - \sum_{i=1}^{\infty}\sum_{j=1}^{\infty}[A_{nij}\dot{\eta}_i\dot{\eta}_j + B_{nij}\eta_i\eta_j] \tag{2.53}$$

The constants D_{ni}, E_{ni}, A_{nij}, B_{nij} depend on the unperturbed node shapes and frequencies. Linear processes *always* lead to the forms shown; the D_{ni}, E_{ni} are linear combinations of the various contributions, some of which are proportional to the Mach number of the mean flow. Others depend on other small parameters. For example, attenuation due to inert particles depends on the properties of the particles and on the mass fraction of condensed material. For the case of longitudinal modes, substitution of (2.53) in (2.52)a,b eventually leads to the equations

$$\begin{aligned}\frac{dA_n}{dt} &= \alpha_n A_n + \theta_n B_n + \frac{\beta_n}{2}\sum_{i=1}^{\infty}[A_i(A_{n-i} - A_{i-n} - A_{i+n}) \\ &\qquad - B_i(B_{n-i} + B_{i-n} - B_{i+n})] \\ \frac{dB_n}{dt} &= \alpha_n B_n - \theta_n A_n + \frac{\beta_n}{2}\sum_{i=1}^{\infty}[A_i(B_{n-i} + B_{i-n} - B_{i+n}) \\ &\qquad + B_i(A_{n-i} - A_{i-n} + A_{i+n})]\end{aligned} \tag{2.54}a,b$$

where

$$\begin{aligned}\alpha_n &= -\frac{1}{2}D_{nn} \\ \theta_n &= -\frac{1}{2}\frac{E_{nn}}{\omega_n}\end{aligned} \tag{2.55}a,b$$

and

$$\beta = \frac{\bar{\gamma}+1}{8\bar{\gamma}}\omega_1 \tag{2.56}$$

The modes will be linearly coupled only if very special influences are present; in general $D_{ni} = E_{ni} = 0$ if $i \neq n$. While equations (2.54)a,b are valid for any linear process, the nonlinear terms are special, representing only the gasdynamics to second order for longitudinal nodes.

With this formulation, the analytical problem for combustion instabilities has come down to constructing the functions h and f - i.e. modeling the contributions processes appearing in the sources $\mathcal{W}$, $\vec{\mathcal{F}}$ and $\mathcal{P}$, equations (2.21) - (2.23) and then carrying out the integrals defining F_n, equation (2.46). As a preliminary step, of course, the natural modes and frequencies must be computed. Because almost all of this paper will be concerned with linear behavior, a few general remarks are in order.

2.3 The Problem of Linear Stability

The nice feature of linear behavior is that the problem can be solved once for all cases. We have, of course, chosen to treat a rather special form of the general problem in order to reach such a conclusion. If, for example, the average Mach number is large, or if the action of the exhaust nozzle causes a substantial shift from the idealized condition for a rigid wall, then the functions h and f, equations (2.32) and (2.34) are not small perturbations of the classical problem. Nevertheless, the approach taken here is a simple first approximation and in any event offers what we really need - a convenient vehicle for comparing the behavior in different systems, and the possible consequences of different mechanisms.

We assume now that h and f are linear functions of the dependent variables p', $\vec{u}'$, ρ', and T'. Thus equation (2.45) is satisfied if all functions have exponential time dependence, so $p'/\bar{p} \sim e^{i\hat{a}kt}$, $\vec{u}' \sim e^{i\hat{a}kt}$, etc. and h, f, η_n have the same dependence:

$$\eta_n = \hat{\eta}_n e^{i\hat{a}kt};\ h = \hat{h}e^{i\hat{a}kt};\ f = \hat{f}e^{i\hat{a}kt} \tag{2.58}a,b,c$$

All amplitudes denoted by ( ) are complex functions - i.e. they are generally not in phase with one another. It is convenient to measure the phase relative to the pressure oscillation and its amplitude $\hat{\eta}_n$ is taken to be real; because coupling between modes is absent we are really treating one term in the series (2.41) and (2.42):

$$\frac{p'(\vec{r},\ t)}{\bar{p}} = \hat{\eta}_n e^{i\hat{a}kt}\psi_n(\vec{r}) \tag{2.59}$$

and

$$\vec{u}'(\vec{r},\ t) = \frac{\dot{\eta}_n}{\bar{\gamma}k_n^2}\nabla\psi_n(\vec{r}) = \frac{i\hat{a}k}{\bar{\gamma}k_n^2}\hat{\eta}_n e^{i\hat{a}kt}\nabla\psi_n$$

Because the actual value of k differs from k_n by small quantitites, we have to first order

$$\frac{\vec{u}'(\vec{r},\ t)}{\bar{a}} = \frac{i}{\bar{\gamma}k_n}\hat{\eta}_n e^{i\hat{a}kt}\nabla\psi_n \tag{2.60}$$

The expressions (2.59) and (2.60) are to be substituted for p', $\vec{u}'$ when F_n is computed from its definition (2.46). Also to the order considered here, $p'/\bar{p}$ and $T'/\bar{T}$ can be approximated by their values for isentropic motions,

$$\frac{\rho'}{\bar{\rho}} \approx \frac{1}{\bar{\gamma}}\frac{p'}{\bar{p}};\ \frac{T'}{\bar{T}} \approx \frac{\bar{\gamma}-1}{\bar{\gamma}}\frac{p'}{\bar{p}} \qquad (2.61)a,b$$

The wave number k is complex,

$$k = \frac{1}{\bar{a}}(\omega - i\alpha) \qquad (2.62)$$

and with the definitions used here, $\alpha > 0$ if the mode is unstable, for then $p'/\bar{p} \sim e^{\alpha t}$. Substitution of (2.58) in (2.45) and (2.46) and cancellation of the common factor $e^{i\bar{a}kt}$ gives the formula for k^2:

$$k^2 = \frac{1}{\bar{a}^2}(\omega - i\alpha)^2 = \frac{\omega_n^2}{\bar{a}^2} + \frac{1}{\bar{\rho}E_n^2}\{\int \frac{\hat{h}}{\hat{\eta}_n}\psi_n\, dV + \oint\!\!\!\oint \frac{\hat{f}}{\hat{\eta}_n}\psi_n dS\} \qquad (2.63)$$

Because we are treating only small perturbations, α/ω and $(\omega-\omega_n)/\omega_n$ are small. With this approximation, the real and imaginary parts of (2.63) give convenient formulas for the frequency and growth constant of the actual motions:

$$\begin{aligned}\omega &= \omega_n + \frac{\bar{a}^2}{2\omega_n\bar{\rho}E_n^2}\{\int \frac{\hat{h}^{(r)}}{\hat{\eta}_n}\psi_n dV + \oint\!\!\!\oint \frac{\hat{f}^{(r)}}{\hat{\eta}_n}\psi_n dS\} \\ \alpha &= \frac{-\bar{a}^2}{2\omega_n\bar{\rho}E_n^2}\{\int \frac{\hat{h}^{(i)}}{\hat{\eta}_n}\psi_n dV + \oint\!\!\!\oint \frac{\hat{f}^{(i)}}{\hat{\eta}_n}\psi_n dS\}\,.\end{aligned} \qquad (2.64)a,b$$

Now we relate these formulas to the results obtained in the preceding section with the method of averaging. First note that η_n, equation (2.5)a can be written:

$$\eta_n = \hat{\eta}_n e^{i\bar{a}kt} = \hat{\eta}_n e^{\omega - i\alpha t} = \hat{\eta}_n e^{\alpha t + i(\omega-\omega_n)t} e^{i\omega_n t}$$

or, if $\delta\omega_n = \omega - \omega_n$ denotes the frequency shift,

$$\eta_n = \hat{\eta}_n e^{\alpha t} e^{i(\omega_n + \delta\omega_n)t} \qquad (2.65)$$

For linear behavior only, equations (2.54)a,b are

$$\begin{aligned}\frac{dA_n}{dt} &= \alpha_n A_n + \theta_n B_n \\ \frac{dB_n}{dt} &= \alpha_n B_n - \theta_n A_n\end{aligned} \qquad (2.66)a,b$$

Direct substitution shows that these equations are satisfied by

$$\begin{aligned}A_n &= A_{n0}e^{\alpha_n t}\cos\theta_n t \\ B_n &= -A_{n0}e^{\alpha_n t}\sin\theta_n t\end{aligned} \qquad (2.67)a,b$$

The assumed form (2.51) for the amplitude is therefore

$$\eta_n(t) = A_{n0}e^{\alpha_n t}\sin(\omega_n + \theta_n)t \qquad (2.68)a,b$$

This is exactly the imaginary part of (2.65). We conclude that the parameter $\alpha_n = -D_{nn}/2$ defined by (2.55)a is the growth constant of the nth perturbed mode equation (2.64)b; and $\theta_n = -E_{nn}/2\omega_n$ defined by (2.53)b is the frequency shift, calculated with equation (2.64)a, $\theta_n = \delta\omega_n \approx \omega - \omega_n$.

All of the above can be summarized in the following steps, a receipe for assessing the consequences of an analysis of linear behavior.

i.) Construct the contributions to the functions h and f by applying the definitions of the source functions W, $\vec{\mathcal{F}}$ and $\mathcal{P}$ and extracting their linear forms;

ii.) Substitute the acoustic approximations $p' = \bar{p}\eta_n\psi_n$ and $\vec{u}' = \dot{\eta}_n\nabla\psi_n/\bar{\gamma}k_n^2$ in f and h; if required, the formulas (2.61)a,b are used for the density and temperature fluctuations;

ii.) Compute F_n according to its definition (2.46). If second derivatives of the amplitudes should arise, they are to be replaced by the zeroth order approximation, $\ddot{\eta}_n \approx -\omega_n^2\eta_n$.

v.) Then F_n will have the form (2.53) with $D_{ni} = E_{ni} = 0$ for $i \neq n$. The values for the growth constant and the frequency shift for the nth mode can be found immediately from the coefficients of $\dot{\eta}_n$ and η_n:

$$\alpha_n = -\frac{1}{2}D_{nn};\ \theta_n = \omega - \omega_n = -\frac{1}{2}\frac{E_{nn}}{\omega_n} \qquad (2.69)$$

In this way the primary information given by a linear analysis can be found in a straightforward manner. It's true that due to approximations made here, there may be quantitative inaccuracies greater than those accompanying a more careful computation of linear behavior. The great advantage of the procedure described above is that comparison of proposed mechanisms can readily be made.

2.4 Evaluating the Linear Contributions to the Frequency Shift and the Growth Constant

In this review we concentrate on the linear behavior. We shall find in Section 3 that proposed mechanisms for instabilities can be properly assessed only within the complete acoustical analysis. It is therefore essential to work out the details for the most general possible forms of the inhomogeneous forcing functions represented by h and f.

Some rearrangement leads to the following result for the linear parts of h and f:

$$\begin{aligned}\int \hat{h}\psi_n dV + \iint \hat{f}\psi_n dS = \bar{\rho}k_n^2 \int (\vec{u}_g \cdot \hat{\vec{u}}_g)\psi_n dV - \bar{\rho}\int (\vec{u}_g \times \nabla \times \vec{u}_g)\cdot \nabla\psi_n dV \\ + i\frac{k_n}{\bar{a}}\int \psi_n[\vec{u}_g \cdot \nabla\hat{p} + \gamma\bar{p}\nabla\cdot\hat{\vec{u}}_g]dV \\ - i\frac{k_n}{\bar{a}}\int \psi_n \hat{P} dV - \int \hat{\mathcal{F}}\cdot\nabla\psi_n dV \\ + i\bar{\rho}\bar{a}k_n \iint \psi_n \hat{\vec{u}}_g \cdot \hat{n} dS\end{aligned}$$

We assume throughout that all terms in h and f are small (e.g. many are of order of the mean flow Mach number) and since k differs from k_n by terms of that order, we replace k by k_n, thereby consistently neglecting terms of order square in small quantities. For the same reason, we replace $\hat{p}$ and $\hat{\vec{u}}$ by their unperturbed values,

$$\hat{p} = \bar{p}\hat{n}_n\psi_n; \quad \hat{\vec{u}} = \frac{i\bar{a}}{\bar{\gamma}k_n}\hat{n}_n\nabla\psi_n \tag{2.70}$$

Taking the real and imaginary parts of the integrals and substituting in (2.64)a,b gives the basic formulas for studying linear stability:

$$\begin{aligned}\omega = \omega_n + \frac{\bar{a}^2}{2\omega_n\bar{p}E_n^2}\{\frac{k_n}{\bar{a}}\int \psi_n \frac{\hat{P}^{(i)}}{\hat{n}_n}dV - \int \frac{1}{\hat{n}_n}\hat{\mathcal{F}}^{(r)}\cdot\nabla\psi_n dV \\ - \bar{\rho}\bar{a}k_n \iint \frac{1}{\hat{n}_n}(\hat{\vec{u}}_g^{(i)}\cdot\hat{n})\psi_n dS\}\end{aligned} \tag{2.71}$$

$$\begin{aligned}\alpha = -\frac{\bar{a}^2}{2\omega_n\bar{p}E_n^2}\{\frac{k_n}{\bar{a}}\int \psi_n \frac{\hat{P}^{(r)}}{\hat{n}_n}dV + \int \hat{\mathcal{F}}^{(i)}\cdot\nabla\psi_n dV \\ - (\bar{\gamma}-1)\frac{k_n}{\bar{a}}\bar{p}\int \psi_n^2(\nabla\cdot\vec{u}_g)dV \\ + \bar{\rho}\bar{a}k_n \iint \frac{1}{\hat{n}_n}(\hat{\vec{u}}_g^{(r)}\cdot\hat{n})\psi_n + \frac{1}{\bar{\gamma}}\psi_n^2(\vec{u}_g\cdot\hat{n})]dS\}\end{aligned} \tag{2.72}$$

The term $\hat{\vec{u}}\cdot\hat{n}$ in the surface integral arises from the contribution $\rho(\partial\vec{u}/\partial t)\cdot\hat{n}$ in f. Here $\vec{u}$ is not replaced by its unperturbed value ($\vec{u}\cdot\hat{n} = 0$) at the surface because in general the boundary is not rigid. It has long been a convention in classical acoustics to replace fluctuations of the velocity at a boundary by admittance functions. That has become common practice in analysis of combustion instabilities with account taken of the mean flow through the boundary, as at a burning surface in solid propellant rockets, and at the exhaust nozzle generally. The admittance function A_N at the nozzle entrance is defined as

$$A_N = \frac{1}{\bar{a}}\frac{\hat{\vec{u}}_g\cdot\hat{n}}{\hat{p}/\bar{\gamma}\bar{p}} = \frac{\bar{\gamma}}{\bar{a}}\frac{\hat{\vec{u}}_g\cdot\hat{n}}{\hat{n}_n\psi_n} \tag{2.73}$$

Thus the combination in the surface integral is

$$\frac{1}{\bar{a}}[\bar{\gamma}\frac{\hat{\vec{u}}_g\cdot\hat{n}}{\hat{n}_n\psi_n} + \vec{u}_g\cdot\hat{n}] = A_N + M_N \tag{2.74}$$

All types of systems treated in this paper use choked exhaust nozzles. Owing to the large gradients of mean flow properties in the convergent section, such a nozzle acts as an efficient reflector of acoustic disturbances under most conditions - but not always. Tsien (1952) first analyzed the unsteady behavior in nozzles, in a paper that set the essential basis for all subsequent calculations. Crocco (1953) and Crocco and Cheng (1956) elaborated on Tsien's treatment of one-dimensional (planar) wave motions. Some chief results of the theory were confirmed with tests performed by Crocco, Grey and Monti (1961). Culick (1961) reported limited results for three-dimensional motions but the most thorough treatment of the subject was given by Crocco and Sirignano (1967). The latter work is particularly useful because fluctuations of vorticity and entropy are accommodated. Some consequences of entropy disturbances incident in a nozzle were later investigated by Marble (1973) and Marble and Candel (1977); that is an issue which arises in connection with analysis of convective waves as a possible mechanism for instabilities. Some aspects of nonlinear behavior of a nozzle have been treated by Crocco and Sirignano (1966) and by Zinn and Crocco (1968a, 1968b); they will not be pursued here.

The exhaust nozzle provides a significant loss of acoustic energy particularly for longitudinal oscillations. Its effects are less clear for three-dimensional motions, particularly when the nozzle is submerged, a common feature in solid propellant rockets. There has therefore been considerable interest in measuring the nozzle admittance, beginning in the late 1960's [Dufflun et al (1967); Culick and Dehority (1969)]. The most elaborate and effective

experimental work has been done using a large impedance tube with flow, a method first used by Zinn et al (1973). For longitudinal modes, for which the wavelength is usually much greater than the nozzle length, the "short nozzle approximation" is quite accurate, $A_N = (\bar{\gamma}-1)\bar{M}_N/2$. There is no experimental data sufficiently accurate to prove or disprove the theoretical prediction that under some conditions transverse oscillations may be amplified by the exhaust nozzle: that is, a small amount of energy is transferred from the mean to the unsteady flow, not an unreasonable possibility (cf. whistles and sirens). For most purposes here the action of the nozzle may be viewed as causing attenuation of acoustic waves with a slight increase of axial wavelength.

Similarly, an admittance function can be introduced to represent the effects of fluctuations of the liquid fuel and oxidizer at the injector. There is no average flow of gas in that case, so we set $\vec{u}\cdot\hat{n}=0$ and define

$$A_I = -\frac{\bar{\gamma}}{\bar{a}}\frac{\vec{u}_g\cdot\hat{n}}{\hat{\eta}_n\psi_n}$$

The minus sign is appended because the normal vector $\hat{n}$ is positive outward but the velocity is positive inward at injector ports. Equations (2.71) and (2.72) are now

$$\omega = \omega_n + \frac{\bar{a}^2}{2\omega_n\bar{p}E_n^2}\{\frac{k_n}{\bar{a}}\int\psi_n\frac{\hat{\mathcal{P}}^{(r)}}{\hat{\eta}_n}dV - \int\frac{1}{\hat{\eta}_n}\hat{\vec{\mathcal{F}}}^{(r)}\cdot\nabla\psi_n dV + k_n\bar{p}\iint A_I^{(i)}\psi_n^2 dS - k_n\bar{p}\iint A_N^{(i)}\psi_n^2 dS\} \tag{2.75}$$

$$\alpha = \frac{\bar{a}^2}{2\omega_n\bar{p}E_n^2}\{\frac{k_n}{\bar{a}}\int\psi_n\frac{\hat{\mathcal{P}}^{(i)}}{\hat{\eta}_n}dV - \int\frac{1}{\hat{\eta}_n}\hat{\vec{\mathcal{F}}}^{(r)}\cdot\nabla\psi_n dV - (\bar{\gamma}-1)\frac{k_n}{\bar{a}}\bar{p}\int\psi_n^2(\nabla\cdot\vec{u}_g)dV + k_n\bar{p}\iint A_I^{(r)}\psi_n^2 dS - k_n\bar{p}\iint(A_N^{(r)}+\bar{M}_N)\psi_n^2 dS\} \tag{2.76}$$

The result (2.75) has not been particularly useful in predictions of linear stability because the frequency shifts $\omega-\omega_n$ are usually so small as not to be noticeable. As we noted earlier, predictions of the frequency are not a true test of a theory. However, 'prediction' means that all contributions on the right hand sides of (2.74) and (2.75) can be calculated. It has been common practice in studies of instabilities in liquid rockets to use both of these equations in the stability boundary ($\alpha=0$) to compute the real and imaginary parts of the function representing unsteady combustion. Hence the matter of prediction is not an issue. We discuss the procedure at greater length in Sections 4 and 5.

First we need to make explicit the contributions to the source functions $\vec{\mathcal{F}}$ and $\vec{\mathcal{P}}$, derived from the definitions (2.32) and (2.33). We make two assumptions to simplify the formulas:

i.) Viscous stresses and heat conduction are negligible within the volume of the chamber. This is true except for sharp fronted waves. Otherwise, viscous effects are important at boundaries, as for gas/particle interactions or at inert walls. Those losses are not included here but are easily taken into account.

ii) In steady state, the liquid droplets are in equilibrium. Thus $\delta\vec{u}_l=0$, an approximation that is valid only after the injected liquid has formed a spray moving with the chamber gases. Thus this approximation is not good over most of the region near the injector. As a result, losses are underestimated.

With these two assumptions, we find to first order in small quantities*

$$\vec{\mathcal{F}}' = \delta\hat{\vec{F}}_l' + \delta\hat{\vec{u}}_l'\bar{w}_l \tag{2.77}$$

$$\mathcal{P}' = \frac{\bar{R}}{\bar{C}_v}[Q' + \delta Q_l' + (\bar{h}_l - \bar{e})w_l' + (h_l' - e')\bar{w}_l] \tag{2.78}$$

Also, we replace $\nabla\cdot\vec{u}$ in the third term of (2.76) by using the averaged form of the continuity equation (2.1) with $\bar{\rho}_g$ approximately constant: then $\nabla\cdot\vec{u}_g = \dot{w}_l/\bar{\rho}_g$. Equation (2.76) is now

$$\alpha = \frac{\bar{a}^2}{2\omega_n\bar{p}E_n^2}\{\frac{k_n}{\bar{a}}\frac{\bar{R}}{\bar{C}_v}\int\frac{\psi_n}{\hat{\eta}_n}[(\dot{Q}+\delta\dot{Q}_l)+(\dot{h}_l-\bar{e})w_l'+(h_l'-e')\bar{w}_l]^{(r)}dV'$$

unsteady energy addition

$$+\int\frac{1}{\hat{\eta}_n}[\delta\hat{\vec{F}}_l+\delta\hat{\vec{u}}_l\bar{w}_l]^{(i)}\cdot\nabla\psi_n d\vec{V}'$$

losses due to gas/liquid interactions

$$-(\bar{\gamma}-1)\frac{k_n}{\bar{a}}\frac{\bar{R}}{\bar{\rho}_g}\int\psi_n^2\dot{\bar{w}}_l dV \tag{2.79}$$

loss associated with vaporization

* To simplify, we have also dropped arbitrarily a term $\bar{C}_v\bar{T}_g\nabla\cdot(\bar{\rho}_l\delta\vec{u}_l')$ in $\mathcal{P}$ representing a fluctuation of energy due to expansion (or contraction) of the droplet cloud.

$$+k_n\bar{p}\iint A_I^{(r)}\psi_n^2 dS - k_n\bar{p}\iint (A_N^{(r)}+\bar{M}_N)\psi_n^2 dS\}$$

injector exhaust nozzle

This result seems to contain all contributions considered in previous works and will therefore serve as the basis for discussion of mechanisms of instabilities in Section 3.

2.5 Rayleigh's Criterion

As a result of his studies of acoustic waves generated and sustained by heat addition, Lord Rayleigh (1878, 1945, Vol. II, p. 226) stated his famous criterion:

> "If heat be communicated to, and abstracted from, a mass of air vibrating (for example) in a cylinder bounded by a piston, the effect produced will depend upon the phase of the vibration at which the transfer of heat takes place. If heat be given to the air at the moment of greatest condensation, or be taken from it at the moment of greatest rarefaction, the vibration is encouraged. On the other hand, if heat be given at the moment of greatest rarefaction, or abstracted at the moment of greatest condensation, the vibration is discouraged."

Probably no other principle has been so widely invoked in studies of combustion instabilities [e.g. Heidmann and Wieber (1966a,b); Putnam(1971); Harrje and Reardon(1972); Zinn(1980)]. Even some success has been achieved. But it seems that in all cases when Rayleigh's criterion has been applied to situations involving exchange of mass as well as heat, the conclusions reached have been incomplete and in some cases seriously misleading. The reason is that not all sources have been properly accounted for - that is, pieces of $\vec{\mathcal{F}}$ and $\mathcal{P}$, equations (2.22) and (2.23), have been omitted. Rayleigh never considered the possible influences of a condensed phase.

The approximate analysis worked out in Section 2.3 provides a convenient basis for deriving an explicit form of Rayleigh's criterion including all contributions [see Culick (1987) for the form accounting only for heat addition and applicable to nonlinear motions]. We begin with equation (2.45) for the time-dependent amplitude of the n^{th} mode,

$$\frac{d^2\eta_n}{dt^2}+\omega_n^2\eta_n = F_n$$

This is the equation for a driven oscillator whose "energy" is $\mathcal{E}_n = (\dot{\eta}_n^2+\omega_n^2\eta_n^2)/2$ which, within a constant multiplier, is the mechanical energy associated with the n^{th} acoustic mode. Energy flows to the mode at the rate $F_n\dot{\eta}_n$ and at time t the rate of change of energy in one period $\tau_n = 2\pi/\omega_n$ of the motion is

$$\Delta\mathcal{E}_n(t) = \int_t^{t+\tau_n} F_n\dot{\eta}_n dt' \tag{2.80}$$

Traditional use of Rayleigh's criterion has involved only heat addition, a strictly literal use of the statement quoted above. Correct application to liquid-fueled systems requires consideration of all contributions associated with heat addition and exchange of mass, momentum and energy between the gas and liquid phases. With only those terms retained, $\vec{\mathcal{F}}'$ and $\mathcal{P}'$ are given by (2.77) and (2.78) so h and f, equations (2.32) and (2.34), are*:

$$h = \nabla\cdot[\delta\vec{F}_l'+\delta\vec{u}_l'\bar{w}_l]-\frac{\bar{R}/\bar{C}_v}{\bar{a}^2}\frac{\partial}{\partial t}[Q'+\delta Q_l'+(\bar{h}_l-\bar{e})w_l'+(h_l'-e'-\frac{p'}{\bar{\rho}_g})\bar{w}_l] \tag{2.81}$$

$$f = -[\delta\vec{F}_l'+\delta\vec{u}_l'\bar{w}_l]\cdot\hat{n} \tag{2.82}$$

Then F_n, equation (2.46), is

$$F_n = \frac{\bar{R}/\bar{C}_v}{\bar{\rho}E_n^2}\int\frac{\partial Q_R}{\partial t}\psi_n dV+\frac{\bar{a}^2}{\bar{\rho}E_n^2}\int\vec{\mathcal{F}}_R\cdot\nabla\psi_n dV \tag{2.83}$$

where

$$Q_R = Q'+\delta Q_l'+(\bar{h}_l-\bar{e})w_l'+(h_l'-e'-\frac{p'}{\bar{\rho}_g})\bar{w}_l$$
$$\vec{\mathcal{F}}_R = \delta\vec{F}_l'+\delta\vec{u}_l'\bar{w}_l \tag{2.84a,b}$$

To find an explicit expression of Rayleigh's criterion, substitute (2.83) in (2.80) and integrate the first term by parts:

$$\Delta\mathcal{E}_n = \frac{\bar{R}/\bar{C}_v}{\bar{\rho}E_n^2}\int\{[Q_R\dot{\eta}_n]_t^{t+\tau_n}-\int_t^{t+\tau_n}\ddot{\eta}_n Q_R dt')\psi_n dV+\frac{\bar{a}^2}{\bar{\rho}E_n^2}\int\int_t^{t+\tau_n}\dot{\eta}_n\vec{\mathcal{F}}_R\cdot\nabla\psi_n dV$$

If the system is executing a steady oscillation, then $Q_R\,\dot{\eta}_n$ is strictly periodic and the term in square brackets vanishes. In the second term we may set $\ddot{\eta}_n = -\omega_n^2\eta_n$ as remarked earlier. With $\bar{R}/\bar{C}_v = \bar{\gamma}-1$, the energy added to the n^{th} mode during one period of oscillation is

* This formula includes the terms that led to the part of equation (2.79) identified as a "loss associated with vaporization".

$$\Delta\mathcal{E}_n = \frac{\omega_n^2}{\bar{p}E_n^2}\int dV \int_t^{t+\tau_n} [(\bar{\gamma}-1)\frac{p_n'}{\bar{p}}Q_R + \bar{\gamma}\vec{\mathcal{F}}_R\cdot\vec{u}_n']dt \tag{2.85}$$

where we have used the definition of the acoustical pressure and velocity: $\eta_n\psi_n = p_n'/\bar{p}_n$, $\vec{u}_n' = \nabla\psi_n/\bar{\gamma}k_n^2$.

Equation (2.85) is an extended form of Rayleigh's criterion. The first term accounts for heat addition with and without charge of phase; the second term represents the effects of momentum transfer between the two phases. If $\Delta\mathcal{E}_n$ is positive, then the amplitude of the mode in questions grows providing the contributions accounted for here exceed the energy losses associated with the injector and the nozzle, the last two terms of equation (2.79).

The derivation of equation (2.85) has involved only some of the terms in h and f, a restriction imposed here only because previous works have emphasized the importance of heat and mass addition. It is evident from the derivation that all of the perturbations can be included. This will produce an extended form of Rayleigh's criterion applicable to all circumstances encompassed by the original conservation equations.

We need simply to use the entire definition (2.46) of F_n in equation (2.80) for $\Delta\mathcal{E}_n$. The contribution from the volume integral over $\psi_n^2\bar{w}_l$ in (2.79) arises from the term in F_n,

$$-\frac{\bar{R}/\bar{C}_v}{\bar{p}E_n^2}\int\frac{\partial p'}{\partial t}\frac{\bar{w}_l}{\bar{p}_g}\psi_l\,dV\,. \tag{2.86}$$

When this is placed in the definition of $\Delta\mathcal{E}_n$, the result can be re-written

$$-\frac{\bar{R}/\bar{C}_v}{\bar{p}E_n^2}\int_t^{t+\tau_n}dt'\int\frac{\bar{w}_l}{\bar{p}_g}\frac{\partial p'}{\partial t}(\dot{\eta}_n\psi_l)dV$$

The combustion $\dot{\eta}_n\psi_n = \partial(p'/\bar{p})/dt$ so this contribution to $\Delta\mathcal{E}_n$ is

$$-\frac{\bar{R}/\bar{C}_v}{E_n^2}\int_t^{t+\tau_n}dt'\int\frac{\bar{w}_l}{\bar{p}_g}\left[\frac{\partial}{\partial t}\left(\frac{p_n'}{\bar{p}}\right)\right]^2 dV \tag{2.87}$$

Similarly, the surface integral involving the real part* of the admittance in F_n is

$$\frac{\bar{a}^2}{\bar{p}E_n^2}\iint\left(\bar{\rho}\frac{\partial\vec{u}_g'}{\partial t}\cdot\hat{n}\right)^{(r)}\psi_n\,dS = \frac{\bar{a}^2}{\bar{p}E_n^2}\iint\bar{\rho}\bar{a}A^{(r)}\frac{\partial}{\partial t}\left(\frac{p'}{\bar{\gamma}\bar{p}}\right)\psi_n\,dS$$

where the definition (2.72) has been used. After substitution in the definition of $\Delta\mathcal{E}_n$, this term gives

$$\frac{\bar{a}^2}{\bar{p}E_n^2}\int_t^{t+\tau_n}dt'\iint\bar{\rho}\bar{a}A^{(r)}\frac{\partial}{\partial t}\left(\frac{p'}{\bar{\gamma}\bar{p}}\right)(\dot{\eta}_n\psi_n)\,dS\,.$$

Again $\dot{\eta}_n\psi_n$ is replaced by $\partial(p'/\bar{p}))\partial t$ and we have the contribution to $\Delta\mathcal{E}_n$

$$\frac{\bar{\rho}\bar{a}}{\rho_g E_n^2}\int dt'\iint A^{(r)}\left[\frac{\partial}{\partial t}\left(\frac{p_n'}{\bar{p}}\right)\right]^2 dS\,. \tag{2.88}$$

This result can be applied to both the injector and the exhaust nozzle, the two contributions appearing in equation (2.79).

With these additional contributions, the extended form of Rayleigh's criterion is now

$$\begin{aligned}\Delta\mathcal{E}_n = \frac{\omega_n^2}{\bar{p}E_n^2}\int dV\int_t^{t+\tau_n}dt'\left[(\bar{\gamma}-1)Q_R\frac{p_n'}{\bar{p}} + \bar{\gamma}\vec{\mathcal{F}}_R\cdot\vec{u}_n\right]\\ -\frac{1}{E_n^2}\int dV\int_t^{t+\tau_n}dt'(\bar{\gamma}-1)\frac{\bar{w}_L}{\bar{p}_g}\left[\frac{\partial}{\partial t}\left(\frac{p_n'}{\bar{p}}\right)\right]^2\\ +\frac{\bar{a}}{E_N^2}\iint dS\int_t^{t+\tau_n}dt'\frac{\bar{\rho}}{\bar{\rho}_g}A_J^{(r)}\left[\frac{\partial}{\partial t}\left(\frac{p_n'}{\bar{p}}\right)\right]^2\\ -\frac{\bar{a}}{E_N^2}\iint dS\int_t^{t+\tau_n}dt'\frac{\bar{\rho}}{\bar{\rho}_g}(A_N^{(r)}+\bar{M}_N)\left[\frac{\partial}{\partial t}\left(\frac{p_n'}{\bar{p}}\right)\right]^2.\end{aligned}$$

This formula for the energy charge* in one period of oscillation contains all the contributions included in the conservation equations (2.8)-(2.26). The statement of the crtierion is now: if $\Delta\mathcal{E}_n$ calculated with (2.80) is positive, then the oscillation is unstable. As the calculations in the following section confirm, this result is equivalent to the condition for stability based on the growth constant.

* Why it is legimate to use the real part follows from the remarks in the next section.

* Actually $\Delta\mathcal{E}_n$ is only proportional to the energy change; because of its definition (2.80), $\Delta\mathcal{E}_n$ has units $\sec^{-2}$

2.6 The Connection Between Rayleigh's Criterion and the Growth Constant

The growth constant, defined as the imaginary part of the frequency, is the exponential rate of growth of the pressure amplitude. It is therefore related to the rate of change of acoustic energy by a formula easily established in the following paragraphs. Further, because Rayleigh's criterion has to do with the time evolution of acoustic energy in the system, there must be a relation between that principle and the growth constant, a result we establish in this section.

Equation (2.45) for the amplitude of the n^{th} mode is the basis for computing both the growth constant α and the change of energy $\Delta\mathcal{E}_n$, and therefore provides the connection between these quantities.

We are concerned here only linear behavior; thus $\eta_n(t)$ is proportional to $e^{i\bar{a}kt}$ and with no loss of generality we can set the constant of proportionality equal to unity*, so $\eta_n = e^{i\bar{a}kt}$, a choice that simplifies the following calculations. Substitute in equation (2.45) to find the formula for k^2:

$$\begin{aligned} k^2 &= \frac{\omega_n^2}{\bar{a}^2} - \frac{F_n}{\bar{a}^2} e^{-i\bar{a}kt} \\ &= \frac{\omega_n^2}{\bar{a}^2} - \frac{\hat{F}_n}{\bar{a}^2} \end{aligned} \tag{2.90}$$

where as usual we write

$$F_n = \hat{F}_n e^{i\bar{a}kt} .$$

The real and imaginary parts of (2.90) give equation (2.64)a,b, here expressed in terms of F_n:

$$\begin{aligned} \omega^2 &= \omega_n^2 - \hat{F}_n^{(r)} \\ \alpha &= \frac{1}{2\omega_n} F_n^{(i)} \end{aligned} \tag{2.91}a,b$$

Now integrate the right hand side of the definition (2.80) of $\Delta\mathcal{E}_n$:

$$\begin{aligned} \Delta\mathcal{E}_n &= \int_t^{t+\tau_n} F_n \dot{\eta}_n dt' \\ &= \int_t^{t+\tau_n} \left[\frac{d}{dt}(F_n\eta_n) - \eta_n \frac{dF_n}{dt'} \right] dt' \\ &= [F_n\eta_n]_t^{t+\tau_n} - \int_t^{t+\tau_n} \eta_n \frac{dF_n}{dt'} dt' . \end{aligned}$$

The first term vanishes because we consider steady oscillations (at most $F_n\eta_n$ changes by a small amount in one period) and

$$\Delta\mathcal{E}_n = -\int_t^{t+\tau_n} \eta_n \frac{dF_n}{dt'} dt' . \tag{2.92}$$

Let ϕ be the phase of F_n (measured relative to the pressure oscillation) and

$$F_n = |F_n| e^{i(\bar{a}kt+\phi)} . \tag{2.93}$$

Real quantities must be used in the right hand side of (2.92); we choose the real parts of complex quantities, so $\eta_n = \cos(\bar{a}kt)$, $F_n = |F_n|\cos(\bar{a}kt + \phi)$. hence (2.92) is

$$\begin{aligned} \Delta\mathcal{E}_n &= -\int_t^{t+\tau_n} \cos(\bar{a}kt')\{-\bar{a}k|F_n|\sin(\bar{a}kt' + \phi)\}dt' \\ &= \bar{a}k \int_t^{t+\tau_n} |F_n|\cos(\bar{a}kt')\{\cos(\bar{a}kt')\sin\phi + \sin(\bar{a}kt')\cos\phi\}dt . \end{aligned}$$

Once again we apply the condition that F_n is a small perturbation so we can set $\bar{a}k \approx \omega_n$ and assume that $|F_n|$ and ϕ are nearly constant during one period of the motion. Hence the integrals can be done; only the first integral is non-zero and we find

$$\Delta\mathcal{E}_n = \omega_n |F_n| \sin\phi \frac{\tau_n}{2} .$$

With $\omega_n\tau_n = 2\pi$, we have the result

$$\Delta\mathcal{E}_n = \pi F_n^{(i)} . \tag{2.94}$$

Finally, comparison of (2.91)b and (2.94) gives the desired relation:

$$\Delta\mathcal{E}_n = 2\pi\omega_n\alpha . \tag{2.95}$$

This result establishes quite generally the connection suggested by the explicit forms (2.79) and (2.89). We should emphasize that as he originally formulated the statement known as his criterion, Rayleigh considered only the matter of heat addition to the acoustic field. It is perhaps stretching the point to account for all energy losses and gains to produce equation (2.95). We have done so here to clarify some abuses that have appeared in the literature; an example is discussed in Section 3.2

* This is usually a matter of normalisation; see also remarks in Section 4.3 after equation (4.10).

3. MECHANISMS OF COMBUSTION INSTABILITIES

Both Rayleigh's criterion and the growth constant provide means of analyzing the stability of unsteady motions. Properly interpreted, Rayleigh's criterion can be applied to nonlinear behavior, but the growth constant is strictly defined for linear instabilities. The results expressed as equations (2.79) and (2.90) are largely formal. Their physical content derives from the assumptions forming the basis for the conservation equations (2.18) - (2.26). To proceed further it is necessary to provide more explicit representations, or models, of the processes dominating the behavior in a combustion chamber.

Apart from differences in geometry, the primary distinctions between different propulsion systems are due to the internal physical processes. Some are independent of geometry, but others - such as flow separation - are not. In this section, we discuss the four main ideas that have been proposed for explaining combustion instabilities in liquid-fueled systems. Although all have been prompted by experimental results, they differ greatly in the extent to which they have been developed. We begin with the most widely used idea, the "time lag model".

3.1 Interpretation With a Time Lag

The basic idea is simple, and quite general, related to the familiar experience that a forced oscillating system will gain energy if the force has a component in phase with the velocity of the point of application. Stability of dynamical systems characterized in some sense by a phase or time lag had been studied prior to the concern with combustion instabilities [for example, see Callender et al (1936) and Minorsky (1942)]. In 1941, Summerfield (1951) had observed low frequency 'chugging" during firings of a liquid rocket. Discussion with von Karman led to the idea of a time lag as a possible explanation. Gunder and Friant (1950) independently introduced a time lag in their analysis of chugging, but it was Summerfield's paper and subsequent work at Princeton by Crocco that established the time lag theory in the firm widely used.

The essential idea in all applications of the time lag is that a finite interval - the lag - exists between the time when an element of propellent enters the chamber and the time when it burns and releases its chemical energy. Such a time lag must exist in steady operation, and, since combustion is distributed throughout the chamber, there is no unique value. Evidently a complete analysis of injection and subsequent processes could then be interpreted in terms of a time lag; results exist only for approximate analyses.

Now suppose that at time t the pressure in the chamber suddenly decreases, causing an increase in the flow of propellant through the injector. The increased mass burns at some later time $t + \tau$, where τ is the time lag. If the pressure is increasing when the added mass burns, the energy released will tend to encourage the pressure increase, a destabilizing tendency. This elementary process is easily interpreted with Rayleigh's criterion. Assume that the pressure varies sinusoidally,

$$p' = \hat{p}\sin\omega t \tag{3.1}$$

and that the energy occurs later with constant time lag τ,

$$Q' = \hat{Q}\sin\omega(t-\tau) \tag{3.2}$$

Integration of the product $p'Q'$ over one period $2\pi/\omega$ gives

$$\int_t^{t+2\pi/\omega} p'Q'dt' = \hat{p}\hat{Q}\int_t^{t+2\pi/\omega} \sin\omega t'\sin(\omega t'-\omega\tau)dt' = \hat{p}\hat{Q}\frac{\pi}{\omega}\cos\omega\tau \tag{3.3}$$

Thus, according to Rayleigh's criterion (2.7), we expect that net energy is added to the oscillation if $\cos\omega\tau$ is positive, so the time lag must lie in the ranges

$$0 < \tau < \frac{\pi}{2\omega}, \qquad \frac{3\pi}{2\omega} < \tau < \frac{5\pi}{2\omega}, \qquad \text{....etc.} \tag{3.4}$$

Suppose that the system is unstable and the τ lies in the range $3\pi/2\omega < \tau < 5\pi/\omega$. Then the strategy for fixing the problem is based on modifying the system so that τ is either increased or decreased, placing its value outside the range for instability.

Because the processes subsequent to injection are surely dependent on the flow variables, pressure, temperature, velocity, ..., it is unrealistic to assume that the time-lag is constant. The most widely used form of the representation with a time lag are dominated by its dependence on pressure.

Figure 3.1, taken from Dipprey (1972), is a sketch illustrating the behavior for a sinusoidal pressure oscillation imposed on the system. The total time delay to burning is supposed in this case to be composed of two parts, due to the propellant feed system, and the combustion delay (injection, atomization, vaporization, mixing, and chemical kinetics). It is the second part that is sensitive to the flow conditions in the chamber.

Let $\dot{m}$ denote the mass flow (mass/sec.) of propellant. At this point we are not concerned with details and we need not distinguish between fuel and oxidizer. The arguments based on the idea of a time lag are directed mainly to constructing a representation of the mass source term w_l(mass/vol. - sec.) in the continuity equation (2.1). Thus the result is intended to express the rate of conversion of liquid to gas in a volume element of the chamber. There is no consideration of combustion processes; the usual assumption is that combustion occurs instantaneously, a view that determines how the time lag model ought to be incorporated in the equations.

Let ($\vec{r}$, dV) denote the volume element at position $\vec{r}$ in the chamber and let (t, dt) denote the small time interval dt at time dt. The idea is that the amount of liquid $w_l dV dt$ converted to gas in the element (r, dV)

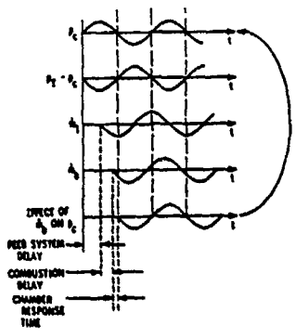


FIGURE 9.1

in the interval (t, dt) was injected as $\delta\dot{m}(t-\tau)d(t-\tau)$ at the time $t-\tau$ in the interval $d(t-\tau)$. Hence by conservation of mass,

$$w_l dV dt = \delta\dot{m}_i(t-\tau)d(t-\tau) \tag{3.5}$$

According to earlier remarks, the time lag is supposed to be variable, and can be written as the sum of average and fluctuating values, $\tau = \bar{\tau} + \tau'$. In steady-state operation, (3.5) is

$$\bar{w}_l dV dt = \delta\dot{m}_i(t-\bar{\tau})d(t-\bar{\tau}) = \delta\dot{m}_i(t-\bar{\tau})dt \tag{3.6}$$

Expanding $\delta\dot{m}(t-\tau)$ in Taylor series for use in (3.5) we have

$$\delta\dot{m}_i(t-\tau) = \delta\dot{m}_i(t-\bar{\tau}) + \tau'\{\frac{d}{dt}\delta\dot{m}_i(t)\}_{t-\tau} + \cdots \tag{3.7}$$

The second term is non-zero if the injected mass flow is not constant. There are many situations (notably for low frequency instabilities) for which variations are important But for the instabilities at high frequencies, variations of the propellant flow are generally not important. Hence we ignore the second term in (3.7) and substitute (3.6) in (3.5) to find

$$w_l(\vec{r},\ t) = \dot{w}_l(1 - \frac{d\tau}{dt}) \tag{3.8}$$

The variations of the local conversion of liquid to gas depend in this simple fashion on the time - dependence of the time lag. Note that τ may in general depend on position: the reasoning here is quite widely applicable.

The difficult problem is of course to predict τ - in fact it has never been done. Crocco introduced the idea that the time lag is the period required for the processes leading to vaporization to be completed. He assumed that this integrated effect can be represented by an integral over the time lag of some function f of the variables affecting the processes

$$\int_{t-\tau}^{t} f\{p,\ T,\ \vec{u},\ \vec{u}_l,\ \ldots\}dt' = E \tag{3.9}$$

The constant E is supposed to be a measure of the level to which the integrated effects must reach in order for vaporization to occur. Almost all applications of the time lag model rest on the assumption that the time lag is sensitive only to the pressure. The function f may then be expanded about its value at the mean pressure.

$$f(p) = f(\bar{p}) + p'\left.\frac{df}{dp}\right|_{\bar{p}} = f(\bar{p})\{1 + p'\frac{1}{f(\bar{p})}\left.\frac{df}{dp}\right|_{\bar{p}}\}$$

If $f = cp^n$ then $df/dp = ncp^{n-1}$ and $(df/dp)/f(p) = n/p$. The **interaction index** n is defined as

$$n = \frac{\bar{p}}{f(\bar{p})}\left.\frac{df}{dp}\right|_{\bar{p}} \tag{3.10}$$

and $f(p)$ is approximated as

$$f(p) = f(\bar{p})\{1 + n\frac{p'}{\bar{p}}\} \tag{3.11}$$

This form is now used in approximate evaluation of (3.9).

First differentiate (3.9) with $f(p) = f(p(t))$ to find

$$f\{p(t)\} - (1 - \frac{d\tau}{dt})f\{p(t-\tau)\} = 0$$

Substitution of (3.11) gives

$$1 - \frac{d\tau}{dt} = \frac{1 + n\frac{p'(t)}{\bar{p}}}{1 + n\frac{p'(t-\tau)}{\bar{p}}} \approx 1 + n\left[\frac{p'(t)}{\bar{p}} - \frac{p'(t-\tau)}{\bar{p}}\right] \tag{3.12}$$

Set $w_l = \bar{w}_l + w_l'$ in (3.8) and substitute (3.12) to find the basic result of the time lag theory:

$$w_l' = \bar{w}_l n\left[\frac{p'(t)}{\bar{p}} - \frac{p'(t-\tau)}{\bar{p}}\right] \tag{3.13}$$

For analyzing linear stability, $p' = \bar{p}e^{i\hat{\omega}t}\psi(\vec{r})$ and $w_l' = \hat{w}_l e^{i\hat{\omega}t}$, so

$$\hat{w}_l = \bar{w}_l n(1 - e^{-i\omega\tau}) \tag{3.14}$$

where the usual approximation has been made, $\alpha\tau << \omega\tau$ in the exponent.

Equation (3.17) is a two-parameter representation of the conversion of liquid to gas. The two parameters, the time lag τ and the interaction or pressure index n, are unknown *a priori*. All work with the time lag theory requires experimental measurements to determine their values. The general idea is simple. After substituting (3.14) in the linearized conservation equations, solution is found for the stability boundary ($\alpha = 0$) with n and τ as parameters. Experimental data for the stability boundary are used to determine n and τ. Crocco, Grey and Harrje (1960) were first to obtain sufficient data to confirm the value of this approach. Figure 3.2 reproduces some of their results for the time lag and interaction index inferred from tests with two injectors. The data were taken for the stability boundary of the fundamental longitudinal mode and show the strong dependence on fuel/oxidizer ratio.

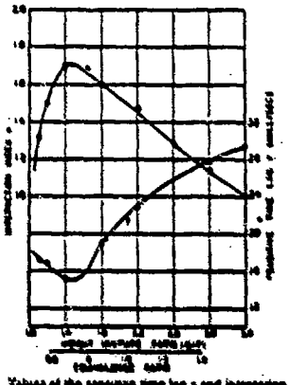


Fig. 11 Values of the crossover time lag τ and interaction index n determined from the experimental inner stability boundary (Fig. 4) for the fundamental longitudinal mode. This figure shows results for the first injector (design $O/F = 2.41$) at a nominal chamber pressure of 300 psia

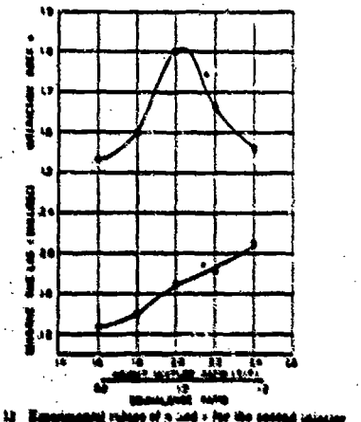


Fig. 12 Experimental values of n and τ for the second injector (design $O/F = 2.8$)

FIGURE 3.2

Obviously, there are many limitations. The analysis leading to (3.14) is entirely phenomenological, the final result containing two parameters only is an enormous simplification of the real situation, but there is no way to assess the imperfections. The formula (3.14) can be extended to include, for example, dependence on velocity fluctuations [Reardon, Crocco, and Harrje (1964)]. Because the values of all parameters must be found from experimental data, the difficulties become prohibitive.

The time lag model (it is, after all, not really a theory) is based on an appealing physical argument but no processes are treated explicitly. Probably the most serious deficiency is that no detailed treatment is given of combustion, which is ultimately the source of the energy driving all combustion instabilities. Nevertheless, the model has been the basis for some success in treating instabilities in liquid rockets, primarily as the basis for correlating data. The two-parameter representation provides a convenient framework for detecting trends of stability with design changes. Its predictive value is very restricted indeed.

3.2 Atomization, Droplet Vaporization and Burning

Some years after the time lag model had been developed, work at the NASA Research Center [Priem and Guentert (1962) and Priem (1963)] showed that the stability of a liquid rocket motor could be controlled by varying the characteristics of the vaporization process. The conclusion followed from the results of numerical solutions to the equations for nonlinear unsteady motions in a chamber. The source terms were approximated with models of the atomization, vaporization and burning. Variations of characteristic parameters showed that atomization and vaporization were the dominant rate processes determining the stability limits. That conclusion led to a series of studies particularly emphasizing vaporization.

Because of the difficulty of extracting precise conclusions from numerical analyses, Heidmann and Wieber (1966a, 1966b) devised a method for assessing the vaporization process alone. A droplet is injected axially in a

steady flow. An acoustic field is superimposed having the form of the lowest first tangential mode for a cylindrical chamber ($\sin\theta\, J_1(\kappa_{11}r)$). The motion and vaporization rate of the droplet is calculated throughout its history. By superimposing the results for an array of injected drops, assumed not to interact with one another, one may find the local fluctuation of vaporization rate throughout the chamber. That is the mass source term w_l' in the continuity equation (2.1) for the gas phase.

Heidmann and Wieber (1966a) defined a "response factor", N, to interpret their results:

$$N = \sum \frac{w_l'/\bar{w}_l}{p'/\bar{p}} \tag{3.15}$$

where $\sum$ here denotes the sum over all droplets in the volume considered. They gave results for N as a function of various parameters. Typically, N shows a peak of about .6-.9 in a frequency range .04-.1 Hertz. Results obtained for n-heptane over fairly wide flow conditions were correlated with a dimensionless parameter containing droplet size, chamber pressure, gas velocity and a dimensionless amplitude of the oscillation.

In a later work, Heidmann and Wieber (1966b) used a restricted form of Rayleigh's criterion and a simpler linear analysis to produce essentially the same conclusions. The new definition of the response factor was

$$N = \sum \frac{\int_0^{2\pi/\omega} \frac{w_l'^{(+)}}{\bar{w}_l} \frac{p}{\bar{p}}\, dt}{\int_0^{2\pi/\omega} \left(\frac{p}{\bar{p}}\right)^2 dt} \tag{3.16}$$

These analyses amount to detailed examination of a particular process contributing to the time lag discussed above. Substitution of the real part of (3.14) in (3.16) gives

$$N = n(1 - \cos\omega\tau) \tag{3.17}$$

Heidmann and Wieber found that their numerical results could be approximated quite well in the range $\tau_m\omega < 1$ by the values

$$\begin{aligned} n &= 0.21 \\ \tau &= 1.5\tau_m \end{aligned} \tag{3.18}$$

where τ_m is the mean droplet lifetime. This comparison is shown in Figure 3.3 taken from Heidmann and Wieber (1966).

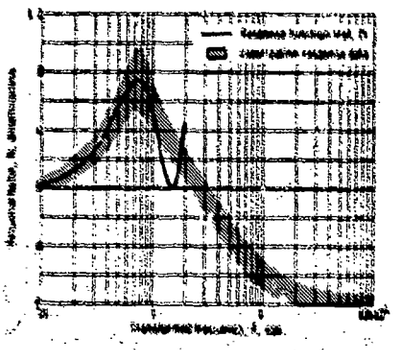


FIGURE 3.3

Note that the function (3.17) oscillates and therefore becomes a poor approximation for $\omega\tau_m > 1$, as does by the solid line in Figure 3.3. The vaporization rates seem physically reasonable for the conditions shown, so one must conclude that the time lag model fails at higher frequencies. Recently Tong and Sirignano (1986a, 1986b, 1987) have re-examined the problem of unsteady vaporization. With their more detailed model including the effects of unsteady heat transfer in the gas phase, they conclude that their vaporization rates are much higher than those found by Heidmann and Wieber.

More strongly, Tong and Sirignano propose that unsteady droplet vaporization is a potential mechanism for driving combustion instabilities. Heidmann and Wieber had earlier noted that the response factor they calculated for the vaporization process was less than that calculated for the nozzle losses. Thus, although vaporization itself did add energy to the acoustic field according to their analysis, the effect was too small to be a mechanism for instabilities. Tong and Sirignano conclude that their results show sufficient energy transfer from the vaporizing droplets to the acoustic field to qualify as a mechanism in actual systems*. Their conclusion is based solely on the $\bar{p}\dot{v}$ = v work done by the process of vaporization and does not include any energy release due to combustion. The proposal is evidently wrong for the following reasons.

* Later application of this work to ramjet combustion is discussed briefly in Section 3.3.4

It is significant that none of the preceding conclusions involved combustion: the assertion is that coupling between pure vaporization and the acoustic field produces net flow of energy to the oscillations in the gas. The contrary conclusion was reached by Marble and Wooten(1970) and Marble (1969), that both condensing and vaporizing droplets attenuate acoustical motions.

The reason for the opposite conclusion seems to be that not all interactions between the droplets and the acoustic field are accounted for in the calculations by Heidmann and Wieber and by Tong and Sirignano. Their conclusions were based on using Rayleigh's criterion, but only one term was considered. They argued that by analogy with Raleigh's original statement concerning fluctuations of heat addition, the same criterion should apply to mass addition. Therefore, as in equation (3.16) only the integral involving w_l' was computed; a positive value indicates the possibility for driving the acoustic field. However, the derivation in Section 2.5 has shown that the correct form of the criterion involves several contributions. Considering only those associated with the conversion of liquid to gas, we combine equations (2.84)a,b and (2.83) to find

$$\Delta\mathcal{E}_n = \frac{\omega_n^2}{\bar{\rho}E_n^2}\int dV \int_t^{t+\tau_n} [(\bar{\gamma}-1)\{\delta Q_l' + (\bar{h}_l - \bar{e})w_l' + (h_l' - e' - \frac{p'}{\bar{\rho}_g})\bar{w}_l\} + \bar{\gamma}(\delta\vec{F}_l' + \bar{w}_l\delta\vec{u}_l')\cdot\vec{u}_n']dt \tag{3.19}$$

There is indeed a term proportional to the integral of $w_l'p'$ but it is multiplied by $(\bar{h}_l - \bar{e})$ which contains the heat of vaporization. There are also significant amounts of energy transfer associated with the terms involving $\delta Q_l' + \delta F_l'$ which for non-vaporizing drops represent the attenuation of sound waves. Those effects are included in the work by Marble and Wooten: their results show that the accompanying energy losses dominate so that in fact if combustion is ignored, vaporizing droplets cause damping, not driving, of unsteady gas motions.

We must emphasize that the conflicting results, and the conclusion that vaporization is not a mechanism for driving combustion instabilities rests on proper computation of the energy transfer. In the earlier work, an incorrect or, rather, incomplete form of Rayleigh's criterion was used. It is certainly true that the process represented by $w_l'p'$ alone does cause driving if the fluctuation of mass release has a component in phase with the pressure fluctuation, but that is only part of the story.

Priem (1988) has recently used Heidmann and Wieber's model of vaporization, combined with the model worked out by Feiler and Heidmann (1967) for a gaseous fuel, to study combustion instabilities in the LOX/methane system. He bases his conclusions concerning stability boundaries on numerical results for the combustion responses, of which that for liquid oxygen is computed with equation (3.16) and the method described above; and on corresponding results found for the losses associated with the exhaust nozzle and baffles. His results seem to compare fairly well with recent experimental work. The reason that this could be so - even though vaporization causes net energy losses if all contributions are accounted for - is that the energy released by combustion, immediately following vaporization, is the dominant factor. That is, in equation (3.17) the terms involving energy transfer are larger than those representing losses. Comparison with experimental results seems always to involve multiplicative factors which are determined to provide best fit to data, or are absent in normalized forms. Then when good agreement is found, it seems that it is largely the qualitative behavior that is being checked.

Despite the heavy emphasis, in many works, on vaporization as the rate controlling process, it is generally recognized that other processes contribute and in some situations may be dominant. The injection process itself may be affected under unsteady conditions due to the varying streams, impact of jets, and atomization all are sensitive to unsteady flow fields. Those problems are extremely complicated difficult to describe in a fashion suitable for use in a general analysis, and are very much dependent on details of the hardware. Thus the work has largely been experimental with some effort to correlate results in a form useful for design [e.g. Levine (1965); Sotter, Woodward and Clayton (1969); Webber (1972); Webber and Hoffman (1972)]. The time lag model has been used essentially as a means of correlating all of those processes without concern for details [Reardon, Crocco and Harrje (1964); Reardon, McBride and Smith (1966)]. Summaries of experimental results obtained prior to 1971 may be found in the reference volume edited by Harrje and Reardon (1972).

Of recent work, the most fundamental and detailed is that carried out at ONERA as a result of problems due to combustion instabilities in the Viking motor. Special effort has been made to understand the unsteady behavior of the injectors used in that engine. The intentions of the research program were described by Souchier, Lemoine and Dorville (1982); and by Lourme and Schmitt (1983). Considerable effort has since been expended to characterize the steady and unsteady behavior as the basis for analyzing instabilities in the engine [Lourme, Schmitt and Brault (1984); Lecourt, Foucaud and Kuentzmann (1986); Lourme (1986); Lecourt and Foucaud (1987)]. The results range from detailed measurements of the spray (droplet size and velocity distributions) to the more global unsteady response of the injector, using a device adapted from a method developed for solid propellant rockets. Incorporation of the results of these works in analysis of the instabilities in engines is in progress.

3.3 Convective Waves

Following work by Kovasznay (1953), Chu and Kovasznay (1957) showed one way of decomposing general small disturbances of a viscous compressible fluid into three classes: acoustic, viscous, and entropy waves. Acoustic waves carry no entropy changes, while viscous and entropy waves have no accompanying pressure fluctuations. The direct effects of viscous stresses and heat conduction on combustion instabilities are generally negligible except in the vicinity of surfaces. That entropy fluctuations evidently have second order effects on the acoustic waves is implied by the formal analysis covered in Section 2; there was no need to introduce the entropy.

However, both viscous effects and nonuniform entropy may affect the acoustic field indirectly through processes at the boundaries. First we examine here the possible influences of entropy fluctuations. These fall within

the general class of convective waves, that is, disturbances that are carried with the mean flow: their propagation speed is the average flow speed. Entropy fluctuations are associated with the portion of temperature fluctuations not related isentropically to the pressure fluctuation; such as non-uniformities of temperature due, for example, to combustion of a mixture having non-uniformities in the fuel/oxidizer ratio. In general, an entropy wave may be regarded as a nonuniformity of temperature carried with the mean flow.

As shown by Chu(1953) pressure waves incident upon a plane flame will cause generation of entropy waves carried downstream in the flow of combustion products. Thus one should expect that when combustion instabilities occur, there must be ample opportunity for the production of entropy fluctuations. That process has negligible effect directly on stability (the coupling between acoustic and entropy waves is second order within the volume) but there has long been interest in the possible consequences of entropy waves for the following reason.

When an entropy wave is incident upon the exhaust nozzle, it must pass through a region containing large gradients of mean flow properties. A fluid element must retain its value of entropy and for this condition to be satisfied, the pressure and density fluctuations cannot be related by the familiar isentropic relation, $\delta p \sim \gamma \delta \rho$. As a result, within the nozzle pressure changes are produced that will generate an acoustic wave that will propagate upstream. Thus, an entropy wave incident upon an exhaust nozzle can produce an acoustic wave in the chamber, augmenting the acoustic field due to other sources.

An artificial elementary example will illustrate the proposition. Consider a chamber admitting uniform constant mean flow at the head end, say through a choked porous plate; the flow exhausts through a choked nozzle (Figure 3.4). Suppose that

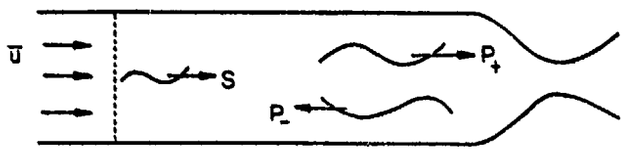


FIGURE 3.4

at the head end a heater is placed, arranged so that its temperature can be varied periodically, with frequency ω. This action produces a continuous temperature or entropy wave convected with the flow. An experimental realization of this situation has been described by Zukoski and Auerbach (1976). We assume no losses within the flow, so a fluid element retains its entropy; small perturbations s' of the entropy satisfy the equation

$$\frac{\partial s'}{\partial t} + u\frac{\partial s'}{\partial z} = 0 \tag{3.18}$$

If S is the amplitude of the fluctuation at the heater ($z = 0$), the solution for s' is

$$s' = S e^{-i\omega(t - \frac{z}{u})} \tag{3.19}$$

To simplify the calculations, assume that the flow speed is vanishingly small so that we may ignore its effect on acoustic waves (we relax this assumption in Section 5). Then the acoustic pressure and velocity fields can be expressed as sums of rightward and leftward traveling plane waves:

$$\begin{aligned} p' &= \{P_+ e^{ikz} + P_- e^{-ikz}\} e^{-i\omega t} \\ u' &= \{U_+ e^{ikz} + U_- e^{-ikz}\} e^{-i\omega t} \end{aligned} \tag{3.20a, b}$$

As usual, the complex wavenumber is $k = (\omega - i\alpha)/a$. The acoustic pressure and velocity must in this problem satisfy the classical acoustic momentum equation, (3.27) with $a_y = F' = 0$:

$$\rho\frac{\partial u'}{\partial t} + \frac{\partial p'}{\partial z} = 0 \tag{3.21}$$

Separate substitution of the forms for the rightward and leftward traveling waves shows that $U_\pm$, $P_\pm$ are related by

$$\rho a U_+ = P_+ \quad ; \qquad \rho a U_- = -P_- \tag{3.22}$$

Assume that the head end acts as a perfect reflector for the acoustic waves, so

$$u' = 0 \; ; \qquad \frac{\partial p'}{\partial z} = 0 \qquad (z = 0) \tag{3.23a, b}$$

In a real case (e.g. if the heater were actually a flame) the pressure fluctuations would cause fluctuations of entropy at the head end. To represent this effect, set s' proportional to p' at $z = 0$:

$$s' = A_{sp} p' \quad (z = 0) \tag{3.24}$$

Tsien (1952), Crocco (1953) and Crocco and Cheng (1956) have shown that the boundary condition at the nozzle entrance may be written in the form

$$p' + \bar{\rho}\bar{a}A_1 u' + A_2 s' = 0 \qquad (z = L) \tag{3.25}$$

We may now show that the problem formulated here admits solutions representing steady acoustic oscillations in the chamber, whose stability depends on the values of the coefficients A_0, A_1, A_2. We eliminate the unknown amplitudes S, P_+, P_- and obtain a characteristic equation for the complex wavenumber k, by satisfying the boundary conditions (3.22)-(3.25). Substitute equations (3.20) and (3.22) into (3.23) to find

$$P_+ - P_- = 0 \tag{3.26}$$

With (3.19) and (3.20)a, the condition (3.24) is satisfied if

$$S = A_0(P_+ + P_-) \tag{3.27}$$

Finally, substitution of (3.19), (3.20)a,b and (3.27) in (3.25) gives

$$[(1 + A_1)e^{ikL} + A_0 A_2 e^{i\frac{\omega}{\bar{u}}L}]P_+ + [(1 - A_1)e^{-ikL} + A_0 A_2 e^{i\frac{\omega}{\bar{u}}L}]P_- = 0 \tag{3.28}$$

With $P_- = P_+$ from (3.26) we have the characteristic equation

$$e^{i2kL} = \frac{-1}{(1 + A_1)}[1 - A_1 + 2A_0 A_2 e^{i(k+\frac{\omega}{\bar{u}})L}] \tag{3.29}$$

Generally A_0, A_1, A_2 are complex numbers. The real and imaginary parts of (3.29) provide transcendental equations for the real and imaginary parts ($\omega/\bar{a}$, $\bar{\alpha}/\bar{a}$) of k. The solutions are unstable if $\alpha > 0$, corresponding to self-excited waves. Note that in the limiting case of no entropy fluctuations ($A_0 = 0$) and a rigid wall ($A_1 \to \infty$) at $z = L$, (3.29) reduces to $e^{i2kL} = +1$ or $\cos 2kL = 1$ and $\sin 2kL = 0$. Then $k = n\pi/L$ and the allowable wavelengths are $\lambda = 2\pi/k = 2L/n$, the correct values for a tube closed at both ends.

This example suggests the possibility for producing instabilities *if* entropy waves are generated and *if* those waves interact with the boundary in such a way as to produce acoustic disturbances. It is in fact a genuine possibility that has been considered both in laboratory tests and as an explanation of instabilities observed in actual engines. The difficulties in applying this idea are largely associated with treating the processes responsible for causing the entropy waves.

In a combustion chamber, possible sources of entropy fluctuations may be distributed throughout the chamber. Burning of non-uniform regions of fuel/oxidizer ratio and interactions of pressure distributions with combustion zones are important causes, both producing non-isentropic temperature fluctuations. Thus in general the property that in inviscid flow free of sources an element of fluid has constant entropy, is inadequate. A proper description of entropy waves should be placed in the broader context accounting also for convective waves of vorticity as worked out first by Chu and Kovasznay (1957). We cannot provide a complete discussion here, but for later purposes in Section 5.3 it is helpful to have at hand the more general equation governing entropy fluctuations.

Combination of the first law of thermodynamics for a perfect gas and the definition $ds = dq/T$, valid if the heat transfer dq is not too abrupt, gives

$$ds = C_v \frac{dT}{T} - \frac{p}{\rho_g}\frac{d\rho_g}{\rho_g}$$

Now introduce the perfect gas law to eliminate the temperature change. Writing the result for motion following a fluid element we have

$$\frac{1}{C_v}\frac{Ds}{Dt} = \frac{1}{p}\frac{Dp}{Dt} - \frac{\bar{\gamma}}{\rho_g}\frac{D\rho_g}{Dt} \tag{3.30}$$

where $D/Dt = \partial/\partial t + \vec{u}_g \cdot \nabla$ is the convective derivative. After substitution of (2.18) and (2.20) we find the equation for entropy,

$$\begin{aligned}\frac{1}{C_v}\frac{Ds}{Dt} = \frac{1}{p}\frac{\dot{R}}{C_v}[Q + \delta Q_l + \nabla\vec{q} + \Phi + \delta\vec{u}_l \cdot \vec{\mathcal{F}}_l + \frac{p}{\rho_g}\nabla\cdot(\rho_l\delta\vec{u}_l) \\ + \{(h_l - \epsilon) + \frac{1}{2}(\delta u_l)^2\}w_l]\end{aligned} \tag{3.31}$$

The right hand side contains all sources of entropy changes including viscous effects, combustion and conversion of liquid to gas.

Equation (3.31) completes the set of equations required for complete analysis of combustion instabilities including entropy waves. The equations governing vorticity waves are obtained by splitting the velocity field into two parts: the acoustic field which is irrotational, and the rotational vorticity field which, if treated in all generality, includes turbulence as well as large vortex structures and shear waves.

The subject of convective waves in the presence of acoustic motions has not been exhaustively treated. Some special examples are discussed in Section 5.3

3.4 Vortex Shedding and Combustion

The presence of swirling, spinning or vortex motions in propulsion systems has long been recognized as a serious problem. They fall broadly into two classes: those with angular momentum directed along the axis, usually (if the rocket itself isn't spinning) related to standing or spinning transverse acoustic modes of the chamber; and those having angular momentum mainly perpendicular to the axis, associated with vortex shedding from bluff bodies or rearward facing steps.

Motions identified as forms of transverse or tangential modes do not normally qualify as mechanisms: they are themselves the combustion instability. Male, Kerslake and Tischler (1954) gave an early summary of severe transverse oscillations ("screaming" at 10K Hertz) and noted what has always been a serious consequence: greatly increased surface heat transfer.

Here we are concerned with vortex motions growing in unstable shear layers. Those vortices, now commonly called "large coherent structures" [Brown and Roshko(1974)] are convected downstream at approximately the average speed of the two streams forming the shear layer. In propulsion systems, the shear layers in question are generally formed in flow past bluff body flame holders (in thrust augmentors) or past rearward facing steps (in ramjet engines).

Observations of vortex shedding from flameholders, and recognition of the importance of this process as a possible mechanism for combustion instabilities were first independently reported by Kaskan and Noreen (1955) and by Rogers (1954) and Rogers and Marble (1956). Both experiments used premixed gaseous fluel and air flowing past a flameholder in a rectangular channel. However, the particular mechanisms proposed were very different. Figures 3.5 and 3.6 taken respectively from Kaskan and Noreen (1955) and Rogers and Marble (1956) clearly show the vortex shedding.

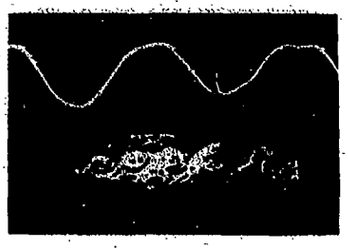


FIGURE 3.5

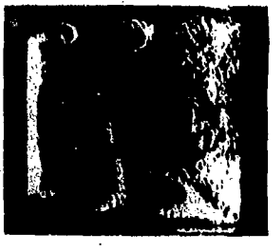


FIGURE 3.6

Motivated partly by earlier observations of Blackshear (1953) and Putnam and Dennis (1953), Kaskan and Noreen speculated that stretching of the flame front accompanying roll-up in the vortex causes a pressure distrubance. Periodic disturbances generated by periodic vortex shedding may then sustain either transverse or longitudinal acoustic fields. (They observed both in their tests.) As a quantitative basis for interpreting their results they modified a theoretical relation derived by Chu (1953) for plane flames. Although they had modest success comparing their reasoning with their data, Kaskan and Noreen did not provide a complete explanation of the closed-loop process required to generate self-excited oscillations. This mechanism has not subsequently received much notice as a cause for combustion instabilities, although the idea has recently been revived in connection with work on ramjet combustion; see remarks in Section 5.3.2.

Rogers and Marble gave detailed reasoning to support their idea that delayed periodic combustion in shed vortices generates periodic pressure pulses that serve as sources of the acoustic field (transverse in their tests).

The fluctuating velocity of the acoustic field itself initiates the vortex shedding, thereby closing the loop. Rogers and Marble drew on earlier data for the ignition delay in flow past bluff bodies [Zukoski and Marble (1955)] to demonstrate that vortex combustion could in fact occur in proper phase to support the acoustic vibrations.

During the past six years, the idea that vortex shedding is a dominant factor in mechanisms for many combustion instabilities has gained growing support. Practically all of the work has been motivated by problems of longitudinal oscillations in ramjet engines. Even though the frequencies are substantially lower than those of the oscillations treated by Rogers and Marble, the essentials of the idea seem to hold true.

The problem of longitudinal oscillations in small ramjet engines was apparently first recognized by Hall (1978). Rogers (1980a, 1980b) gave thorough summaries of the available experimental work. Those reports served as the basis for an early analysis of the problem by Culick and Rogers (1983); that work did not include a satisfactory mechanism. Concurrently, Byrne (1981, 1983) proposed that vortex shedding in a dump combustor appeared to be a likely cause of the observed instabilities. Apparently unaware of the earlier work by Rogers and Marble on transverse oscillations, he based his argument on known results for cold jet flows.

Since the early 1980's a great deal of attention has been given to the role of vortex shedding in dump combustors, both in cold flow and in laboratory combustion tests [e.g. Keller et al (1982); Smith and Zukoski (1985); Biron et al (1986); Schadow et al (1987); Sterling and Zukoski (1987); Poinsot et al (1987); Yu et al (1987)]. There is little doubt now that indeed the coupling between periodic energy released by combustion in shed vortices and the acoustic field is the dominant mechanism in dump combustors. The extent to which the same mechanism is active in contemporary thrust augmentors is less well-established but there is good reason to believe that it is often, if not usually, the main cause.

Extensive experimental work on vortex shedding in shear layers and jets at room temperature has provided a fairly complete picture of the formation of vortices; vortex pairing; and the general features of the flow without heat addition [see Schadow et al (1987) for a brief review of the literature relevant to problems in ramjet engines]. Tests in various configurations, including those appropriate to ramjets [e.g. Flandro et al (1972); Culick and Magiawala (1979); Dunlap and Brown (1981); Brown et al (1981, 1983); Schadow et al (1984)] established the ability of shed vortices to drive acoustic resonances over a broad range of flow conditions. The works cited above have extended that conclusion to flows with large heat addition accompanying combustion under circumstances simulating those found in actual ramjet engines. We shall discuss those results further in Section 5.3.2.

The obvious qualitative importance of combustion in large vortices has prompted several recent analytical investigations of the process. Broadly the idea is that the shear layer is formed at the edge of a bluff body, the high speed stream consisting of an unburnt mixture of reactants; the low speed stream is composed largely of hot combustion products forming the recirculation zone behind the body. As Smith and Zukoski (1985) and Sterling and Zukoski (1987) have shown, the shear layer exhibits widely varying degrees of stability depending on the operating conditions. We are concerned here with cases when the layer is highly unstable, a situation encouraged by the action of the acoustic velocity forcing oscillations of the layer at the lip. Large vortices may then rapidly form, entraining unburnt mixture on one side of an interface, with the combustion products on the other side. A flame is initiated at the interface and the question to be answered is: how does the rate of combustion, and therefore heat release, vary as the vortex rolls up and propagates downstream?

Marble (1984) treated an idealized case of a diffusion flame initiated along a horizontal plane when simultaneously the velocity field of a line vortex is imposed along an axis in the interface. Elements of flame initially in the interface are caused to execute circular motions and are stretched by the vortex field, causing an increase in the rate at which reactants are consumed. The expanding core contains combustion products but as the vortex roll-up continues, the rate of consumption always remains greater than that for flame in the flat interface having the same length as that in the rolled-up vortex. Karagozian and Marble (1986) carried out a similar analysis accounting for the influence of stretching along the axis of the vortex. They found that, following a transient period during which the core grows to its asymptotic form, the augmented consumption rate is unaffected by axial stretching. In those cases the rate of heat release reached a constant value monotonically: there is no distinguished period of pulsed combustion as required for the mechanism for instability described above.

More recently, Laverdant and Candel (1987, 1988) have treated both diffusion and premixed flames in the presence of vortex motion with finite chemical kinetics. Their analysis is entirely numerical giving good agreement with those of Karagozian and Marble and Karagozian and Manda (1986) for a vortex pair.

Perry (1983) also analysed the influence of finite chemical kinetics in the problem posed and solved by Marble (1984) who had assumed infinite reaction rates. Under some conditions, the heart release rate shows a modest peak in time. However, neither his results, nor those of Laverdant and Candel, suggest the sort of time delay to pulsed combustion one might like to see to complete the picture.

No work has been accomplished to determine whether or not the augmented reaction rates found in the analysis are sufficient to explain the mechanism of instabilities driven by vortex combustion. On the other hand, the experimental results reported by Smith and Zukoski (1985), Sterling and Zukoski (1987), and Yu et al (1987) show vividly and beyond doubt that unsteady combustion associated with vortex motions is a vigorous source indeed. Figure 3.7 is a sequence of photographs taken by Smith and Zukoski during one cycle of a high amplitude oscillation. They propose the following mechanism. A vortex is initiated at the edge of the step at a time determined partly by the local acoustic velocity. The vortex propagates downstream, releasing energy of a rate that seems to reach maximum when the vortex impinges on the wall. In order for impingement to occur at a favorable time during the acoustic oscillation, the propagation rate and hence strength of the vortex must increase with frequency. Because the vortex strength depends on the magnitude of velocity fluctuation initiating the motion at the lip, it is necessary that the steady amplitude of the acoustic field increase with frequency. That behavior is observed. Moreover, numerical calculations by Hendricks (1986) have shown quite similar behavior for the unsteady flow induced by an abrupt change of velocity past a rearward facing step. Figure 3.8 is a sketch

taken from Hendricks' work showing the development of a vortex calculated for those conditions.

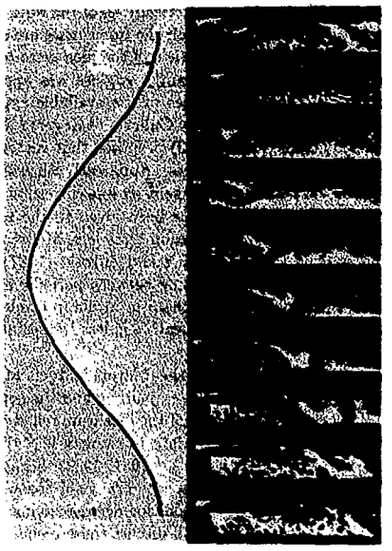


FIGURE 3.7

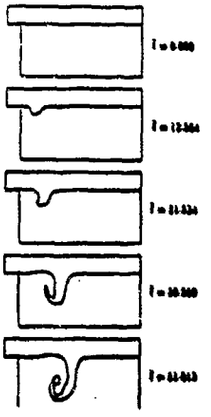


FIGURE 3.8

The essential ideas of vortex combustion as a mechanism for driving instabilities can be easily incorporated in the approximate analysis summarized in Sections 2.2 and 2.3. There is ample experimental evidence that large vortices in cold flow can sustain resonances in a duct; Flandro (1986) has shown one means of handling the process analytically based on direct fluid mechanical coupling between vortical and acoustic motions. See also Aaron and Culick (1985) for an elementary model of coupling associated in the impingement of a vortex on an obstacle. Tests with combustors have shown, however, that the amplitudes of oscillation are substantially greater when burning occurs. That result is most likely due to the unsteady energy release. We therefore assume that this is the main source of the driving.

Hence in the forcing function F_n, equations (2.45) and (2.46), we retain only the term Q' in P, equation (2.23); Equation (2.45) for the time-dependent amplitude of the n^{th} mode is

$$\frac{d^2\eta_n}{dt^2} + \omega_n^2\eta_n = \frac{\bar{\gamma}-1}{\bar{p}\bar{E}_n^2}\int \psi_n \frac{\partial Q'}{\partial t}dV \qquad (3.32)$$

A formula for Q' must be constructed to account for the trajectory of the vortex and its associated rate of energy release along the trajectory. To illustrate with a simple example, we consider excitation of longitudinal modes and assume that the vortex travels parallel to the axis. Within the one-dimensional approximation, that implies averaging the presence of the vortex over planes transverse to the axis. The situation is sketched in Figure 3.9. The origin $z = 0$ is at the step, which is not the location of a pressure anti-node. In fact, we must allow the acoustic velocity to be non-zero at the beginning of the shear layer at $z = 0$, so the mode shape is

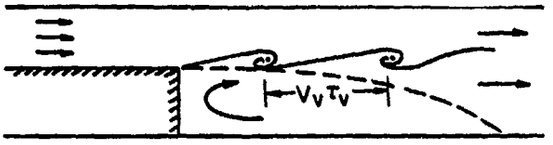


FIGURE 3.9

$$\psi_n(z) = \cos(k_n z + \phi) \tag{3.33}$$

The values of k_n and ϕ can be set by imposing a boundary condition at $z = l$ and choosing some location $z < 0$ for a pressure anti-node. For example, if pressure anti-nodes occur at $z = -\delta L_0$ and $z = L + \delta L_1$, the two conditions must be satisfied

$$\begin{aligned} \sin(-k_n \delta L_0 + \phi) &= 0 \\ \sin[k_n(L + \delta L_1) + \phi] &= 0 \end{aligned} \tag{3.32}$$

from which k_n and ϕ can be determined. For the purposes here, the particular values of k_n and ϕ are immaterial. With (3.33), the acoustic pressure and velocity are

$$\begin{aligned} p' &= \bar{p}\eta_n(t)\cos(k_n z + \phi) \\ u' &= -\frac{\dot{\eta}_n}{\bar{\gamma} k_n}\sin(k_n z + \phi) \end{aligned} \tag{3.33a, b}$$

For simplicity, assume that the vortices propagate with constant speed v_v and are launched periodically with period τ_v, at the times $t = 0, \tau_v, 2\tau_v, \cdots$. Assume further that these are point vortices releasing energy at the rate $q(t)$ each. Hence the energy release associated with a train of shed vortices can be represented by δ-functions moving with speed v_v multiplying the energy release:

$$\begin{aligned} Q'(z,t) &= q_1(t)\delta[z - v_v t] + q_2(t)\delta[z - v_v(t - \tau_v)] + q_3(t)\delta[z - v_v(t - 2\tau_v)] + \cdots \\ &= \sum_{j=0}^{\infty} q_j(t)\delta[z - v_v(t - j\tau_v)] \end{aligned} \tag{3.34}$$

In accordance with the behavior reported by Smith and Zukoski we should relate the strength of each vortex and, therefore by assumption its energy release to the velocity fluctuation causing its birth. For simplicity we ignore the influence of the mean flow speed and set q_j proportional to the acoustic velocity at the step and at the time when the vortex is launched. Hence, we assume

$$q_j(t) = \bar{q}_j(t)u'(0, j\tau_v) = -\bar{q}_j(t)\frac{\dot{\eta}_n(j\tau_v)}{\bar{\gamma} k_n}\sin\phi \tag{3.35}$$

where $q(t)$ is supposed to be common to all vortices. With (3.37) for $q_j(t)$, differentiate (3.36):

$$\frac{\partial Q'}{\partial t} = -\sum_{j=0}^{\infty}\frac{\dot{\eta}_n(j\tau_v)}{\bar{\gamma} k_n}\sin\phi\{\dot{\bar{q}}_j\delta[z - v_v(t - j\tau_v)] - \bar{q}_j v_v\delta'[z - v_v(t - j\tau_v)]\} \tag{3.38}$$

Now substitute (3.33) and (3.38) in the integral on the right hand side of (3.30), with $dV = S_c dz$ where S_c is the cross-section area of the chamber:

$$\begin{aligned} \int \psi_n \frac{\partial Q'}{\partial t} dV = S_c \int_0^L \cos(k_n z + \phi) \sum_{j=0}^{\infty} \frac{\dot{\eta}_n(j\tau_v)}{\bar{\gamma} k_n} \sin\phi\{\dot{\bar{q}}_j\delta[z - v_v(t - j\tau_v)] \\ - \bar{q}_j v_v \delta'[z - v_v - v_v\delta(t - j\tau_v)]\} dz \end{aligned}$$

Use the properties

$$\int \delta(x - a)f(x)dx = f(a); \qquad \int \delta'(x - a)f(x)dx = -f'(a)$$

to find:

$$\int \psi_n \frac{\partial Q'}{\partial t} dV = -S_c \sum_{j=0}^{\infty} \zeta_{nj} \{\dot{\bar{q}}_j(t) \cos[k_n v_v (t - j\tau_v)] + \bar{q}_j(t) k_n v_v \sin[k_n v_v (t - j\tau_v)]\} \tag{3.39}$$

with

$$\zeta_{nj} = \frac{\dot{\eta}_n(j\tau_v)}{\bar{\gamma} k_{1_n}} \sin\phi \tag{3.40}$$

Thus we have an expression for the right hand side of (3.30) representing the forcing due to a train of burning vortices, launched at $t = 0, \tau_v, 2\tau_v, \cdots$ from the lip of the step at $z = 0$.

The results (2.52)a,b of time averaging may now be used to determine the functions $A_n(t)$, $B_n(t)$ in the form (2.51) for $\eta_n(t)$. To find explicit results, the time dependence $q(t)$ for the energy release rate of each vortex must be prescribed. Although contrary to the results for vortex combustion cited earlier, we assume for simplicity that negligible energy is released by each vortex until some time τ_c later, the time delay for this process. Hence we set all $q_j(t)$ equal except for the difference in the times of initiation:

$$\bar{q}_j(t) \doteq q_v \delta[t - j(\tau_v + \tau_c)] \tag{3.41}$$

With this form the integrals in (2.52)a,b can be carried out explicitly. In this step, consistent with the approximations required for the method of time averaging we set

$$\dot{\eta}_n(j\tau_v) = -\omega_n [A_n(t) \cos\omega_n j\tau_v - B_n(t) \sin\omega_n j\tau_v]$$

and take $A_n(t)$, $B_n(t)$ to be constant when the integrals are performed. As a result, the formulas (2.52)a,b lead to the results always found for linear behavior,

$$\frac{dA_n}{dt} = \alpha_n A_n + \theta_n B_n$$
$$\frac{dB_n}{dt} = \alpha_n B_n - \theta_n B_n \tag{3.42}a,b$$

Hence the α_n, θ_n depend on the various parameters k_n, ϕ_n, τ_v, τ_c etc. introduced to define the mode shape and the stream of vortices. Their particular forms are unimportant here. The point is that the idea of producing combustion instabilities by unsteady combustion in vortex shedding can be translated to an approximate description allowing correlation and interpretation of data. The details of applying this analysis to experimental data are presently incomplete. It would be particularly interesting to determine whether this model of the process predicts frequency shifts as large as those sometimes observed in laboratory tests.

4. METHODS OF ANALYSIS

Ultimately the purpose of research on combustion instabilities is to provide the basis for understanding and curing the problem in actual propulsion systems. Experimental data taken with laboratory or full-scale devices, combined with analytical estimates, have suggested the most likely mechanisms for instabilities. Analysis based on the conservation equations incorporating one or more of those mechanisms provides the means for translating empirical results to a form useful in design and development.

Thus the analyses of unsteady motions that have been carried out have been conditioned to a considerable extent by the *a priori* view of the mechanism, or model, chosen to represent the unsteady combustion processes. (That is not entirely a necessary rule, but seems to be partly a social matter or a question of taste.) In this section we shall cover briefly four classes of analysis that seem to encompass almost all of the work that has been done on combustion instabilities in liquid rockets. Historically, the problems were first treated for liquid rockets, research in the subject was particularly active during the 1960's because of the needs of the Apollo program. Some of the ideas have since been adapted with suitable modifications, to analyze instabilities in augmentors and ramjets. We shall discuss those subjects in Section 5.

4.1 Numerical Analysis and Simulation of Combustion Instabilities

By 'numerical analysis' we mean works that are devoted to solving the differential conservation equations, usually in nonlinear forms. Thus, it is necessary to prescribe in complete detail the mechanism selected as the cause for the instabilities. In view of the discussions in Section 3, it is therefore not surprising that numerical analyses have uniformly been concerned with mechanisms emphasizing injection, atomization, vaporization, and combustion of liquid propellants.

Priem and Guentert (1962) were first to treat combustion instabilities in liquid rockets by solving numerically the conservation equations. Their approach was later adopted by others [notably by Hoffman, Wright and Breen (1968) based on work reported by Beltran, Wright, and Breen (1966)] with some important detailed changes, but the strategy remained unchanged. The work has been summarized in Harrje and Reardon (1972), pp. 194-207 and pp. 286-293.

Because of computational limitations, only one- or two- dimensional problems were treated. The two-dimensional problem was formulated for concentric annuli in the chamber (Figure 4.1) The nonlinear conservation equations were solved with source terms representing vaporization and combustion. Hoffman, Wright, and Breen distinguished the liquid fuel and oxidizer and were able to represent the energy release somewhat more

realistically: for example, they were able to account for variable oxider/fuel ratio and conditions when either fuel or oxidizer may be excess. Moreover, they included the droplet drag and momentum thransfer between the liquid and gas phases. They assumed, with Priem, that the vaporization rate was quasi-steady, but they improved the representation by including a dependence on Reynolds number. Like Priem, they assumed also that combustion occurred immediately upon vaporization. As an improvement in detail, they used a lognormal distribution of sizes for both the fuel and oxidizer droplets. Break-up and atomization of the injected liquids were ignored.

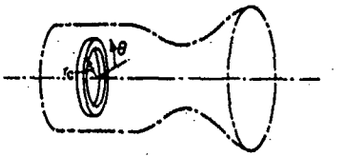


FIGURE 4.1

The same initial value problem was treated in all these works: a wave having sinusoidal amplitude distribution around the annulus is initiated with maximum amplitude $\Delta\bar{p}/\bar{p}$. It is time evolution is calculated as it propagatees around the annulus. The annulus can be placed anywhere along the axis of the chamber, but axial propagation of the wave is not treated. Axial locations are distinguished because the properties of the droplet sprays vary as the flow proceeds from the injector. The average properties of the spray are assumed uniform within an annulus.

Thus the wave is confined to an annulus and the chief results are the waveform as a function of time and space. From that can be determined the growth or decay of the wave and the dependence on the various parameters characterizing the system. It's a curious result - never satisfactorily explained - that all calculations apparently showed linear stability. The initial disturbance had to have finite amplitude in order to be amplified. When unstable, the wave steepened, as shown by Figure 4.2 taken from Hoffman, Wright, and Breen. Owing to the constraints placed in the problem (especially the required propagation in an annulus) it is not very surprising that the possibility of finite amplitude transverse waves without shocks, predicted by Maslen and Moore (1956) was not confirmed; their results always show substantial steeping after short times.

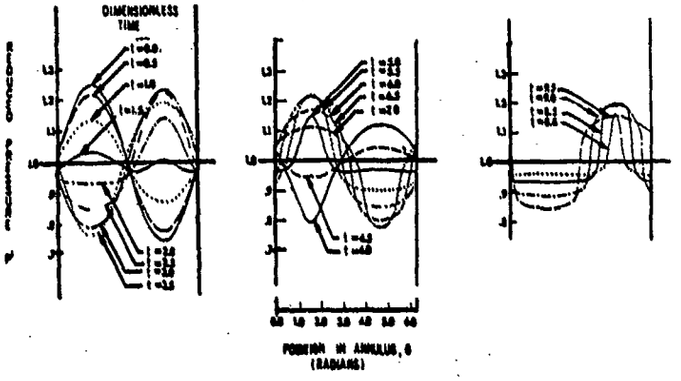


FIGURE 4.2

Figure 4.3 shows some of the main results found by Hoffman, Wright, and Breen. The initial maximum amplitude of the wave is plotted versus a burning rate parameter, essentially a measure of the average energy release rate in unit volume. The curves are stability boundaries: for values of amplitude below the curve, the wave decays. Several boundaries are shown for values for a 'drag parameter' equal to 1, 10 and 100. The drag parameter is a dimensionless measure of the momentum exchange per unit volume between the liquid and gas phases. Figure 4.3 illustrates the obvious result that the region of instability is decreased as the momentum exhange increases.

Transverse waves have long been troublesome and destructive instabilities in liquid rockets [Male, Kerslake and Tischler (1954); Reardon, Crosco and Harrje (1964); Levine (1965); Clayton, Rogers, and Sotter (1968)]. The problem had motivated the analyses described above, and for similar reasons Burstein, Chinitz and Schechter (1972) also carries out a numerical analysis. Like the earlier formulations, they treated wave propagation in an annulus, including the influences of a droplet cloud, but with the added feature that they could include axial

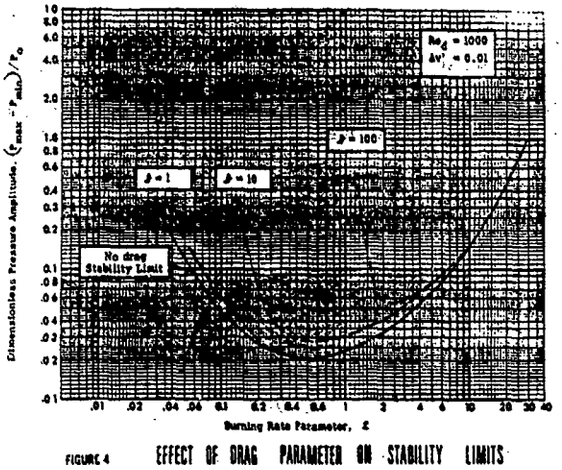


FIGURE 4 EFFECT OF DRAG PARAMETER ON STABILITY LIMITS

FIGURE 4.3

baffles. Thus their main contribution seems to have been their more extensive treatment of propagation in the axial direction. They too evidently found that small amplitude waves were stable.

The serious constraints placed on those earlier works, mainly due to the limitations of computational resources, cause them to be of limited value. It is not clear that the problems solved have been formulated in a physically consistent fashion, causing one to question the meaning of the results. In particular, the restriction to wave propagation in an annulus is no longer an acceptable approximation. Habiballah, Lourme and Pit (1988) have recently reported their most recent progress in a program devoted to modern numerical analysis - or numerical simulation - of instabilities. Although the calculations are being done specifically for the Viking engine, the ideas are more general and the essentials of the approach are broadly applicable.

This sequence of works has been previously described in several places [Schmitt and Lourme (1981); Habiballah and Monin (1984); Habiballah, Maraffa, and Monin (1985)] and we shall not cover the details here: the results are yet to be completed. The work amounts to be as thorough as possible analysis of both the liquid and gas phases in unsteady flow, including the influences of turbulence and combustion based on recent analysis and experiment. A series of two-dimensional and three-dimensional computer programs is being constructed. Ultimately, solutions (simulations) will be obtained for the conservation equations discussed in Section 2, but with careful account taken of chemical species. This seems clearly to be the proper direction for current and future numerical analysis of combustion instabilities. Only with full use of modern computational resources will it be possible to include the necessary details of the processes from injection to combustion.

4.2 Analyses Based on the Time Lag Model

By 'time lag model' we mean here the most common form, expressed by equation (3.14) for the unsteady conversion of liquid to gas. Crocco and Cheng (1956) examined various elaborations, including spatial variations of the sensitive time lag, but here we shall assume τ to be uniform everywhere and the same for all elements of injected propellant. Also we shall not distinguish between oxidizer and fuel. Both assumptions have been adopted in almost all applications, a notable exception being an analysis of chugging in which two time lags were introduced [Wenzel and Szuch (1965)].

Although some analysis has been done of nonlinear behavior with the time lag model [Sirignano and Crocco (1964); Mitchell, Crocco and Sirignano (1969); Mitchell and Crocco (1969)] by far most results, and all applications, have been worked out for linear behavior. To illustrate here we use the approximate analysis described in Sections 2.2 and 2.3. Although differences in detail will arise, the results will contain all the essential ideas discussed in previous works.

Broadly, the central idea is to use the formula (2.72) for the growth constant, α, *evaluated on the stability boundary*, so $\alpha = 0$. Those terms containing ω will of course depend on the interaction index, n, and the time lag, τ. If we assume that all other contributions to the formula are known, then the condition $\alpha = 0$ provides a relation between n and τ that must, within the approximations used, hold on the stability boundary.

There is no need to work out all details. Comparison of equations (2.90) and (2.96) shows that equation (2.72) will take the form

$$\alpha = C_1 \int \psi_n \dot{w}_l^{(r)} dV - C_2$$

where C_1, C_2 are constants. The constant C_2 contains the various effects of liquid/gas interactions, the nozzle, mean flow/acoustics interactions and damping devices. Now with $\dot{w}_l$ given by (3.13), its real part is $n(1-\cos\omega\tau)$, and for $\alpha = 0$, (4.1) gives

$$n(1-\cos\omega\tau) = \frac{C_1}{C_2 \int \dot{w}_l \psi_n^2 dV} = G_R \qquad (4.1)$$

since E_n^2 is defined by (2.44)b and therefore becomes a common factor. The function G_R is supposed to be known, with value depending on the various parameters (geometrical, etc....) defining the system. Then equation (4.1) is the relation between n and τ referred to above.

Figure 4.4 shows the unstable regions defined by equation (4.1). This is a reproduction of Figure 4.2.2a, p.180, in an article prepared by Crocco [Harrje and Reardon (1972)]. The calculations carried out by Crocco were quite different from those summarized here, but the result has the same form, another illustration of the fact that, there is, in certain deep sense, only one 'linear stability problem'. Differences in detail among analyses arise only because representations of processes, and therefore characteristic parameters, may differ.

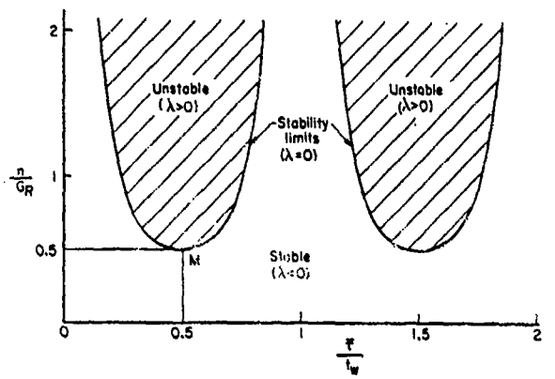


FIGURE 4.4

In this normalized form, Figure 4.4 is a kind of universal chart for the $n-\tau$ model. The multiple regions appear because of the factor $1-\cos\omega\tau$ in (4.2) and correspond to the multiple peaks in the response, noted in respect to Figure 3.3. They are usually not physically realistic and are another reflection of limitations of the elementary time lag model. A formulation of the $n-\tau$ model showing only a single peak was reported by Crocco (1966) but need not be discussed here.

For applications, equation (4.1) and Figure 4.4 have always been unfolded to give plots of n versus τ; n and τ versus some characteristic parameter, such as the fuel/oxidizer ratio as in Figure 3.2 above; or in some cases the stability boundaries have been presented in terms of system variables, with n and τ parameters along the curves.

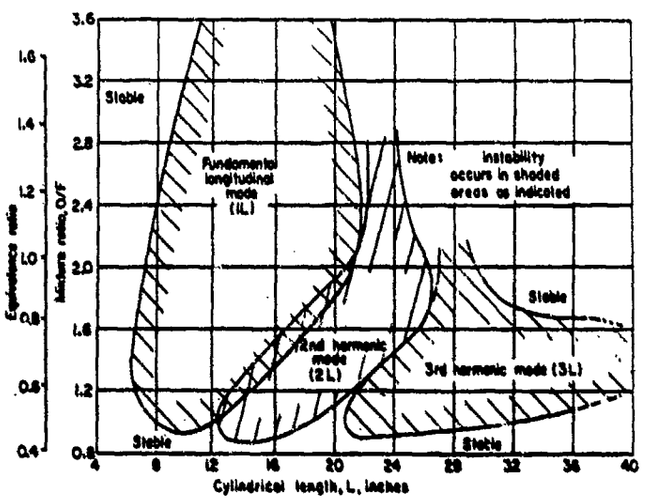


FIGURE 4.5

An example of the latter is reproduced in Figure 4.5 taken from Crocco, Grey and Harrje (1960). The preparation of this figure, and other quantitative results for n and τ, rests on extensive experimental work. In

all cases the strategy is the same: the stability boundary, marking the transition between stable and unstable small amplitude waves, is located experimentally, as a function of the variables defining the instabilities. Then the theoretical relation (4.1) is used to compute the required values of n and τ along the boundary.

That procedure has been used successfully to interpret longitudinal modes [Crocco, Grey and Harrje (1960)] and transverse modes [Crocco, Harrje and Reardon (1962) and Reardon, Crocco and Harrje (1964)]. By applying the method to large numbers of tests, extensive correlations have been worked out for the interaction index and time lag as functions of geometric variables, injector design, propellant types and operating conditions. A brief summary has been given by Reardon in Harrje and Reardon (1972), pp.277-286. Figure 4.6 is an example, of results for n and τ determined from tests for storable hypergolic propellants, with various types of injectors.

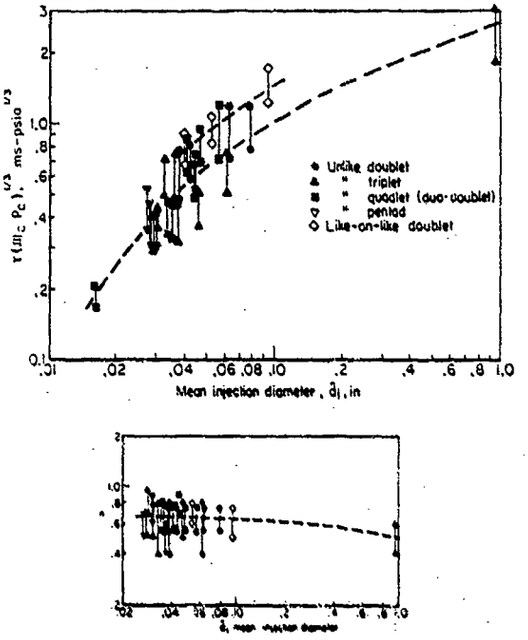


FIGURE 4.6

Having values of n and τ, one is now presumably in a position to return to the theoretical result for the growth constant and apply the results to designing new systems. An obvious shortcoming is that the data correlations can be assumed valid only for the systems actually tested. How far the results can be extrapolated cannot be known with great confidence. Nevertheless, this semi-empirical approach has been apparently used successfully both as a framework for correlating data and as an aid to design. It is essential in this procedure that the same theoretical result for the growth constant be used for correlating the data and for subsequent predictions. Otherwise, inconsistent and meaningless results will be obtained.

Although the ideas leading to the definitions of n and τ are appealing, the time lag model should be regarded truly as a framework for correlating data and not as a theory explaining fundamental mechanisms of combustion instabilities. With a different two-parameter representation of the unsteady process, the left hand side of (4.1) might have a different functional form, but the formula could be used in the same fashion to interpret stability boundaries. Only the forms of the correlations would be changed.

We must also note that because only the single formula for the growth constant (2.79) or (4.1) has been used, the method described above uses one equation to determine two unknowns (n, τ). Thus in practice, some difficulties may arise in obtaining consistent restuls. That trouble is avoided if, more correctly, both the real and imaginary parts, (2.75) and (2.76) of the complex wavenumber are used. In that event, measured values of the frequency are used and since (2.75) contains the imaginary part of the unsteady mass source (3.14), the two equations (2.75) and (2.76) have the form

$$\omega = \omega_n + C_3 \int \phi_n \tilde{w}_j^{(1)} dV - C_4$$

$$a = C_1 \int \phi_n \tilde{w}_j^{(1)} dV - C_2$$

Hence with (3.14)

$$n\sin\omega\tau = \frac{\omega - \omega_n + C_4}{C_3 \int \psi_n^2 \bar{w}_l dV}$$
$$n(1-\cos\omega\tau) = \frac{C_2}{C_3 \int \psi_n^2 \bar{w}_l dV} \qquad (4.2)a,b$$

The left hand sides could equally be regarded, within a multiplier, as the real and imaginary parts of the mass source,

$$\hat{w}_l^{(r)} = \bar{w}_l n(1-\cos\omega\tau)$$
$$\hat{w}_l^{(i)} = \bar{w}_l n\sin\omega\tau \qquad (4.4)a,b$$

and correlations could be done with $\hat{w}_r = n(1-\cos\omega\tau)$ and $\hat{w}_i = n\sin\omega\tau$ instead of (n, τ). Thus, even though the heuristic argument leading to $\hat{w}_l$ in the form (4.4) is based on a time lag associated with motions of the propellant (a Lagrangian view), the end result is equivalent to a purely Eulerian representation of local combustion process. The time lag associated with motions in space can be reinterpreted as a phase lag in time at a fixed location in space.

The formulas (4.3)a,b have been deduced from the approximate analysis discussed in Section 2 and therefore have a particularly simple form. Although it is true that a linear analysis will always produce two formulas, for the real and imaginary parts of complex wavenumber, the forms may be wildly different in detail, depending in the method of solution. Crocco, Grey and Harrje (1960) solved their differential equations directly, a method used later by Crocco, Harrje and Reardon (1962) and Reardon, Crocco and Harrje (1964) to study transverse modes.

The time lag models of the combustion process has been used also in analysis of nonlinear behavior, both for longitudinal oscillations [Sirignano and Crocco (1964); Mitchell, Crocco and Sirignano (1969); Crocco and Mitchell (1969)] and for transverse oscillations [Zinn (1966); Zinn and Savell (1968)]. In those and other works discussed in the following two sections, either n and τ are assigned values; or the unsteady behavior is studied as a function of n and τ. Thus, sufficient experimental data had been gained to support the time lag model that it could be used in a general fashion for theoretical work. However, remarks above emphasize that this practice really amounts to using any combustion response having real and imaginary parts related to n and τ by equations (4.4)a,b. Expressing results and interpreting behavior in terms of n and τ carries no uniqueness.

4.3 Use of Green's Function to Compute Linear Stability

Beginning in the late 1960's, Mitchell and co-workers (1972, 1975, 1979, 1984, 1985, 1986, 1987) introduced use of a Green's function to produce an integral equation solved by iteration. Good summaries of this approach have been given by Mitchell and Eckert (1979) and by Mitchell (1984). The time lag model was assumed to represent the combustion response, the reason for mentioning these works here. Apart from that matter, the method is attractive for analying complications such as baffles and resonators that are quite awkward to handle when differential equations are used.

The approximate results (2.63) and (3.64)a,b are in fact the first order terms in an iterative procedure like that used by Mitchell. They are also, as the discussion in Section 2 showed, found by applying Galerkin's method to the problem of linear stability of sinusoidal disturbances. We therefore end this section with brief resumes of those two methods.

With the introduction of Green's function, a differential equation is converted to an integral equation that may be conveniently solved by iteration. The general theory, with applications, is thoroughly described by Morse and Feshbach (1953). Culick (1963) first applied the method to problems of combustion instabilities; it was later adopted by Oberg and Kulaws (1969, 1971) to study acoustic liners.

Mitchell and his co-workers (e.g., 1969, 1979, 1984, 1985) have chosen to express the acoustic field terms of a velocity potential, an unnecessary limitation to irrotational flows, as the developments in Section 2 demonstrate. We can illustrate the essentials of his method with the formulation derived here. The problem is to solve the inhomogeneous equation (2.31) for the pressure, subject to the boundary condition (2.33). For steady waves, all dependent variable are proportional to $e^{i\omega t}$; $p' = \hat{p}e^{i\omega t}$ and equation (2.31) is

$$\nabla^2\hat{p} + k^2\hat{p} = \hat{h} \qquad (4.5)$$

Define the Green's function satisfying the same equation as $\hat{p}$ but with a unit source at position $\vec{r}_0$ and homogeneous boundary conditions

$$\nabla^2 G(\vec{r}\,|\,\vec{r}_0) + k^2 G(\vec{r}\,|\,\vec{r}_0) = \delta(\vec{r} - \vec{r}_0)$$
$$\hat{n}\cdot\nabla G(\vec{r}\,|\,\vec{r}_0) = 0 \qquad (4.6)a,b$$

Now multiply (4.5) by $G(\vec{r}\,|\,\vec{r}_0)$, (4.6) by $\hat{p}$, integrate over the chamber, use Green's theorem and insert the boundary conditions (2.33) and (4.6)b to find* the 'solution' for $\hat{p}$

$$\hat{p} = \int G(\vec{r}\,|\,\vec{r}_0)\hat{h}(\vec{r}_0)dV_0 + \iint_S G(\vec{r}\,|\,\vec{r}_0)f(\vec{r}_0)dS_0 \qquad (4.7)$$

* In these manipulations, the exchange of variables is made, $\vec{r} \leftrightarrow \vec{r}_0$, and the reciprocity property of G is used: $G(\vec{r}\,|\,\vec{r}_0) = G(\vec{r}_0\,|\,\vec{r})$.

It is convenient to express $G(\vec{r}' \mid \vec{r}_0')$ as an expansion in the normal modes ψ_n of the system, satisfying (2.35)a,b. That is, assume the form

$$G(\vec{r}' \mid \vec{r}_0') = \sum A_n(\vec{r}_0')\psi_n(\vec{r}_0')$$

Substitution in (4.6)a, multiplication by ψ_m, and integration over the chamber gives

$$A_n = \frac{\psi_n(\vec{r}_0')}{k^2 - k_n^2}$$

so the Green's function is

$$G(\vec{r}' \mid \vec{r}_0') = \sum \frac{\psi_m(\vec{r}_0')}{k^2 - k_m^2}\psi_m(\vec{r}') \tag{4.8}$$

Now insert (4.8) in (4.7) and assume that we are examining that mode which, when the perturbations vanish, reduces to the nth classical acoustic mode. Split that term from the remainder of the expansion and apply the normalization $\hat{p} \to \psi_n$ in the limit $\hat{h} = \hat{f} = 0$. Those operations give the formulas for $\hat{p}$ and k^2.

$$p(\vec{r}') = \psi_n(\vec{r}') + \sum_{m \neq n} \frac{\psi_m(\vec{r}')}{k^2 - k_n^2}\left\{\int \psi_n(\vec{r}_0')\hat{h}(\vec{r}_0')dV_0 + \iint \psi_n(\vec{r}_0')\hat{f}(\vec{r}_0')dS_0\right\} \tag{4.9}$$

$$k^2 = k_n^2 + \frac{1}{E_n^2}\left\{\int \psi_n(\vec{r}_0')\hat{h}(\vec{r}_0')dV_0 + \iint \psi_n(\vec{r}_0')\hat{f}(\vec{r}_0')dS_0\right\} \tag{4.10}$$

Equation (4.10) is exactly equation (2.63), except for the factor $p\hat{\eta}_n$ which appeared because to obtain (2.63) equation (2.59) was used, $p' = p\hat{\eta}_n e^{ikt}\psi_n$ (i.e. here $p\hat{\eta}_n = 1$, allowed because there is an arbitrary factor in the normalization; thus $\hat{p} \to \psi_n$ in (4.9) while in (2.59), $\hat{p} = p\hat{\eta}_n\psi_n$).

Equation (4.9) shows explicitly the perturbations of the classical mode shape, ψ_n, giving the actual mode shape $\hat{p}$. Because $\hat{h}$ and $\hat{f}$ depend on p' and $\vec{u}'$ (i.e. $\hat{p}$ and $\hat{\vec{u}}$), equation (4.9) is an integral equation for $\hat{p}$ and of course k^2 cannot be calculated with (4.9) until $\hat{p}$ and $\hat{\vec{u}}(\vec{r}')$ are known. In the approximate method discussed in Section 2, we simply set $\hat{p} \approx \psi_n$, $\hat{\vec{u}} \approx i(a/\gamma k_n)\nabla\psi_n$ and use (4.10) directly. To proceed further, the integral equation (4.9) must be solved. That is where most of the labor in Mitchell's work is expended. He solves the equation numerically using an iteration procedure. We shall not discuss the details further.

We must note, however, that when an iteration procedure is used, care must be exercised that *all* terms of consistent order are retained. The small parameter here is a Mach number, M_r, characterizing the average flow. Corrections to $\hat{p} = \psi_n$ are thus of order M_r; that is, if the successive steps in the iteration are labeled $\hat{p}^{(r)}$, the procedure gives:

$$\hat{p}^{(0)} = \psi_n$$
$$\hat{p}^{(1)} = \psi_n + M_r\phi^{(1)}$$
$$\hat{p}^{(2)} = \psi_n + M_r\phi^{(1)} + M_r^2\phi^{(2)} \quad \text{...etc}$$

The functions $\hat{h}$ and $\hat{f}$ are constructed by expansion of the primitive conservation equations according to remarks in Section 2.2. If they are not carried to order higher than M_r, then it is *not* correct to proceed beyond the zeroth approximation $\hat{p}^{(0)} = \psi_n$ of the mode shape to compute k^2 with (4.10). That is why the approximate method discussed in Sections 2.2-2.4 was not carried to higher order. To carry $\hat{p}$ and $\hat{\vec{u}}$ to higher order than allowed by the construction of $\hat{h}$ and $\hat{f}$ may yield misleading and incorrect results.

Properly used, the formulation based in Green's function is a powerful method to obtain results for complicated problems. For practical purposes it is much superior to solution of the differential equations owing to the ease with which arbitrary boundary conditions and volumetric sources can be accommodated. In that respect, this method has the same advantages as the approximate method discussed earlier, except that use of Green's function as described here and in Mitchell's work is strictly limited to linear problems. On the other hand, the approximate method given earlier is a form of Galerkin's method and can be used to analyze nonlinear behavior.

4.4 Application of Galerkin's Method

Zinn and Powell (1968, 1970) first published work applying a form of Galerkin's method to combustion instabilities. The chief difference from the classical Galerkin's method was addition of a recipe for handling the inhomogeneous boundary conditions. In a subsequent series of papers, the method was used to investigate both longitudinal and transverse instabilities, with main emphasis on special aspects of nonlinear behavior [Powell and Zinn (1971, 1974); Lores and Zinn (1972, 1973)].

Because the purpose of this review is mainly to cover characteristics of linear stability, space does not permit a survey of nonlinear problems. That is not intended to imply that nonlinear behavior is unimportant. On the contrary, there is much to be learned both theoretically and for applications to design. As implied by the discussion of the approximate method in Section 2, this author believes that the most promising method on both counts is some form of Galerkin's method.

Best Available Copy

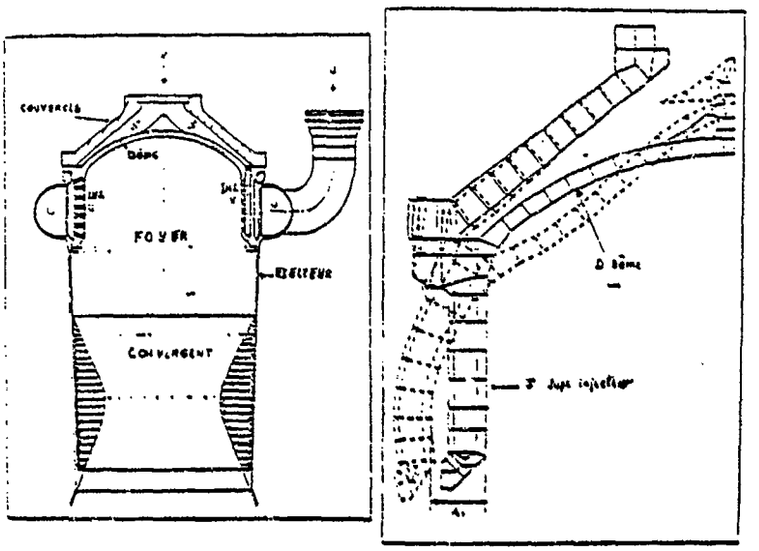
5. REMARKS ON INSTABILITIES IN THE THREE TYPES OF SYSTEMS

Most of the preceding discussion has been concerned with matters common to all three types of systems. Much of the work was in fact carried out originally for liquid-fueled rockets, the strongest motivation being applications to engines intended for the Apollo vehicle. Some of the ideas and methods developed for liquid rockets have been modified or extended for analysis of combustion instabilities in augmentors and ramjets. Moreover, there are special problems peculiar to the different systems themselves. We therefore examine now those particular matters.

5.1 Combustion Instabilities in Liquid Rockets

We have covered almost all the basic material related to liquid rockets. Little work was done in the problem in the later 1970's. With the flight failure of an Ariane vehicle due to combustion instability in a first stage Viking motor, a comprehensive research program was initiated in France in 1981. Most of the available reports of that work have already been referred to and little more needs to be added here.

Within the present context, the most important parts of the French work are the experimental and analytical efforts to characterize the liquid spray; and the extensive numerical simulations of unsteady motions, incorporating the results obtained for the propellant sprays. The problem causing the failure involved coupling between the pressure oscillations in the chamber and structural vibrations of the injector which is placed in the lateral boundary [Figure 5.1 taken from Souchier, Lemoine and Dorville (1982)] Figure 5.1(b) shows the computed distortion of the injector plane. As a result, the fuel and oxidizer jets were shaken, causing (apparently) perturbations of the distribution and phase of the energy release, therby closing the loop and making possible self-excited motions.



(a) (b)

FIGURE 5.1

Such effects on the injection processes have long been known to be a potential cause of instabilities [Levine (1965); Harrje and Reardon (1972)] but they have yet to be well-characterized. They are likely to be particularly important in cases when the amplitudes of motion are large. It is quite possible that the *forms* of the representation of the unsteady sources of mass and energy are strongly dependent on the amplitudes of motion as well as on the hardware design. Such behavior is far outside any successes of the time lag model and is likely to remain so. Careful experimental work is essential to clarify the situation.

During the past several years, serious interest in developing new liquid-fueled rockets has grown in the U.S. primarily for use in proposed heavy lift launch vehicles. Because of their high densities and good performance, liquid oxygen and hydrocarbon fuels are being considered as propellants. In particular, methane has been selected by the NASA Lewis Research Center is the favored fuel. As a result, studies of combustion instabilities are in progress at the Aerojet TechSystems Company and at the Rocketdyne Division of Rockwell International.

Rocketdyne has designed and fabricated two engines, for the Lewis Research Center (LeRC) and for the Marshall Space Flight Center(MSFC). Both use LOX/methane and have identical thrust chambers but different injectors. The MFSC engine has an acoustic resonator; the LeRC engine has no damping device. A small number of firings directed to determining stability characteristics have been completed [Jensen, Dodson and Trueblood (1988); Philippart and Moser (1988)].

Development of computer programs for analysis of instabilities is in progress and only incomplete reports have been used. [Fang (1984, 1987); Fang and Jones (1987); Mitchell, Howell and Fang (1987); Nguyen (1988)]. The program IFAR (Injector Face Acoustic Resonator) has been in existence for some years; the time lag model was used to represent the combustion process. That program has been revised and modified for application to both retangular and axisymmetric chambers to become HIFI (High Frequency Intrinsic Stability) [Nguyen (1988)].

These computer programs are being used in the manner described in Section 4.2. With all other variables and parameters specified, the values of n and τ are calculated on the stability boundary. Then to predict whether the engine is stable or not, the values of n and τ must be determined. Traditionally this has been done with correlations exists for injectors using hydrocarbon fuels, so as part of their work the group at Aerojet has been performing sub-scale tests and carrying out analysis of the injector response [Muss and Pieper (1987); Nguyen and Muss (1987)]. The analysis and tests is intended to provide correlations of n and τ for the injector with those on the stability boundary calculated with the analyses cited above.

Aerojet is pursuing a program combining analysis, sub-scale tests using both retangular and axisymmetric chambers prior to full- scale firings. The chief purpose is to provide as certain as possible basis for confidently predicting the stability of the large engines, thereby reducing development costs. This program has been recently described by Muss and Pieper (1988).

Philippart (1987) and Philippart and Moser (1988) have reported comparisons of predictions of the sort mentioned above, with firings of the two Rocketdyne engines. One operating condition was examined for which the LeRC engine was stable and the MSFC engine was unstable. Three calculations of the stability boundary in the $n - \tau$ plane were done, using the programs IFAR, HIFI and a modified from (NDORC) of Mitchell and Eckert's (1979) MODULE. Figure 5.2, taken from Philippart and Moser, shows the results obtained with HIFI for the two engines. Results obtained with the other two programs

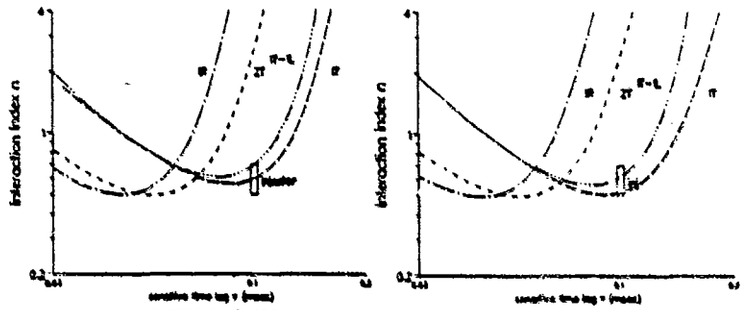


Fig. 9: HIFI MSFC Analysis (1/4 wave axial cavity)

Fig. 9: HIFI Analysis LeRC Engine (no cavity)

FIGURE 5.2

differ in details that are unimportant here. Also shown as filled boxes are estimates of the 'combustor response' (i.e. the values of $n = \tau$) based on correlations for LOX/hydrogen injectors. Apparently the predictions of the three codes agreed fairly well. However, there are uncertainities owing to differences between the codes; a significant distinction is that IFAR and HIFI assume that combustion is concentrated in a transverse plane, while MODULE is written for distributed combustion. Comparison with the test data is ambiguous and must be viewed as preliminary because the true characteristics of the injectors are unknown.

Jensen, Dodson and Trueblood (1988) have given an early progress report in their tests with the LeRDCF engine. They have measured growth rates (α) and, using the MODULE program, have inferred the necessary values of n and τ. Two examples are shown in Figure 5.3. The striking result is that the values of the interaction index are found to be considerably greater than those computed by Philippart and Moser and those provided previous correlations of data. It is impossible at this point to determine the cause for these differences.

Also at Rocketdyne some interesting work is in progress to analyze the characteristics of sprays vaporizing and burning under steady conditions [Liang et al (1986, 1987)]. The calculations are being done for various injector types placed in chambers with provision for computing the internal flow field. When extended to cover transient motions, this work is potentially an important contribution to analysis of combustion instabilities. Indeed, it appears that one of the most important outstanding problems in the subject is the prediction of the liquid drops; unsteady spray combustion; and incorporation of the results in a complete formation allowing realistic numerical simulations.

5.1.1 Pogo Instabilities

The problem of low frequency POGO instabilities is well- documented and understood. Due to the POGO instability in the Apollo vehicle, it is also probably the best known among people otherwise not familiar with combustion instabilities.

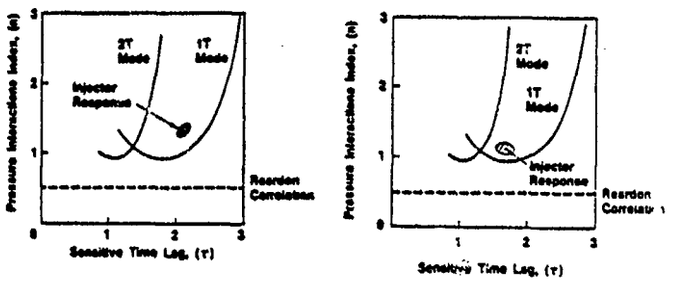


FIGURE 5.3

Low frequency instabilities ('chugging') arise due to coupling between the fluid dynamics in the combustion chamber, and the propellant supply system. They are perhaps the first sort of combustion instability definitely identified and analyzed for liquid rockets (see the remarks at the beginning of Section 3.1). POGO instabilities involve the further complication of coupling between the propulsion system and the structure of the vehicle. The low frequency structural vibrations are the origin of the name, by analogy with the motions of a POGO stick.

During the 1960's, the POGO instability received much attention as a serious problem in several vehicles including the Thor, Atlas, and Titan vehicles. Rubin (1966) has given a clear brief summary, including particular emphasis on pump cavitation and wave propagation in the propellant feed lines. Those are matters often overlooked by those concerned with motions in the combustion chamber. Yet they provide significant contributions to time lags in the system.

More recent work in France has been reported by Dordain, Lourme and Estoureig (1974) for the Europa II and Diamant B vehicles; and by Ordonneau (1966) for the Ariane.

5.2 Combustion Instabilities in Thrust Augmentors

It has long been standard practice that acoustic liners are integral parts of thrust augmentors. Since high frequency or 'screech' instabilities were first encountered as a serious problem in the late 1940's and early 1950's, liners have been developed largely by trial and error to act as passive control devices designed to suppress the oscillations. The staff of the Lewis Laboratory (1954) compiled most of the existing data and performed some tests to provide a basis for general guidelines for design; Harp et al. (1954) reported the results of extensive tests, also at Lewis Laboratory. Of the methods investigated to solve the problem, including baffles and vanes as well as adjusting the distribution of injectors, perforated liners worked best. Groups at Pratt and Whitney Aircraft and the United Aircraft Research Laboratory had already tried Helmholtz resonators and in 1953 demonstrated the first successful use of perforated liners is a full-scale afterburner on a J57. The physical basis for the success of liners is explained in Section 6.1.

Despite several attempts to develope analytical methods and a more quantitative basis for design, treatment of combustion instabilities in thrust augmentors has remained almost entirely an empirical matter. Kenworthy, Woltmann and Corley (1974) reported the results of an experimental program devoted to studying screech instabilities in 3 different designs of augmentors. The report also contains analysis used to correlate data and to provide some guidance for design of acoustic liners. This seems to be the last extended work on high frequency instabilities in full-scale augmentors; the mechanisms remain obscure. Chamberlain (1983) has given the most recent status report: little has changed in the past decade, it seems.

Perforated liners effectively attenuate the high frequency oscillations related to radial and tangential acoustic modes. Low frequency instabilities, often called 'rumble', tend to be more troublesome. Liners are ineffective at low frequencies and the problem of rumble is solved or reduced in practice by careful control and coordination of the distribution of injected fuel and the nozzle opening. It's a costly process to develop the system, inevitably requiring several designs of the injection system and flameholders, and expensive full-scale tests in altitude simulation test facilities

The problem of combustion instabilities in thrust augmentors is arguably more difficult then that in liquids rockets for at least two reasons: the processes involved in flame stabilizations are sensitive to pressure and velocity fluctuations; and the device is usually required to perform over a wider range of operating conditions. The first explains the importance of injector and flameholder design. As a result of the second, the high and low frequency instabilities are typically found in different regions of the flight envelope. Figure 5.4, reproduced from the excellent summary (as of 1971) by Bonnell, Marshall and Riecke (1971) illustrates the point.

Instabilities in the lower frequency range became increasingly troublesome with the development of turbofan engines, a consequence of the geometry (see Figure 5.5 taken from Bonnell, Marshall and Riecke (1971) and Figure 5.6 taken from Zukoski (1985). In the pure turbojet, the fluctuations may propagate upstream past the turbine disk but the turbine generally seems to act as a good reflector. In fan engines, it is common that the entire length of the fan duct participates in the oscillations, reducing the frequencies sometimes as low as 80 Hz. See Nicholson and Radcliffe (1953) for an early report of very low frequency oscillations; observations in turbofans have been discussed by Bonnell, Marshall and Riecke (1971); Mach (1971); Ernst (1976); Underwood et al (1977); and Cullom and Johnsen (1979). Figure 5.7 reproduces power spectral densities taken from turbofan augmentors [Bonnell, Marshall and Riecke (1971)]. Because of the rotating parts, spectra of the acoustic field in gas turbine

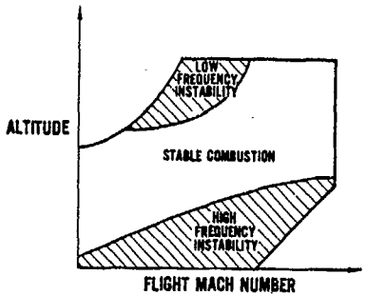


FIGURE 5.4

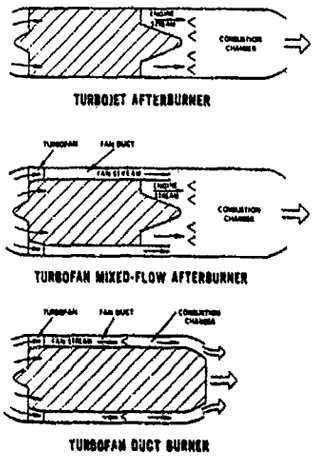


FIGURE 5.5

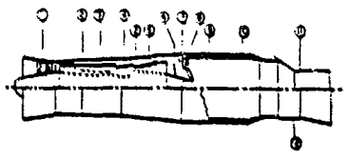
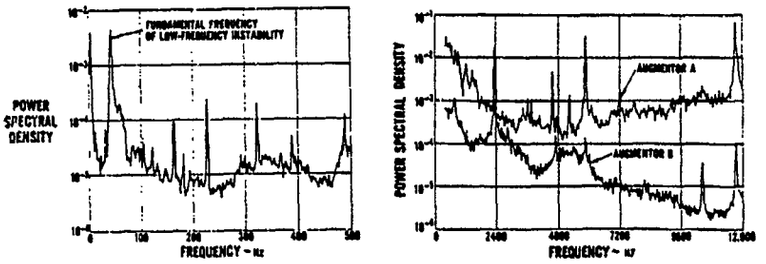


Figure 21.0.2 Pratt and Whitney F100-PW-100 augmented turbofan engine. (1) Three stage fan; (2) bypass air duct; core engine compressor (3), burner (4), and turbine (5); (6) fuel injectors for core engine gas stream; (7) fuel injectors for bypass air stream; (8) flame stabilizer for afterburner; (9) perforated afterburner liner; (10) afterburner case; nozzle closed to minimum area (11) and opened to maximum area (12).

FIGURE 5.6

engines tend to exhibit a greater variety of discrete oscillations than do those for liquid rockets. The peaks at the higher frequencies in Figure 5.7(a) are 'screech' modes.

The combustion processes in an augmentor differ in several fundamental respects from those in a liquid rocket. Only fuel is injected as liquid; the oxidizer is unburnt oxygen in the fuel-lean flows from the bypass and the core engine. There are no impinging fuel and oxidizer liquid streams, but the formation of drops and



(a) (b)

FIGURE 5.7

vaporization of the fuel must obviously occur. Normally, it is intended that the fuel drops should be entirely vaporized prior to ignition in the core flow so burning occurs in the fuel/air gaseous mixture. Because the flame propagation speed is less than the flow speed, a continuous source of ignition is required, normally supplied by the wake of a bluff body, the flame holder. Clearly, the performance of such a system depends not only on the flow conditions and physical properties of the fuel but also very strongly on the geometry of the injectors and flame holders. In the cooler bypass flow, vaporization is not completed upstream and liquid impinges on the flameholders; the liquid layer then vaporizes. Zukoski (1985) has provided a thorough and readable discussion of the combustion processes in afterburners. Figure 5.8 taken from his article, illustrates the general features of the flow in the vicinity of various flame holders.

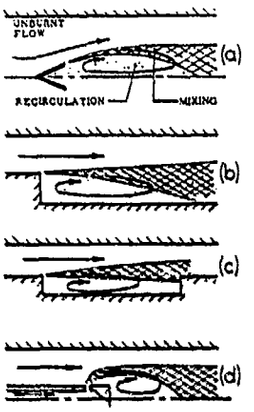


FIGURE 5.8

According to the preceding remarks, it appears unlikely that vaporization of the fuel droplets is a dominant mechanism for combustion instabilities in augmentors. Nevertheless, it is certainly quite possible that interaction of the acoustic field with the injection system could produce fluctuations of the fuel flow and hence subsequent fluctuations of fuel/oxidizer ratio and heat release in combustion. The process might be modeled in terms of a time lag but there seems to be no treatment of this sort in the published literature.

One would suspect that processes associated with the flame holder may dominate. That view is generally supported by practical experience with the strong effects of flame holder design on instabilities. We have discussed in Section 3.4 the mechanism based on vortex shedding and combustion suggested by Rogers and Marble (1956). Their argument is persuasive and there has never been evidence disproving that process as a possible mechanism. Theoretical developments and the necessary laboratory tests have not been carried far enough to incorporate the proposal in an analysis suitable for general design work with arbitrary geometries.

Russell, Brant and Ernst (1978), have worked out a one-dimensional analysis of instabilities in augmentors: the work is also discussed by Underhill et al (1977). Broadly the analysis represents the acoustic field as a synthesis of up and downstream traveling acoustic waves, and entropy waves, as in the example discussed earlier here in Section 3.3. The unsteady heat sources are derived as models of mixing and combustion in the wakes of the flame holders. Bypass and core flows are treated separately and superposed in parallel. It's a linear analysis; the equations for the time-dependent variables are solved by applying the Laplace transform. Conditions for stability are determined by applying the Nyquist criterion. It is difficult to understand all details of the analysis from the available (abbreviated) description. Although some success was evidently achieved with this work, it

seems not to have been widely applied. Moreover, the results are mainly in a computer program which has not furthered general understanding of the problem although it may have been useful in treating particular cases.

Over a period of several years Dix and Smith and co-workers developed an analysis based on the formulation published by Culick (1963) for liquid rockets. See Dix and Smith (1971) and references cited there for a description of the work. Although that sort of approach should be useful in treating augmentors, that analysis has also not be widely applied. It is important to note that while their linear analysis is correct, Dix and Smith committed some basic errors in trying to extend their calculations to nonlinear behavior. The results they have reported for the influences of the amplitudes of oscillations are wrong.

The most recent work in instabilities in augmentors seems to be that reported by Dowling and Bloxsidge (1984); Langhorne (1988) and Bloxsidge, Dowling, and Langhorne (1988) at Cambridge University. Laboratory experiments were done in a configuration intended, roughly, to represent a longitudinal segment of an augmentor (Figure 5.9). A flame stabilized on a single vee gutter in a duct supplied with premixed gaseous reactants entering through a choked nozzle. With modifications

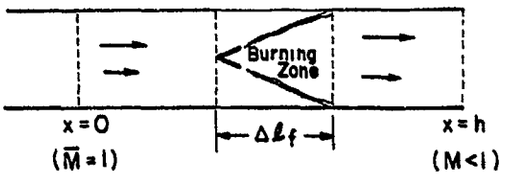


FIGURE 5.9

that may have significant influences on the unsteady behavior, this is a common configuration [Kaskan and Noreen (1954); Hegde et al (1986, 1987, 1988); Reuter et al (1988)]. The work by Kaskan and Noreen has already been described briefly (see Figure 3.5). They worked with a flame stabilized on a vee gutter whereas Hegde, Reuter, and their co-workers at Georgia Tech have been using one or two wires to stabilize the burning, although their work has presumably been directed to applications in ramjet engines and is mentioned further in Section 5.3.2.

All of these works are concerned in some broad sense with flames and flame instabilities the instabilities are ultimately manifested as vortices, so the mechanism for the instabilities discussed here could be classified as vortex shedding and combustion, as discussed in Section 3.4. Another similarity among these works is the use of electromagnetic radiation to identify the heat released by combustion products.

Langhorne (1988) concludes that for the device shown in Figure 5.9, two types of coupling exist between the burning processes and pressure oscillations. The transition between the two occurred in a narrow range of stoichiometric ratio around 0.65. For $\phi < 0.65$ a convective wave of entropy or spots of high temperature appeared to propagate well downstream of the flame holder. With increasing ϕ, that convective aspect seemed to have been confined to a short length and in the remainder of the duct the heat release (as measured by radiation from C_2 and $C(t)$ seemed to be in phase with the pressure oscillation. No results of flow visualization are available to confirm the behavior directly, but vortex shedding apparently may be involved.

At least partly as a result of the two kinds of coupling, two frequencies of instability were observed with larger amplitudes produced at higher stoichiometric ratios. Bloxsidge, Dowling, and Langhorne (1988) have worked out an interesting and useful one-dimensional analysis to interpret their observations.

Certain aspects of the Cambridge results are similar to those reported by Heitor, Taylor, and Whitelaw (1984). Sivesegaram and Whitelaw (1987) and by the Georgia Tech groups. The reasons for the similarities and reconciliation of differences are not known; a sufficiently general analysis has not been constructed to accommodate all the results on a common basis. There is little doubt that more than one mechanism may act, one or another dominant under different conditions. Because this is a relatively well-defined situation, (a premixed flame in a duct) the problem merits further attention both experimentally and theoretically to bring clearer understanding of the behavior.

5.3 Combustion Instabilities in Ramjet Engines

During the past decade, substantially more attention has been paid to combustion instabilities in ramjet engines than can be discussed in this paper. Much progress has been made but several essential problems remain unsolved, mainly associated with the conversion of liquid fuel to gaseous reactants; coupling between combustion processes and the unsteady motions; and the inlet/diffuser.

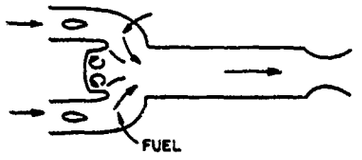
Sketches of two typical configurations are shown in Figure 5.10. Most contemporary liquid-fueled ramjets are "integral ramjet engines". The combustion chamber is initially filled with solid propellant that is burnt to boost the vehicle to supersonic speed. Liquid propellant is injected upstream of the region where the flow area abruptly increases at the "dump plane". Flame stabilization is achieved through continuous ignition by the hot combustion products in the recirculation zone. In some designs additional bluff body flame holders may also be used; and occasionally continuous burning of a pilot light may be required.

Zukoski (1985) has given a thorough discussion of steady flame stabilization in thrust augmentors. Much of that material applies with virtually no change to the corresponding problems in ramjet engines. The presence of the rearward facing step and the sensitivity of shear layers and recirculation zones to fluctuations in the flow are major factors in the problem of combustion instabilities in ramjet engines.

Much of the material we have covered for liquid-fueled rockets and thrust augmentors is relevant as well to ramjet engines. There are, however, several distinguishing features. First, unlike the case for liquid rockets



COAXIAL DUMP COMBUSTOR



SIDE DUMP COMBUSTOR

FIGURE 5.10

but similar to that for afterburners, spray combustion seems a lesser issue. Although the published evidence is perhaps not wholly conclusive, [see,e.g, Edelman (1981); Edelman et al (1981); Harsha et al (1981)], it appears that in operating engines, the liquid droplets are largely vaporized before the flow reaches the zones of flame stabilization and combustion. Hence the processes in those regions involve mostly gaseous reactants, a great simplification for carrying out research on combustion instabilities; very little experimental work has been done recently in the coupling between spray combustion and unsteady motions. Laboratory tests have for the most part used gaseous fuels.

That is not to say that transient processes of droplet heating and vaporization are unimportant, for they are surely influential in arranging the distribution of fuel over the plane at the entrance to the combustor. But there is no operational or experimental evidence to support the proposal by Tong and Sirignano (1986a, 1986b, 1987) that the unsteady conversion of liquid to vapor is a potential mechanism for instabilities. This matter has already been discussed in Section 3.2 with the chief conclusion that if all processes *except combustion* are accounted for, the presence of evaporating liquid drops is a stabilizing influence on unsteady motions. We shall not consider further problems associated with injection, atomization and vaporization. However, it is true that insufficient attention has been paid to the distribution of fuel/oxidizer ratio in the flow. Little is known of the details, either theoretically or experimentally; yet laboratory tests [e.g. Schadow et al (1987)] have shown that the distribution of fuel can have a substantial effect on instabilities , a fact that has long been known qualitatively from experience gained in engine development. [Rogers (1980a, 1980b); Grenleski et al (1977)]. There seems to be no evidence of coupling between oscillations in the flow and the fuel supply system. Thus no oscillations have been observed in ramjets corresponding to 'chugging' or POGO instabilities in liquid rockets.

5.3.1 Unsteady Behavior of the Inlet/Diffuser

So far as combustion instabilities are concerned, the principal feature distinguishing ramjet engines from liquid-fuel rockets and afterburners is the inlet/diffuser. Within the inlet a system of shock waves exists to provide the mass flow and stagnation conditions demanded by the conditions set in the combustion chamber and exhaust nozzle. Under normal operating conditions the shocks are located downstream of the geometric throat in the expanding supersonic flow. The position of the shock depends chiefly in the stagnation pressure in the combustion chamber; increasing the stagnation pressure causes the shocks to move upstream where the Mach number and therefore loss of stagnation pressure are less. It is this sensitivity of the flow in the inlet to pressure changes downstream that has caused longitudinal oscillations to be such a serious concern in ramjet engines. In the late 1970's [Hall (1978, 1980); Rogers (1980a, 1980b)] first qualitative and later limited quantitative relations were established between the amplitudes of pressure oscillations and the loss of dynamic pressure margin.

Since those early works, extensive tests by Sajben and co-workers [Chen, Sajben and Kroutil (1979); Sajben, Bogan and Kroutil (1984); Bogan, Sajben and Kroutil (1983a, 1983b)] have shown that the unsteady behavior is greatly more complicated due to flow separation and instability of shear layers. High speed schlieren pictures [see also Schadow et al (1981)] have shown large shock oscillations as well as the formation of vortex structures. Although computations based in the one-dimensional approximation to flow in the diffuser [Culick and Rogers (1983); Yang (1984); Yang and Culick (1984, 1985, 1986)] are useful and seem to capture some of the dominant features of the behavior, it is quite clear that the true motions can be simulated well only by numerical analysis based on the Navier-Stokes equations for two-or three-dimensional flows [Hsieh, Wardlaw and Coakley (1984); Hsieh and Coakley (1987), and references cited there].

There is evidence that under some conditions inlets exhibit self- excited or 'natural' oscillations. Energy is transferred from the mean flow to the fluctuations associated at least partly with separated flow. Although a one-dimensional calculation [Culick and Rogers (1983)] and an approximation to some of Sajben's data by Waugh et al (1983, Appendix D) suggest the possibility that the inlet may drive combustion instabilities, there is no firm evidence from tests with combustors that those conclusions hold. Most experimental results strongly suggest that the major source of driving unstable motions is likely associated with processes in the combustion chamber.

Nevertheless, because the flow from the inlet is the initial state for flow in the chamber, it is fundsmentally important that processes in the inlet be well- understood. In that respect, as we remarked above, perhaps the greatest deficiency is knowledge of the history of the injected fuel and the distribution of liquid droplets and gaseous fuel at the inlet phase.

5.3.2 Vortex Shedding and Combustion Instabilities

By far most attention has been directed to vortex shedding as the most likely mechanism for combustion instabilities in ramjet engines. In addition to extensive experimental work related to those ideas, much has been done, both with laboratory tests and analysis, to clarify the acoustical characteristics of the modes of oscillation. Much more is known, and understood, about vortex shedding and its role as a mechanism for causing combustion instabilities chiefly because that phenomenon is easily identified in experiments and is commonly encountered. Although vortex shedding is arguably the dominant feature causing instabilities in dump combustors - and might therefore be termed the most important mechanism - it cannot be separated completely from convective waves. Furthermore, neither mechanism can be understood apart from the acoustics of the chamber in which they occur; the type of mode that is unstable always provides some clues about the mechanism. For convenience here we nevertheless treat the phenomena separately and defer discussion of convective waves to Section 5.3.5. One distinction between the two mechanisms that seems to be true is that if direct coupling between large vortices and the acoustics field dominates, the frequencies of oscillations tend to be close to those of classical resonances. If convective waves are involved, the frequencies may be quite different, as shown with the elementary example in Section 3.3.

In Section 3.4 we discussed vortex shedding as a mechanism for combustion instabilities. The earliest ideas were developed in the 1950's to explain the occurrence of high frequency transverse or tangential waves in afterburners. Periodic combustion of reactants entrained in large vortex structures served as sources of acoustic energy. If properly phased, the sources may supply energy to an acoustic mode of the chamber. The fluctuations of velocity associated with the mode initiate vortex shedding, completing the cycle.

Roughly two decades later vortex shedding was again proposed as a possible mechanism for instabilities, but now periodic combustion was not part of the argument [Flandro and Jacobs (1975); Culick and Magiawala (1979)]. Laboratory tests in cold flow established the result that if vortices shed from a step or corner impinge on an obstacle downstream, there is sufficient coupling with unsteady motions to excite the sustain standing acoustic modes in a duct [Culick and Magiawala (1979); Dunlap and Brown (1981); Dunlap et al (1981); Nomoto and Culick (1982); Aaron and Culick (1985)]. In all those cases, longitudinal modes were drive. Large "vortex-like" structures were observed in some flow visualization work on dump combustors at AFWAL sometime in the late 1970's [Private communication, F.D. Stull].

It was therefore logical that vortex shedding should be proposed as a possible mechanism for causing the longitudinal modes in a ramjet engine. The idea seems to have been discussed first in this connection at a JANNAF workshop [Culick (1980)] in 1979. Byrne (1981, 1983) gave the first detailed discussion of the mechanism. He used known results for the stability of shear layers and jets, vortex shedding and vortex merging to argue that the frequencies of those processes taking place under the conditions occurring in ramjet engines are in the range of frequencies of the oscillation actually observed. He supported his conclusions by good comparisons of his estimated frequencies with data taken by others for both coaxial and side-dump configurations. Waugh et al (1983, Appendix B) showed modest success correlating amplitudes of instabilities with Strouhal number.

Since 1980, a large number of experimental works have established both by visualization and quantitative measurements that vortex shedding is a distinctive feature of dump combustors. [Schadow et al (1985, 1987); Smith and Zukoski (1985); Brown et al (1985); Biron et al (1986); Sterling and Zukoski (1987); Poinsot et al (1987); Yu et al (1987); Davis and Strahle (1987)]. All of those tests were performed either in cold flow or with premixed gaseous reactants. The most extensive summary of the subject has been given by Schadow et al (1987) who included also references to related work not discussed here.

The work by Schadow and co-workers at NWC is particularly noteworthy for its systematic progression from tests in cold flow to experiments in dump combustors with burning, as well as studies of vortex combustion in diffusion flames. Their program has used four different experimental facilities and has involved both forced and self-excited oscillations. They have also done limited tests in a water tunnel to show the formation of large vortices in their configuration. Overall, the work at NWC has established the existence of vortex shedding at the frequencies of instabilities in realistic coaxial configurations. Moreover, they have shown that combustion processes drive oscillations to much higher amplitudes than found in the cold flow tests. We should note that for the cases cited earlier, of oscillations driven by votex shedding in solid rocket motors, the vortices were formed in essentially non-reacting combustion products. The amplitudes of such instabilities have always been relatively small (<5% of mean pressure). Thus it seems true, as found also in the work by others cited above that truly large amplitude oscillations require the presence of combustion processes and the conversion of heat released to mechanical energy.

Hegde et al (1986, 1987) and Reuter et al (1983) have studied oscillations in a duct driven by a flame, in a situation similar to that devised by Kaskan and Noreen (1955) and by Dowling and co-workers at Cambridge for afterburners (Figure 5.9). In the Georgia Techo tests, the flame (or flames) is stabilized on one or two wires spanning a duct. Under broad conditions, the flame is unstable and vortices grow in the sheet. Interactions with the flow field are sufficiently strong to excite acoustic waves in the duct. The authors have proposed that fluctuations of the flame surface area - and hence of the reaction rate are responsible. They have given data based on emitted radiation, showing that the oscillations of surface area are in phase with the pressure variations. By Rayleigh's criterion for heat addition, it follows that the heat addition encourages growth of acoustic waves, a result established also by Sterling and Zukoski (1987) for a dump combustor.

Although most experimental work related to vortex shedding in ramjets has been done with coaxial configurations, the phenomenon has also been found in side-dump combustors. Stull et al (1983) have reported early work with that geometry and Nosseir and Behar (1986) have examined similar cases in a small scale. More extensive results with full-scale hardware were discussed by Zetterström and Sjöblum (1986) who investigated configuration having two or four inlets. Visualization in a water tunnel revealed the presence of vortex shedding. Instabilities in the operating engines were avoided by modifying the fuel injection systems in such a fashion as to minimize combustion within the vortices. That's an important practical result clearly supporting the general picture of vortex shedding as a dominant mechanism.

5.3.3 Mode Shapes: Experimental and Calculated

In practice, the first indications of combustion instabilities are almost always fluctuations in recordings of the pressure. If there is only one pressure transducer, one can infer only the amplitude and frequency - best displayed as a power spectral density. While the frequency alone may suggest what modes are involved, the configurations used for ramjet combustors are sufficiently complicated that the modes are not always easily identified. Moreover, in laboratory tests there may be an upstream plenum chamber and other parts of the apparatus that participate in the oscillations. As a general rule, it is essential that measurements of the pressure be taken at several locations in order to provide unambiguous identification of the modes. Sufficient care should be taken that distributions of both the amplitude and relative phase can be determined. This information has also proven extremely useful for confirming the results of analyses.

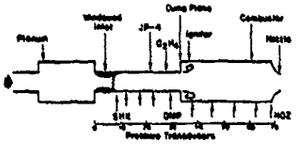
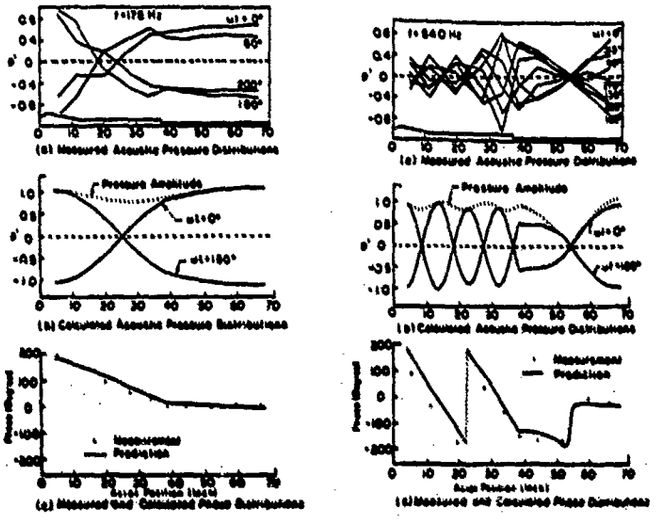


FIGURE 5.11

The most extensive measurements of mode shapes in dump combustors were made at the Naval Weapons Center by Schadow and co-workers. A summary of the results, with references to the previous work, was published by Crump et al (1986). Figure 5.11 shows the geometry of the sub-scale laboratory device; some results of measurements and analysis are reproduced in Figure 5.12. A case in which a bulk mode is excited in the combustion chamber (175 Hz) is shown in Figure 5.12(a); the fundamental wave mode was excited in the chamber excited for the case shown in Figure 5.12(b) (540 Hz). The calculated



(a) (b)

FIGURE 5.12

results were based on a one-dimensional analysis [Yang (1984)] in which combustion was ignored and the mean flow was accounted for only in the inlet. The good agreement is further evidence of the point emphasized in Sections 1 and 2, that the mode shapes and frequencies for combustion instabilities are often well-approximated by results based on classical acoustics. Here we also find that the one-dimensional approximation works well. For those calculations, the inlet shock was represented with the admittance function computed by Culick and Rogers (1983). It is apparently a good approximation that for these cases, the shock system is highly absorbing: the reflected wave has much smaller amplitude than the upstream-traveling incident wave. That fact, and the presence of the high speed average flow, explains why the relative phase varies linearly in the inlet.

Clark and Humphrey (1986) have also reported fairly good results obtained with a one-dimensional analysis applied to a side-dump configuration. The engine was supplied from a large plenum through inlets that were not always choked. Although the frequencies of oscillation, phase distributions throughout the device, and amplitude distributions within the combustor were predicted well, the amplitude distributions within the inlets diffuser considerably from the measured results. The reasons for the differences are not known. Yang and Culick (1985) later carried out a numerical analysis including vaporization of the liquid fuel and were able to predict quite well both the distribution and level of the pressure field.

A series of tests in a coaxial combustor have been reported by Sivasegaram and Whitelaw (1987), intended to examine the consequences of changing geometric parameters and fuel/air ratio. Data are given for frequencies and sound intensity at one location. Mode shapes were evidently not measured and no results of analysis are cited. It would appear that these data offer an opportunity for a straightforward application of a simple one-dimensional analysis.

The one-dimensional approximation works suprisingly well for rapid estimates of mode shapes and frequencies. It is worthwhile remarking on its application. Equation (2.25) and (2.26) with $\mathcal{F}_1 = \mathcal{P}_1 = 0$ determine the classical mode shapes. Few exact solutions exist for arbitrary variations of cross-section area $S_c(z)$, but in the case of ramjet configurations it is generally required to obtain results for piecewise variations. The problem comes down to solving the wave equation

$$\frac{d^2\hat{p}}{dz^2} + k_l^2\hat{p} = -\frac{d\hat{p}}{dz}\frac{1}{S_c}\frac{dS_c}{dz}$$

where dS_c/dz vanishes everywhere except at discontinuities of area where it is infinite.

Hence the general procedure is straightforward to find normal modes of the chamber. In uniform sections, the pressure field is represented by the usual forms, $A_i\cos(k_l z+\phi_i)$ or its equivalents, where A_i, ϕ_i are associated with segment i, and k_l is the wavenumber for mode l. These solutions are matched at the discontinuities by requiring continuity of the acoustic pressure and mass flow. Eventually the amplitudes A_i can be found to within a multiplicative constant, and the values of k_l are determined as roots of the characteristic equation.

This sort of analysis has long been known to give satisfactory results if the changes of area are not too large [Culick, Derr, Price (1972); Derr and Mathes (1974)]. Simple resonance tests at room temperature have confirmed the calculations, a method that is still useful for investigating the acoustic modes of combustion chambers. For application to actual systems, significant differences between these approximate results and observed values may arise due to uncertainties in the boundary conditions at the inlet and exhaust.

5.3.4 Numerical Analysis of Flows in Ramjet Combustors

It is the nature of the sort of approximate analysis discussed in Section 2 that reasonable results for the frequencies of oscillations can be obtained with rather crude approximations to the actual mode shapes. Furthermore, the stability of small amplitude notions can be assessed with some confidence if all the important processes are modeled reasonably well. The approximate analysis of course provides no information about the details of the situation in an actual combustor. Indeed, qualitative knowledge of the real state of affairs is required to make this sort of approach productive. Independently of experimental results, the only other source of information is numerical analysis based on the complete conservation equations. More importantly, results of accurate numerical analysis provide the only basis for judging the accuracy of an approximate analysis.

Thus, thorough numerical analysis of both the steady and unsteady flows in a combustion chamber is potentially extraordinarily important for investigating combustion instabilities. Even with recent developments in high speed computers, capabilities and resources fall considerably short of those required to handle "real" problems. For example, it is still not realistic to treat three-dimensional problems, even without combustion; and of course proper accounting of turbulence and combustion processes already taxes available resources beyond practical limits even for flows that are two-dimensional in the mean.

Numerical analysis, or simulation - really the application of computational fluid dynamics to investigate internal flows - has never been seriously pursued either for liquid rockets or for thrust augmenters. Because the surge of interest in treating combustion instabilities in ramjet engines has been quite recent, application of CFD has become a sensible endeavor. Although results obtained to date do not approach closely the goals cited above, some progress has been made.

The most advanced works have been reported by Kailasanath et al (1985, 1986, 1987) and by Jou and Menon (1986, 1988). Although eventually combustion processes will be accounted for, results published to date are only for cold flow, in the configuration tested by Schadow et al, Figure 5.11. The two chief differences between the two works are that Kailasanath et al solve the inviscid (Euler) equations, arguing that the effects of nonlinear damping of the numerical scheme gives a high (but not infinite) "effective Reynolds number", while Jou and Menon solve the full Navier-Stokes equations; and while Khailasanath et al assume multiple exhaust nozzles, Jou and Menon treat a single nozzle smoothly joined to the chamber as in the experimental apparatus. Both analyses are carried out for axisymmetric flows using similar grid sizes. Figure 5.13, reproduced from Kailasanath et al

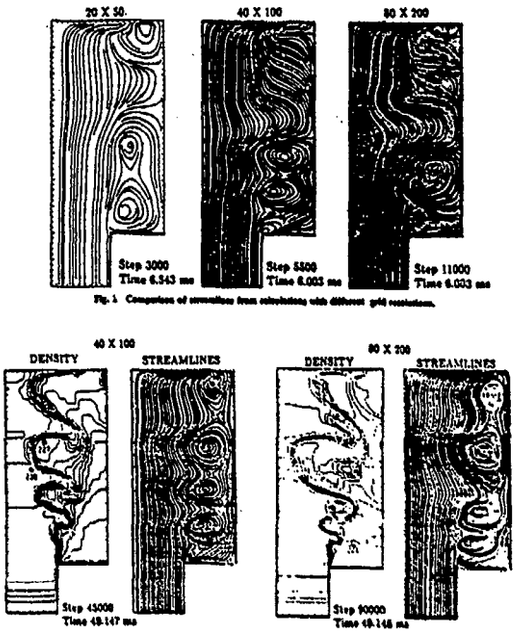


FIGURE 5.13

(1987b) shows density contours and streamlines for two different meshes. Figure 5.14 shows a time-sequence of vorticity contours computed by Jou and Menon (1988a). Obviously both results show the generation of large vortex structures.

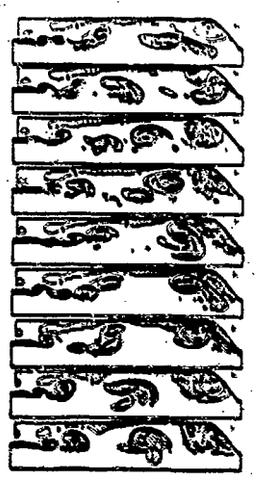


FIGURE 5.14

These numerical results have not been subject to any objective detailed comparison, and it is impossible to do so here. Both works have concentrated in the vortex/acoustics interactions. much of the discussion of the results tends to descriptive. There are of course both similarities and differences between the two sets of works. At this time, one might be inclined to favor calculations based on the Navier-Stokes equations for which all boundary conditions can be correctly satisfied.

For some purposes, it can be an awkward feature that numerical analysis produces results for the total values - mean plus fluctuating - of the flow variables. Perhaps the easiest way to display the properties of the unsteady flow is with power spectral densities and various correlations. Power spectral densities are computed in the works cited, showing peaks not all of which can be related to classical acoustic modes. Jou and Menon (1988b) have attempted the more difficult task of extracting the acoustic field itself by computing the solenoidal and potential parts of the velocity field. Their results show that the large vortices are approximately quadrupole

sources of the acoustic field; and that impingement of a vortex on a choked nozzle appears as a dipole source. They have used the latter conclusion, and an approximation to the influence of the acoustic field on separation of the shear layer, to construct a model for coupled acoustic/vorticity modes. This is a form of an instability based on a mechanism involving convected waves (in this case vorticity waves). Evidence of such coupled modes appears in the numerical results: their frequencies are not particularly close to those of classical acoustic modes.

More recently, Molavi and Sirignano (1988) have published their initial results for numerical analysis of the unsteady field in a two-dimensional dump configuration. The $k-\epsilon$ model is used to describe the gas flow. Vaporization of liquid fuel drops is accounted for, followed by combustion with finite reaction rate. Calculations of the gas motions were done using codes written by others (a "Teach-based algorithm with the Simple method for solving the pressure field").

Unlike the analyses discussed above, there is no evidence of vortex shedding and no discussion of that striking difference from previous calculations and experimental results. The emphasis in the work is on the behavior of the liquid phase. No oscillations appear spontaneously, and forced oscillations (i.e. unsteady motions numerically superimposed on the steady solutions) decay rapidly.

Two recent analyses have been done to demonstrate the existence of recirculation zones (confined or trapped vortex motions) in the head end of a side-dump combustor [Liou et al (1988) and Hong et al (1988)]. Those works use the same or similar computer codes as those used by Molavi and Sirignano; the results show steady vortex motions apparently in good agreement with observations of flow visualization tests [Stull et al (1983); Vanka et al (1983, 1985); Liou and Wu (1985)]. The calculations do not include combustion. Like another recent work by Vanka et al (1988), these analyses have to do with the steady flow in a ramjet combustor and make no attempt to treat combustion instabilities. In that respect they are nevertheless relevant because knowledge of the steady flow field is prerequisite to understanding unsteady motions.

It is not possible to reconcile the preceding numerical analyses. While all must contain some realism, the results show only limited qualitative agreement with experimental results and among themselves. The calculations are difficult, time consuming and as always are subject to peculiar - sometimes unpredictive - influences of numerical schemes. Others not involved in performing the calculations can only assume that the published results are in fact numerical solutions to the formulated physical problems and do not reflect in any significant fashion the computational procedures. Success with computational fluid dynamics applied to internal flows can be an enormously important contribution to treating problems of combustion instabilities.

5.3.5 Convective Waves of Entropy and Vorticity

We gave in Section 3.3 an elementary example showing the possibility for exciting instabilities by coupling entropy and acoustic disturbance at the exhaust nozzle. The calculations carried out there are equally valid for vorticity: just replace the entropy fluctuation by the vorticity fluctuation. That is essentially the gist of the model discussed by Jou and Menon (1988) cited above in Section 5.3.4.

Those computations have produced two main results: they confirm the view that convective waves constitute a possible mechanism for instabilities; and they show that the frequencies of coupled acoustic/convective wave modes can be significantly different from those of perturbed classical acoustic modes. Some of the numerical results cited in Section 5.3.4, and some experimental tests as well, have shown peaks in power spectral densities that apparently are not related to excitation of classical modes. Those observations strongly suggest that convective waves participate in some combustion instabilities, although incontrovertible proof has not been given.

Waugh treated two models of instabilities associated with entropy waves [Waugh et al (1983); Waugh and Brown (1984)]. In one model, the source of entropy fluctuations was concentrated at a single axial location, and in the second, several concentrated sources were used. The calculations required are modest extensions of the example given in Section 3.3. According to those results, distributed combustion tends to more stable than concentrated combustion when the chief mechanism for instability is the convected entropy wave.

In a work intended to investigate the stability of unsteady motions with combustion in a dump combustor, Humphrey and Cullick (1986, 1987) used the results worked out by Chu (1953) for the unsteady behavior of a plane flame. The upstream boundary condition at the inlet was set with the one-dimensional analysis of the shock response [Cullick and Rogers (1983)]. These works once again established the existence of coupled acoustic/entropy modes that do not reduce to classical modes when the entropy fluctuations vanish: they arise in addition to the classical modes which themselves are of course slightly modified when entropy fluctuations are present.

Prompted by high speed films of the unsteady flow in a dump combustor [Davis (1981)], Abouseif, Keklak and Toong (1984) postulated that the instabilities were due to coupling between entropy waves and acoustic waves. The basic model was essentially that described in Section 3.3. Periodic shedding of hot spots from the recirculation zone near the dump plane was interpreted as a consequence of periodic heat release causing oscillations of temperature. Predictions of the frequency were about 10 per cent below the observed values. The authors speculated that the difference may be due to their assumption that the combustion zone - and hence the source of entropy waves - was concentrated at the dump plane. Apparently no effort was made to model a distributed combustion zone and no comparison was made between those coupled modes and classical acoustic modes that could be excited directly by interaction with shed vortices. The stability of the modes was calculated (i.e. values of the growth constant) but data was not available for comparison.

Waugh and Brown (1984) also applied their analysis of acoustics with convective waves to Davis's data. They noted that Abouseif et al had used an incorrect boundary condition at the nozzle. The corrected calculations produced frequencies quite close to those observed, and the mode shapes as well showed better agreement with test results.

5.3.6 The Time Lag Model Applied to Combustion Instabilities in Ramjet Engines

During the past seven years, Reardon (1981, 1983, 1984, 1985, 1988) has used the time lag model to correlate and interpret the extensive data taken by Davis (1981). Because the work is summarized in a paper given at this conference [Reardon (1988)], there is little to add here apart from noting the general approach and how it fits with other works.

The time lag model is unwieldy (at best) to use if combustion is allowed to be distributed and the time lag is variable. Hence as in many previous applications to liquid rockets, Reardon assumes that the energy release is concentrated in a transverse plane, that the parameters $(n,\ \tau)$ are constant, and that the flow field is one-dimensional. Then the combustion response is given by the part of equation (3.14) depending on frequency; to represent concentrated combustion, the average distribution $\bar{w}_l$ is replaced by δ-function. A modest change in the argument allows one to use this form for the unsteady conversion of liquid to vapor, or for unsteady energy release.

Reardon assumes that the oscillations observed by Davis are bulk modes in the combustor: the pressure is essentially uniform in space and pulsates in time. Hence the mode shape $\psi(\vec{r})$ is approximately constant and one may assume that the total unsteady energy release due to combustion processes in the chamber, E_c, is given by

$$\dot{E}_c = \dot{E}_0 n(1 - e^{-i\omega\tau})\frac{p'}{\bar{p}}$$

The rate of change of energy in the chamber is the net result of energy released by combustion and the rates at which energy is convected in and out of combustor:

$$\frac{dE}{dt} = \dot{E}_c + \dot{E}_{in} - \dot{E}_{out}$$

This relation is the basis for Reardon's treatment of the experimental results.

As we discussed in Section 4, in applications of the time lag model to instabilities in liquid rockets, both parameters $(n,\ \tau)$ were determined by matching a theoretical result to experimental results for the stability boundary. The idea then is that those values of $(n,\ \tau)$ can be used to predict the stability characteristics for new (but in some sense similar) designs. Here, Reardon has chosen to use values of n calculated by Crocco and Cheng (1956) and to compute the time lag independently, using previous results obtained by others. In short, Reardon essentially assumes that the combustion model is known (defined by the two parameters $(n,\ \tau)$ with concentrated combustion) and then uses the relation for the balance of energy in the chamber to correlate data.

Stability of oscillations may be determined by application of the Nyquist criterion after the unsteady energy balance is re-written by using the Laplace transform. This possibility arises because, as we have briefly described earlier, the problem of self-excited combustion instabilities can be interpreted as a linear system with a negative feedback loop. The stability criterion, expressed with the growth constant α, depends on other processes included in the energy balance. The formal result may therefore be used to test the importance of those processes by comparison with data.

Reardon has used this procedure to study the effects of several processes and geometrical parameters, with mixed results. It seems that this sort of approach suffers from the intrinsic limitation noted earlier: it is really only a method for correlating data and therefore in the first instance has little predictive value without assurance that the models used are accurate. Confidence in the results comes only from good correlations with data over broad ranges of parameters. The results to date do not seem to provide that confidence.

6. PASSIVE AND ACTIVE CONTROL OF COMBUSTION INSTABILITIES

There are two general strategies to follow in treating a combustion instability: change the design of the system to reduce the amplitudes of the self-excited oscillations, or introduce some form of control. When instabilities are encountered in a development program, significant design changes usually cannot be accepted. Moreover, even after nearly fifty years' experience with the general problem, it is often difficult to recommend effective modifications with great confidence. Since the earliest instances of serious instabilities, much effort has therefore been devoted to controlling the oscillations, generally by passive means.

Small solid propellant rockets produced during World War II posed serious problems of high frequency transverse modes. They were usually eliminated by incorporating 'resonance rods' extending along the axis of the chamber, or baffles, extending radially from the outer case. Perforated liners were evidently first used in about 1950 to reduce the amplitudes of screech oscillations in amplitudes of screech oscillations in afterburners [Lewis Laboratory Staff (1954)]. At about the same time, individual resonating cavities were first used in a small supersonic inlet to reduce shock oscillations ("buzz") [Fox (1951)]. During the 1960's, much was accomplished on the use of liners and damping cavities in liquid rocket engines, motivated chiefly by applications to the F-1 and lunar ascent engines of the Apollo program [Oberg (1971); Oberg and Kuhnle (1971)].

It is now standard practice to incorporate acoustic liners in the design of afterburners to attenuate screech oscillations. Baffles and resonating cavities, or liners are used in many liquid rockets, particularly larger engines. The way in which these devices work is quite well understood. Reasonably good designs can be produced if the mode shapes and frequencies of the troublesome oscillations are known, but in practice, successful applications always requires testing and modifications for reasons we shall explain below.

The two greatest disadvantages of passive devices are the space required to fit them in the combustion chamber, a constraint that limits their use in solid propellant rockets; and the added mass, which is effective only

over a fairly narrow frequency range. It is possible to design baffles for operation at low frequencies, but acoustic liners and resonators can be used only to treat high frequency oscillations because their linear dimensions increase as the frequency is reduced. Generally, the necessary sizes are too large for application at frequencies below, say, 500-1000 Hz in actual propulsion systems.

Greater difficulties with low-frequency combustion instabilities during the past few years has generated serious interest in active control. The idea is not new, dating at least back to a proposal by Tsien (1953) for servo-stabilization of low- frequency chugging modes. In sensors, instrumentation and microprocessors make active control an attractive possibility for treating combustion instabilities over broad ranges of frequency and operating conditions. Recent research on this subject has just begun and only a few results have been obtained.

6.1 Passive Control Devices

The design and operation of **baffles**, resonators and acoustic liners for liquid-fueled rockets have been thoroughly covered in two lengthy summaries: Chapter 8 of Harrje and Reardon (1972), and a report prepared largely by the group at Rocketdyne with the collaboration of other organizations [NASA Design Criteria Office (1974)]. In liquid rocket engines, baffles are mounted on the injector face along radii and extending some distance downstream. Figure 6.1 taken from Harrje and Reardon (1972, p. 428) shows the installation in the Lunar Module Ascent engine manufactured by Rocketdyne. The design also included slots around the periphery that acted as acoustic resonators. It has often been the practice to use both baffles and resonators or acoustic liners in liquid rocket engines. The liners may extend along the chamber wall to the nozzle entrance, an example of which is shown in Figure 6.2 [Mitchell (1965)]

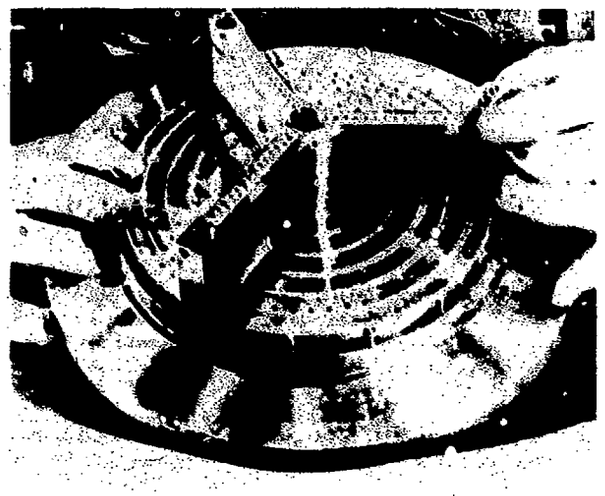


FIGURE 6.1

The number and orientation of baffles depends on the modes to be treated. Figure 6.3 taken from NASA Design Criteria Office (1974) shows the three most common cases encountered in practice. The idea is that the baffles are essentially rigid walls, changing the geometry locally and therefore allowing fewer modes than possible in the unobstructed chamber. For example, a single baffle extending over a diameter prevents traveling or spinning modes, Figure 6.3(a). If more baffles are added, as in Figure 6.3(b), a limited number of the lower modes are eliminated. Thus, if there are three radial baffles, the first and second tangential modes cannot exist, but the boundary conditions do allow the third tangential mode.

Because of performance losses and the practical problem of maintaining structure integrity, baffles can extend only part way along the axis of the chamber, so they cannot be totally effective. A measure of their operation is the rate at which a mode decays after excitation by injecting a pulse. Figure 6.4 [Oberg et al (1969)]. The time required for a mode to damp to 1/e of its initial value must obviously decrease as the length of baffle is increased in the axial direction.

In addition to discouraging the presence of some resonances - purely a geometrical effect - baffles also are sources of energy losses due to viscous effects. While skin friction may have some contribution, probably the largest effects are due to oscillating flow past edges and the associated formation of shear layers and vortex shedding.

Preventing certain modes is beneficial if the coupling between combustion process and the unsteady motions is primarily in the frequency range of those modes. Because the baffles are mounted on the injector, they may also affect the coupling directly by shielding the sensitive regions near the injector face from oscillating disturbances. Thus baffles are evidently effective both because they provide damping of unsteady motions and because they influence the processes tending to excite the motions.

In contrast to baffles, resonant acoustic cavities and acoustic liners have essentially no effects on energy transfer from combustion processes to the acoustic field. Their intended function is entirely to provide energy

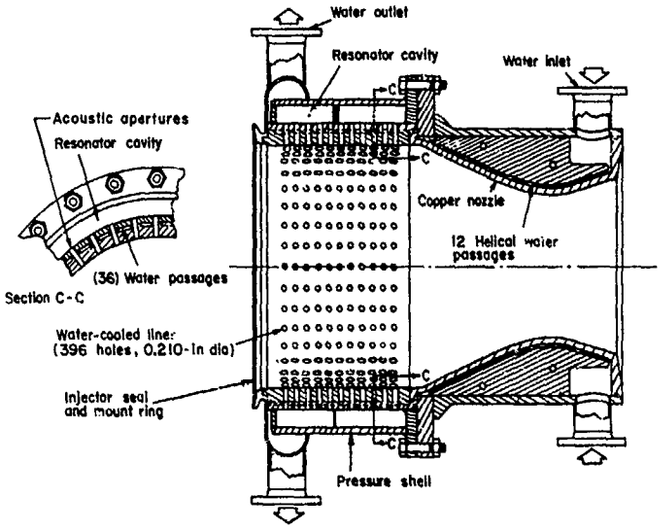
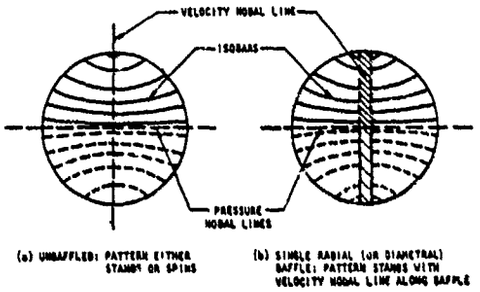
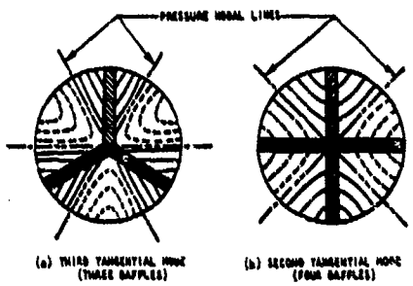


FIGURE 6.2



(a)



(b)

FIGURE 6.3

losses in the frequency range of instabilities. Their effectiveness depends on the local flow field induced by the unsteady field in the chamber, and in the consequent action of viscous forces to dampen the motions. The elementary cavity is the Helmholtz resonator, sketched in Figure 6.5. Its action can be visualized most simply as a mass/spring/dashpot system. The mass is the plug of gas in the orifice and the spring is provided by the compressibility of the gas in the volume of the chamber. Hence, one should expect that the natural frequency should decrease as the volume of the cavity increases(because a given displacement of the plug is a smaller fraction of the volume); and should also decrease as the mass of the plug increases. [frequency ~ (spring constant/mass)$^{\frac{1}{2}}$]. The formula for the resonant frequency is

$$\omega_r = \frac{a}{l_0}\sqrt{\frac{V_0}{V_c}} \tag{6.1}$$

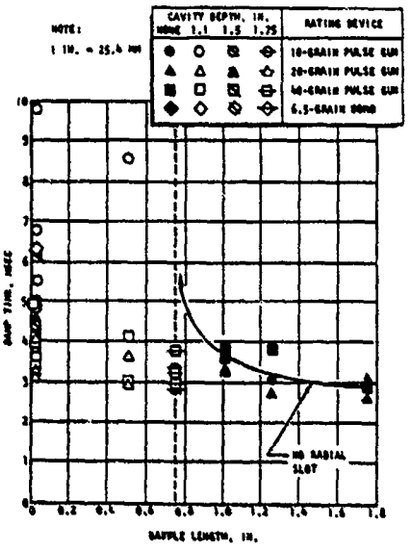


FIGURE 6.4

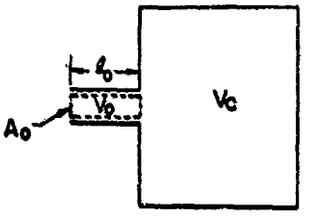


FIGURE 6.5

where l_0 is the length of the orifice, V_0 is its volume and V_c is the volume of the cavity. This formula is quite a good approximation to observed values providing the average temperature is everywhere the same, and if l_0 is assigned an approximate value. The length is really an effective length of the plug of gas, so in a sense, (6.1) really defines l_0. Theoretical estimates for l_0 may be found in several of the references cited, e.g. Harrje and Reardon (1972, p. 410).

Damping of the motions occurs primarily because of the motion of the plug of gas in the orifice. It is strongly a function of the amplitude of motions because of flow separation in the orifice [Ingaard and Labate (1950); Ingaard (1953); Sirignano et al (1967); Zinn (1969)].

Acoustic liners are essentially arrays of small acoustic resonators. Figure 6.6 [Harrje and Reardon (1972, p. 410) is a sketch of a typical configuration. Each
backing cavity has several orifices. Equation (6.1) is the basic formula for designing resonators and liners but clearly many compromises must be made in specific applications.

The design issues for liners are thoroughly discussed in the references. In addition to the obvious geometrical variables, we should mention that special consideration must be given to the effects of the amplitude of motion, mean flow past or into the orifices, and temperature variations. The influence of temperature is important because it determines the speed of sound and hence the resonant frequency. Tuning cavities and liners is therefore seriously affected by the temperatures of the gases in the orifices and cavities. That is a major reason why acoustic resonators have not been successfully used in solid propellant rockets. Because of the short firing times, resonators are almost always operating under changing conditions.

A practical limitation of resonators is the finite bandwidth: a given geometrical configuration effectively attenuates only over a relatively narrow band of frequencies. Figure 6.7 [Nestlerode and Oberg (1969)] shows the influence of changing geometry of a liner used in the Lance Booster engine.

Increasing the amplitude of motions tends to reduce the peak of the resonance curve for a liner, but broadens the bandwidth. Figure 6.8 [Blackman (1960)] shows data taken at room temperature for a small section of liner in an impedance tube. Agreement with calculations is fairly good (θ is essentially the real part of the admittance function for the liner.)

Calculation of the influences of resonators and acoustic liners have appeared in many publications [e.g. Oberg et al (1969, 1971, 1972); Baer and Mitchell (1974, 1977); Harrje and Reardon (1972, Chapter 8); and NASA Design Criteria Office (1974)]. Whatever the details of the computations, the results eventually come

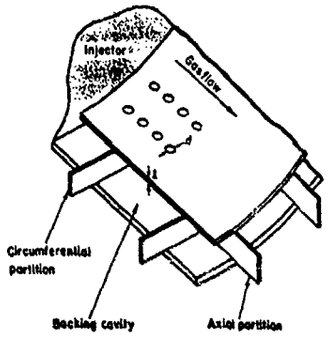


FIGURE 6.6

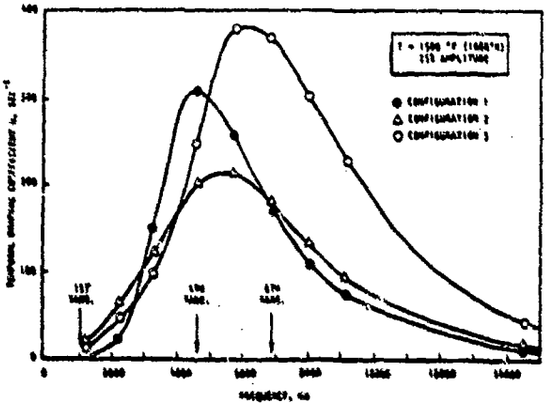
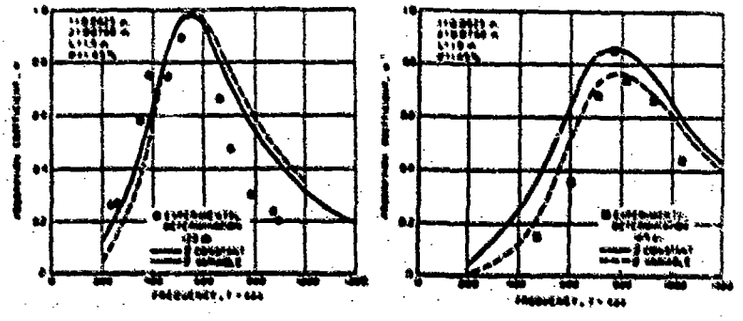


FIGURE 6.7



(a) (b)

FIGURE 6.8

down to a form of the last term in equation (7.79). Although it might appear that there are formal difficulties when the basic acoustic velocity is parallel to the surface, it can be shown that the same formula is valid (Cullick

(1973)]. Thus, assuming no average flow normal to the plane of the liner, the attenuation constant is

$$\alpha_{\text{liner}} = -\frac{\bar{a}}{2E_n^2}\iint A_l^{(r)}\psi_n^2 dS \tag{6.2}$$

where $A_l^{(r)}$ is the real part of the admittance function defined for a unit area of liner; that is, it is an average of the admittance function for the orifices and the solid surface. If the impermeable surface is rigid, $A_l = 0$, and (6.2) can be written

$$\alpha_{\text{liner}} = -\frac{\bar{a}}{2E_n^2}\left(\frac{S_0}{S_l}\right)\iint A_l^{(r)}\psi_n^2 dS \tag{6.3}$$

where S_0 is the total open area and S_l is the total area covered by the liner. Obviously the liner is more effective if placed where the mode shapes (i.e. pressure fluctuation) is largest. We emphasize that this result is strictly valid only for linear behavior; nonlinear behavior is accomodated by the approximate analysis given in Section 2, but no results are available.

In view of the widespead use of baffles and liners, perhaps the most remarkable liquid rocket engine design is that used for the Lunar Module Descent engine [Cherne (1967); Elverum et al (1967)]. Neither baffles nor liners nor any other damping device was required: the engine possessed very robust intrinsic stability over its entire range of throttling, from 1000.pounds to 10,000 pounds thrust. Moreover, the design has been scaled to 50,000 pounds and still exhibited complete stability in static tests (the large engine has never been flown).

The chief reason for the stability seems to be the feature that the propellants are injected through a single (large) coaxial element located in the axis of the combustion chamber. As a result, the distribution of energy release tends to be concentrated near the axis of the chamber where the tangential modes have pressure nodes and even the radial modes have smaller pressure anti-nodes than at the periphery. Refer to the first term representing the main source of excitation in equation (2.79) and consider only the unsteady energy addition,

$$\alpha_e \sim \int \psi_n \dot{Q}^{(r)} dV \tag{6.4}$$

The integral is reduced if the energy release $\dot{Q}$ is small where ψ_n is large, and vice-versa. Figure 6.9(a) taken from Elverum et al is a sketch of the situation for the first radial mode. As shown in Figure 6.9(b), the

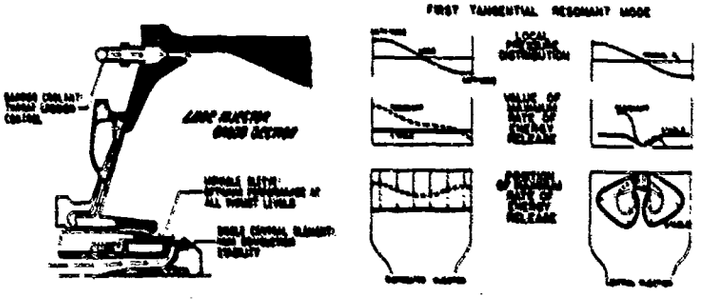


FIGURE 6.9

energy release has this distribution because fuel is injected axially along the periphery of the injector. Oxidizer is injected radially through 36 holes. Thus, the liquids impinge at the intersection of a sheet with 36 jets. As suggest in Figure 6.9(a), the axial momentum of the fuel sheet tends to bias the energy release in the axial direction, the oxidizer jets cause spreading also towards the chamber walls. Although the injector projecting into the chamber acts as a baffle against the radial modes, it can have little influence on the tangential modes. Hence one must conclude that the high level of stability in the absence of baffles and liners derives from the low value of the driving, equation (6.4). Yodis (1968) gave an interesting brief comparison of the stability characteristics of three engines in the Apollo vehicle.

6.2 Active Control of Combustion Instabilities

It is a fundamental property that combustion instabilities are self-excited oscillations. Their excitation occurs because the energy transferred from the combustion processes and mean flow to the unsteady motions depends on the unsteady motions themselves. That is why a small amplitude disturbance grows exponentially in time until a nonlinear process limits its amplitude, commonly producing a periodic limit cycle.

Prediction of instabilities in combustion chambers is difficult and is always accompanied by large uncertainties. Consequently, any strategy of design or correction must in practice rely heavily on experimental work, and on analysis providing a framework for basic understanding, interpretation of data and designing experiments.

The very nature of the instabilities, that they are self-excited, causes considerable trouble both for treating problems in propulsion systems and for laboratory experiments. Experimental work is time consuming and expensive, due to the difficulty of performing controlled and reproducible tests.

Passive measures, as described in the preceding section, were the earliest and continue to be the only practical means of treating combustion instabilities in operational propulsion systems. While often effective, they have the disadvantages noted above: there is no widely applicable theory for passive control; development is always a costly trial and error process; and the effectiveness of a particular design is inevitably limited to a relatively narrow range of frequency and operating conditions.

Active control is an attractive strategy for use in both practical and research problems. It is not a new idea and has appeared in several limited forms in the past 35 years. Tsien (1953) showed how the chugging instability in a liquid rocket motor could be stabilized by controlling the supply of liquid propellant. His proposal was based on the time lag model of the supply and combustion dynamics. As Figure 3.1 shows, the overall time lag in the system is composed of several contributions. Consequently, it is not necessary to affect only the combustion processes or the pump characteristics to alter the stability. Tsien's idea was to manipulate the propellant flow in the supply lines by controlling the capacitance, Figure 6.10.

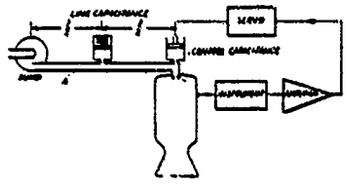


FIGURE 6.10

The theoretical basis is readily established by writing the equation for the chamber pressure, a result that can be obtained either by considering conservation of mass or energy, or by specializing the approximate analysis described in Section 2. Then we expect that pressure fluctuations will satisfy the equation for a damped oscillator, and if we include an excitation due to combustion with a time lag, the behavior is governed by

$$\ddot{p} + 2\alpha\dot{p} + \omega_0^2 p = \beta p(t-\tau) + u(t) \tag{6.5}$$

where $u(t)$ is an unspecified input control function. The damping coefficient is $\alpha > 0$, ω_0 is the resonant frequency of the chamber and β is a constant, something like the interaction index. Now take the Laplace transform, with s the transform variable and $P(s), V(s)$ denoting transforms of $p(t), u(t)$, to find

$$P(s)\left[s^2 + 2\alpha s + \omega_0^2\right] = \beta e^{-s\tau} P(s) + U(s) \tag{6.6}$$

This equation can be interpreted with the block diagram drawn in Figure 6.11.

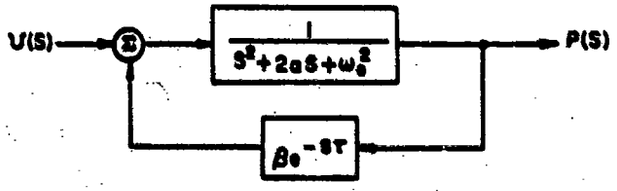


FIGURE 6.11

Equation (6.6) and the block diagram can be solved to give

$$P(s) = \frac{\beta e^{-s\tau} G}{1 + \beta e^{-s\tau} G} U(s) \tag{6.7}$$

where G denotes the transform function of the chamber (the "plant" in the terminology of control theory):

$$G(s) = \frac{1}{s^2 + 2\alpha s + \omega_0^2} \tag{6.8}$$

The solution (6.7) can be re-written as

$$\frac{P(s)}{U(s)} = \frac{\beta e^{-s\tau}}{s^2 + 2\alpha s + (\omega_0^2 + \beta e^{-s\tau})} \tag{6.9}$$

Stability of the system requires that the roots of the denominator have negative real parts.

For the case of a purely bulk mode or chugging, the term s^2 is missing from the denominator of $G(s)$. Tsien treated the problem of stability by applying the Nyquist criterion to the denominator of (6.9). For a system with time delay, the form due to Satche (1949) is required; see Tsien (1953, 1956). This method was applied by Marble and Cox (1953) and Marble (1955) to more complicated forms of the low frequency stability problem.

This example, progressing from formulation of wave motions in a chamber, as expressed by equation (6.5), to the block diagram in Figure 6.11 and the transfer function (6.9) for the closed loop system is the simplest illustration connecting combustion instabilities to control theory. There is no point pursuing details here, but this brief discussion should make appealing the application of modern control theory suggested below.

Application of "servo-stabilization" as proposed by Tsien may have been attempted in a laboratory somewhere, but it appears that no results have been published, and certainly this method has never been adopted in practice. The primary reasons seem to be inadequate sensors and instrumentation. That situation is very different now, with the recent developments in solid state devices and microprocessors. While practical applications may still be some time from realization, there is ample reason to pursue research on the problem, and indeed some interesting results have already been reported.

Short of the sort of intelligent control systems envisioned here, there have been several efforts in research programs to gain control over self-excited instabilities in order to obtain better data. A device invented at ONERA [Kuentzmann and Nadaut (1975)] used a rotating exhaust valve to modulate the flow and impose pressure oscillations on a burning solid propellant. The purpose was to provide a controllable means of measuring the frequency response of a burning surface. Subsequently the method was modified and used by several groups in the U.S. and England. Another technique for switching oscillations on and off involves a moveable baffle [described in the reference manual edited by Culick (1974)]. This technique has been used to produce several growth and decay periods of oscillations during a firing lasting less than one minute. Similar results have been obtained with a resonator, but with much greater difficulty because the temperature in the orifice and cavity changes rapidly during a test, causing great problems with tuning. All such methods are motivated by the need to gain some measure of control over unstable oscillations in laboratory tests. Here we are more concerned with techniques that have promise for application to full-scale propulsion systems.

Ffowcs-Williams (1984, 1986) has described his own successes and those of others in the use of active control to manipulate acoustic fields at normal temperatures and pressures by using acoustical interference. The essential idea — simply stated but not always easily realized in practice — is to determine the characteristics of the given acoustic field and use that information to control secondary sources of sound so as to produce desired results by interference. Most obviously a "desired result" is to reduce unwanted noise to silence—all parents' Holy Grail. Ffowcs-Williams calls "anti-sound" the acoustic field injected as the input to control the subject field.

In principle, the idea should be applicable to combustion systems, and some apparent examples have already been reported. The principle of interference will cover many situations, but not clearly in those just cited. When the primary sources of the acoustic waves are themselves sensitive to pressure and velocity disturbances - as the case is for all combustion instabilities - then interactions between the injected "control" field and the sources become a central issue. Consequently, although some authors may (possibly with justification) cite their results as examples of the application of "anti-sound," it seems that one might reasonably be skeptical.

Sreenivasan, Raghu and Chu (1985) demonstrated control of oscillations generated in a Rijke tube by introducing a secondary heater. The idea has been at least discussed for many years and likely tried informally; some earlier results were reported by Collyer and Ayres (1972) but not in the context of control. If the fluctuation q' has the proper phase and spacial distribution, then the contribution $\int \dot{q}^{(1)}\psi_n dV$ in α, equation (2.79), and the first term in (2.85) can be made negative, so disturbances are attenuated. In the Rijke tube, the control heater need not be oscillated by external means. If the source is placed in the upper half of the tube, the fluctuating heat addition arises from interactions with the velocity and automatically has the phase necessary to attenuate the waves. That is, the heat source in fact extracts energy from the field, on the average. Similar results were obtained by Sreenivasan it et al. with secondary heaters installed in an organ pipe and a "whistler-nozzle." The experiments are interesting and useful demonstrations but, if only because true external control is not exercised, application to propulsion systems seems a doubtful enterprise.

True active control of instabilities has been demonstrated in a series of works carried out at Cambridge University. Dines (1983) and Heckl (1985, 1986) injected acoustic waves with a loudspeaker placed near the end of the tube. The speaker was placed in a feedback loop allowing controllable gain and phase. Dines used a sensor to monitor the light emission as a measure of heat release. That information was processed to adjust the loop gain and phase. Heckl used the output of a microphone, sensing pressure fluctuations, as the signal in the feedback loop and showed that the instabilities could be suppressed over a broad range of phase. That result demonstrated that control of that combustion instability is not explained by the principle of "anti-sound," which requires a well-defined phase relation. Evidently the injected field had significant effects on the heat transferred to the oscillations.

More recently, Blaxidge et al (1987) have controlled instabilities in the laboratory burner described in Section 5.2 (Figure 5.9). Control was exerted with an oscillating plug inserted in the choked inlet nozzle. Technically this amounts to controlling the inlet mass flow: its average value is always zero but the amplitude and phase of the oscillations can be varied. Those oscillations generate pressure waves that serve the same

purpose as those produced by a loudspeaker (which itself actually appears as an oscillatory source of mass). The system was only partially successful in suppressing the instabilities, reducing the amplitude of the fundamental mode by somewhat more than half.

Lang et al (1987) and Poinsot et al (1988) have reported control of instabilities in a subsonic laboratory burner supplied with gaseous reactants. Two different flameholders have been used: a plate having 80 orifices, set in a stream of premixed gases; and a more realistic configuration comprising an array of three rearward facing steps through which fuel is injected into an air stream. In each case a microphone was used as sensor to excite loudspeakers placed upstream of the flames. Not only was suppression of the instabilities demonstrated, but in the most recent work, the authors have shown the great usefulness of control to study the transient behavior of the motions. Active control will no doubt be a useful tool in laboratory research.

Langhorne, Dowling, and Hooper (1988) have given an initial report of their results for a method which may well prove to be the most effective approach to controlling combustion instabilities in full-scale systems. Using the apparatus described in Sectin 52 [see Figure 5.9] they successfully reduced the amplitudes of an instability by introducing a controlled secondary supply of fuel upstream of the flameholder. That this is an attractive method follows from the discussion in the Introduction. Instabilities are encouraged in combustion chambers because of the high densities of energy release. The power involved cannot be matched by mechanical systems, such as loudspeakers, and response times as well may be inadequate. Evidentally the most direct method of control should be based on manipulating the source of energy. The work by Langhorne *et al.* is thoroughly discussed in a paper at this meeting.

In their work intended primarily for study the noise produced by convection of entropy fluctuations through a supersonic nozzle, Zuloski and Auerback (1976) demonstrated a form of control in a laboratory device. They produced entropy fluctuations by oscillating the temperature of a nichrome wire heater. The heat addition caused fluctuations of both temperature and pressure, the latter accompanying the unavoidable density fluctuations. With an oscillatory bleed valve, they were able to compensate the pressure fluctuations, leaving nearly pure temperature or entropy waves. Thus they demonstrated simultaneous control of mass and energy sources.

The approximate analysis developed in Section 2 has a form that is naturally adapted to applying the theory of control of distributed systems [Murray-Lasso (1966); Gould and Murray-Lasso (1966); Balas (1977; 1982)]. State-feedback control can be applied to distributed systems after decomposition of the general motion into modes, as accomplished in Section 2. The state of the system is then specified by the matrix of amplitudes η_n and amplitude velocities $\{\eta_1, \eta_2, \ldots; \dot\eta_1, \dot\eta_2, \ldots\}^T$. Yang, Sinha and Fung (1988) have first discussed the application of modal control to the problem of combustion instabilities and have given some preliminary results of a simulation. It appears that neither this nor any similar method has been tested on an actual combustion instability.

The basic ideas are easily explained, but successful application will require considerable further research. Simply incorporating some sort of feedback control is by no means a guarantee that the system can be stabilized — for example, a stable oscillator can be converted to an amplifier with the addition of feedback. In order to achieve success with active control of combustion instabilities, it is essential to have a thorough understanding of the system in question, particularly of the responsible mechanisms. There is no point here in speculating on possible control laws, or on the potential problems that may arise with use of modal control, but we can at least indicate why this appears to be a sensible strategy to pursue.

To control combustion instabilities means to exert external influence on the unsteady mass, momentum or energy in the chamber. Whatever physical means may be devised, the control inputs must theoretically appear as sources in the conservation equations (2.1) - (2.4) and in subsequent forms. Thus, in equations (2.18) - (2.20), we may add control inputs $W_c, \vec{F}_c$ and P_c on the right hand sides, their particular forms depending on the kind of control used.

In the examples treated above, Sreenivasan et al used control (limited) of an energy source; all others worked with a mass source, except in their most recent work, Langhorne *et al.* controle the energy source by modulating a secondary fuel supply. In order to give a complete analysis of their results, it would be necessary also to analyze the basic mechanisms of the instabilities, for they were clearly affected by the motions induced by the control inputs.

The control source terms add contributions to h and f, and the wave equation (2.31) with its boundary condition (2.33) become

$$\nabla^2 p' - \frac{1}{a^2}\frac{\partial^2 p'}{\partial t^2} = h + h_c \qquad \hat{n}\cdot\nabla p' = -f - f_c \qquad (6.10)a,b$$

Application of the expansion in the modes $q_n(t)\psi_n(\vec{r})$ proceeds as in Section 2.2, leading now, instead of (2.45), to the system of equations for the amplitudes:

$$\frac{d^2 q_n}{dt^2} + \omega_n^2 q_n = F_n + u_n(t) \qquad (6.11)$$

where $u_n(t)$ is the control input to the n^{th} mode:

$$u_n(t) = -\frac{\bar{a}^2}{\bar{\rho}E_n^2}\left\{\int h_c\psi_n dV + \oint f_c\psi_n dS\right\} \qquad (6.12)$$

If there is no linear or coupling between modes, the equations (2.53) and (2.55) a, b give the linear part of F_n as $-D_{nn}\dot{q}_n - E_{nn}q_n = 2\alpha_n\dot{q}_n + 2\omega_n\theta_n q_n$ and (6.11) is

$$\frac{d^2 q_n}{dt^2} - 2\alpha_n\omega_n\frac{dq_n}{dt} + (\omega_n^2 - 2\omega_n\theta_n)q_n = F_n^{NL} + u_n(t) \qquad (6.13)$$

where F_n^{NL} stands for the nonlinear part of the forcing function. If nonlinear behavior is ignored, each of the oscillator equations has the same form as (6.5) – it is trivial to incorporate a time lag model, and of course α_n here contains both energy sources and damping, for which the contributions are negative.

To incorporate feedback control, the state of the system must be sensed: that is, the unsteady pressure and its rate of change must be measured, say at S points, and the output signal is the matrix $\{y_1, y_2, \ldots, y_S\}$, where the s^{th} element is the signal measured at the position $\vec{r}_m$ in the chamber:

$$y_s^{(t)} = c_s \frac{p'(\vec{r}_s, t)}{\bar{p}} + d_s \frac{1}{\bar{p}} \frac{\partial p'(\vec{r}_s, t)}{\partial t} \tag{6.15}$$

Because the pressure field is represented by an expansion in modes, and in practice only a finite number, N, can be treated, (6.13)

$$y_s(t) = c_s \sum_{n=1}^{N} \eta_n(t) \psi_n(\vec{r}_s) + d_s \sum_{n=1}^{N} \dot{\eta}(t) \psi_n(\vec{r}_s) \tag{6.16}$$

In matrix form, the sensor output is

$$\{y\} = [C] \begin{Bmatrix} \eta \\ \dot{\eta} \end{Bmatrix} \tag{6.16}$$

where C is an $S \times 2N$ matrix.

The control input (6.12) is due to a finite number of actuators; in the earlier examples, heaters or loudspeakers were used. Their presence can be represented in h_c and f_c, so $U_n(t)$ can be made explicit, except that the amplitudes for the actuator motions depend on the control law chosen. In practical systems, it is hardly likely that simple heaters or loudspeakers will be effective in combating combustion instabilities. The fast response necessary, and the energy requirements, probably will dictate either active control of the fuel supply, or some other method of directly affecting the mechanism of the instability.

Whatever the form of physical control chosen, the control matrix $\{u\}$ can be computed according to equation (6.12). In general, all actuators will affect all modes, and all $u_n(t)$ are non-zero. Yang *et al.* outlined the use of this formulism as the basis for a digital control system using a zero-order-hold technique. Their analysis is entirely formal, with a simulation to confirm their proposal. Neither they nor anyone else have attacked the far more difficult problems of applying these ideas to suppress combustion instabilities in a full-scale system. It's an area of research that holds much promise for productive results in the near future, a possible solution to the problem of combustion instabilities whose time has arrived.

7. Concluding Remarks

The operating conditions in high performance combustion chambers are such that there will always be high probabilities for disturbances to be unstable. Experience during the past four decades has clearly shown that one must expect a new design always exhibit instabilities. While research has established the principles for constructing stable combustion chambers, in practice the requirements may be poorly understood or violated in efforts to improve steady-state performance.

It is therefore essential that continuing work on these problems be directed to deeper understanding of the mechanisms of combustion instabilities; constructing more powerful and widely applicable analysis; and development of new methods for suppressing instabilities when they arise in full-scale systems. Recent progress in sensors, instrumentation and computing resources offer significant new opportunities.

Understanding mechanisms requires extensive and careful laboratory experiments as well as thorough analysis of instabilities in full-scale systems. Three dominant mechanisms have been emphasized here: liquid droplet formation, vaporization and combustion; vortex shedding and combustion; and convective waves. For many years, mechanisms have been interpreted with a time lag model. This representation of the coupling between gasdynamics and unsteady mass and energy release has been successfully used in both research and design. However, as emphasized in Section 3.1, the use of the two parameters n, the interaction index, and τ, the time lag, is not to be confused with understanding what is really happening. Global correlations of data without firm basis on fundamental processes have limited predictive value and ranges of application.

With the development of higher performance propulsion systems, the most effective strategy (and cheapest in the long run) to treat combustion instabilities must be founded on research devoted to basic problems. It seems clear that for all three types of liquid-fueled systems, it is essential first to understand thoroughly the steady and unsteady processes leading from injected liquid to combustion of gaseous reactants. Already much has been learned in recent research on these subjects that has not been incorporated in studies of combustion instabilities. Much remains to be done, but the main point is that it should no longer be necessary to rely so heavily on vague applications of the $n - \tau$ model. Modern experimental methods, including high speed non-intrusive measurements and flow visualization, provide wide opportunities for obtaining closer definition of the processes.

The recent work on vortex shedding and combustion in dump combustors is an indication of the possibilities. In addition to tests on realistic configurations, related laboratory tests and detailed numerical analysis have provided the beginnings for understanding the basic processes involved. The research is certainly not complete, and satisfactory connections with design yet to be made, but the direction of progress is correct. Work on this subject and on the processes of spray formation and combustion should be directly applicable to thrust augmentors as well.

Analysis of the complete problem in combustors serves as a global framework important to both research and design. It is essential that proposed mechanisms be checked thoroughly with all relevant processes accounted

for; failure to do so will quite likely produce incorrect and misleading results as discussed in Section 3.2. Modern computing resources are now capable of handling full three-dimensional problems and the time has arrived for serious application of computational fluid dynamics to problems of combustion instabilties.

Such calculations are expensive and will not in the forseeable future be useful for routine design work. Moreover, it will likely always be true that significant uncertainties will accompany some of the necessary input information, especially for the unsteady combustion processes. And of course there is always the feature that each numerical calculation provides results only for one case.

Nevertheless, numerical analysis is important for several purposes. As for the external aerodynamics of a missile or aircraft, CFD can be used in the design process. However, the corresponding application to combustion instabilities must await further progress in understanding the fundamental processes in a combustion chamber.

Recent work on the flow fields in dump combustors, and similar calculations for solid fueled rockets, have demonstrated that much can be learned even at this stage. Equally important, although incomplete and limited, the analyses serve as necessary steps in continued development of analytical tools.

For most applications and theoretical work, approximate analysis in one form or other will probably always be the primary method of doing calculations. One framework has been described here in Section 2; its usefulness has been illustrated in several places. It affords a rapid and simple way of assessing mechanisms and predicting trends of behavior; and in combination with test results, it provides guidelines for design.

An important step that has yet to be taken is close coordination of approximate and numerical analyses. Because of the assumptions required to simplify the equations, any approximate analysis is always accompanied by uncertainties in the results that are not completely known. The only way to assess accuracy is to compare approximate results with those obtained by an accurate numerical analysis. Limited comparisons of this sort have been done for instabilities in solid rockets, showing that the approximate analysis is accurate under broad useful conditions and can also be helpful in understanding unexpected numerical results.

Nonlinear behavior of combustion instabilities is an important topic not covered in this survey. Because combustion instabilities are self-excited oscillations, they reach limiting amplitudes only because one or more nonlinear processes are active. There are two classes of nonlinear problems to be considered theoretically: 1) what are the conditions for existence and stability of limit cycles?; and 2) under what conditions is a linearly stable system unstable to a sufficiently large initial disturbance? These problems have received some attention, chiefly with approximate analysis, but much remains to be learned. The subject of nonlinear behavior is fascinating theoretically, and already some results useful in practical situations have been obtained.

It appears that the confluence of modern experimental and analytical research will provide the basis for applying methods of active control to problems of combustion instabilities. The possibility is attractive, and may seem almost obvious, but practical realization is far off. Initial results obtained in laboratory tests with and without combustion have illustrated the premise. However, the differences between the conditions in these devices and in full-scale propulsion systems must be recognized. Successful applications will surely require thorough understanding of the mechanisms causing instabilities in the actual systems; results will be required of all the subjects covered in this review.

Acknowledgments

During preparation of this paper I have benefitted from numerous conversations (and arguments) with my colleagues Professors Marble and Zukoski.

This work has been supported partly by the California Institute of Technology; by the Office of Naval Research; by the Air Force Office of Scientific Research; by the Naval Weapons Center under a Personal Services Contract; and by Hersh Acoustical Engineering under contract to the Air Force Astronautics Laboratory. I am indebted to Mmes. Cynde Herman, Jan Patterson, Elizabeth Wood, and Dana Young for all the extraordinary help they gave me in the typing and preparation of this manuscript.

REFERENCES

Liquid Rocket Motors

Ashurswurd, B. (1972) "The Missile Liquid Rocket Propulsion Unit VR35 and Some of Its Development Problems," AIAA/SAE 8th Joint Propulsion Specialist Conference, AIAA Paper No. 72-1102.

Artamunov, K.I. (1963) "Stability of Liquid Fuel Rocket Engine Operation," *AIAA J.*, Vol. 1, No. 1, pp. 263-266.

Bairamov, F.D. (1978) "On Stability of Operation of Liquid Rocket Engine (LRE) with Turbopump Assembly (TPA), *Soviet Aeronautics*, Vol. 21, pp. 10-15.

Barrère, M. and Williams, F.A. (1969) "Comparison of Combustion Instabilities Found in Various Types of Combustion Chambers," International Symposium on Combustion.

Barrére, M. (1976) "Analysis of Rocket Engine Transient Regimes," XXVII Congress, International Astronautical Federation, Paper IAF-76-160.

Bastress, E.K., Harris, G.H. and Miller, I. (1967) "Statistical Derivation of Design Criteria for Liquid Rocket Combustion Instability," NASA CR-72370.

Beltran, M.P., Wright, R.O. and Breen, B.P. (1966) "Combustion Stability Limits Calculated Utilizing a Non-linear Model," Dynamic Science Report No. SN-70-F, Final Report in Contract NAS 7-366.

Bénoit, A., Collin, G. and Mestie, A. (1974) "Etude de la stabilitde la combustion dans un foyer à flux giratoire," *La Recherche Aérospatiale*, No. 1 (Janvier-Février), pp. 37 à 48.

Bracco, F.V. (1975) "Standing Acoustic Waves in a confined Non-Uniform Gas," *J. Sound and Vibration*, Vol. 41, No. 3, pp. 301-309.

Burstein, S.A., Chinitz, W. and Schechter, H.S. (1972) "A Nonlinear Model of Combustion Instability in Liquid Propellant Rocket Engines," AIAA/SAE 8th Joint Propulsion Specialist Conference, AIAA Paper No. 72-1146.

Callender, A., Hartree, D.R. and Porter, A. (1938) "Time Lag in a Control System," *Trans. Roy. Soc. London*, Vol. A235, pp. 415-444.

Cherne, J.M. (1967) "Mechanical Design of the Lunar Module Descent Engine," XVIII International Astronautical Congress, IAF.

Chu, B.-T. (1953) "On the Generation of Pressure Waves at a Plane Flame," *Fourth Int. Symp. on Comb.*, pp. 603-612.

Chu, B.-T. and Kovasznay, L.S.G. (1957) "Non-linear Interactions in a Viscous Heat-Conducting Compressible Gas," *J. Fluid Mech.*, Vol. 3, No. 5, pp. 494-512.

Clayton, R.M., Rogers, R.S. and Sotter, J.G. (1968) "An Experimental Description of Destructive Liquid Rocket Resonant Combustion," *AIAA Journal*, Vol. 6, No. 7, pp. 1252-1259.

Crocco, L. (1952) "Aspects of Combustion Instability in Liquid Propellant Rockets," JARS Part I, Vol. 21, No. 1951, Part II, Vol. 22.

Crocco, L. (1953) "Supercritical Gas Discharge with High Frequency Oscillations," *Aerotecnica*, Vol. 33, pp. 46-53.

Crocco, L. (1956) "Considerations on the Problem of Scaling Rocket Motors," AGARD Selected Combustion Problems, Vol. 2, Butterworths Scientific Publications, London, pp. 457-468.

Crocco, L. and Cheng, S.I. (1956) *Theory of Combustion Instability in Liquid Propellant Rocket Motors*. AGARDOGRAPH, No. 8, Butterworths Scientific Publications, London.

Crocco, L. (1958) "Comments on the Zucrow-Osborn Paper on Combustion Oscillations," Jet Propulsion, Vol. 28, No. 12, p. 843.

Crocco, L., Grey, J. and Harrje, D.T. (1960) "Theory of Liquid Propellant Rocket Combustion Instability and Its Experimental Verification," ARS J., Vol. 30, No. 2, pp. 159-168.

Crocco, L., Monti, R. and Grey, J. (1961) "Verification of Nozzle Admittance Theory by Exact Measurement of the Admittance Parameter," ARS J., Vol. 31, No. 6, pp. 771-775.

Crocco, L., Harrje, D.T. and Reardon, F.H. (1962) "Transverse Combustion Instability in Liquid Propellant Rocket Motors," ARS J. Vol. 32, No. 3, pp. 366-373.

Crocco, L. (1965) "Theoretical Studies on Liquid-Propellant Rocket Instability," *Tenth Symposium (International) on Combustion*, The Combustion Institute, pp. 1101-1128.

Crocco, L., Grey, J. and Matthews, G.B. (1963) "Preliminary Measurement of the Combustion Time Lag in a Monopropellant Rocket Motor," Fifth Symposium (International) on Combustion, Reinhold.

Crocco, L. (1966) "The Relevance of a Characteristic Time in Combustion Instability," 2nd ICRPG Combustion Conference.

Crocco, L. and Sirignano, W.A. (1966) "Effects of the Transverse Velocity Component on the Nonlinear Behavior of Short Nozzles," AIAA J., Vol. 4, No. 8, pp. 1428-1430.

Crocco, L., Harrje, D.T., Sirignano, W.A. et al (1967) "Nonlinear Aspects of Combustion Instability in Liquid Propellant Rocket Motors," NASA CR 72270.

Crocco, L., Harrje, D.T., Sirignano, W.A. et al (1968) "Nonlinear Aspects of Combustion Instability in Liquid Propellant Rocket Motors," NASA CR 72426.

Crocco, L. and Mitchell, C.E. (1969) "Nonlinear Periodic Oscillations in Rocket Motors with Distributed Combustion," *Combustion Science and Technology*, Vol. 1, pp. 147-169.

Culick, F.E.C. (1963) "High Frequency Oscillations in Liquid Rockets," *AIAA J.*, Vol. 1, NO. 5, pp. 1097-1104.

Culick, F.E.C. (1971) "Nonlinear Growth and Limiting Amplitude of Acoustic Oscillations in Combustion Chambers," *Combustion Science and Technology*, Vol. 3, pp. 1-16.

Culick, F.E.C. (1975) "Stability of Three-Dimensional Motions in a Combustion Chamber," *Combustion Science and Technology*, Vol. 10, pp. 109-124.

Culick, F.E.C. (1976) "Nonlinear Behavior of Acoustic Waves in Combustion Chambers," Parts I and II, *Acta Astronautica*, Vol. 3, pp. 714-757.

Dipprey, D.F. (1972) "Liquid Propellant Rockets," in *Chemistry in Space Research* (R.F. Landel and A. Rembaum, Ed.), American Elsevier Publishing, Inc.

Dombrowski, N. and Hooper, P.C. (1964) "A Study of the Sprays Formed by Impinging Jets in Laminar and Turbulant Flows," *J. Fluid Mech.*, Vol. 18, pp. 392-406.

Dordain, J.J., Lourme, D. and Estoueig, C. (1974) "Etude de l'Effet POGO sur les Lanceurs EUROPA II et DIAMANT B," *Acta Astronautica*, Vol. 1, pp. 1357-1384.

Elverum, G., Jr., Staudhammer, P., Miller, J., Hoffman, A. and Rockow, R. (1967) "The Descent Engine for the Lunar Module," AIAA 3rd Propulsion Joint Specialist Conference, AIAA Paper No. 67-521.

Epstein, P.S. and Carhart, P.R. (1953) "The Absorption of Sound in Suspensions and Emulsions. I. Water Fog in Air," *J. Acoust. Soc. Am.*, Vol. 25, pp. 553-565.

Fang, J.J. (1984) "Application of Combustion Time-Lag Theory to Combustion Stability Analysis of Liquid and Gaseous Propellant Rocket Engines," AIAA 22nd Aerospace Sciences Meeting, AIAA Paper No. 84-0510.

Fang, J.J. (1987) "Combustion Instability Model Study," Phase I Repoort (September 1986 - October 1987) Contract NAS 8-36274, NASA Marshall Space Flight Center.

Fang, J.J. and Jones, Y.T. (1984) "Comparison of Analytical Modeling Results with O_2/H_2 Combustion Stability Data," 21st JANNAF Combustion Meeting.

Fang, J.J. and Jones, Y.T. (1987) "Development of a Generic Combustion Stability Code for Liquid Propellant Rocket Engines," 24th JANNAF Combustion Meeting.

Feiler, C.E. and Heidmann, M.F. (1967) "Dynamic Response of Gaseous-Hydrogen Flow System and its Application to High Frequency Combustion Instability," NASA TN D-4040.

Filimonov, V.I. (1968) "Investigation of Instability of Combustion of Liquid-Propellant Rocket Motors," *Soviet Applied Mechanics*, Vol. 4, No. 9, pp. 80-81.

Flandro, G.A. (1964) "Roll Torque and Normal Force Generation in Acoustically Unstable Rocket Motors," *AIAA J.*, Vol. 2, No. 7, pp. 1303-1306.

Flandro, G.A. (1967) "Rotating Flows in Acoustically Unstable Rocket Motors," Ph.D. Thesis, California Institute of Technology.

Fontaine, R.J., Levine, R.S. and Combs, L.P. (1968) "Secondary Non Destructive Instability in Medium Size Liquid Fuel Rocket Engines," Chapter 3, AGARD Conference Proceedings, *Advances in Tactical Rocket Propulsion*.

Ganichev, A.I. (1984) "Influence of Liquid Rocket Engine Hot Wall Compliance on Low-Frequency Instability," *Soviet Aeronautics*, Vol. 27, pp. 24-28.

Gunder, D.F. and Friant, D.R. (1950) "Stability of Flow in a Rocket Motor," *J. App. Mech.*, Vol. 17, No. 3, pp. 327-333.

Habiballah, M. and Menin, H. (1984) "Two-dimensional Model for the Two Phase Flow Simulation in a Viking Rocket Engine Combustion Chamber," 9th International Conference on Numerical Methods in Fluid Dynamics, SACLAY.

Habiballah, M. Maraffa, L. and Menin, H. (1985) "Numerical Simulation of High Frequencies Instabilities in a Liquid Propellant Engine Through a Combustion Pressure Coupling," 10th International Colloquium on Dynamics of Explosions and Reactive Systems, Berkeley.

Habiballah, M., Lourme, D. and Pit, F. (1988) "A Comprehensive Model for Combustion Stability Studies Applied to the Ariane Viking Engine," AIAA 26th Aerospace Sciences Meeting, Reno.

Hardesty, D.R. (1970) "Unsteady Combustion in Gaseous Propellant Rocket Motors," Princeton University Department of Aerospace and Mechanical Sciences, Report T-963.

Hartje, D.J. and Reardon, F.H. (Ed.) (1972) *Liquid Propellant Rocket Instability*, NASA SP-194.

Heiser, R.J. (1966) "Review of Combustion Stability Development with Storable Propellants," *J. Spacecraft*, Vol. 3, No. 7, pp. 1046-1051.

Heidmann, M.F. and Feiler, C.E. (1960) "Evaluation of Tangential Velocity Effects on Spinning Transverse Combustion Instability," NASA TN D-3406.

Heidmann, M.F. and Wieber, P.R. (1966a) "Analysis of n-Heptane Vaporization in Unstable Combustor With Traveling Transverse Oscillations," NASA TN D-3424.

Heidmann, M.F. and Wieber, P.R. (1966b) "Analysis of Frequency Response Characteristics of Propellant Vaporization," NASA TN D-3749.

Hoehn, F.W. (1972) "Experimental Evaluation of a 600 LBF Spacecraft Rocket Engine," AIAA/SAE 8th Joint Propulsion Specialist Conference, AIAA Paper No. 72-1129.

Hoffman, R.J., Wright, R.O. and Breen, B.P. (1968) "Combustion Instability Prediction Using a Bipropellant Vaproization Model," NASA CR-920.

Jensen, R.J., Dodson, H. and Trueblood, B. (1988) "Oxygen/Methane Combustion Stability Investigation," Advanced Earth-to-Orbit Technology Conference, Huntsville, AL (May 1988).

Kovasznay, L.S.G. (1953) "Turbulance in Supersonic Flow," *J. Aero. Sci.*, Vol. 20, pp. 657-682.

Krylov, N. and Bogoliubov, N. (1947) *Introduction to Nonlinear Mechanics*, Princeton University Press.

Landau, L.D. and Lifschitz, E.M. (1959) *Fluid Mechanics*, Addison-Wesley Publishing Co.

Lecourt, R., Fouceud, R. and Keuntzmann, P. (1986) "Experimental Study of the Acoustical Sensitivity of Liquid Fuel Rocket Motors Injectors," *La Recherche Aerospatiale* (English edition), pp. 11-22.

Lecourt, R. and Foucaud, R. (1987) "Experiments on Stability of Liquid Propellant Rocket Motors," AIAA Paper No. 87-1772, AIAA/SAE/ASME/ASEE 23rd Joint Propulsion Conference, San Diego, California.

Levine, R.S. (1965) "Experimental Status of High Frequency Liquid Rocket Combustion Instability," *Tenth Symposium (International) on Combustion*, The Combustion Institute, pp. 1083-1099.

Liang, P.-Y., Fisher, S. and Chang, Y.M. (1986) "Comprehensive Modeling of a Liquid Rocket Combustion Chamber," *J. Propulsion*, Vol. 2, No. 2, pp. 97-104.

Liang, P.-Y., Charakhani, A. and Jensen, R. (1987) "A Finite Difference Analysis of Wave Damping and Acoustic Cavities," 24th JANNAF Combustion Meeting.

Liang, P.-Y., Fisher, S. and Chang, Y.M. (1987) "Numerical Analysis of SSME Preburner Injector Atomization and Combustion Processes," *J. Propulsion*, Vol. 3, No. 6, pp. 508-513.

Liang, P.-Y. and Schumann, M.D. (1987) "A Numerical Investigation of the Flame-Holding Mechanism Downstream of a Coaxial Injection Element," 24th JANNAF Combustion Meeting.

Lores, E.M. and Zinn, B.T. (1972) "The Prediction of Nonlinear Longitudinal Combustion Instability in Liquid Propellant Rockets," NASA CR 12094.

Lores, E.M. and Zinn, B.T. (1973) "Nonlinear Longitudinal Combustion Instability in Rocket Motors," *Combustion Science and Technology*, Vol. 7, pp. 245-256.

Lourme, D. and Schmitt, D. (1983) "Les moyens nécessaires à l'étude fondamentale des instabilités de combustion d'une moteur biliquide," IAF Paper NO. 82-304, 33rd IAF Congress, Paris, 1982, and Astronautica Acta, Vol. 10, No. 12, pp. 761-775.

Lourme, D., Schmitt, D. and Brault, F. (1984) "Experimental Characterization of the Spray Originating from an Impinging-Jet Injector in a Liquid Rocket Engine," *Acta Astronautica*, Vol. 11, pp. 469-482.

Lourme, D., Schmitt, D. and Brault, F. (1985) "Experimental Characterization of a Spray Formed by Two Impinging Jets in Liquid Rocket Injector," 3rd International Conference on Liquid Atomization and Spray Systems (ICLASS), London.

Lourme, D. (1986) "Like-on-like Injector Spray Characterization for the Ariane Viking Engine," AIAA Paper No. 86-1444, AIAA/SAE/ASME 22nd Joint Propulsion Conference, Huntsville, Alabama.

Male, T., Kerslake, W.P. and Tischler, A.O. (1954) "Photographic Study of Rotary Screaming and Other Oscillations in a Rocket Engine," NACA RM E54A29.

Marble, F.E. (1969) "Some Gasdynamic Problems in the Flow of Condensing Vapors," *Astronautica Acta*, Vol. 14, pp. 585-614.

Marble, F.E. (1970) "The Dynamics of Dusty Gases," *Annual Reviews of Fluid Mechanics*, Vol. 2, pp. 397-446.

Marble, F.E. and Wooten, D.C. (1970) "Sound Attenuation in a Condensing Vapor," *Physics of Fluids*, Vol. 13, pp. 2657-2664.

Marble, F.E. (1973) "Acoustic Disturbance From Gas Non-Uniformities Convecting Through a Nozzle," *Symposium on Transportation Noise, Stanford University*, Vol. 1.

Masden, S.H. and Moore, F.K. (1956) "On Strong Transverse Waves Without Shocks in a Circular Cylinder," *J. Aero Sci.*, Vol. 23, pp. 583-593.

Mikolowsky, W.T. (1968) "Three-Dimensional Combustion Instability in Liquid Propellant Rocket Engines: Parametric Study," *AIAA Student Journal*, Vol. 7, pp. 179-184.

Minorsky, N. (1942) "Self-Excited Oscillations in Dynamical Systems Possessing Retarded Actions," *Transactions ASME, J. App. Mech.*, pp. A65-A71.

Mitchell, C.E. (1969) "Stability Limits for a Liquid Rocket Engine Using a Droplet Vaporization Model," AIAA 5th Joint Propulsion Specialist Conference, AIAA Paper No. 69-483.

Mitchell, C.E., Crocco, L. and Sirignano, W.A. (1969) "Nonlinear Longitudinal Instability in Rocket Motors with Concentrated Combustion," *Combustion Science and Technology*, Vol. 1, pp. 35-64.

Mitchell, C.E. (1970) "The Effect of Entropy Waves on High Frequency Pressure Oscillations in Liquid Rocket Motors," *Combustion Science and Technology*, Vol. 1, pp. 269-275.

Mitchell, C.E. and Jotiben, Y. (1976) "Wave Distortion Effects on Vaporization Limited Combustion Stability," 13th JANNAF Combustion Meeting.

Mitchell, C.E. and Eckert, K. (1979) "A Simplified Computer Program for the Prediction of the Linear Stability Behavior of Liquid Propellant Combustors," NASA CR 3169.

Mitchell, C.E. (1984) "An Integral Closed Loop Combustion Stability Model - Status and Review," 21st JANNAF Combustion Meeting.

Mitchell, C.E. (1985) "Improvement of and Integral Stability Model," 22nd JANNAF Combustion Meeting.

Morse, P. and Ingard, L. (1968) *Theoretical Acoustics*, McGraw-Hill, Inc.

Muss, J.A. and Pe'per, J.L. (1987) "Performance and Stability Characterization of LOX/ Hydrocarbon Injectors," 1987 JANNAF Propulsion Conference.

Muss, J.A. and Peiper, J.L. (1988) "Performance and Stability Characterization of LOX/ Hydrocarbon Injectors," AIAA/SAE/ASME/ASEE 24th Joint Propulsion Specialist Conference.

Nguyen, T.V. and Muss, J.A. (1987) "Modification of the Agosta-Hammer Vaporization Response Model for the Prediction of High Frequency Combustion Stability," 24th JANNAF Combustion Meeting.

Nguyen, T.V. (1988) "An Improved High-Frequency Combustion Stability Model," AIAA/ASME/SAE/ASEE 24th Joint Propulsion Conference, AIAA Paper No. 88-2853.

Nickerson, G. and Nguyen, T.K. (1984a) "A Computer Program for Modeling Steady-State Combustion in a Rocket Engine Thrust Chamber," Software and Engineering Associates, Inc.

Nickerson, G. and Nguyen, T.K. (1984b) "A Computer Program for Prediction of Combustion Instability Using a Nonlinear Bipropellant Vaporization Model," Software and Engineering Associates, Inc.

Perry, E.H. and Culick, F.E.C. (1974) "Measurement of Wall Heat Transfer in the Presence of Large Amplitude Combustion - Driven Oscillations," *Combustion Science and Technology*, Vol. 9, pp. 49-53.

Philippart, K.D. (1987) "Stability Characteristics and Analysis of Liquid Oxygen/Methane Injectors," 24th JANNAF Combustion Meeting.

Philippart, K.D. and Moser, M.D. (1988) "Stability Analysis of Liquid Oxygen/Methane Injectors Using Currently Available Analytical Tools," AIAA/ASME/SAE/ASEE 24th Joint Propulsion Conference, AIAA Paper No. 88-2851.

Pieper, J.L. and Fang, J.J. (1986) "Combustion Characterization Methodology for LOX/ Hydrocarbon Engines," 1986 JANNAF Propulsion Conference.

Powell, E.A. and Zinn, B.T. (1971) "A Single Mode Approximation in the Solution of Nonlinear Combustion Instability Problems," *Combustion Science and Technology*, Vol. 3, pp. 121-132.

Powell, E.A. and Zinn, B.T. (1974) "Theoretical Investigation of Nonlinear Three-Dimensional Instabilities in Liquid Rockets with Real Nozzles," *Acta Astronautica*, Vol. 1, pp. 1051-1073.

Priem, R.J. and Heidmann, M.F. (1960) "Propellant Vaporization as a Design Criterion for Rocket-Engine Combustion Chambers," NASA Technical Report R-67.

Priem, R.J. and Guentert, D.C. (1962) "Combustion Instability Limits Determined by a Nonlinear Theory and a One-Dimensional Model," NASA TN D-1409.

Priem, R.J. and Rice, E.J. (1963) "Combustion Instability with Finite Mach Number Flow and Acoustic Liners," NASA TMX 52412.

Priem, R.J. and Breisacher, K.J. (1988) "Combustion Instability Coupling with Feed System Acoustics," Earth-to-Orbit Technology Conference, Huntsville, AL (May, 1988).

Ranz, W.E. and Marshall, W.R., Jr. (1952) "Evaporation from Drops, Part I," *Chem. Eng. Prog.*, Vol. 48, No. 3, pp. 141-146.

Razumeyenkh, B.V. (1963) *Vibrational Combustion*, Air Force Systems Command, Foreign Technology Division, Report FTD-TT-63-942.

Lord Rayleigh (1878) "The Explanation of Certain Acoustic Phenomena," *Royal Institution Proceedings*, Vol. VIII, pp. 536-542.

Lord Rayleigh (1945) *The Theory of Sound*, Dover Publications, New York.

Reardon, F.H., Crocco, L. and Harrje, D.T. (1964) "Velocity Effects in Transverse Mode Liquid Propellant Rocket Combustion Instability," *AIAA J.*, Vol. 2, pp. 1631-1641.

Reardon, F.H., McBride, J.M. and Smith, A.J., Jr. (1966) "Effect of Injection Distribution on Combustion Stability," *AIAA J.*, Vol. 4, No. 3, pp. 506-512.

Reardon, F.H. (1973) "Guidelines for Combustion Stability Specifications and Verification Procedures," J.P.J.A. Publication 247, NASA CR 136745.

Reichel, R.H., Hague, D.S., Jones, R.T. and Glatt, C.R. (1973) "Program User's Manual for Optimizing the Design of a Liquid or Gaseous Propellant Rocket Engine with the Automated Combustor Design Code AUTOCOM," NASA CR-2293.

Reichel, R.H., Hague, D.S., Jones, R.T. and Glatt, C.R. (1974) "System Oriented Design Optimization for Liquid Propellant Rocket Engines," *Raumfahrtforschung*, Vol. 1/1974, pp. 16-24.

Rubin, S. (1966) "Longitudinal Instability of Liquid Rockets Due to Propulsion Feedback (POGO)," *AIAA J. Spacecraft*, Vol. 3, No. 8, pp. 1188-1195.

Rubin, S., Wagner, R.G. and Payne, J.C. (1973) POGO Suppression on Space Shuttle - Early Studies," NASA CR-2210.

Rupe, J.H. (1967) "An Experimental Correlation of the Nonreactive Properties of Injection Schemes and Combustion Effects in a Liquid Propellant Rocket Engine. Part V. On the Influence of Vanes on Combustion and Combustion Instability," Caltech Jet Propulsion Laboratory Report TR 32-255.

Sabersky, R.H. (1954) "Effect of Wave Propagation in Feed Lines on Low Frequency Rocket Instability," *Jet Propulsion*, Vol. 24, pp. 172-174.

Saluri, R.J., Wanhainen, J.P. and Hannum, N.P. (1968) "Effect of Thrust per Element in Combustion Stability Characteristics of Hydrogen-Oxygen Rocket Engines," NASA TN D-4851.

Scherrer, D. (1953) "Combustion d'une goutte en milieu réactif avec décomposition exothermique préalable du combustible," *Journées sur la Simulation Numérique des Phénomènes de Combustion*, Sophia-Antipolis, 1983.

Scherrer, D. (1983) "Combustion d'une goutte immobile: etude numerique de l'influence des hypothèses conduisant a la 'Loi en D^2'," *La Recherche Aerospatiale*, 1983, No. 5, pp. 331-337.

Scherrer, D. (1986) "Effet de la convection sur l'evaporation et la combustion d'une goutte de combustible," 70th AGARD P.E.P. Symposium on Combustion and Fuel in Gas Turbine Engines.

Schmitt, D. and Lourme, D. (1952) "A Model of Instability of Liquid Propellant Engine with Radial Injection," IAF Paper No. 81-302, 32nd IAF Congress, Rome, 1981, and *Astronautica Acta*, Vol. 9, No. 6-7, pp. 445-454.

Shuen, J.-S. (1987) "Prediction of the Structure of Fuel Sprays in Cylindrical Combustion Chambers," *J. Propulsion*, Vol. 3, pp. 105-112.

Strignano, W.A. and Crocco, L. (1964) "A Shock Wave Model of Unstable Rocket Combustors," *AIAA J.*, Vol. 2, No. 7, pp. 1285-1296.

Smith, L.O., Jr., Parker, F.P. and O'Hara, J.C. (1975) "Analysis of Liquid Rocket Combustion Chamber Turbulence Levels from Diffusion Data," *Combustion and Flame*, Vol. 25, pp. 161-176.

Sotter, J.G., Woodward, J.W. and Clayton, R.M. (1969) "Injector Response to Strong High-Frequency Pressure Oscillations," *J. Spacecraft*, Vol. 6, NO. 4, pp. 504-506.

Sotter, J.G. and Flandro, G.A. (1968) "Resonant Combustion in Rockets," *Scientific American*, Vol. 219, No. 12, pp. 93-103.

Sowdier, A., Lemoine, J.C. and Derville, G. (1982) "Résolution du problème des instabilités sur le moteur Viking," IAF Paper No. 82-363, 33rd IAF Congress, Paris.

Sternfeld, H.J. (1971) "Leistungsverhalten koaxialer Einspritzsysteme in LO_2/GH_2 - Raketentriebwerken," Deutsche Luft-und Raumfahrt DLR FB 71-38.

Summerfield, M. (1951) "A Theory of Unstable Propulsion in Liquid Propellant Rocket Systems," *ARS J.*, Vol. 21, No. 5, pp. 108-114.

Sutton, R.D., Hines, W.S. and Combs, L.P. (1972) "Development and Application of a Comprehensive Analysis of Liquid-Rocket Combustion," *AIAA J.*, Vol. 10, No. 2, pp. 194-203.

Swithenbank, J. and Sotter, G. (1963) "Vortices in Solid Propellant Rocket Motors," *AIAA J.*, Vol. 1, pp. 1682-1684.

Szuch, J.R. and Wenzel, L.M. (1968) "Experimental Verification of a Double Dead-Time Model Describing Chugging in Liquid Bipropellant Rocket Engines," NASA TN D-5303.

Szuch, J.R. (1969) "Application of a Double Dead-Time Model Describing Chugging to Liquid Propellant Rocket Engines Having Multielement Injectors," NASA TN D-5303.

Temkin, S. and Dobbins, R.A. (1966) "Attenuation and Dispersion of Sound by Particulate-Relaxation Processes," *J. Acoust. Soc. Am.*, Vol. 40, pp. 317-324.

Tong, A.Y. and Strignano, W.A. (1986a) "Multicomponent Droplet Vaporization in a High Temperature Gas," *Combustion and Flame*, Vol. 66, pp. 221-235.

Tong, A.Y. and Sirignano, W.A. (1986b) "Multicomponent Transient Droplet Vaporization: Integral Equation Formulation and Approximate Solution," *Numerical Heat Transfer*, Vol. 10, pp. 253-278.

Tong, A.Y. and Sirignano, W.A. (1987) "Vaporization Response of Fuel Droplet in Oscillatory Field," ASME National Heat Transfer Conference, Paper No. 87-HT-58.

Tsien, H.S. (1952) "The Transfer Functions of Rocket Nozzles," *J. Am. Rocket Soc.*, Vol. 22, pp. 139-143.

Valentine, R.S. (1972) "Liquid Rocket Performance, Stability, and Compatibility," *J. Spacecraft*, Vol. 9, No. 5, pp. 295-307.

Webber, W.T. (1972) "Calculation of Low Frequency Unsteady Behavior of Liquid Rockets from Droplet Combustion Parameters," *J. Spacecraft*, Vol. 9, No. 4, pp. 231-237.

Webber, W.T. and Hoffman, R.J. (1972) "A Mechanistic Model for Analysis of Pulse-Mode Engine Operation," 8th AIAA/SAE Joint Propulsion Specialist Conference, AIAA Paper No. 72-1184.

Williams, F.A. (1985) *Combustion Theory* (Second Edition), The Benjamin/Cummings Publishing Co., Inc., Menlo Park, CA.

Wuerker, R.F. and Briones, R.A. (1978) "Application of Holography to the Combustion Characterization of Solid Rocket Propellants," TRW, Inc., Report AFRPL-TR-77-90.

Yodzis, C.W. (1968) "Engines for Manned Spacecraft, AIAA 4th Propulsion Joint Specialist Conference, AIAA Paper No. 68-567.

Zinn, B.T. (1966) "A Theoretical Study of Nonlinear Transverse Combustion Instability in Liquid Propellant Rocket Motors," Ph.D. Thesis, Princeton University.

Zinn, B.T. and Crocco, L. (1968) "The Nozzle Boundary Condition in the Nonlinear Rocket Instability Problem," *Astronautica Acta*, Vol. 13, pp. 489-496.

Zinn, B.T. and Powell, E.A. (1968) "Application of the Galerkin Method in the Solution of Combustion Instability Problems," Proceedings, XIX Congress, International Astronautical Federation.

Zinn, B.T. and Savell, C.T. (1968) "A Theoretical Study of Three-Dimensional Combustion Instability in Liquid-Propellant Rocket Engines," *Twelfth Symposium (International) on Combustion*, The Combustion Institute, pp. 139-147.

Zinn, B.T. and Powell, E.A. (1970) "Nonlinear Combustion Instability in Liquid- Propellant Rocket Engines," *Thirteenth Symposium (International) on Combustion*, The Combustion Institute, pp. 491-503.

Zinn, B.T., Bell, W.A., Daniel, B.R. and Smith, A.J., Jr. (1973) "Experimental Determination of Three-Dimensional Liquid Rocket Nozzle Admittances," *AIAA J.*, Vol. 11, No. 3, pp. 267-272.

Zukoski, E.E. and Auerbach, J.M. (1976) "Experiments Concerning the Response of Supersonic Nozzles to Fluctuating Inlet Conditions," Transactions of the ASME, *Journal of Engineering for Power*, Vol. , pp. 61-64.

Thrust Augmentors

Blackshear, P.L. (1953) Driving Standing Waves by Heat Addition," *Fourth Symposium (International) on Combustion*, pp.

Blackshear, P.L., Rayle, W.D. and Tower, L.K. (1953) "Experimental Determination of Gas Motion Accompanying Screeching Combustion in a 6 in. Simulated Afterburner," NACA-RM 53I28.

Blackshear, P.L., Jr. and Rayle, W.D. (1957) "Oscillations in Combustors," Chapter VIII, NACA TR 1300.

Bonnell, J.M., Marshall, R.L. and Rieche, G.T. (1971) "Combustion Instability in Turbojet and Turbofan Augmentors," AIAA/SAE 7th Propulsion Jount Specialist Conference, AIAA Paper No. 71-698.

Chamberlain, J. (1983) "Combustion Instability in Turbine Engine Afterburners and Ramjets," ONR/AFOSR Workshop.

Clapp, C.J. (1967) "Full Scale Turbofan Duct Burner Test Program," NASA CR-54637.

Cullom, R.R. and Johnsen, R.L. (1979) "Operating Condition and Geometry Effects on Low-Frequency Afterburner Combustion Instability in a Turbofan at Altitude," NASA TP-1475.

Cumpsty, N.A. (1979) "Jet Engine Combustion Noise: Pressure, Entropy and Vorticity Perturbations Produced by Unsteady Combustion or heat Addition" *J. of Sound and Vibration*, Vol. 66 No. 4, pp. 527-544.

Dix, D.M. and Smith, G.E. (1971) "Analysis of Combustion Instability in Aircraft Engine Augmentors," AIAA/SAE 7th Propulsion Joint Specialist Conference, AIAA Paper No. 71-700.

Dowling, A.P. and Bloxsidge, G.J. (1984) "Reheat Buzz — An Acoustically Driven Combustion Instability," AIAA/NASA 9th Aeroacoustics Conference, AIAA Paper No. 84-2321.

Duroshenko, V.E. and Silverstov, V.M. (1982) "Experimental Investigation of Entropy Waves During Unstable Combustion in the Chamber of a Gas Turbine Engine," *Combustion, Explosion and Shock Waves*, Vol. 18, pp. 20-25.

Ernst, R.C. (1976) "A Combustion Model for Low Frequency Instability in Turbofan Augmentors," AIAA/SAE 12th Propulsion Conference, AIAA Paper No. 76-680.

Garrison, G.D., Russell, P.L. and Stettler (1972) "Investigation of Damping Methods for Augmentor Combustion Instability," Air Force Aero Propulsion Laboratory, Report AFAPL-TR-72-84.

Harp, J.L., Jr., Velie, W.W. and Bryant, L. (1954) "Investigation of Combustion Screech and a Method of its Control," NACA RM E35L24b.

Kaskan, W.E. and Noreen, A.E. (1955) "High Frequency Oscillations of a Flame Held by a Bluff Body," *ASME Transactions*, Vol. 77, pp. 885-895.

Kenworthy, M.J., Woltmann, I.E. and Corley, R.C. (1974) "Augmentor Combustion Stability Investigation," Air Force Aero Propulsion Laboratory, Report AFAPL-TR-74-61.

Legendre, D. (1986) "Internal Acoustics in Turbomachinery," *Rech Aerosp*, 1986-3, 75-79.

Lewis Laboratory Staff (1954) "Summary of Preliminary Investigations into the Characteristics of Combustion Screech in Ducted Burners," NACA TR 1384.

Mach, K.D. (1971) "Systems Aspects of Augmentor Combustion Instability," AIAA/SAE 7th Propulsion Joint Specialist Conference, AIAA Paper No. 71-697.

Moreau, R., Candel, S., Piquemal, J.P. and Borghi, R. (1981) "Phénomènes d'inotabilité dans un foyee turbulent," First International Specialists Meeting of the Cumbustion Institute, Bordeaux.

Nagel, R.T., Denham, J.W. and Papothanasion, A.G. (1983) "Supersonic Jet Screech Tone Cancellation," *AIAA Journal*, Vol. 21, No. 11, pp. 1541-1545.

Newton, R.T. and Truman, J.J. (1956) "An Approach to the Problem of Screech in Ducted Engines," Transactions of the ASME, Vol. 78.

Nicholson, H.M. and Radcliffe, A. (1953) "Pressure Fluctuations in a Jet Engine," *British J. App. Phys.*, Vol. 4, pp. 359-364.

Putnam, A.A. and Dennis, W.R. (1953) "A Study of Burner Oscillations of the Organ-Pipe Type," Transactions of the ASME, Vol. 73, pp. 15-26.

Russell, P.L., Brant, G. and Ernst, R. (1978) "Low-Frequency Augmentor Instability Study," AIAA/SAE 14th Joint Propulsion Conference, AIAA Paper No. 78-996.

Smart, A.E. and Jones, B. (1976) "Measurement of Unsteady Parameters in a Rig Designed to Study Reheat Combustion Instabilities," 14th AIAA Aerospace Sciences Meeting, AIAA Paper No. 76-141.

Underwood, F.N., Rusnak, J.P., Ernst, P.C., Petrino, E.A., Russell, P.L. and Murphy, P., Jr. (1977) "Low Frequency Combustion Instability in Augmentors," AGARD CP 229, *High Temperature Problems in Gas Turbine Engines*.

Usow, K.H., Meyer, C.L. and Schulze, F.W. (1953) "Experimental Investigation of Screeching Combustion in Full-Scale Afterburner," NACA RM-E53I01.

Zukoski, E.E. (1985) "Afterburners," Chapter 2 of *Aerothermodynamics of Aircraft Engine Components*, G. Oates (Ed.), AIAA Education Series.

Ramjet Engines

Aaron, K. and Culick, F.E.C. (1985) "Coupled Vortex Shedding and Acoustic Resonances in a Duct," 22nd JANNAF Combustion Meeting.

Abouseif, G.E., Keklak, J.A. and Toong, T.Y. (1984) "Ramjet Rumble: The Low-Frequency Instability Mechanism in Coaxial Dump Combustors," *Combustion Science and Technology*, Vol. 36, pp. 83-108.

Biron, D., Hébrard, P., Pauzin, S. and Laverdant, A. (1986) "Etude du couplage acoustique - instabilities arodynamiques sur une maquette de statoréacteur," IUTAM Symposium Aero et Hydro-acoustique, Ecole Centrale de Lyon, 1986, Proceedings edited by Springer-Verlag.

Biron, D., Hébrard, P., Pauzin, S. and Laverdant, A. (1986) "Couplage acoustique - structures coherentes: une approche expérimentale et théorique sur une configuration de base," 7ème Journées d'etudes sur la Propagation Ecoustique (JESPA), Lyon.

Bogar, T.J., Sajben, M. and Krontil, J.C. (1983) "Characteristic Frequencies of Transonic Diffuser Flow Oscillations," *AIAA J.*, Vol. 21, No. 9, pp. 1232-1240.

Bogar, T.J., Sajben, M. and Krontil, J.C. (1983) "Response of a Supersonic Inlet to Downstream Puturbations," AIAA/SAE/ASME 19th Joint Propulsion Conference, AIAA Paper No. 83-2017.

Bogar, T.J. and Sajben, M. (1986) "Response of Transonic Diffuser Flows to Abrupt Increases of Back Pressure: Wall-Pressure Measurements," 23rd JANNAF Combustion Meeting.

Brown, G.L. and Roshko, A. (1974) "On Density Effects and Large Structure in Turbulent Mixing Layers," Journal of Fluid Mechanics, Vol. 64, p. 775.

Brown, R.S., Dunlap, R., Young, S.W. and Waugh, R.C. (1981) "Vortex Shedding as a Source of Acoustic Energy in Segmented Solid Rockets," *J. Spacecraft*, Vol. 18, No. 4, pp. 312-319.

Brown, R.S., et al (1983) "Ramjet Combustor Instability Investigation," Final Report for Period 1 October 1981 - 31 March 1983, AFWAL-TR-83-2056, Vol. II.

Brown, R.S., Dunlap, R. Young, S.W. and Waugh, R.C. (1985) "Periodic Vortex Shedding in Simulated Coaxial Dump Combustors," *J. Prop. and Power*, Vol. 1, pp. 413-415.

Byrne, R.W. (1981) "A Note on Longitudinal Pressure Oscillations in Ramjet combustors," 18th JANNAF Combustion Meeting.

Byrne, R.W. (1983) AIAA/SAE/ASME 19th Joint Propulsion Conference, Seattle, Washington, AIAA Paper 83-2018.

Chen, C.P., Sajben, M. and Krontil, J.C. (1979) "Shock-Wave Oscillations in a Transonic Diffuser Flow," *AIAA J.*, Vol. 17, No. 10, pp. 1079-1083.

Clark, W.H. (1982) "Experimental Investigation of Pressure Oscillations in a Side Dump Ramjet Combustor," *J. of Spacecraft and Rockets*, Vol. 19, No. 1, pp. 47-53.

Clark, W.H. (1982) "Geometric Scale Effects on a Side Dump Liquid Fuel Ramjet," 19th JANNAF Combustion Meeting.

Clark, W.H. and Humphrey, J.W. (1986) "Identification of Longitudinal Acoustic Modes Associated with Pressure Oscillations in Ramjets," *AIAA J. Propulsion*, Vol. 2, No. 3, pp. 199-205.

Crow, S.C. and Champagne, F.H. (1971) "Orderly Structure in Jet Turbulence," Journal of Fluid Mechanics, Vol. 48, p. 547.

Crump, J.E., Schadow, K.C., Blomshield, F.S. and Bicker, C.J. (1981) "Combustion Instability in a Research Dump Combustor: Pressure Oscillations," 18th JANNAF Combustion Meeting.

Crump, J.E., Schadow, K.C., Yang, V. and Culick, F.E.C. (1986) "Longitudinal Combustion Instabilities in Ramjet Engines: Identification of Acoustic Modes," *Journal of Propulsion and Power*, Vol. 2, No. 2, pp. 105.

Culick, F.E.C., Derr, R.L. and Price, C.F. (1972) "Linear Analysis of One-Dimensional Oscillations in a Variable-Area T-Burner," 9th JANNAF Combustion Meeting.

Culick, F.E.C. and Magiawala, K. (1979) "Excitation of Acoustic Modes in a Chamber by Vortex Shedding," *Journal of Vibration and Sound*, Vol. 64, No. 3, pp. 455-457.

Culick, F.E.C. (1980) Report of the JANNAF Workshop on Pressure Oscillations in Ramjets," 17th JANNAF Combustion Meeting.

Culick, F.E.C. and Rogers, T. (1980) "Modeling Pressure Oscillations in Ramjets," AIAA/SAE/ASME 16th Joint Propulsion Conference, Hartford, Connecticut, AIAA Paper 80-1192.

Culick, F.E.C. and Rogers, T. (1983) "The Response of Normal Shocks in Diffusers," *AIAA J.*, Vol. 21, No. 10, pp. 1382-1390.

Culick, F.E.C. (1987) "A Note on Rayleigh's Criterion," *Combustion Science and Technology*, Vol. 56, pp. 159-166.

Curran, E.T. (1979) "An Investigation of Flame Stability in a Coaxial Dump Combustor," Ph.D. Dissertation, Air Force Institute of Technology, Report AFIT/AE/DS79-1.

Davis, D.L. (1981) "Coaxial Dump Combustors Combustion Instabilities, Part I - Parametric Test Data," Aero Propulsion Laboratory Air Force Wright Aeronautical Laboratories, Wright-Patterson AFB, Ohio, Interim Report.

Davis, J.A. and Strahle, W.C. (1987) "Acoustic Vortical Interaction in a Complex Turbulent Flow."

Derr, R.L. and Mathes, H.B. (1974) "Cold Gas Acoustic Tests for Resolving T-Burner Uncertainties," 11th JANNAF Combustion Meeting.

Dunlap, R. and Brown, R.S. (1981) "Exploratory Experiments on Acoustic Oscillations Driven by Periodic Vortex Shedding," *AIAA Journal*, Vol. 19, No. 3, p. 408.

Edelman, R. (1981) "Spray Combustion in Ramjet Environments," Report of a JANNAF Workshop, C.P.I.A. Publication No 343.

Edelman, R.B., Harsha, P.T. and Schmotolocka, S.N. (1981) "Modeling Techniques for the Analysis of Ramjet Combustion Processes," *AIAA J.*, Vol. 19, No. 5, pp. 601-609.

Flandro, G.A., Isaacson, L.K., Boys, D.L. and Lin, P.T. (1972) "The Influence of Mean Flow on Rocket Motor Combustion Instability," AFRPL-TR-72-103, Vol. 3, Contract No. FO4611-71-C-0047, University of Utah.

Flandro, G.A. and Jacobs, H.R. (1975) "Vortex Generated Sound in Cavities," in *Aeroacoustics: Jet and Combustion Noise*, Vol. 37 of AIAA Series, *Progress in Astronautics and Aeronautics*.

Flandro, G.A. (1986) "Vortex Driving Mechanism in Oscillatory Rocket Flows," *J. Propulsion*, Vol. 2, No. 3, pp. 206-214.

Grenleski, S.E., Kiersey, J.L., Stevens, C.E. and Dale, L.A. (1977) "Effect of Fuel Injector-Flameholder Configuration on Pressure Distributions in ASAR-ER Combustor," 14th JANNAF Combustion Meeting, Vol. 3, pp. 49-67.

Gutmark, E., Parr, T.P., Parr, D.M. and Schadow, K.C. (1986) "Visualization of Vortex Dynamics in Flame Combustion," *Bulletin of the American Physical Society*, Vol. 31, No. 10, p. 1681.

Gutmark, E., Parr, T.P, Hanson-Parr, D. and Schadow, K.C. (1987) "Azimuthal Structure of an Annular Diffusion Flame," Western States Section of the Combustion Institute Spring Meeting, Paper 87-27.

Hall, P.H. (1978) "Generic Ordnance Ramjet Engine - GORJE Tests of the Inlet Combustor," Naval Weapons Center, China Lake, NWC TP-6068.

Hall, P.H. (1980) "Response of Supercritical Inlets to Downstream Pressure Fluctuations," AIAA/SAE/ASME 16*th* Joint Propulsion Conference, AIAA Paper 80-1118.

Hanson, R.K., Vandsburger, V., Allen, M.G. and McManus, K. (1986) "Effects of Fuel Spray Characteristics and Vaporization on Energy Release Rates and Flow Field Structure in a Dump Combustor," 23rd JANNAF Combustion Meeting.

Harsha, P.T. and Edelman, R.B. (1982) "Assessment of Modular Ramjet Combustor Model," *J. Spacecraft and Rockets*, Vol. 19, No. 5, pp. 430-436.

Hegde, U.G., Reuter, D., Daniel, B.R. and Zinn, B.T. (1986) "Flame Driving of Longitudinal Instabilities in Dump Type Ramjet Combustors," AIAA 24th Aerospace Sciences Meeting, AIAA Paper 86-0371.

Hegde, U.G., Reuter, D., Zinn, B.T. and Daniel, B.R. (1987) "Fluid Mechanically Coupled Combustion-Instabilities in Ramjet Combustors," AIAA 25th Aerospace Sciences Meeting, Reno, Nevada, AIAA 87-0216.

Hegde, R.G., Reuter, D. and Zinn, B.T. (1988) "Combustion Instability Mechanisms in Ramjets," AIAA 26th Aerospace Sciences Meeting, AIAA Paper No. 88-0150.

Heitor, M.V., Taylor, A.M.K.P. and Whitelaw, J.W. (1984) "Influence of Confinement in Combustion Instabilities of Premixed Flames Stabilized on Axisymmetric Baffles," *Combustion and Flame*, Vol. 57, pp. 109-121.

Hendricks, G.J. (1986) "Two Mechanisms of Vorticity Generation in Combusting Flow Fields," Ph.D. Thesis, California Institute of Technology.

Ho, C.M. and Huang, L.S. (1982) "Subharmonics and Vortex Merging in Mixing Layers," *Journal of Fluid Mechanics*, Vol. 119, p. 443.

Ho, C.M. and Huerre, P. (1984) "Perturbed Free Shear Layers," *Annual Review of Fluid Mechanics*, Vol. 16, p. 365-424.

Hong, Z.-C. and Ko, T.-H. (1988) "A Numerical Study on the Three-Dimensional Vortex Motion in a Side-Inlet Dump Combustor," AIAA/ASME/SAE/ASEE 24th Joint Propulsion Specialist Meeting, AIAA Paper No. 88-3009.

Hsieh, T., Wardlaw, A.B., Jr. and Coakley, T. (1984) "Numerical Simulation of a Ramjet Inlet Flowfield in Response to Large Amplitude Combustion Pressure Oscillations," AIAA/ASME/SAE 20th Joint Propulsion Specialist Conference, AIAA Paper No. 84-1363.

Hsieh, T. (1986) "Downstream Boundary Effects on the Frequency of Self-Excited Oscillations in Transonic Diffuser Flow," 23rd JANNAF Combustion Meeting.

Hsieh, T. and Coakley, T.J. (1987) "Downstream Boundary Effects on the Frequency of Self-Excited Oscillations in Transonic Diffuser Flows," AIAA 25th Aerospace Sciences Meeting, AIAA Paper No. 87-0161.

Humphrey, J.W. and Culick, F.E.C. (1986) "Linear Coupling of Acoustics and Entropy and Acoustic Stability in Ramjet Combustion Chambers Containing a Plane Flame," 23rd JANNAF Combustion Meeting.

Humphrey, J.W. and Culick, F.E.C. (1987a) "Linear and Nonlinear Stability of Acoustics with Nonuniform Entropy in Chambers with Mean Flow," AIAA 19th Fluid Dynamics, Plasma Dynamics and Laser Conference, AIAA Paper No. 87-1417.

Humphrey, J.W. and Culick, F.E.C. (1987b) "Acoustic-Energy Interactions in Ramjet Combustion Chambers," AIAA/SAE/ASME/ASEE 23rd Joint Propulsion Meeting, AIAA Paper 87-1872.

Jou, W.-H. and Menon, S. (1986) "Numerical Simulation of the Vortex Acoustic Wave Interaction in a Dump Combustor," AIAA 24th Aerospace Sciences Meeting, Reno, Nevada, AIAA Paper 86-0002.

Jou, W.-H. and Menon, S. (1988) "Modes of Oscillation in a Non-Reacting Ramjet Combustor Flow," Submitted to *Physics of Fluids*; based on AIAA Paper No. 87-1422, AIAA 19th Fluid Dynamics, Plasma Dynamics and Lasers Conference (1987).

Kailasanath, K., Gardner, J.H., Boris, J.P. and Oran, E.S. (1985) "Acoustic-Vortex Interactions in an Idealized Ramjet Combustor," 22nd JANNAF Combustion Meeting.

Kailasanath, K., Gardner, J., Boris, J. and Oran, E (1986) "Numerical Simulations of hte Flowfield in a Central-Dump Ramjet Combustor. I. Tests of the Model and Effects of Forcing," Naval Research Laboratory, Washington, D.C., NRL Memorandum Report.

Kailasanath, K., Gardner, J.H., Oran, E.S. and Boris, J.P. (1986) "Numerical Simulation of Combustion Oscillation in Compact Ramjets," Proceedings of the 1986 JANNAF Propulsion Meeting.

Kailasanath, K., Gardner, J.H., Boris, J.P. and Oran, E.S. (1987a) "Acoustic-Vortex Interactions and Low Frequency Oscillations in Axisymmetric Combustors," 25th AIAA Aerospace Sciences Meeting, AIAA Paper No. 87-0165.

Kailasanath, K., Gardner, J.H., Boris, J.P. and Oran, E.S. (1987b) "Numerical Simulations of Acoustic-Vortex Interactions in a Central-Dump Combustor," *J. Propulsion*, Vol. 3, No. 6, pp. 525-533.

Karagozian, A.R. and Manda, V.S. (1986) "Flame Structure and Fuel Consumption in the Field of a Vortex Pair," *Combustion Science and Technology*, Vol. 49, pp. 185-200.

Karagozian, A.R. and Marble, F.E. (1986) "Study of a Diffusion Flame in a Stretched Vortex," *Combustion Science and Technology*, Vol. 45, pp. 65-84.

Keller, J.O., Vaneveld, L., Korschelt, D., Hubbard, G.L., Ghoniem, A.F., Daily, J.W. and Oppenheim, A.K. (1982) "Mechanisms of Instabilities in Turbulent Combustion Leading to Flashback," *AIAA Journal*, Vol. 20, No. 2, pp. 254-262.

Keller, J.O. and Daily, J.W. (1985) "The Effects of Highly Exothermic Chemical Reaction on a Two-Dimensional Mixing Layer," *AIAA Journal*, Vol. 23, No. 12, pp. 1937-1945.

Kychakoff, G., Howe, R.D., Hanson, R.K. and McDaniel, J.C. (1982) "Quantitative Visualization of Combustion Species in a Plane," *Applied Optics*, Vol. 21, pp. 3225-3227.

Laverdant, A., Poinsot, T. and Candel, S. (1986) "Influence of the Mean Temperature Field on the Acoustic Mode Structure in a Dump Combustor," AIAA/SAE/ASME 21st Joint Propulsion Conference, Monterey, CA, also in Journal of Propulsion and Power, Vol. 2, July-August.

Laverdant, A. and Candel, S. (1987a) "A Numerical Analysis of a Diffusion Flame Vortex Interaction," SIAM Conference on Numerical Combustion, San Francisco, CA.

Laverdant, A. and Candel, S. (1987b) "Computation of Diffusion and Premixed Flames Rolled up in Vortex Structures," 23rd AIAA/SAE/ASME/ASEE Joint Propulsion Conference, San Diego, CA.

Laverdant, A.M. and Candel, S.M. (1988) "A Numerical Analysis of a Diffusion Flame-Vortex Interaction," *Combustion Science and Technology*

Liou, T.-M., Hwang, Y.-H. and Hung, Y.-H. (1988) "Computational Study of Flow Field in Side Inlet Ramjet Combustors," AIAA/ASME/SAE/ASEE 24th Joint Propulsion Specialist Meeting, AIAA Paper No. 88-3010.

Liou, T.-M. and Wu, S.-M. (1988) "Flow Field in a Dual-Inlet Side-Dump Combustor," *J. Propulsion and Power*.

Marble, F.E. (1985) "Growth of a Diffusion Flame in the Field of a Vortex," *Recent Advances in the Aerospace Sciences* (C. Casci, Ed.), pp. 395-413.

Menon, S. and Jou, W.-H. (1988) "Simulations of Self-Sustained Oscillatory Non-Reacting Flows in a Ramjet Combustor," Submitted to *Physics of Fluids*; based on AIAA Paper No. 87-1421, AIAA 19th Fluid Dynamics, Plasma Dynamics and Lasers Conference (1987).

Molavi, K. and Sirignano, W.A. (1988) "Computational Analysis of Acoustic Instabilities in Dump Combustor Configuration," AIAA/ASME/SAE/ASEE 24th Joint Propulsion Specialist Meeting, AIAA Paper No. 88-2856.

Nomoto, H. and Culick, F.E.C. (1982) "An Experimental Investigation of Pure Tone Generation by Vortex Shedding in a Duct," *J. Sound and Vib.*, Vol. 84, No. 2, pp. 247-252.

Norton, O.P. (1983) "The Effects of a Vortex Field on Flames with Finite Kinetics," Ph.D. Thesis, California Institute of Technology.

Nosseir, N.S. and Behar, S. (1986) "Characteristics of Jet Impingement in a Side-Dump Combustor," *AIAA Journal*, Vol. 24, No. 11, pp. 1752-1757.

ONR/AFOSR (1983) "Workshop on Mechanisms of Instability in Liquid-Fueled Ramjets," C.P.I.A. Publication 375, Strahle, W.A. (Organizer).

Parker, J. Sawyer, R.F. and Ganji, A.R. (1979) "Measurement of Vortex Frequencies in a Lean, Premixed Prevaporized Combustor," *Combustion Science and Technology*, Vol. 20, pp. 235-241.

Poinsot, T., Trouvé, A.C., Veynante, D.P., Candel, S.M. and Esposito, E.J. (1987) "Vortex Driven Acoustically Coupled Combustion Instabilities," *J. Fluid Mech.*, Vol. 177, pp. 265-292.

Putnam, A.A. (1964) "General Considerations of Autonomous Combustion Oscillations," Chapter F of *Non-Steady Flame Propagation*, G.F. Markstein (Ed.), The MacMillian Co., N.Y.

Putnam, A.A. (1971) *Combustion Driven Oscillations in Industry*, American Elsevier.

Putnam, A.A. and Faulkner, L. (1982) "An Overview of Combustion Noise," 3rd AIAA/ASME Joint Thermophysics, Fluids, Plasma and Heat Transfer Conference, AIAA Paper No. 82-0927.

Lord Rayleigh (1945) "Theory of Sound,"Vol. 2, Dover, New York, Section 322g, pp. 232-234.

Reardon, F.H. (1981) "Analysis of Very Low Frequency Oscillations in a Ramjet Combustor by Use of a Sensitive Time Lag Model," 18th JANNAF Combustion Meeting.

Reardon, F.H. (1983) "The Sensitive Time Lag Model Applied to Very Low Frequency Oscillations in Side-Dump Liquid-Fuiled Ramjet Engines," 20th JANNAF Combustion Meeting.

Reardon, F.H. (1984) "Modeling of Very Low Frequency Oscillations in Side-Dump Liquid-Fueled Ramjet Engines," California State University, report prepared for Universal Energy Systems, Dayton, OH.

Reardon, F.H. (1985) "An Examination of Some Possible Mechanisms of Combustion Instability in Liquid-Fueled Ramjets," 22nd JANNAF Combustion Meeting.

Reardon, F.H. (1988) "Very Low Frequency Oscillations in Liquid-Fueled Ramjets," 72B Specialists' Meeting of the AGARD Propulsion and Energetics Panel, "Combustion Instabilities in Liquid-Fueled Propulsion Systems."

Reuter, D.M., Hegde, D.E., and Zinn, B.T. (1988) "Flowfield Measurements in an Unstable Ramjet Burner," AIAA/ASME/SAE/ASEE 24th Joint Propulsion Conference, AIAA Paper No. 88-2855.

Rogers, D.E. and Marble, F.E. (1956) "A Mechanism for High Frequency Oscillations in Ramjet Combustors and Afterburners," Jet Propulsion, Vol. 26, pp. 456-462.

Rogers, T. (1980a) "Ramjet Inlet/Combustor Pulsations Study," Naval Weapons Center, China Lake, NWC Report TP-6053.

Rogers, T. (1980b) "Ramjet Inlet/Combustor Pulsations Test and Analysis," Naval Weapons Center, China Lake, NWC Report TP-6155.

Sajben, M., Bogar, T.J. and Krontil, J.C. (1984) "Forced Oscillation Experiments in Supercritical Diffuser Flows," *AIAA J.*, Vol. 22, No. 4, pp. 465-474.

Schadow,K.C., Crump, J.E. and Blomshield, F.S. (1981) "Combustion Instability in a Research Dump Combustor: Inlet Shock Oscillations," 18th JANNAF Combustion Meeting.

Schadow, K.C., Crump, J.E. and Blomshield, F.S. (1983) "Effect of Dump Plane Design on Pressure Oscillations in a Sudden Expansion Ramjet Combustor," 1983 JANNAF Propulsion Meeting.

Schadow, K.C., Wilson, K.J., Crump, J.E., Foster, J.B. and Gutmark, E. (1984) "Interaction Between Acoustics and Subsonic Ducted Flow with Dump," AIAA 22nd Aerospace Sciences Meeting, Reno, Nevada, AIAA Paper 84-0530.

Schadow, K.C., Crump, J.E., Mahan, V.A., Nabity, J.A., Wilson, K.J. and Gutmark, E. (1985) "Large-Scale, Coherent Structures as Drivers of Ramjet Combustion Instabilities," 1985 JANNAF Propulsion Meeting.

Schadow, K.C., Wilson, K.J. and Gutmark, E. (1985) "Characterization of Large-Scale Structures in a Forced Ducted Flow with Dump," AIAA 23rd Aerospace Sciences Meeting, Reno, Nevada, AIAA Paper 85-0080.

Schadow, K.C., Gutmark, E., Parr, D.M. and Mahan, V.A. (1987) "Effect of Shear-Flow Dynamics in Combustion Processes," to be presented at the 8th International Symposium on Airbreathing Engines.

Schadow, K.C., Gutmark, E., Parr, T.P., Parr, D.M., Wilson, K.J. and Crump, J.H. (1987) "Large Scale Coherent Structures as Drivers of Combustion Instability," AIAA 19th Fluid Dynamics, Plasma Dynamics and Lasers Conference, AIAA Paper No. 87-1326.

Shaeffer, C.W., Flandro, G.A. and Brown, R.S. (1987) "Ramjet Combustion Instability Investigation," Final Report for Period July 1985-December 1986, AFWAL-TR-85-2017.

Sirignano, W.A., Abramzon, B., Raju, M. and Molavi, K. (1986) "Spray Combustion: A Driving Mechanism for Ramjet Combustion Instability," 23rd JANNAF Combustion Meeting.

Sivasegaram, S. and Whitelaw, J.H. (1987) "Suppression of Oscillations in Confined Disk-Stabilized Flames," *J. Propulsion*, Vol. 3, No. 4, pp. 291-295.

Sreenivasan, K.R., Raghy, S. and Chu, B.T. (1983) "The Control of Pressure Oscillations in Combustion and Fluid Dynamical Systems," AIAA Shear Flow Control Conference, AIAA Paper 85-0540.

Smith, D.A. and Zukoski, E.E. (1985) "Combustion Instability Sustained by Unsteady Vortex Combustion," AIAA/SAE/ASME/ASEE 21st Joint Propulsion Conference, AIAA Paper 85-1248.

Sterling, J.D. and Zukoski, E.E. (1987) "Longitudinal Mode Combustion Instabilities in a Dump Combustor," AIAA 25th Aerospace Sciences Meeting, AIAA Paper No. 87-0220.

Stull, F.D., Craig, R.R., Wtreby, G.D. and Vanka, S.P. (1983) "Investigation of a Dual Inlet Side Dump Combustor Using Liquid Fuel Injection," 21st AIAA Aerospace Sciences Meeting, AIAA Paper No. 83-0420.

Trouvé, A., Candel, S.M. and Daily, J.W. (1988) "Linear Stability of the Inlet Jet in a Ramjet Dump Combustor," AIAA 26th Aerospace Sciences Meeting, AIAA Paper No. 88-0149.

Vanka, S.P., Stull, F.D. and Craig, R.R. (1983) "Analytical Characterization of Flow Fields in Side Inlet Dump Combustors," AIAA/SAE/ASME 19th Joint Propulsion Conference, AIAA Paper No. 83-1399.

Vanka, S.P., Craig, R.R. and Stull, F.S. (1985) "Mixing, Chemical Reaction and Flow Field Development in Ducted Rockets," AIAA/SAE/ASME/ASEE 21st Joint Propulsion Conference, AIAA Paper No. 85-1271.

Vanka, S.P., Krazinski, J.L. and Nejad, A.S. (1988) "An Efficient Computational tool for Ramjet Combustor Research," AIAA 26th Aerospace Sciences Meeting, AIAA Paper No. 88-0060.

Waugh, R.C., et al (1983) "Ramjet Combustor Instability Investigation: Literature Survey and Preliminary Design Study," Final Report for Period 1 October 1981-31 March 1983, AFWAL-TR-83-2056, Vol. I.

Waugh, R.C. and Brown, R.S. (1984) "Ramjet Combustor Instability – Comparison of Data and Analysis," 21st JANNAF Combustion Meeting.

Wong, K., Peddieson, J., Jr. and Ventrice, M. (1980) "Analysis of Combustion Instabilikty in Liquid Fuel Rocket Motors," NASA CR-159733.

Yang, V. and Culick, F.E.C. (1983) "Linear Theory of Pressure Oscillations in Liquid-Fueled Ramjet Engines," AIAA 21st Aerospace Sciences Meeting, AIAA Paper No. 83-0574.

Yang, V. (1984) "Pressure Oscillations in Liquid-Fueled Ramjet Engines," Ph.D. Thesis, California Institute of Technology.

Yang, V. and Culick, F.E.C. (1985) "Analysis of Unsteady Inviscid Diffuser Flow with a Shock Wave," *J. of Propulsion and Power*, Vol. 1, No. 3, pp. 222-228.

Yang, V. and Culick, F.E.C. (1984) "Analysis of Low Frequency Oscillations in a Laboratory Ramjet Combustor," *Comb. Sci. and Tech.*, Vol. 45, pp. 1-25.

Yang, V. and Culick, F.E.C (1986) "Nonlinear Analysis of Pressure Oscillations in Ramjet Engines," AIAA 24th Aerospace Sciences Meeting, AIAA Paper No. 86-0001.

Yang, V., Kim, S.-I. and Culick, F.E.C. (1987) "Third-Order Nonlinear Acoustic Instabilities in Combustion Chambers, Part I: Longitudinal Modes," AIAA/SAE/ASME/ASEE 23rd Joint Propulsion Specialist Conference, AIAA Paper No. 87-1873.

Yang, V., Kim, S.-I. and Culick, F.E.C. (1987) "Third-Order Nonlinear Acoustic Instabilities in Combustion Chambers, Part II: Transverse Modes," 24th JANNAF Combustion Meeting.

Yu, K., Trouve, A. and Daily, J.W. (1987) "Low Frequency Pressure Oscillations in a Model Ramjet Combustor," 24th JANNAF Combustion Meeting.

Yu, K., Lee, S., Trouve, A., Stewart, H. and Daily, J.W. (1987) "Vortex-Nozzle Interactions in Ramjet Combustors," AIAA/SAE/ASME/ASEE 23rd Joint Propulsion Conference, AIAA Paper No. 87-1871.

Zikikout, S., Candel, S., Poinsot, T., Trouvé, A. and Esposito, E. (1988) "High-Frequency Combustion Oscillations Produced by Mode Selective Acoustic Excitation," *21st Symposium (International) on Combustion*, The Combustion Institute, pp. 1427-1434.

Zetterström, K.-A. and Sjöblom, B. (1985) "An Experimental Study of Side Dump Ramjet Combustors," International Symposium on Airbreathing Engines, Paper 85-7024.

Zukoski, E.E. and Marble, F.E. (1955) "Experiments Concerning the Mechanism of Flame Stabilization in the Wakes of Bluff Bodies," Proceedings of the Symposium on Gas Dynamics, Northwestern University.

Passive and Active Control of Combustion Instabilities

Baer, M.R., Mitchell, C.E. and Espander, W.R. (1974) "Stability of Partially Lined Combustors with Distributed Combustion," *AIAA Journal*, Vol. 12, No. 4, pp. 475-480.

Baer, M.R. and Mitchell, C.E. (1977) "Theoretical Evaluation of Rigid Baffles in Suppression of Combustion Instability," *AIAA Journal*, Vol. 15, No. 2, pp. 135-136.

Balas, M.J. (1978) "Feedback Control of Flexible Systems," *IEEE Transactions on Automatic Control*, Vol. AC-23, No. 4, pp. 673-679.

Balas, M.J. (1982) "Trends in Large Space Structure Control Theory: Fondest Hopes, Wildest Dreams," *IEEE Transactions on Automatic Control*, Vol. AC-27, No. 3, pp. 522-535.

Blackman, A.W. (1960) "Effect of Nonlinear Losses on the Design of Absorbers for Combustion Instabilities," *ARS J.*, Vol. 30, No. 11, pp. 1022-1028.

Bloxsidge, G.J., Dowling, A.P., Hooper, N. and Langhorne, P.J. (1987) "Active Control of Reheat Buzz," AIAA 25th Aerospace Sciences Meeting, Paper No. AIAA-87-0433.

Bloxsidge, G.J., Dowling, A.P, Hooper, N. and Langhorne, P.J. (1987) "Active Control of an Acoustically Driven Combustion Instability," *J. Theor. and App. Mech.*, Supplement to Vol. 6, pp. 161-175.

Collyer, A.A. and Ayres, D.J. (1972) "The Generation of Sound in a Rijke Tube Using Two Heating Coils," *J. Phys. D.*, Vol. 5, pp. L73-L75.

Combs, L.P., Oberg, C.L., Coultas, T.A. and Evers, W.H., Jr. (1974) "Liquid Rocket Engine Combustion Stabilization Devices," NASA SP-8113.

Culick, F.E.C. (1973) "The Stability of One-Dimensional Motions in a Rocket Motor," *Combustion Science and Technology*, Vol. 7, pp. 165-175.

Culick, F.E.C., Ed. (1974) "T-Burner Testing of Metallized Solid Propellants," Air Force Rocket Propulsion Laboratory, Report AFRPL-TR-74-28.

Dines, P.J. (1983) "Active Control of Flame Noise," Ph.D. Thesis, Cambridge University.

Epstein, A.H., Ffowcs Williams, J.E., and Greitzer, E.M. (1986): "Active Suppression of Compression Instabilities,"AIAA 10th Aeroacoustics Conference, Paper No. AIAA-86-1994.

Ffowcs-Williams, J.E. (1984): "Anti-Sound," *Proc. Roy. Soc. London*, A395, pp. 63-88.

Ffowcs-Williams, J.E. (1986): "The Aerodynamic Potential of Anti-Sound," ICAS-86-0.1.

Fox, J.L. (1951) "Preliminary Investigation of Helmholtz Resonators for Damping Pressure Fluctuations in 3.6 Inch Ram Jet at Mach Number 1.90," NACA RM E51C05.

Gould, L.A. and Murray-Lasso, M.A. (1966) "On the Modal Control of Distributed Systems with Distributed Feedback," *IEEE Transactions on Automatic Control*, Vol. AC-11, No. 4, pp. 729-737.

Harp, J. L., Jr., Velie, W. W. and Bryant, L. (1954) "Investigation of Combustion Screech and a Method of its Control" NACA RM E53L24b

Heckl, M.A. (1985) "Heat Sources in Acoustic Resonators," Ph.D. Thesis, Cambridge University.

Heckl, M.A. (1986) "Active Control of the Noise From a Rijhe Tube," IUTAM Symposium on Aero and Hydro-Acoustics, Lyon 1985, Springer-Verlag, pp. 211-216.

Hersh, A.S. and Walker, B. (1979) "Effect of Grazing Flow in the Acoustical Impedance of Helmholtz Resonators Consisting of Single and Clustered Orifices," NASA Report CR 3177.

Ingaard, U. and Labate, S. (1950) "Acoustic Circulation Effects and the Nonlinear Impedance of Orifices," *J. Acoust. Soc. of Amer.*, Vol. 22, No. 2, pp. 211-218.

Ingaard, U. (1953) "On the Theory and Design of Acoustic Resonators," *J. Acoust. Soc. of Amer.*, Vol. 25, No. 6, pp. 1037-1061.

Kuentzmann, P. and Nadaud, L. (1975) "Réponse des Propergols Solides aux Oscillations de Pression et de Vitesse," *Combustion Science and Technology*, Vol. 11, pp. 119-139.

Lang, W., Poinsot, T., and Candel, S. (1987): "Active Control of Combustion Instability," *Combustion and Flame*, Vol. 70, pp. 281-289.

Marble, F.E. and Cox, D.W., Jr. (1953) "Servo-Stabilization of Low-Frequency Oscillations in a Liquid Bipropellant Rocket Motor," *ARS J.*, pp. 63-81.

Marble, F.E. (1955) "Servo-Stabilization of Low-Frequency Oscillations in Liquid Propellant Rocket Motors," *ZAMP*, Vol. VI/1, pp. 1-35.

Mitchell, C.E. (1972) "Stability of Combustors With Partial Length Acoustic Liners," *Combustion Science and Technology*, Vol. 6, pp. 61-70.

Mitchell, C.E. and Baer, M.R. (1975) "Stability Predictions for Combustors with Acoustic Absorbers and Continuous Combustion Distributions," *AIAA Journal*, Vol. 13, No. 8, pp. 1107-1109.

Mitchell, C.E., Dodd, F.E., Hudson, T.J. and Howell, D.J. (1986) "Acoustic Cavity Model Development," 23rd JANNAF Combustion Meeting.

Mitchell, C.E., Dodd, F.E. (1987) "Two Dimensional Acoustic Cavity Models," 24th JANNAF Combustion Meeting.

Mitchell, C.E., Howell, D.J. and Fang, J.J. (1987) "An Improved Predictive Model for Injector Face Baffles," 24th JANNAF Combustion Meeting.

Mitchell, J.P. (1965) "Advanced Throttling Concept Study," Pratt and Whitney, Report AFRPL-TR-65-98.

Murray-Lasso, M.A. (1966) "The Modal Analysis and Synthesis of Linear Distributed Control Systems," Sc.D. Dissertation, Massachusetts Institute of Technology.

NASA Design Criteria Office (1974) "Liquid Rocket Engine Combustion Stabilization Devices," NASA SP-8113.

Nestlerode, J.A. and Oberg, C.L. (1969) "Combustion Instability in an Annular Engine," 6th ICRPG Combustion Conference.

Oberg, C.L. (1969) "Final Report - Lunar Module Ascent Engine Acoustic Cavity Study," Rocketdyne Division, North American Rockwell, Report R-7935.

Oberg, C.L. and Kukula, N.M. (1969) "Acoustic Liners for Large Engines," Rocketdyne Report No. K-7792.

Oberg, C.L. (1971) "Combustion Stabilization with Acoustic Cavities," *J. Spacecraft*, Vol. 8, No. 12, pp. 1220-1225.

Oberg, C.L. and Kukula, N.M. (1971) "Analysis of the F-1 Acoustic Liner," *J. Spacecraft*, Vol. 8, No. 12, pp. 1138-1143.

Oberg, C.L., Wong, T.L. and Ford, W.M. (1972) "Evaluation of Acoustic Cavities for Combustion Stabilization," AIAA/SAE 8th Joint Propulsion Specialist Conference, AIAA Paper No. 72-1147.

Oberg, C.L., Kesselring, R.C. and Warner, C. III (1974) "Analysis of combustion Instability in Liquid Propellant Engines With or Without Acoustic Cavities," Rocketdyne Division, Rockwell International, Report R-9353.

Poinsot, T. Lang, W., Bourienne, F., Candel, S., and Esposito, E. (1987): "Suppression of Combustion Instabilities by Active Control," AIAA/SAE/ASME/ASEE 23rd Joint Propulsion Conference, Paper No. AIAA-87-1876.

Poinsot, T., Veynante, D., Bourienne, F., Candel, S., and Esposito, E. (1988): "Initiation and Suppression of Combustion Instabilities by Active Control," *22nd International Symposium in Combustion*.

Satche, M. (1949) discussion of "Stability of Linear Oscillating Systems With Constant Time Lag," by H.I. Ansoff, *J. App. Mech.*, Vol. 16 (Dec. 1949), pp. 419-420.

Sirignano, W.A., Crocco, L. and Harrje (1967) "Acoustic Lines Studies," 3rd ICRPG Combustion Conference.

Sivasegaram, S. and Whitelaw, J.H. (1987): "Suppression of Oscillations in Confined Disk-Stabilized Flames," AIAA 25th Aerospace Sciences Meeting, Paper No. 87-0434; *J. Propulsion*, Vol. 3, No. 4, pp. 291-295.

Sreenivasan, K.R., Raghu, S. and Chu, B.T. (1985) "The Control of Pressure Oscillations in Combustion and Fluid Dynamical Systems," AIAA Shear Flow Conference, AIAA Paper No. 85-0340.

Tang, P.K. and Sirignano, W.A. (1971) "Theory of a Generalized Helmholtz Resonator," *J. Vib. and Sound*, Vol. 26, No. 2, pp. 817- .

Tonen, T.S., Tang, P.K., Sirignano, W.A. and Harrje, D.T. (1971) "Acoustic Liner Design from a Fluid Mechanics Approach," AIAA/SAE 7th Propulsion Joint Specialist Conference, AIAA Paper No. 71-757.

Tsien, H.S. (1952) "Servo-Stabilization of Combustion in Rocket Motors," *ARS J.*, pp. 256-263.

Tsien, H.S. (1956) *Engineering Cybernetics*, McGraw-Hill Book Co., New York.

Utvik, D.H., Ford, H.J. and Blackman, A.W. (1966) "Evaluation of Absorption Liners for Suppression of Combustion Instability in Rocket Engines," *J. Spacecraft*, Vol. 3, No. 7, pp. 1039-1045.

Yang, V., Sinha, A. and Fung, Y.T. (1988): "Linear Theory of Active Control of Pressure Oscillations in Combustion Chambers," AIAA/ASME/SAE/ASEE 24th Joint Propulsion Conference, AIAA Paper No. 88-2944.

Zinn, B.T. (1969) "A Theoretical Study of Nonlinear Damping by Helmholtz Resonators," AIAA 5th Propulsion Specialist Meeting, AIAA Paper No. 69-481.

DISCUSSION

A. P. Dowling, UK

> I am surprised by your statement that the design of a successful active controller requires a detailed understanding of local combustion-flow interactions. Usually the implementation of 'anti-sound' or active control requires only global properties, and the transfer functions are more frequently measured than predicted. Would you care to elaborate?

Author's Reply:

> I base my comment on the notion that the most effective control of a complicated physical system generally requires understanding the system itself. That forms part of the basis for designing the controller. While it's true that knowing only the transfer functions may on occasion be adequate, that information already implies at least partial knowledge of the system. Especially if, as the case is for combustion chambers, nonlinear processes may be important, I suspect that success will rest substantially on knowledge of the physical behavior.

COMBUSTOR INFLUENCE ON FIGHTER ENGINE OPERABILITY

by
Thomas L. DuBell
Pratt & Whitney - Government Engine Business
United Technologies
P.O. Box 109600
West Palm Beach, Florida 33410-9600
and
Anthony J. Cifone PE31
Naval Air Propulsion Center
1440 Parkway Avenue
Trenton, New Jersey 08628
USA

SUMMARY

This paper discusses an aspect of combustion instability that is generally unrecognized, but which has a critical influence on aircraft gas turbine engine operability. The basic lean combustion limit (static stability) of a combustor, when coupled with engine system dynamics, can result in the inability of an engine to recover from a compressor stall. This is a most serious event for a tactical fighter/attack aircraft engaged in air combat.

The coupling of combustor static stability characteristics with engine system dynamics is reviewed, a hypothesis presented, solution approaches suggested and plans to address this challenge discussed.

INTRODUCTION

Combustor designers are generally concerned with two aspects of stability. The first is static stability which is the range of conditions over which combustion process is stable. Outside of this range, the combustion device will not release energy. The second aspect is dynamic stability which is often referred to as resonance in main combustors and screech in augmentors. Dynamic instability must be avoided because of its destructive nature.

There is another stability characteristic that is not usually recognized. It is pseudo dynamic stability which has a strong influence on engine operability. It may manifest itself during fighter aircraft combat maneuvers which result in an engine compressor stall. If the combustor does not continue to deliver energy during the highly dynamic stall event (it blows out), then the engine may not recover from the stall. Loss of power during combat can be catastrophic.

During a stall event, the fuel flow remains relatively stable, but the airflow varies widely from positive through-flow to negative back-flow in the combustor. For the combustor process to continue, there must always be a region of reaction to pilot the bulk stream. If the heat loss from the pilot area exceeds the heat release, or if the pilot is removed completely, then the combustion process will be extinguished and the engine will cease to operate.

Engine system dynamic stall events and their influences on the combustion process are not normally considered by combustion system designers. The purpose of this paper is to draw attention to this issue and to suggest the combustion system design should include consideration of combustion influence on compressor stall recovery; this will be referred to as "operability".

THE MAIN COMBUSTION SYSTEM

The typical turbojet engine contains a combustor which appears to be a simple component, but which is fundamentally the most complex component in the engine. As a result, it is not well understood. Figure 1 illustrates why this device has earned its "black art" nickname. The combustor designer/developer must satisfy many conflicting requirements while dealing with three dimensional and locally separated flows, multiphase chemically reacting flows, velocities that vary from Mach .4 to less than Mach .4, temperatures that range from -65 deg. F to more than 4000 deg. F, pressures that range from 3 PSIA to more than 600 PSIA, and fuel/air ratios that cover up to an A/1 range. The combustor must deliver near 100% chemical efficiency over a wide operating range and produce low exhaust smoke emission.

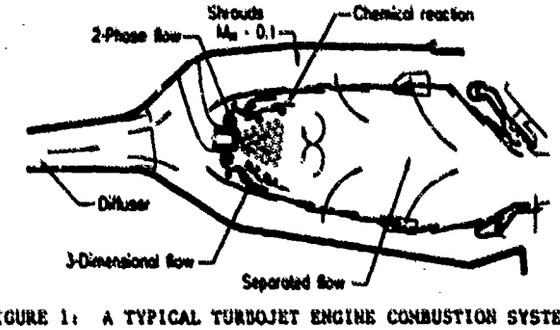


FIGURE 1: A TYPICAL TURBOJET ENGINE COMBUSTION SYSTEM

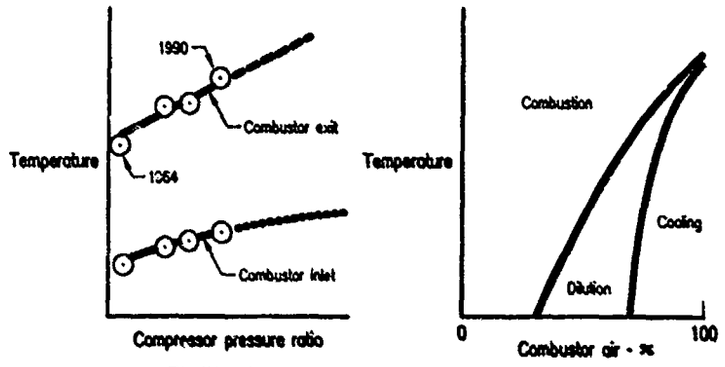


FIGURE 2: COMBUSTOR REQUIREMENT TRENDS

Figure 2 shows that future designs will be even more of a challenge. Temperature rise, hence fuel/air ratio is increasing which causes the amount of airflow used in the combustion process to increase. This trend toward increased combustion process airflow and higher overall fuel/air ratio increases the engine operability challenge.

COMBUSTOR STATIC STABILITY

A combustor, once started, will continue to release energy as long as the energy release in the reacting gases is equal to or greater than the energy loss from the reacting gases. When energy loss exceeds energy release, the reacting gas temperatures drop below the level at which combustion can occur.

The environment in which combustion is desired is very important. Reducing pressure and/or inlet gas temperature reduces the probability of achieving a self sustaining reaction, as does increasing the through-flow velocities in the combustor. Therefore, static stability is a function of reacting fuel/air ratio, pressure, temperature and through-flow velocity. Figure 3 shows a typical combustor stability envelope: combustion inside the envelope is possible, but stable combustion outside the envelope is not attainable.

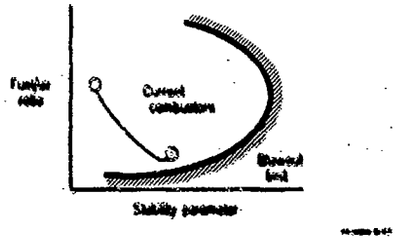


FIGURE 3: COMBUSTOR STABILITY ENVELOPE

If a turbojet engine had to operate at only a single design point within the stability envelope, there would be no static stability challenge. Design of such a device would be relatively easy. However, the engine must be started from ground level through high altitudes and power level must be variable from maximum to idle. Transients such as deceleration from maximum to idle power must be possible. This places severe demands on the combustor. Figure 3 also shows the path a transient might take on a combustor stability map. The path must remain within the "combustion possible" region.

The challenge to satisfy this requirement is made more difficult by increasing the temperature rise. The effect of this is shown by Figure 4. A larger turn down of the fuel/air must be accommodated which results in operation nearer the stability limit of the combustor.

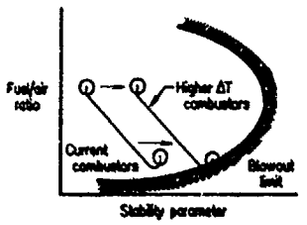
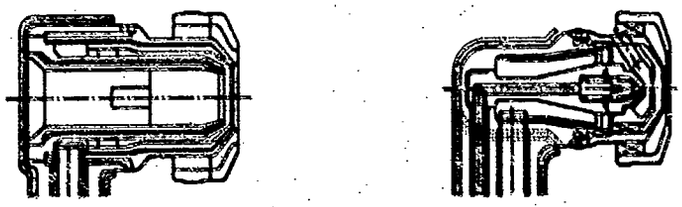


FIGURE 4: COMBUSTOR STABILITY AT HIGHER TEMPERATORE RISE

The static stability requirement is not new;combustion systems have been successfully accommodating this since the Whittle engine. What is new is a recognition that engine system dynamics during a transient can couple with the combustor static stability characteristic to result in a blow out where none would be predicted.

ENGINE STALL RECOVERY

During violent maneuvers, such as those typical of fighter aircraft in combat, airflow into the compressor can become so distorted that the compressor stalls or ceases to pump air into the engine. The high pressure air in and aft of the compressor reverses flow direction; pressure in and downstream of the compressor drops rapidly which "clears" the stall and allows the compressor to resume pumping airflow into the engine. If the cause of the original stall is removed, the engine will operate normally; if not, stall cycles may continue to repeat until the system recovers. Should the engine power level deteriorate too far during stall cycles, the compressor may suffer local circumferential stalls known as rotating stall. The engine system must be shut down and restarted to clear this stall. It is desired the engine recover from a stall without shutdown; shutdown is a loss of operability.



Air blast		Hybrid
84/27	Stall/non-recoverable	45/0
68	Percent recovered	100

FIGURE 5: ENGINE STALL RECOVERY EXPERIENCE

Experience has taught that combustion system modifications can result in improved engine recovery from stalls. Figure 5 shows that one typical engine was far more successful using fuel nozzles having part of the fuel atomized by fuel pressure drop than when using more advanced and desirable air blast fuel nozzles. A clear understanding of why this is so may provide insight to enable design of combustion systems that contribute to engine stall recovery.

COMBUSTOR BEHAVIOR DURING A STALL

Figure 6 shows a time history of combustor pressure during a stall. The stall occurred when fuel was added causing an increase in combustor exit temperature. The increased exit temperature resulted in increased combustor pressure which caused the compressor to stall. Upon stall, pressure dropped to a very much lower value which allowed the stall to clear and pressure increased back toward the level needed to satisfy flow function requirements in the turbine.

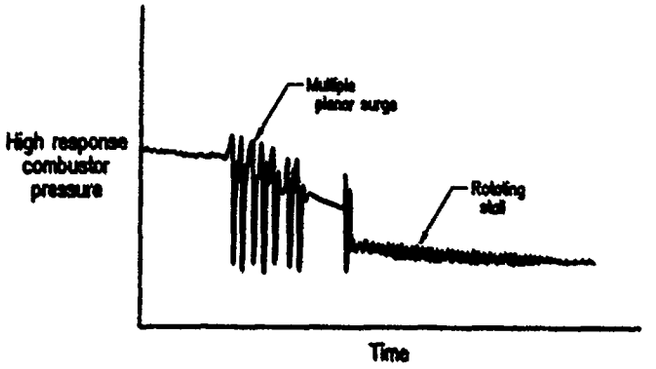


FIGURE 6: COMBUSTOR PRESSURE DURING ENGINE STALL

The data show a momentary drop in combustion pressure as the pressure increased toward the point where another stall cycle was initiated. After several of these cycles, this system recovered to a "steady state" level below that demanded by combusting flow; the combustor had "blown out". The combustion process was reinitiated (by a spark) and the stall cycles started again, but quickly changed character to a stable rotating stall from which engine recovery does not occur. The engine must be shut down and restarted.

Close examination of such data leads to the conclusion that the combustor experienced partial blow outs on recovery from each stall event and finally suffered complete blow out. Study of similar data from stall events where the engine recovered shows complete blow outs did not occur. The engine has a chance to recover if combustion can be maintained. Investigations were initiated to determine why blow out occurs where the engine metered fuel/air ratio remained well within the stability envelope of the combustor. One clue was provided by the engine data that indicated one type of fuel nozzle was better than another (Figure 5).

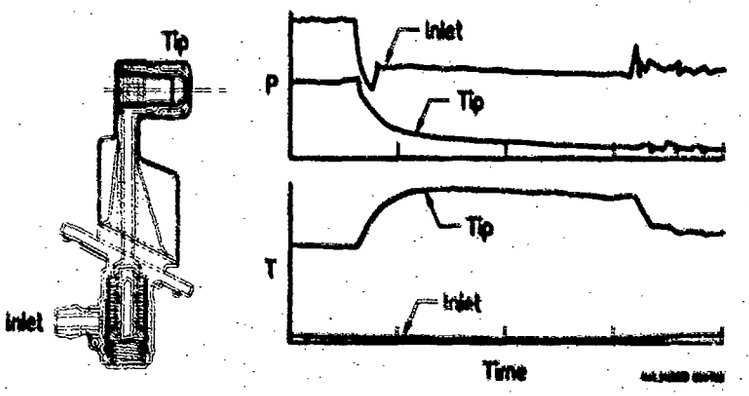


FIGURE 7: FUEL NOZZLE RESPONSE DURING ENGINE STALL

An air blast fuel nozzle was extensively instrumented and data taken during engine stall testing. Figure 7 shows some typical data which indicates the fuel pressure in the nozzle tip is very near that in the combustor, and the fuel temperature in the tip initially increases significantly during the transient. Analysis of fuel pressure and temperature data taken during a stall showed that some fuel vaporization could be expected. As the engine recovered from a stall, fuel vapor existed in the fuel nozzle. Combustor pressure increased and caused the vapor to compress into a liquid. As fuel vapor compression occurred, less fuel was delivered to the combustor than was metered by the engine. The metered flow was within the combustor stability zone, but the transiently delivered fuel/air ratio was below the blow out limit. This hypothesis has been confirmed by testing with heated and cooled fuel and by testing with fuels having different vaporization temperatures.

CLOSING REMARKS

A new requirement for the combustor designer to consider has been presented. The combustion system pseudo dynamic characteristics play a very important roll in enabling an engine to recover from a stall event. Stall recovery is especially important for fighter aircraft engines where the probability of encountering stalls will always be high.

The combustor static stability characteristic and the fuel system dynamic behavior appear to be fundamental to enabling an engine to recover from a stall. The combustor fuel/air ratio must remain in the stable range. How to achieve that is the challenge; some possible improvement approaches include:

- o Improve combustor stability
- o Reduce fuel temperature
- o Reduce fuel volatility
- o Increase pressure in the fuel nozzle.

The U.S. Navy is supporting efforts to investigate how to achieve improvement through research programs using a new dynamic combustion facility. Figure 8 shows the basic facility arrangement, and Figure 9 illustrates its capability. A complete description of this facility and its operation is presented in Reference 1. This unique facility is capable of imposing normal engine transients and engine stall transients on a model combustor so that behavior can be studied.

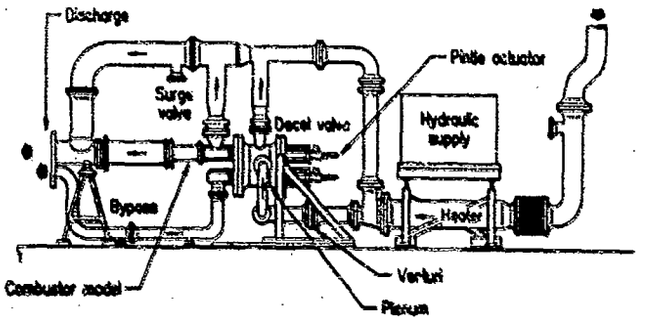


FIGURE 8: COMBUSTOR TRANSIENT TEST FACILITY

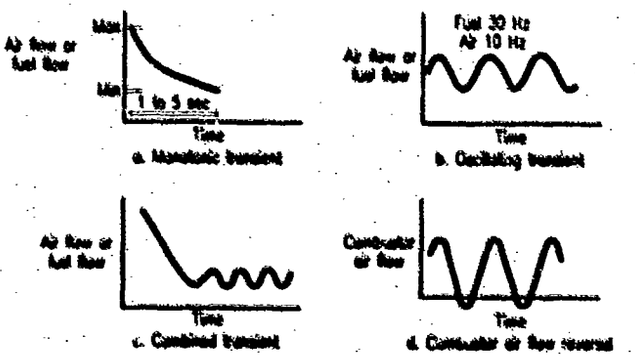


FIGURE 9: COMBUSTOR TRANSIENT FACILITY CAPABILITY

The results of this work are expected to provide the technology foundation for guiding the design and development of current and advanced turbojet combustion engines having significantly improved operability.

REFERENCES:

1) Nonfjord, T.J., Haley, Jr. J., Mennell, J.M., "Unique Transient Test Combustor Capability", AIAA Paper 88-3197, AIAA/ASEE/ASME/SAE 24th Joint Propulsion Conference, July 1988.

2) Whittle, Sir Frank, "Jet, The Story of a Pioneer", Frederick Muller, Ltd., London, 1953.

3) Steele, L.L., Grant, Jr. J.M., Harrold, D.P., and Erhart, J.J., "Application of System Identification Techniques to Combustor Post Stall Dynamics", AFWAL TR-86-2105, September, 1987.

CHARACTERISTICS OF COMBUSTION DRIVEN PRESSURE OSCILLATIONS IN ADVANCED TURBO-FAN ENGINES WITH AFTERBURNER.

B E HENDERSON AND J S LEWIS
Rolls-Royce plc, Filton, Bristol

SUMMARY

Development of a high trust to weight ratio engine requires that the maximum afterburner thrust boost is achieved. The achievement of this thrust boost must be free of potentially damaging pressure oscillations.

The characteristics of both low and high frequency combustion driven pressure oscillations associated with the afterburner of an advanced turbo-fan engine are described. These oscillations are related to the geometry and flow conditions of the afterburner and engine.

Models of the characteristics have been developed based on experimental and theoretical techniques. It is shown how these have been used to ensure unrestricted operation of the afterburner system throughout the required operating range.

AFTERBURNER DESCRIPTION

The development of the turbofan afterburner system being considered is well documented in REF 1, a brief description follows.

The afterburner is described as a mix/burn system (Fig 1) the essential feature of which is to keep the bypass and core streams of the turbofan engine separate until the flameholder plane. The degree of mixing between the two streams is limited to ensure that once fuel is injected into a stream it remains with the airflow. Problems have been observed, particularly with injection of fuel into the cold bypass stream, where droplets take up the initial air direction but do not follow subsequent mixing patterns resulting in non-ideal fuel-air ratio distributions.

An advantage of this style of afterburner is that flameholders and fuel injectors appropriate to the local gas conditions can be specified. Referring to Fig 1 simple annular 'V' section flameholders with upstream fuel injection are provided in the core stream whilst the more difficult combustion conditions in the bypass stream are accommodated by a separately fuelled vaporising primary zone with injection of the main fill fuel co-planar with the primary zone.

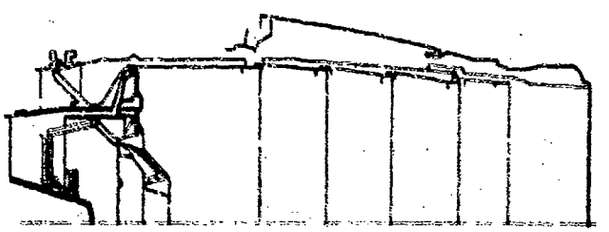


Figure 1 Turbofan Afterburner System

The jet pipe is protected by a screech damper in the vicinity of the flameholder and then by a film cooled liner. This liner also provides cooling air to protect the propelling nozzle.

CLASSIFICATION OF COMBUSTION INSTABILITIES

If one examines the pressure signal from an afterburner under normal operating conditions some random variation will be present, ie there is always an element of instability present in the combustion process. Therefore pressure fluctuation in itself is not an adequate definition of combustion instability. As afterburner fuel air ratio is increased discrete peaks appear in the pressure-frequency spectrum and it is with these instabilities at discrete frequency that this paper is concerned.

These discrete frequencies are acoustic in nature, being pressure waves travelling between boundaries within the afterburner/engine. For the purpose of this paper they have been classified into two types.

The lower range of frequencies, typically 50-200 Hz, are characterised as acoustic waves travelling axially along the engine/afterburner and bounded by the Fan or Turbine and Propelling Nozzle. These instabilities are known as buzz.

The higher range of frequencies, 500-5K Hz, are acoustic waves in a plane at right angles to the jet pipe axis and flow direction and are termed screech. As will be shown later a number of discrete frequencies can exist during screech events, some of these are harmonics of one acoustic mode but it is also apparent that different modes can exist, transverse, radial, tangential, etc. The formation of these modes is linked to geometric features within the afterburner.

BUZZ

It has already been stated that afterburner buzz is a low frequency acoustic wave. Its presence, magnitude and frequency, has been detected by monitoring pressure within the jet pipe. A piezo-electric transducer, which measures the fluctuating portion of the pressure signal, was flush mounted on the jet pipe skin. It was positioned upstream of the flameholder to avoid environmental problems for the transducer.

A typical output (Fig 2) shows how the signal develops as the afterburner fuel air ratio is increased. The signal changes from being random in nature to exhibiting a frequency peak which then increased in amplitude.

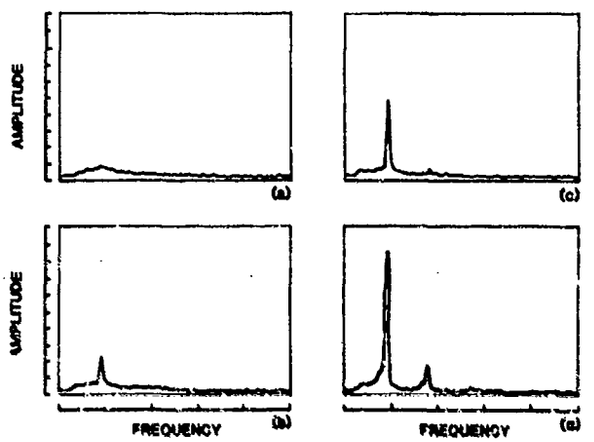


Figure 2 Development of Pressure Spectrum with Increasing Afterburner Fuel Air Ratio (a) to (d)

Why are we concerned about afterburner buzz? If it were allowed to continue unchecked the cyclic pressure loads produced could severely limit the life of the afterburner. If the buzz frequency were to be coincident with the natural frequency of a component in the afterburner, or indeed any part of the engine, the effect of the pressure variation would be magnified. Examining the engine installed in an airframe buzz appears as a peak in the noise spectrum from the engine exhaust and will impose cyclic pressure loads on the aircraft structure. Finally low levels of buzz (of the order of 2% pressure variation) have been reported as audible and deemed unacceptable by pilots.

STEADY STATE BUZZ

The onset and severity of afterburner buzz has been related to fuel air ratio. On mix then burn turbofan afterburners the mean applied fuel air ratio is used to describe buzz onset limits. One advantage of the previously described mix/burn system is that the fuel air ratio in the two streams, bypass and core, is separately controlled. This has enabled a more precise definition of fuel air ratio at the buzz onset point to be made. The analysis of steady state buzz data from full scale rig and engine afterburner testing has resulted in model of buzz onset (Fig 3).

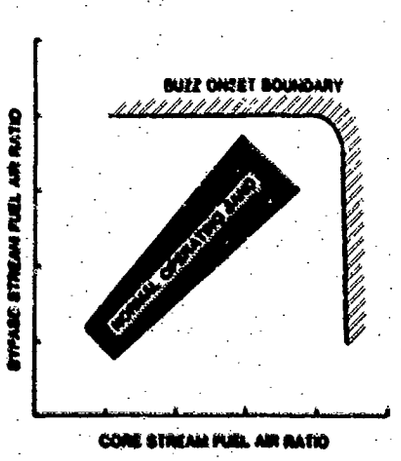


Figure 3 Steady State Buzz Characteristic

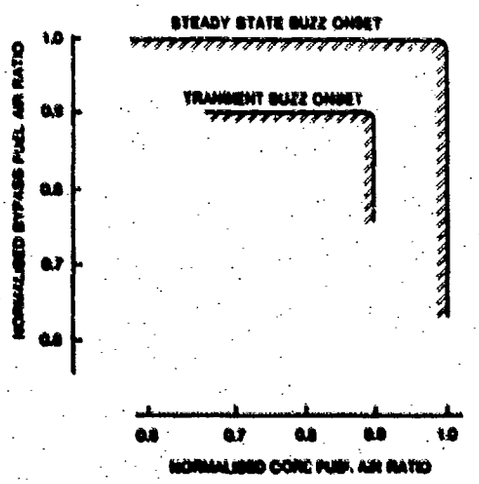


Figure 4 Transient Buzz Characteristic

The characteristic shows that buzz can be induced by increasing the fuel air ratio in either stream and that onset is independent of the conditions in the other stream. The testing also showed that buzz onset in the two streams was accompanied by different frequencies, separate acoustic paths being excited. A buzz characteristic of this form coupled with the ability, in a mix/burn system, to devise fuelling laws around the flight envelope to match the characteristic, results in optimum afterburner fuelling at all flight points. This ensures that the maximum afterburner performance is always achieved.

TRANSIENT BUZZ

When rapid handling of the engine/afterburner was carried out the buzz characteristic changed. With the afterburner control laws set to give fuelling conditions below the steady state buzz limits, buzz was apparent during transients. The reduction in buzz onset fuel air ratio was greatest during an idle to combat slam acceleration (Fig 4).

Examination of the engine transient (Fig 5) revealed the following. The stability characteristics of the control system allowed overshooting of reheat fuel flow at the end of the transient, this overshoot was found to vary with control system. However when modifications were introduced to prevent the afterburner fuel overshoot a reduction in buzz onset fuel air ratio was still observed. The transient also reveals that engine speeds, and therefore mass flows, are not stable this will give rise to variations in fuel air ratio. Examination of the main engine fuel flow trace shows that the overfuelling necessary to accelerate the engine is still occurring at the time that maximum reheat is achieved.

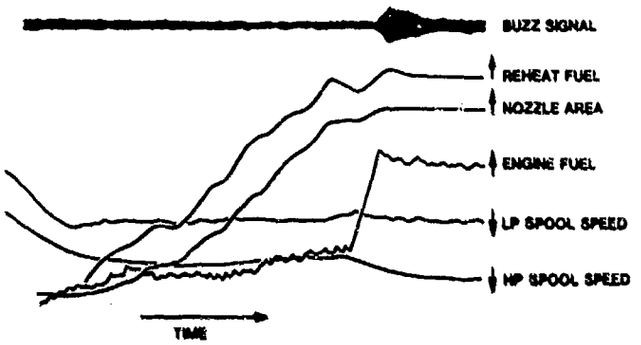


Figure 5 Engine/Afterburner Transient

The effects of inlet vitiation level on the buzz characteristic were examined on a full scale afterburner rig. It was possible to operate the rig at constant entry conditions in terms of mass flow, pressure and temperature whilst varying the level of vitiation in the core stream. This was achieved by injecting water into the core stream thereby increasing the preheater fuel flow required to achieve the core stream entry temperature. A buzz onset characteristic was generated for the rig operated in this way (Fig 6)

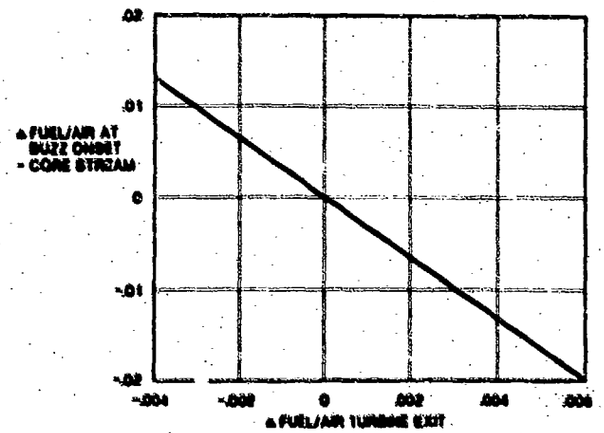


Figure 6 Effect of Inlet Vitiation on Buzz Onset (Rig Derived)

This shows that inlet vitiation has a powerful influence on the buzz onset point. Inlet vitiation and afterburner fuel cannot be exchanged on a 1:1 basis, the rig results indicate a ratio of 3:1.

To reduce the influence of the transient on buzz onset the control laws were modified such that the points of engine overfuel and achievement of maximum reheat fuel air ratio were separated in time

BUZZ ONSET VARIABILITY

Having established an afterburner/control system standard that gave acceptable performance in development it was found that when the engine entered the production phase a variation in afterburner fuel air ratio at buzz onset was evident. Over a sample of 50 engines a variation in fuel air ratio at +9% about the mean value was found. A detailed examination of production engine pass off statistics was carried out.

Initially the ambient atmospheric conditions at the time of pass test were examined (Figs 7 and 8) but as can be seen pressure and temperature level bore no obvious relationship to buzz onset fuel air ratio. Detailed geometric measurements of the afterburner systems were compared but again no obvious trends were found. Internal engine parameters, pressures, temperatures and bypass ratios (Fig 9) again showed no conclusive trend. Although later investigation revealed an underlying trend masked by other influences.

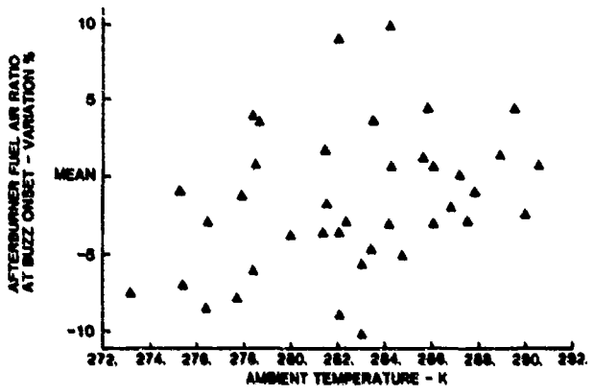


Figure 7 Influence of Ambient Temperature on Buzz Onset Fuel Air Ratio

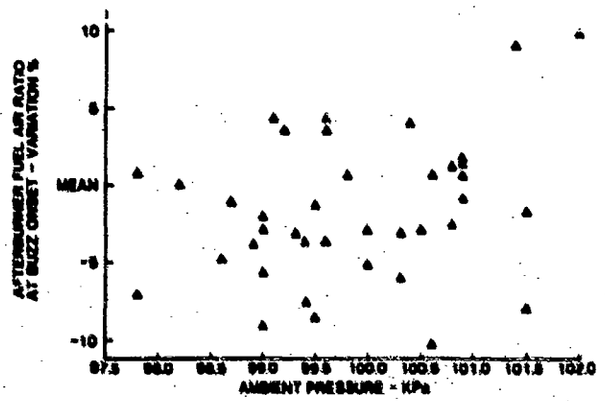


Figure 8 Influence of Ambient Pressure on Buzz Onset Fuel Air Ratio

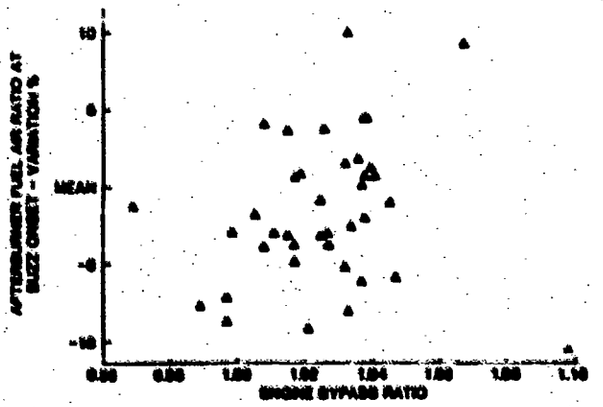


Figure 9 Influence of Engine Bypass Ratio on Buzz Onset Fuel Air Ratio

At this point a model of the engine and control system was set up into which variations in key parameters could be fed. This was coupled to a fixed buzz onset characteristic of the form shown in Fig 4. By systematically examining the effect variations in key parameters had on the afterburner fuel air ratio at buzz onset a picture of how the ±9% variation in fuel air ratio could occur was built up (Fig 10). This shows that some parameters have a strong effect whilst other key parameters have no effect on buzz onset fuel air ratio. This approach showed that the buzz characteristic could remain constant yet other factors could influence the onset fuel air ratio.

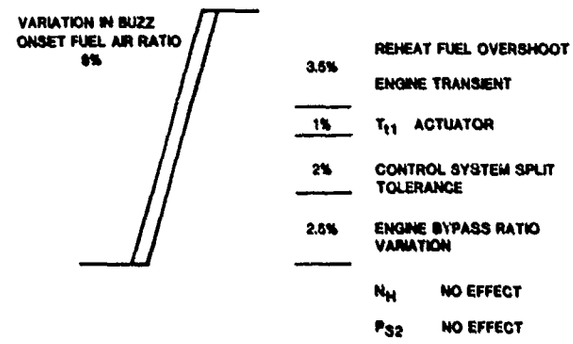


Figure 10 Effect of Engine and Control System Parameters on Buzz Onset Fuel Air Ratio

HARDWARE MODIFICATION

As part of the investigation into buzz onset variability the effect of build tolerances was examined No systematic dependence on any build detail was found, the afterburner was insensitive to build tolerances

During flow visualisation associated with this investigation it was noted that flow in the bypass stream had a radially outward component as it passed through the flameholder. As has been observed previously (Ref 1) fuel injected into such a stream follows the initial direction of the stream but in the cold bypass air, where vaporisation is low, the fuel does not subsequently follow the air flow. This results in fuel concentrations which it is known can lead to premature buzz onset.

A CFD model of the afterburner was set up to examine the flow in the bypass stream The flow paths produced by the model show (Fig 11) that the flow at the point of injection is angled at 12^0 to the axis. Changes were then made to the CFD model to determine if a simple modification to the hardware could eliminate the outward flow component. It was shown that a change to the flameholder profile (Fig 12) resulted in axial flow at the point of fuel injection.



Figure 11 Bypass Air Flowpath from CFD Model with Standard Flameholder Profile

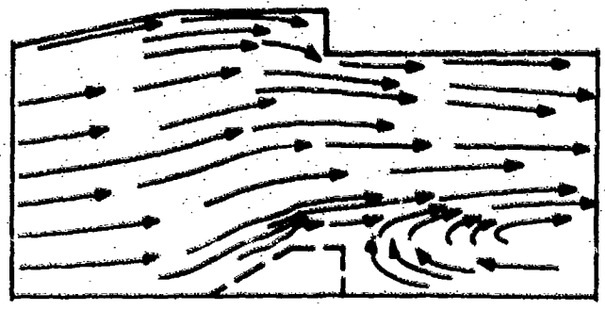


Figure 12 Bypass Air Flowpath from CFD Model with Modified Flameholder Profile

This flameholder profile was converted into engine hardware and its buzz onset characteristic compared with the standard system (Fig 13). This demonstrates an improvement in buzz onset of 22%.

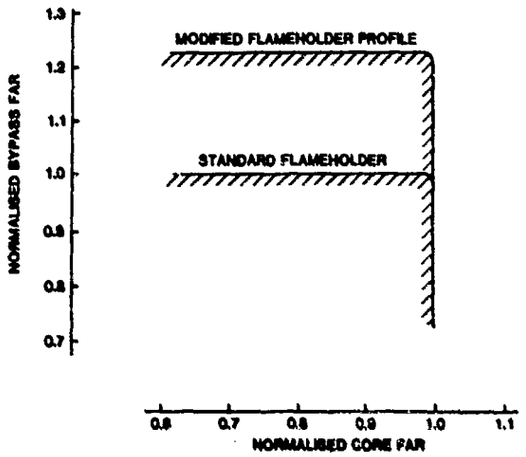


Figure 13 Effect of the Modified Flameholder Profile on the Transient Buzz Onset Characteristic

SCREECH

It has already been stated that screech is associated with acoustic waves in a plane at right angles to the jet pipe axis. If allowed to continue unchecked it's amplitude can rise very rapidly and severe damage follows (Fig 14). Failure is often associated with holes appearing in heatshields when the metal has cracked because of the cyclic pressure acting on overheated areas. A typical pressure spectrum taken during a screech event (Fig 15) contains several pressure peaks.

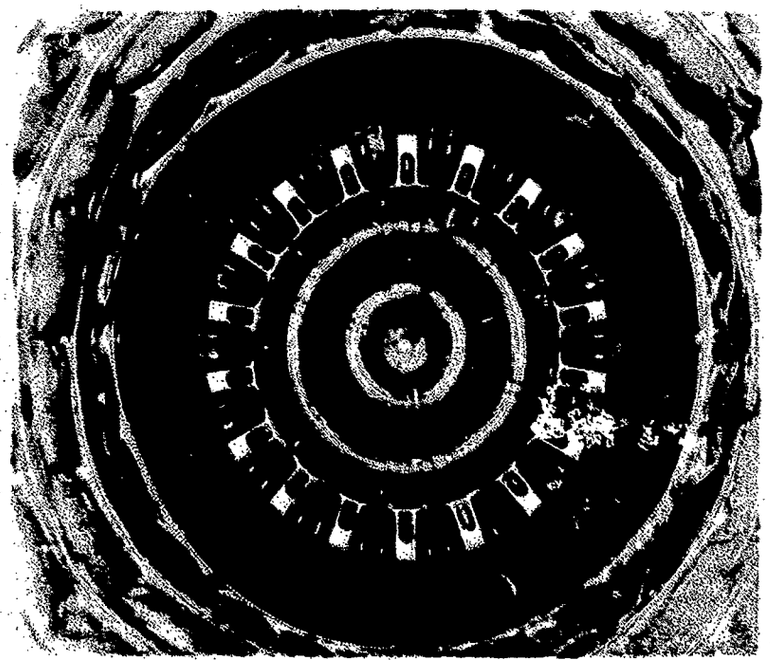


Figure 14 Typical Screech Damage

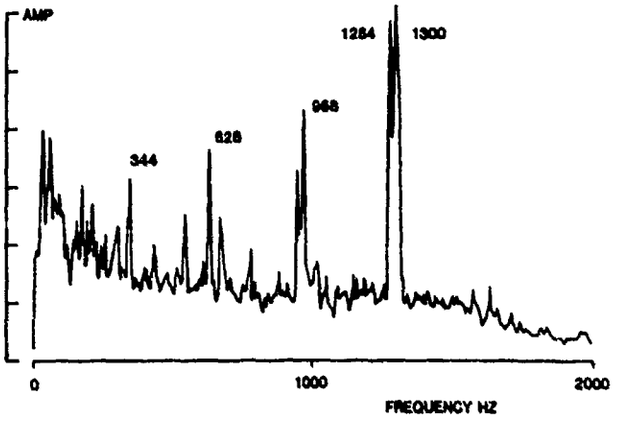


Figure 15 Typical Screech Frequency Spectrum

One approach to limiting the problem has been to provide passive damping using a perforated liner within the jet pipe. Cells associated with the holes in the liner act as helmholtz resonators and in this way limit screech amplitudes. Initially the liner geometry was configured such that the resonators were tuned to the dominant screech frequency. This resulted in a low porosity liner which was limited in effectiveness. It was found that as porosity was increased the screech damper became more effective although its helmholtz frequency was moving away from the measured screech frequency.

To explain this it is necessary to examine the damping curves of such screech liners. It is found that the low porosity liner has a very narrow peak to its damping capability, whilst as the porosity increases the damping curve broadens. This happens to the extent that higher degrees of damping can be achieved at the screech frequencies with a high porosity liner than with a "tuned" liner. This would not be true of a liner exactly matched to a screech frequency but this situation is difficult to achieve in practice.

In examining the factors which govern screech onset it was found, for a turbofan afterburner, that it was most dependent on bypass stream fuel air ratio and temperature (Fig 16). This suggested that the instability was being initiated in the bypass stream. This was further supported by the fact that when features were introduced into the bypass duct which resulted in varying but symmetrical pressure and temperature profiles at afterburner entry a reduction in the screech onset boundary was apparent.

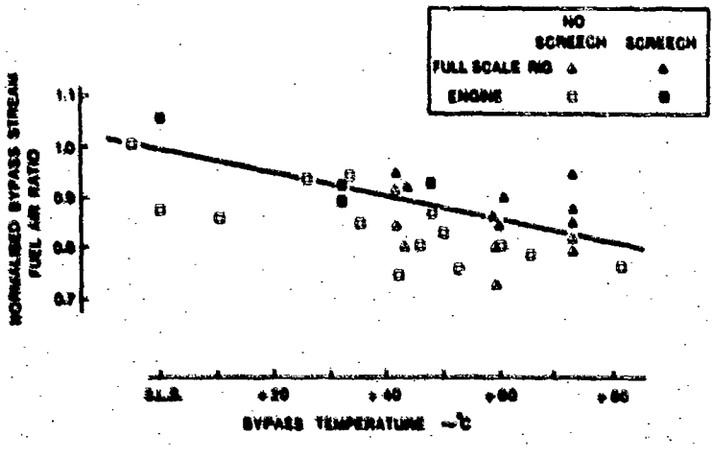


Figure 16 Screech Characteristic

REFERENCE

1 A SOTHERAN
High Performance Turbofan Afterburner Systems
AIAA-87-1830 23rd Joint Propulsion Conference

ACKNOWLEDGEMENT

This work has been carried out with the support of the Procurement Executive, Ministry of Defence.

DISCUSSION

S. Candel, Fr

Could you please explain how the prevaporizing system works.

Author's Reply:

The primary zone is fed by hot combustion products - the core gases. We have a mixing tube or vaporizer into which hot gas is fed with the fuel and in that way we get a relatively pre-vaporized stable primary zone.

C. M. Coats, UK

What is the reason for the flow separation on the upstream surface of the stabilizer in your flow-field calculation.

Author's Reply:

The flow separation is caused by the presence within the model, of a fuel manifold at this position.

DYNAMIC INSTABILITY CHARACTERISTICS OF AIRCRAFT TURBINE ENGINE COMBUSTORS

by

MJ Kenworthy, DW Bahr, P. Mungur, DL Burrus, and JM Mehta

GE Aircraft Engines
1 Neumann Way
POB 156301
Cincinnati, Ohio - 45215-6301

AJ Cifone

Naval Air Propulsion Center
POB 7176
Trenton, NJ - 08628

SUMMARY

Many aircraft turbine engine combustors exhibit dynamic instabilities at subidle and idle operating conditions. These instabilities can result in objectionable noise and, in some instances, compressor stall problems. To permit analytical assessments of these phenomena, an aeroacoustic model of these combustor instabilities was developed. To calibrate and validate this model, sector rig tests of the CF6-80A engine combustor were conducted. In these tests, the frequencies and amplitudes of the instabilities and the acoustic characteristics of the combustor were measured. Additional tests in a F101/F110/CFM56 sector combustor rig are planned.

The test results compare well with the theory. The following conclusions are drawn from the portion of the work completed to date.

1. Audible noise is a resonant acoustic wave within the cavity as predicted by the analytical model.

2. The acoustic wave responds strongly at the fuel-air ratio with the optimum time lag between the fuel injector and the heat release region, consistent with the analytical model.

3. The analytical model predictions are in generally good agreement with the CF6-80A combustor test data, but further experiments with better defined end conditions are being obtained for a more complete validation.

INTRODUCTION

Audible, dynamic pressure oscillations associated with the combustion process frequently occur in turbine engines, particularly development engines, at subidle and near idle conditions. These pressure oscillations are in the frequency range of 50 to 500 Hz. At GE Aircraft Engines, they are called growl at subidle and howl near idle.

These dynamic pressure oscillations can cause compressor stall margins to be affected resulting in engine stall. They can also result in increased start times, objectionable noise levels, and in some cases hardware failure. This phenomena could become more severe for future gas turbine combustion systems having substantially wider operating ranges.

The problem is not always duplicated in combustor component or sector tests and this has greatly limited exploration. These oscillations are often first identified in initial engine tests which typically have only one or a very few dynamic pressure measurements. Subsequent testing has also had less instrumentation than needed to verify analytical models. These data are not sufficient to estimate the combustor end reflection characteristics and other detailed features of the acoustic mode present.

The effort described herein involves the acquisition of this needed detailed data in sector combustor test rigs. The objective of this effort is to document the character of the acoustic noise in sector combustor test rigs and to relate these findings to an available analytical model. Ultimately, the intent is to apply the analytical model to engines as a means of identifying design modifications to correct instability problems in existing engines and of avoiding such problems in the design of combustors for new engines. To permit the use of the analytical model for this program in any given engine, data on the acoustic and reflection characteristics of the engine compressor and turbine will also be needed.

The growl-howl phenomena is believed to correspond to a standing acoustic wave in the combustor and is influenced by the acoustic reflection characteristics of the compressor engine inlet region and of the turbine. The wave is also influenced by the cross sectional area variation in the combustor, the combustor temperature rise along the length, and the specific acoustic driving effort of the combustion heat release itself. An analytical model

is available for evaluating the various acoustic resonant modes that are possible. The tendency of the combustion heat release to drive one or more of these resonances is then explored by examining the phase relationship between the source of fuel-air variations at the fuel injector, which result in a fluctuating heat release, and the associated fluctuating pressure.

This investigation was initially conducted with a CF6-80A sector combustor, which was found to have a howl frequency near the frequency encountered in an engine. It was, therefore, postulated that this sector would be suitable for investigating the phenomena. The experimental results acquired with this test rig are presented in this paper.

In addition, the US Navy under its Aircraft Propulsion Exploratory Development Project, is sponsoring a more detailed effort to investigate dynamic instabilities in an advanced military combustion system. The program objectives are: (1) Characterize the combustor system dynamic aerothermoacoustic instability phenomenon; and, (2) Incorporate the results into the overall combustor design methodology utilized for current and future systems. Testing under this program is currently being carried out with a sector of another combustor, the F110/F101/CFM56 engine combustor. In this case, blockage is provided at the combustor exit to simulate the turbine stator, which generally operates with choked conditions in the engine. Variable inlet lengths are also provided to permit fine tuning of acoustic resonances, and to permit different fuel-air conditions in the combustor to be studied. The effect of fuel type will be investigated. In addition to the frequencies excited naturally by the combustion process, the system will also be excited by modulating the fuel flow and modulating the air flow. The planned scope and content of these investigations are also presented in this paper.

The prior related work includes the analytical model derived basically for augmentors, Reference 1, and the further exploration of that model together with experimental augmentor work, Reference 2. A specific exploration of CF6-50 combustor noise in an engine was provided in Reference 3. However, none of the available references involved specific instabilities in the main combustor or detailed instrumentation such as provided in this report.

ANALYTICAL MODEL

The intent of these efforts is to relate the sector combustor test results to an available analytical model. This model was developed previously at GE Aircraft Engines, but was never adequately validated by test data.

The analytical model representing the growl-howl phenomena is a combustion dynamics model concerned with the physics of unsteady combustion. It involves making estimates of the unsteady pressure and unsteady velocity fields excited by an unsteady heat release rate in a ducted environment.

If the unsteady heat release rate $\dot{Q}(x,t)$ is specified as a function of time (t) at some spatial location (x), the unsteady pressure field may be evaluated by solving the appropriate governing equation with unsteady heat release as a source term. The unsteady pressure field must satisfy not only the governing equation but also boundary conditions at the compressor, at the turbine inlet nozzle, and across the flame/source plane where the heat release is specified.

Governing Equation - The analytical model is based on a general equation governing the unsteady compressible pressure field excited by unsteady heat release rate, unsteady mass flux and unsteady aerodynamic forces, and may be derived from the conservation of mass, momentum and energy equations. It may be expressed as an inhomogeneous convected wave equation in the form:

$$\nabla^2 p - \frac{1}{\bar{\rho}} \frac{\partial \bar{\rho}}{\partial x_i} \frac{\partial p}{\partial x_i} - \bar{\rho} \frac{D}{Dt}\left(\frac{1}{\bar{\rho}\bar{c}^2} \frac{Dp}{Dt}\right) + \bar{\rho} \frac{D}{Dt}\left(\frac{1}{\bar{c}_p T} \dot{Q}\right) + \frac{\partial \dot{F}_i}{\partial x_i} + \bar{\rho} \frac{\partial \dot{u}_j}{\partial x_i} \frac{\partial u_j}{\partial x_i} \qquad (1)$$

where ∇^2 = three-dimensional laplacian

and $\frac{D}{Dt} = \frac{\partial}{\partial t} + u_i \frac{\partial}{\partial x_i}$

In the above equation, the left side represents the convected wave equation for the unsteady pressure field $P(x_i,t)$ and includes interactions with nonuniform mean flow and nonuniform mean temperature fields. The right side of the above equation corresponds to various possible sources of excitation. The first source is associated with unsteady heat release rate.

The second term is associated with rate of change of mass flux associated with vibrating surfaces or rotating blades of finite thickness. The third term is associated with unsteady aerodynamic forces, such as those induced on fan and compressor blades in the presence of unsteady flow fields; it is relevant when modeling the dynamics of compressors or fans. The fourth term is associated with Lighthill's turbulent noise source and is relevant in estimating jet noise.

For a coupled compressor-combustor system with unsteady heat release and unsteady blade force, Equation 1 must be solved with these two source terms specified independently or evaluated in a feedback loop. Depending on the nature and phasing of such a feedback loop, the coupled system may be stable or unstable.

For the combustor dynamic model, only the unsteady heat release term is relevant. The compressor duct acts only as an acoustic load to the combustor in the form of a complex reflection coefficient at the inlet diffuser of the combustor. In this way, the combustor dynamic analysis may be restricted to the combustion chamber.

Unsteady Heat Release - Before evaluating the unsteady pressure and velocity fields from the solution of Equation 1 driven only by the first or the unsteady heat release term, some comments about the unsteady heat release term are appropriate.

The heat release rate may be estimated from a quasi-steady perturbation of the steady state heat release characteristics as a function of fuel-air ratio. The amplitude of unsteady heat release rate may then be related to the amplitude of fluctuations of the fuel-air ratio and the slope of steady state heat release characteristics. Fluctuations in fuel-air ratio may originate from any of the following possibilities:

1. Steady compressor discharge air mixing with time dependent fuel flow.
2. Unsteady compressor discharge air mixing with steady fuel flow.
3. Unsteady mixing of steady air and steady fuel flow (includes laminar or turbulent mixing).

In any case, an unsteady fuel-air ratio produces unsteady heat release rate, which in turn produces an unsteady pressure field. The estimation of this unsteady pressure field is discussed next as a solution of Equation 1, driven only by the unsteady heat release rate. Whether in a transient or a periodic form, the unsteady heat release rate can always be reduced to its frequency components.

To solve Equation 1, the source term is assumed to be spatially localized at the flame region. This allows Equation 1 to be solved by a Green function method with boundary conditions on either side of the flame in addition to those at the inlet and exhaust planes.

The governing equation (1) has been solved in the frequency domain for time harmonic variation of the heat release rate. The analysis requires specification of the axial distributions of the flow Mach number, of the temperature including a temperature jump at the flame, of the cross sectional area variations, and of the complex reflection coefficients (amplitude and phase) of the inlet and exhaust. Figure 1 shows the distributions used. The unsteady pressure field may be expressed as the sum of modal solutions:

$$P(R,\theta,z,t) = \frac{\dot{q}(\omega)}{c_p T} \sum_m \sum_n A_{mn}(\omega,\ldots)\, \psi_{mn}(R,z,\omega)\, e^{-j\omega t + jm\theta} \qquad (2)$$

where

$A_{mn}(\omega,\ldots)$ = spatial distribution of each mode

$\psi_{mn}(R,z,\omega)$ = spatial distribution of the relevant mode. It is made up of Bessel functions and numerically integrated modified cosine functions

$\dot{q}(\omega)$ = Fourier transform of the rate of change of the unsteady heat release rate $\dot{q}(x,t)$

The spatial and spectral distributions of each mode are obtained by numerical integration of a reduced form of Equation 1. The computer programs for generating these distributions exist.

The solution for the unsteady pressure field as expressed in Equation 2 corresponds to a forced response of the combustor fluid excited by the unsteady heat release spectrum $\dot{q}(\omega)$.

Standing Wave Driven by Heat Release - Up to this point, discussion has focused on the normalized forced response of the combustor. The actual spectrum of the unsteady pressure field may be evaluated from Equation 2 which involves the product of the unsteady heat release spectrum $\Delta\dot{q}(\omega)$ and the normalized response spectrum $A_{mn}(\omega)$. For a given combustor, $A_{mn}(\omega)$ is fixed. The unsteady heat release spectrum, however, does depend on the manner by which the fuel-air ratio is changed.

Under some conditions, combustors are known to be unstable and become self-excited. In such situations, a positive feedback loop is necessary. The fuel-air ratio becomes modulated by either the unsteady pressure or unsteady velocity produced by the unsteady heat release. The selected frequency of instability is governed by a time lag made up of different mechanisms, including acoustic propagation, fluid convective transport, and thermal rate of vaporization.

If a simple and lossless standing wave exists in a constant area duct, the wave would have a sine or cosine wave shape perhaps as shown in Figure 2a. The amplitude changes from positive to negative with time. A null or zero pressure condition may exist at one or more points along the duct. The phase is constant from one null to the next if it exists, and changes by 180° at the null.

At the same time, the velocity varies as illustrated in Figure 2b. The velocity variation is maximum where the pressure is null. The velocity variation becomes zero where the pressure is maximum.

In Figure 2c the pressure variation versus time is plotted. The fuel flow will be affected by the pressure of this standing wave. When the pressure is lowest the fuel will be highest. This will create a maximum fuel-air ratio. The heat release in the combustion process does not occur immediately. The fuel air mixture travels at least part way around the recirculation zone in the dome region of the combustor before releasing the major portion of its heat. Some reaction may also occur downstream of the recirculating zone. If the average travel time to the heat release, as illustrated in Figure 2c, occurs when the pressure is at maximum, then the heat release will drive the standing wave. If it were to occur when the pressure was at minimum it would counteract or damp the standing wave. Thus, a time equal to that of one-half wavelength would need to exist between the fuel nozzle and the heat release region for maximum driving.

It should be noted that this phenomena will be affected by the exact configuration of the fuel system. If the fuel nozzle pressure drop is not located at the rig but is upstream at the fuel nozzle distributer, then the speed of sound in the fuel will cause a slight phase lag. However, as will be seen the fuel pressure drop is so high that this fuel flow modulation is not the driving mechanism in the present experiments.

Figure 2d illustrates a second mechanism for driving the standing wave. In this case the air velocity is seen to vary at the fuel nozzle position. If the fuel flow is nearly constant then this air flow variation will result in a fuel-air variation. Again, if the travel time for this fuel-air ratio variation is such that the heat is released primarily at the high pressure portion of the wave, then the heat release will drive the standing wave. This travel time would be three-fourths of that wavelength. However, if the pressure node were downstream instead of upstream of the fuel nozzle region, then the time for driving would be equal to that of one-fourth wavelength.

While the above is the mechanism utilized in this paper, one more mechanism should be mentioned. With a choked burner exit, the high fuel-air region could reach the burner exit as the high pressure region of the wave. It would then drive the standing wave. More mixing of the dynamic fuel-air mixture would take place by the exit, and this might mitigate the effect.

In the real case the standing wave is not so simple. Flow, flow gradients, temperature gradients and acoustic losses are also present. These effects modify the amplitude and relative phase distributions along the duct. No longer will there be a 180° phase shift at a null. The phase is constantly changing with axial distance and the phase relationship between velocity and pressure is affected. The analytical model for the standing wave calculates these complexities. It also accounts for cross sectional area variations. It does not as yet account for the presence of the combustor liner and its exact effect on the standing wave. With these changing phases, the time lag between the fuel nozzle and the heat release region will also have an acoustic time lag associated with the phase difference between the two locations. The average time to the heat release region includes not only the travel time, but also any additional time required to vaporize, mix, and burn this fuel. Thus, the major effect of fuel type is expected to be associated with the time to vaporize the fuel.

EXPERIMENTAL TEST RIG

The testing completed to date involved the use of a five-swirl cup (60°) sector of a CF6-50A combustor. The test rig is shown in Figures 3 and 4. This test rig featured an inlet plenum section, a prediffuser section, combustor chamber housing, and an exhaust section. The inlet plenum was attached to a heated nonvitiated air supply. The exhaust section contained a water quench system to cool the combustor exhaust gases prior to passing through the

downstream back pressure control valve, and out of the test facility exhaust. JP5 fuel was supplied through a manifold feeding a set of five engine-type fuel nozzles. Each fuel nozzle was flow calibrated prior to installation in the test rig.

The test rig consisted of a true 60° sector of the combustion system of the CF6-80A engine. However, the combustor inlet and outlet conditions of the engine were not duplicated. Specifically: (1) The prediffuser section inlet provided no simulation of the blockage from the compressor outlet guide vanes; (2) The exhaust section inlet provided no simulation of the blockage from the high pressure turbine nozzle diaphragm. These two features obviously affected the acoustic reflection characteristics at these two extremities of the test rig. Being a 60° sector of a full annular combustor, the test rig featured side walls. As such, the test rig did not afford a representative simulation of the circumferential acoustic wave characteristics that might occur in a full annular combustor.

As shown in Figure 5, the test rig instrumentation included two Plane 3.0 total pressure probes; one Plane 3.0 gas stream thermocouple; four combustor dome static pressures providing a pair of measurements of the combustor dome pressure drop; and one gas stream thermocouple in the exhaust section. This static instrumentation was used to establish and monitor the combustor test rig operating conditions. Combustor fuel flows were set using a turbine type fuel meter calibrated in the range of 0 to 1,000 pounds per hour. In addition to this static instrumentation, an array of dynamic pressure instrumentation was employed to monitor and record resonance activity within the combustor test rig. Included in this array of dynamic pressure instrumentation were six dynamic air flow type sensors.

Test rig static instrumentation was hooked up to digital display devices as well as a multichannel Sanborn recorder. The digital displays were monitored and recorded to document the combustor operating conditions at each test point. The Sanborn recording provided a continuous time history of the operating conditions. All dynamic instrumentation included a set of amplifiers to boost sensor output signals. The amplified signals were then split to a 14 channel tape recorder for postprocessing going to a spectrum analyzer device with channel selector to provide on line reduction of signals from the individual sensors into their frequency spectrums. A hard copy device was attached to provide hard copies of the spectrum displays. A photograph of the dynamic instrumentation data acquisition equipment is shown in Figure 4.

Data could be obtained through the complete range of fuel-air ratios from lean blowout to very high levels corresponding to engine accelerations. The pressure levels could be varied through the subidle region from one atmosphere to three atmospheres with unvitiated inlet air up to 300°F.

EXPERIMENTAL RESULTS

The test results obtained with the CF6-80A sector combustor showed a significant amplitude at one fuel-air ratio. A similar but slightly different frequency occurred at other fuel-air ratios, but with much lower amplitude. Figure 6 shows these results.

While the approximate frequency near 300 Hz exists at all fuel-air ratios, only one of these fuel-air ratios resulted in a high amplitude. The specific characteristics associated with this one fuel-air ratio were examined in detail with the analytical model.

Figure 7 shows spectrums from the dynamic pressure instrumentation along the axial length of the test rig. These data show that a single sharp discrete frequency, was measured at every measurement station. They are all at the same frequency, but at different amplitudes.

Figure 8 shows the amplitude and the phase relationship for these measurements. These data were used for comparison with the analytical model. These data show a gradual change in phase from the front to the back of the sector. As shown in the next section, this is consistent with an acoustic mode standing in the sector.

A reproducible oscillation was encountered and its characteristics were documented with dynamic pressure measurements showing consistent phase relationships along the length and a unique fuel-air ratio at which this resonant standing wave in the sector is driven to high amplitudes. This data base permits the use of the analytical model to analyze the measured waves, to determine the end reflection characteristics of the test rig and to relate the acoustic driving mechanism to the unique phase relationship between the fuel nozzle and heat release region at the driven fuel-air ratio.

COMPARISON WITH ANALYTICAL MODEL

The measured results were compared with the analytical model for the standing acoustic wave in the test rig. The calculation of this standing acoustic wave, requires assumptions for the end reflections at the front and the back of the test rig.

At the inlet, the entrance is approximately an open end. The reflection coefficient, however, needs correction factors to account for the exact shape of the opening, the flow effects, and any effects of the inlet plenum. Estimation of the reflection coefficient at the exit end is more complicated. In the passages around the combustor, the passage ends at an acoustically hard end. However, in the hot gas path of the combustor, the passage ends in an

approximately open end, 6 inches downstream of the inner and outer passage end. Thus, some combination of these two different ends must be used in the model. In addition, the open end, corrections are needed for the exit shape, through flow effects, and exit plenum effects. Also, corrections for the temperature differences between the burner and the quenched plenum are needed.

Calculated reflection coefficients using shape and through-flow corrections were estimated, References 4 and 5. However, the actual reflection coefficients finally adopted were determined by comparing theoretical calculations to the measurements. Figure 9 shows the results of these calculations. The best match with the data, particularly the frequency data, was selected for making further data-theory comparisons. The final reflection coefficients used were $0.5\ \exp(200^{o})$ for the inlet and $1.33\ \exp(165^{o})$ for the exhaust. These coefficient values include a real part, which is the first constant and represents the fraction of energy reflected, and an imaginary part as a power of the natural logarithm base, which represents the phase of the reflected wave.

With these reflection coefficients, the model predictions compare with the data as shown in Figure 10. The amplitudes and phase relationships are in reasonable agreement. Figure 7 shows a low amplitude near the dilution holes and a high amplitude near the locally closed aft end, measurement Station 7. The region through the combustor liner is more complicated and is beyond the scope of the present analytical capabilities. Amplitude data are compared, therefore, only in the earlier portion of the test rig, measurement Stations 1 - 3.

An explanation in terms of the acoustic wave present for the high amplitude case shown previously in Figure 6 is as follows. For the frequency of 285 Hz, the associated time period for one wavelength is 3.6 msecs. The time lag between the fuel-air variation at the fuel injector and the heat release at the flamefront, may be one-half wavelength or 1.8 msecs or perhaps even one-quarter wavelength, as indicated in Figure 1. This 1.8 msec is on the order of the time for fuel to travel around the recirculation zone to reach the burning region. For flow Mach number of 0.2 and convection Mach number of 0.5 of the free stream, a time lag of 1.8 msec is calculated if the flame region is 2.4 inches downstream of the fuel nozzle.

Now if the time lag is optimum at a fuel-air ratio of 0.020 then at other lower amplitude fuel-air ratios, it must not be optimum. As the fuel-air ratio becomes richer, more oxygen is consumed and the average distance to the heat release region must increase to finally reach the additional oxygen. This will increase the time lag. Also as the burning temperature goes up because of increased fuel-air ratio, the frequency of the standing wave resonant in the test rig will increase and hence, the optimum time lag will in fact decrease as indicated in Figure 11. Thus, the time to reach the flamefront does not drive in phase with the standing wave at fuel-air ratios either above or below the strong resonance condition of the heat release. Accordingly, the optimum fuel-air ratio can be attributed to the time lag of the heat release.

FUTURE WORK

The next effort will be conducted with the F110/F101/CFM56 sector combustor. The test rig exit will have the turbine stator blockage simulated. Thus, at sufficiently high fuel-air ratios the exit will be choked corresponding to a close acoustic end. With both the combustor and the inner and outer passages ending closed the downstream end reflection will be much better defined.

The inlet end will be variable permitting the optimum fuel-air ratio to be varied due to the frequency change. This will provide some quantification of the time lag The end reflection will also be better determined in the constant area inlet region. At some condition this reflection will simulate the reflection from the engine compressor.

The F110/F101/CFM56 sector combustor test rig configuration is shown in Figure 12. The internal portion of the adjustable length inlet section is housed entirely within the plenum chamber section. Threaded rods, driven from outside the plenum section, are used to move the male portion of the inlet section into or out of the external portion. Inlet length adjustments up to 15 inches can be obtained.

A total of 13 dynamic pressure transducers are available to monitor and record the dynamic response characteristics of the combustor. Three of these transducers are incorporated into a probe to be installed inside the male portion of the adjustable length inlet section. Nine additional transducers are located along the test rig cold flowpath. A single specialized transducer (No. 6 indicated in Figure 12), is immersed flush with the inside surface of the combustor outer cooling liner. Access for this probe is obtained by using one of two spark igniter ports featured on the test rig. The purpose of this probe is to monitor and record the dynamic response activity within the hot flowpath of the combustor and later correlate with measurements made in the cold flowpath. This specialized probe has been used for similar purposes on full engine tests, and will be available for use in this testing effort. In general, all transducers are circumferentially centrally located along the 90^{o} (five cup) sector combustor test rig. Transducers No. 8a and No. 8c (refer to Figure 12) will be located near the side wall of the sector to monitor transverse mode activity.

Best Available Copy

As a part of the planned testing, the effects of fuel type will be determined. Also, the effect of driving the acoustic wave by fuel modulation and air modulation will be documented.

CONCLUSIONS

1. Audible noise is a resonant acoustic wave within the cavity consistent with the analytical model.

2. The acoustic wave responds strongly at the fuel-air ratio with the optimum time lag between the fuel injector and the heat release region, consistent with the analytical model.

3. The analytical model seems to be well verified by the CF6-80A combustor test data, but further data with better defined end conditions are needed for a more complete validation.

5. Further experiments, which will be even more definitive, are in progress.

REFERENCES

1. Smith, GE and Bastress, EK, "Propulsion System Flow Stability Program (Dynamic), Phase II Final Technical Report, Part X Combustion Instability Model Program User's Manual", Report No. AFAPL-TR-69-113, Feb., 1970.

2. Kenworthy, MJ, Woltmann, JE, and Corley, RG "Augmentor Combustion Stability Investigation", Report No. AFAPL-74-TR-61, August, 1974.

3. Huff, RG, "The Effect of Acoustic Reflections on Combustor Noise Measurements", Paper No. 84-2323, J. Prop., Vol. 2, No. 1, Jan., 1986.

4. Morse, PM and Ingard, K, "Theoretical Acoustics", McGraw Hill Publishers, 1968.

5. Munger, P and Plumblee, HE, "Influence of the Jet Exhaust Flow Field on the Acoustic Radiation Impedance of a Jet Pipe Opening", AIAA Paper No. 79-0676, March, 1979.

Governing Equation:

$$\nabla^2 p + a(z)\frac{\partial p}{\partial t} + b(z)\frac{\partial p}{\partial t} - \frac{\partial}{\partial t}\left[\frac{1}{c^2}\frac{\partial p}{\partial t}\right] = \frac{\rho_0}{C_p T}\frac{\partial \dot{Q}}{\partial t}$$

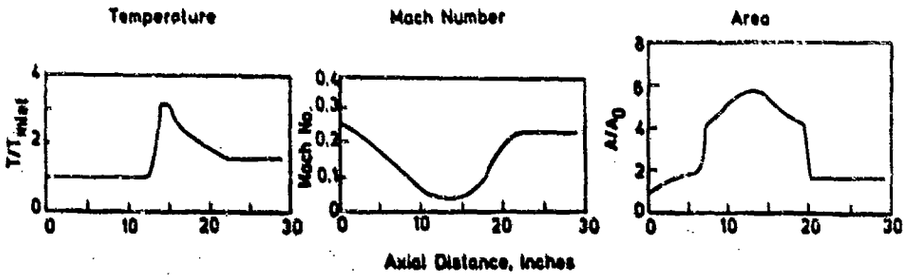


Figure 1. Inputs to Governing Equation.

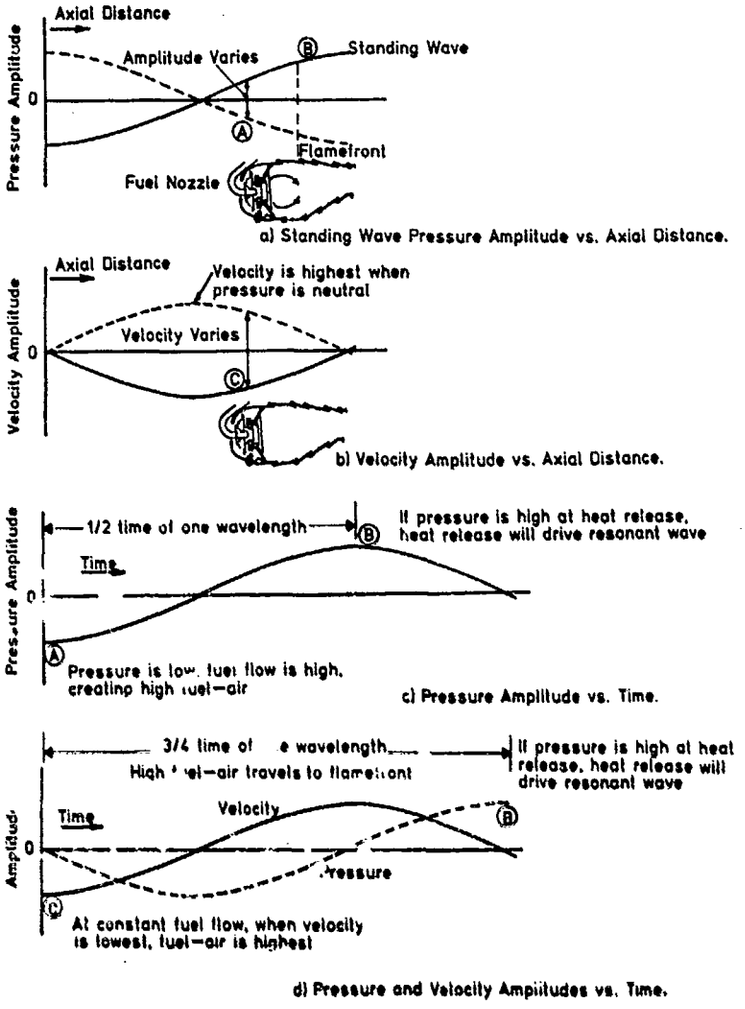


Figure 2. Simple Standing Wave in Straight Duct with No Acoustic Losses.

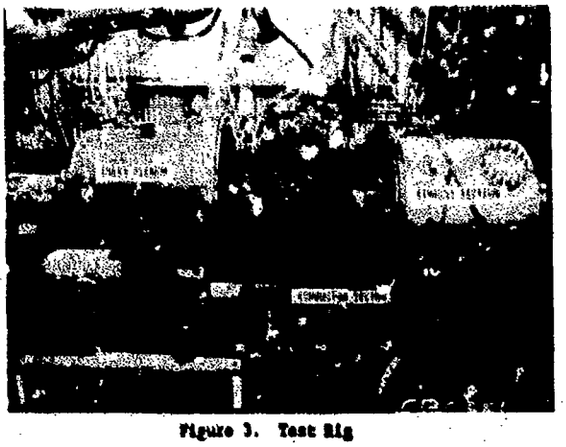


Figure 3. Test Rig

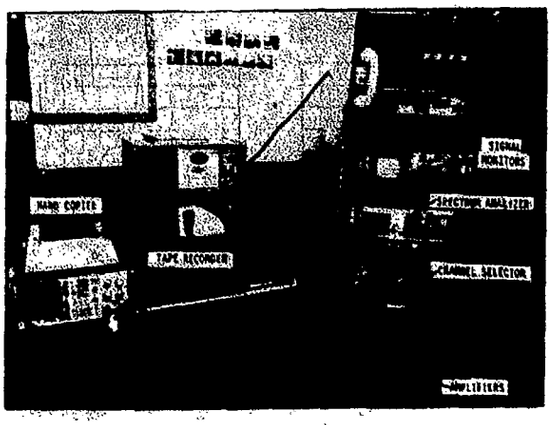


Figure 4. Resonance Reading in Control Room.

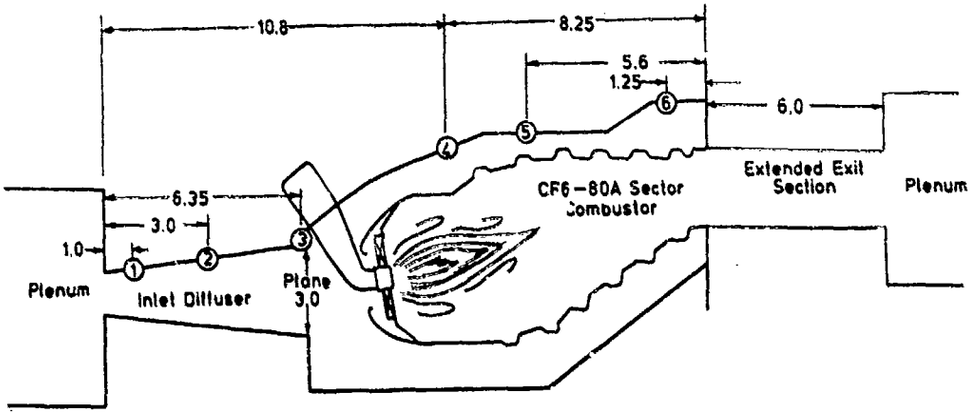


Figure 5. Test Rig/Instrumentation Schematic (dimensions in inches).

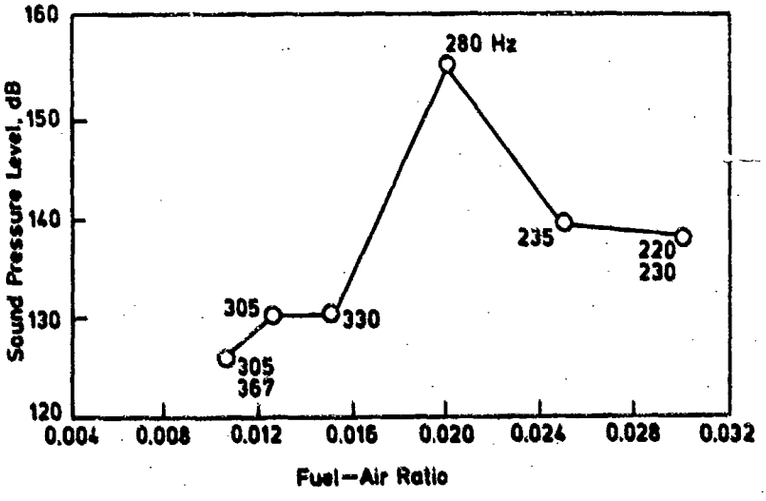


Figure 6. High Amplitude Shown at One Fuel-Air Ratio.

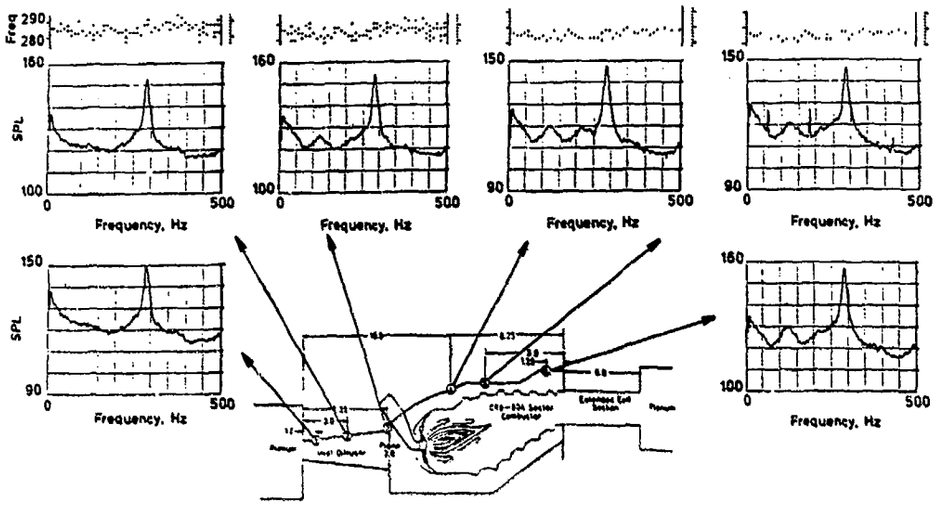


Figure 7. Natural Howl Spectra at Different Spatial Locations Inside Combustor (dimensions in inches).

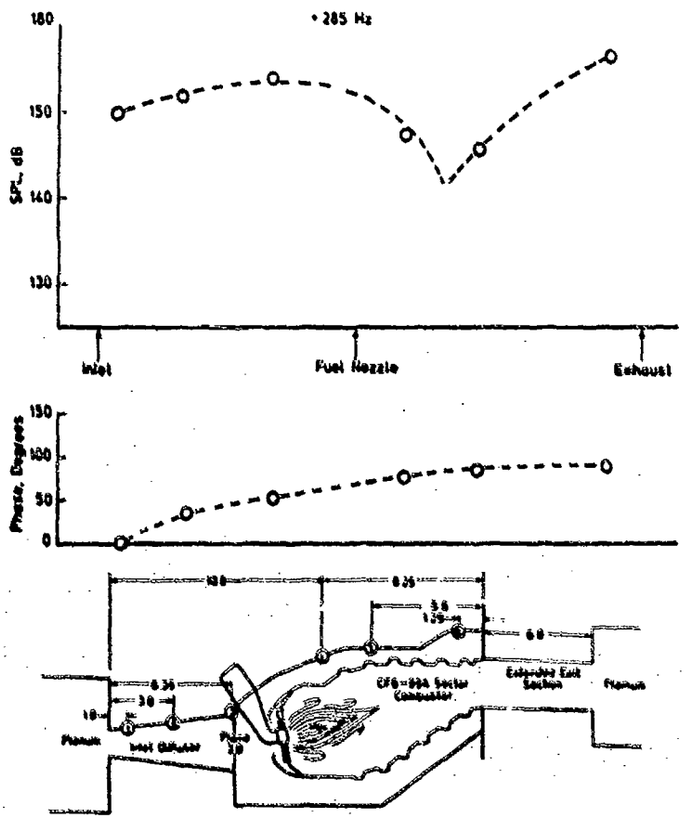
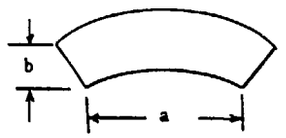


Figure 8. Spatial Distribution of SPL and Relative Phase (dimensions in inches).

$$z = \frac{1}{16} k^2 (a^2 + b^2) - j \frac{k}{\pi} \left[\frac{a^2 + ab + b^2}{a + b} \right]$$

$$\sigma = \frac{z - 1}{z + 1}$$



AT 300 Hz, INLET: $0.77 \exp(j\ 131^0)$
EXHAUST: $0.83 \exp(j\ 139^0)$

AFTER CORRECTIONS DUE TO FLOW:
INLET: $0.40 \exp(j\ 131^0)$
EXHAUST: $1.31 \exp(j\ 139^0)$

DATA MATCHED VALUES; GUIDED BY ABOVE ANALYSIS:
INLET: $0.50 \exp(j\ 200^0)$
EXHAUST: $1.31 \exp(j\ 165^0)$

Reference 4. Morse, PM and Ingard, K. "Theoretical Acoustics," McGraw Hill Publishers, 1968.

Reference 5. Mungur, P and Plumblee, HE. AIAA Paper No. 79—0676, March 1979.

Figure 9. Analytical Evaluation of Reflection Coefficients.

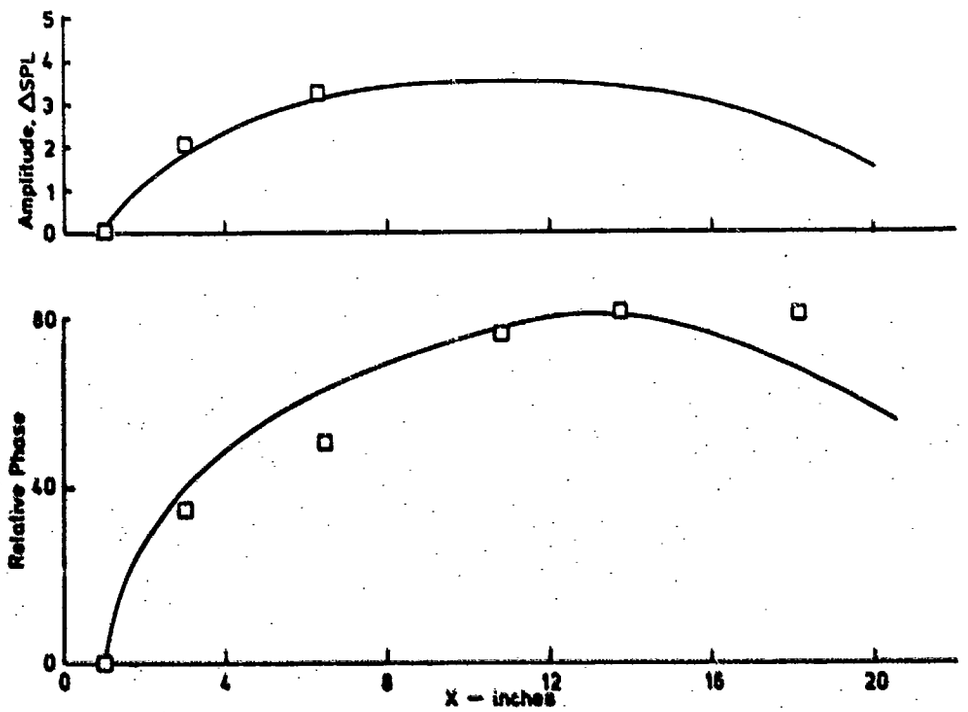


Figure 10. Comparison of Measured and Calculated Amplitude and Phase Relationship.

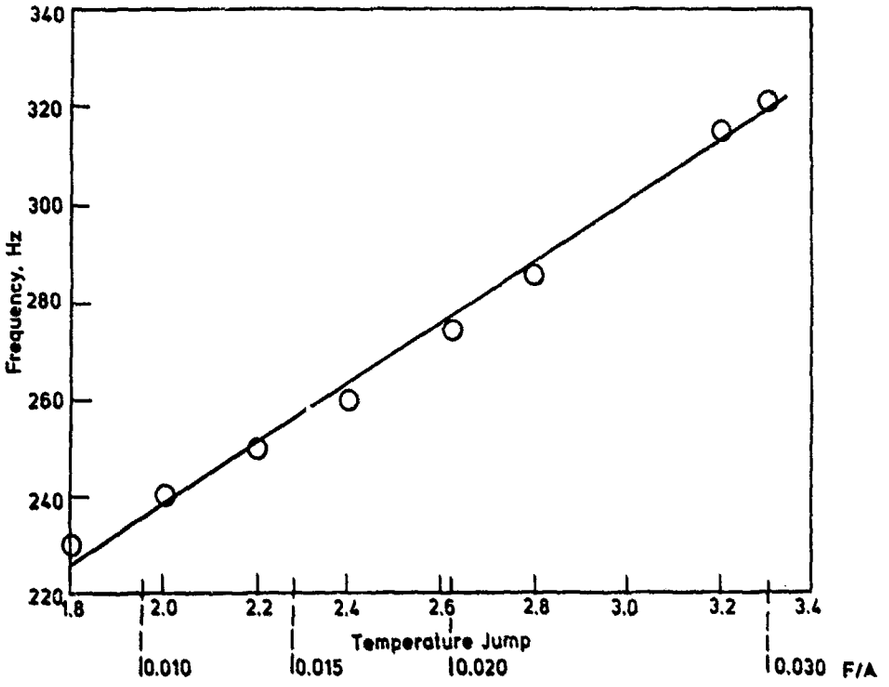


Figure 11. Time Lag Variations with Fuel-Air Ratio.

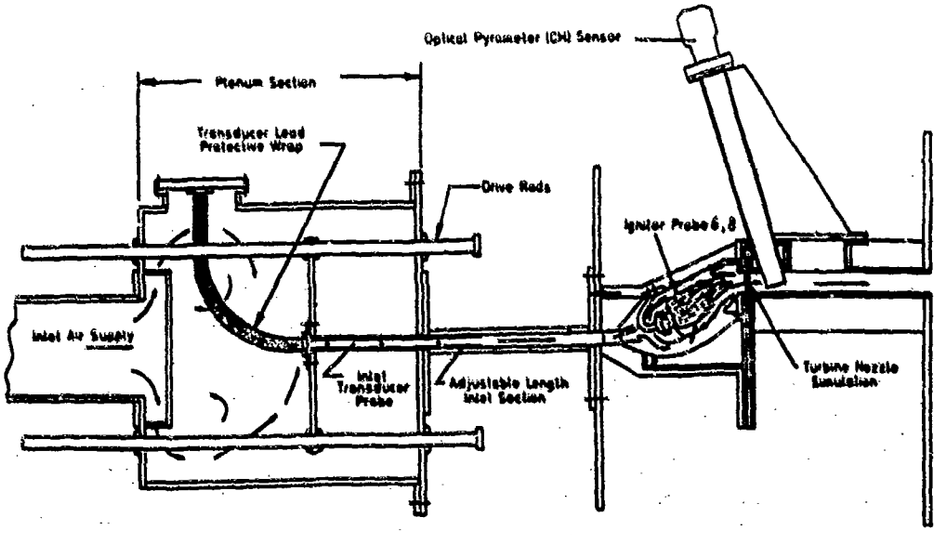


Figure 12. Test Rig Configuration for Elevated Pressure/Temperature Operation.

DISCUSSION

S. Candel, Fr

The data presented in your paper essentially describes the influence of the fuel-air ratio. Experiments performed at our laboratory on a small scale combustor indicate that the mass flow rate also determines which instabilities become dominant in the low frequency range. Did you also vary the mass flow rate and could you describe its influence?

Author's Reply:

Yes, we have done experiments with the mass flow rate changed. The mass flow change does cause the resonant frequency to change a bit and you will see that result in the data. I did not show that data here.

RECHERCHE EXPERIMENTALE SUR LA STABILITE DES PETITS MOTEURS FUSEES A ERGOLS STOCKABLES

par Robert FOUCAUD, Renaud LECOURT

Office National d'Etudes et de Recherches Aérospatiales
29, Avenue de la Division Leclerc
92320 CHATILLON (FRANCE)

Résumé

Un montage a été développé à l'ONERA pour quantifier la stabilité du fonctionnement d'un petit moteur fusée à ergols stockables et déterminer la sensibilité de l'injection aux phénomènes acoustiques. La méthode utilisée consiste à déstabiliser périodiquement un petit propulseur autour de son premier mode longitudinal, par une modulation intermittente du col de la tuyère, et à mesurer l'amortissement des oscillations ainsi déclenchées. Les dimensions du moteur sont choisies pour que la fréquence excitée soit très voisine de celle susceptible d'apparaître naturellement, en mode tangentiel, sur le moteur réel étudié en parallèle.

Deux types d'injecteurs ont été essayés : le premier correspond à une injection axiale au fond avant de la chambre, où le phénomène acoustique prépondérant est une oscillation de pression ; le second est caractérisé par une injection radiale effectuée à mi-chambre afin que les oscillations acoustiques portent de façon préférentielle sur la vitesse. Une étude paramétrique a été menée en changeant successivement : la pression moyenne de fonctionnement, les caractéristiques de l'injecteur, les ergols, la longueur de chambre et l'amplitude initiale des oscillations.

Les résultats obtenus constituent une base précise pour valider les codes de calcul, et ils mettent en évidence l'importance relative des oscillations de pression et de vitesse sur l'injection. En outre, les tendances enregistrées se comparent assez favorablement aux observations faites sur le moteur réel. Le montage mis au point s'avère donc un outil potentiel précieux pour l'aide au développement des propulseurs biliquides.

EXPERIMENTS ON STABILITY OF SMALL STORABLE LIQUID PROPELLANT ROCKET MOTORS

Abstract

An experimental device was developed at ONERA in order to quantify the stability of a storable liquid propellants rocket motor and to measure the sensitivity of the injection zone to an acoustic disturbance. The method consists in a periodic destabilization of a small rocket near its first longitudinal acoustic mode by means of an intermittent modulation of the throat. The sensivity of the injection zone is quantified by the measurement of the damping of the pressure oscillations. The length of the small rocket motor is choosen so that its firts longitudinal mode has the same frequency than the expected instable mode, generally tangential, in the large scale motor.

Two types of injectors were tested : axial ones at the aft end of the chamber, where the acoustic disturbance is mainly a pressure oscillation, and radial ones at mid-length of the chamber, where the acoustic disturbance is mainly a velocity oscillation. The studied parameters were the mean chamber pressure, two designs of injectors, the fuels, the length of the chamber and the triggering amplitude of oscillations.

All the date obtained constitute an accurate basic mean to test the validity of the numerical models. Moreover, a good agreement can be established between the small scale data and the ones obtained on stability of the large scale motor. The device can be a profitable tool for the development of liquid propellant rocket motor.

Nomenclature

a celerité du son

A_T admittance de tuyère (adimensionnelle)

L Longueur de la partie cylindrique de la chambre de combustion

M Nombre de Mach à l'entrée de la tuyère

Re Partie réelle

α amortissement

α_{c_L} amortissement dû à la couche limite acoustique

Δ^{95} intervalle de confiance à 95 %.

INTRODUCTION

L'apparition d'instabilités de combustion à haute fréquence pendant le fonctionnement d'un moteur fusée à ergols liquides constitue un risque majeur pour la vie de ce moteur et de l'engin qu'il propulse, car elle entraine généralement leur destruction. De nombreux travaux expérimentaux et théoriques ont été conduits, [1], pour se prémunir contre l'apparition d'instabilités de combustion. Les références [2] et [3] résument les efforts accomplis récemment à l'ONERA dans ce domaine, dans le cadre du programme Viking.

Par analogie avec des travaux réalisés à l'ONERA sur les propulseurs à propergol solide, [4] et [5], une démarche expérimentale a été proposée à la DRET, dans le cadre du développement d'un moteur à injection "unlike", afin de tenter de quantifier globalement la réponse de la zone proche de l'injecteur à une excitation acoustique. Dans ce but, l'ONERA a développé et mis au point un montage, fig. 1, décrit en détail dans les références [6] et [7]. Avec ce montage on simule un mode acoustique quelconque d'un propulseur par le premier mode longitudinal d'un petit propulseur.

La plupart des moteurs à ergols liquides réalisés possèdent une injection au fond avant. Dans ces moteurs, les instabilités de combustion à haute fréquence, lorsqu'elles apparaissent, s'organisent principalement sous forme de modes acoustiques tangentiels. Dans cette configuration, injecteur au fond avant-mode tangentiel, chaque injecteur élémentaire est soumis à des oscillations de la pression statique et de la vitesse tangentielle.

Pour cette raison, deux configurations de propulseurs ont été étudiées. L'une comporte un injecteur axial placé au fond avant afin de soumettre principalement la zone d'injection au ventre de pression acoustique du premier mode longitudinal, l'autre comporte un injecteur radial à différentes abcisses de la longueur de la chambre de combustion afin de soumettre la zone d'injection au ventre de vitesse acoustique du même mode ou à une combinaison de ces deux grandeurs. Après une modification du propulseur, l'étude paramétrique du montage à injection axiale (type d'injecteur, nature du combustible, pression moyenne de fonctionnement) a montré qu'il était possible d'obtenir des mesures précises de l'amortissement du premier mode longitudinal. De plus, les configurations étudiées ont pu être classées en fonction de l'amortissement, donc de leur stabilité et ce classement s'est, dans l'ensemble, révélé cohérent avec les résultats de stabilité obtenus d'après les essais réalisés sur le moteur à échelle 1, [6]. La même modification n'a pas été effectuée, jusqu'à présent, sur le propulseur à injection radiale en raison de sa complexité dans ce cas. L'étude paramétrique de cette configuration a donc été réalisée sur le propulseur originel ce qui n'a pas donné de résultats très satisfaisants [7]. Nous avons donc choisi, d'une part de poursuivre l'étude paramétrique avec le seul propulseur à injection axiale, d'autre part de mettre en oeuvre des méthodes d'analyse des mesures plus approfondies afin de pouvoir transposer plus sûrement les indications de stabilité fournies par le petit propulseur au moteur à échelle 1. Cet article présente donc les travaux actuellement réalisés dans ces deux voies.

PROGRAMME EXPERIMENTAL

Au cours du développement du propulseur réel, celui-ci s'est révélé instable sur son premier mode tangentiel dans certaines configurations de fonctionnement. De plus l'adjonction de cavités acoustiques pour supprimer ce mode, a fait apparaître les modes tangentiels supérieurs. Il est donc apparu intéressant de compléter l'étude paramétrique de la réponse des injecteurs par la mesure des amortissements en fonction de la fréquence de l'excitation acoustique. Nous avons choisi une plage de fréquence allant de 5 à 12 kHz qui englobe les fréquences des deux premiers modes tangentiels du propulseur à échelle 1. Cette étude a été réalisée avec le petit propulseur à injection axiale qui présentait seul une bonne garantie de qualité des mesures. Le petit propulseur est muni de chambres de combustion de longueurs différentes de façon à obtenir un premier mode longitudinal de fréquence appropriée. L'objectif principal de cette campagne d'essai étant de déterminer l'évolution de la réponse d'injecteurs en fonction de la fréquence, l'éventail des paramètres a été réduit par rapport aux deux études précédentes, [6] et [7]. Ainsi il n'a été retenu qu'un injecteur sur deux et un combustible sur deux. Par contre les mesures sont toujours effectuées pour deux valeurs de pression moyenne dans la chambre de combustion. Le tableau I récapitule les paramètres étudiés.

Sur huit configurations nous n'avons testé jusqu'à présent que les quatre chambres de combustion les plus longues. Des difficultés rencontrées avec le système de modulation pour les hautes fréquences n'ont pas encore été résolues et retardent donc l'exécution des essais entre 9 et 12 kHz. Les mesures de fréquence et d'amortissement global effectuées avec ces configurations de propulseurs sont présentées dans le tableau II. On rappelle qu'au cours de chaque essai, et donc pour chaque configuration, on

réalise entre quarante et cinquante mesures du couple fréquence-amortissement. Les valeurs indiquées dans le tableau II sont donc des valeurs moyennes pour chaque montage. On constate que les fréquences obtenues sont proches de celles qui étaient visées. Comme pour tous les essais précédents, les fréquences propres du mode sont un peu plus élevées à haute pression qu'à basse pression. De même les amortissements sont plus faibles à haute pression qu'à basse pression. En fonction de la fréquence, l'amortissement augmente. On verra plus loin que cette évolution est due à l'acoustique des chambres de combustion. Enfin on notera que les mesures de fréquence comme celles d'amortissement sont de bonne qualité ainsi que l'attestent les faibles valeurs des intervalles de confiance.

APPLICATION DES RESULTATS A UN PROPULSEUR REEL

L'objectif original de l'étude était de quantifier la sensibilité de l'injection d'ergols liquides à un champ acoustique. Cela devait permettre, d'un point de vue fondamental, d'améliorer nos connaissances sur la zone d'injection et, d'un point de vue appliqué, de mettre au point un outil de développement des propulseurs à ergols liquides à petite échelle et donc bon marché. La précision insuffisante des mesures effectuées avec les propulseurs à injection radiale n'a pas permis de comparer les couplage-pression et couplage-vitesse et donc de progresser sur le premier point. Par contre, les résultats obtenus avec les propulseurs à injection axiale peuvent être confrontés au comportement du propulseur réel vis-à-vis des instabilités de combustion. Cette confrontation démontrera ou infirmera la validité de la conception du montage expérimental en ce qui concerne le deuxième point.

APPLICATION DES MESURES D'AMORTISSEMENT BRUTES

La première façon simple d'appliquer les résultats obtenus à l'aide du montage à petite échelle au propulseur réel est de comparer les indications de stabilité données par les mesures d'amortissement avec le comportement stable ou instable du propulseur réel. Les travaux décrits en [6] ont permis, pour une fréquence donnée de 6500 Hz, fréquence du premier mode tangentiel du moteur réel, de classer les différentes configurations possibles de fonctionnement de ce propulseur en fonction de l'amortissement du premier mode longitudinal du petit propulseur. Cette classification est rappelée dans le tableau III. Elle indique que les configurations avec l'injecteur à doublets, avec la MMH comme combustible et à basse pression sont plus stables que les configurations avec l'injecteur à quintuplets, avec l'UDMH et à haute pression. Or le propulseur réel s'est révélé stable avec la MMH comme combustible, et instable avec l'UDMH, quel que soit le type d'injecteur. De plus l'augmentation des risques d'instabilités avec l'élévation de la pression moyenne de chambre est aussi un phénomène bien connu des motoristes. En ce qui concerne le type d'injecteur, le nombre trop réduit d'essais de stabilité du propulseur réel avec l'injecteur à doublets ne permet pas de connaître l'influence de ce paramètre à échelle 1.

Le propulseur réel a été aussi instable sur son second, voire son troisième mode tangentiel. Ces faits ont motivé la mesure, sur le petit propulseur, de l'évolution de l'amortissement en fonction de la fréquence.

Mais cette fois ci une confrontation directe des mesures d'amortissement obtenues sur le petit propulseur avec le comportement stable ou instable du moteur réel n'est pas possible. En effet la modification de la longueur de chambre des propulseurs et le changement de la fréquence des oscillations font que les petits propulseurs ne sont plus équivalents du point de vue acoustique comme dans le cas précédent. La transposition des mesures d'amortissement au cas du propulseur réel nécessite alors de s'affranchir de cette différence acoustique.

EVALUATION DE L'AMORTISSEMENT DU A L'ACOUSTIQUE

Pour évaluer correctement cette réponse, il faut pouvoir estimer correctement la part due à l'acoustique de la chambre de combustion des petits propulseurs dans la mesure globale de l'amortissement. Cette part est principalement constituée par les pertes acoustiques de tuyère qui peuvent être calculées avec une bonne précision dans le cas des modes acoustiques longitudinaux. C'est d'ailleurs l'un des avantages du montage.

Deux méthodes ont été utilisées pour estimer la part d'amortissement des oscillations due à l'acoustique de la chambre de combustion. La première méthode est celle du bilan acoustique, développée par Culick [8]. La seconde est celle de la simulation numérique directe des phénomènes acoustiques dans un propulseur. Pour la méthode du bilan acoustique, les admittances de tuyères ont été calculées à l'aide d'un programme mettant en oeuvre la théorie de Crocco et Sirignano [9]. Le programme de simulation numérique, développé pour une application aux propulseurs à propergol solide, résout les équations d'Euler dans une description bidimensionnelle axisymétrique et monophasique de l'écoulement dans des propulseurs complets. Après une évaluation poussée des performances instationnaires de ce programme de calcul, du fait que les phénomènes acoustiques pour les modes longitudinaux sont fortement monodimensionnels et pour réduire les temps de calcul, les différentes simulations des petits propulseurs ont été effectuées avec une description monodimensionnelle de l'écoulement. Chaque simulation a été réalisée de la façon suivante, par analogie avec la méthode utilisée sur le montage expérimental : calcul de l'état stationnaire de l'écoulement dans le propulseur, excitation du premier mode longitudinal par une modulation sinusoïdale du débit au fond avant sur trois périodes, calcul de l'évolution de l'écoulement pendant le retour à l'état stationnaire. La figure 2 représente l'évolution de la composante instationnaire de la pression à l'entrée du convergent pendant les deux dernières phases de la simulation. Cette figure est à comparer aux enregistrements expérimentaux présentés en [6] et [7]. Pour les deux méthodes, l'amortissement dû à la couche limite a été estimé à l'aide des résultats de Morse et Ingard [10]. En résumé, avec la méthode du bilan, l'amortissement acoustique se présente sous la forme d'une somme de trois termes :

$$\alpha_{acoustique} = \frac{a}{L} M + \frac{a}{L} \mathcal{R}_e(\mathcal{B}_t) + \alpha_{c.l.}$$

$\frac{\omega}{c}M$ amortissement dû à la convection des ondes, $\frac{\omega}{c}R_e(\beta_T)$ amortissement dû à la radiation des ondes par le convergent de la tuyère, α_{CL} amortissement dû à la couche limite. Avec la simulation numérique qui donne globalement l'amortissement dû à la convection et à la radiation des ondes, l'amortissement acoustique se réduit à la somme de deux termes :

$$\alpha_{acoustique} = \alpha_{numérique} + \alpha_{CL}$$

Ces deux méthodes ont été utilisées de façon à la fois complémentaire et concurrente. En effet, en cherchant à retrouver les fréquences mesurées expérimentalement, la simulation numérique a permis une évaluation correcte de la valeur de la célérité du son nécessaire pour la méthode du bilan acoustique. Et la comparaison des résultats des deux méthodes a donné la possibilité de juger de leur validité, sachant que les calculs d'admittances de tuyère ont déjà été confirmés sur le plan expérimental [11].

Ces calculs ont donc été effectués pour les petits propulseurs à injection axiale. Les simulations numériques ont d'abord permis d'estimer la célérité moyenne du son dans les propulseurs, de l'ordre de 1070 m/s pour les configurations avec l'injecteur à doublets et 1100 m/s avec l'injecteur à quintuplets. Le tableau IV récapitule les résultats pour les propulseurs utilisés dans la première étude, [6]. On constate que les valeurs d'amortissement acoustique sont très proches pour les deux configurations de propulseur avec l'injecteur à doublets ou à quintuplets. Cela reflète le fait que, bien que les chambres de combustion aient des géométries différentes pour être adaptées aux injecteurs, elles ont été conçues de façon à être acoustiquement équivalentes. Enfin, les deux méthodes, bilan acoustique et simulation numérique, donnent des résultats concordants à quelques pour-cent près. Dans ce cas cela donne un avantage certain à la méthode du bilan acoustique, beaucoup plus rapide et moins coûteuse que les simulations numériques.

Le tableau V récapitule les mêmes calculs effectués pour les propulseurs muni de l'injecteur à quintuplets mais avec des chambres de combustion de longueurs différentes. Ces chambres, bien sûr, ne sont pas acoustiquement équivalentes d'où l'intérêt d'estimer avec précision l'amortissement d'origine acoustique. Cette fois-ci les deux méthodes, bilan acoustique et simulation numérique, donnent des résultats qui divergent un peu notamment pour les longueurs de chambres les plus extrêmes. Des simulations bidimensionnelles effectuées pour des chambres de longueurs 52 et 89 mm semblent indiquer que le calcul monodimensionnel sous-estime l'amortissement par rapport au calcul bidimensionnel. En ce qui concerne la chambre de 52 mm, la simulation bidimensionnelle donne un amortissement intermédiaire entre le résultat du calcul monodimensionnel et du bilan acoustique. Dans le cas présent, afin de bien exploiter les mesures expérimentales obtenues sur les petits propulseurs, il semble judicieux de prendre pour l'amortissement acoustique la moyenne des valeurs données par les deux méthodes. Dans un cas général, l'attitude à suivre dépend de la précision désirée. En raison du coût des simulations bidimensionnelles, la méthode du bilan acoustique est d'excellente qualité.

<u>EVALUATION DE LA REPONSE DE LA ZONE D'INJECTION, APPLICATION AU PROPULSEUR A ECHELLE 1</u>

En ce qui concerne les propulseurs réalisés pour simuler le premier mode tangentiel, à 6500 Hz, du propulseur réel, le classement des différentes configurations en fonction de l'amortissement global, tableau II, ou en fonction de la réponse de la zone d'injection, tableau VI, ne change pas puisque ces propulseurs sont acoustiquement semblables. A la lecture du tableau VI, on constate que l'ensemble des phénomènes d'injection et de combustion ont un effet amortisseur dans le cas des quatre premières configurations car leur contribution à l'amortissement global est négative. Par contre, avec une contribution positive, ils ont un effet amplificateur dans le cas des trois configurations suivantes. La dernière configuration (QU20) s'est révélée naturellement instable sur son premier mode tangentiel.

En ce qui concerne les petits propulseurs de longueurs différentes et pour les essais réalisés à ce jour on constate comme précédemment que les phénomènes d'injection et de combustion ont une action plus déstabilisatrice à 25 atmosphères qu'à 15 atmosphères, tableau VII. Par contre si l'on regarde l'évolution en fonction de la longueur de chambre, donc de la fréquence, il semble que cette action soit constante.

Si cette tendance se confirme pour les fréquences les plus élevées, de 9 à 12 kHz, sachant de plus que nos petits propulseurs se sont révélés naturellement instables à 31 et 35 kHz, cela pourrait signifier que la réponse des phénomènes d'injection et de combustion est constante dans un très large domaine de fréquence, tant que leurs temps caractéristiques sont compatibles avec la fréquence du mode acoustique. Dans ce cas et du point de vue de la stabilité, il serait plus facile d'appréhender des modifications géométriques des moteurs, de concevoir des moteurs dérivés avec les mêmes injecteurs élémentaires qu'un propulseur déjà développé et de prévoir la stabilité des propulseurs pour les modes acoustiques d'ordre supérieur. En moyenne, pour les quatre essais réalisés, l'amortissement dû aux phénomènes d'injection et de combustion est proche de 0 S^{-1} pour une pression de chambre de 15 atm. et de 450 S^{-1} pour 25 atm.

Si les évaluations de la réponse de la zone d'injection obtenues pour le premier mode longitudinal des petits propulseurs peuvent être appliquées aux modes transverses du propulseur réel, du point de vue de la stabilité on peut faire les recommandations suivantes :

- premièrement, il est préférable de choisir l'injecteur à doublets, d'utiliser le combustible HMH et de faire fonctionner le moteur à basse pression,
- deuxièmement, la contribution des phénomènes d'injection semble constante quelque soit la fréquence, il suffit, dans le cas étudié (injecteur à quintuplets, combustible HMH) de dimensionner la chambre de combustion de façon à rendre maximal son amortissement acoustique pour les modes transverses.

CONCLUSION

Le montage, décrit en référence [6], a permis de mesurer l'amortissement du premier mode longitudinal d'un petit propulseur dans différentes configurations. Après avoir soustrait à ces mesures la contribution due à l'acoustique des chambres de combustion utilisées, la réponse globale de la zone d'injection a pu être déterminée pour cette excitation longitudinale. Ces résultats sont actuellement qualitativement cohérents avec le comportement stable ou instable du propulseur réel. Pour les appliquer de façon quantitative à ce propulseur, il est nécessaire de résoudre d'abord plusieurs problèmes. Tout d'abord, pour un mode transverse, l'instabilité de combustion peut être considérée comme la composition de deux couplages, pression et vitesse acoustique, avec la zone d'injection. Or il n'a été obtenu de données expérimentales exploitables qu'avec les propulseurs concernés principalement par le couplage pression. De plus, même disposant de données pour le couplage vitesse, la méthode de la transposition de ces données de couplage au cas d'un mode transverse d'un propulseur à échelle 1 reste à déterminer. Enfin l'approche expérimentale réalisée avec le montage ONERA est linéaire et il faut s'interroger sur son domaine de validité vis-à-vis de phénomènes rapidement non linéaires à échelle 1.

D'un point de vue fondamental, les travaux expérimentaux continueront par la reprise des essais avec les injecteurs radiaux mais avec des chambres de combustion mieux adaptées du point de vue de l'acoustique. Ces essais auront donc pour but de déterminer l'existence ou non d'un effet de couplage vitesse et dans l'affirmative de la mesurer. Ensuite, il est envisagé d'utiliser le programme de calcul de la référence [3], d'une part dans le cas des petits propulseurs afin d'améliorer la compréhension des phénomènes qui s'y déroulent pendant leur fonctionnement instationnaire, d'autre part, au cas du propulseur réel pour étudier une méthode de transposition des mesures obtenues à échelle réduite à l'aide d'un mode acoustique longitudinal. Enfin, la confrontation entre les mesures d'amortissement sur le montage ONERA et les simulations numériques permettra de construire et de valider des modélisations instationnaires de la vaporisation et de la combustion dans les propulseurs biliquides.

D'un point de vue industriel, en raison de la cohérence des mesures d'amortissement obtenues sur petits propulseurs avec le comportement instationnaire à échelle 1, le montage sera utilisé pour effectuer un tri d'injecteurs en fonction de leur sensibilité acoustique.

Références

[1] D.T. HARRJE et F.H. REARDON. Liquid propellant rocket combustion instability. NASA SP-194 (1972)

[2] D. LOUHME et D. SCHMITT. Les moyens nécessaires à l'étude fondamentale des instabilités de combustion d'un moteur biliquide. Acta Astronautica, vol. 10, n° 12 (1983), p 761-775.

[3] M. HABIBALLAH, D. LOUHME et F. PIT. A comprehensive model for combustion stability studies applied to the Ariane Viking engine. AIAA - 26th Aerospace Sciences Meeting, RENO (USA), 1988.

[4] P. KUENTZMANN et A. LAVERSANT. Détermination expérimentale de la réponse d'un propergol solide aux oscillations de pression de haute fréquence. La Recherche Aérospatiale n° 1, 1984-1, French and English Editions.

[5] F. VUILLOT et P. KUENTZMANN. Flow turning and admittance correction : an experimental comparison. Journal of Propulsion and Power, vol. 2, n° 4.

[6] B. LECOURT, R. FONCAUD et P. KUENTZMANN. Etude expérimentale de la sensibilité acoustique d'injecteurs de moteurs fusées à ergols liquides. La Recherche Aérospatiale n° 1984-5.

[7] B. LECOURT et R. FONCAUD. Experiments on stability of liquid propellant rocket motors. AIAA Paper 87-1772, AIAA/SAE/ASME/ASEE 23rd joint propulsion conference, SAN DIEGO (California) USA (1987).

[8] F.E.C. CULICK. Stability of three-dimensional motions in a combustion chamber. Combustion Science and Technology, 1975, vol. 10.

[9] CROCCO-SIRIGNANO. Behaviour of supercritical nozzles under three dimensional oscillatory conditions. AGARDOGRAPH n° 117.

[10] P.M. MORSE and K.U. INGARD. Theoretical Acoustics. Mc Graw-Hill Book Co. New York.

[11] A. BELL et B.T. ZINN. The prediction of three dimensional liquid propellant rocket nozzle admittances. NASA CR-121129 Feb. 1973.

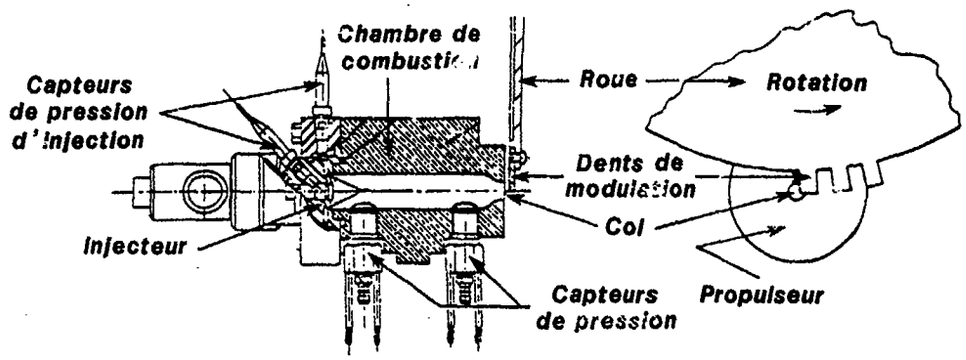


Fig. 1 - Schéma de fonctionnement du montage

Paramètres communs à tous les essais :
- injecteur à quintuplets
- combustible MMH
- comburant N_2O_4

L_{ch} (mm)	120		102		87		77		69		63		57		52	
FREQUENCE VISEE (kHZ)	5		6		7		8		9		10		11		12	
P_{ch} (atm)	15	25	15	25	15	25	15	25	15	25	15	25	15	25	15	25

Tableau I - Récapitulation des paramètres de l'étude de la sensibilité acoustique des injecteurs en fonction de la fréquence

	P_{ch} = 15 atm				P_{ch} = 25 atm			
L_{ch} (mm)	f (Hz)	Δ_f^{95} (Hz)	α (S^{-1})	Δ_α^{95} (S^{-1})	f (Hz)	Δ_f^{95} (Hz)	α (S^{-1})	Δ_α (S^{-1})
52	----	---	----	---	----	---	----	---
57	----	---	----	---	---	---	---	---
63	----	---	----	---	---	---	---	---
69	----	---	---	---	---	---	---	---
77	7770	30	- 2060	80	7845	33	- 1400	110
87	6820	26	- 1530	30	6930	30	- 1150	83
102	5815	22	- 1190	85	5920	20	- 750	60
120	4895	15	- 1010	66	4985	11	- 810	60

Tableau II - Résultats des dépouillements en fréquence et en amortissement des essais de l'injecteur à quintuplets avec les chambres de différentes longueurs

MONTAGE	$\bar{\alpha}$ (s^{-1})
DM16	- 3060
DM27	- 2090
DU16	- 1990
QM15	- 1650
DU26	- 1350
QM23	- 1110
QU15	- 740
QU20	instable

D : injecteur à doublets
Q : injecteur à quintuplets
M : combustible MMH
U : combustible UDMH
15 : pression chambre en atm

Tableau III - Classement des configurations testées en fonction de $\bar{\alpha}$ pour les injecteurs axiaux

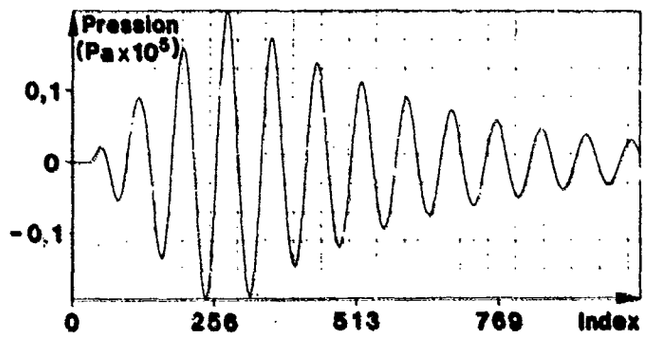


Fig. 2 - Simulation numérique de l'amortissement du premier mode longitudinal d'un propulseur : évolution de la composante instationnaire de pression à l'entrée du convergent

CONFIGURATION EXPERIMENTALE	α_{CL} (s^{-1})	α_M (s^{-1})	α_{AT} (s^{-1})	α_{sup} (s^{-1})	$\alpha_{exper.\ min.}$ (s^{-1})	$\alpha_{exper.\ M.A.}$ (s^{-1})
DM16	- 100	- 1130	- 260	- 1420	- 1520	- 1490
DM27	- 75	- 1130	- 260	- 1420	- 1495	- 1465
DU16	- 100	- 1130	- 260	- 1420	- 1520	- 1490
DU27	- 75	- 1130	- 260	- 1420	- 1495	- 1465
QM15	- 90	- 1130	- 300	- 1475	- 1565	- 1520
QM25	- 70	- 1130	- 300	- 1475	- 1545	- 1500
QU15 *	- 90	- 1130	- 300	- 1475	- 1565	- 1520
QU20	- 70	- 1130	- 300	- 1475	- 1545	- 1500

D : injecteur à doublets — M : combustible MMH
Q : injecteur à quintuplets — U : combustible UDMH
15 : pression chambre en atmosphère

Tableau IV - Estimation de l'amortissement d'origine acoustique dans les petits propulseurs tels que $f_{1L} \approx 4500$ Hz, par les méthodes du bilan acoustique et de la simulation numérique

L_{ch} (mm)	α_M (s^{-1})	α_{AT} (s^{-1})	α_{num} (s^{-1})	P_{ch} (atm)	α_{CL} (s^{-1})	$\alpha_{acous.\ num}$ (s^{-1})	$\alpha_{acous.\ B.A.}$ (s^{-1})	$\frac{\Delta\alpha}{\alpha}$ (%)
52	- 2265	- 1395	- 3120	15	- 115	- 3235	- 3775	- 15,4
				25	- 90	- 3210	- 3750	- 15,5
57	- 1995	- 1020	- 2730	15	- 110	- 2840	- 3125	- 9,6
				25	- 85	- 2815	- 3100	- 9,6
63	- 1745	- 740	- 2330	15	- 105	- 2435	- 2590	- 6,2
				25	- 80	- 2410	- 2565	- 6,2
69	- 1550	- 550	- 2065	15	- 100	- 2165	- 2200	- 1,6
				25	- 75	- 2140	- 2175	- 1,6
77	- 1350	- 400	- 1775	15	- 95	- 1870	- 1845	1,3
				25	- 70	- 1845	- 1820	1,3
87	- 1165	- 290	- 1520	15	- 85	- 1605	- 1540	4,1
				25	- 70	- 1590	- 1525	4,2
102	- 965	- 200	- 1265	15	- 80	- 1345	- 1245	7,7
				25	- 60	- 1325	- 1225	7,8
120	- 800	- 140	- 1050	15	- 75	- 1125	- 1015	10,3
				25	- 60	- 1110	- 1000	10,4

D : injecteur à quintuplets M : combustible à MMH

Tableau V - Estimation de l'amortissement d'origine acoustique dans les petits propulseurs de longueur différente, par les méthodes du bilan acoustique et de la simulation numérique

CONFIGURATION EXPERIMENTALE	α acoustique (s^{-1})	α expérimental (s^{-1})	α zone d'injection (s^{-1})
DM16	- 1505	- 3060	- 1555
DM27	- 1480	- 2090	- 610
DU16	- 1505	- 1990	- 485
QM15	- 1545	- 1650	- 105
DU26	- 1480	- 1350	130
QM23	- 1525	- 1110	415
QU15	- 1545	- 740	805
QU20	- 1525	Instable	---

Tableau VI - Evaluation de la réponse de la zone d'injection dans les petits propulseurs tels que f_{1L} = 6500 Hz

	$\alpha_{acoustique}$ (s^{-1})		$\alpha_{expérimental}$ (s^{-1})		$\alpha_{zone\ d'injection}$ (s^{-1})	
L_{ch} (mm)	15 atm	25 atm	15 atm	25 atm	15 atm	25 atm
52	- 3505	- 3480	---	---	---	---
57	- 2985	- 2960	---	---	---	---
63	- 2515	- 2490	---	---	---	---
69	- 2165	- 2160	---	---	---	---
77	- 1880	- 1835	- 2060	- 1400	- 200	435
87	- 1575	- 1560	- 1530	- 1150	45	410
102	- 1295	- 1275	- 1190	- 750	105	525
120	- 1070	- 1055	- 1010	- 610	60	445

Tableau VII - Evaluation de la réponse de la zone d'injection dans les petits propulseurs de longueurs différentes

LOW FREQUENCY AND HIGH FREQUENCY COMBUSTION OSCILLATION PHENOMENA INSIDE A ROCKET COMBUSTION CHAMBER FED BY LIQUID OR GASEOUS PROPELLANTS

by

D. Preclik and P. Spagna
MESSERSCHMITT-BOELKOW-BLOHM GMBH
Kommunikationssysteme und Antriebe

Postfach 80 11 69
8000 München 80

ABSTRACT

The article presents an investigation of combustion instability phenomena inside a rocket combustion chamber fed by liquid or gaseous propellants.

The interpretation relies, among others, on the combustion time lag theory and the use of linear transfer functions for the different elements building the closed loop transfer function of the system.

1. INTRODUCTION

Rocket chamber fed by gaseous or/and liquid propellant types are normally designed to exhibit a stable operational working mode, as well during transition (start, shutdown) as at main stage. However, under some circumstances, organized pressure oscillations, at low respectively high frequency, appear inside the combustion chamber with undesirable consequences and side effects which may result, in the burn-out or mechanical damage of the hardware under test. Therefore, it is essential to understand the causes of those phenomena in order to provide against them and dispose of a sufficient operational margin with respect to the instability domain.

This paper presents an investigation of the above mentioned phenomena using, among others, the combustion time lag theory as an analysing tool. After giving some comments related to the forms, observation and effects of combustion instability, it summarizes the theoretical background necessary to the understanding of the described phenomena. Subsequently, the LF-respectively HF-behaviour of an oxygen-hydrogen combustor is analysed, finally some remarks about the measures to be taken in order of preventing instability oscillations are made.

2. FORMS, OBSERVATION AND EFFECTS OF COMBUSTION INSTABILITY

● Inside a rocket combustion chamber in the transient phases or in steady state at main stage, the pressure at a given point of the chamber is always the sum between a mean value and a fluctuation, the mean pressure being approximately uniform throughout the chamber:

$$P_c(x,t) = \overline{P_c(t)} + \tilde{p}_c(x,t) \qquad (1)$$

where $x = \rho, \theta, z$ are the cylindrical coordinates.

● The fluctuation is generally random and displays an almost "continuous" power density spectrum $d\tilde{p}_c(x)_{RMS}/d\omega$ V.S. the frequency. The level of fluctuation is usually defined by means of the fluctuation rate:

$$\frac{\left(\frac{1}{\tau}\int_0^\tau [\tilde{p}_c(x,t)]^2\right)^{\frac{1}{2}}}{\overline{P_c(t)}} = \frac{|\tilde{p}_c(x)|_{RMS}}{\overline{P_c(t)}} \qquad (2)$$

● Under specific conditions, the oscillations cease to be random and take an organized character, i.e. the power density spectrum displays large discrete lines of a definite breadth (a definite energy is contained under the excited mode) and the value of the fluctuation rate, for the same combustor, increases (for two different combustors however, it cannot be excluded that the fluctuation rate of the one combustor under random oscillation mode is not larger than the fluctuation rate of the other combustor under organized oscillation mode, i.e. combustion roughness does not automatically mean combustion instability).

● There principally are two cases of organized oscillations, which can pratically be encountered, namely the low frequency case (LF) and the high frequency case (HF). Intermediate frequencies (IF) are mentioned in the literature (Ref. 2) but have only rarely been observed.

● In the LF-case, the frequencies observed lie in a range up to a few hundred Hertz. This means the wavelength of the oscillation is generally large compared to the geometrical size (length, radius) of the chamber. Consequently, the fluctuation will sensibly be the same throughout the chamber / i.e. not position related: $\tilde{p}_c(t)$ /.

● In the HF-case, on the other hand, the frequencies observed usually closely match the acoustic modes of the chamber (common range: 2–20 KHz), which include purely transversal/tangential (standing, spinning), radial/and longitudinal modes, as well as their different combinations (tangential : radial, tangential : longitudinal, etc. ...), the transversal ones, particularly the 1st and 2nd tangentials being generally more crucial than the other modes (the longitudinal modes are normally well damped by the convergent part of the nozzle). In the HF-case, the wavelength of the oscillation is no more large compared to the geometrical size of the chamber and the pressure fluctuation will be position dependent: $\tilde{p}_c(x, t)$.

● LF-oscillation phenomena can usually adequately be observed by means of the pressure pick-ups foreseen for the measurement of the mean combustion pressure, provided the corresponding signals are FM-recorded or the sampling rate is high enough.

● For the HF-case, on the other hand, the correct observation of the pressure fluctuation (mode shape) requires the availability of flush- or nearly flush-mounted pressure transducers, which, because of the chamber cooling channels, cannot always be installed on the hardware under investigation (exception: uncooled chamber or better water-cooled chamber enabling the adjunction of a so-called instrumentation ring between body of the watercooled chamber and injector plate).

An alternative consists in using acceleration pick-ups adequately mounted on the injector head or possibly on the chamber body itself. Since the expected frequencies are high, the acceleration levels will be important (order of magnitude of the instantaneous acceleration signals: without organized HF-oscillation around 100 g; under the presence of HF instability around 1000 g). The accelerometers will generally permit to recognize the main excited mode(s) by means of the measured frequencies. An accelerometer signal will however be "polluted" by oscillations which are proper to the structure of the chamber and of the injector themselves and the higher the frequency, the more difficult it will be to separate what belongs to the combustion and what stems from the structure alone.

● Since during the HF-oscillation phenomenon the burnt gases are swept to and fro around the droplets, the mixing rate of the propellants will be modified and the efficiency of combustion affected.

If the combustion efficiency is relatively low (storable propellants), the HF-oscillations will exhibit a tendency to increase it. If, on the other hand, the combustion efficiency is very high (cryogenic propellants), HF-oscillations will occasion a sensible degradation (decrease of $\overline{P_c(t)}$).

Through the destruction of the boundary layer along the chamber wall and the abscence of a well positioned burnfront, which enables the flame to leap to the injector plate, the heat transfer to the structure will significantly be increased with the risk of an immediate burn-out of the chamber and/or injector. (This last possibility is specially critical for storable propellants, less severe, however, for cryogenic propellants). Moreover, mechanical resonance phenomena can be induced, which can lead to the rupture of parts either on the chamber itself or its interface environment, including the facility. This last remark is also true for LF-oscillations.

3. THEORETICAL BACKGROUND

● Combustion time lag

An element of propellant injected into the combustion chamber only burns after a certain amount of time, referred to as the total time lag, has elapsed. During this amount of time, the element of propellant undergoes several transformations, which typically are the following: propellant injection, atomization, heating, vaporization, mixing, chemical reaction. Each of those transformations can schematically be represented by an individual time lag and in a simplified manner, the total time lag can be contemplated as being the sum of those individual time lags:

$$\tau_T = \tau_J + \tau_A + \tau_H + \tau_V + \tau_M + \tau_R \qquad (3)$$

The injection time lag τ_J accounts for the delay elapsed between the instant the propellant leaves the injector plate and the moment it is transformed into liquid sheets (liquid jet break-up time). The atomization time lag τ_A is the time necessary for a liquid sheet to break-up into droplets (spray formation).

Generally, injection time lag and atomization time lag are insensitive to the surrounding process conditions (pressure). On the other hand, the heating and vaporizing phenomena are sensitive to the process environment.

If we consider an element of propellant being presently vaporized under fixed environmental conditions (i.e. vaporized flowrate in steady state) and that we suddenly (i.e. with a step variation) modify those conditions, the time required by the vaporized flowrate to reach the new steady state value can be interpreted as the sum of the heating and vaporization time lags.

The time lag occasioned by the chemical reaction is usually negligible compared to the other time lags. The vapor mixing, which is controlled by turbulent processes, is also normally small compared to the vaporization time lag. Thus following Crocco (Ref. 1), we can split the total time lag into two parts, one insensitive and the other one sensitive to the environmental process conditions:

$$\tau_T = \tau_i + \tau_b \tag{4}$$

$$\tau_i = \tau_J + \tau_A \tag{4-1}$$

$$\left.\begin{aligned} \tau_b &= \tau_H + \tau_V + \tau_M + \tau_R \\ &\simeq \tau_H + \tau_V \end{aligned}\right\} \tag{4-2}$$

τ_i is the insensitive time lag, τ_b (where the index b stands for "burning") is the sensitive or "burning" time lag (Ref. 6). In this sense, τ_i can be interpreted as the "pre-burning" time lag.

If gaseous propellants are injected into the combustion chamber, the expression for the total time lag reduces to:

$$\tau_T = \tau_J + \tau_H + \tau_M + \tau_R \tag{5}$$

due to the absence of atomization and vaporization phenomena.

In case of an impinging injector type, τ_J can, according to J. Fang (Ref. 6), be interpreted as the so-called unlike impingement time lag, which is generally larger than the remaining time lags and consequently controls the gaseous propellant combustion instability.

In case of a coaxial injector type, our opinion is that τ_J is negligible, so that the sum of the remaining heating and mixing time lags in this case controls the instability process (see paragraph 4).

● Mass conservation

An element of propellant which burns between the instant t and the instant t + dt has been introduced into the chamber, according to what has been said about the total time lag, between $t - \tau_T$ and $(t + dt) - (\tau_T + d\tau_T)$, i.e. during the interval $dt - d\tau_T$.

This enables to write (Crocco Ref. 1, Reardon Ref. 2) the relationship between burning and injection rates as:

$$\dot{m}_b(t)\,dt = \dot{m}_i(t - \tau_T)\,d(t - \tau_T) \tag{6}$$

Taking the instantaneous rate $\dot{m}$ as the sum between a mean value $\bar{\dot{m}}$ and a perturbation $\tilde{\dot{m}}$, supposed small with respect to the mean value, yields, by neglecting the second order terms:

$$\tilde{\dot{m}}_b(t) \simeq \tilde{\dot{m}}_i(t - \tau_T) - \bar{\dot{m}}\,\frac{d\tau_T}{dt} \tag{7}$$

(where: $\bar{\dot{m}} = \bar{\dot{m}}_b = \bar{\dot{m}}_i$)

or by replacing $d\tau_T/dt$ by the equivalent quantity $d\tau_b/dt$ and writing $t - \bar{\tau}_T$ instead of $t - \tau_T$ (which only introduces higher order terms):

$$\tilde{\dot{m}}_b(t) \simeq \tilde{\dot{m}}_i(t - \bar{\tau}_T) - \bar{\dot{m}}\,\frac{d\tau_b}{dt} \tag{8}$$

Relationship (8) can be adapted to the case of a bipropellant (fuel F, oxydator O) chamber (Fang Ref. 6) such as:

$$\dot{m}_b(t)\,dt = \dot{m}_{iO}(t - \tau_{OT})\,d(t - \tau_{OT}) + \dot{m}_{iF}(t - \tau_{FT})\,d(t - \tau_{FT}) \tag{9}$$

or after replacement by equivalent quantities and introduction of the mean mixture ratio $\bar{r} = \bar{\dot{m}}_O/\bar{\dot{m}}_F$ and mean flowrate $\bar{\dot{m}} = \bar{\dot{m}}_O + \bar{\dot{m}}_F$:

$$\frac{\tilde{\dot{m}}_b(t)}{\bar{\dot{m}}} = \frac{\tilde{\dot{m}}_{iO}(t - \bar{\tau}_{OT}) + \tilde{\dot{m}}_{iF}(t - \bar{\tau}_{FT})}{\bar{\dot{m}}} - \frac{\bar{r}}{\bar{r} + 1}\,\frac{d\tau_{Ob}}{dt} - \frac{1}{\bar{r} + 1}\,\frac{d\tau_{Fb}}{dt} \tag{10}$$

Equations (9) and (10) represent the basic relationships of the combustion time lag theory.

The above expression can be related to the corresponding pressure perturbation in the chamber, using Crocco's relationship (Ref. 1):

$$-\frac{d\tau_b}{dt} = n \cdot \frac{\tilde{p}_c(x_i, t) - \tilde{p}_c(x_{i-\bar{\tau}_b}, t - \bar{\tau}_b)}{\bar{p}_c} \tag{11}$$

Where n is the so-called pressure interaction index. This approximately yields (considering only the transversal modes):

$$\tilde{m}_b(t) = \tilde{m}_{io}(t - \bar{\tau}_{oT}) + \tilde{m}_{iF}(t - \bar{\tau}_{FT}) + \frac{\bar{r}}{\bar{r}+1} n_o \frac{\tilde{p}_c(t) - \tilde{p}_c(t - \bar{\tau}_{ob})}{\frac{\bar{p}_c}{\bar{m}}} + \frac{1}{\bar{r}+1} n_F \frac{\tilde{p}_c(t) - \tilde{p}_c(t - \bar{\tau}_{Fb})}{\frac{\bar{p}_c}{\bar{m}}} \tag{12}$$

Where two interaction indices n_o and n_F have been introduced.

● Linear analysis

The combustion instability phenomenon can be investigated by means of a linear analysis. According to this technique, any dependent variable is represented, as tacitly supposed above, by the sum of a mean value and a small perturbation. In order to obtain damped or growing oscillations, the time dependence of the perturbation has to be exponential:

$$u(t) = \bar{u} + \tilde{u}(t) \tag{13-1}$$

$$\tilde{u}(t) = u' \exp(st) \tag{13-2}$$

Where $s = \lambda + i\omega$ is the complex frequency.

Applying this technique to equation (12) one obtains:

$$\frac{\dot{m}'_b(s)}{p'_c(s)} = A^i_{nm}\left[\frac{\dot{m}'_{io}(s)}{p'_c(s)} \exp(-\bar{\tau}_{oT}s) + \frac{\dot{m}'_{iF}(s)}{p'_c(s)} \exp(-\bar{\tau}_{FT}s)\right] + \ldots$$

$$\ldots + A^e_{nm} \frac{\bar{m}}{\bar{p}_c}\left\{\frac{\bar{r}}{\bar{r}+1} n_o [1 - \exp(-\bar{\tau}_{ob}s)] + \frac{1}{\bar{r}+1} n_F [1 - \exp(-\bar{\tau}_{Fb}s)]\right\} \tag{14-1}$$

or by introducing the chamber and injection admittances:

$$Y_c(s) = -A^i_{nm}[Y_{io}(s) \exp(-\bar{\tau}_{oT}s) + Y_{iF}(s) \exp(-\bar{\tau}_{FT}s)] + \ldots$$

$$\ldots + A^e_{nm} \frac{\bar{m}}{\bar{p}_c}\left\{\frac{\bar{r}}{\bar{r}+1} n_o [1 - \exp(-\bar{\tau}_{ob}s)] + \frac{1}{\bar{r}+1} n_F [1 - \exp(-\bar{\tau}_{Fb}s)]\right\} \tag{14-2}$$

A^i_{nm} and A^e_{nm} are amplification coefficients which depend on the nm-mode considered and on the injection distribution density function $\mu(p, \theta)$ (Ref. 2, Ref. 3) or $f(\rho)$ (Ref. 4). The introduction of those coefficients is made necessary when the spreading of the burning droplets within a chamber cross-section is taken into account (Equations (10) and (12) are primarily valid at a given point $x(p, \theta, z)$ only).

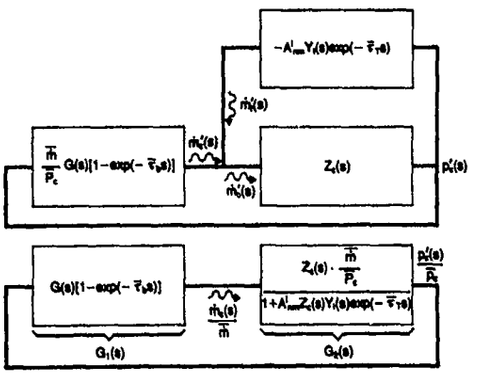
If we, as simplification, drop the differences between fuel and oxidiser, equation (14-2) reduces to:

$$Y_c(s) = -A^i_{nm} Y_i(s) \exp(-\bar{\tau}_T s) + A^e_{nm} \frac{\bar{m}}{\bar{p}_c} n[1 - \exp(-\bar{\tau}_b s)] \tag{14-3}$$

Which can be reshuffled to

$$A^e_{nm} \cdot n[1 - \exp(-\bar{\tau}_b s)] = \frac{1 + A^i_{nm} Z_c(s) Y_i(s) \exp(-\bar{\tau}_T s)}{\frac{\bar{m}}{\bar{p}_c} Z_c(s)} \tag{14-4}$$

corresponding to the transition condition of the following equivalent control loops:



- $Z_c(s)$: chamber impedance
- $Y_i(s)$: injection admittance
- $G(s)$: intrinsic comb. gain
  $G(s) \approx f[n, l_r, l_\theta, \mu(r,\theta)]$
- A^i_{nm} [$\mu(r,\theta)$] amplif. coeff. (injection)
- $\bar{\tau}_T$: total time lag (mean val.)
- $\bar{\tau}_b$: „sensitive" time lag (mean val.)
- $\dot{m}'(s)$: flowrate perturbation (complex value)
- $p'(s)$: pressure perturbation (complex value)

- Transition to instability for $G_1(s).G_2(s) = -1$
- Stability task
  - reduce $Z_c(s)$ [i.e. increase $Y_c(s)$]
  - reduce $G(s)$
  - reduce $Y_i(s)$
  - detune $G_1(s)$ from $Z_c(s)$

Fig. 1 LF & HF-stability control loops

In those loops, $G(s) = A^c_{nm} \cdot n \ldots$ is the combustion gain and $Z_c(s) = 1/Y_c(s)$ is the impedance of the chamber.

Improving the stability conditions implies:

- Minimization of the chamber impedance (i.e. increase of the corresponding admittance).
- Minimization of the injection admittance $Y_i(s)$.

(For $Y_i(s) = 0$, the loop reduces to Crocco's intrinsic case (Ref. 1, Ref. 2)). On the other hand, for $1 + A^i_{nm}Z_c(s) \cdot Y_i(s) \cdot \exp(-\bar{\tau}_T s) = 0$, the chamber pressure is instable, independently of the value taken by the burning transfer function $G(s)[1 - \exp(-\bar{\tau}_b s)]\,\bar{m}/\bar{p}_c$, where $G(s)\,\bar{m}/\bar{p}_c$ can be interpreted as the burning admittance. $Y_i(s) \neq 0$ signifies a degradation of the intrinsic stability conditions.

- Minimization of the combustion gain (the higher $A^c_{nm} \cdot n \ldots$, the easier instability will take place).

- Detuning combustion and chamber impedance through the shifting of the sensitive time lag $\bar{\tau}_b$ with respect to $T_{nm}/2$ ($f_{nm} \approx 1/T_{nm}$ being the chamber acoustic frequency of the corresponding nm-mode) or vice versa, in order no resonance phenomenon between combustion process and combustion chamber can occur.

● Combustion gain

The spray produced by an injector is generally not homogeneous and a certain stratification of the mixture ratio exists in the vapour surrounding the droplets. If a transverse acoustic field is superposed onto the spray, the vapor will oscillate with respect to the droplets causing mixture ratio oscillations around each droplet and accordingly affecting the burning rate, the oscillation of which can be expressed by means of a radial respectively a tangential velocity index l_r and l_θ (Ref. 2). When the injection density distribution function $\mu(\rho, \theta)$ is taken into account, additional amplification coefficients B^c_{nm} and C^c_{nm}, similar to A^c_{nm}, are introduced (Ref. 3), so that for the transition case ($\lambda = 0$, with $s = \lambda + i\omega$) the combustion gain can be expressed by:

$$G(i\omega) \approx n\left[A^c_{nm} + \frac{1}{\gamma\omega}\left(B^c_{nm} \cdot \frac{l_r}{n} + C^c_{nm} \cdot \frac{l_\theta}{n}\right)\right] \qquad (15\text{-}1)$$

According to Ref. 3, A_{nm} and B_{nm} are real numbers and $C^c_{nm} = (C^c_{Re} - i\,C^c_{Im})_{nm}$ is complex ($C^c_{Im} \leqslant 0$). This yields:

$$G(i\omega) \approx n\left\{\left[A^c_{nm} + \frac{(C^c_{Im})_{nm}}{\gamma\omega} \cdot \frac{l_\theta}{n}\right] + \frac{1}{\gamma\omega}\left[B^c_{nm} \cdot \frac{l_r}{n} + (C^c_{Re})_{nm} \cdot \frac{l_\theta}{n}\right]\right\} \qquad (15\text{-}2)$$

The pressure interaction index n and the velocity indices l_r and l_θ are generally unknown.

It is expected that the effect of the velocity indices is much larger for the impinging injector types than for the coaxial ones, since the latter are more symmetrical.

● Chamber impedance

The chamber impedance $Z_c(s) = p'_c(s)/\dot{m}'_b(s)$ (or in dimensionless form $[p'_c(s)/\dot{m}'_b(s)]\ [\dot{m}\sqrt{\bar{p}_c}]$) can be established by solving the conservation equations for a diphasic flow (combustion gas and propellant droplets) within the combustion chamber, the latter providing the necessary boundary conditions).

If the frequency range of interest is low, with respect to the acoustic frequencies of the chamber, the oscillations (as already mentioned under paragraph 2) are not position-dependent and the chamber impedance is primarily function of the gas residence time within the chamber. Increasing the residence time augments the chamber admittance and will improve the stability behaviour.

If the frequency range of interest covers the acoustic frequencies of the chamber, the wave propagation velocity a_o has to be taken into account. The axial boundary conditions are provided downstream by the convergent part of the nozzle (irrotational nozzle admittance Ref. 5), upstream by the injection admittance at the injector plate, the chamber wall determining the radial boundary conditions. Acoustic cavities and baffles if any, will modify the chamber geometry and consequently alter the chamber impedance (generally, they will increase the damping and occasion a frequency shift of a few percent with respect to the pure acoustic frequency of the chamber). Thus, in a first approximation, the impedance of the chamber will mainly depend on the geometrical shape of the chamber and on the combustion gas properties $[a_o(\overline{P_c}, \bar{r}), \gamma]$ (see Ref. 1, Ref. 2, Ref. 4 for the case the admittance at the injection plate is neglected).

In the control loops represented on Fig. 1, instability will occur for those frequencies yielding impedance values of the combustion chamber, which, together with the corresponding values of the injection admittance and the $(n, \bar{\tau}_b)$-combustion pair, enable an open loop gain equal to or larger than unity. Normally these frequencies sensibly match the acoustic frequencies of the chamber at which the absolute impedance value usually peaks.

Equations 14 and Fig. 1 neither take into account the contribution to the unsteady burning rate provided by the oscillation of the mixture ratio of the injected propellants (secondary effect) nor that occasioned by the perturbation of the injection velocities, the impact of which is difficult to ascertain with precision in a real case (see Reardon's simplified treatment in Ref. 2).

● Injection admittance

For high frequency oscillations (range of the chamber acoustic modes), the injection admittance is generally governed by the resistance $2\overline{\Delta P}/\bar{m}_i$ respectively the inertance $1/N[\Sigma_K(l_K/A_K)]$ of the injector elements, considered in parallel, together with the capacitance v/a_i^2 of the distribution manifold. Further upstream, the HF-oscillations are usually damped out i.e. feedline and combustion chamber are uncoupled).

For low frequency oscillations, on the other hand, the wave propagation upstream into the feed-system has to be taken into account, usually up to a clear boundary condition provided either by a propellant pump or a cavitating venturi, and, depending on the value of the injector resistance, a coupling between feed-system and combustion chamber is existing (main cause of the "chugging" phenomenon) or not.

In both cases (HF and LF), increasing the injector resistance (i.e. for a given $\bar{m}_i$ value, increasing the pressure drop across the injector plate) will improve the stability behaviour of the chamber.

4. HF- AND LF-OSCILLATION PHENOMENA IN A GASEOUS HYDROGEN, LIQUID OXYGEN (GH_2:LOX) COMBUSTION CHAMBER

To illustrate the theory summarized under paragraph 3, we describe and interpret in this section the HF-respectively LF-stability behaviour of the GH_2:LOX HM7-combustion chamber developed at MBB-Ottobrunn for the 3rd-stage propulsion system (Ref. 8) of the Ariane launcher.

● Chamber configuration and feedsystem

Fig. 2 shows an axial cross section through the combustion chamber and the injector head.

The liquid oxygen (LOX) is fed to the combustion chamber by means of the LOX-dome, which enables a uniform distribution of propellant through the injector head.

The chamber assembly is regeneratively cooled by liquid hydrogen (LH_2).

At the outlet of the cooling channels, the hydrogen, having been heated up by means of the heat transferred from the chamber, is gaseous and feeds the hydrogen outlet manifold respectively distributor, which similarly to the LOX-dome, enables a uniform propellant injection into the chamber through the injector.

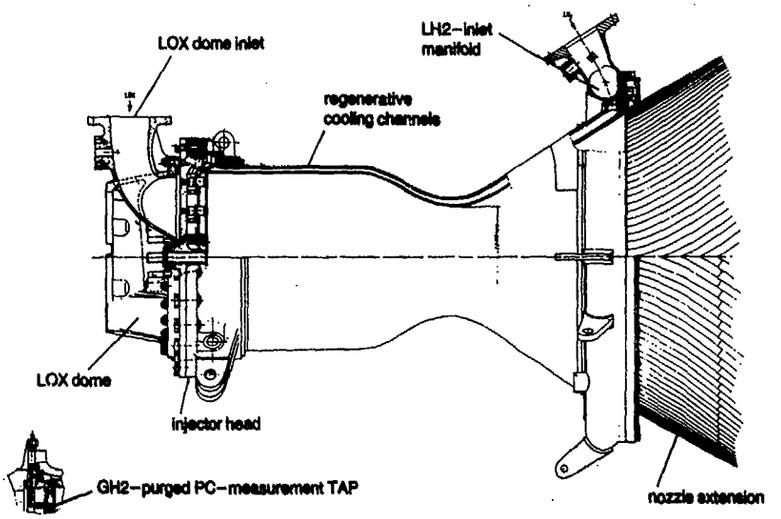


Fig. 2 LH2 ÷ LOX thrust chamber configuration

Both LOX- and LH_2 feedsystems include control valves and cavitating venturis, as represented on Fig. 3, so that the combustion chamber and the feed-systems upstream of the venturis are uncoupled.

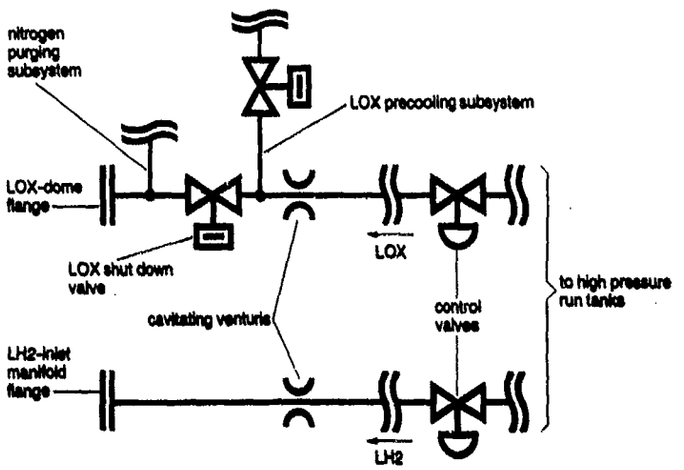


Fig. 3 LOX- & LH2-feedsystems

● Injector configuration

The HM7-thrust chamber (Ref. 8) uses a coaxial type injector element, a typical version of which is represented on Fig. 4 (other configuration variantes are described in detail in Ref. 9).

In the concentric tube element injector type, the oxydizer (liquid oxygen) is injected in the central tube, whereas the fuel (gaseous hydrogen) is injected at the periphery. While entering the combustion chamber, the low velocity liquid (LOX) jet is thus surrounded by a high velocity gas annulus and the atomization process takes place by means of a shearing mechanism between the two jets (as a result of the momentum exchange between fuel and oxider, liquid sheets are separated from the central jet and break into ligaments, the ligaments breaking themselves into droplets).

Additionally, the atomization process can be enhanced by the inclusion of a ribbon swirler in the oxidizer central tube (Fig. 4).

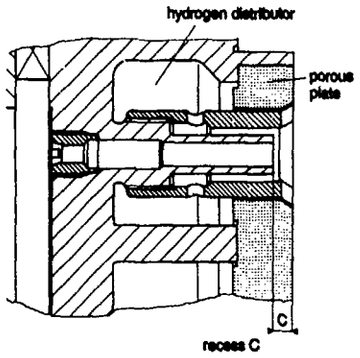


Fig. 4 Typical injector element configuration

As far as the propellants are concerned, the atomization efficiency primarily depends on density, surface tension and dynamic viscosity of the liquid repectively on density of the gas and differential velocity between the two jets. Moreover, it is in the design largely influenced by the value of the LOX-post recess c with respect to the hydrogen sleeve (Fig. 4) and the presence of cylindrical or tapered LOX-post elements (Ref. 9) and their diameter.

The pressure drop across the injector is mainly provided by restrictors disposed at the element's inlet but a fraction of it is also distributed along the element itself.

- Start-respectively shutdown sequence

Fig. 5 represents the start-respectively shut-down sequence used during the developement tests of the thrust chamber.

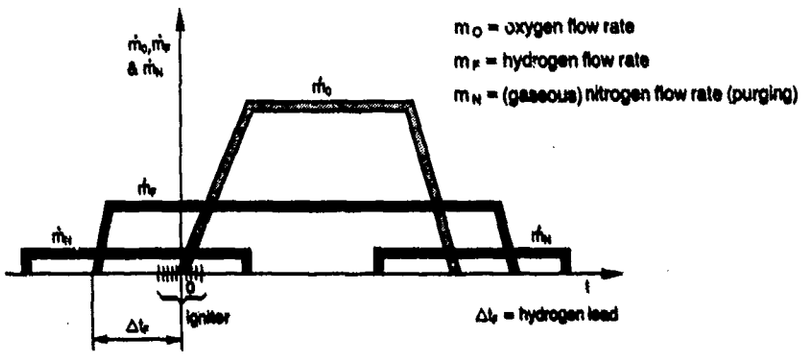


Fig. 5 Start-respectively shut-down sequence

For safety reasons (mixture ratio value, cooling problems), the chamber is started with an hydrogen lead (time duration Δt_F) ignited by means of an electrical torch igniter with a very high mixture ratio (Ref. 8). At the moment of ignition, the hydrogen flowrate injected into the chamber has reached its nominal value. As soom as ignition has been detected, the oxygen-"shutdown" valve is opened and oxygen is fed into the chamber. During the start-sequence, a gaseous nitrogen purge (flowrate $\dot{m}_N$ on Fig. 5) is activated to prevent a backflow over the injector into the oxidizer feedsystem. At the end of the test, the oxygen-shut-down valve is closed whereas the hydrogen flowrate has still its nominal value (hydrogen lag) and the nitrogen purge is simlarly activated as during start.

- Observed oscillation phenomena of the chamber pressure

  - LF oscillation phenomenon

Has been practically observed in each hot-run during the start and the shut-down phases, as shown on Fig. 6. It has been established, during the development test campaign, that the LF-oscillation corresponding to the start phase results from the coupling between the combustion chamber and the oxygen feedline, as the pressure drop across the oxygen injector goes through a minimum value. This minimum value is occasioned by the sudden liquefaction of the injected oxygen

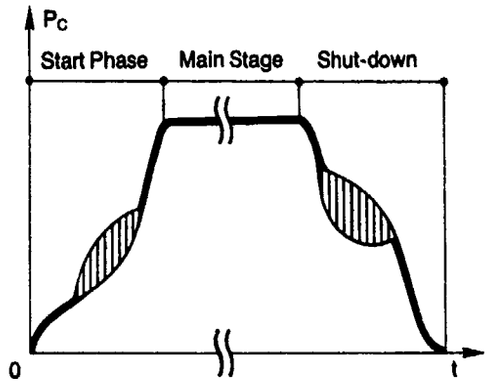


Fig. 6 Chugging phenomenon

propellant (during the precooling phase of the oxygen feedline, the shut-down valve – Fig. 3 – remains closed and the feedline section between valve and thrust chamber is not cooled down. At time t = 0, just after ignition, the valve opens and the heat stored in the hardware is high enough to vaporize the oxygen propellant, which, as a consequence, is injected under gaseous form for nearly 0.5 sec.). The coupling of the combustion chamber and the hydrogen feedsystem remains uncritical, as far as the LF-oscillation phenomenon is concerned (as the "chugging" oscillation is triggered, the pressure drop across the hydrogen injector is high enough due first, to the nominal flowrate of hydrogen, second, to the "high"-temperature at the outlet of the cooling channels occasioned by the combustion phenomenon itself. Furthermore, the pressure drop along the cooling channels themselves additionally enhances the uncoupling between combustion chamber and hydrogen feedsystem).

The LF-oscillation during the shut-down sequence, also results from the same coupling between chamber and oxygen feedsystem as during the start phase. However, the preponderant rôle played by the nitrogen purging subsystem has been clearly demonstrated, whereas this influence was negligible during the start phase.

– HF-oscillation phenomenon

Has only been observed during the chamber start sequence if the hydrogen injection temperature at the instant of ignition (more exactly at the opening of the oxygen "shut-down" valve – Fig. 3–, i.e. for t = 0) lay underneath a critical value $T_{if} \leq T_{if\ critical}$ function of the injector configuration.

Action on the value of T_{if} (t = 0) was provided by varying the time duration Δt_p of the hydrogen lead (Fig. 5), i.e. the precooling phase of the chamber assembly.

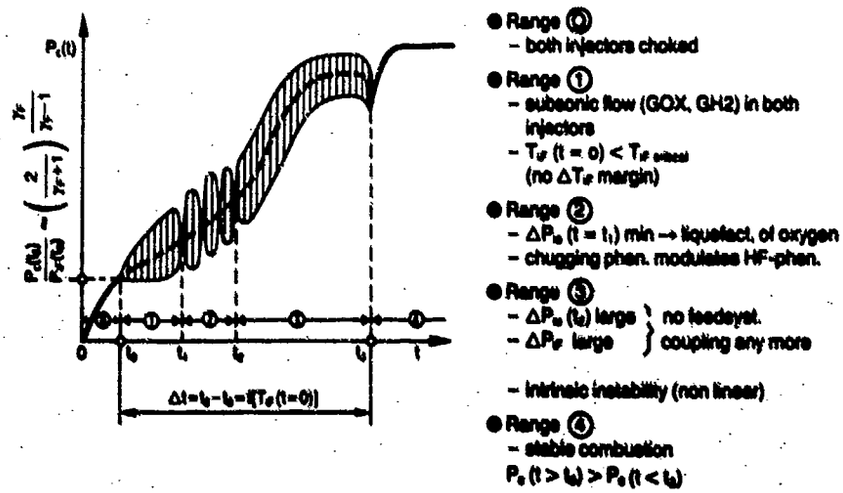
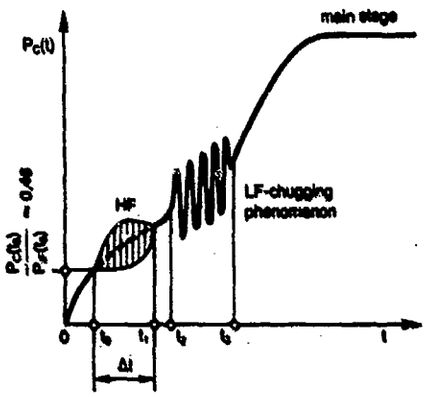


Fig. 7-1 HF-case A : T_{if} (t = o) < $T_{if\ critical}$ no ΔT_{if} (t = o) margin: full developed HF-phenomenon

The critical temperature condition for hydrogen injection being fulfilled, the HF-phenomenon was always triggered for a value of the ratio chamber pressure to hydrogen injection pressure sensibly equal to 0.46, i.e. exactly matching the ratio value $(P_c/P_{iF}) \approx \left(\frac{2}{\gamma_F+1}\right)^{\frac{\gamma_F}{\gamma_F-1}}$ at which the gaseous hydrogen in the injector switched over from the choked condition to the subsonic flow. Because the transition between the two flow types, in the hydrogen injector, always took place before the appearance of the "chugging" phenomenon in the chamber, the oxygen injected at that moment into the chamber was also gaseous, the transition between choked and subsonic flows in the oxygen injector sensibly occuring at the same time as for hydrogen.

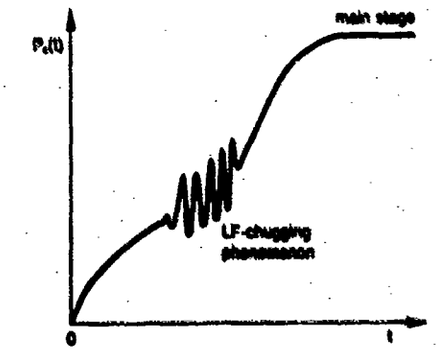
Since, as far as oxygen is concerned, the start sequence was repeatable from test to test, and, alone considered, had no action on the genesis of the HF-oscillation phenomenon, we can conclude that GH_2-feedsystem coupling with the combustion chamber was necessary to trigger the instability phenomenon.

According to the type of injector employed, the 2nd acoustic respectively 1st acoustic tangential mode of the chamber has been observed. The diagrams (Fig. 7) explain, for a given hardware configuration, the 3 encountered cases.



- $T_{iF}(t = o) \approx T_{iF\ critical}$
- $\Delta T_{iF}(t = o)$ margin insufficient
- Transition to HF-instability for $\frac{P_{c(t_1)}}{P_{iF(t_0)}} \approx 0{,}46$ (choked to subsonic transition)
- Short duration Δt of HF-phenomenon (HF-disappears before LF-genesis).
- 1T-mode (high injection velocity ratio)
- 2T-mode (low injection velocity ratio)

Fig. 7-2 HF-case B : $T_{iF}(t = o) \approx T_{iF\ critical}$: transient HF-phenomenon



- $T_{iF}(t = o) > T_{iF\ critical}$
- $\Delta T_{iF}(t = o)$ margin sufficient
- ΔP_{iF} large enough (no GH_2-feedsystem coupling)
- No HF-phenomenon
- LF-chugging initiated when ΔP_{iF} too low (liquefaction).

Fig. 7-3 HF-case C : $T_{iF}(t = o) > T_{iF\ critical}$: no HF-phenomenon observed

- Interpretation of the LF ("chugging") oscillation phenomenon

A possibility to make the interpretation of the "chugging" phenomenon would consist as reshuffling equation (14-2) (i.e. neglecting the intrinsic part and introducing a correction to take into account the contribution to the unsteady burning rate of the mixture ratio fluctuation – magnitude estimated to around 4 to 5 per cent of the total fluctuation –) and further performing an analysis of the so modified open loop transfer function using Nyquist's stability criterion.

However, knowing already, as explained above, the "chugging" phenomenon is mainly occasioned by the coupling between chamber and oxidizer feedsystem, when the pressure drop across the oxygen injector is insufficient, and remarking $(\dot{P}_c/\dot{m})\ Y_{io} \sim (\dot{P}_c/2\,\Delta\dot{P}_{io})$ is identical with a gain (i.e. a critical parameter), we choose as stability diagram a representation of the form $(\Delta\dot{P}_{io}/\dot{P}_c) = f(\Delta\dot{P}_{io}/\dot{P}_c)$, which shows the reduced fuel injector pressure drop as a function of the

reduced oxidizer pressure drop, a classical stability diagram displaying for low frequency oscillations (Ref. 2). We have two cases to consider: first, sea-level development tests; second, altitude simulation tests. With respect to the oxidizer feedsystem, the two test configurations differ as far as, for the altitude simulation case, the cavitating venturi (Fig. 3) has been deported upstream from around one meter so as to be situated outside of the vacuum cell.

In order of calculating the frequency of the pressure oscillations, we consider an homogeneous feed-line delimited on the one side by the cavitating venturi and on the other one by the thrust chamber and we solve the wave propagation equation

$$\frac{\delta^2 \tilde{Q}(z,t)}{\delta t^2} = \frac{1}{a^2_{LOx}} \frac{\delta^2 \tilde{Q}(z,t)}{\delta z^2} \tag{16-1}$$

with the boundary conditions

– for z = 0 (cavitating venturi):

$$\tilde{m}(z=o,t)=0 \tag{16-2}$$

(stating the cavitating venturi has an infinite impedance).

– for z = l (thrust chamber):

$$\tilde{p}(z=l,t)=\tilde{p}_0(t)+\tilde{p}_c(t) \tag{16-3}$$

(stating the pressure fluctuation in the feed-line for z = l is the sum of the corresponding fluctuations along the oxidizer injector and in the chamber)

where

$$\tilde{p}(z,t)=\frac{1}{C'}\frac{\delta \tilde{Q}(z,t)}{\delta z} \tag{16-4}$$

$$\tilde{m}(z,t)=-\frac{\delta \tilde{Q}(z,t)}{\delta t} \tag{16-5}$$

we obtain

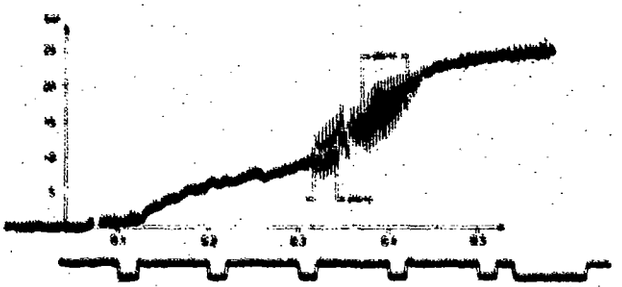
$$\mu \operatorname{cotg} \mu + \frac{C'l}{C_c} - \frac{L_0}{L'l}\mu^2 = 0 \tag{16-6}$$

provided $\overline{\Delta P_c}$ is negligibly small and (dP_c/dm_c) very large.

C'l is the capacitance of the feed-line (length l), repectively L'l its inertance, C_c the chamber capacitance and L_0 the injector inertance. The angular frequency ω is related to μ by

$$\omega^2 = \frac{\mu^2}{L'l \cdot C'l} \tag{16-7}$$

– Results of the sea-level configuration testing



T_{LOx} / K	125	120.8	114	105	
F_1 = (Hz) (1^{st}wave or fundamental wave)	226.2	226.2	230.0	267.1	excited mode
F_2 = (Hz) (2^{nd}wave or harmonic wave)	518.1	547.5	599.0	688.3	

Fig. 6-1 Calculated frequency and observed pressure oscillation in the chamber during start phase of the facility sea-level testing

Fig. 8-1 shows the chamber pressure fluctuations during the start phase, respectively the calculated oscillation frequency v.s. the temperature of the LOX-propellant inside the feed-line. It can be seen the first feed-line mode is excited, the correspondence between measured and calculated frequencies being satisfactory. (Note the strong influence of the propellant temperature – over the velocity of sound – on frequency.)

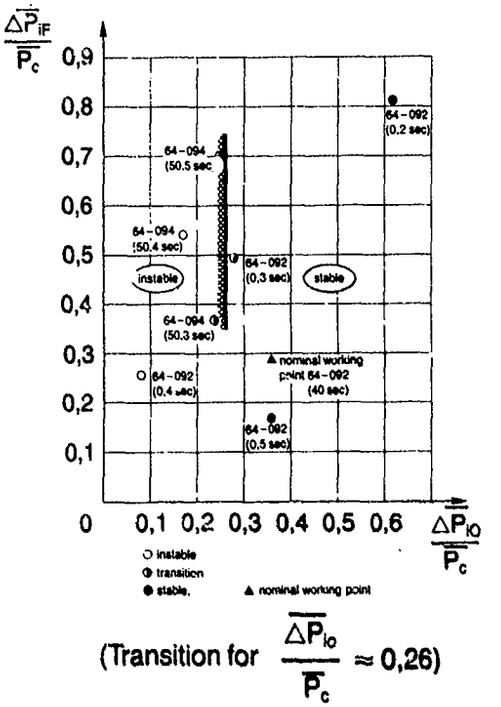


Fig. 8-2 Stability diagram of the combustion chamber during the facility sea-level testing.

Fig. 8-2 displays the stability diagram of the combustion chamber for the facility sea-level configuration. Transition between instability and stability occurs for:

$$\left(\frac{\overline{\Delta P_{io}}}{\overline{P_c}}\right)_{critical} \approx 0.26 \pm 0.02$$

As noticed before, $(\overline{\Delta P_{iF}}/\overline{P_c})$ in the range 0.4 to 0.7 has little influence on transition.

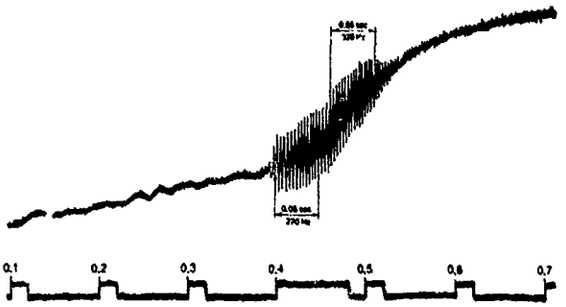
At the nominal working point, $\left(\frac{\overline{\Delta P_{io}}}{\overline{P_c}}\right)_{nominal} \approx 0.35$, which provides enough margin for a smooth operational use of the chamber.

– Results of the altitude simulation testing

Fig. 9-1 shows the chamber pressure oscillations during the start phase as well as the corresponding calculated mode frequencies. It is apparent that the frequency of the feed-line modes is lowered, with respect to the sea-level testing configuration, due to the increased length of the line.

On the other hand, this time the second feed-line mode is excited, which corresponds to a higher oscillation frequency than in the sea-level case.

Calculated and measured frequencies are in satisfactory condordance (similarly, note the strong temperature effect on the frequency value of the feed-line modes).



$\frac{T_{LOX}}{K}$	125	120.8	114	105	
F_1 = (Hz) (1^{st}wave)	123.2	128.3	136.2	145.0	
F_2 = (Hz) (2^{nd}wave)	260.7	275.3	299.2	327.0	excited mode

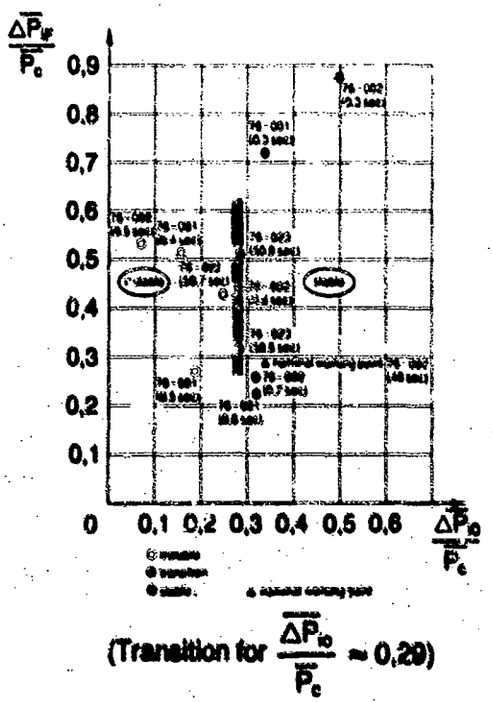
Fig. 9-1 Calculated frequency and observed pressure oscillation in the chamber during start phase of the facility altitude simulation testing.

Fig. 9-2 illustrates the instability respectively the stability domain of the combustion chamber for the altitude simulation testing configuration of the facility.

Transition between instability and stability sensibly occurs for

$$\left(\frac{\overline{\Delta P}_{ip}}{\overline{P}_c}\right)_{critical} \approx 0.29$$

which represents a degradation of around 12 per cent with respect to the sea-level testing configuration of the facility.



(Transition for $\frac{\overline{\Delta P}_{ip}}{\overline{P}_c} \approx 0{,}29$)

Fig. 9-2 Stability diagram of the combustion chamber during the facility altitude simulation testing.

As in the previous case, $(\Delta P_{if}/P_c)$ (between 0.3 and 0.6) has no noticeable effect on the transition line. At the nominal working point,

$$\left(\frac{\overline{\Delta P}_{io}}{\overline{P}_c}\right)_{nominal} \approx 0.33$$

which provides enough margin for a smooth operational use of the chamber.

– For both facility configurations (sea-level and altitude simulation) in the starting transient phase, the gaseous oxygen injected into the chamber generally switches over from the choked condition to the subsonic flow in the injector less than 0.2 sec after ignition.

As of now, although the injected flowrate is low, the corresponding pressure drop across the injector $\overline{\Delta P}_{io}$ is relatively high, due to the low value of the gas density, and the ratio $(\overline{\Delta P}_{io}/\overline{P}_c)$ has an order of magnitude around 0.5 : 0.6, the combustion chamber being stable.

When the injected oxygen liquefies, the pressure drop across the injector collapses (due to the higher fluid density), the ratio $(\overline{\Delta P}_{io}/\overline{P}_c)$ taking typical values of 0.1 : 0.2 and the chamber is instable.

Since the injected flowrate keeps increasing, the pressure drop across the injector increasing faster than the chamber pressure, the oscillation disappears (transition value of $(\overline{\Delta P}_{io}/\overline{P}_c)$ from 0.26 to 0.29). Above the transition value of $(\overline{\Delta P}_{io}/\overline{P}_c)$, the chamber is stable.

– When the mean pressure drop $\overline{\Delta P}_{io}$ across the injector is negligible, whereas $(dP_c/d\dot{m}_o)$ is large (the mean mixture ratio being very low), we can interpret the LF-oscillation as a resonance phenomenon between the oxygen-feedsystem and the thrust chamber (assimilated then to the pair LOX-injector inertance and chamber capacitance, presenting the undamped natural frequency Ω). Among the modes which can be excited in the feedsystem (equations 16-), the thrust chamber picks-up the next neighbour ω_K of its natural frequency Ω. The nearer ω_K lies from Ω, the stronger is the resonance phenomenon involved.

This simplified reasoning neglects the total time lag and one needs, as "power" source, an increase of the flowrate v.s. time at the cavitating venturi, a condition which indeed is fulfilled during the start phase of the chamber (Fig. 5), in order an oscillation be triggered in the chamber (open loop system).

However, we actually have to deal with a closed loop system exhibiting moreover a dead time (the total time lag). Consequently, an oscillation can be triggered without necessitating an increase of the flowrate v.s. time at the cavitating venturi, the transition to instability sensibly taking place for $1 + Z_c(s)\,[1 + \varepsilon]\,Y_{io}(s) \exp(-\bar{\tau}_{oT} s) = 0$, which is a variante of equation (14-3), where $Z_c(s)$ primarily depends on the residence time of the combustion gas within the chamber, respectively ε ($\bar{r}$, c^*, $\delta c^*/\delta r$) represents the contribution of the mixture ratio oscillation of the propellants at the injection, and, the intrinsic part has been neglected.

● Interpretation of the HF-oscillation phenomenon

– HF-oscillation genesis (gaseous propellants)

We have seen above, that a "GH_2-feedsystem coupling" with the chamber was necessary to trigger the HF-oscillation phenomenon (start of phenomenon for $(P_c/P_{if}) \approx \left(\frac{2}{\gamma_F + 1}\right)^{\frac{\gamma_F}{\gamma_F - 1}}$ as both propellants injected into the chamber were gaseous. The question which now arises is to know wether this coupling is sufficient or, in other words, wether a certain contribution of the intrinsic loop (Fig. 1) is indispensable (the trouble being of course, that the combustion gain of the latter is unknown).

In oder to investigate this question, we first suppose the contribution of the feedsystem coupling alone is sufficient to start and sustain instability. Doing this, we obtain a critical value of the total time lag which, in this case, practically reduces to the sum of the heating and mixing elementary time lags, if we suppose, a) the time lag corresponding to the chemical reaction is negligibly small, b) admit the injection time lag (equation (5)) has no real significance for a coaxial injector type fed by gaseous propellants. Second, having obtained the critical value of the corresponding total time lag and remarking "burning time lag" and "total time lag" are for our case practically alike, we will compare this critical value with the period duration of the corresponding HF-oscillation.

If we suppose the main part of the combustion gain (equation (15-2)) is a real number, then the order of magnitude of the necessary "burning time lag" should sensibly be equivalent to $T_{nm}/2$, where T_{nm} is the oscillation period of the involved nm-mode.

Consequently if $(\bar{\tau}_T)_{critical}$ has an order of magnitude similar to or larger than $T_{nm}/2$, we will conclude that a contribution of the intrinsic loop is involved in the triggering of the HF-phenomenon. If, on the other hand, $(\bar{\tau}_T)_{critical}$ is far smaller than $T_{nm}/2$, we will conclude, within the scope of our hypothesis, that no contribution of the intrinsic loop is necessary to start the HF-phenomenon.

Considering the equation $1 + A^i_{nm} Z_o(s)\, Y_i(s) \exp(-\bar{\tau}_T s) = 0$, we can express the amplification coefficient λ of the complex frequency s as well as the shift ω_1 of the angular frequency with respect to the value of the pure acoustic mode ω_o as follows:

$$2\frac{l}{a_o}\lambda \approx A^i_{nm}\,\gamma\, M_e \left\{ \left[\frac{K_{ox} D_{ox}}{1+D_{ox}^2} + \frac{K_F D_F}{1+D_F^2} \right] \sin \bar{\tau}_T \omega - \left[\frac{K_{ox}}{1+D_{ox}^2} + \frac{K_F}{1+D_F^2} \right] \cos \bar{\tau}_1 \omega - \frac{1 + \frac{\alpha_r(\omega)}{M_e}}{A^i_{nm}\,\gamma} \right\} \qquad (17\text{-}1)$$

respectively

$$2\frac{l}{a_o}\omega_1 \approx A^i_{nm}\,\gamma\, M_e \left\{ \left[\frac{K_{ox}}{1+D_{ox}^2} + \frac{K_F}{1+D_F^2} \right] \sin \bar{\tau}_T \omega_o + \left[\frac{K_{ox} D_{ox}}{1+D_{ox}^2} + \frac{K_F D_F}{1+D_F^2} \right] \cos \bar{\tau}_T \omega_o - \frac{\frac{\alpha_i(\omega_o)}{M_e}}{A^i_{nm}\,\gamma} \right\} \qquad (17\text{-}2)$$

where

ω = $\omega_o + \omega_1$ = angular frequency
l = cylindrical length of the chamber
a_o = velocity of sound in the chamber
γ = $(c_p/c_v)_{chamber}$
M_e = Mach number at the inlet of the convergent
α = $\alpha_r + i\alpha_i$ = irrotational admittance of the convergent part of the nozzle

$$D_K \approx \tau_K \omega - \frac{1}{T_K \omega + \frac{2\,\overline{\Delta P}_{iK}}{\bar{m}_K} (Y_{Im})_{KFL}} \qquad (K = O \text{ or } F)$$

τ_K = time constant of the corresponding injector

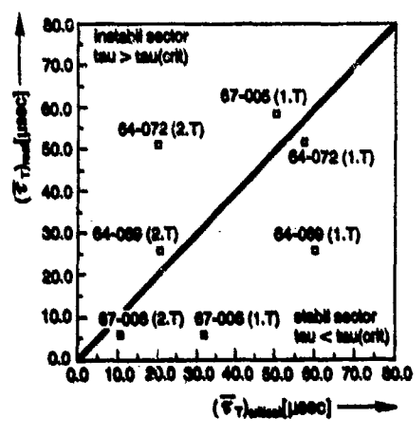
$$K_K \approx \left[\frac{\bar{P}_c}{2\,\overline{\Delta P}_{iK}} \cdot \frac{\bar{r}}{\bar{r}+1} \right] \left[1 - \frac{1}{\gamma_K} \cdot \frac{\overline{\Delta P}_{iK}}{\bar{P}_c} \right]$$

T_K = time constant of the pair injector-dome (k = O) or injector distributor (k = F)
$\overline{\Delta P}_{iK}$ = mean pressure drop across the corresponding injector
$\bar{m}_K$ = mean injected mass flow in the corresponding injector
$(Y_{Im})_{KFL}$ = imaginary part of the feedsystem admittance seen from dome or distributor.
$\bar{r}$ = mean mixture ratio in the chamber
γ_K = $(c_p/c_v)_K$
A^i_{nm} = amplification coefficient (nm-mode) related to the feedsystem coupling, introduced by the injection distribution density function.

Using equations (17) for the instant at which the hydrogen flow in the injector switches from the choked condition to the subsonic flow, we find, for the injector configuration leading to the excitation of the 2nd tangential mode ($A^i_{21} \approx 2{,}510$ for a uniform injection distribution density), a critical value of the total time lag $(\bar{\tau}_T)_{critical} \approx 20$ usec, whereas $\omega = \omega_{21} \approx 50369$ sec^{-1} corresponds to $(T_{21}/2) \approx 62.4$ usec.

For the injector configuration leading to the excitation of the 1st tangential chamber mode ($A^i_{11} \approx 1{,}980$ for a uniform injection), we find, under the same conditions $(\bar{\tau}_T)_{critical} \approx 50$ usec, whereas $\omega = \omega_{11} \approx 31532$ sec^{-1} corresponds to $(T_{11}/2) \approx 99.6$ usec.

In both cases, we see $(\bar{\tau}_T)_{critical}$ is smaller than $(T_{nm}/2)$, however, it is not small enough in order $(1 - \cos \bar{\tau}_b \omega)$ be completely negligible, which means the intrinsic loop, depending on the combustion gain $G(\omega)$, could contribute to the genesis of the HF-phenomenon. when both injected propellants are gaseous.



● Complex frequency $s = \lambda + i\omega$
– λ : amplification coeff.
– ω : angular frequency

$$\omega = \omega_0 + \omega_1 \begin{cases} \omega_0 = \text{acoust. value} \\ \omega_1 = \text{shift} \end{cases}$$

● Characteristic equation
$1 + A^i_{nm} Z_o(s) y_i(s) \exp(-\bar{\tau}_T S) = 0$
$\lambda = 0 \rightarrow (\bar{\tau}_T)_{critical}$

● $(\bar{\tau}_T)_{real} \approx \tau_o \left(\frac{E_{ignition}}{E_{chamber}} \right)^k$

(τ_H & τ_M partially overlapped)

Fig. 10 Correlation tentative $(\bar{\tau}_T)_{real} = f(\bar{\tau}_T)_{critical}$ for different tests results with gaseous propellants (GOX, GH2)

On Fig. 10, we have tentatively tried to correlate several test results by drawing the diagram $(\bar{\tau}_T)_{real} = f(\bar{\tau}_T)_{critical}$.

In this diagram, if $(\bar{\tau})_{real} < (\bar{\tau}_T)_{critical}$, the chamber is stable. If $(\bar{\tau}_T)_{real} \geq (\bar{\tau}_T)_{critical}$ the chamber is instable.

Remarking that in the relationship $\tau_T = \tau_H + \tau_M$ the two different operations of propellant heating and propellant mixing (corresponding to the two elementary time lags) are probably more overlapped than separated, we have expressed $(\bar{\tau}_T)_{real}$ as a function of the ratio between the energy which is necessary to heat the injected cold hydrogen up to the ignition level and the heat contained in the combustion chamber at the same time:

$$(\bar{\tau}_T)_{real} \approx \tau_o \left(\frac{E_{ignition}}{E_{chamber}} \right)^a \tag{18}$$

where the constant τ_o and the exponent a have been chosen in order the total time lag $(\bar{\tau}_T)_{real}$ of the injector configuration leading to the excitation of the 1st chamber tangential mode be situated lightly beyond the instability border in the instable sector. The correlation, although relatively simple, works surprisingly good and enables a correct interpretation of the test results (Fig. 10), which shows the contribution of the intrinsic loop seems to be marginal and consequently in the expression $\gamma M_e G(\omega)[1 - \cos \bar{\tau}_b \omega]$ (which should be added to the RHS of equation 17-1 in order to take into account the contribution of the intrinsic loop) the gain $G(\omega)$ should be small enough to be neglected.

– HF-oscillation during the liquefaction of the injected oxidizer

Fig. 11 presents the case of an injector configuration resulting in the excitation of the 2nd tangential mode of the chamber (see also Fig. 7-1). The figure shows the acceleration of the chamber assembly at the instant where both HF-oscillation and LF-oscillation are fully developed in the combustion chamber. On this picture, it is apparent that the HF-oscillation is amplitude modulated by the LF-signal. This signifies, that at this time, the contribution of the intrinsic loop to the HF-oscillation phenomenon can still be neglected, whereas the influence of the hydrogen feedsystem decreases due to the

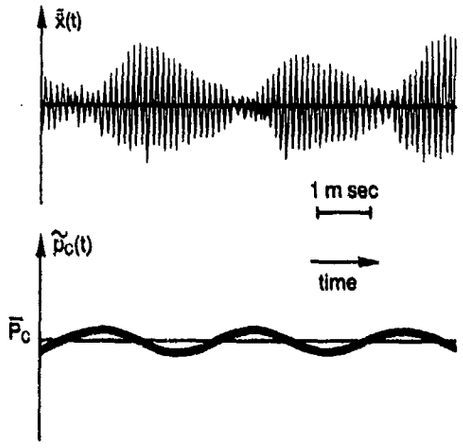


Fig. 11 Structure acceleration and "chugging"-phenomenon during liquefaction of the injected oxidizer and simultaneous HF-instability (Test 64-069)

increasing pressure drop $\overline{\Delta P}_{if}$ across the hydrogen injector, occasioned by the increasing injection temperature, the main cause of the HF-instability being now provided by the coupling with the oxygen feedsystem/equation (14-2) practically reduces to $1 + A^1_{nm} Z_c(s)\ Y_{io}(s)\ \exp(-\bar{\tau}_{To} s) = o$ where $Y_{io}(s) \cdot (\bar{P}_c/\bar{m}) \sim (\bar{P}_c/2\,\overline{\Delta P}_{io})$, $\overline{\Delta P}_{io}$ being, from the HF-view point, modulated by the LF-fluctuation $\tilde{m}_{io}(\Omega)$ of the injected flowrate: $\overline{\Delta P}_{io} \sim (\xi/2\rho A^2)(\bar{m}^2_{io} + 2\bar{m}_{io}\tilde{m}_{io} + \cdots)$

This similarly modulates the gain $K_{ox} \sim (\bar{P}_c/2\,\overline{\Delta P}_{io})(\tilde{f}/f + 1)$ on which the amplification coefficient of the complex high frequency $s = \lambda + i\omega$ depends/.

Note that the observed predominance of the LOX-feedsystem coupling, in this section of the chamber start phase, is probably enhanced by the influence of the injection velocity perturbation on the total time lag (Reardon Ref. 2).

– HF-oscillation after the disappearance of the "chugging"-phenomenon (Fig. 7-1)

After the disappearance of the "chugging"-phenomenon, the mean pressure drop across the LOX-injector, $\overline{\Delta P}_{io}$, has practically reached its nominal value, whereas $\overline{\Delta P}_{if}$, the mean pressure drop along the hydrogen injector, is sensibly higher than its nominal value, due to the increased heat transfer to the cooling channels occasioned by the HF-phenomenon. Under those circumstances no coupling between combustion chamber and feedsystem exists any more and the HF-oscillation, if it persists, is solely controlled by the intrinsic loop, where non-linear phenomena limit the amplitude of the fluctuation.

During the transition back to stability, equation (14-2) reduces to $Y_c(s) = A^o_{nm}(\bar{m}/\bar{P}_c)\,(\tilde{f}/f + 1)\,(n_o[1 - \exp(-\bar{\tau}_{to} s)] + \cdots)$.

Where $A^{o}_{nm} \approx 1$ (Ref. 4), because of the uniform injection density, and the contribution of hydrogen has been omitted, due to the low value of $\bar{\tau}_{Fb}$ with respect to $\bar{\tau}_{ob}$.

At main stage and under the assumption the HF-phenomenon, if any, initiated during the start phase of the chamber has ceased, the chamber is always stable for all injector configurations. This means the intrinsic loop alone, to the contrary of what is known for the storable propellants (Ref. 2, Ref. 4), is insufficient to trigger instability. In other words, the combustion gain, mainly affected here by the pressure interaction index, is always too low.

5. POSSIBLE MEASURES TO BE TAKEN IN ORDER OF INFLUENCING COMBUSTION INSTABILITY

● LF-case

– Action on the injection admittance

As mentioned under paragraph 3, the injection admittance has to be minimized in order of improving the stability behaviour.

Since $(\bar{P}_c/\bar{m})\ Y_i(s) \sim (\bar{P}_c/2\,\overline{\Delta P_i})$, this implies increasing: a) the pressure drop across the injector by reducing the cross-sectional area of the injector orifices, b) the pressure drop in the feedsystem by inserting restrictors in the feedlines (in both cases, the limitation factor being the maximum injection pressure drop tolerated by the turbopumps or equivalent feed-systems), c) if possible, for a given pressure drop $\overline{\Delta P_i}$, decreasing the combustion pressure (difficult to realize since chamber pressure is generally dictated by other considerations). Moreover we have seen a variation (increase or reduction) of the length of the feedline tubing also affects the stability limit.

– Action on the chamber impedance

As seen under paragraph 3, the chamber impedance has to be minimized. Since $(1/Z_c(s)) = Y_c(s) \approx (1 + \theta_c s)/\gamma(\bar{P}_c/\bar{m})$, where θ_c is the combustion gas residence time, increasing this relaxation time, by increasing the combustion chamber volume, will improve the stability behaviour.

– Action on the total time lag

In order of improving the stability behaviour, the total time lag /equation (3)/ has to be held as small as possible. This can be achieved in a given case either by modifying the propellant properties [use of a more volatile propellant, addition of catalytic substances etc. (Ref. 10)] or more likely, by means of geometrical trimming of the injector in view of reducing the insensitive time lag /equation (4-1)/ and improving the mixing process /for examp. in the case of a coaxial injector with the GH_2 : LOX propellant combination, action on the value of the recess parameter c (Fig. 4) will affect atomization and mixing processes/.

A recirculation of the combustion gases will alike enhance heating/vaporizing and mixing mechanisms and so doing, affects the sensitive time lag /equation (4-2)/. It must be remarked that the effects of the injector trimming have, in a large manner, to be experimentally determined. Moreover they will generally influence the efficiency of combustion.

● HF-case

All that has been said above, with respect to the injection admittance, remains true. Additionally, increasing the inertance of the injector elements will also enhance stability.

As far as the chamber impedance is concerned, the main action, in order of improving the HF-stability behaviour, will consist in inserting, in the combustion zone of the chamber damping devices such as acoustic cavities and baffles (problem areas: for the cavities, temperature and gas composition inside the cavity itself must be precisely known since they influence the corresponding velocity of sound; for the baffles, mechanical integrity and cooling problems). In case of a regeneratively cooled combustion chamber, a modification c' the shape of the convergent part of the nozzle /action on $\alpha_t(\omega)$, real part of the irrotational nozzle admittance, in equation (17-1)/ will generally not be possible since this shape is largely conditioned by the chamber cooling.

A modification of the injector parameters (injection areas, propellant velocities, injection angles if any, etc. ...) will affect the spray quality and therefore modify the combustion gain and associated time lag. As mentioned above, the influence of this injector "trimming" has to be empirically determined during the experimental investigation of the stability and efficiency behaviour of different injector sets.

6. CONCLUSION

In the present paper, we have tried to explain the instability behaviour of a combustion chamber fed by gaseous or liquid propellants, using, among others, the combustion time lag theory as an investigating tool.

To illustrate the theory, the concrete example of a hydrogen/oxygen thrust chamber was considered. It was shown the theory enables a satisfactory interpretation of the experimentally observed instability processes.

7. ACKNOWLEDGEMENTS

The authors wish to thank the direction of MBB's propulsion department for permission to publish this paper although the views expressed are only their own.

8. LITERATURE

1. **Crocco & Cheng:** "Theory of Combustion Instability in Liquid Propellant Rocket Motors ".
Agardograph N° 8 Butterworths scientific publications 1956.

2. **Harrje D. T. & F. H. Reardon:** "Liquid Propellant Rocket
Combustion Instability".
NASA SP-194, 1972.

3. **F. H. Reardon, J. M. Mcbride & A. J. Smith JR.**
"Effect of Injection Distribution on Combustion Stability".
AIAA-Journal March 1966, Vol. 4, N° 3.

4. **D. Schmitt, D. Lourme**
"A Model of Instability of Liquid Propellant Engine with Radial Injection"
32nd International Aeronautical Congress
IAF-Paper N° 81-362.

5. **L. Crocco & W. A. Sirignano**
"Behaviour of Supercritical Nozzles under Three Dimensional Oscillatory Conditions".
Agardograph N° 117.

6. **J. Fang**
"Application of Combustion Time-Lag Theory to Combustion Stability Analysis of Liquid and Gaseous Propellant Rocket Engines".
AIAA 22nd Aerospace Sciences Meeting.
AIAA-84-0510.

7. **L. Crocco**
"The Relevance of a Characteristic Time in Combustion Instability".
2nd Combustion Conference.
CPIA-Publication N° 105, May 1966.

8. **H. Dederra & E. Kirner**
"Test Results with a Regeneratively Cooled LOX/LH, Thrust Chamber for the Ariane 3rd Stage Propulsion System".
AIAA-Paper N° 75-1189, AIAA/SAE 11th Propulsion Conference, Anaheim California, Sept. 29 - Oct. 1, 1975.

9. **G. S. Gill**
"A Qualitative Technique for Concentric Tube Element Optimization, Utilizing the Factor (Dynamic Head Ratio-1)".
AIAA 16th Aerospace Sciences Meeting, Huntsville Alabama, January 16-18, 1978.

10. **M. Summerfield**
"A Theory of Unstable Combustion in Liquid Propellant Rocket Systems".
ARS-Journal pp. 138-114, September 1951

EFFETS DES INSTABILITES DE BASSE FREQUENCE SUR LE FONCTIONNEMENT DES PRISES D'AIR DE STATOREACTEUR

par

C.Sans
Office National d'Etudes et de Recherches Aérospatiales
Boite Postal No.72, 92322 Châtillon CEDEX
France

RESUME

La propulsion par statoréacteur est un moyen idéal pour certains types de missiles de moyenne et longue portée. Ce type de moteur fait apparaître, sous certaines conditions, des instabilités générées par la chambre de combustion. Pour certaines géométries, des basses fréquences sont émises.

Le problème posé consiste donc à savoir si celles-ci peuvent modifier les performances des prises d'air.

Des essais réalisés à Mach 2,0 sur une prise d'air circulaire permettent grâce à un système mécanique de réaliser des fluctuations de pression importantes à des fréquences variant entre 0 et 200 Hz.

Les principaux résultats de cette étude montrent que les instabilités engendrées ne déclenchent pas le pompage de la prise d'air, sauf pour des régimes de fonctionnement très subcritiques. Le piège à couche limite interne atténue très nettement les fluctuations de pression.

ABSTRACT

Ramjet propulsion has proven to be very efficient at least for some types of missile and especially for intermediate or long range missiles. However instabilities can be generated in the combustion chamber under particular flight test conditions. Depending on the geometry, low frequency instabilities can occur.

It is necessary to know the influence of these low frequency instabilities on the inlet performance.

In order to investigate this problem, tests have been carried out on an axysymmetric inlet equipped with a mechanical device providing large pressure fluctuations between 0 and 200 Hz.

The tests were performed at a Mach number of 2.

The analysis of the results shows that the instabilities do not lead to the buzz of the inlet for usual operating conditions. The internal boundary layer bleed reduces drastically the pressure fluctuations.

1 - INTRODUCTION

La propulsion par statoréacteur est un moyen idéal pour certains types de missile de moyenne et longue portée.

Ce type de moteur peut laisser apparaître sous certaines conditions des instabilités de basse fréquence générées par la chambre de combustion.

L'expérience acquise, montre qu'en général, ces basses fréquences sont voisines de 100 à 200 Hz, qu'elles se manifestent principalement à bas nombre de Mach, par temps froid et peuvent atteindre des amplitudes proches de 30 %, comme le montre les diagrammes de la figure 1.

Si ces perturbations sont importantes, on peut penser qu'elles peuvent modifier le comportement des prises d'air en diminuant le rendement ou même, dans certains cas provoquer le décrochage et le pompage.

L'ONERA a développé des moyens d'essais ; les résultats présentés sont ceux obtenus lors des essais de ces dernières années.

2 - ETUDE PRELIMINAIRE - PRISE D'AIR BIDIMENSIONNELLE

Une première étude a été effectuée avec une maquette de prise d'air bidimensionnelle existante, placée dans un écoulement à un nombre de Mach relativement élevé, voisin de 3 et en incidence.

Cette maquette était installée sur la paroi latérale de la veine de mesure figure 2.

L'écoulement capté par la prise d'air est dévié vers un caisson extérieur à la veine d'essai qui se termine par un obturateur permettant de modifier le régime de fonctionnement de la prise d'air et également de mesurer le débit.

Ce caisson est pourvu d'un haut-parleur pneumatique qui a été choisi comme moyen d'excitation de l'écoulement. Celui-ci, comme le montre la figure 3 présente une plage d'énergie maximale entre 300 et 1000 Hz qui correspond à environ 120 db à la pression atmosphérique.

Ce moyen d'essai, bien que séduisant, présentait toutefois quelques inconvénients :

- en premier lieu, le débit d'air nécessaire au fonctionnement du haut-parleur devait être soustrait, après mesure, du débit global.
- la pression du caisson étant relativement faible, les performances du haut-parleur étaient diminuées d'autant ;
- la gamme de fréquence correspondant à l'énergie maximale était trop élevée.

Malgré ces inconvénients, de nombreuses mesures ont pu être effectuées pour différents points de fonctionnement de la prise d'air, du régime supercritique au régime subcritique.

Dans aucun des cas, les fluctuations de pression engendrées à l'aval, dans le caisson, n'ont provoqué un pompage de la prise d'air.

A titre d'exemple, on a reproduit sur la figure 4, les signaux obtenus pour différents capteurs situés entre le point d'émission et le plan d'entrée de la prise d'air. La zone sombre représente la différence entre les configurations avec et sans instabilités.

On remarque l'atténuation progressive de la perturbation aval, lorsque l'on se déplace vers l'amont. Sur les capteurs n° 1 et n°2, on observe l'apparition à des fréquences plus faibles d'une nouvelle perturbation qui correspond à la proximité du choc de recompression et au piège à couche limite dans lequel un jet assez turbulent existe.

Ces résultats ne permettant pas de conclure définitivement sur le bien-fondé du problème, ceci en partie à cause du système générateur d'instabilités qui conduit à des Δp trop faibles, à sa fréquence d'utilisation trop élevée, ainsi qu'à cause de l'équipement trop restreint de la prise d'air, une nouvelle série d'essais a été décidée.

3 - REPRISE DES ESSAIS - PRISE D'AIR CIRCULAIRE

Pour simplifier le problème et pour se mettre dans les conditions les plus favorables, il a été décidé de reprendre ces essais avec une prise d'air circulaire. Celles-ci sont, en général, présentées comme nettement plus instables.

De même, pour rester dans le domaine incriminé, le nombre de Mach de 2,0 a été choisi.

3.1. Présentation du montage

La figure 5 présente ce nouveau montage, qui va être détaillé ensuite.

Le principe de base reste le même que précédemment : l'écoulement capté par la prise d'air passe, après un coude de liaison, dans un caisson extérieur à la veine d'essai. Celui-ci se termine par un obturateur assurant deux fonctions :

- la variation du régime de fonctionnement de la prise d'air,

- la mesure du débit après un tarage du col.

La partie arrière de la maquette, au niveau du coude a été aménagée pour y installer un nouveau générateur d'instabilités de type mécanique.

La maquette proprement dite est présentée sur la figure 6.

A l'amont, se trouve la prise d'air circulaire à pointe conique qui peut prendre deux configurations géométriques distinctes avec ou sans piège à couche limite interne. Elle est suivie d'une manchette interchangeable qui permet d'effectuer, au choix, des mesures stationnaires ou instationnaires.

A l'aval, on trouve le coude, aménagé pour qu'une partie de l'écoulement passe par un col sonique auxiliaire.

Ce dispositif est défini sur la figure 7 qui montre les divers éléments constitutifs du système.

Celui-ci comprend, après la dérivation :

- le col sonique auxiliaire interchangeable en forme de lunule,

- un disque perforé par deux lumières dont la rotation est assurée par un moteur électrique.

Cette rotation détermine les fréquences de fluctuation de débit comprises entre quelques hertz et 200 Hz maximum.

La forme de la lunule assure des fluctuations de type sinusoïdal, sa taille autorise des Δp plus ou moins importants.

3.2. Moyens de mesure

Les mesures sont principalement regroupées dans deux zones bien distinctes :

- la première correspond à la prise d'air, figure 8. Les mesures de la pression pariétale sont effectuées sur le profil interne de la carène et sur le corps central. Comme nous le verrons ultérieurement, cet équipement assez complet permet d'estimer la position du choc interne pour chaque point de fonctionnement et de connaître les déplacements de ce choc en présence des instabilités de pression engendrées à l'aval ;

- la deuxième zone est située dans le plan appelé "fin de diffuseur" dans lequel on caractérise le fonctionnement de la prise d'air. C'est dans ce plan que sont calculés les coefficients de débit et surtout l'efficacité de la prise d'air. La figure 9 illustre les moyens utilisés, tant stationnaires qu'instationnaires.

3.3. Résultats stationnaires

Lors de ces essais, on s'est d'abord attaché à caractériser la prise d'air dans tout son domaine de fonctionnement pour les deux configurations, avec et sans piège interne.

Les résultats obtenus sont présentés sur la figure 10. Les courbes caractéristiques montrent bien l'intérêt de la configuration avec piège à couche limite interne qui permet d'augmenter sensiblement l'efficacité au prix, il est vrai, d'une perte de débit , mais celle-ci peut-être compensée par une légère augmentation de la section d'entrée.

L'utilisation de la composante continue des mesures instationnaires effectuées sur le corps central et la carène permet d'obtenir, pour chaque point de fonctionnement repéré sur la caractéristique, la répartition des pressions internes correspondantes, figure 11.

Ces tracés, outre la compréhension de l'écoulement interne renseignent, avec plus ou moins de précision selon les cas, sur la position du choc de recompression.

Ceci nous amène à la figure 12 qui présente, pour les configurations avec et sans piège interne, les courbes relatives au déplacement du choc et donne l'efficacité correspondante.

On peut remarquer :

- que la limite de pompage est obtenue pour la même position longitudinale du choc sur le cône à l'amont de la carène, quelle que soit la configuration.
  Ceci est logique, si l'on admet qu'une des causes connues du déclenchement du pompage est l'ingestion par la prise d'air de la ligne de glissement formée par la rencontre du choc droit et du choc conique issu de la pointe.

- que dans la phase de fonctionnement critique, les débattements longitudinaux sont plus faibles dans la configuration avec piège où l'on observe une augmentation sensible de l'efficacité lorsque le choc se trouve situé au niveau du piège interne.

- que les positions du choc sont équivalentes, à même efficacité, dans tout le domaine supercritique.

3.4. Résultats instationnaires

Le fonctionnement de la prise d'air, sans instabilités forcées étant maintenant bien connu, nous allons dans cette deuxième partie aborder la phase instationnaire de ces essais, et tout d'abord caractériser à son tour le système générateur d'instabilités.

Sur la figure 13, on a reporté les points de fonctionnements obtenus avec les deux lunules (col auxiliaire) pour des positions de celles-ci soit grande ouverte, soit fermée et ceci pour différentes positions fixes de l'obturateur principal.

Les points de fonctionnement choisis, dans cet exemple, au nombre de 3, ont été déterminés pour obtenir trois zones : l'une en supercritique à partir du point n°1, l'autre proche du point critique et le troisième pour donner en position fermée de la lunule, un point de fonctionnement le plus proche possible du pompage. L'amplitude obtenue est bien sûr dépendante de la taille de la lunule utilisée.

Les sections des lunules représentent 14 et 17,5 % de la section d'entrée A1, ce qui entraine des débattements maximaux de l'ordre de 20 % de l'efficacité.

Les courbes de la figure 14 sont un exemple des signaux temporels obtenus au moyen des capteurs installés sur les parois du corps central et de la carène.

A l'aval, d'autres capteurs permettent la mesure de la pression statique et de la pression d'arrêt moyenne en fin de diffuseur et également d'obtenir une référence proche du générateur d'instabilités (pv).

Sur les tracés, les niveaux des prises 1 et 2 montrent que l'écoulement au droit de ces prises est encore supersonique et, le tracé très plat, que les fluctuations engendrées à l'aval sont bloquées par le choc. On peut nettement voir passer celui-ci sur les prises n°3, n°4 et n°5, les pressions correspondent alternativement soit à un écoulement supersonique soit à un écoulement subsonique.

Les niveaux de pression des prises n° 6 à 12 indiquent par contre que celles-ci sont toujours situées dans un écoulement subsonique.

Lorsque l'on superpose les fluctuations RMS sur les répartitions longitudinales des pressions moyennées, pour un point de fonctionnement et une fréquence donnée, on obtient les courbes de la figure 15.

Pour l'exemple choisi, on remarque que :

- en subcritique (zone A de la courbe caractéristique), les fluctuations maximales sont obtenues sur les premières prises, juste à proximité du choc de recompression, la prise n°1 bien que toujours en supersonique est la plus interactionnée. Aucun pompage n'est décelé.

- en supercritique (zone B de la courbe caractéristique), le maximum est décalé et situé sur les prises n°8 et n°9, où se trouve le choc terminal pour ce point de fonctionnement. Le taux de RMS baisse rapidement à l'amont du choc. Les fluctuations observées, dans la zone correspondant à un écoulement supersonique, indiquent que le choc provoque un décollement de la couche limite qui s'est développée sur le corps central.

Ceci nous amène à la comparaison des taux de RMS pour les deux configurations avec et sans piège interne. Un exemple est présenté figure 16 pour des fonctionnements équivalents et proches du régime critique.

Le taux de fluctuation, dans la configuration sans piège est nettement plus élevé au passage du choc de recompression et plus faible à l'aval de celui-ci.

Le piège qui stabilise le choc joue donc également un rôle en diminuant le pic de RMS et en étalant le processus.

Lorsque ces mêmes valeurs de RMS sont tracées, figure 17, en fonction de la fréquence des instabilités, on observe le même décalage entre les deux configurations, avec en plus une amplification du phénomène pour une fréquence proche de 100 Hz. Celle-ci correspond à un couplage avec la fréquence fondamentale du conduit. Celui-ci n'a jamais déclenché le pompage, mais il est bien évident que l'on a intérêt à éviter cette difficulté si l'on connait par ailleurs les fréquences émises par la combustion. Il pourrait donc être judicieux soit de modifier le réglage du moteur (en déplaçant par exemple les injecteurs) soit de prévoir une longueur de manche à air différentes pour éviter tout couplage intempestif.

4 - SYNTHESE DES RESULTATS

Les courbes et schémas des figures 18 et 19 présentent la synthèse de ces résultats pour les deux configurations étudiées.

Elles regroupent les indications de positionnement du choc obtenues en stationnaire, avec l'efficacité correspondante.

Elles indiquent, pour un col auxiliaire donné, les écarts réalisés en statique.

Elles donnent enfin, pour différentes fréquences, les débattements du choc et les écarts d'efficacité correspondants.

On peut noter que les valeurs d'efficacité semblent toujours plus faibles que celles obtenues en statique ; en fait les écarts observés ne sont pas nécessairement significatifs.

Les précisions obtenues tant sur la position des chocs que sur le rendement peuvent être la cause de ceux-ci.

Dans la configuration sans piège interne, figure 18, on peut remarquer que :

- les déplacements du choc (quelle que soit la fréquence comprise entre 10 et 200 Hz) sont moins étendus en instationnaire et n'atteignent jamais les limites stationnaires.

Il faut également dire que si en stationnaire, on obtient des fluctuations de pression de l'ordre de 20 %, celles-ci tombent rapidement à un niveau beaucoup plus faible en instationnaire, principalement à cause du coefficient de striction du col auxiliaire. Il est donc normal que les mesures de l'efficacité soient également comprises dans la fourchette stationnaire. Elles sont toutefois assez comparables aux résultats que l'on aurait déduits de la position stationnaire du choc, aux remarques près, faites précédemment sur la précision.

En supercritique, le débattement est centré sur la zone stationnaire.

En subcritique, par contre, les débattements du choc sont proches de la position la plus avancée.

Pour la configuration avec piège interne, figure 19, les mêmes remarques générales peuvent être faites, mais des différences sensibles existent :

- en stationnaire, la vitesse de déplacement du choc ne suit pas une loi continue,
- en instationnaire, pour le régime subcritique, les débattements du choc, pour toutes les fréquences d'essais, se font dans la zone aval de la plage stationnaire.

Le piège interne a donc deux fonctions primordiales qui sont :

- l'amélioration de l'efficacité,
- l'amortissement et l'effet tampon vis-à-vis des instabilités aval.

Par ailleurs, la couche limite étant moins épaisse sur le corps central, les interactions et donc le taux de RMS est plus faible au droit du choc de recompression.

5 - MESURES EFFECTUEES PENDANT LE POMPAGE

Des mesures ont été effectuées pendant un cycle de pompage. Celui-ci a été obtenu en recherchant une position de l'obturateur principal suffisamment fermée pour le provoquer. La fréquence de ce pompage peut être modulée en fonction de la position de l'obturateur jusqu'à des valeurs très basses (f = 0,5 Hz) comme le montre la figure 20a. Ces points ne correspondent pas à un fonctionnement habituel de la prise d'air, mais leur intérêt réside dans le fait qu'ils permettent d'obtenir tous les régimes de fonctionnement pendant un cycle de pompage.

Ce dernier se décompose en trois phases :

- dans un premier temps, à partir d'une position stable du choc à l'amont de la carène, dans un fonctionnement très subcritique, on assiste à un amorçage très rapide, une fréquence de 2000 Hz apparait alors (figure 20b). La vitesse de déplacement du choc est alors de 6,7 m/s ;

- ensuite, pendant quelques fractions de secondes, l'écoulement est très stable même dans sa partie subsonique ;

- enfin, on assiste à un désamorçage avec des signaux de nouveau plus perturbés, le choc se déplaçant alors à 0,4 m/s pour reprendre sa position primitive.

Pendant ce cycle, le choc passe donc de l'amont de la prise n°1 sur le cône à la prise n°9 dans le diffuseur.

Un zoom de la zone à 2000 Hz permet figure 21 de suivre la position du choc.

6 - CONCLUSIONS

En conclusion, il faut remarquer que le deuxième montage utilisé pour créer les instabilités et la technique d'essai sont mieux adaptés au but recherché, que les fréquences d'excitation correspondaient bien au problème posé, mais que par contre, bien que les différences de pression obtenues en stationnaire soient très élevées (environ 20 %), les fluctuations de pression réalisées, tant en statique qu'en pression d'arrêt en fin de diffuseur restent relativement faibles, même pour des fréquences très basses.

Les nombreux enregistrements effectués ont permis d'approfondir le fonctionnement de la prise d'air pour deux configurations géométriques internes : dans la gamme des fréquences réalisées, le pompage de la prise d'air n'a jamais été déclenché pour les points de fonctionnement habituels, le choc ayant alors tendance à se déplacer entre les bornes des régimes stationnaires sans aucune amplification.

Le seul point sensible, où une augmentation du niveau des fluctuations a été entrevue correspond à la fréquence propre du conduit.

Le piège interne qui limite d'une façon importante le déplacement du choc de recompression est d'une utilité évidente dans la stabilité de l'écoulement.

Il faut toutefois se méfier : les résultats obtenus sur cette prise d'air ne sont pas obligatoirement et directement transposables à d'autres prises d'air même si celles-ci sont circulaires. Il faut au préalable s'assurer que les écoulements internes sont comparables : c'est-à-dire même nombre de Mach devant le choc droit, loi de section méridienne, position et forme du piège analogue. Si ces conditions ne sont pas remplies, les résultats précédents ne sont utilisables qu'avec la plus grande prudence.

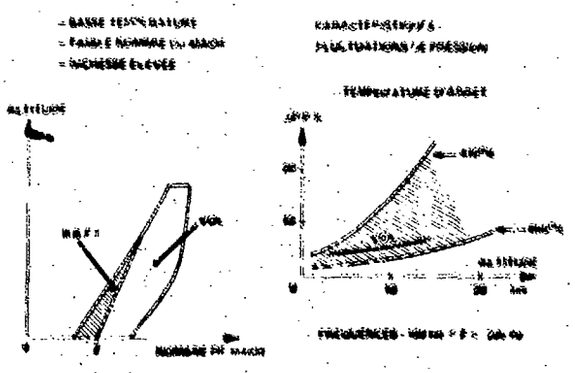


Fig. 1 - Domaine des instabilités de basse fréquence

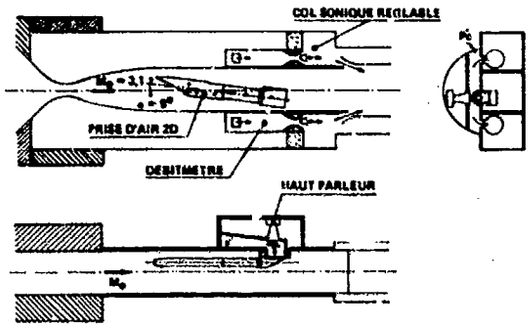


Fig. 2 - Première série d'essais. Prise d'air bidimensionnelle.

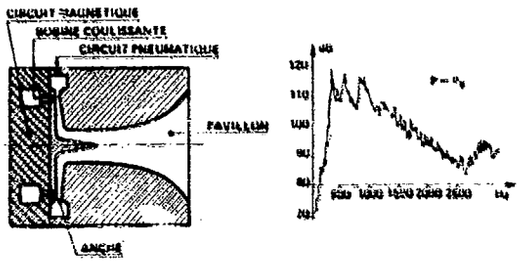


Fig. 3 - Caractérisation du haut parleur pneumatique.

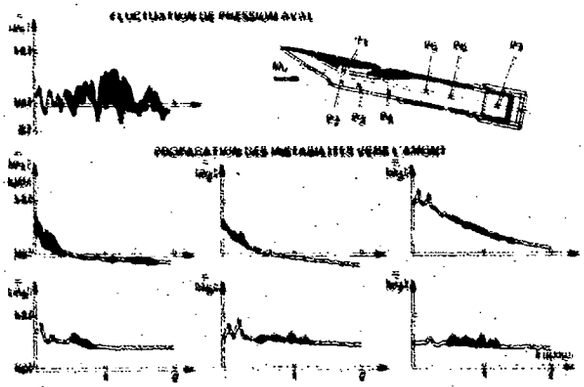


Fig. 4 - Fluctuations de pression dans le diffuseur.

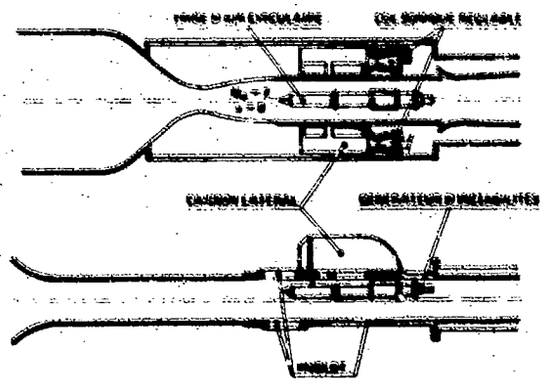


Fig. 5 - Deuxième série d'essais. Prise d'air circulaire.

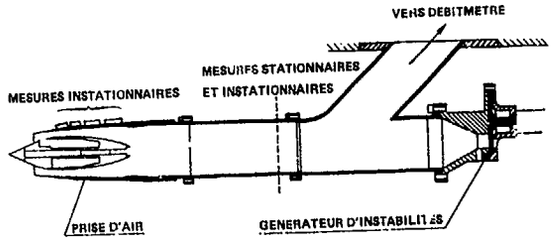


Fig. 6 - Prise d'air et générateur d'instabilités.

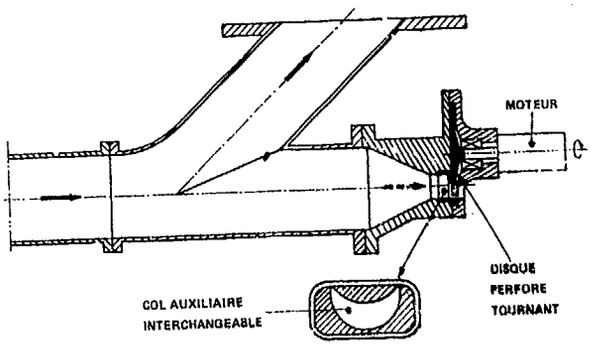


Fig. 7 - Générateur d'instabilités.

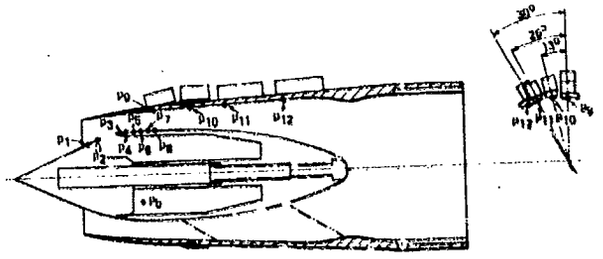


Fig. 8 - Equipement de la prise d'air en mesures instationnaires.

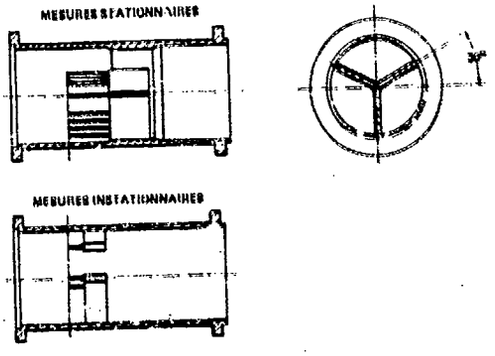


Fig. 9 - Mesures en fin de diffuseur.

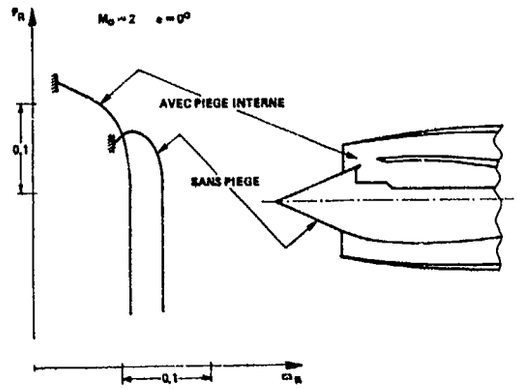


Fig. 10 - Prise d'air circulaire.

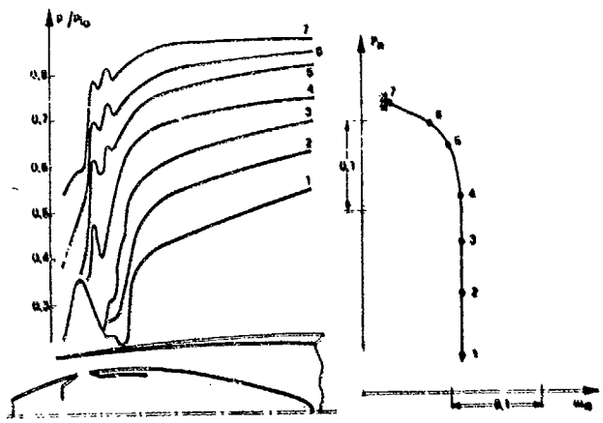


Fig. 11 - Répartitions de pression pour différents points de fonctionnement.

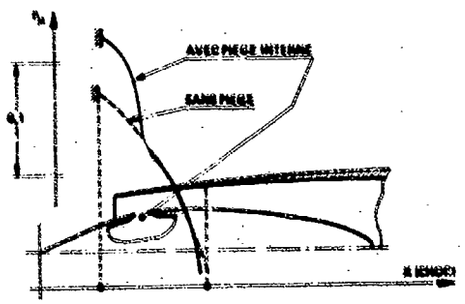


Fig. 12 - Position du choc interne.

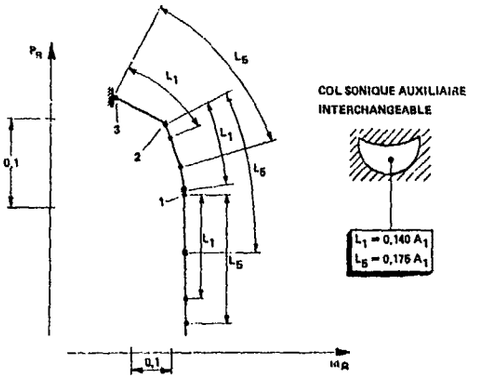


Fig. 13 - Amplitude stationnaire des perturbations.

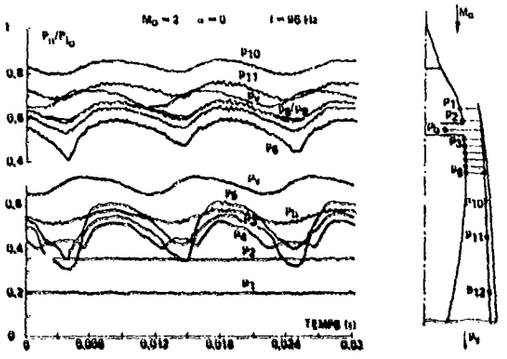


Fig. 14 - Mesures instationnaires.

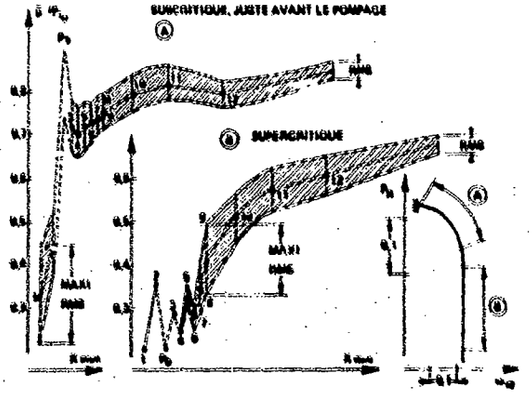


Fig. 15 - Moyennes des répartitions de pression et fluctuations.

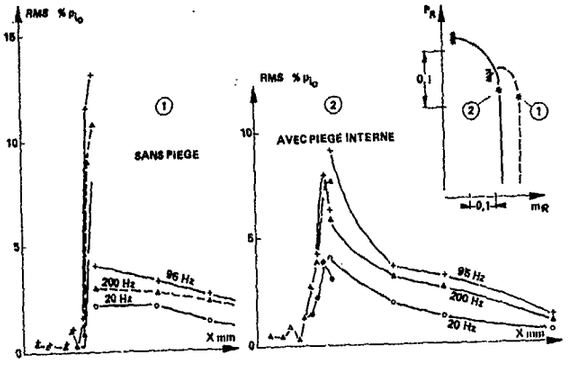


Fig.16 - Fluctuations de pression, fonctionnement proche du point critique

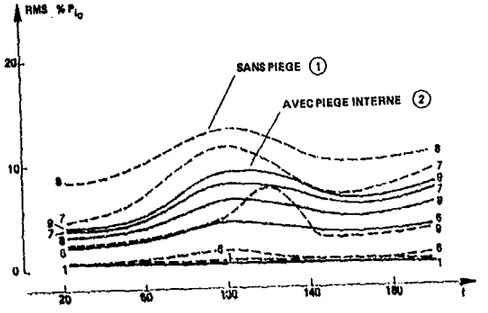


Fig. 17 - Effet de la fréquence sur les fluctuations de pression (fonctionnement proche du point circulaire).

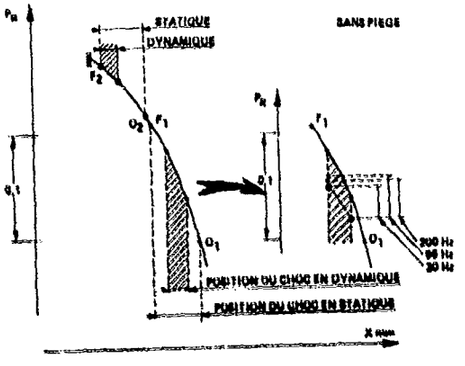


Fig. 18 - Positions du choc interne et efficacité correspondante (configuration sans piège).

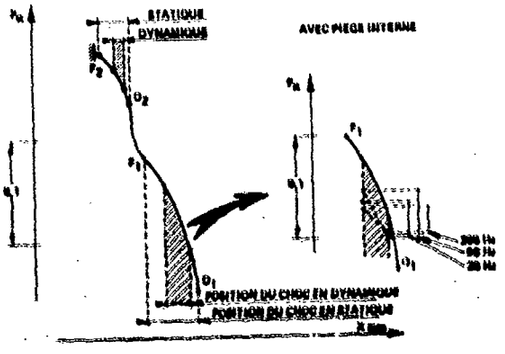


Fig. 19 - Positions du choc interne et efficacité correspondante (configuration avec piège).

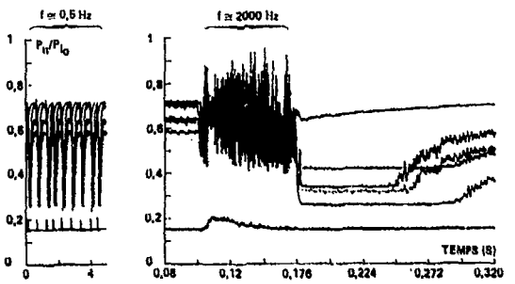


Fig. 20 - Mesures pendant la phase de pompage.

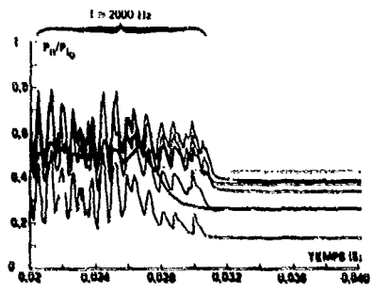


Fig. 21 - Mesures pendant la phase de pompage.

RECENT DEVELOPMENTS IN RAMJET PRESSURE OSCILLATION TECHNOLOGY

by
P. A. Chun, J. A. Loundagin, J. A. Nabity, S. E. Ayler
Airbreathing Propulsion Branch
Naval Weapons Center
China Lake, California, 93555-6001
USA

SUMMARY

Dynamic matching of a supersonic inlet and combustor is a major consideration in ramjet propulsion development. The inlet shock system present under supersonic speeds must be kept stable under all engine operating conditions. An unstable shock system could result in inlet unstart and/or buzz and undesirable pressure oscillations in the ramjet engine. To date, there is no technique for determining if a particular ramjet engine configuration will have combustion-induced pressure oscillations.

This paper summarizes current experimental and theoretical techniques applied to the characterization of liquid fuel ramjet combustors. Comparisons between steady-state and dynamic data are provided to show how both types of information are used to interpret engine behavior.

LIST OF SYMBOLS

APTF	Airbreathing Propulsion Test Facility
A_3	Combustor chamber flow area
A_5	Exit nozzle flow area
F/A	Fuel-to-air
FM	Frequency modulation
GN_2	Gaseous nitrogen
IRIG	Inter-Range Instrumentation Group
LVDT	Linear voltage displacement transducer
NWC	Naval Weapons Center
PF1	Fuel control valve inlet static pressure
$P_{1.54}$	Inlet static pressure at location 1.54, psia
$P_{1.72}$	Diffuser static pressure at location 1.72, psia
$P_{4.4}$	Combustor static pressure at location 4.4, psia
RMS	Root mean square
WF1	Flowmeter

INTRODUCTION

Depending upon the frequency and amplitude, an unstable inlet shock system could not only affect the inlet performance and margin, but also could have a detrimental effect on the combustor thermal protection system and the guidance and control components. Although no technique is currently available to determine if a particular ramjet configuration will be susceptible to combustion-induced pressure oscillations, work summarized in Reference 1 has shown that oscillations depend on a number of factors, including F/A ratio, temperatures, pressures, and geometries. Data indicate that the amplitude of the oscillations increases as the fuel-to-air ratio increases up to the stoichiometric value. Some correlation has been seen between higher amplitude oscillations and lower inlet temperatures and pressures. The frequencies of the oscillations increase with both F/A ratio and inlet temperature. Data, however, are still incomplete since fuel management, fuel injection system, and flameholder responses have not been established.

This paper discusses techniques and results of both steady-state and dynamic measurements for characterizing the stability of a ramjet combustor.

BACKGROUND

These results were obtained during three series of experimental investigations of a small-diameter (approximately 8 inches) center-dump combustor. Testing was accomplished at NWC using the T-Range high-pressure air facility and the Airbreathing Propulsion Test Facility (APTF). Based on previous tests of similar engine configurations, low-frequency longitudinal mode pressure oscillations were anticipated

Approved for public release; distribution is unlimited.

in this combustor. These did not occur. However, the combustor exhibited pressure oscillations tentatively identified as tangential or "soreeoh" mode combustion instabilities. These instabilities, at a frequency of approximately 2000 hertz, did not degrade the overall combustor performance. However, there was concern that the vibrations due to the combustion instabilities could have a detrimental effect on the guidance and control components of a missile. The three series of technology investigation tests and experiments provided a follow-on to the original combustor baseline development; they were designed to characterize the combustor flow, identify modes of instability, and evaluate methods for suppressing the instabilities. During these tests and evaluations it was apparent that great care had to be taken in obtaining and evaluating high-frequency response pressure data.

TEST CONFIGURATIONS AND PROCEDURES

The baseline combustor configuration shown in Figures 1 and 2 was tested in a direct-connect, or connected pipe, mode. Figure 1 is the horizontal configuration tested at the NWC T-Range facility, and Figure 2 is the vertical configuration tested at the NWC APTF. The thick walled combustor case allowed a "heat sink" mode of testing with typical combustion run times of approximately one minute. The configuration used one two-dimensional inlet, which transitions to a circular cross section, that dumps into the combustor. During the testing, heated air simulating the desired flight Mach number and altitude conditions entered a plenum chamber prior to being supplied to the engine through a direct-connect inlet.

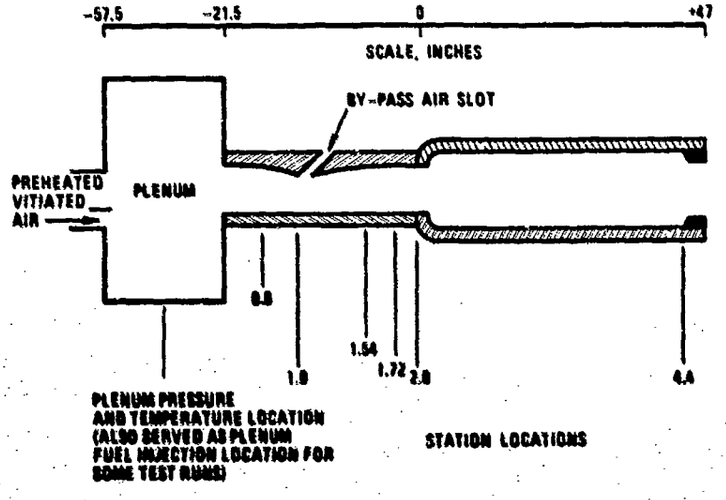


Figure 1. Horizontal Configuration for Direct Connect or Connected Pipe Combustor Test Setup.

As standard test procedure, the facility air was heated in a propane burner during the T-Range tests and in a hydrogen-fueled burner during the APTF tests. Oxygen was then added to establish the appropriate oxygen mass fraction to the air. The ramjet fuel flow rate was next set to give the required equivalence ratio, and the mixture was ignited with an H_2/O_2 torch. After ignition, the fuel flow was swept over the desired range of fuel-to-air ratios.

Inlet

The connected pipe inlet section included the bypass air slot, as shown in Figures 1 and 2. The amount of air actually passing through the bypass slot was not measured directly. Instead, the airflow entering the combustor was estimated using a correlation of inlet static measurements at station 1.54 ($P_{1.54}$). The bypass airflow was computed as the difference between the total airflow entering the plenum and the airflow entering the combustor.

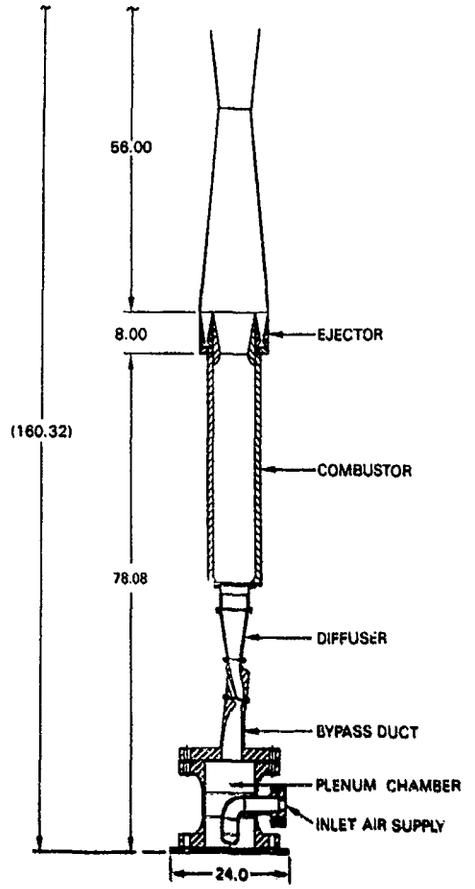


Figure 2. Vertical Configuration for Direct-Connect or Connected-Pipe Combustor Test Setup.

Fuel System

Figure 3 is a schematic of the fuel system hardware used in the combustor tests at the T-Range facility. RJ-4 fuel could be delivered to the engine from either of two fuel supply vessels. One vessel was the standard facility fuel tank pressurized by compressed nitrogen, and the other was a 2-ft^3 expulsion cylinder pressurized by fuel from the facility fuel tank. This dual supply system was used to investigate the effects of dissolved nitrogen in the fuel on engine performance. RJ-4 fuel pressurized directly by nitrogen can contain gas in solution-up to 15% by volume-measured at the conditions of the solution. It was theorized that, when fuel pressure was decreased downstream of the fuel control valve, large volumes of gas would evolve from the saturated fuel and cause uneven fuel flow through the fuel injectors. Fuel supplied by the expulsion cylinder was driven by a free-floating piston and was devoid of dissolved nitrogen. Preliminary analysis of engine performance using the two fuel supply vessels has shown no difference in operation between nitrogen-rich and nitrogen-free fuel.

From the supply vessel, the fuel was directed through a flightweight type fuel control valve, which metered the fuel flow rate. The valve was an electromechanical, cavitating venturi type, designed and fabricated by The Marquardt Company (TMC). It was operated either manually or automatically from a digital electronic fuel controller. In the manual mode, the valve pintle position was controlled directly via a potentiometer on the fuel controller, with fuel flow rate through the WF1 flowmeter visually monitored for feedback. In the automatic mode, pressure transducer outputs from P1.5^6 in the inlet diffuser and PF^1 at the fuel control valve inlet, along with a desired F/A ratio command signal from a potentiometer, were input to the fuel controller digital computer. The computer used engine and valve calibrations to

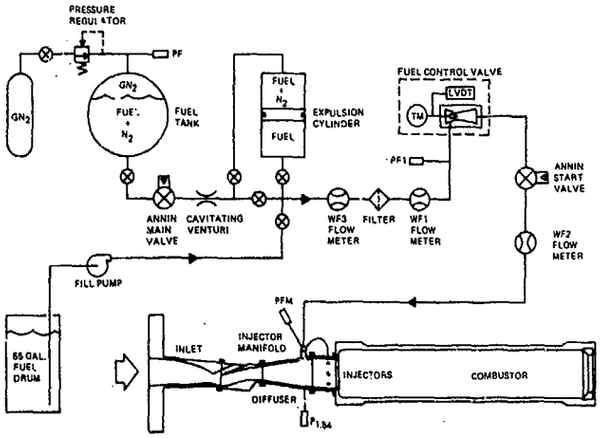


Figure 3. 1-Range Fuel System Hardware Schematic.

calculate the valve pintle position for the desired F/A ratio. An analog feedback servo system then drove the valve pintle to the commanded position.

Fuel from the valve entered the injector manifold. It was distributed to six flush wall variable area poppet injector nozzles for fuel atomization into the combustor.

The fuel supply system used at the APTF is shown in schematic in Figure 4. It consisted of a high-pressure fuel expulsion tank with a gaseous nitrogen pressurization system, a fuel pressure regulator, a network of four parallel cavitating venturis of various sizes with remotely operated Annin air-operated on/off valves located in series with each venturi, and numerous valves, filters, and pressure and flow rate sensors. The fuel flow rate to the engine was controlled by the fuel pressure regulator upstream of the venturis, and by the four Annin valves, which directed flow through the venturis either singularly or in various combinations. With four venturis, a total of 16 discrete flow metering areas could be selected. The Annin valves were controlled by a 16-position rotary switch that commanded flow areas.

Tests were conducted by pressurizing the fuel expulsion tank and setting the fuel pressure regulator to a predetermined value. The initial fuel flow rate was selected by opening the desired combination of Annin valves, and then opening the main fuel valve. When the airflow conditions through the engine were stabilized at the desired values, fuel flow to the injectors was initiated by opening the start valve. During the test, the F/A ratio was varied by turning the rotary switch to change the combination of venturis present in the fuel metering system.

Instrumentation

Figures 5 through 7 show the available instrumentation locations on the test hardware. Depicted in these figures are the static pressure and thermocouple locations and the high-frequency response pressure transducer locations. Not all of the high-frequency pressure locations were used in these tests. The following high-frequency pressure locations were used through these two series of tests: plenum, bypass exit, PK 0.0, PK 1.2, PK 1.5, PK 1.72, PK 1.75A, PK 1.75B, PK 2.0, PK 3.0 (five locations), PK 4.0, and PK 4.3. The water-cooled high-frequency transducers were manufactured by PCB Piezotronics, Inc. (Model 124A21). The probes in the plenum, bypass exit, PK 1.75A, and PK 1.75B used the nonresonant, semi-infinite tube technique. The remainder were wall mounted on the combustor.

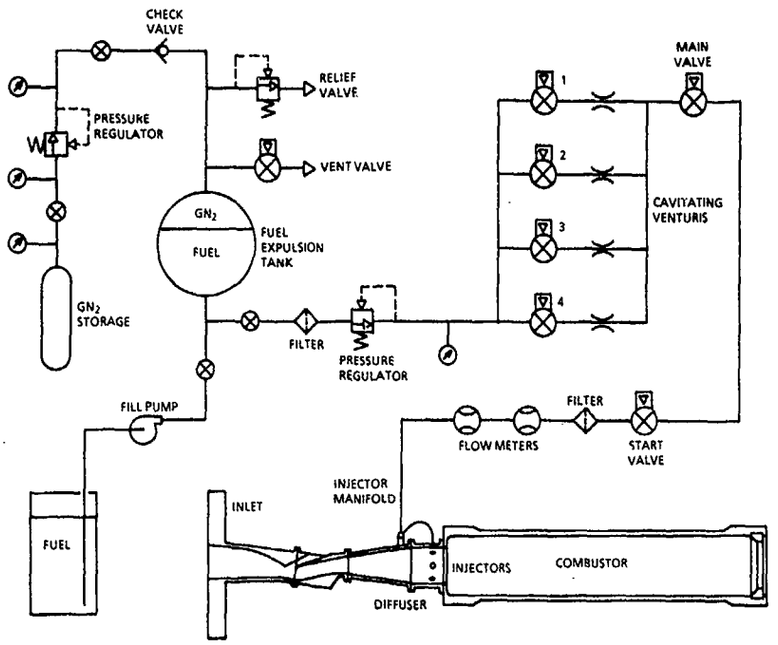


Figure 4. APTF Fuel System Hardware Schematic.

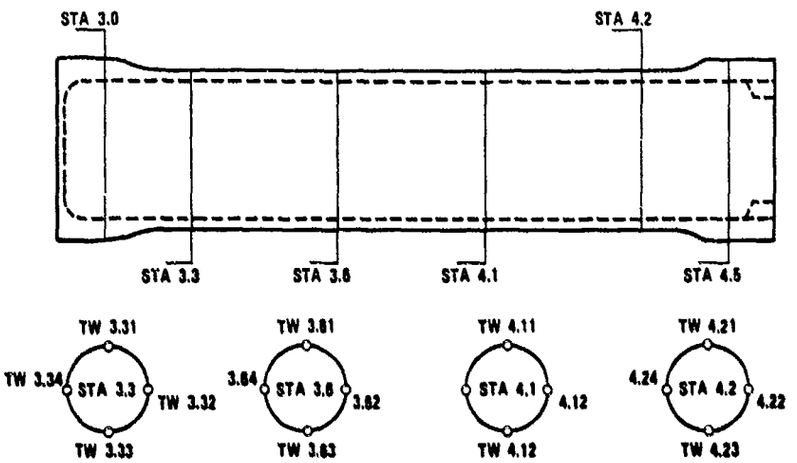
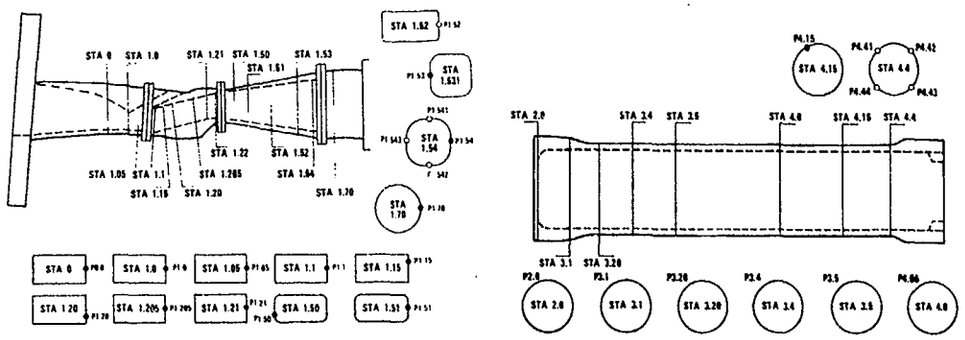


Figure 5. Locations of Combustor Wall Thermocouples.

The nonresonant, semi-infinite tube technique has been used to measure high-frequency pressure oscillations in turbojet engines (References. 2 and 3). In this technique, a long tube is used as a waveguide for the fluctuations. The tube is long enough that the fluctuations dissipate before reaching the end. The technique ensures that there will be no reflections and thus no resonance. This means that the acoustic impedance, which is the product of the gas density and the velocity of sound divided by the cross-sectional area, must approach a constant. This is accomplished by minimizing cross-sectional area changes, especially at the pressure transducer inlet port, and avoiding major changes in the gas properties.



a. Inlet.

b. Combustor.

Figure 6. Locations of Static Pressure Transducers.

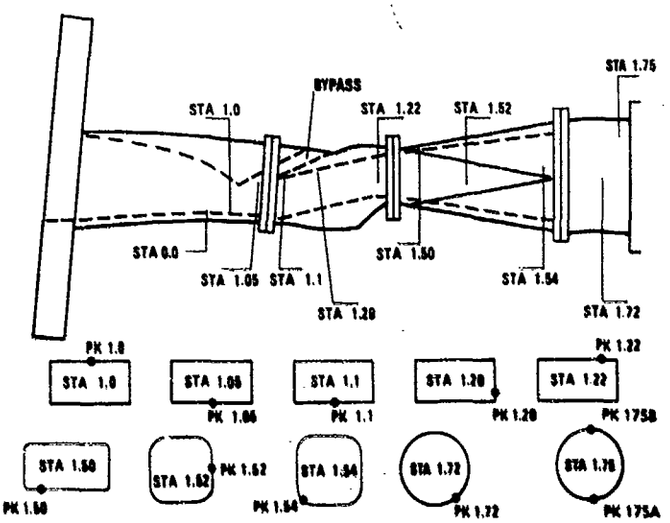


Figure 7a. Locations of Inlet High-Frequency-Response Pressure Transducers.

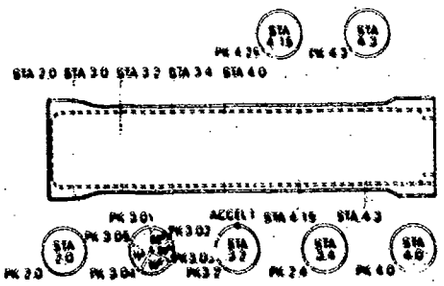


Figure 7b. Locations of Combustor High-Frequency-Response Pressure Transducers.

Figure 8 is a schematic of the installation and location of the high-frequency total pressure probes. The probe at location 1.75 consisted of a 1/4-inch-diameter pitot tube with a right angle turn that faced upstream into the airflow and was located 3/8 inch into the airflow from the diffuser wall. This stainless steel tube was attached to a drilled block of stainless steel (1 inch by 1 inch by 3 inches). To accomplish this installation, a 0.187-inch hole was drilled through 3 inches of the block. This hole was then drilled and tapped to accept a 1/4-inch flare fitting. The 0.25-inch stainless steel probe was then silver soldered into the flare fitting. Throughout this internal flow path, there could be no cross-sectional area differing from the interior of the stainless steel tube; that is, there were to be no projected areas. At the other end of the drilled 0.187-inch-diameter hole, a 50-foot line of stainless steel tubing was attached with the end plugged to provide a nonresonating chamber.

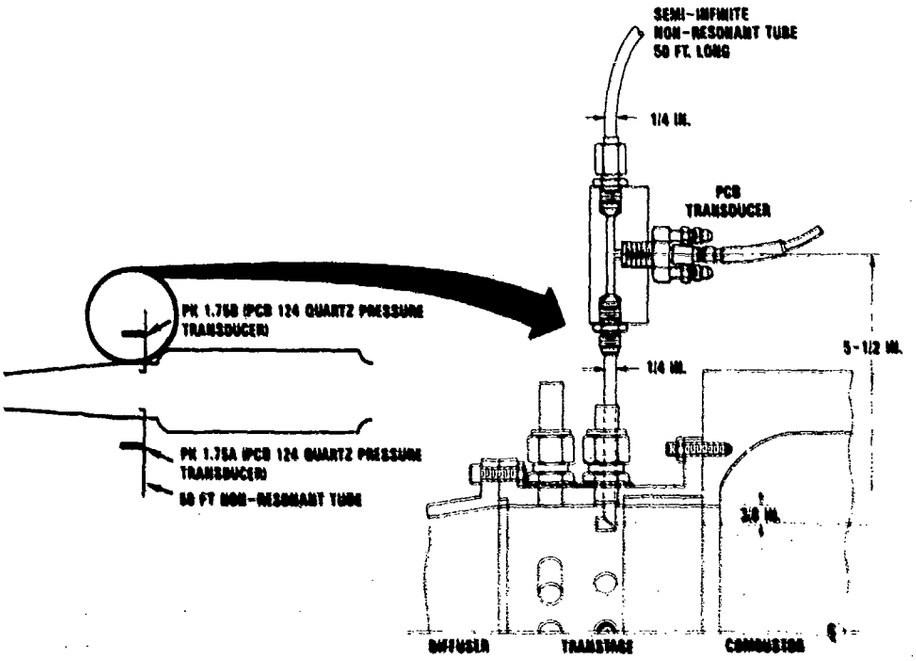


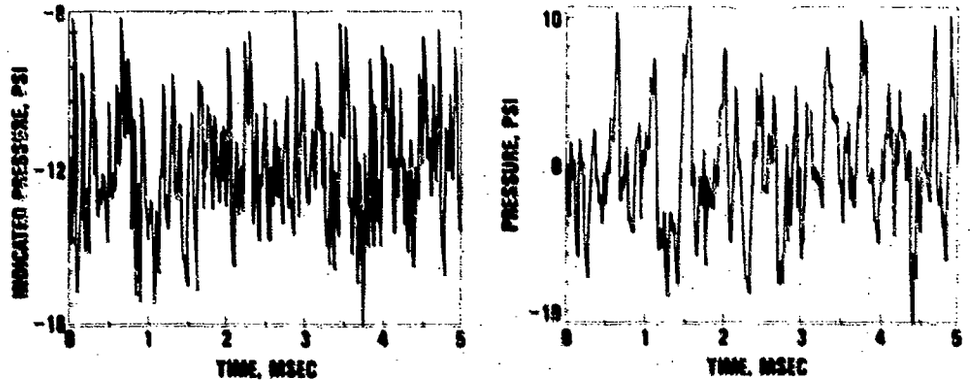
Figure 8. Installation and Location of High-Frequency-Response Total Pressure Probes.

The water-cooled high-frequency transducer was mounted by tapping a 0.50-inch-diameter by 20-thread-per-inch hole into the side of the stainless steel block at an angle of 90 degrees to the 0.187-inch-diameter hole. A 0.050-inch hole was used to connect the 0.187-inch-diameter flow path to the transducer port. The high-frequency pressure signals and IRIG reference time were recorded on a FM 14-track analog tape recorder. Analysis of the resulting data was accomplished using a fast Fourier transform digital signal analyzer.

The effect of vibration levels on the high-frequency instrumentation was extensively studied because two test facilities were used and because the combustor stand was changed from horizontal to vertical. To effectively measure pressure oscillations in a ramjet combustor, inlet and plenum during combustion, the acoustic response must be isolated from the vibration response of the high-frequency pressure transducers. The semi-infinite, nonresonant tube technique is difficult to implement without having specific criteria (such as materials to use, standoff distances, tube diameters, etc.) for decreasing the response of the transducer to vibration. The goal was to identify these criteria and to reduce the vibration response to an acceptable level or to identify the minimum level attainable. The details of this investigation are contained in Reference 4. The results were that the semi-infinite, nonresonant tube technique can effectively be used for reducing vibration response of the

transducer and producing a clean acoustic signal. Oscillation amplitudes of less than 5% of the total pressure can be resolved as acoustic in origin.

Figure 9 shows the results of two high-frequency pressure transducers directly mounted such that one was measuring in the actual airflow with acoustic and vibration input and the other was plugged, responding only to the vibration spectrum. This was for a system with an acceleration of several thousand *g*s at high frequency. Note that the ordinate scales are different on the two plots. This graphically illustrates the contribution to the data of the vibration component. The vibration component can be significantly reduced with proper implementation of the semi-infinite, nonresonant tube technique. The vibration levels have to be established to provide understanding of the acoustic levels and to interpret high-frequency pressure measurements correctly. Vibration data must not be superimposed on the pressure data. Otherwise, the result would be overstatement of the actual dynamic pressure fluctuations.



a. Vibration Input Only (Plugged Port). b. Vibration and Acoustic Input Included (Unplugged Port).

Figure 9. High-Frequency Pressure Transducer Response.

TEST RESULTS

The testing at the APTF was able to replicate conditions tested at T-Range. Fuel-to-air ratio sweeps were conducted at the appropriate conditions; however, at the APTF the run durations were nominally 25 seconds, compared with longer durations at T-Range. Figure 10 shows a comparison of the variation of the RMS pressure oscillation at location 1.72 as a function of F/A ratio. The RMS pressure oscillations are normalized by the static pressure at location 4.3. As shown, there is an increase in levels at APTF over T-Range. The cause is unclear, but it may be an increase in vibration at APTF; the high-frequency transducer at location 1.72 did not use the semi-infinite, nonresonant tube technique. As had been observed in all the testing, the oscillations were dominated by frequency components in the 1600- to 2200-hertz range. They appear to be driven by a coupling between the fuel distribution system and the primary combustion zone, temporally and spatially. The amplitudes of the oscillations decrease rapidly with increasing distance from the combustor dump region. The pressure amplitude peaks at 1800 and 2100 hertz were identified as closely spaced acoustic modes of the first tangential/first longitudinal and first tangential/second longitudinal mixed mode frequencies. Figure 11 shows the spectrum in the inlet at location 1.72 and in the combustor at location 3.0 for the baseline condition at the APTF. This result was similar to that observed at T-Range.

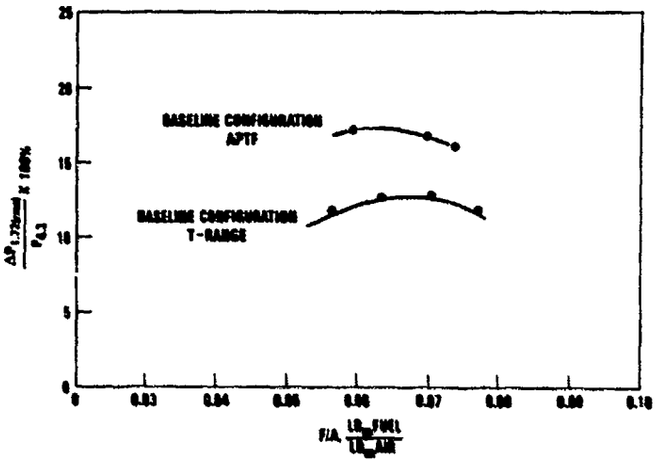
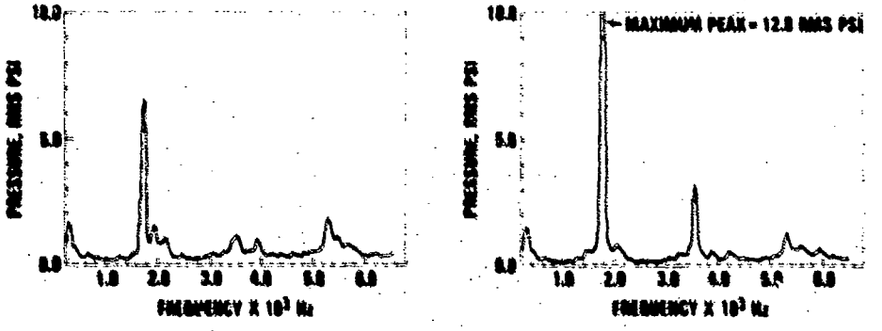


Figure 10. Comparison of Broadband (30-6400 Hz RMS) Pressure Oscillation at Location 1.72 at T-Range and APTF.



a. Location 1.72. b. Location 3.0.

Figure 11. Spectral Distribution of Pressures.

The dynamic oscillation data at location 1.75 (PK 1.75A and PK 1.75B) were compared on the basis of pressure amplitude versus time, as shown for the baseline in Figure 12. This comparison showed that the dynamic distortion measured by PK 1.75A and PK 1.75B is 180 degrees out of phase from one side of the duct to the other. Such a result was viewed as a forced transitory stall, which is a time-dependent, three-dimensional flow, as discussed in Reference 5. The implications of this in terms of the data interpretation were critical. Without use of the two total pressure dynamic probes, flipping of the flow from side to side would not have been observed. Because there are only two dynamic probes instead of a complete rake across the diffuser section at location 1.75, the total dynamic distortion profile at the combustor dump plane still is not obvious. What has been seen is that the flow through the duct is not uniform. This nonuniformity would not have been seen with only one high-frequency pressure probe at this location.

Another comparison of high-frequency data was made in which the total pressure in the plenum was compared to the high-frequency pressure at locations 1.72 and 1.75. From the plots, Figure 13, it is seen that pressure in the constant area duct exceeds plenum pressure. In order for the total pressure of the constant area duct to exceed the plenum total pressure, a constant volume combustion process must be occurring, and a shock wave, or detonation-type wave, must be traveling upstream. The wave does not appear to be traveling past the diffuser. Also, if the combustor pressure is greater than the plenum pressure, then the flow must be momentarily reversed.

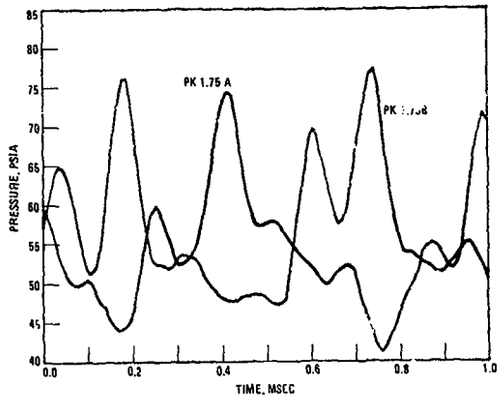


Figure 12. Pressure Amplitude Versus Time Distribution for Dynamic Total Pressure Probe Measurements PK1.75A and PK1.75B.

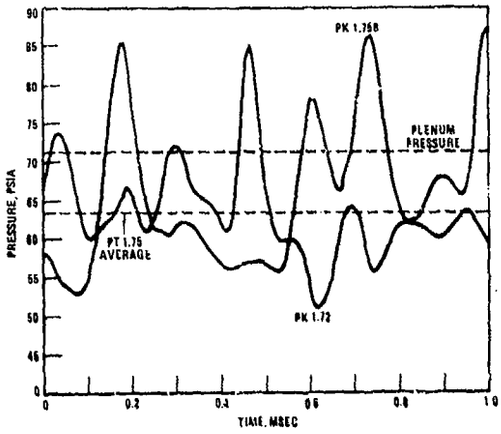
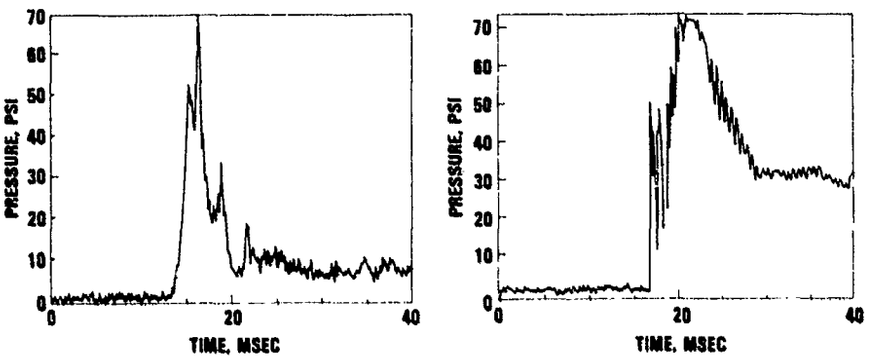


Figure 13. Comparison of High-Frequency Pressure Amplitudes at Locations 1.75 and 1.72 with Plenum Total Pressure and Average Total Pressure at Location 1.75 (Without Aerodynamic Grid).

One diagnostic technique that would be very desirable when engine performance is being investigated is the capability to determine the maximum combustion efficiency of any given combustor configuration, independent of the fuel injector configuration. This diagnostic technique would provide design goals for optimization of fuel injector configurations and other mixing devices. For this technology investigation, a technique was used that consisted of injecting fuel into the plenum instead of through the fuel injectors. The fuel injectors were removed, and the ports were plugged. The fuel was injected through two swirl orifice injectors, 160 degrees apart, into the plenum. Ample residence time was provided for the fuel and air to be premixed prior to entering the combustor. There appeared to be a flameholding zone residing upstream of the combustor in the plenum. A pressure wave traveled upstream, igniting the fuel in the plenum. Figure 14 shows the ignition spike characteristic observed during this type of test in the combustor and in the plenum. Comparison of the two shows the time delay between the two locations, and it is noted that the levels after ignition are

quieter in the combustor than in the plenum while burning and flameholding are exclusively in the plenum. Further refinements to this technique will include instream and contrastream fuel injection in the inlet/diffuser through orifices and use of swirl devices to premix the fuel and air better.

Testing was conducted in which the diffuser was instrumented with high-frequency pressure instrumentation. This was done to determine whether the oscillations observed in the duct were also present upstream. Figure 15 shows the spectrum in the diffuser at the bypass. There is no indication of an instability at the bypass.



a. Ignition Spike in Combustor. b. Ignition Spike in Plenum.

Figure 14. Pressure Amplitude Versus Time While Fuel Was Being Injected into the Plenum.

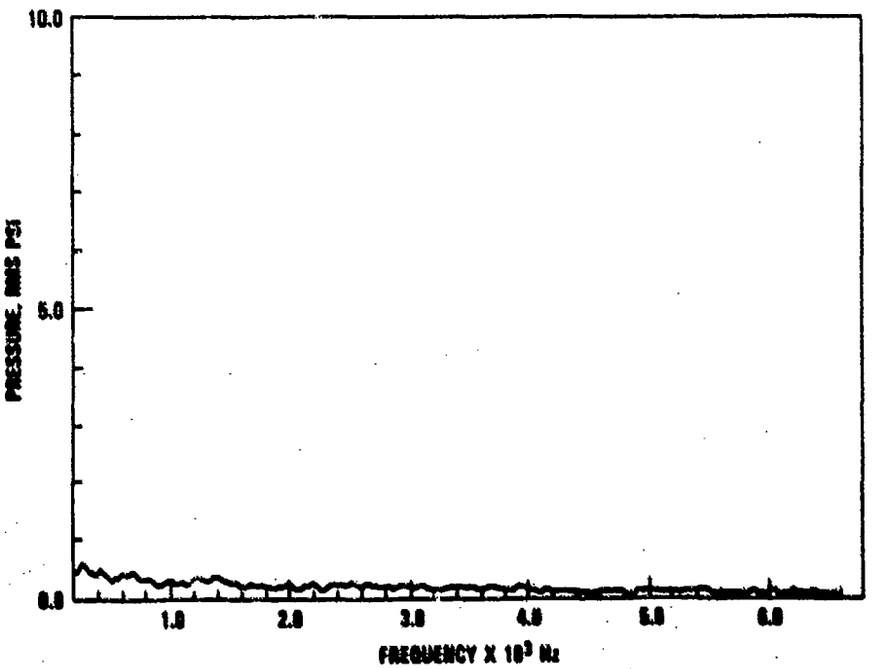


Figure 15. Spectral Distribution at the Bypass Slot.

CONCLUSIONS

This paper summarizes the dynamic and steady-state experimental techniques used in the technology investigations of a small-diameter liquid fuel ramjet combustor. The results of these investigations give insight into the complicated nature of the actual flowfields and provide techniques for characterizing them.

The techniques for measuring high-frequency pressure oscillations in ramjet engines are being studied and refined. The nonresonant, semi-infinite tube technique described in the test has provided a method of eliminating enhancement of the pressure oscillation measurement magnitude due to reflections and resonance in the instrumentation lines.

If the test hardware has mechanical vibration, the acoustic response must be isolated from the vibration response of the high-frequency pressure transducers during measurement of pressure oscillations. The nonresonant, semi-infinite tube technique is difficult to implement without having specific criteria (such as materials to use, standoff distances, tube diameters, etc.) for decreasing the response of the transducer to vibration. If the test hardware is characterized well, the nonresonant, semi-infinite tube technique will provide valuable and accurate information.

Dynamic measurements are imperative when studying flowfield phenomena; steady-state instrumentation alone cannot provide complete characterization. However, the techniques of utilizing dynamic instrumentation must be thoroughly understood.

REFERENCES

1. F. E. C. Culick, "Report of the JANNAF Workshop on Pressure Oscillations in Ramjets," 7-8 September 1980, Monterey, California.

2. W. M. Shaffernocker, "Current State-of-the Art for Airbreathing Combustor Measurements." Presented at the Symposium in Instrumentation for Airbreathing Propulsion, September 1972, and published in Instrumentation for Airbreathing Propulsion, Vol. 34, 1974, MIT Press, Cambridge, Massachusetts.

3. D. R. Englund and W. B. Richards, "The Infinite Line Pressure Probe." 30th International Instrumentation Symposium, May 1984, Vol. 21, pp. 115-124.

4. James Nabity and James Loundagin, Naval Weapons Center, China Lake, California, Implementation of a Semi-infinite, Nonresonant Tube Probe for High Frequency Measurement, November 1987. (NWC TM 6126.)

5. Stephen J. Kline, "On the Nature of Stall." Journal of Basic Engineering, September 1959, pp. 305-320.

ACKNOWLEDGEMENTS

The authors wish to gratefully acknowledge work done by J. G. Bendot, R. K. Dunlop, and T. G. Piercy of The Marquardt Company and by W. H. Clark, J. N. Matson, W. K. Jaul, and R. D. Coleman of the Naval Weapons Center. Results of their work provided technical data, information, direction, and insight to the technology investigations.

DISCUSSION

LeBlond, Fr.

1. What was the position of the injectors in the test facilities?
2. Did you change their position?
3. What is then the influence on the instabilities?

Author's Reply:

The fuel injector positions were varied, axially and radially. There were also varying combinations of flush-wall, contra-stream and in-stream mounted fuel injectors. Those configurations which promoted a more uniform fuel/air mixture decreased the amplitude of the pressure oscillation.

H. B. Weyer, Gr.

You have been using 50ft long lines to measure the steady-state pressures. Have you been aware of the fact that those techniques read mean pressures at considerable error depending on fluctuating amplitude and pressure wave shape?

Author's Reply:

The semi-infinite, nonresonant tube technique does introduce errors in attenuation, distortion and time delay, but these errors are less than those errors which are introduced by similar-sized transducers which do not use the semi-infinite, nonresonant tube technique. In our frequency range of interest (0 to 3000 Hz), we find there is about a 3-4% distortion.

REHEAT BUZZ - AN ACOUSTICALLY COUPLED COMBUSTION INSTABILITY

A.P. Dowling
Reader
University Engineering Department
Trumpington Street
Cambridge
CB2 1PZ
United Kingdom

SUMMARY

Reheat buzz is a low frequency instability of afterburners. It is caused by the interaction of combustion and acoustic waves within the reheat duct. The acoustic waves perturb the combustion, while the unsteady combustion generates yet more sound leading to the possibility of instability. A simple theory has been developed and tested by comparison with results obtained on a premixed rig. The theory is able to predict the frequency of the instability and the mode shape, accurately reproducing the effect of changes in flow rate, inlet temperature, duct length and fuel-air ratio.

1. INTRODUCTION

Reheat buzz is a combustion instability involving the propagation of longitudinal pressure waves in a duct. A similar instability has been observed when a premixed flame burns in the wake of a bluff body in a duct. These schlieren photographs (1) show that oncoming acoustic waves perturb the flame, causing it to move and change in surface area, thereby altering the instantaneous heat release rate. Rayleigh's criterion (2) states that if heat is added unsteadily in phase with the high pressure part of a sound wave, the wave will grow in magnitude. Therefore, provided the phase relationship between the pressure disturbances and the unsteady combustion is suitable, the pressure waves in the duct gain energy. Disturbances grow in time if their energy gain from the combustion is greater than the energy radiated from the ends of the duct.

A linear stability analysis for a flame burning in a duct has been developed by Bloxsidge, Dowling & Langhorne (3) and compared satisfactorily with the experimental results of Langhorne (4). The work presented here simplifies the theory of Bloxsidge et al, while retaining all its essential features.

The equations of motion for linear disturbances of frequency ω, in a duct with heat release and mean flow are derived in section 2. These equations can be readily solved once the boundary conditions and the heat release rate are specified. It is found that only certain discrete values of ω can exist as free modes of the flame/duct arrangement. If the imaginary part of ω is negative the disturbance grows in time and the system is unstable; Real ω gives the frequency of this unstable mode. The relationship between the perturbation in heat release rate and the flow must be specified. Rayleigh emphasized the importance of this relationship. It not only determines the stability but also affects the frequency of the oscillation (2). Models describing the dependence of the rate of heat release on flow perturbations are well developed for gas and oil burner ports (5-7) and for rocket systems (8). Bloxsidge et al (3) determined a flame model for the afterburner geometry in which there is an appreciable mean flow and the combustion is distributed. We use their model in this work.

In section 3 the theory is tested by comparison with experimental results on a premixed rig. The effects of some differences between the rig and an afterburner are discussed in section 4.

2. UNSTEADY FLOW IN A DUCT WITH HEAT RELEASE

Consider perturbations to a flow in a duct of uniform cross-sectional area A. Since our interest is primarily in the onset of instability, when the amplitude of the oscillations is small, only linear disturbances to the mean flow will be considered. Then each Fourier element may be analysed separately and it is sufficient just to consider disturbances with time dependence $e^{i\omega t}$. The frequency of the buzz mode is low and its wavelength is long in comparison with the duct diameter. Therefore only plane acoustic waves carry energy and we treat the flow as one-dimensional. Mean values will be denoted by an overbar so that the axial velocity $u(x,t)$, for example, can be expressed as

$$u(x,t) = \bar{u}(x) + u'(x,t)$$

where the fluctuating component $u'(x,t) = \mathrm{Re}\{\hat{u}(x)e^{i\omega t}\}$. The pressure p, density ρ and temperature T may be expanded in a similar way.

Experimental results on a laboratory rig (4) show that burning persists throughout the region downstream of the flame-holder, a length which can be an appreciable fraction of the wavelength. We therefore consider distributed heat release. The equations of mass,

momentum and energy conservation for the mean flow are respectively:

$$\frac{d}{dx}(\bar{\rho}\bar{u}) = 0 \tag{2.1}$$

$$\frac{d}{dx}(\bar{p} + \bar{\rho}\bar{u}^2) = 0 \tag{2.2}$$

and

$$\frac{d}{dx}(c_p\bar{T} + \tfrac{1}{2}\bar{u}^2) = \frac{\bar{q}(x)}{\bar{\rho}\bar{u}\bar{A}} . \tag{2.3}$$

c_p is the specific heat capacity at constant pressure and $\bar{q}(x)$ is the rate of heat release per unit axial length of duct. In addition to these equations we have the perfect gas law

$$\bar{p} = R\bar{\rho}\bar{T} . \tag{2.4}$$

When $\bar{q}(x)$ is specified as a function of x, and the flow is given at one axial position, $x = 0$ say, equations (2.1) - (2.3) can be integrated with respect to x in a straightforward way to determine the mean flow at all positions downstream.

We will now go on to consider perturbations from this mean condition. For a mean flow satisfying (2.1) and a linear disturbance proportional to $e^{i\omega t}$, the one-dimensional equation of mass conservation reduces to

$$\frac{d}{dx}(\hat{\rho}\bar{u} + \bar{\rho}\hat{u}) = -i\omega\hat{\rho} . \tag{2.5}$$

Similarly the momentum equation simplifies to

$$\frac{d}{dx}(\hat{p} + \hat{\rho}\bar{u}^2 + 2\bar{\rho}\bar{u}\hat{u}) = -i\omega(\hat{\rho}\bar{u} + \bar{\rho}\hat{u}) , \tag{2.6}$$

while the energy equation becomes

$$\frac{d}{dx}\left[(\hat{\rho}\bar{u} + \bar{\rho}\hat{u})(c_p\bar{T} + \tfrac{1}{2}\bar{u}^2) + \bar{\rho}\bar{u}(c_p\hat{T} + \bar{u}\hat{u})\right] = \frac{\hat{q}}{A} - i\omega\left[\hat{\rho}(c_v\bar{T} + \tfrac{1}{2}\bar{u}^2) + \bar{\rho}(c_v\hat{T} + \bar{u}\hat{u})\right] \tag{2.7}$$

$q'(x,t) = \mathrm{Re}(\hat{q}(x)e^{i\omega t})$, is the perturbation in the rate of heat release per unit axial length. c_v is the specific heat capacity at constant volume. For a linear disturbance the perfect gas law gives

$$\frac{\hat{p}}{\bar{p}} = \frac{\hat{T}}{\bar{T}} + \frac{\hat{\rho}}{\bar{\rho}} . \tag{2.8}$$

When the mean flow, the frequency ω and the relationship between $\hat{q}(x)$ and the flow are specified and the flow perturbations are given at one axial position, these equations can be integrated numerically with respect to x to determine the flow perturbations at all positions downstream.

We see then that if, for a given ω, the flow is known at one position in the duct and we have a flame model to determine $q(x,t)$, both the mean and fluctuating flow can be calculated at all other axial positions by integrating equations (2.1) - (2.3) and (2.5) - (2.7) numerically. In the next section we will demonstrate how this can be used to determine the buzz frequency in a premixed laboratory rig.

3. COMPARISON OF THEORY AND EXPERIMENT FOR A PREMIXED RIG

The geometry of the Cambridge Reheat Buzz Rig has been described in detail by Langhorne (4) and is illustrated in Figure 1. The working section is a duct of circular cross-section, whose length L can be varied. Air is supplied at constant pressure to a choked nozzle at the upstream end of the working section. In a similar way, the fuel (ethylene) is injected at constant temperature and pressure through choked holes. The fuel and air mix effectively in the nozzle, thus supplying a premixed gas of uniform fuel-air ratio and constant mass flow rate to the working section. The flame is stabilized in the wake of a bluff body consisting of a conical gutter supported on a stem, and all the burning length is visible through quartz ducting.

We choose a coordinate system in which the origin, $x = 0$, is at the inlet of the working section and x increases towards the hot duct exit. A running condition is defined by specifying the inlet Mach number and stagnation temperature and the mean heat release rate. The exit pressure is atmospheric. The axial distribution of the mean heat release rate can be determined from the measurements. Bloxsidge et al (3) showed that, at least for this rig, it is a good approximation to take the instantaneous heat release rate to be proportional to the light emission by C_2 radicals. The ultimate aim of the work at Cambridge is to develop a prediction scheme for buzz onset and frequencies in afterburners, for which there are existing codes to calculate the axial distribution of the mean heat release rate. So, rather than develop a theory to calculate $\bar{q}(x)$ for the rig geometry,

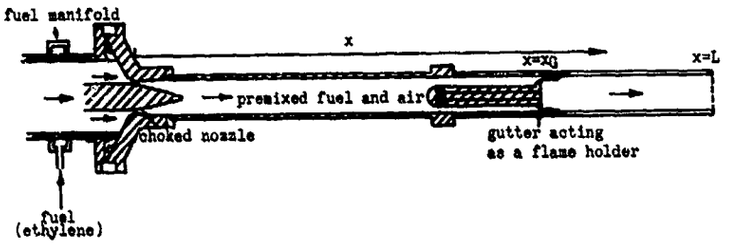


Figure 1 The geometry of the rig

Bloxsidge et al simply approximated it by three straight lines choosing the break-points and slopes to fit the light emission data. However, at some running conditions, the fit was poor. When the mean heat release distribution was refined to give better agreement with experiment the predicted frequency changed considerably. In order to eliminate this arbitrariness, we choose to use the measured light emission to describe the mean heat release rate precisely. We fit a spline to the distributed light emission data, and take the local mean heat release rate to be proportional to the local mean light emission. A measurement of the stagnation temperature rise across the burning region enables the constant of proportionality to be determined.

Once the axial distribution of the mean heat release rate has been specified, the mean flow can be calculated. The mean flow satisfies mixed point boundary conditions: the inlet Mach number and temperature are known and the exit pressure is atmospheric. The scheme adopted is to guess the upstream pressure, integrate down the duct and then iterate in the value of the guess for the mean upstream pressure until the mean exit pressure is atmospheric. We now turn our attention to the unsteady flow.

The nozzle at the upstream end of the duct is choked. This means that acoustic perturbations within the working section will not alter the mass flow rate at inlet which therefore remains constant and we have

$$\frac{\hat{\rho}(0)}{\bar{\rho}(0)} + \frac{\hat{u}(0)}{\bar{u}(0)} = 0 \quad . \tag{3.1}$$

Moreover, care was taken to ensure that the flow was only just choked, so that any shocks are weak and there is negligible entropy production. The flow is therefore isentropic and, with γ denoting the ratio of specific heat capacities,

$$\frac{\hat{p}(0)}{\bar{p}(0)} = \gamma \frac{\hat{\rho}(0)}{\bar{\rho}(0)} \quad . \tag{3.2}$$

Since the theory is linear, if $\hat{p}(x)e^{i\omega t}$ satisfies the homogeneous equations of motion, so will $\alpha\hat{p}(x)e^{i\omega t}$, for any complex constant α. Consequently we may choose without loss of generality, that

$$\hat{p}(0) = 1 \quad . \tag{3.3}$$

When (3.1) - (3.3) are combined with the perfect gas equation they completely specify the unsteady inlet flow.

The downstream end of the working section is open and has an appreciable mean flow with a temperature higher than ambient through it. Cargill (9) has shown that for such a geometry the appropriate boundary condition is

$$\hat{p}(L) = 0 \quad . \tag{3.4}$$

This arises purely as a consequence of application of the Kutta condition at the duct exit The same boundary condition was deduced intuitively by Bechert (10).

The development of the unsteady flow along the duct depends crucially on the unsteady heat release. Bloxsidge et al (3) investigated this important parameter experimentally. They ran their rig at a low fuel-air ratio for which the buzz mode was stable and there was no discernible narrow-band peak in the pressure spectrum. Acoustic waves were then generated in the rig by a movable centre-body, and the response of the flame investigated. The unsteady heat release rate along the duct was found to be related to the perturbation in the heat release rate at the flame-holder at an earlier time. Bloxsidge et al gave an explicit form for this time delay, $\tau(x)$. Once the perturbations in the heat release rate

at the flame-holder are known, the time delay can be used to determine the unsteady combustion throughout the duct.

Near the flame-holder the heat release rate responds to changes in particle velocity, pressure and temperature. But when the Mach number of the mean flow is low, the fractional change in velocity is much larger than the fractional change in pressure and temperature near the flame-holder. This was evident in Langhorne's experimental results (4), where the flame was observed to move intermittently upstream of the flame-holder (indicating velocity perturbations of the order of the mean velocity), while fractional changes in pressure were less than 10 %. Since the fractional changes in velocity are so much larger than the other fractional changes in the flow, Bloxsidge et al assumed the unsteady combustion to be determined principally by velocity fluctuations near the flame-holder. This supposition was confirmed by their data collapsing into a universal form when expressed in this way. By exciting the flame at a range of frequencies Bloxsidge et al found the relationship between the heat release rate at their flame-holder and local velocity perturbations to be a function of Strouhal number and gave an explicit form for that relationship (see reference (3) equation (3.8)). We will use Bloxsidge et al's flame model and write

$$\frac{\hat{q}(x)}{\bar{q}(x)} = \frac{1}{1St}\left(1 + \frac{e^{-i\omega\pi St/2}}{1St}\right)\frac{\hat{u}_G}{\bar{u}_G} e^{-i\omega\tau(x)} \quad . \tag{3.5}$$

St is the Strouhal number $\omega 2\pi r_G/\bar{u}_G$, where the suffix G denotes conditions at the gutter lip. r_G is the radius of the gutter.

Two distinct forms for the time delay $\tau(x)$ were observed. At low fuel-air ratios

$$\tau(x) = (x - x_G)/\bar{u}_G \quad . \tag{3.6}$$

Bloxsidge et al (3) and Langhorne (4) termed this 'weak buzz'. For higher fuel-air ratios at which the natural oscillations have a larger amplitude, the time delay was only found to have the form shown in (3.6) for positions near the flame-holder. Further downstream the phase of the heat release rate was nearly uniform. In the earlier work this was called 'established buzz' and following Bloxsidge et al we will describe it by

$$\tau(x) = \frac{x_o - x_G}{\bar{u}_G} + \int_{x_o}^{x} \frac{dx}{\bar{c}(x)} \quad , \tag{3.7}$$

where $\bar{c}(x)$ is the local speed of sound and x_o is the axial position at which $\hat{q}(x)$ first lags $\hat{p}(x)$.

With the unsteady inlet flow determined by equations (3.1) - (3.3) and the flame model in (3.5) - (3.7), equations (2.5) - (2.7) can be integrated along the duct. At a general value of ω, the exit boundary condition (3.4) is not satisfied. We therefore iterate in ω, at each step calculating the flow in the duct, until we determine the complex value of ω for which the exit pressure perturbation vanishes. Only disturbances with these particular frequencies satisfy all the boundary conditions and can exist as free modes of the duct/flame arrangement. The mode shape has also been determined.

Bloxsidge et al integrated the one-dimensional equations of mass, momentum and energy conservation in a similar way. Their theory was complicated by consideration of the gutter blockage and inclusion of a spreading flame zone. It is evident from their results that these extensions had little effect. Their treatment of them, however, involved the introduction of additional constants (control volume lengths and a flame spreading angle among others). Our aim here has been not only to simplify the theory of unnecessary complications, but also to avoid the introduction of extra arbitrary constants. By using an experimentally determined mean heat release rate, the only modelling required in the theory is the adoption of the flame model as described in equations (3.5) - (3.7).

The predictions of this simple theory have been checked by comparison with Langhorne's data (4), where the changes in the buzz frequency and mode shape for different mean flows and duct lengths are reported. The geometries and mean flow conditions investigated are summarized in Table 1, which also compares the calculated frequency and growth rate with those of Bloxsidge et al. In all but one case the simple theory improves the frequency prediction. The largest error between theory and experiment is 4.6 Hz (6%). The predicted mode shapes are displayed in Figures 2 - 6 and compared with Langhorne's experimental data (4).

TABLE 1

	Configuration 1	Configuration 2 (lower fuel-air ratio)	Configuration 2 (higher fuel-air ratio)	Configuration 3	Configuration 4
Equivalence ratio	0.70	0.65	0.66	0.65	0.71
Inlet Mach number	0.08	0.08	0.08	0.08	0.15
x_0 (m)	1.18	0.74	0.74	1.19	1.18
L (m)	1.92	1.48	1.48	2.18	1.92
x_{ref} (m)	0.75	0.49	0.49	0.75	0.75
Experimental frequency (Hz)	77	81	103	77	109
Calculated frequency (Hz)	81.6	78.3	102.8	81.2	110.1
Calculated growth rate (s^{-1})	-1.9	-3.5	-5.0	-1.0	93.2
Frequency calculated by Bloxsidge et al. (Hz)	81.7	75.5	88.3 (108 with improved mean heat release rate)	80.1	113.1
Growth rate calculated by Bloxsidge et al. (s^{-1})	1.1	-4.4	68.1 (79 with improved mean heat release rate)	33.1	86.6

The inlet static temperature is 288K, the duct radius 35mm and the gutter radius, r_0, 17mm for all configurations.

Results for Configuration 1 are illustrated in Figure 2. The spline fit to the measured mean heat release rate is shown in Figure 2c, while the comparison between the flame model in equations (3.5) and (3.7) and the measured unsteady heat release rate is displayed in Figures 2a and b. The flame model clearly describes the phase of the unsteady combustion accurately, but overestimates its amplitude in the downstream portion of the duct. However, the satisfactory agreement between the predicted frequency of 81.6 Hz and the measured value of 77 Hz suggests that this inaccuracy is not important. The calculated and measured pressure mode shapes at the buzz frequency are illustrated in Figures 2d and e.

Figure 3 shows comparison between theory and experiment for Configuration 2 at the lower fuel-air ratio. At this fuel-air ratio 'weak buzz' occurs. Figure 3b demonstrates that the flame model in equations (3.5) and (3.6) describes the phase of the unsteady heat release rate well. The agreement between the theoretical and measured buzz frequencies (78.3 and 81 Hz respectively) is good and the pressure mode shape is accurately reproduced. At a higher fuel-air ratio established buzz occurs. This case is illustrated in Figure 4. Now the established flame model in equations (3.5) and (3.7) is required. The theoretical frequency of 102.8 Hz is in excellent agreement with the measured value of 103 Hz.

Configuration 3 has a longer length of working section downstream of the flame-holder. The results for this geometry are shown in Figure 5. We see that once again the theory predicts the unsteady heat release rate and pressure mode shapes accurately, and the theoretical frequency, 81.2 Hz, is reasonably close to the experimental value of 77 Hz.

Results for Configuration 4 are shown in Figure 6. Here the geometry is the same as that in Configuration 1 but the inlet Mach number has been increased to 0.15. This has an appreciable effect on the experimental frequency which increases from 77 Hz for an inlet Mach number of 0.08 to 109 Hz at this running condition. This increase is accurately reproduced by the theoretical frequency which rises from 81.6 to 110.1 Hz. A comparison of the pressure mode shapes in Figures 2d and 6d is interesting. Figure 2d shows that at low Mach numbers the pressure perturbation appears to have a node near the flame-holder. This has been used by Heiter, Taylor & Whitelaw [11] to obtain the frequency of combustion oscillations in their rig. We see from Figure 6d that at higher flow rates the minimum in the pressure amplitude occurs further upstream.

Macquisten (private communication) has recently obtained new results on this rig at higher inlet temperatures. He produced these inlet temperatures by burning in a preheater upstream of the working section. The afterburner fuel-air ratio is quantified by a parameter ϕ, which is the afterburner fuel-oxygen ratio divided by the value for stoichiometric burning. ϕ includes the effects of oxygen consumption in the preheater and the small amount of unburnt preheat fuel entering the working section. Macquisten's measured heat release rates and pressure mode shapes are illustrated in Figure 7 for an inlet stagnation temperature of 620 K with $\phi = 0.75$ and the same inlet Mach number and geometry as Configuration 4. It is reassuring how well the flame model, which was developed from observations for an inlet velocity of 25 m/s, is able to describe unsteady combustion in an oncoming stream over 2½ times faster, an indirect confirmation of the Strouhal number scaling in equation (3.5). At this running condition the agreement between the measured frequency (156 Hz) and the predicted frequency (154.5 Hz) is excellent.

Figure 8 shows a comparison between theory and Macquisten's experimental results for a range of afterburner fuel-air ratios and three inlet temperatures. At low afterburner fuel-air ratios, near buzz onset, when a narrow-band peak is first discernible in the pressure spectrum, the agreement between theory and experiment is good. As the afterburner fuel flow rate is increased, the amplitude of the oscillations grows, with in particular

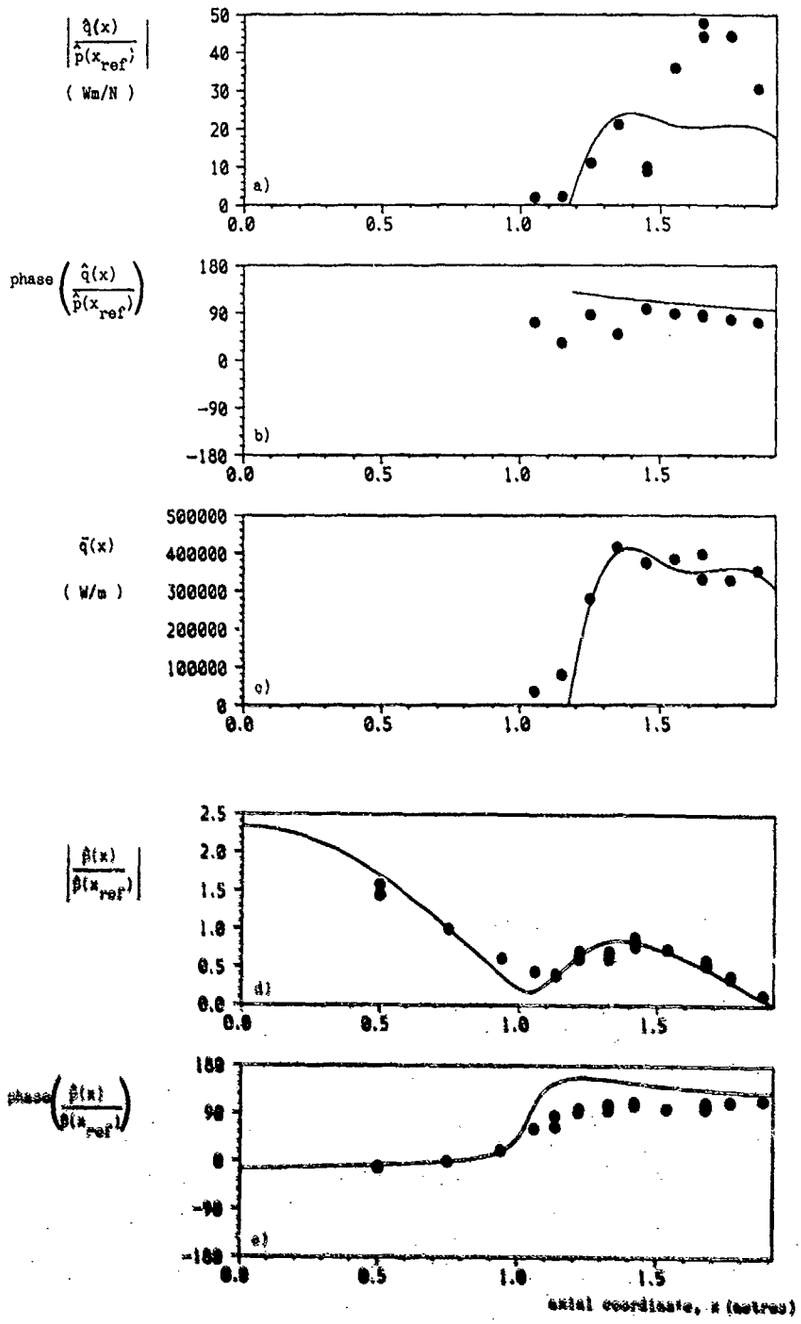


Figure 2 The heat release rate/unit length and pressure variation along the duct at the burn frequency for Configuration 1 .

theory

● Langhorne's experimental data

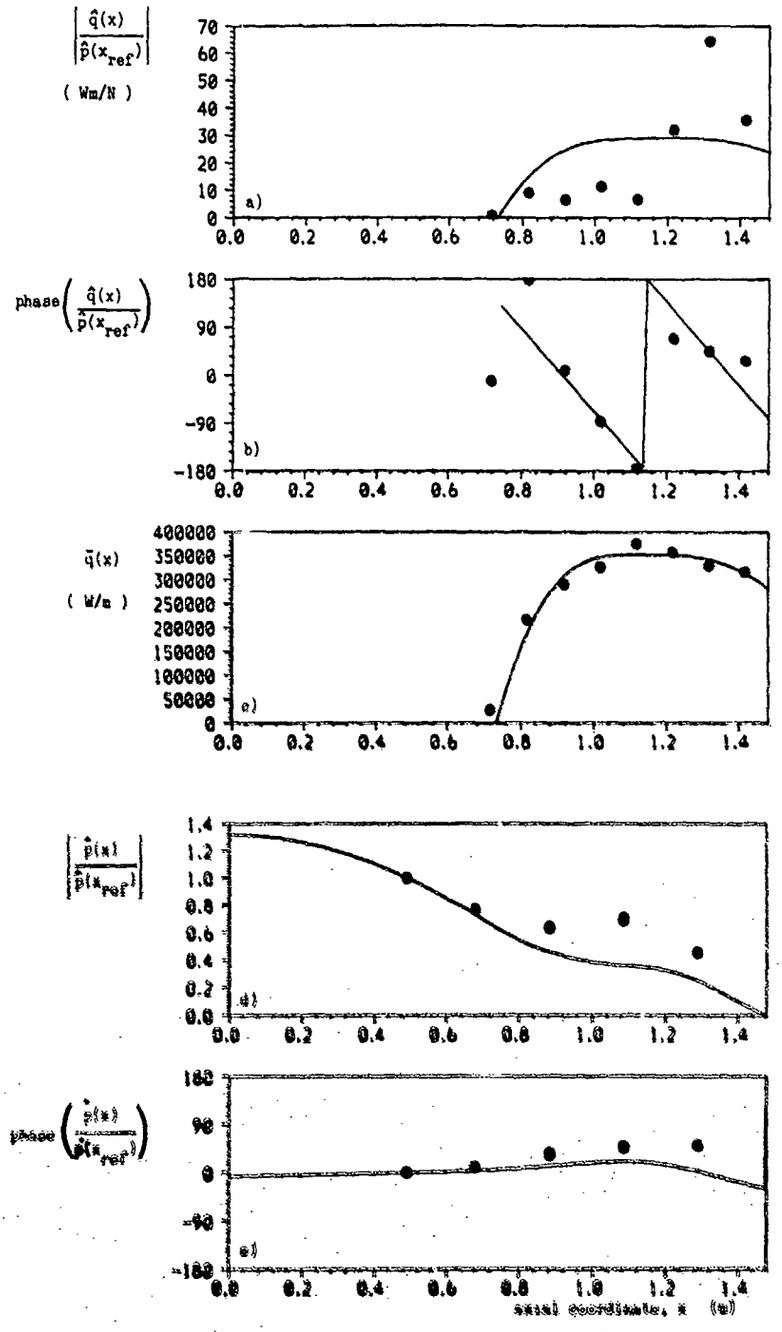


Figure 3 The heat release rate/unit length and pressure variation along the duct at the buzz frequency for Configuration 2 at the low fuel-air ratio.

——— theory

● Langhorne's experimental data

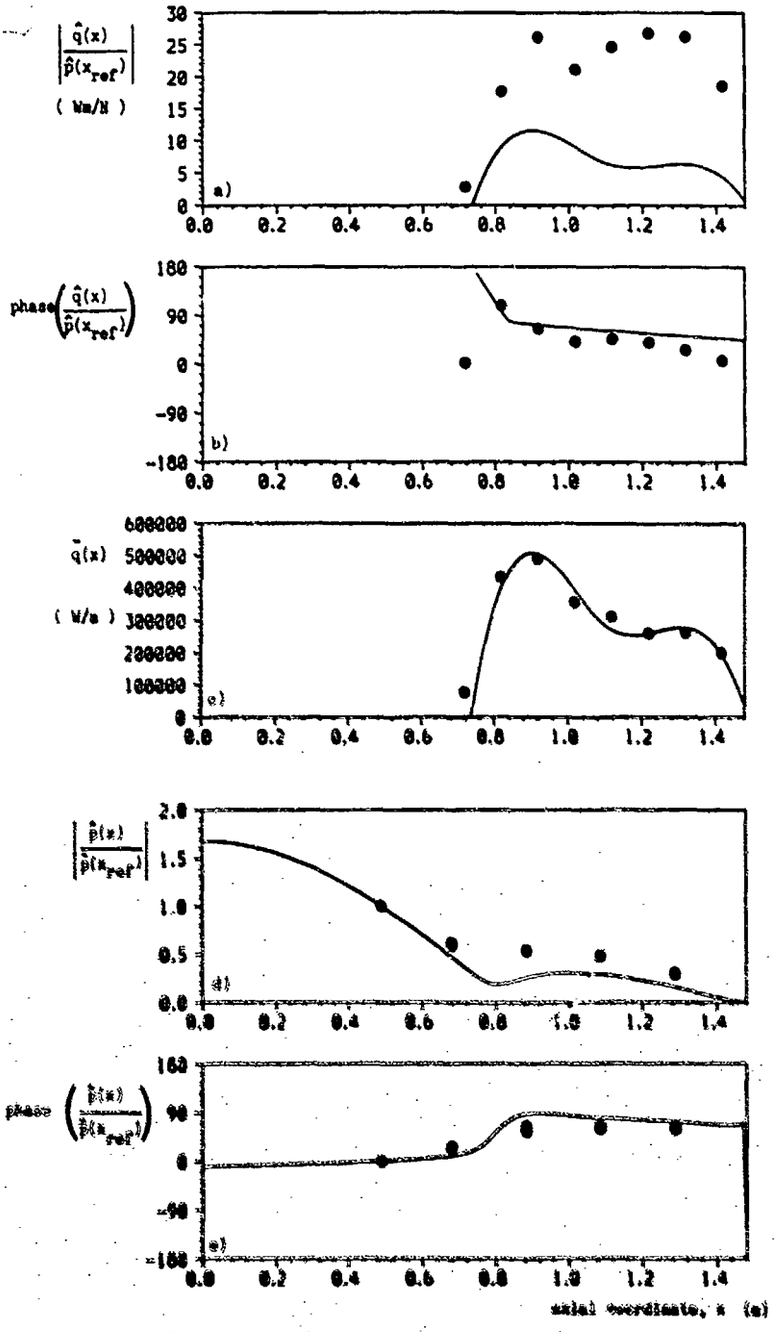


Figure 4. The heat release rate/unit length and pressure variation along the duct at the buzz frequency for Configuration 2 at the higher fuel-air ratio.

——— theory

● Langhorne's experimental data

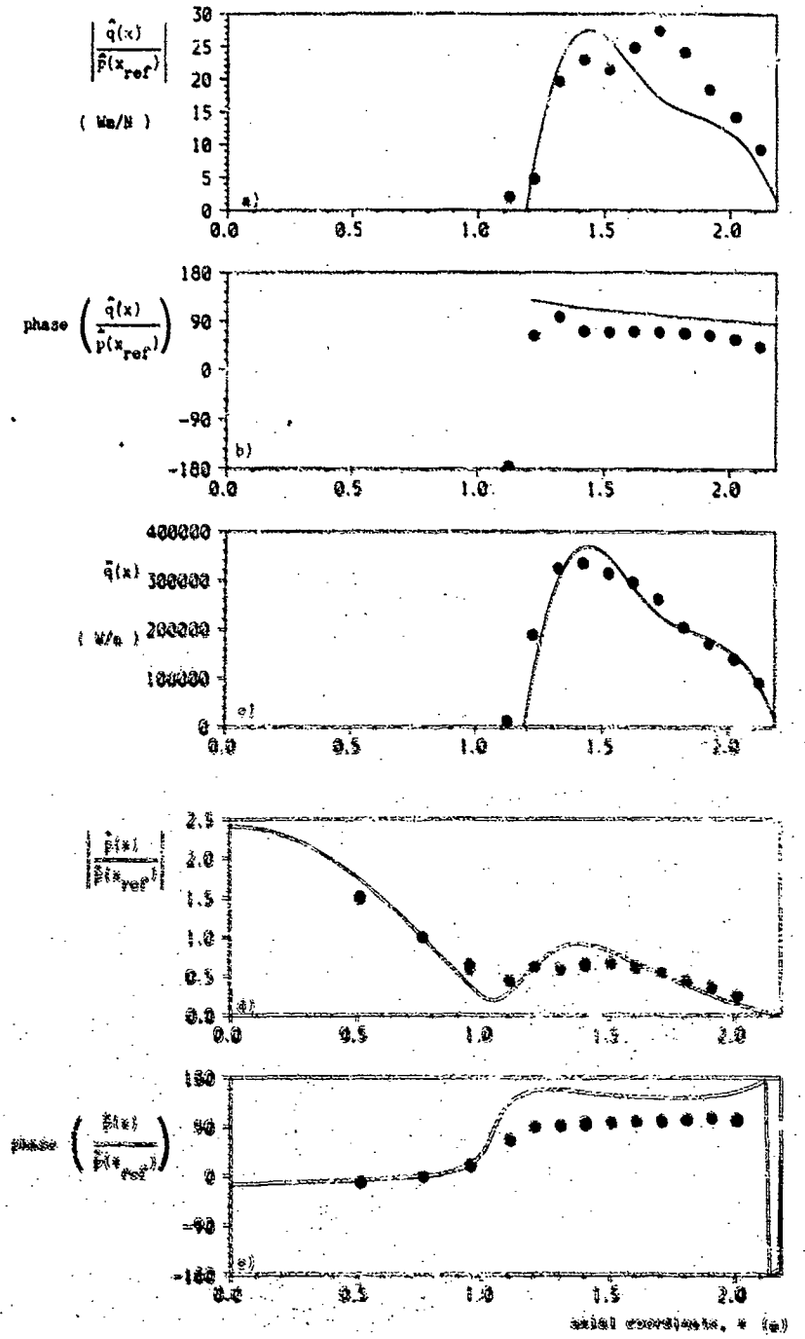


Figure 5. The heat release rate, unit length and pressure variation along the duct at the buzz frequency for Configuration 3.

Theory

Langhorne's experimental data

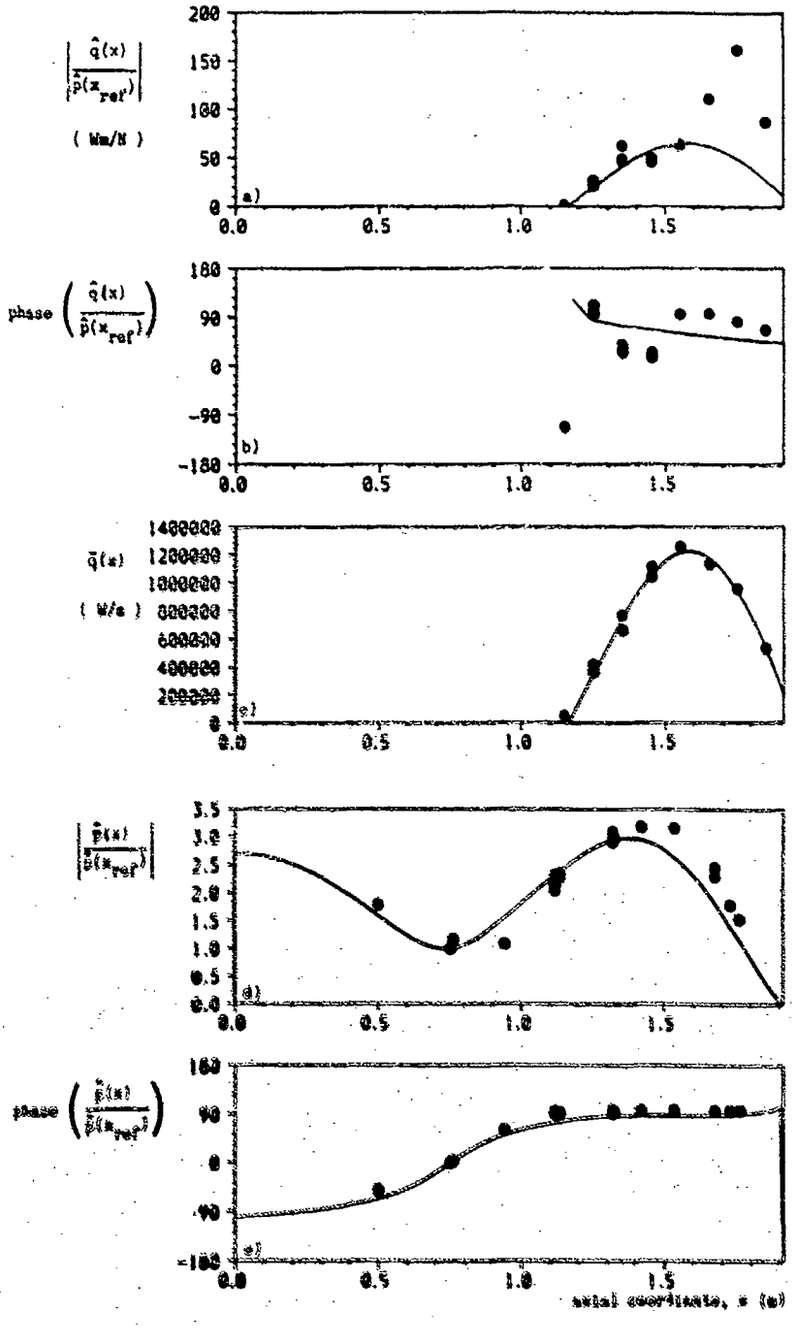


Figure 6. The heat release rate/unit length and pressure variation along the duct at the [illegible] frequency for Configuration 4 .

——— theory

● Langhorne's experimental data

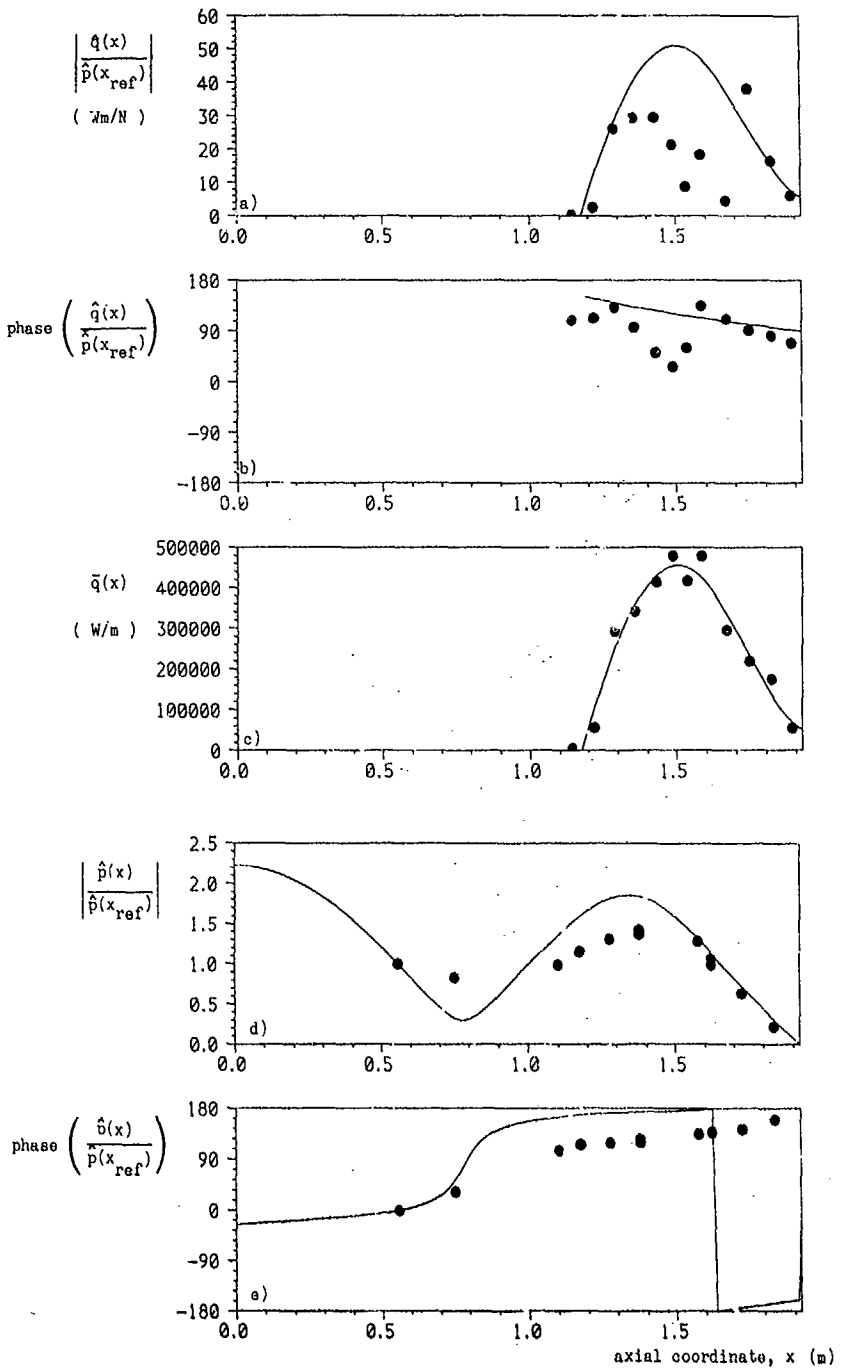


Figure 7 The heat release rate/unit length and pressure variation along the duct at the buzz frequency for an inlet stagnation temperature of 620K, ϕ=0.75 and the same geometry and inlet Mach number as Configuration 4.

theory

● Macquisten's experimental data

nonlinear fluctuations in the heat release rate. The linear theory then underestimates the frequency.

We have simplified the theory developed by Bloxsidge et al without degrading the agreement between theory and Langhorne's experimental results. This simple theory has also been able to predict correctly the significant rise in frequency measured by Macquisten as the temperature at inlet to the working section is increased.

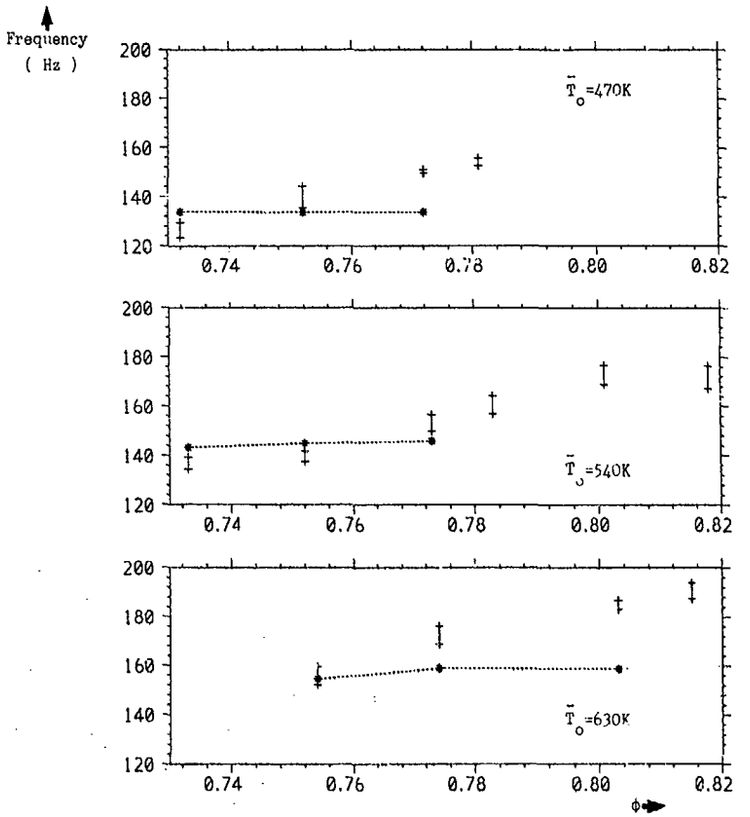


Figure 5 Comparison between theory and experiment for various afterburner fuel-air ratios and three values of the inlet stagnation temperature, $\bar{T}_o$.

‡ Macquisten's experimental results

-- theory

4. DIFFERENCES BETWEEN THE RIG AND AN ENGINE AFTERBURNER

In this section we investigate the effects on the buzz frequency and mode shape of two differences between the rig and an aeroengine afterburner. Our aim here is not to include a realistic engine afterburner geometry (although it can be incorporated into a similar calculation as shown by Bloxsidge (12)). Instead we aim to highlight the effects of two simple changes when the rest of the geometry and mean flow is unchanged.

Firstly an engine afterburner is terminated by a choked nozzle rather than the open end on the rig. The boundary condition at a choked nozzle is that of constant non-dimensional mass flow, which Marble & Candel (13) have shown reduces to

$$\frac{\hat{p}}{\bar{p}} - 2\frac{\hat{u}}{\bar{u}} - \frac{\hat{\rho}}{\bar{\rho}} = 0 \qquad (4.1)$$

for linear perturbations. We have replaced the exit boundary condition (3.4) by (4.1) and repeated the calculations for Configuration 1. The flame model retains the form in (3.5) - (3.7). This use of the same flame model emphasizes an advantage of the procedure

developed by Bloxsidge et al (3). Poinsot, Le Chatelier, Candel & Esposito (14) also excited a flame in a duct for a range of frequencies. They used their data to determine a reflection coefficient. But as they point out, this reflection coefficient depends not only on the flame but also on the downstream geometry. In determining the relationship between fluctuations in heat release rate and particle velocity Bloxsidge et al have determined a more general flame model which can be applied to different geometries and mean flows.

The frequency of combustion oscillations with the choked-nozzle end condition (4.1) is found to be much lower than that for an open end. The two lowest roots are now 40.9 Hz and 63.0 Hz with growth rates of $37.1\ s^{-1}$ and $-7.8\ s^{-1}$ respectively. These results are consistent with the observations of Sivasegaram & Whitelaw (15) who found that their rig was susceptible to a lower frequency instability when they installed an exit nozzle. The pressure mode shape at the lowest eigenfrequency is shown in Figure 9. We see that the pressure fluctuations at this low frequency are in phase throughout the duct.

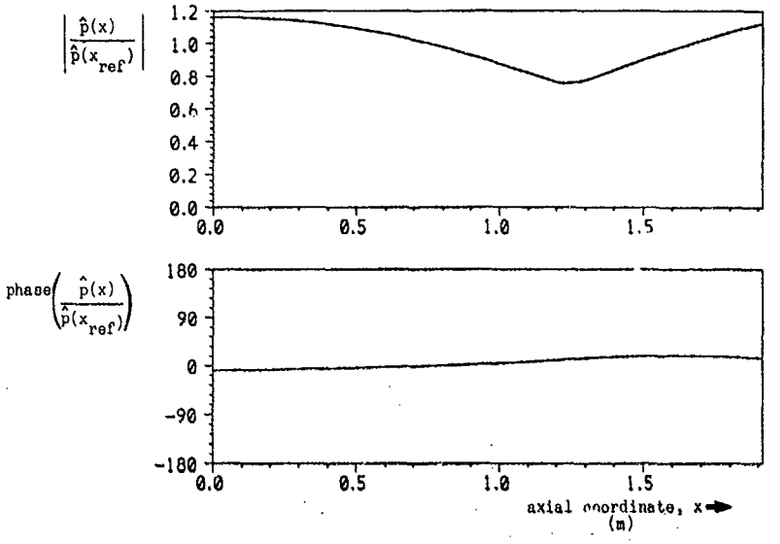


Figure 9. The pressure variation along the duct at the buzz frequency of 40.9 Hz for Configuration 1 with a choked nozzle at exit.

Another difference between the rig and an aeroengine afterburner is that, while the rig uses gaseous fuel, the engine is liquid-fuelled. The liquid is injected at a constant flow rate into a high temperature air stream in the afterburner. The liquid can be expected to evaporate quickly at these temperatures, but as the combustion oscillations modify the local air flow rate past the fuel injectors variations in fuel-air ratio will occur. In contrast the rig is premixed with a uniform fuel-air ratio.

For the premixed rig, we used a flame model in which changes in heat release rate near the flame-holder were described by

$$\frac{\hat{q}_G}{\bar{q}_G} = f(St)\ \frac{\hat{u}_G}{\bar{u}_G}\ , \tag{4.2}$$

where f is a function of the Strouhal number $\omega 2\pi r_G/\bar{u}_G$.
The explicit form of f is given in (3.5):

$$f(St) = \frac{1}{iSt}\left(1 + \frac{a}{iSt}\,e^{-ii\pi St/2}\right)\ . \tag{4.3}$$

Part of this fluctuation occurs because, for the premixed gas, the fuel flow arriving at the flame-holder in unit time modulates with the changing air flow.

Let $\hat{Q}(x)$ denote the unsteady heat release rate per unit length when fuel is injected at the flame-holder. Then

$$\frac{\hat{Q}_G}{\bar{Q}_G} = -\frac{\hat{\rho}_G}{\bar{\rho}_G} - \frac{\hat{u}_G}{\bar{u}_G} + \frac{\hat{q}_G}{\bar{q}_G} \quad . \quad . \qquad (4.4)$$

After making the usual approximation that for a low Mach number flow $\hat{\rho}_G/\bar{\rho}_G$ is small in comparison with $\hat{u}_G/\bar{u}_G$, equations (4.3) and (4.4) can be combined to give a fuel-injection flame model

$$\frac{\hat{Q}_G}{\bar{Q}_G} = (f(St) - 1)\frac{\hat{u}_G}{\bar{u}_G} \quad . \qquad (4.5)$$

For simplicity we will again use the time delays in equations (3.6) and (3.7) to describe the combustion downstream of the flame-holder

When this flame model is used, the frequency of the combustion oscillation is found to be shifted slightly from that predicted for a premixed flame, and the growth rate is increased. For example, for the weak buzz at the low fuel-air ratio in Configuration 2 the frequency becomes 74.0 Hz with a growth rate of 20.3 s^{-1}. The effect of injecting fuel directly into the working section is predicted to be destabilizing, but only to lead to a modest change in frequency.

CONCLUSIONS

The linear stability analysis of a flame burning in a duct developed by Bloxsidge et al has been simplified, while retaining all its essential features. The theory is able to predict the frequency of the instability and the mode shape. It accurately describes the effects of changes in flow rate, inlet temperature, duct length and fuel-air ratio.

REFERENCES

(1) Smart, AE, Jones, B & Jewell, NT 1976 Measurements of unsteady parameters in a rig designed to study reheat combustion instabilities. AIAA-76-141

(2) Rayleigh, JWS 1945 The Theory of Sound: Vol. II, 224-227, Dover Publications

(3) Bloxsidge, GJ, Dowling, AP & Langhorne, PJ 1988 Reheat buzz: an acoustically coupled combustion instability. Part 2. Theory. J. Fluid Mech. 193, 445-473

(4) Langhorne, PJ 1988 Reheat buzz: an acoustically coupled combustion instability. Part 1. Experiment. J. Fluid Mech. 193, 417-443

(5) Merk, HJ 1956 Analysis of heat-driven oscillations. Appl. Sci. Res. A7, 175-191

(6) Hadvig, S 1971 Combustion instability: system analysis. J. Inst. Fuel, 44, 550-558

(7) Mugridge, BD 1980 Combustion driven oscillations. J. Sound Vib. 70, 437-452

(8) Crocco, L 1965 Theoretical studies on liquid-propellant rocket instability. 10th Symposium (International) on Combustion, 1101-1128

(9) Cargill, AM 1982 Low-frequency sound radiation and generation due to the interaction of unsteady flow with a jet pipe. J. Fluid Mech. 121, 59-105

(10) Bechert, DW 1980 Sound absorption caused by vorticity shedding, demonstrated with a jet flow. J. Sound Vib. 70, 389-405

(11) Heitor, MV, Taylor, AMKP & Whitelaw, JH 1984 Influence of confinement on combustion instabilities of premixed flames stabilized on axisymmetric baffles. Combust. Flame 57, 109-121

(12) Bloxsidge, GJ 1987 Reheat buzz - an acoustically driven combustion instability. Ph.D. thesis, University of Cambridge

(13) Marble, FM & Candel, SM 1977 Acoustic disturbance from gas non-uniformities convected through a nozzle. J. Sound Vib. 52, 235-243

(14) Poinsot, T, Le Chatelier, C, Candel, SM & Esposito, E 1986 Experimental determination of the reflection coefficient of a premixed flame in a duct. J. Sound Vib. 107, 265-278

(15) Sivasegaram, S & Whitelaw, JH 1987 Combustion oscillations of relevance to augmentors. AIAA-87-2107

ACKNOWLEDGEMENT

I am grateful to Dr M.A. Macquisten for allowing me to use his as yet unpublished data in Figures 7 and 8. This work has been carried out with the support of Rolls-Royce plc and the Procurement Executive, Ministry of Defence.

DISCUSSION

S. Candel, Fr

1. What are the main differences between weak and strong buzz?

2. What is the meaning of x in the time lag expression. Does x vary with the equivalence ratio or with the other upstream conditions?

Author's Reply:

1. The main difference between weak and established buzz is in the form of the time delay between unsteady heat release along the duct and that at the flame-holder (as described by equations 3.6 and 3.7).

2. x is the axial position at which the heat release rate/unit length first lags the pressure perturbation. Physically it seems to represent the axial extent of effective flame-holding. Both our flow visualization and the photomultiplier measurements of C emission show that combustion is intermittently extinguished during the buzz cycle at all positions downstream of x .

   The position of x is a function of upstream conditions and in particular it moves downstream as the Mach number is increased (Langhorne (4)).

G. Winterfeld, Gr

Do you think that your heat relase model applies equally well to saturated hydrocarbon fuels (e.g. keresene) as it does to ethylene which has rather different ignition and combustion characteristics?

Author's Reply:

We have not used saturated hydrocarbon fuels in our rig. However, it is clear that it is the response of the ethylene flame to perturbations in the oncoming flow velocity that leads to unsteadiness in the heat release rate, and that the details of the chemistry are not relevant. If that were still true for a saturated hydrocarbon flame we would expect to be able to use the same model.

C. N. Coats, UK

Your oscillating flame model assumes the same correlation between C_2 chemiluminescence and heat release for the oscillating flame as for the stationary flame. Can you justify this assumption and does it make any difference to your predictions?

Author's Reply:

In fact we do not assume the same correlation between light emission by C_2 radicals and heat release rate for each running condition. The details are given in Bloxsidge et al (3), where the constant of proportionality between light emission and heat release rate is determined for each running condition from the measured stagnation temperature rise.

[An additional comment was made by Dr. P. J. Langhorne.]

P. Langhorne, New Zealand

We do not expect to be able to change the fuel to air ratio substantially and still use the same constant of proportionality between the light emission from C_2 radicals and the heat release rate.

Author's Reply:

Work is currently in progress at extending the results to higher Mach numbers. However we think that, because our flame model describes the relationship between the flow and the perturbation in heat release rate, it is in fact a description of the dynamics of the flame. But, like you, we believe that it is worth testing the model at higher Mach numbers.

S. Sivasegaram, UK

1. If the bulk mode frequency associated with the instability is to be calculated, can the same assumption as for the longitudinal frequency be made about the heat release distribution?

2. Is it not possible that the mechanisms of instability are different for the bulk mode and longitudinal modes?

Author's Reply:

Both these questions can be answered in the same way. Bloxsidge et al (3) developed the flame model in equation (3.5) by investigating the response of the flame to excitation at a wide range of frequencies (15-95Hz). We can therefore have confidence that this flame model does describe the unsteady heat release even for the low frequency of the bulk mode shown in Figure 9.

K. Kailasanath, US

I noticed that you had varied the inflow Mach number at least up to 0.15. Have you looked at the effects of increasing the Mach number furtrher? Our results (presented at this meeting, paper No. 16) show that for higher Mach numbers, the natural dynamics of the shear layer might play a greater role than at lower Mack numbers. Would you comment on the validity of your analysis for such a flow field.

ATTENUATION OF REHEAT BUZZ BY ACTIVE CONTROL

P.J. Langhorne
Department of Physics, University of Otago, P.O. Box 56, Dunedin, New Zealand.

and

N. Hooper
Whittle Laboratory, Cambridge University Engineering Department, Madingley Rd., Cambridge CB3 0DY, England.

SUMMARY
Reheat buzz is a low frequency longitudinal pressure fluctuation which can be excited by flame/sound field interaction in the afterburner of a jet aeroengine operating at high fuel to air ratios. Active control techniques have already been applied to control a similar combustion instability on a rig. In this previous case the controller modified the upstream boundary condition by unsteadily altering the mass flow of premixed gas. This method is not readily applicable to an engine. In this paper we demonstrate that similar achievements are possible with the suitably-phased addition of extra fuel. The mechanical power requirements of this controller are modest and the system is easy to implement.

1. INTRODUCTION

When combustion takes place within an acoustic resonator, the interaction between acoustic waves and unsteady combustion may lead to oscillations of damaging intensity. Such a combustion instability can occur in the afterburners of jet aeroengines, where it has a low frequency and is termed 'reheat buzz'. The existence of this particular instability does not depend on any property peculiar to liquid fuels, such as atomisation. Indeed similar oscillations have been observed on premixed laboratory rigs with gaseous fuel. There the flame burns in the wake of a bluff body in a duct and Schlieren photographs (see for example Smart et al.[1]) show that the flame is perturbed by velocity fluctuations at the flame holder, which alter the instantaneous heat release rate. If this unsteady heat release rate is in phase with local pressure perturbations, Rayleigh's criterion[2] states that the disturbances will grow. Longitudinal pressure waves propagating in the duct can then become destructively large in magnitude. Since passive dampers are uneffective at these low frequencies, the traditional solution has been to modify the aerodynamics of the burner to reduce the coupling between the heat release rate and the unsteady flow. However, there are frequently constraints on burner/flame-stabiliser design and the only alternative is to limit the heat release in the duct. In afterburners this means that a limit is placed on the available thrust.

A low frequency combustion instability in a duct lends itself to the techniques of active control. In this, a feedback signal taken from the unstable system is suitably processed and used to drive an actuator so as to reduce the instability. This may be done either by changing the boundary conditions so that more energy is lost at the boundaries or by altering the unsteady heat release rate so that the energy gain is reduced.

There have now been a number of demonstrations of the success of active control techniques in suppressing combustion instabilities on laboratory-scale apparatus. One of the simplest of these is the Rijke tube[3]. This is a vertical pipe, open at both ends, which contains a heated gauze or a flame. Such a pipe has a natural, half-wave resonance. The perturbations associated with this resonance induce fluctuations in the heat release rate that lag the unsteady velocity. Thus when the heat source is in the lower half of the pipe, the unsteady pressure and heat release rate are in phase and, according to Rayleigh's criterion, any linear perturbations will grow. The pressure fluctuations are sinusoidal with little cycle-to-cycle variation and it is possible to use active control to reduce the oscillations to negligible levels. This has been carried out in two different ways. Collyer and Ayres[3], Heckl[4] and Screenivasan et al[5] introduced a second controlling heat source into the upper half of the tube. The unsteady heating associated with this second heat source is out of phase with the pressure perturbations and dampens any oscillations. Alternatively, Dines[6] altered the energetics of linear perturbations by actively modifying the boundary condition at the end of the tube using a loudspeaker. The feedback signal here was the light emission from CH radicals in the flame, which has been shown to be a measure of heat release rate[7]. Heckl[8] has achieved noise reduction in essentially the same way as Dines, but using pressure fluctuations as the feedback signal to the loudspeaker.

In addition to the work on the Rijke tube, combustion instabilities have been controlled on other small scale apparatus. Kidin et al[9] have used a novel technique for generating the controlling pressure fluctuations, the expansion from a DC discharge. More conventional methods, very similar to Heckl's were used on a 1 kW laminar premixed burner by Lang et al[10]. They restated the encouraging observation for the application of active control techniques to practical devices, that the energy consumption of the controller is very small.

Consequently Poinsot et al[11] progressed to a more realistic and practical burner. The apparatus is a diffusion turbulent combustor with an air flow rate of 0.024 kgs $^{-1}$ and a fuel-to-air ratio which is 40% of the stoichiometric value for propane. Pressure oscillations were sensed by a microphone, suitably filtered, delayed and amplified and fed into a pair of loudspeakers. At the frequency of the combustion oscillation, the uncontrolled peak of 125dB was reduced by 24dB by the application of their control system.

Active control techniques have also been used successfully on a laboratory rig designed to model some of the essential features of the reheat system of a jet aeroengine[12,13]. The rig is illustrated in figure 1 and has been described in detail in Langhorne[14]. Air and ethylene are introduced at constant mass flow rates upstream of a choked nozzle. The gases mix as they enter the working section so there is a uniform fuel-to-air ratio across the duct. The experiments of Bloxsidge and others were performed with a premixed mass flow of 0.135 kgs^{-1} (i.e. about 27 ms^{-1} upstream of the flame holder) and a fuel-to-air ratio of 66% of the stoichiometric ratio. The premixed flame is stabilised in the wake of a conical gutter and undergoes an acoustically coupled combustion instability called 'buzz'. Control was applied by actively changing the boundary condition at the upstream end of the working section. In these experiments the fixed nozzle was replaced by a moveable one. The mass flow rate of premixed gas entering the working section could then be changed by altering the axial position of this nozzle, thereby modifying the upstream boundary condition. The nozzle was driven by a suitably processed pressure signal from the rig. Once implemented, the 162dB peak in the pressure spectrum due to the buzz was reduced by 20dB. In addition, the acoustic energy in the bandwidth 0-800 Hz was diminished to 10% of its value without control. Furthermore the modified 'buzz' frequency and modal pressure distribution with control were successfully predicted using the calculations described in Bloxsidge et al[15].

Although this method of control was successful on a 1/4 MW turbulent premixed burner with significant cycle-to-cycle variations, the method of implementation is not a practical proposition for full-scale afterburners. Mass flow fluctuations of the order of 3% of the mean mass flow are required in order to produce stability aerodynamically. Likewise it is impractical to consider the use of loudspeakers to produce significant pressure fluctuations in environments where mass flows of many kilogrammes per second are to be handled. In this paper we describe the results of a series of experiments to investigate a more practical means of implementing the feedback. The basic rig is identical to that used by Bloxsidge et al[12,13] (and illustrated in Figure 1), but control is achieved by the unsteady addition of fuel near the flame-holder. We exploit the fact that unsteady combustion is very effective at producing high intensity sound levels. In this case a pressure perturbation measured by a transducer upstream of the flame is a suitable input to the control circuit. This choice is not unique and successful control has been accomplished with other signals from the rig. The idea of the control is to use fast-response solenoid valves to pulse fuel into the rig in response to this input. This produces an additional unsteady rate of heat release which, if the control circuit is suitably designed, stabilises the flame.

2. A PRACTICAL CONTROL SYSTEM

The use of unsteady addition of fuel as a means of controlling combustion instabilities has been tested on the rig illustrated in Figure 1. In the basic configuration the fuel (gaseous ethylene) and air are introduced at constant mass flow rates upstream of a nozzle. This nozzle is choked to ensure that the supplies of fuel and air are acoustically isolated from the working section. The ethylene and air mix well in the constriction and enter the working section as a premixed gas. The working section is just a straight duct in which a flame is stabilised in the wake of a conical gutter. The experiments were performed with a premixed mass flow rate of 0.135 kgs^{-1} and equivalence ratios (defined as the ratio of mass of fuel to mass of air as a fraction of the ratio required for stoichiometric burning) in the range 0.63 to 0.70.

The pressure perturbation, $p'(x,t)$, is measured at various axial distances x downstream of the choked nozzle. In addition, the light emission from short-lived C_2 radicals in the flame is monitored. The optical arrangement is straightforward. A screen blanks off all but a 75mm length of flame. An image of this portion is focussed through a filter onto the photocathode of a photomultiplier. Two nominally identical systems are available. The filters are centred on 516.7 and 518.0nm with bandwidths of 3.2 and 3.6nm respectively, to

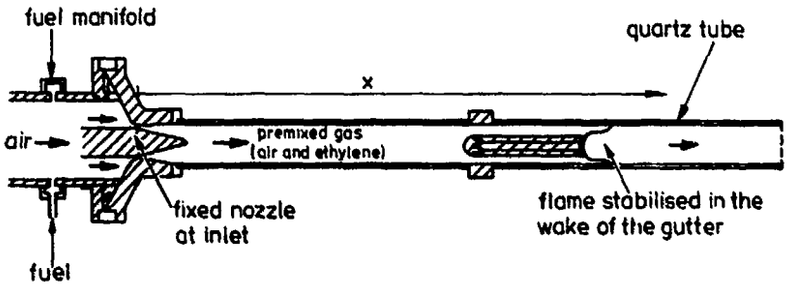


Figure 1. The reheat buzz rig.

pass the light emitted in the main C_2 transition. I(x,t) denotes the output from the photomultiplier for the window centred on x. Hurle et al[7] have shown that under certain conditions, the heat release rate is proportional to this light emission. Previous work[14,15] has shown that this is a valid assumption for this apparatus under limited conditions, although the constant of proportionality is not independent of large changes in fuel to air ratio. However a measurement of the stagnation temperature rise across the duct length enables the photomultiplier output in volts to be converted into heat release rate. We denote the heat release rate in the window centred on x by Q(x,t), which may be decomposed into its mean and fluctuating components, $\overline{Q}(x)$ and Q'(x,t) respectively.

The combustion oscillations on this rig have significant cycle-to-cycle variations and if they are to be successfully controlled by feedback, the time delay in the feedback system must be kept as short as possible. In earlier work, Bloxsidge and others noted that an additional time delay of one cycle (about 13 ms) led to a 10dB degradation in the performance of the controller. We aim to use the fluctuations in heat release rate due to imposed variations in fuel-air ratio as our control. These non-uniformities will convect with the fluid from the solenoid valves to the flame. The primary fuel manifold is so far upstream of the flame in our premixed rig that the time delay between the primary injection of fuel and its combustion is prohibitively large. Consequently when implementing the control the primary supplies of fuel and air are kept steady and a secondary unsteady supply of fuel is introduced close to the flame holder.

We chose to use automotive fuel injectors to pulse this secondary fuel. These direct-acting solenoid valves are cheap, robust and readily available. They have the advantage of being electrically operated with a response time of less than 1 ms[15]. Design calculations showed that four injectors were required to provide sufficient fuel flow rate to control the instability. The operation of a fuel injector is controlled by a preset threshold voltage. Whenever the input voltage is higher than this threshold the injectors open. The delivered mass flow of fuel depends both on the pressure in the supply feeding the injectors and on the length of time they are open, and is related to the input voltage in a non-linear way. Since the pressure in the supply cannot be changed rapidly, the cycle-to-cycle variations in the delivery of secondary fuel is purely a function of the length of time the injectors are open. There are two disadvantages to the injectors. The first is that they only have two modes of operation: they are either fully open or closed. Second, Hands[15] has shown that nominally identical injectors require different pulse widths in order to deliver the same volume flow rate of fuel. These differences can be of the order of 0.5 ms. This means that there would be radial variations in fuel to air ratio if the injectors discharged directly into the rig.

The addition of a secondary supply of heat fuel in a premixed gas at a location close to the flame will create local rich spots and destabilise the flame. We must therefore ensure that the secondary fuel is well mixed with air before it is incident on the flame. This also ensures that the effects of radial differences in volume flow rates from the injectors are reduced by mixing. Consequently air is added to the secondary fuel in a chamber prior to injection into the rig (see figure 2). Rapid and complete mixing is required in this chamber. Air flows steadily into the chamber through a choked orifice which isolates the air supply. The fuel enters unsteadily through the choked injectors. The two streams meet in perpendicular directions to maximise mixing. If the control is to be effective the mixing chamber must be flushed in a fraction of a cycle. This time is estimated to be about 2 ms. The chamber was designed so that this time delay and the opening time of the

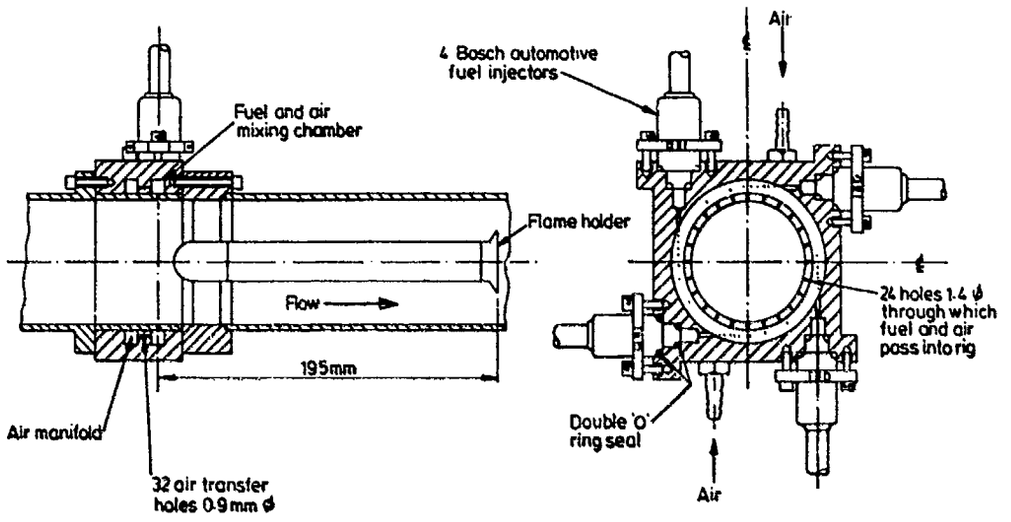


Figure 2. Detail of mixing device for the secondary fuel and air.

injectors are small in comparison with the time taken for the secondary fuel to convect along the working section to the flame holder. This is of the order of 7 ms, or half a cycle at a typical frequency of the combustion instability. The delay represents a reasonable compromise between the conflicting requirements of minimising the time delay while ensuring that the jets of secondary gas enter the working section sufficiently far upstream of the combustion zone to prevent the flame from stabilising in their wakes. It is difficult to avoid the production of such an aerodynamic disturbance since it is important that there is a pressure drop between the mixing chamber and the rig. This means that the secondary gas supply is insensitive to pressure fluctuations in the rig.

It is worth noting that the requirement of a secondary fuel and air supply for control is peculiar to a premixed rig and would not apply to an afterburner. There the primary fuel is injected sufficiently close to the combustion region for modulations in this fuel flow rate to be used for control.

An unsteady signal is taken from the rig and used as input to the control circuit. The main criterion for the choice of control signal is that it should have a large signal-to-noise ratio at the buzz frequency. The unsteady light emission from C_2 radicals close to the exit of the duct and a pressure upstream of the region of combustion have both been successfully used as control signals. The DC component is removed from this unsteady signal. It is then amplified and a suitable time delay is imposed (see figure 3). A variable offset is then applied to this signal so that it can be adjusted relative to the fuel injector's threshold voltage. The offset voltage is set as close to the threshold voltage as is practically possible since the difference between them will limit the effectiveness of the control. When the signal exceeds this threshold voltage the gate of a power transistor controlling the current to the injectors is opened. Thus the larger the amplitude of the control signal, the longer the injectors remain open. The secondary air enters the rig steadily and continuously so that the fuel-to-air ratio of secondary gas is varied. Once the time delay and offset voltage have been chosen to give optimum control, they are fixed during an experiment.

In the experiments to be described in this paper the primary mass flow of premixed gas, M_1, and primary equivalence ratio, ϕ_1, are set to produce a flame of the required stability. Secondary air flows steadily into the rig with a mass flow rate, m_{a2}, which is unchanged throughout all the experiments. The mass flow of secondary fuel, m_{f2}, not only depends on the proportion of a cycle over which the injectors are open, but also on the pressure in a feedring joining the inlets of the four injectors denoted by p_{inj}. The slow response of the pressure regulator controlling p_{inj} means that it decreases whenever the injectors are open and rises again as they shut. We will denote the mean and fluctuating components of p_{inj} by

$\overline{p_{inj}}$ and p_{inj}' respectively. The secondary mass flow, M_2, and its equivalence ratio $\phi_2 = \overline{\phi_2} + \phi_2'$, can be altered in the following four ways.

(i) the injectors are closed and there is no secondary fuel flow, m_{f2}, so that $\phi_2 = 0.0$.

(ii) the injectors are held open so that m_{f2} is steady and $\phi_2 = \overline{\phi_2}$ with no unsteady component ϕ_2'.

(iii) the injectors are driven by the signal from a function generator at a range of frequencies so that m_{f2} and $\phi_2 = \overline{\phi_2} + \phi_2'$ have a mean component and unsteady component of constant amplitude.

(iv) the injectors are driven from a feedback signal from the rig so that $\phi_2 = \overline{\phi_2} + \phi_2'$, where the magnitude of both the mean and unsteady components depends on the effectiveness of the control.

Under all four types of condition, the premixed gas downstream of the secondary supply will have a total mean equivalence ratio ϕ_T associated with it, where

$$\phi_T = \frac{m_{f1} + \overline{m}_{f2}}{(m_{a1} + m_{a2}) \times 0.0675} \qquad (1)$$

ϕ_T can therefore be increased by an increase in either ϕ_1 or ϕ_2.

The mass flow rate of the secondary premixed gas is approximately 7% of the mass flow rate of the primary. It was found that when the control had taken effect the injectors were open for approximately one fifth of the time. Thus the maximum value ϕ_2 would attain is approximately 1.3. Since ϕ_1 lies in the range 0.6 to 0.70, the secondary ϕ_2 is changing by

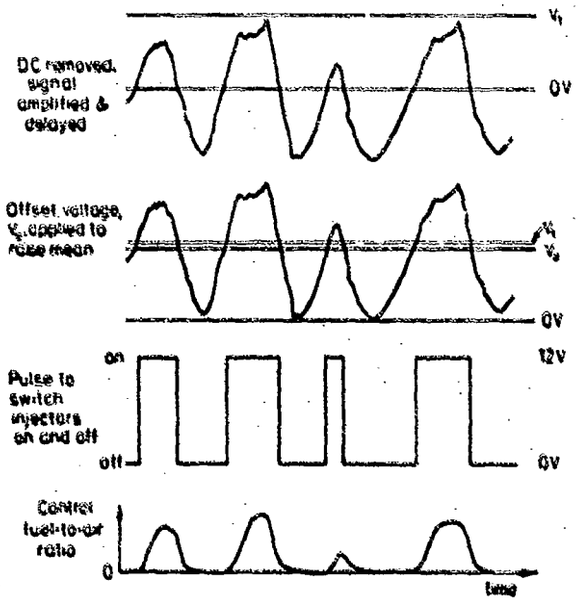


Figure 3.
The control system.

approximately $2\phi_1$. The total equivalence ratio then has a maximum possible range of 0.63 to 0.73 for $\phi_1 = 0.68$. This range will be significantly reduced by time delays in the valves and by turbulent diffusion.

3. PERFORMANCE OF THE CONTROL SYSTEM

The time delays throughout the system without feedback are shown in figure 4 in which the response to a pulse in V(t), the input voltage to the fuel injectors, is recorded. In the example the primary fuel-air ratio is low, $\phi_1 = 0.64$, and the combustion is stable. This can be seen in figure 4(c) to (e) where linear disturbances decay after the pulse of fuel. The injectors begin to open when 6V is exceeded in figure 4(a). Figure 4(b) shows that there is a delay of 1.3 ms before p_{inj}, the pressure behind the injectors, begins to drop indicating a flow through the injectors. It takes between 9 and 10 ms before the unsteady pressure 0.725 metres downstream of the choked nozzle, $p'(0.725,t)$ in figure 4(c), registers a deviation from the previous pattern of low intensity oscillations. Figure 4(d) shows the response of light emission from C_2 radicals from a 75 mm length in the flame located 225 mm downstream of the flame stabiliser. The rapid rise in the light emission, and hence in heat release rate, at this location occurs almost instantaneously with the rise in pressure. At a downstream location, x = 1.71m, the rise in heat release rate occurs 1 to 2 milliseconds later as shown in Figure 4(e). However these delay times are not determined very accurately.

The control system can be described as simply imposing a gain and time delay on the control transducer output to produce the fuel injector input. More complete and accurate information on the required control system can be obtained by driving the injectors at single frequencies as in (iii) to obtain the transfer function between V(t), the input voltage to the injectors, and the control signal, which is chosen in what follows as the pressure perturbation at x = 0.725m and will be denoted by $p(x_{ref},t)$. The transfer function between $\tilde{V}(\omega)$ and $\tilde{p}_{ref}$ (the Fourier transforms of V(t) and $p_{ref}(t)$ respectively) can be constructed from this information. Standard control theory can then be used to calculate the required characteristics of the control circuit. The gain in this analysis is related, rather loosely, to the value of the mean backpressure, $\bar{p}_{inj}$.

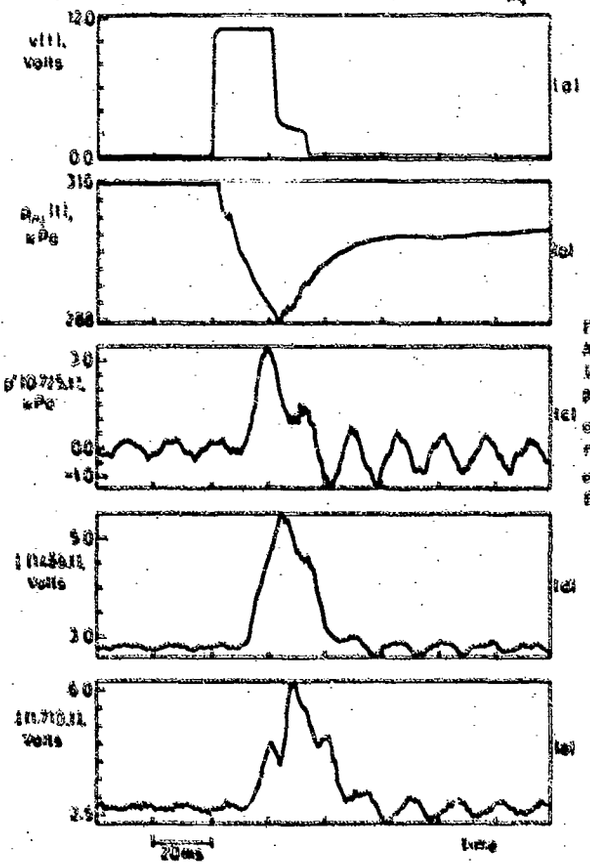


Figure 4.
A 22ms pulse is applied to the injectors (a), causing a drop in p_{inj} (b). The effect of this pulse of additional secondary fuel on the reference pressure, (c), and C_2 emission at two locations in the flame, (d) and (e), is also shown.

The same optimization can be performed experimentally and this is the approach in this paper. Langhorne, Dowling and Hooper[18] describe the comparison of experimental results with the predictions of control theory. The effect of the time delay across the feedback circuit on the measured pressure band level PBL in the range 0-400 Hz at x = 0.725m is shown in figure 5. The experimentally determined optimum delay is near 3.5ms and values in the range 3.4 to 3.6ms have been used in the remaining experiments. We can see from figure 5 that the time delay need not be set with great precision in order to obtain a reduction in sound level.

The optimum value of the gain is also determined experimentally. The data of figure 5 are for two values of the mean backpressure to the injectors, $\bar{p}_{inj}$, that is for two values of the gain of the control system. At the higher value of $\bar{p}_{inj}$, a significant reduction in PBL occurs over a wider range of delay times. When $\bar{p}_{inj}$ is reduced the data become more scattered and the range of delays over which a reduction in sound is possible is smaller. Thus, for this experiment the flame can be stabilised with a range of possible values of control system gain. This latitude in the choice of control system time delay and gain is reassuring in the application to practical devices where it may not be possible to maintain constant conditions.

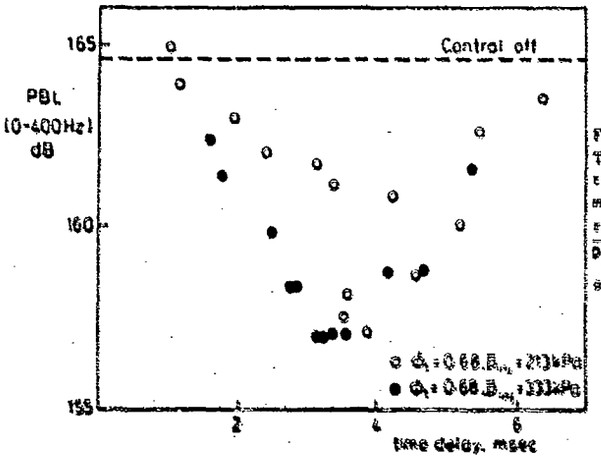
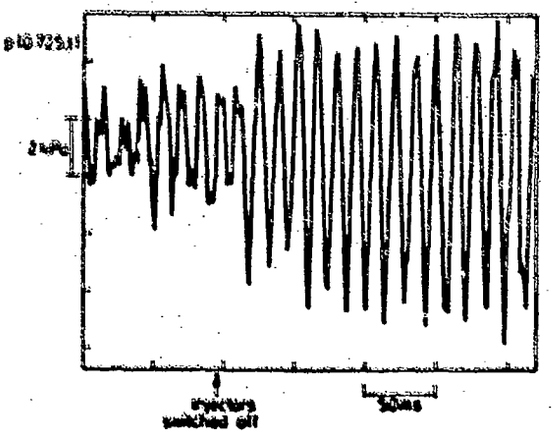


Figure 5.
The effect of the time delay across the feedback circuit on the measured pressure band level on the range 0 to 400 Hz for two values of $\bar{p}_{inj}$. The PBL without control is shown by the dotted line.

Once the control system has stabilised the flame, it is possible to measure the growth rate of linear disturbances when the control is switched off. This is illustrated in figure 6. The growth rate is an important parameter in determining the stability of the flame. We may also examine the effect of the control on the unsteady heat release rate. Since the fluctuations in fuel to air ratio are being convected with the fluid, it is reasonable that regions just downstream of the gutter lip would be most influenced by the application of the control. Figure 7 shows that at a position 0.1m downstream of the gutter lip, the imposition of suitably-phased fluctuations in fuel to air ratio reduces the distinct troughs in the heat release rate. These troughs represent partial extinction of the flame at this position and are characteristic of a highly perturbed flame[4].



$\bar{\Phi}_1 = 0.68$, $\bar{p}_{inj} = 213$kPa, $t = 3.6$msec

Figure 6.
The effect of switching off the control on the pressure at x=0.725m. The growth rate of linear disturbances can be deduced from this result.

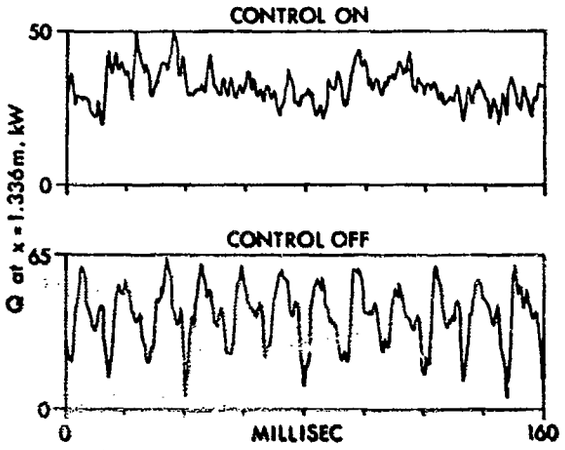


Figure 7.
The effect of switching off the control on the C_2 emission at x=1.336m. Note the change of scale between control on and control off. Running conditions in Table 1.

Figure 8 shows that the application of control changes the axial distribution of mean heat release rate, as well as increasing its overall level due to the increase in ϕ_T. Without control the mean heat release rate has a maximum close to the gutter lip and then decreases, this is also a characteristic of a highly perturbed flame[4]. The application of control moves the maximum in mean heat release rate downstream, a feature which is typical of a more stable flame.

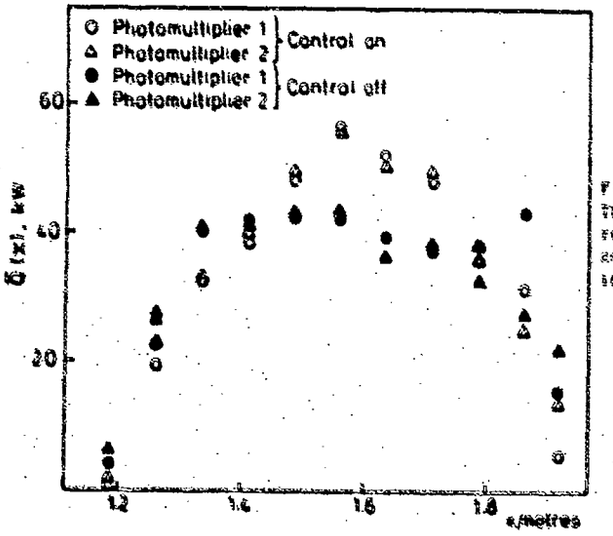
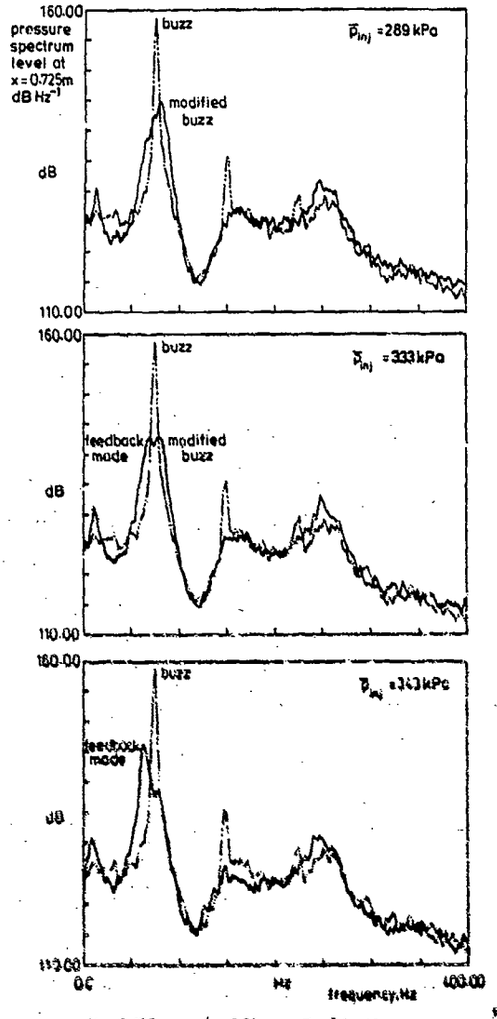


Figure 8.
The axial distribution of mean heat release rate with and without control for the running condition in Table 1.

When control is applied two modes appear in the spectrum. The behaviour of these two peaks is clearly seen in the experimental results in figure 9 for a time delay of 3.6ms. The primary equivalence ratio was kept constant at 0.65 in these tests. No secondary fuel is added when the control is off. The uncontrolled spectra in figure 9 show a narrow band peak near 74Hz due to a combustion instability. We call this the 'buzz' mode. 'Control on' involves the unsteady injection of secondary fuel and hence a higher total fuel-air ratio. For this value of time delay it is seen that at low values of $\bar{P}_{reg}$, which is related to gain, the amplitude of the modified buzz mode is less than the uncontrolled buzz peak. As 'gain' is increased the modified buzz peak is further reduced but a second peak due to a feedback mode begins to appear. The optimum 'gain' for our control system is approximately $\bar{P}_{reg}$ = 333 kPa. If $\bar{P}_{reg}$ is increased above this, the feedback peak becomes significantly large. The existence and behaviour of these two frequencies at various values of the "gain" can also be predicted from control theory[5]. A more sophisticated control circuit is required for complete stability. We have not pursued this further optimisation. Our aim has been simply to demonstrate that the unsteady addition of fuel is a suitable way of implementing the feedback.



$M_1 = 0.125$, $\phi_1 = 0.68$, $\tau = 3.4$ msec

Figure 9. The effect of an increase in the injector back pressure on the pressure spectrum level upstream of the flame. Dotted curves are spectra without control while solid curves show the effect of control.

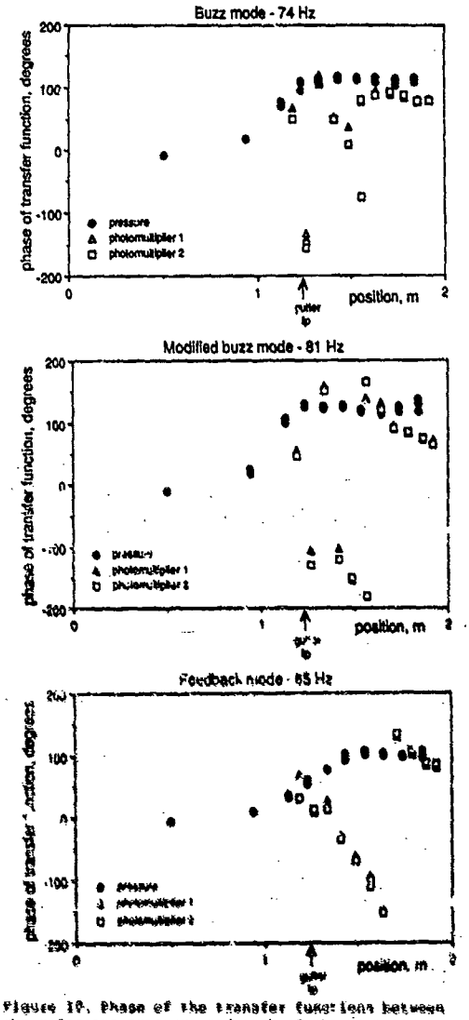


Figure 10. Phase of the transfer functions between the reference pressure and each of the unsteady pressure and the unsteady heat release rate. Data are given for (a) the buzz frequency with control off and (b) the modified buzz frequency and (c) the feedback frequency with control on. Running conditions in Table 1.

Transfer functions between the pressure at axial positions x along the duct and the reference pressure, $\hat{p}(x,\omega)/\hat{p}(x_{ref},\omega)$, have been measured. Similarly transfer functions, $\hat{q}(x,\omega)/\hat{p}(x_{ref},\omega)$, between the unsteady heat release rate in 75mm long windows centered on x and the reference pressure have been obtained. An effective controller should have a large value of the modulus of the transfer function, $\left|\hat{q}(x,\omega)/\hat{p}(x_{ref},\omega)\right|$, but ensure that $\hat{q}(x,\omega)$ is out of phase with $\hat{p}(x,\omega)$ to provide effective damping of any disturbances[3-5]. We therefore examine the modulus and phase of these transfer functions. The phase of the transfer functions is shown in figure 10(a) for the buzz frequency without control and in figures 10(b) and (c) respectively for the modified buzz frequency and the feedback frequency with control. For both the buzz mode without control and the modified buzz mode with control the phase of the pressure and heat release rate lie within 10° of each other from x=1.5m to the end of the duct. However in the case of the feedback mode, the axial distribution of the phase of the C_2 emission is indicative of the convection of a 'hot spot' with a speed of approximately $31ms^{-1}$. This is the velocity of the fluid at the gutter lip. This is similar to the behaviour of low intensity buzz[14] observed on the basic configuration of this rig.

When the controller is on, the modulus of the transfer function, $\left| \hat{Q}(x,\omega)/\hat{p}(x_{ref},\omega) \right|$, has larger values for the modified buzz and feedback modes than its value in the buzz mode with the controller off. This is illustrated in figure 11(a). Thus our controller exhibits similar properties to the controllers of references 3 to 5. When $\left| \hat{Q}(x,\omega)/\hat{p}(x_{ref}) \right|$ is multiplied by the square root of the power spectral density, $\sqrt{S_p(\omega)}$ we obtain a measure of the unsteady heat release rate from each 75mm window in the flame. This quantity is plotted for the three pertinent frequencies in figure 11(b). At a position just downstream of the gutter lip ($x \approx 1.3$m), the unsteady heat release rate at the buzz frequency without control exceeds that at the modified buzz and feedback peaks with control. This results in a significant reduction in the unsteady heat release rate towards the end of the duct when the control is applied.

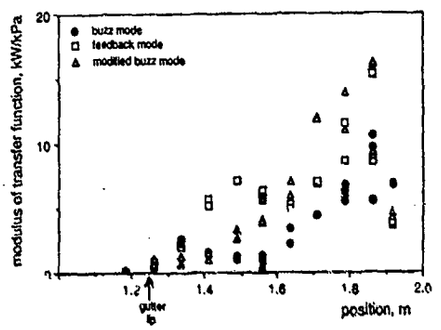


Figure 11(a). Modulus of the transfer function between the unsteady heat release rate and the reference pressure. Running conditions given in Table 1.

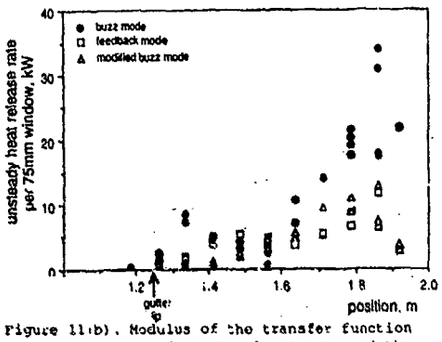


Figure 11(b). Modulus of the transfer function between the unsteady heat release rate and the reference pressure, multiplied by the square root of the power spectral density of the reference pressure. This is a measure of unsteady heat release rate. Running conditions given in Table 1.

The origin of the two low frequency peaks in the controlled spectrum can be further illustrated by examining the Rayleigh source term at these frequencies. This source term has been written down by Chu[9] and is

$$\int_0^L \frac{(\gamma - 1)}{\bar{\rho}\bar{c}^2} \overline{q' p'} \, dx \qquad (2)$$

where γ is the ratio of specific heat capacities
L is the duct length
$\bar{\rho}$ is the local mean density
$\bar{c}$ is the local mean sound speed
q' is the fluctuating component of heat release rate per unit length
p' is the fluctuating component of pressure.

The overbar denotes a short time average over one period of the oscillation. If this integral is negative, it indicates that, on average, the acoustic disturbances are dampened by the unsteady combustion and the system is stable. When it is positive, however, disturbances gain energy from the combustion. If this energy gain is greater than that lost on reflection at the boundaries, linear perturbations will be unstable.

The Rayleigh source term can be calculated from two sets of transfer functions, $\hat{p}(x,\omega)/\hat{p}_{ref}(\omega)$ and $\hat{Q}(x,\omega)/\hat{p}_{ref}(\omega)$, for each of the frequencies of interest. The product $(\gamma-1)/\overline{\rho c}^2$ only changes by about 3% along the duct and this variation will be ignored. The quantity

$$S_{pQ}(x,\omega) = \left| \frac{\hat{p}(x,\omega)}{\hat{p}_{ref}(\omega)} \right| \left| \frac{\hat{Q}(x,\omega)}{\hat{p}_{ref}(\omega)} \right| \cos\Delta\theta \; S_p(\omega) \qquad (3)$$

has been calculated for each window at the buzz frequency without control and at the frequencies of both the feedback mode and the modified buzz mode with control. The results of evaluating equation (3) are plotted in Figure 12. Again $S_p(\omega)$ denotes the power spectral density of the reference pressure, while $\Delta\theta$ is the phase difference between $\hat{p}(x,\omega)$ and $\hat{Q}(x,\omega)$. $S_{pQ}(x,\omega)$ is the real part of the cross-power spectral density of $p(x,t)$ and $Q(x,t)$. When it is

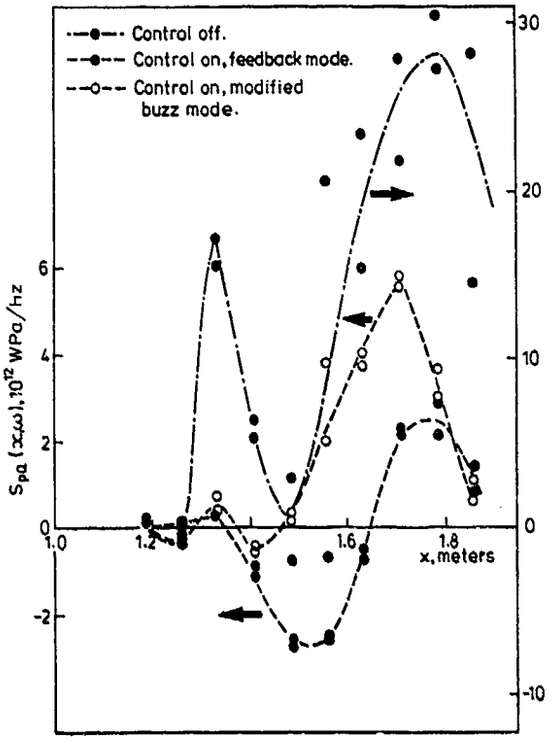


Figure 12.
The cross-power spectral density of $p(x,t)$ and $Q(x,t)$ plotted as a function of axial position for the buzz mode without control and for the modified buzz and feedback modes with control for the running conditions in Table 1.

multiplied by $(\gamma-1)/\overline{\rho c^2}$, it gives the contribution to the Rayleigh source term in equation (2) from disturbances of frequency ω in the window centred on x. Hence when data for each frequency in Figure 12 are summed along the duct, they indicate the net energy gained from the combustion by acoustic disturbances.

It is apparent from Figure 12 that without control the Rayleigh source term is large and positive at the buzz frequency. This source term is clearly reduced in amplitude when the controller is switched on (note the change of scale). However, it is undoubtedly still positive at the higher of the two frequencies indicating some driving from the combustion. This is the disturbance we have identified as the modified buzz mode. At the lower frequency there is little net destabilising contribution along the duct. This mode is at such a frequency that it is augmented by the addition of fuel with the time delay required to cancel the buzz frequency. We have therefore called this the feedback mode.

Figure 9 illustrates that the application of control has significantly reduced the sharp peak in the uncontrolled pressure spectrum. Table 1 summarises the performance of the controller for the case $\bar{p}_{inj}$ = 333kPa. With the total air flow rate and the primary equivalence ratio constant, the addition of 3% more fuel has reduced the PBL within 3dB of the peak at the buzz frequency by at least 12dB. In the range 0-400Hz the controlled acoustic power is reduced to 18% of its uncontrolled value. In the previous experiments on this rig where the instability was controlled purely by aerodynamic fluctuations, the unsteady mass flow required was at least 3% of the total mass flow. This is well over 20 times the amount of fluid which now must be fluxed unsteadily. As well as the reductions in sound level there is an increase of 10% in the gauge pressure, Δp, upstream of the flame. This indicates that more combustion occurs within the duct when controller is on.

In Table 1 we have only considered the effect of applying active control on the broadband sound power at the reference position. The PBL over the bandwidth 0-400Hz along the entire working section is shown in figure 13. The application of active control reduces the PBL at all locations in the duct, despite the changes in frequency and mode shape.

We saw in Table 1 that, Δp, the gauge pressure just upstream of the flame increased by 10% when the controller was switched on. This means that more heat is released within the duct and the thrust is increased. Figure 14 explains why this occurs. It shows Δp to be roughly proportional to the overall equivalence ratio, ϕ_T, and that a similar improvement in

TABLE 1

Table of typical running conditions. Where it is significant to the number of decimal places quoted, the variability between experiments is given.

	Control on		Control off	Change
	Feedback	Modified buzz		
Frequency	65±1	81±2	74±1	
Δp, kPa	6.95±0.05		6.28±0.10	+10%
M_1, kgs^{-1}	0.135		0.135	
ϕ_1	0.68		0.68	
M_2, kgs^{-1}	10.0×10^{-3}		10.0×10^{-3}	
$\bar{\phi}_2$	0.28±0.01		-	
M_T, kgs^{-1}	0.145		0.145	
ϕ_T	0.65		0.63	+3%
$\bar{p}_{inj}$, kPa	333±4		-	
τ, msec	3.6±0.1		-	
$\bar{m}_{f2}/m_{f1}$	3%		-	
PBL(-3dB), dB at x=0.75m	151.6±0.6	152.0±1.3	164.1±0.4	-12.5 -12.1
PBL(0-400Hz), dB at x=0.75m	157.2±0.5		164.6±0.4	-7.4
controlled acoustic power / uncontrolled acoustic power (0-400Hz)				18%

thrust can be made by the steady addition of fuel at the injectors; that is case (ii) in our classification. This is not to say that steady addition of secondary fuel is as effective as fuel addition with feedback since the resultant level of the instability must also be considered.

So far the comparison has been made with an uncontrolled case in which the secondary fuel is switched off, $m_{f2} = 0$; an example of (i) in our classification. When the control is on, secondary fuel is added unsteadily, while M_1, ϕ_1 and m_{a2} are held at the same constant values as in the no control case. This results in an increase in ϕ_T and leads to the question of

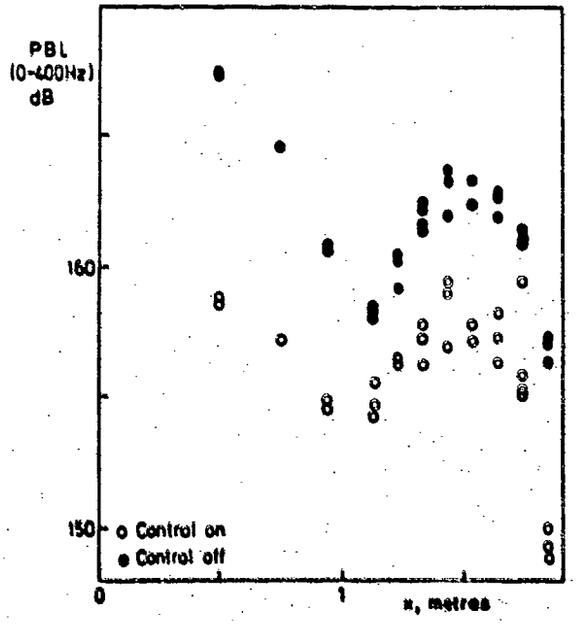


Figure 13.
Pressure band level over 0 to 400 Hz plotted as a function of axial position with and without control for the running conditions in Table 1.

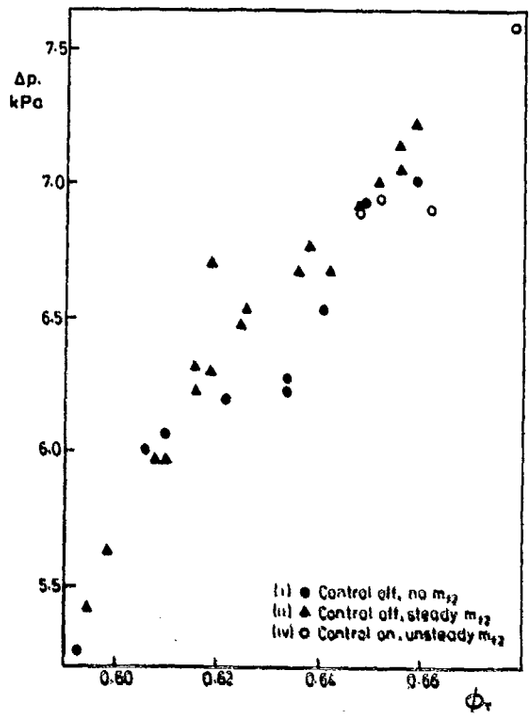


Figure 14.
The effect of total fuel to air ratio on Δp, the gauge pressure upstream of the flame, for various methods of fuel addition.

how the controlled case compares with alternative fuelling schemes for the same overall equivalence ratio. The same value of ϕ_T could be achieved by adding more primary fuel or by the steady injection of secondary fuel as in (ii).

Figure 15 shows data collected by injecting the secondary mass flow as in cases (ii), (iii) and (iv) above, and plotting buzz frequency against ϕ_T calculated from equation (1). As we

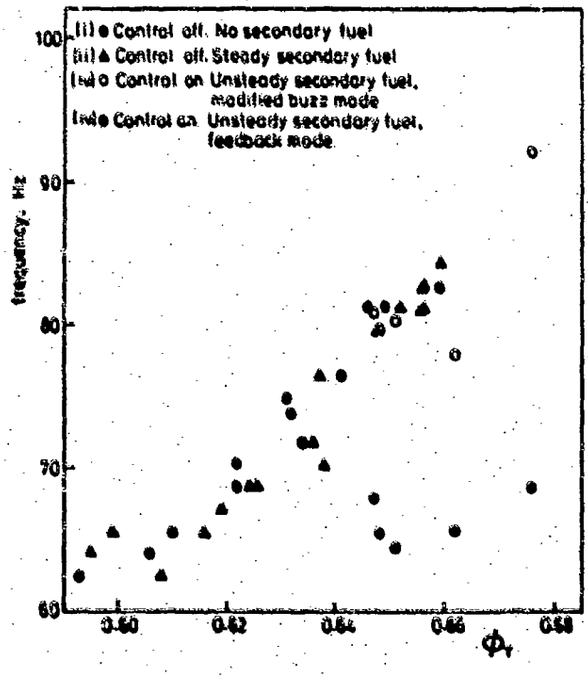


Figure 15.
The effect of total fuel to air ratio on the dominant frequency. Data are shown for various methods of fuel addition.

have seen in figure 9 for case (iv) when the control is on, there are two frequencies at each value of ϕ_T. Clearly the data for the modified buzz frequency, along with that for cases (i) and (ii) show that the buzz frequency is determined primarily by the total equivalence ratio rather than the location at which fuel is added. As we might expect, the feedback frequency is anomalous on this figure.

In contrast to the frequency, Figure 16 shows that the stability of the flame/duct configuration with steady fuelling is influenced by the proportions of primary and secondary

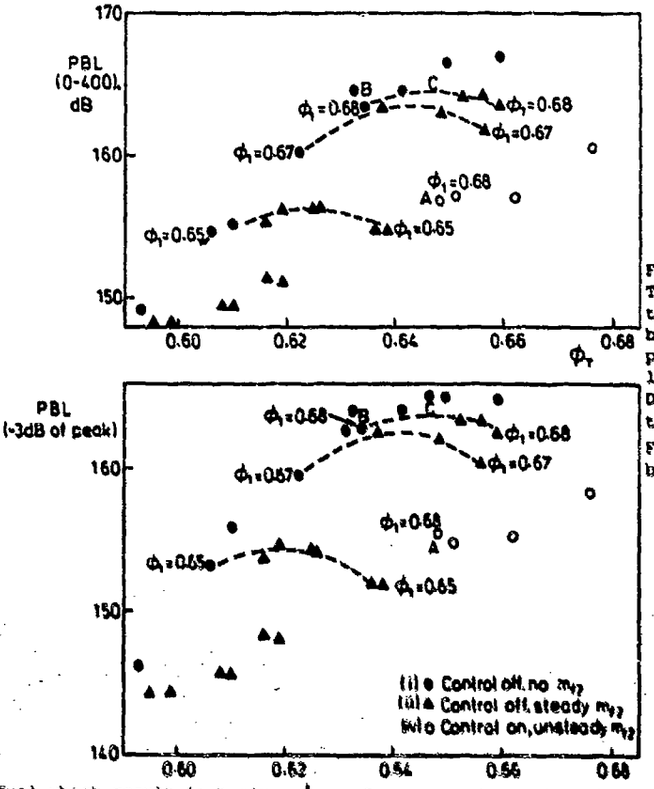


Figure 16.
The effect of the total fuel to air ratio on the pressure band level within 3dB of the peak and on the pressure band level over 0 to 400 Hz. Dotted curves are drawn through data at constant ϕ_1. Fuel is added to the system by various methods.

fuel which result in a given ϕ_T. Curves are drawn through points at a constant value of ϕ_1, with ϕ_T being increased by the steady addition of secondary fuel. For example, all values of PBL are higher for $\phi_1 = 0.67$ than they are for $\phi_1 = 0.65$ despite the fact that there is region where the values of ϕ_T overlap. Therefore, this diagram shows that addition of fuel at the location of the secondary injectors is less destabilising than mixing the same amount into the primary flow. If this were simply due to the fact that less combustion took place in the duct, then the gauge pressure upstream of the flame should also be relatively insensitive to the addition of fuel at the secondary injectors. Figure 14 shows that this is not the case and that Δp is a function of ϕ_T, independent of the location of fuel addition. It is likely that the distribution of the fuel at the flame holder is the important factor in determining the stability in this case.

In Table 1 we compared results at the same ϕ_1, with $\dot{m}_{f2} = 0$ in the no control case. An alternative test for the effectiveness of the controller would be to compare results for the same ϕ_1 and ϕ_T with and without control. In this comparison the no control case would involve the steady addition of secondary fuel to give the same value of $\dot{m}_{f2}$ as when the controller switched on. For example, the controlled case for $\phi_1 = 0.68$ (point A on figure 16) is compared with point B in Table 1. If the comparison is performed at constant ϕ_1 and ϕ_T then the effectiveness of the controller would be measured as the difference between point A and point C. It is apparent from Figure 16 that these two different comparisons lead to no appreciable difference in the measured effectiveness of the controller.

Ultimately the question we must ask is whether increased thrust can be obtained while maintaining reasonable noise levels. Figure 17 compares thrust with pressure spectrum level over the 0 to 400Hz range for various methods of fuel addition. An ideal controller would place points in the top left hand quadrant of this diagram. In spite of its simplicity, our controller produces the greatest thrust for a given value of pressure band level. The main advantage of the controller is also illustrated in this figure. It enables a flame to burn in the rig at a higher total fuel-air ratio than is possible without control. This results in an increase in the maximum available thrust.

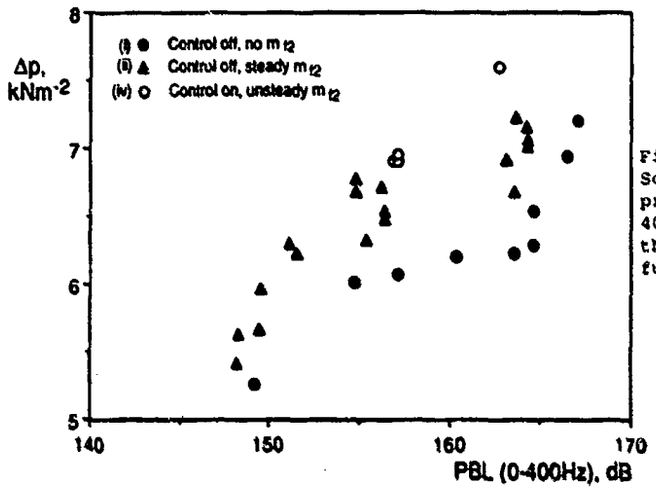


Figure 17.
Scatter diagram of the pressure band level over 0 to 400 Hz compared with the thrust for various methods of fuel addition.

4. CONCLUSIONS

Combustion oscillations in a 1/4 MW burner can be stabilised by the unsteady addition of extra fuel. A suitably-phased addition of 3% more fuel reduces the 164dB peak in the pressure spectrum due to the combustion oscillations by about 14dB. The acoustic energy in the 0-400Hz bandwidth is reduced to 18% of its uncontrolled value. The controller enables the rig to run at high fuel-air ratios at which it is impossible to stabilise a flame without control. This leads to an increase in the maximum available thrust.

The control system exploits the chemical energy in the fuel to alter the acoustic energy balance in the duct. Relatively little mechanical power is needed to produce the required unsteady fuel injection. Hence this method of feedback has considerable potential for full-scale applications.

5. REFERENCES

1. Swart, L.E., D. Jones & N.T. Jewell. Measurements of unsteady parameters in a rig designed to study reheat combustion instabilities. *AIAA-76-1141*. 1976.

2. Rayleigh, J.W.S. The Theory of Sound: Vol II. Dover Publications. 1945.

3. Collyer, A.A. & D.J. Ayres. The generation of sound in a Rijke tube using two heating coils. *J. Phys. D*, 5. 1972. L73-L75.

4. Heckl, M.A. Heat sources in acoustic resonators. Ph.D. thesis, University of Cambridge. 1985.

5. Screenivasan, K.R., S. Raghu & B.T. Chu. The control of pressure oscillations in combustion and fluid dynamical systems. *AIAA-85-0540*. 1985.

6. Dines, P.J. Active control of flame noise. Ph.D. thesis, University of Cambridge. 1983.

7. Hurle, I.R., R.B. Price, T.M. Sudgen & A. Thomas. Sound emission from open turbulent premixed flames. *Proc. Roy. Soc.*, A, 303. 1968. 409-427.

8. Heckl, M.A. Active control of the noise from a Rijke tube. IUTAM Symposium on Aero and Hydro-acoustics, Lyon. Springer-Verlag. 1986.

9. Kidin, N., V. Librovich, N. Nedvedev, J. Roberts & M. Vuillermoz. An anti-sound technique for controlling combustion system instabilities. Workshop on gas flame structure, Novosibirsk. 1986.

10. Lang, W., T. Poinsot & S. Candel. Active control of combustion instability. *Combustion and Flame*, 70. 1987. 281-289.

11. Poinsot, T., F. Bourienne, E. Esposito, S. Candel & W. Lang. Suppression of combustion instabilities by active control. *AIAA-87-1876*, 1987.

12. Bloxsidge, G.J., A.P. Dowling, N. Hooper & P.J. Langhorne. Active control of an acoustically driven combustion instability. *J. Theoretical and Applied Mechanics*, supplement to 6. 1987. 161-175.

13. Bloxsidge, G.J., A.P. Dowling, N. Hooper & P.J. Langhorne. Active control of reheat buzz. *AIAA J.* 1988.(in press)

14. Langhorne, P.J. Reheat buzz - an acoustically coupled combustion instability. Part 1, Experiment. *J. Fluid Mech.* 1988. (in press)

15. Bloxsidge, G.J., A.P. Dowling & P.J. Langhorne. Reheat Buzz - an acoustically coupled combustion instability. Part 2, Theory. *J. Fluid Mech.* 1988. (in press)

16. Norbye, J.P. Automotive Fuel Injection Systems - A Technical Guide. Haynes Pub., England. 1982.

17. Hands, T. The control of spark-injection engines using in-cylinder ionisation sensors. Ph.D. thesis, University of Cambridge. 1987.

18. Langhorne, P.J., A.P. Dowling & N. Hooper. A practical active control system for combustion oscillations. (Submitted to *AIAA J. Propulsion and Power*)

19. Chu, B.T. On the energy transfer to small disturbances in fluid flow (Part I). *Acta Mechanica*, 1. 1964. 215-234.

ACKNOWLEDGEMENTS

This project was funded by Rolls-Royce plc. It was carried out at the Whittle Laboratory, Cambridge University Engineering Department (CUED) while PJL was the Rolls-Royce Research Fellow in Engineering at Newnham College. The authors thank Mr. A. Sotheran and Mr. Lewis of Rolls-Royce for their stimulating interest in this work. Dr. P. Palmer of CUED helped with electronic design. We are especially grateful to Dr. A. Dowling for her enthusiastic guidance of the reheat buzz project.

DISCUSSION

N. L. Besser, Ge

Is it possible, to apply the presented method of instability attenuation to higher frequencies - perhaps with a modified equipment. This could be of interest for applications, when passive dampers cannot be used, e.g. due to cooling problems.

Author's Reply:

There is no reason, in principle, why this method could not be applied to attenuate higher frequencies. However, the time delay between the input signal to the actuator and the response of the combustion system should be small with respect to the period of the oscillation. Of course, the higher the frequency the shorter this period.

LeBlond, Fr

Did you make any experimentation to control by an active mean the first tangential mode? (higher scale 2000-3000 Hz). Do you know if this kind of experimentation has been done before?

Author's Reply:

No, we have not attempted to control anything other than the longitudinal mode. I am sorry but I do not know of any such experiments.

C. M. Coats, UK

With the particular method of control you are using you are adding both heat and mass at the position of the stabiliser at a particular point in the cycle - can you be sure that it is the heat and not the mass addition that is suppressing the oscillation?

Author's Reply:

Yes, there is the doubt that it is the addition of heat rather than the addition of mass at the flameholder which is stabilizing the flame. In previous experiments on this rig in which the instability was controlled purely by aerodynamic fluctuations, Bloxsidge et al (15) found it necessary to unsteadily modulate over 20 times the amount of fluid being fluxed in these experiments. To make absolutely certain, we have also performed a test with pulsed air replacing the pulsed fuel. Since this additional pulsed supply is only 0.1% of the total flow rate it had no effect of the measured pressure spectrum.

NUMERICAL SIMULATION OF PRESSURE OSCILLATIONS IN A RAMJET COMBUSTOR

Wen-Huei Jou, Vice President/Senior Research Scientist
Suresh Menon, Research Scientist
Flow Research, Inc.
21414 - 68th Avenue South
Kent, Washington 98032
U.S.A.

SUMMARY

Large-eddy simulations of compressible cold flow in a ramjet combustor configuration were performed. The objectives were to investigate the mechanisms for vortex-acoustic interaction in such a device and to develop a simulation method that can be extended to cases with combustion heat release to study combustion instability. From the simulations, it was found that the separated shear layer rolls up into concentrated vortices that merge to form large coherent structures. These vortices interact with the choked nozzle downstream to produce an axial acoustic dipole. The spectrum of the pressure fluctuation at the base of the backward-facing step shows that there are two types of oscillations: an acoustic resonant mode and a vortex-acoustic coupled mode. Based on the flow physics observed in the simulations, a simple one-dimensional model for the vortex-acoustic coupled mode was proposed. The eigenvalue problem based on this model was solved to obtain the frequency of the coupled mode.

ABSTRACT

A numerical simulation technique has been developed for investigating the oscillatory cold flow in a ramjet combustor configuration. Simulations were conducted, and the results are presented and analyzed here. The main objective of the simulations was to investigate the interaction between the vorticity component and the acoustic component of the flow field when the reduced frequency of the flow based on the speed of sound is of the order of unity. In constructing the numerical model, it was found that the interior of the combustor must be isolated from the external region by a choked nozzle. The resulting numerical simulations are able to exclude the effects of the artificially imposed boundary conditions at the outflow boundary.

Flow visualizations and frequency spectra of the vorticity and pressure fluctuations have been analyzed to understand the flow field. It appears that the pressure fluctuation at the base of the backward-facing step, a signal taken as acoustic in nature, contains only low-frequency components. This is in contrast to the frequency spectrum of the vorticity fluctuation in the free shear layer near the separation point, which contains both high-frequency and low-frequency components. The vorticity fluctuation at the location where the shear layer impinges on the nozzle wall also contains only low-frequency components. The unsteady flow fields near the shear layer separation point and in the nozzle region have also been investigated. It appears that the boundary layer immediately upstream of the separation point is perturbed by the low-frequency pressure fluctuation at the base of the step. The perturbation is then amplified downstream by the shear layer instability. In the nozzle region, the Mach number in the subsonic region fluctuates at a high amplitude when a vortical structure impinges on the nozzle. However, the Mach number in the supersonic region downstream of the throat remains stationary.

Mean flow quantities and higher moments were computed by averaging the running time to evaluate the contribution of the coherent structures to the transport of momentum. The results, when compared to available experimental data for a two-dimensional backward-facing step configuration, show good agreement over the majority of the flow region; the large-scale structures are faithfully simulated and are the main contributor to the transport of momentum.

An attempt was made to extract acoustic information from the results of the numerical simulations by computing the instantaneous dilatation field, which is shown to drive the unsteady potential flow, i.e., acoustic disturbances. It turns out that the near-field dilatation contains mainly the characteristics of the sound sources. The quadrupole nature of the sound source around each large-scale vortex in the flow field is clearly demonstrated. The complex distributed dilatation field near the impingement point of the shear layer on the nozzle wall is considered as a compact acoustic source and is analyzed by multipole expansion of the distributed field. The results show a strong axial acoustic dipole at the nozzle. The dipole fluctuation is 180 degrees out of

phase with the impinging vorticity fluctuations. This result can be applied as the impedance for the vorticity-acoustic fluctuations at the nozzle. However, the propagation aspects of the sound field cannot easily be visualized in a near field. The spectra of the pressure and vorticity fluctuations at selective points were analyzed to reveal the existence of two types of fluctuations. One is the resonant acoustic mode, in which the vortical disturbances excite the acoustic free modes. The other is the coupled mode, in which the acoustic disturbances and the vortical disturbances are coupled through the dipole radiation at the nozzle and the acoustic susceptibility of the separating shear layer at the dump plane. A simple model for the coupled mode is proposed to explain the latter mechanism and to provide an approximate method for estimating its frequency.

1. INTRODUCTION

A substantial research effort has been initiated to increase our understanding of the mechanism for instability in ramjet combustor flow fields. This effort could lead to the development of methods for suppressing the instability and, hence, to improvements in the performance of ramjet engines. Typically, the instability manifests itself in the form of large-amplitude pressure oscillations in the low-frequency range of a few hundred hertz. These pressure oscillations can cause structural damage or result in system failure caused by the expulsion of the inlet shock. The exact mechanism of these self-excited oscillations is not entirely clear. According to the linear canonical decomposition of the governing equations for small disturbances in an infinite compressible medium, three types of waves can be sustained in a moving medium.[1] These are the two families of acoustic waves, the vorticity wave, and the entropy wave. In a free space, these infinitesimal wave motions are linearly independent. However, in nonlinear cases and in a closed domain such as a ramjet combustor, these disturbances may interact through resonant phenomena and/or through boundary effects. Therefore, there is a fundamental question of how these wave phenomena may couple together in a finite bound domain to form eigenmode oscillations with a discrete frequency spectrum. These eigenmodes are potential candidates for high-amplitude excitation when combustion occurs.

Eigenmode oscillations involving only one wave component have been explored extensively. Examples including only acoustic waves are the well-known acoustic duct modes. These oscillations may be excited by distributed sources in a closed domain and are called "resonant oscillations" in the present paper. Examples including only vorticity waves can be found in the so-called edge tone oscillations, which have been studied extensively (e.g., Rockwell and Naudascher[2]) and have recently been simulated numerically by Ohring,[3] who considered the incompressible fluid. The interaction between an impinging vortex and the leading edge of a plate produces disturbances that provide the perturbation at the jet exit upstream for the initiation of a new vortex. This upstream feedback mechanism in the incompressible flow is through Biot-Savart induction. The feedback is instantaneous, as the speed of signal transmission in the incompressible limit is infinite.

Biot-Savart induction is dynamically meaningful only in the incompressible limit when the reduced frequency based on the speed of sound approaches zero, i.e.,

$$\frac{\omega l}{c} \ll 1 \tag{1}$$

where f is the frequency, l is the characteristic length of the domain of interest, which is considered as one-quarter of a wavelength for acoustic waves, and c is the speed of sound. This criterion certainly cannot be met when the entire spectrum of turbulent flow fluctuations is considered. For example, the pressure fluctuations under a turbulent boundary layer were considered by Ffowcs Williams.[4] He showed that the low-frequency spectrum is dominated by the propagating acoustic waves. When the above condition is not satisfied, the transmission speed of flow information upstream is limited by the speed of sound, and a phase difference between the signal at the source location and at the point of interest may exist. Therefore, acoustic waves must be considered as part of the system. The resulting oscillation may consist of both convective components and acoustic components. This type of oscillation is referred to as a "coupled mode" oscillation in the present paper. In a typical combustor, the reduced frequency is of the order of unity. The incompressible model is then inappropriate.

Resonant acoustic modes excited by turbulent combustion have been studied as a mechanism for combustion instability. However, the frequency of the observed oscillations, in many cases, differs from the eigenfrequency of the acoustic duct modes. More complex physics involving convective waves, i.e., entropy and vorticity waves, may be the cause of the deviation. Entropy wave/acoustic wave coupling was suggested by Abouseif et al.[5] as a mechanism for combustion instability. However, the role of vortex shedding was not considered. In contrast to the model by Abouseif et al.,[5] some experimental evidence points to the participation of vortex shedding in combustion processes.[6,7] The

vorticity fluctuations may interact with the acoustic wave directly and may also affect combustion through their effects on mass and heat transport. The unsteady combustion related to vortex shedding may generate acoustic disturbances. Vortex shedding and the vortex-nozzle interaction were suggested as parts of the system important to combustion instability.[8] This possible coupling between acoustic waves and vortical disturbances prompted Crocco and Sirignano[9] to study theoretically the acoustic reflection coefficient of a choked nozzle subject to impingement by a vortical disturbance. The study of vortex-acoustic interactions in a nozzle under a cold-flow configuration, such as the theoretical work of Crocco and Sirignano,[9] is an essential first step to untangling the intricate interactions among all wave components leading to combustion instability.

The objective of the present investigation is to understand the interaction between the vortex dynamics and acoustic waves in a generic combustor geometry. Since at present combustion has not been considered in this investigation, direct inference from the results of this investigation to combustion instabilities is inappropriate. However, the basic understanding of the cold flow as well as the methodology developed in the present investigation may provide a sound basis for extending the analysis to a combustion flow field.

Because of the complexity of the problem, an analytical solution to the governing equations with complex boundary conditions is not possible. In particular, complex vortex-merging processes and the resulting acoustic disturbances are difficult to analyze unless drastic approximations are used. Numerical simulations, if performed properly, may provide important information for understanding the physics. In this paper, we report the results of our attempt to develop a numerical methodology and methods of extracting the physics from the numerical simulations. We also present a detailed analysis of the simulation results to extract information on the vortex-acoustic interaction.

2. NUMERICAL MODEL

The governing equations are the unsteady, compressible Navier-Stokes equations:

$$\frac{\partial \rho}{\partial t} + \nabla \cdot \rho \vec{v} = 0 \tag{2}$$

$$\frac{\partial (\rho \vec{v})}{\partial t} + \nabla \cdot (\rho \vec{v}\vec{v} + p\vec{\vec{I}}) = \nabla \cdot \vec{\vec{\tau}} \tag{3}$$

$$\frac{\partial \rho E}{\partial t} + \nabla \cdot (\rho \vec{v} H + \vec{q} - \vec{v}\vec{\vec{\tau}}) = 0 \tag{4}$$

where flow variables are given by their conventional notations and $\vec{\vec{I}}$ is the identity dyadics, $\vec{\vec{\tau}}$ is the shear stress tensor, $\vec{q}$ is the heat flux vector, E is the total energy and H is the total enthalpy. These equations are supplemented by the following relations:

$$\vec{\vec{\tau}} = \mu(\nabla \vec{v} + \nabla \vec{v}) + \lambda \nabla \cdot \vec{v}\vec{\vec{I}} \tag{5}$$

$$\vec{q} = -\kappa \nabla T \tag{6}$$

$$E = C_v T + \frac{1}{2} \vec{v} \cdot \vec{v} \tag{7}$$

$$H = E + \frac{p}{\rho} \tag{8}$$

$$p = \rho R T \tag{9}$$

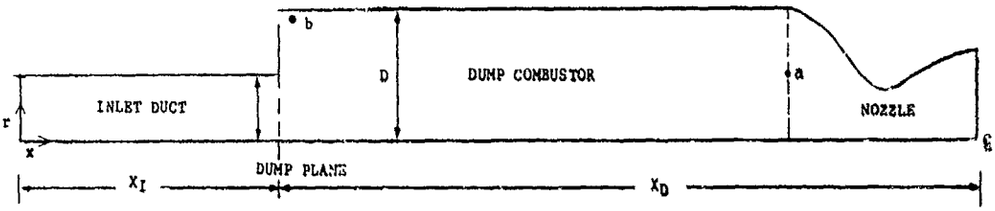
where ν and κ are the coefficients of kinematic viscosity and thermal conductivity, respectively. The above equations were solved in axisymmetric form. The approximation of an axisymmetric configuration requires justification. Our objective is to investigate the interaction between low-frequency pressure oscillations and the dynamics of large vortices. Low frequency is usually associated with longitudinal acoustic waves, which are likely to propagate in an axisymmetric manner. If large vortices are coupled to these acoustic waves, the coupling is likely to be approximately axisymmetric. While the small-scale turbulence is three-dimensional in nature, it is assumed to provide only a dissipative mechanism to the large-scale phenomenon. Whether the dynamics of the large-scale phenomena is critically dependent on the amount of dissipation can be later examined by varying the dissipation coefficients in the governing equations. In this manner, the laminar dissipative coefficients are used as a simple subgrid model.[10] Therefore, the present model only qualifies as a large-eddy simulation model, which contains a degree of uncertainty. However, we believe that the essential physics of the vortex-acoustic interaction is contained in this model.

These equations are solved in the domain shown in Figure 1a. On all solid-wall boundaries, no-slip and adiabatic boundary conditions are applied, i.e.,

$$\vec{v} = 0 \qquad \text{on Solid Surfaces} \tag{10}$$

$$\vec{n} \cdot \vec{q} = 0 \qquad \text{on Solid Surfaces} \tag{11}$$

At the entrance of the inlet pipe, the flow is assumed to be parallel with the prescribed uniform stagnation pressure and stagnation temperature. We are aware that the notion of "stagnation pressure" is not well defined in an unsteady flow. The application of these upstream conditions implies certain "impedance" conditions.[11] In practice, the impedance condition depends on the flow field upstream of the computational domain. It is important that this boundary condition does not artificially excite flow oscillations inside the computational domain. The characteristics of the impedance condition as applied here were examined[11] using a linearized analysis, and the condition was proven to be of the damping type. Hence, the simulated flow field is only a particular class of solutions under the assumed upstream impedance condition. Because of the damping boundary condition, the computed sustained oscillation in the computational domain is self-generated. It is conceivable that, in a practical device, inlet diffuser oscillations such as those reported by Bogar and Sajben[12] may participate in the flow oscillations in the combustion chamber. Specific upstream impedance conditions can be derived if this kind of flow field is completely understood. We have not investigated the effects of upstream impedance on the vortex-acoustic interaction problem and have not experimented with other possible boundary conditions. Since the downstream boundary is at supersonic conditions, no boundary conditions are required there. However, during the transient period and before the supersonic flow is established there, an exit pressure is specified. In fact, the specification of this intermediate exit pressure determines the Mach number in the combustor. The initial condition is a stationary flow with stagnation conditions everywhere in the flow field. The exit pressure is then impulsively lowered to a prescribed value to start the flow. Meanwhile, a complex orchestration involving variation of the throat area and the exit pressure establishes the supersonic flow downstream of the throat.[13]



a. Dimensions of ramjet combustor



b. 256x64 computational grid

Figure 1. Configuration of Ramjet Combustor

MacCormack's explicit unsplit scheme[14] is used for the integration of the conservation equations in time. The scheme is second order in time and in space. Its properties are well-known and are described elsewhere.[14,15] We used the finite volume form of the scheme on a boundary-conforming grid. Aside from the well-known "built-in" artificial dissipation of the scheme, no explicit artificial dissipation has been added. Numerical stability of the time integration can be maintained with a Courant-Frederich-Levy number of 0.6.

A typical grid used in the simulations is shown in Figure 1b. Grid lines are clustered in the critical regions, such as the boundary layer in the inlet duct, the shear layer separation point, i.e., the corner of the backward-facing step, and the nozzle. These are the flow regions where the length scale of the flow features is expected to be small. The clustering of grid lines enables us to resolve the important large-

scale features without an excessively large computational mesh. Large-scale structures with length scales on the order of the boundary layer thickness or larger can be resolved. These are the large-scale vortical structures of interest to the present investigation.

Details of the simulation technique have been described previously.[13] Important features of the numerical model are summarized here. An important issue of numerical simulations of compressible flows is how the boundary conditions affect the solution inside the computational domain. If the outflow boundary is subsonic, boundary conditions are required there. If the local velocity vector is pointing outward, the vorticity and the entropy are convected outward. Among two families of acoustic waves, one family is outgoing and carries the appropriate characteristic variable from the interior, and the other is propagating inward from the downstream representing the reflected wave on the boundary. Therefore, one boundary condition must be supplied. This boundary condition represents, again, some "impedance" condition as was discussed previously for the inflow boundary. Unfortunately, unlike a fairly uniform inflow, the outflow is highly nonuniform and unsteady. The flow field in the combustion chamber is then critically dependent on the arbitrary "impedance" condition for subsonic flows. Even worse is the subsonic outflow in which a vortex may exit at low speed causing locally reversed flow. The vorticity and the entropy are convected from downstream into the computational domain in this case. Three boundary conditions are required there. These boundary conditions are difficult to specify and the resulting simulations not reliable. In the present simulation model, the downstream boundary is at supersonic state. The flow inside the combustor is independent of the boundary conditions at the outflow boundary.

Two questions need to be answered before the simulation model can be applied. The first is the question of grid resolution. We performed simulations of the flow under the same conditions using computational grids of 129x42, 192x64 and 256x64. The spectra of the pressure fluctuations at the base of the step as well as the spectra of vorticity at a point in the flow field are chosen as the basis for comparison. It was found that a 129x42 [illegible] adequate in producing the same spectra as those using a 256x64 grid. However, the contour plots of the flow variables using the 129x42 grid lack the detail and smoothness of the higher-resolution simulations. All results presented here are based on simulations using either 192x64 or 256x64 grids. The second question is how sensitive are the observed spectra on the dissipation. Two simulations were performed, one with a Reynolds number of 10,000 and the other with a Reynolds number of 33,000. The pressure spectra and the vorticity spectra were compared. Again, the results are insensitive to the variation of dissipation in that range.

In the process of simulation, flow quantities are monitored at various locations to determine whether the flow has reached a stationary oscillation. The data in the transient period were discarded so that the data could be analyzed in terms of frequency spectra.

The numerical model constructed above is capable of capturing the essential large-scale unsteady phenomena of interest and can be applied to study the vortex-acoustic interaction.

3. LARGE-SCALE UNSTEADY FLOW STRUCTURES

The vorticity dynamics of the flow inside the combustor is given by a time sequence of vorticity contour plots in Figure 2. The boundary layer separates from the surface at the corner of the backward-facing step. The resulting free shear layer rolls up into concentrated vortices. Subsequently, these vortices merge several times to eventually form large structures that impinge on the nozzle wall. As each vortex impinges on the wall, a secondary vortex of opposite sign is generated, forming a vortex pair that subsequently lifts itself away from the wall. These observations are consistent with the experimental observations of Didden and Ho.[16] They also indicated that strong acoustic radiation may result from the process of generating the secondary vortex.

The frequency spectrum of the vorticity fluctuation at the entrance of the nozzle (point "a" in Figure 1a) near the vortex impingement point is shown in Figure 3a. (The original Fourier spectra in this article have been filtered by using a "maximum entropy method," so the relative intensity of the spectral peaks may not be accurate.) Near the nozzle, the vortices merged into large structures at a reduced frequency of 370 Hz. This frequency, if converted to a Strouhal number based on the jet diameter (i.e., $St = fD/U$), is approximately 0.2, which is in the reported range of "jet preferred mode" values of 0.2 to 0.7.[17] In a confined jet configuration such as the ramjet combustor, the jet preferred mode may be more complex than that for a free-jet configuration because of the additional length scale, i.e., the length of the chamber involved. The selection of the preferred mode frequency from the possible range may depend on the axial length scale.

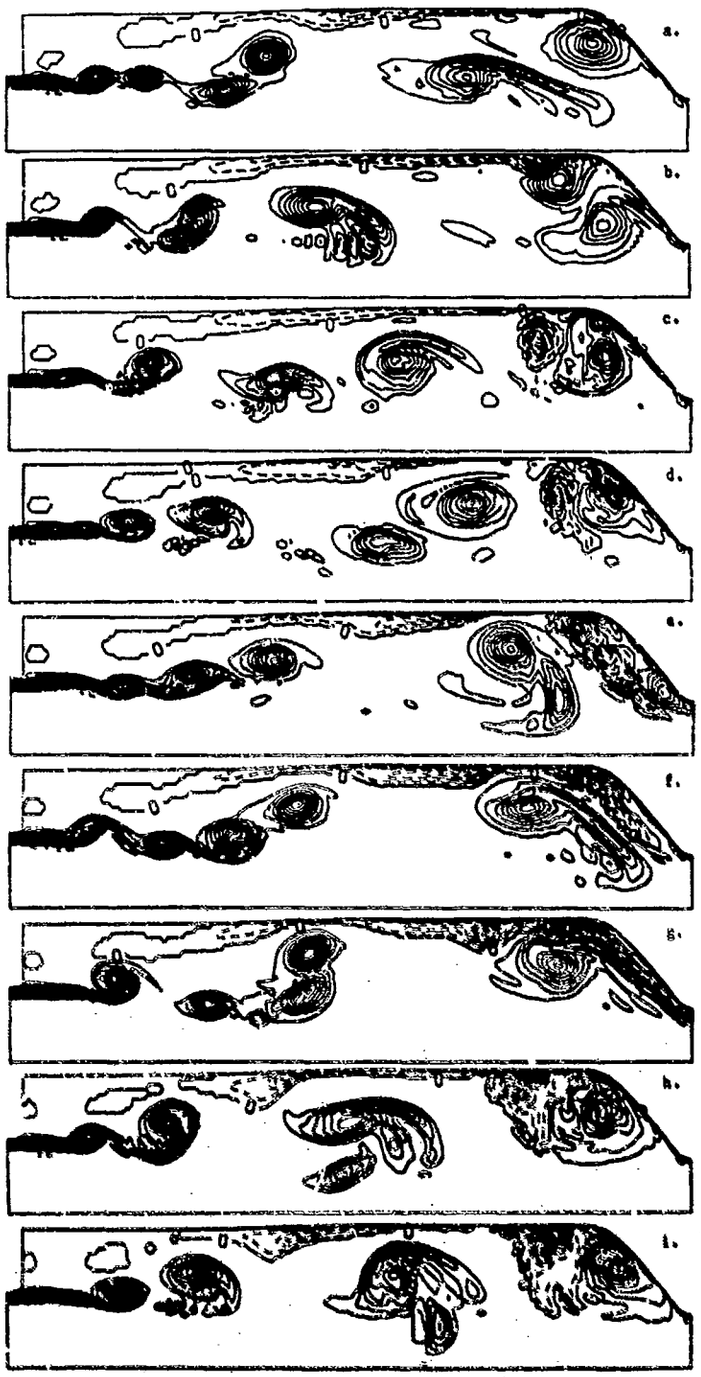
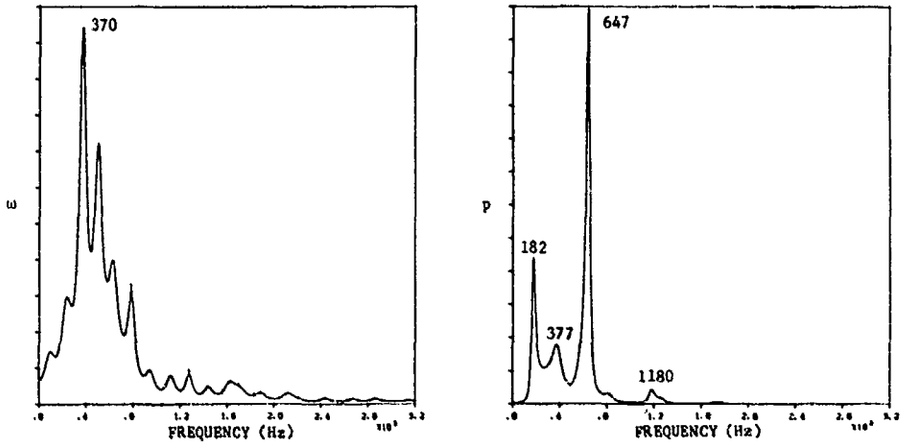


Figure 2. Time Sequence of Vorticity Contours in the Combustor (M = 0.32 Re = 10,000)



a. Vorticity spectrum at entrance of nozzle

b. Pressure spectrum at base of step

Figure 3. Vorticity and Pressure Spectra (192x64 grid)

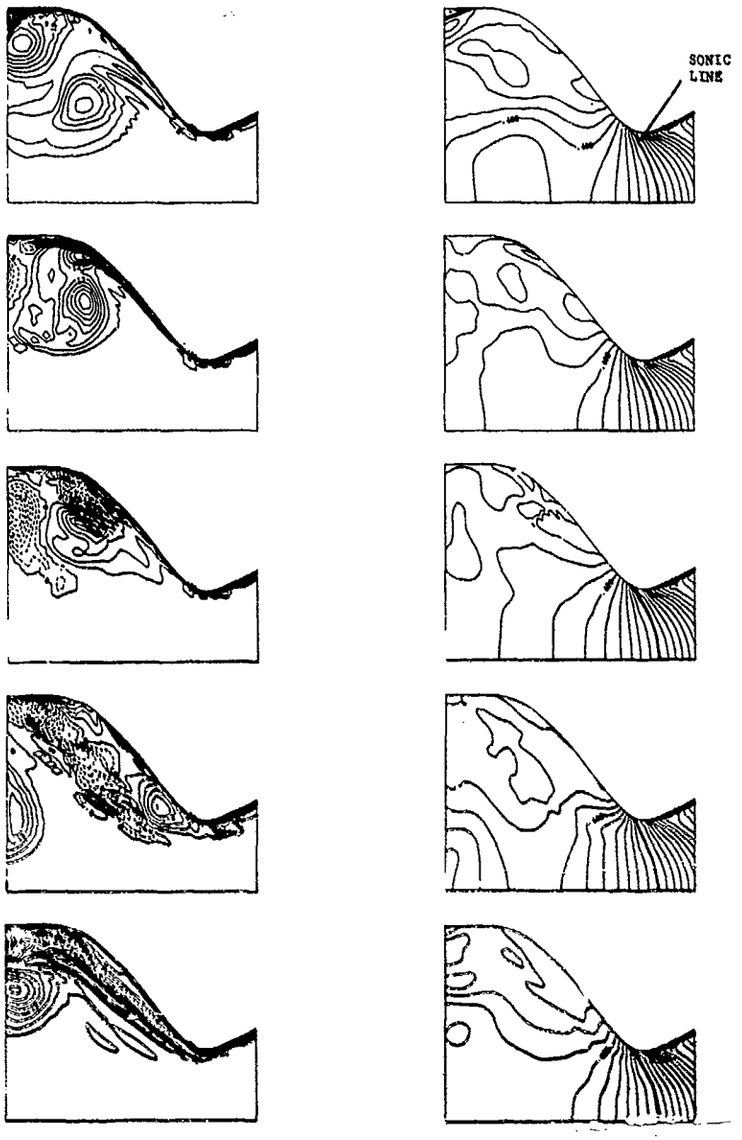
Gutmark and Ho[17] investigated in detail the preferred mode frequency of a jet. They found that the frequency is strongly facility dependent. The fact that the first rollup frequency is not 2^n of the frequency of the large structure indicates that the merging of vortices is more complex than a sequence of simple pairings of vortices. The process may involve the collective interaction as discussed by Ho and Huerre.[18] Since there is no external perturbation imposed on the system and the computation is deterministic, this low-frequency, large vortical structure may be the result of a self-sustained mechanism. Several researchers[17,19] have found that the acoustic disturbance generated during vortex merging may serve as a feedback mechanism for perturbing the shear layer at the jet exit. Later in this paper (Section 7), we suggest that the feedback mechanism may be an acoustic disturbance that is generated by a vortex-choked-nozzle interaction.

It is informative to examine the spectrum of the pressure fluctuation behind the backward-facing step. The vorticity fluctuation at the base of the step is low. Therefore, the pressure fluctuation there is considered an acoustic fluctuation, i.e., that corresponding to the unsteady potential flow.[20,21] The spectrum is shown in Figure 3b. It appears that the rollup and merging of the vortices in the interior of the chamber do not contribute to the acoustic fluctuation directly. In the pressure spectrum, a high peak at the frequency of 647 Hz dominates, and two low-frequency components at 377 Hz and 182 Hz also appear. It will be shown later that these peaks are possibly the results of a resonant acoustic oscillation and the coupled oscillations, respectively.

The interaction of the impinging vortex and the choked throat can be visualized by the time sequence of vorticity contour plots and the corresponding Mach number contour plots shown in Figure 4. As can be seen, the Mach number contours in the subsonic portion of the nozzle fluctuate at large amplitude during the period of vortex-nozzle interaction. However, the Mach number contours remain relatively stationary in the supersonic region.

4. MEAN FLOW

In a large-eddy simulation, the dynamics of the coherent structures in a turbulent flow is captured by the unsteady computation. If sufficiently long time-accurate data are available, the time-averaging process provides a means to evaluate the contributions of these large structures to the transport of mass and momentum. Therefore, the mean flow variables and the higher moments are computed by carrying out a running time average. If experimental data are available, the mean flow quantities and higher moments computed can be compared to the data to assess whether the main characteristics of the flow are faithfully computed. Because of the lack of comprehensive experimental data for a circular jet in a sudden expansion (backward-facing step), the experimental results for flows in a two-dimensional backward-facing step[22] were used for comparison with the computational results.

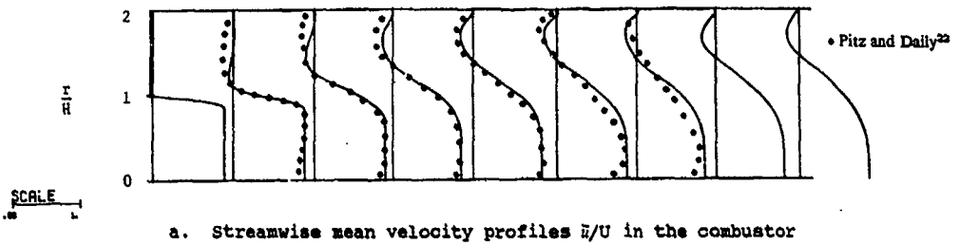


a. Time sequence of vorticity contours in the nozzle (contour interval is 3000 sec^{-1}).

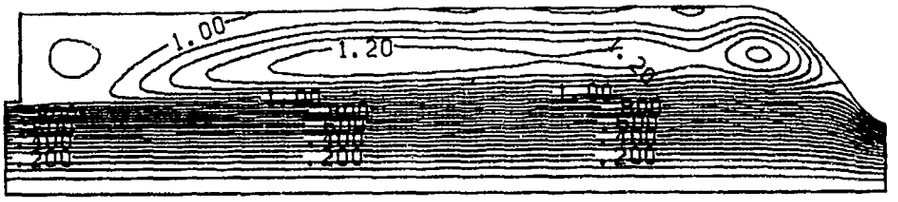
b. Time sequence of Mach number contours in the nozzle (contour interval is 0.1).

Figure 4. Time Sequence of Vorticity and Mach Number Contours Near the Choked Nozzle

Figure 5a shows the mean axial velocity profiles $\bar{u}/U$ as a function of the axial locations x/H in a combustor; only the region between the dump plane ($x/H = 0$) and the entrance to the nozzle ($x/H \approx 8$) is shown. The experimentally obtained profiles[22] are also shown in this figure. The agreement between the computational results and the experiments for $x/H \leq 4$ is good. For $x/H \geq 5$, the spreading rate of the shear layer in the experiments seems to be much faster than in the computed results. There are several factors that may contribute to this difference between the experimental results and the computational results. First, the three-dimensional breakdown of the vortical structure, which cannot be modeled by an axisymmetric computation, may become important



a. Streamwise mean velocity profiles $\bar{u}/U$ in the combustor



b. Normalized stream function ψ in the combustor

Figure 5. Axial Variation of Mean Flow

at the downstream location. Also, the difference between an axisymmetric configuration and a planar configuration may become prominent at the downstream location where the coherent ring vortices are stretched due to the radial motion. The maximum reversed axial velocity in the recirculation region is approximately $0.21\,U$. This value is within the experimentally observed range of $0.2\,U$ to $0.25\,U$.

The mean stream function ψ can be obtained by solving the following equations:

$$\overline{\rho u}\, r = \frac{\partial \psi}{\partial r}, \quad \overline{\rho v}\, r = -\frac{\partial \psi}{\partial z} \tag{12}$$

subject to the appropriate boundary conditions:

$$\psi = 0 \quad \text{at the centerline} \quad (r=0) \tag{13}$$

$$\psi = 1 \quad \text{on the solid wall} \tag{14}$$

where ψ is normalized by the mass flux across the upstream inflow boundary. Figure 5b shows the streamline pattern. Within the elongated recirculation zone, a closed streamline domain with a free-standing stagnation point near the nozzle is indicated. A secondary recirculation zone near the step, with a circulation in the opposite direction of the primary recirculation zone, is also observed. The secondary recirculation zone has been reported in many previous experiments.[23-25] Although the averaged streamline pattern contains several regions of closed streamlines, it is not clear how these affect the mass and heat transport. As will be seen later, the momentum transport by the coherent structures is very strong in the nozzle region where the shear layer reattaches. It is expected that the mass transport is equally strong there. The rate of mass exchange in and out of the closed streamline region is expected to be very large.

To compare quantitatively the shear layer spreading rate to that obtained in the experiments,[22] the vorticity thickness is estimated by

$$\delta_\omega = \frac{\Delta U}{\left|\frac{\partial \bar{u}}{\partial r}\right|_{max}} \tag{15}$$

where ΔU is the difference in axial velocity across the shear layer. Figure 6 shows the computed results compared to the experimental results. The agreement is reasonably good. The shear layer spreading rate, $d\delta_\omega/dx$, in the region $x/H < 3$ is approximately 0.24. Experimental values of 0.26 to 0.29 were reported by Pitz and Daily,[22] whereas a lower rate was reported by Eaton and Johnston.[23] The values reported for the backward-facing step configuration are substantially higher than the spreading rate of 0.125 to 0.2 reported by Gutmark and Ho[17] for a free jet. Beyond $x/H > 5$, the size of the coherent structures is comparable to the step height, and the spreading of the shear layer is inhibited by the wall.

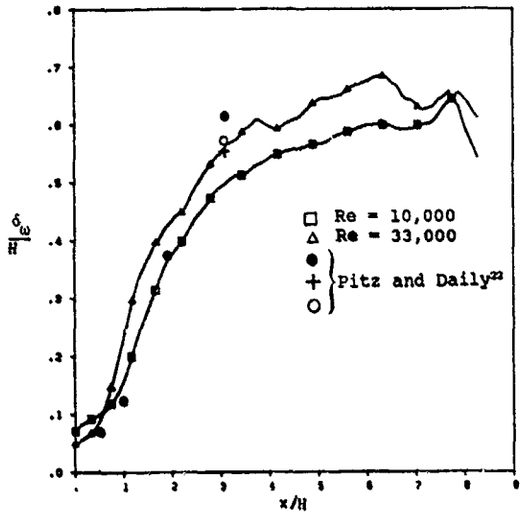
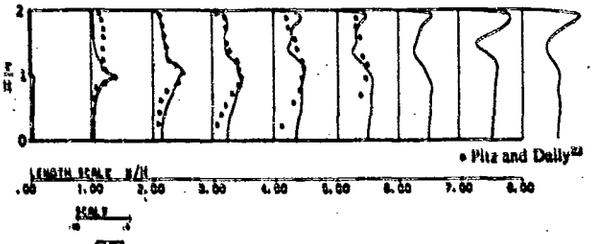
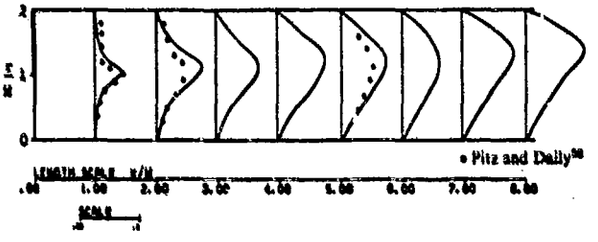


Figure 6. Axial Variation of Vorticity Thickness in the Combustor

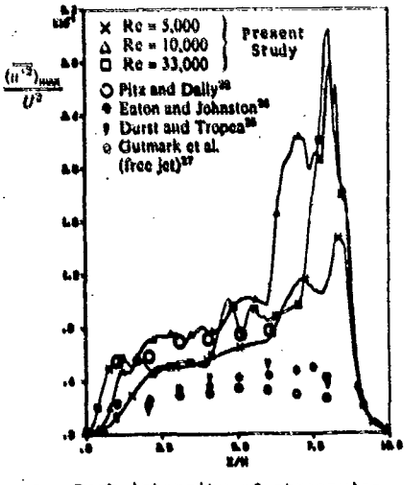
The Reynolds stress tensors $\overline{u_i' u_j'}$ were also evaluated by a running time average. Figure 7a presents the profiles of the streamwise "turbulence" intensity $\sqrt{\overline{u'^2}}/U$ for the Re = 10,000 simulation. The experimental data of Pitz and Daily[22] are also shown for comparison. A similar comparison for the transverse velocity component is also shown in Figure 7b. A few observations are important. The fluctuation of the longitudinal velocity is quite intense along the axis of the combustor, while the mean velocity profiles in Figure 5a show no decay of the mean axial velocity. Along the axis, the fluctuation in axial velocity is the result of the induced flow by the passage of the coherent vortex ring. It does not contribute to the momentum transport across the cross sections. Hence, there is a strong velocity fluctuation even in the potential core in the axisymmetric case. In contrast to the present case, the experimental results by Pitz and Daily[22] for the two-dimensional mixing layer do not show this phenomenon.



a. $\sqrt{u'^2}/U$ profiles (M = 0.32, Re = 10,000)



b. $\sqrt{v'^2}/U$ profiles (M = 0.32, Re = 10,000)

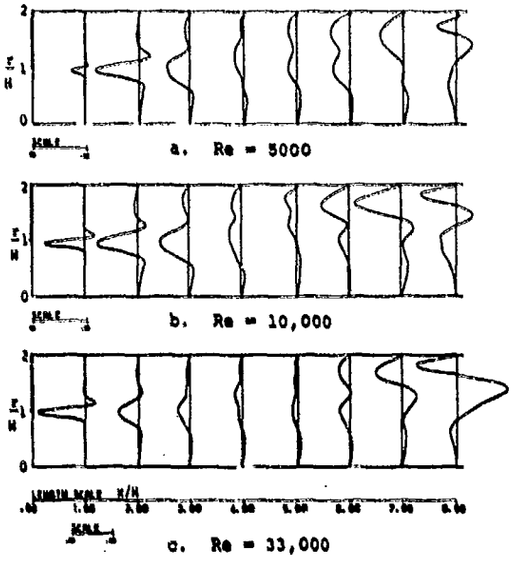


c. Peak intensity of streamwise velocity fluctuation, $(\overline{u'^2}_{max}/U^2)$

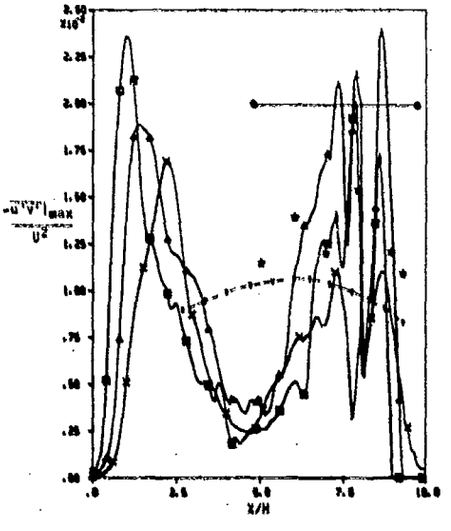
Figure 7. Intensity of Fluctuating Velocity Field

Figure 7c shows the variation of peak intensity $(\overline{u'^2})_{max}/U^2$ as a function of axial location. The results for the three different Reynolds number cases are shown. Because the simulations with different Reynolds numbers were essentially performed to generate a shear layer with different initial thicknesses, the comparison between the different Reynolds number cases is discussed in that context. The peak value of the streamwise fluctuations in the shear layer is in the range of 0.04 to 0.06. This is in agreement with the reported experimental value of 0.04. A global maximum occurs near the dump wall at $x/H \approx 8$, which is about one step height upstream of the reattachment point. This appears to agree with the results of Eaton and Johnston,[26] who also reported a maximum turbulence intensity at one step height upstream of the reattachment point. The streamwise turbulence intensity continues to decrease beyond the reattachment point and through the nozzle throat, as is consistent with experimental observations.[26,28]

Figures 8a through 8c show, respectively, the shear stress profiles $-\overline{u'v'}/U^2$ in the combustor for the three simulations with different Reynolds numbers. The maximum in the shear stress profiles occurs in the shear layer in the initial region of its development. Further downstream, another maximum occurs in the recirculation region. In general, the transverse profiles of the shear stress are similar in all three simulations. The variation of the peak shear stress, $-(\overline{u'v'})_{max}/U^2$, as a function of axial location is shown in Figure 8d. The maximum value of the shear stress increases to a global peak at the location $x = 2.5H$ for the Re = 5000 simulation. With increase in Reynolds number, this peak value increases, and the location shifts closer to the dump plane. This peak shear stress occurs in the region where, in an average sense, the primary vortices undergo pairing. Since the increase in Reynolds number results in a thinner initial shear layer, the rollup and pairing also occur closer to the dump plane, resulting in the shift of the peak shear stress closer to the dump plane. For comparison, some experimental data[25,26,29] are shown in this figure. Beyond $x = 2H$, the peak value of the shear stress begins to decrease, reaching a local minimum at $x \approx 5H$, after which it starts to increase again to reach another maximum in the impingement region. A maximum value of 0.022 at $x \approx 2H$ is observed. The peak near the reattachment point is in approximately the same range.



a-c. Reynolds stress $-\overline{u'v'}/U^2$ profiles in the combustor



d. Axial variation of peak Reynolds stress in the combustor;
●—● Arie and Rouse[26];
★ Durst and Tropea[25];
▸—▸ Best estimate curve[26].

Figure 8. Distribution of Reynolds Stress

As can be seen in Figures 8a through 8c, the Reynolds shear stress profiles change their sign in the transverse direction. Figure 9 shows the transverse profiles for the nondimensional mean velocity gradient $\partial\bar{u}/\partial r$ superimposed on the profiles for the shear

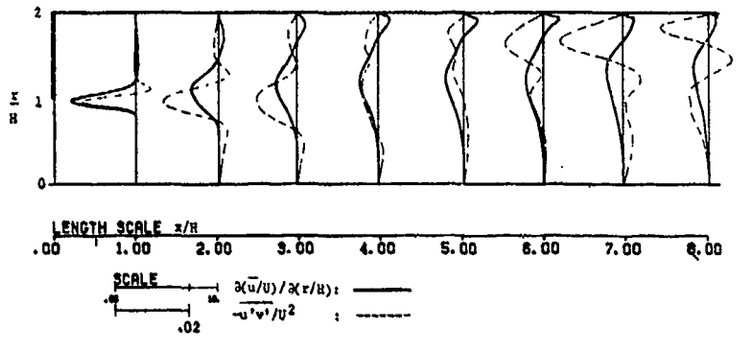


Figure 9. Comparison of Slope Profiles of the Streamwise Mean Velocity $\partial\bar{u}/\partial r$ and the Reynolds Stress $-\overline{u'v'}/U^2$ in the Combustor

stress $-\overline{u'v'}/U^2$. Comparison of these two sets of profiles shows that the shear stress and the slope of the mean profile have opposite signs in the recirculation zone, thus indicating a region of counter-gradient diffusion of momentum. Counter-gradient diffusion is also observed in the region around $x \approx 7H$ across almost the entire cross section. Thus, the gradient hypothesis of the Reynolds stress closure, i.e., $-\overline{u'v'} = \nu_t \partial\bar{u}/\partial r$, where ν_t is the eddy viscosity, is clearly not generally applicable in the combustor. Counter-gradient diffusion has been experimentally observed and is a direct consequence of the presence of large-scale coherent structures (e.g., Hussain[30]). Counter-gradient diffusion has been shown to occur during pairing processes. Furthermore, the local orientation of the traveling, generally noncircular vortices relative to the mean velocity profile determines whether co-gradient or counter-gradient diffusion of momentum will dominate (e.g., Ho and Huerre[18]; Hussain[30]). For example, if the major axis of a vortex with an elliptic shape is oriented opposite to the slope of the mean velocity profile, co-gradient diffusion dominates and energy is extracted from the mean field by the fluctuating field. When the structure is aligned with the mean velocity slope, counter-gradient diffusion dominates and a transfer of energy from the fluctuations back to the mean flow occurs. It has also been shown that the Reynolds stress increases to a peak during pairing and decreases thereafter.[18,30]

This experimentally observed relationship between large-scale structures and shear stress variation is also seen in the present numerical simulations. For example, in Figure 8d there is a peak in Reynolds stress at $x/H \approx 2$, which is around the region where the first pairing occurs. In this region, co-gradient production of kinetic energy dominates with only small local regions of counter-gradient production. Further downstream, the maximum in the shear stress distribution decreases in the shear layer as the pairing is completed and more regions of counter-gradient diffusion appear, as can be seen in Figures 8a through 8c. The peak shear stress increases again as the second merging process occurs, which results in the large structure observed in the region $x/H \approx 7$. In the region near the reattachment point, counter-gradient production dominates due to the relative orientation of the large structures. The characteristic noncircular shape and orientation of the large structure in the combustor can be visualized from the time sequence shown in Figure 2. A point to note is that for counter-gradient production to dominate in an average sense during unsteady motion, the large-scale structures must have the same orientation near the same location during the course of a long simulation. The time-averaged results obtained here indicate that this occurs near the nozzle entrance. Near the dump wall, there is a small region where counter-gradient diffusion always appears to dominate.

The failure of the gradient hypothesis in the recirculation zone and near the impingement region is consistent with past observations. A similar analysis was also carried out to determine the relation between $-\overline{\rho'u'}$ and $\partial\bar{\rho}/\partial x$ and also between $-\overline{\rho'v'}$ and $\partial\bar{\rho}/\partial r$. The results, which are not shown here, also clearly indicate that the gradient approximation for scalar diffusion is not valid in the recirculation region nor near the impingement region.

5. EXTRACTING ACOUSTIC INFORMATION

The major difference between the present simulations and the direct numerical simulations of incompressible turbulent flows extensively investigated in the past[2,3] is the existence of acoustic disturbances in the computational domain when the reduced frequency

of the system based on the speed of sound is of the order of unity. New methods must be developed to extract acoustic information from the results of numerical simulations so that physical phenomena associated with the compressibility effects can be uncovered. Our attempt in that direction is discussed in this section.

Since an acoustic disturbance is identified with the unsteady potential flow in a linearized system, it is natural to attempt to define the acoustic disturbance by working with the velocity field. It is well-known (e.g., Goldstein[21]) that a vector field $\vec{u}$ can be decomposed into a solenoidal field $\vec{v}$ and a potential component $\nabla\phi$ as

$$\vec{u} = \vec{v} + \nabla\phi \tag{16}$$

The solenoidal field $\vec{v}$ satisfies the incompressible condition

$$\nabla \cdot \vec{v} = 0 \tag{17}$$

and the vorticity of the vector field $\vec{u}$ is included by $\vec{v}$ so that the following relation is satisfied:

$$\nabla \times \vec{v} = \nabla \times \vec{u} = \vec{\Omega} \tag{18}$$

From the above equation, the vorticity $\vec{\Omega}$ can be identified as the source term in determining the vortical component of the velocity field $\vec{v}$. In particular, a stream function ψ can be defined for the solenoidal field $\vec{v}$ in two-dimensional or axisymmetric flow so that

$$\nabla^2\psi = -\Omega \tag{19}$$

where the vorticity is the source term for determining the vortical stream function ψ.

While the solenoidal field contains all of the vortical field of the given vector field, the potential field ϕ includes all of the dilatation field of $\vec{u}$. Therefore,

$$\nabla^2\phi = \nabla \cdot \vec{u} = \Delta \tag{20}$$

where Δ is the dilatation field. This decomposition is arbitrary up to a solenoidal-potential field. In other words, the classification of an irrotational-incompressible flow field into one of the two components is arbitrary. This decomposition of the velocity field is kinematic in nature and is valid for both the linear and nonlinear cases.

The definition of acoustic disturbance is given as the unsteady portion of the velocity potential.[20,31] Goldstein[21] further constrained this decomposition by defining the vortical velocity as that governed by a pure convective equation. The pressure variation is attributed to the "acoustic" velocity field. This constraint attaches dynamic significance to the original kinematic decomposition and therefore removes its arbitrariness.

By subtracting the time-averaged part from Eq. (20), the equation for the acoustic potential ϕ' can be given as

$$\nabla^2\phi' = \Delta - \langle\Delta\rangle = \Delta' \tag{21}$$

where the instantaneous fluctuating dilatation field Δ' acts as a source.

In analyzing the results of simulations, we used vorticity contours as a representative quantity for visualization of the vortical disturbance in the flow field. From the parallel between Eqs. (19) and (21), it appears that the unsteady part of the dilatation field may serve as a representative quantity for visualizing the acoustic disturbance.

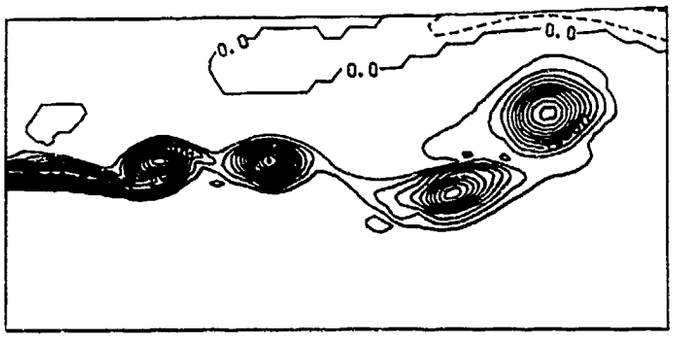
In our numerical simulations, the dilatation field is recorded. Using these data, a running time average of the field is performed. The mean field is then subtracted from the instantaneous field to give the instantaneous fluctuating component. The instantaneous dilatation field in the combustor is shown in Figure 10. The two regions of high instantaneous dilatation field shown in this figure are identified and analyzed in detail below.

The first region is the shear layer near the dump plane where the rollup occurs. A careful examination of the closeups of the dilatation and vorticity fields there reveals that the dilatation field around each concentrated vortex is a quadrupole. Figures 11a

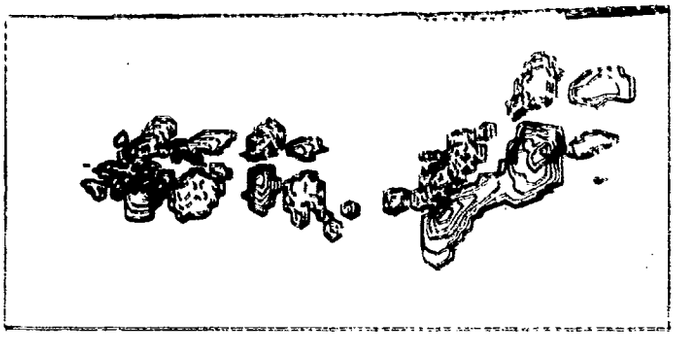


Figure 10. Instantaneous Dilatation Field in the Combustor

and 11b, respectively, show closeups of a vorticity field and the corresponding dilatation field near the dump plane. The quadrupole nature of the dilatation field around a rolled-up vortex is clearly shown. This visual pattern of the dilatation field travels with the vorticity pattern, an observation in contradiction to the general notion of an acoustic disturbance.



a. Vorticity contours



b. Dilatation contours

Figure 11. Comparison of Vorticity and Dilatation Fields Near the Dump Plane

Consider Lighthill's acoustic analogy[32]:

$$\frac{1}{c^2}\frac{D^2\phi}{Dt^2} - \nabla^2\phi = S \qquad (22)$$

The source term S of this equation involves the fluctuation of "Bernoulli enthalpy".[20,31] In the present case, where combustion is absent, this source term mainly consists of the vortical disturbances. In the near field, these sources are not negligible. The length and time scales of the sources dominate this region so that the acoustic equation (22) must be scaled accordingly. It follows immediately that the first term of the acoustic equation is of $O(M^2)$, as compared to the other terms, and is negligible in low subsonic flows. The acoustic potential is governed by a Poisson's equation, with vorticity disturbances acting as a source term. The propagation aspects of the acoustic wave are lost under this scaling, and the acoustic potential field, which is dominated by the sources in the near field, travels with the characteristic velocity of a vortical field instead of the speed of sound. This is usually called a pseudosound[33] and is not an acoustic wave in the conventional sense. The quadrupole behavior of the dilatation field around a concentrated vortex essentially reflects the source behavior discussed by Lighthill.[32] It is worthwhile to mention that the quadrupole sources are weak radiators of sound, and perhaps the resulting acoustic waves interact only weakly with the vortical motion.

The visualization of the dilatation field probably can be used to detect a propagating short acoustic wave such as a shock wave. In general, the long wave in a subsonic flow is difficult to visualize by this method. If the short-wavelength pseudosound disturbances caused by the vortical field can be filtered from the computed dilatation field, the long acoustic wave may be revealed. This filtering process requires integra-

tion of the dilatation field over a sampling volume that is small compared to the wavelength and yet large compared to the scale of the vortical disturbance. In the simulations, a suitable spatial average over a sampling volume is difficult to define, and the deduction of long acoustic waves from the results of simulations has not been attempted.

The dilemma of separating acoustic information from the vortical disturbances, as in the case of pseudosound discussed above, is not new. Crow[20] posed the problem of the formulation of an acoustic equation as follows: given a vorticity field Ω, find the density field and the velocity potential. He considered the subsonic cases in which the eddy length scale and the length scale of the region of vortical disturbances are much smaller than the acoustic wavelength. The acoustic analogy of Lighthill[32] is the result of a matched asymptotic expansion based on the smallness of the characteristic lengths in comparison to the acoustic wavelength. For a source region with dimensions comparable to the wavelength, he concluded that the separation of the acoustic disturbance from the vortical disturbance is dubious. Although it is purely speculative, a multiple-scale expansion may lead to a better formulation for the problem where the region of vortical disturbances is as large as the acoustic wavelength while the eddy size remains small. This is, of course, beyond the scope of the present work.

Since the propagation aspects of acoustic waves are difficult to visualize for a low subsonic flow, the dilatation field is used to find the characteristics of the sources in the near field. The detection of an acoustic disturbance in our simulations relies mainly on the point records of pressure fluctuations at locations where the vortical disturbances are believed to be small.

The second region of high-level dilatation field is near the location where the coherent vortical structures impinge on the solid surface. The structure of the dilatation field in that region is also very complex, as shown in Figure 12. If the eddy size is small compared to the acoustic wavelength, the source can be considered compact. Its behavior can be represented by a multipole expansion of the distributed sources.[21] The lower-order singular sources are known to be more effective sound radiators than quadrupoles. The strengths of the first two terms of the expansion can be given by taking spatial moments of the distributed dilatation field over a sampling volume. The strength of the monopole ϕ_0 and the dipole $\vec{\phi}_1$ can be computed by the following integrals:

$$\phi_0 = \int_V \Delta \, dV \tag{23}$$

$$\vec{\phi}_1 = -\int_V \Delta \, \vec{r} \, dV + \frac{\phi_0}{V} \int_V \vec{r} \, dV \tag{24}$$

where V is the sampling volume containing the vortex impingement point. The time variation of the strength of the monopole and the axial component of the dipole, together with the vorticity integrated over the same volume, are displayed in Figure 13 to show their relationship. It appears that, as the large vortical structure impinges on the wall, a strong fluctuating dipole is generated there. The dipole field is 180 degrees out of phase with the vorticity fluctuation.

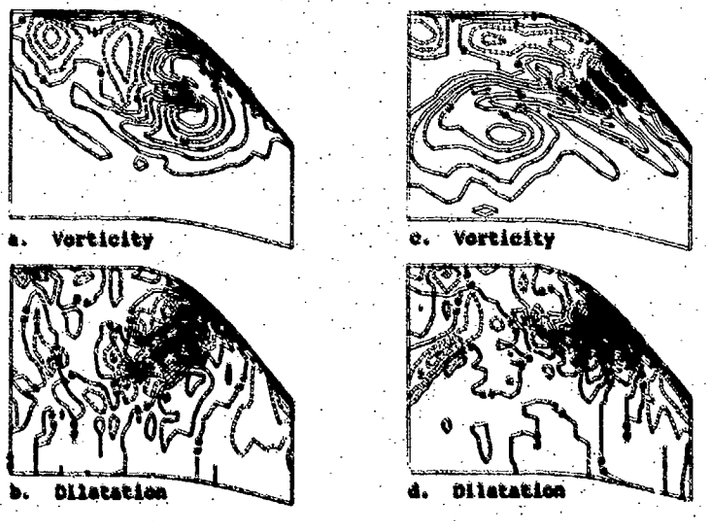


Figure 13. Vorticity and Dilatation Fields Near the Nozzle

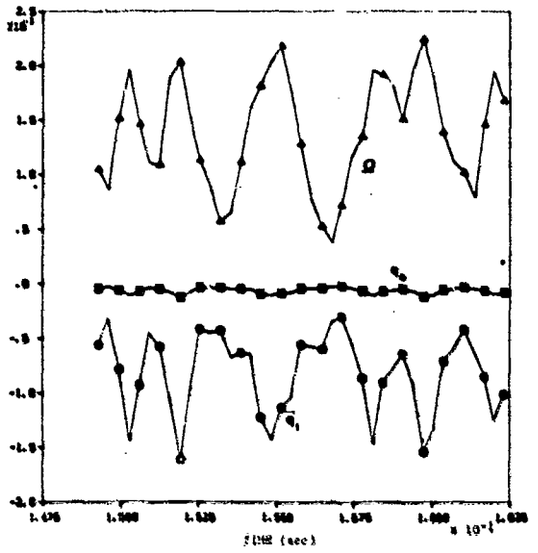


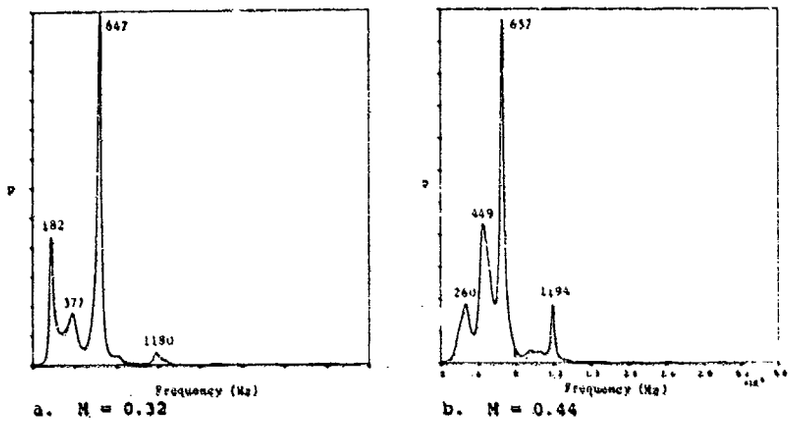
Figure 13. Time Variations of Vorticity Ω, Acoustic Monopole q_0, and Acoustic Dipole q_1.

In carefully performed wind tunnel experiments, Willis[34] observed upstream propagating acoustic disturbances generated at the downstream diffuser even at a low flow speed of 30 m/s. Crighton,[35] in studying the problem of "excess jet noise," found that turbulence causes a fluctuation in the thrust of a jet and that this fluctuation is acoustically equivalent to a strong dipole, and the unsteady mass flux corresponds to a weak monopole. In the present problem, the interaction between the impinging vortices and the nozzle causes fluctuating forces on the nozzle. Acoustically, the fluctuating force is equivalent to a dipole, as shown by the above analysis. These results provide some insight into the nature of sound generation due to vortex impingement on a nozzle. This knowledge of the acoustic behavior of the nozzle resulting from the interaction between impinging vortices and the nozzle can be used to construct a model for the pressure oscillations, as will be discussed later.

6. MODE OF OSCILLATIONS

In the previous section, we discussed our attempt to extract acoustic information from the results of simulations and found that the behavior of the sound sources can be visualized and analyzed. However, the propagation aspects of the long acoustic wave are difficult to visualize. Therefore, point pressure data may be a better representative quantity for the analysis of long acoustic waves. We have decided to use the power spectra of various flow quantities computed at a set of discrete points in the flow field for analysis of our simulation results. The flow quantities we have chosen to analyze are the vorticity and the pressure. The first quantity represents the vortical component of the flow field, while the second quantity is more ambiguous. Again, in the near field, both the vortical component and the acoustic component, if such a distinction can still be made, contribute simultaneously to the fluctuation of the static pressure. As Ffowcs Williams[4] pointed out, the low-frequency components of the pressure fluctuation must contain acoustic waves. There are locations where the vorticity is locally at a very low level. Since the flow is locally a potential flow, the pressure fluctuations computed there are assumed to represent acoustic oscillations. Since the acoustic wavelength is comparable to the length of the combustor, the Biot-Savart law may not give the correct phase relation between the source and the pressure fluctuation at the dump plane. The Biot-Savart law is applicable only when the acoustic wavelength for the given frequency is much larger than the distance between an observer and the source. In the present simulations, the pressure fluctuation at the base of the backward-facing step, where the vorticity fluctuation is small, is considered an acoustic fluctuation.

Figure 14a shows the computed spectrum of pressure at the base of the step. The Mach number in the inlet duct for this simulation is 0.12, and the other conditions were discussed earlier. There are three distinct peaks in the spectrum at approximately 650, 370 and 180 Hz. Although the level of the pressure oscillations is low, at only 4 percent of the static pressure, the existence of such distinct frequencies deserves careful consideration. We attempt to clarify the nature of these spectral peaks of pressure oscillations.



a. M = 0.32 b. M = 0.44

Figure 14. Pressure Spectra at the Base of the Step

There are several ways in which vortical motions of the fluid elements can contribute to the coherent acoustic oscillations. The easiest mechanism to identify is that of a resonant oscillation. Consider Lighthill's acoustic analogy equation (22). The vortices are considered a source independent of acoustic waves. Their presence merely excites the acoustic disturbances. When the space-time distribution of the sources contains one of the "free modes" defined by the eigensolutions of the homogeneous acoustic equation and boundary conditions, a resonant condition is satisfied. The acoustic oscillations in the duct accumulate, and large-amplitude oscillations may result. The frequency of this class of oscillations is that of a free mode.

There is another mechanism by which vortical disturbances can cause pressure fluctuations in a bounded domain such as a dump combustor. In this mechanism, a vortical disturbance may couple with the acoustic disturbance at the boundary to form a type of oscillation in which the vortical disturbance is part of the eigenvector and the frequency depends on the eigenvalue of the combined vortical-acoustic wave operator and, therefore, strongly on the phase speed of the vortical disturbance. This coupling between vorticity and acoustic waves at the solid boundary was discussed in its linearized form by Goldstein[21] in his general discussion of the sound generated by a blade row. This type of oscillation is designated as a coupled-mode oscillation. The detailed mechanisms of this mode will be discussed in the next section by using a simple model.

We used the following simulation method to clarify the nature of the observed spectral peaks. The frequency of a resonant oscillation depends on the speed of sound and only weakly on the convective speed. A variation in Mach number with the same stagnation conditions will not substantially alter the temperature of the chamber, and thus the frequency of an acoustic free mode, if the Mach number is kept reasonably low. However, the variation in the flow velocity is almost proportional to that in the Mach number. The frequency of a coupled-mode oscillation will then be shifted substantially with variations in the Mach number. To take advantage of this property, we performed two simulations: one at an inlet Mach number of 0.32 and the other at 0.44. By comparing the frequency spectra of the oscillations from these two simulations, we can identify the resonant modes and the coupled modes.

The spectra of pressure oscillations at the base of the step from these two simulations are shown in Figures 14a and 14b. The peaks in the 650-Hz range for both simulations are almost identical. These peaks are identified as acoustic resonant oscillations. To investigate the properties of this mode further, we obtained pressure spectra at a set of discrete points along the wall of the combustion chamber. The amplitudes of the 650-Hz peaks were plotted against the axial distance in Figure 15. From this figure, the sonic throat appears to serve as a nodal point for this particular mode of oscillation. There is also another minimum in the dump region. Since we do not have the phase information, we assumed that this minimum is possibly a node. The frequency estimate using the distance between these two node points as one-half of an acoustic wavelength is approximately 650 Hz, which agrees with that obtained from the spectra. We have not attempted to develop an accurate method of predicting the frequencies of the eigen acoustic modes for the combustor combined with an inlet duct. The dump has a slenderness ratio of approximately 5 and has a sonic nozzle located downstream. A one-dimensional model may not give an accurate estimate of the frequency even for the lowest few modes. The results of our numerical simulations, as shown in Figure 15, provide an approximate mode shape for the excited acoustic resonant mode near the combustor wall. Further investigation is required to substantiate this conclusion.

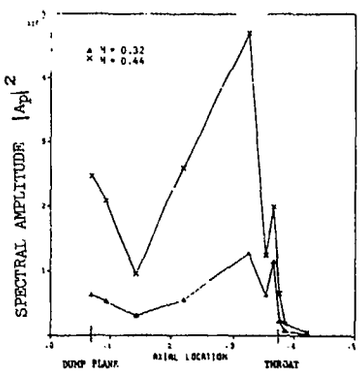


Figure 15. Wall Pressure Amplitude for the 650-Hz Oscillation

Figure 14 also shows that the frequency peaks in the range of 180 and 370 Hz in simulations with a Mach number of 0.32 shifted upward with an increase in the Mach number to the range of 260 and 450 Hz. These are identified as the coupled-mode oscillations. To further substantiate that these lower-frequency peaks are related to the vortex motion, we recorded the time history of vorticity at a location near the entrance of the nozzle. The power spectra of the vorticity fluctuations for the two Mach numbers show that, in the neighborhood of the low-frequency ranges of 370 and 450 Hz, strong vortical activities are evident.

In addition, we showed in the last section that, as a large vortical structure impinges on the wall, the local instantaneous fluctuating dilatation field behaves collectively as a dipole there. A strong sound radiation may originate from that region. This observation suggests that the low-frequency pressure fluctuations at the base of the step correlate with the vorticity impingement at the downstream nozzle. In the following section, we propose a model to describe the coupled-mode oscillations.

7. COUPLED-MODE OSCILLATION

We demonstrated in the previous section that, at the base of the backward-facing step, the pressure oscillations appear to contain frequency components that correlate well with those of the vorticity fluctuations near the impingement point. The frequencies of these components depend on the convective speed of the large vortices. This correlation suggests that the vorticity fluctuations may participate directly in the oscillation mode. Although the details of the interaction process can be quite complex, the essential mechanism can be described in the following simple manner. Upon impinging on the nozzle, a vortex generates an acoustic disturbance. This acoustic disturbance propagates upstream and is locally amplified by the diffraction around the corner of the backward-facing step. The resulting large acoustically induced velocity perturbs the shear layer near the separation point. This perturbation propagates downstream as an unstable vorticity wave, which results in the formation of a large vortical structure. The process is thus self-sustaining. We call this class of oscillations the coupled mode.

Coupled-mode oscillations have been described in many different terms for various flow conditions. For example, Rockwell and Naudascher[2] made an extensive review of the self-sustaining edge tone or cavity oscillations. Culick and Magiavala[36] discussed the pressure oscillations in a solid propellant rocket in which the spacer of the grain sheds vortices that, upon impinging on the downstream spacer, generate upstream-propagating acoustic disturbances that initiate new vortices. Ho and Nosseir[37] investigated experimentally a similar feedback mechanism for a jet impinging on a flat plate. Abouseif et al.[5] studied the generation of acoustic upstream feedback by the interaction of an entropy wave with a nozzle. Martin et al.[38] identified a similar mechanism as the source of wind tunnel pumping observed in an open jet tunnel with a downstream diffuser. Tam and Block[39] investigated the origin of the pressure oscillations in a cavity with external flow. Bogar and Sajben[12] used this mechanism to explain the experimentally observed oscillations in a diffuser with a frequency not associated with the acoustic modes. Williams[40] pointed out the possibility of combined vorticity-acoustic oscillations in a combustion chamber.

We present here a model that utilizes the information on the characteristics of the acoustic source resulting from the interaction between impinging vortices and the nozzle discussed earlier. We also include the inlet duct as part of the acoustic system in the

coupled-mode oscillations. This model not only clearly demonstrates the physical mechanism of the interaction between the acoustic wave and the vortical disturbance but also provides a method for evaluating approximately the frequencies of the coupled modes.

Eq. (22) is rewritten in the following form:

$$\nabla^2 \phi = \frac{1}{c^2}\frac{D^2\phi}{Dt^2} + \Delta_s' \tag{25}$$

where Δ_s' is the distributed dilatation field contributed by the source. As discussed earlier, the contribution of the propagation term to the dilatation field is small compared to the source term in the source region. Hence, the dilatation field computed from the simulations mainly consists of the latter. To investigate the propagation aspects of the acoustic wave, the above equation is filtered to reveal the long-wave behavior. This results in restoration of the propagation term, and the small-scale sources are compact and can be represented by the Dirac delta function or other generalized functions.

It is perhaps more illustrative to use acoustic pressure than to use acoustic potential as the acoustic variable for this simple one-dimensional model. Hence, we have

$$\frac{1}{c^2}\frac{\partial^2 p}{\partial t^2} - \frac{\partial^2 p}{\partial x^2} = \rho\frac{\partial \Delta'}{\partial t} \tag{26}$$

In the above equation, the convection of acoustic disturbances by the mean flow is neglected for low subsonic flows, and Δ' is the filtered dilatation field. Previously, we found that a strong dipole source for dilatation is generated by the impingement of vortices on the nozzle wall. The dimensions of the nozzle are assumed to be small relative to the acoustic wavelength. Therefore, the multipole expansion of the computed dilatation field can be applied by using the entire nozzle region, from the entrance to the throat, as the sampling volume. The results can be interpreted as the acoustic response of the complete vortex-nozzle-acoustic interaction, since the dilatation field is computed by solving the nonlinear flow equations and by satisfying the exact boundary conditions on the nozzle wall. Hence, we have

$$\Delta' = -\alpha\Omega(x_n)\frac{\partial}{\partial x}\delta(x - x_n) \tag{27}$$

where α is a transfer coefficient and x_n is the axial location of the nozzle. The sign in the above expression is determined by the fact that the dipole source is 180 degrees out of phase with the vorticity fluctuations.

For a vortical disturbance, the following convective equation is assumed:

$$\frac{\partial \Omega}{\partial t} + u_0\frac{\partial \Omega}{\partial x} = \sigma\Omega \tag{28}$$

where u_0 is the convective velocity for the vorticity. In this one-dimensional model, the detailed dynamics of the vorticity is lost. For example, the instability of a vortex sheet, or a shear layer, cannot be included in one-dimensional dynamics. Instead, an ad hoc model of a growth rate σ for the vorticity disturbance is included in the above equation to reflect the spatial growth of a vortical disturbance. From Michalke,[41] the growth rate of the vortical disturbance is related to the thickness of the shear layer; it is larger for a thinner shear layer and vice versa. The phase speed of the vortices u_0 was computed by a two-point correlation of the vorticity fluctuations. It was found that the convective speed for the vorticity in the dump is approximately 0.6 of the velocity in the inlet duct and is substantially slower at 0.5 when approaching the impingement point.

The acoustic equation (26) is applied to both the dump region and the inlet duct separately. The solutions in two regions are matched by the continuity conditions at the dump plane. Thus, if p_1 and p_2 are the solutions in the duct and the dump region, respectively, the following boundary conditions are applied:

$$p_1 = p_2 \qquad \text{at } x = 0 \tag{29}$$

$$d_1^2\frac{\partial p_1}{\partial x} = d_2^2\frac{\partial p_2}{\partial x} \qquad \text{at } x = 0 \tag{30}$$

where the dump plane is located at $x = 0$ and the diameters of the inlet duct and the dump are d_1 and d_2, respectively.

Numerically, we applied a constant stagnation pressure boundary condition at the inlet in our simulations. This condition can be formulated in terms of a homogeneous boundary condition by linearization of the steady-state isentropic relation as

$$\frac{p_1}{p} + \gamma M\frac{u'}{c} = 0 \tag{31}$$

where u' is the acoustic velocity and M is the Mach number at the inlet. In an unsteady calculation, the stagnation pressure as defined by the steady-state form, strictly speak-

ing, is not applicable. However, without better implementation of the inflow boundary condition, this boundary condition can be considered as an ad hoc assumption. It is important that this condition does not input energy into the acoustic oscillations in the interior of the computational domain. It turns out that this boundary condition has a damping effect on the acoustic waves in the system. The boundary condition does not generate spurious acoustic waves, which could otherwise be mistaken as self-sustained oscillations.

The nozzle and the supersonic region downstream of the throat are replaced by a dipole source in the acoustic equation. Since the behavior of the dipole source has been computed by a direct numerical simulation, the left-running waves resulting from the complex vortex-nozzle-acoustic interaction are included in the radiated waves by the source. Thus, no additional left-running "free wave" from the homogeneous solution of the acoustic equation is required.

The remaining boundary condition is the mechanism of perturbing the shear layer by an acoustic wave at the dump plane. At the step where the boundary layer separates from the surface to form a free shear layer, an acoustic disturbance is amplified locally by the diffraction around the sharp convex corner. In fact, a linear acoustic theory will predict an infinite acoustic velocity at the corner. Research in the past had been directed toward the issue of so-called acoustic susceptibility at the separation point. For example, Orszag and Crow[42] addressed the problem in the incompressible limit by examining the shear layer behind a trailing edge. They found that the infinite flow velocity at the trailing edge induced by the instability wave of the vortex sheet must be compensated by the initiation of a new vorticity disturbance. Crighton and Leppinton[43] investigated the acoustic susceptibility of the shear layer behind a trailing edge of a flat plate. Again, the Kutta condition at the trailing edge determines the vorticity disturbance that eventually grows into a large-scale coherent structure. This mechanism can be represented by the following boundary condition:

$$\Omega|_{x=0} - \beta u' = 0 \tag{32}$$

where u' is the acoustic-induced velocity at the dump plane and is related to the gradient of acoustic pressure by

$$\rho_0 \frac{\partial u'}{\partial t} = -\frac{\partial p_2}{\partial x} \tag{33}$$

The vorticity dynamics and the acoustic oscillations are coupled through the dipole source and the boundary condition at the dump plane. The system of equations with the boundary conditions is homogeneous. We seek an eigensolution of the form

$$\begin{bmatrix} p \\ \Omega \end{bmatrix} = \begin{bmatrix} \hat{p}(x) \\ \hat{\Omega}(x) \end{bmatrix} e^{i\beta t} \tag{34}$$

where β is the frequency. The variables in the remainder of this article are all nondimensionalized by the reference quantities (e.g., the velocity by c, the spatial coordinate by x_0, time by x_0/c) and use the same nomenclature as the dimensional quantities.

The vorticity equation (28) can be integrated easily to give

$$\hat{\Omega} = a_1 e^{-\frac{i\beta x}{M_c} + \frac{\sigma}{M_c} x} \tag{35}$$

where a_1 is an arbitrary integration constant, M_c is the Mach number of the vortex convective speed and σ stands for the nondimensional growth rate of vortical disturbances.

To solve the acoustic equation (26), we first realize that the Green's function for the equation is given by a retarded potential as

$$G(x, x_0, t, \tau) = \delta(\tau - t + |x - x_0|) \tag{36}$$

where δ is the Dirac delta function. Thus, the particular solution for the forced wave equation (26) can be given by

$$p_2 = -\alpha \frac{\partial^2}{\partial t \, \partial x} \int_{-\infty}^{\infty} \int_{-\infty}^{\infty} d\tau \, dx_0 \, \Omega(\tau, x_0) H(x_0 - x_s)$$

$$\cdot \delta(\tau - t + |x - x_0|) \tag{37}$$

or

$$p_2 = \frac{\alpha}{4} \Omega'' (t - |x - x_s|) \quad \begin{matrix} x \le x_s \\ x > x_s \end{matrix} \tag{38}$$

where the prime denotes the derivative with respect to the argument. Note that there is a 180-degree phase shift in the acoustic pressure across the nozzle. This is due to the dipole nature of the source. We are only interested in the region $x < x_s$.

By using Eqs. (35) and (38), the general solution of the forced acoustic equation in the dump region can be given as

$$\hat{p}_2 = a_3 e^{ifx} + a_4 e^{-ifx} \pm a_5 \frac{A}{\beta} F e^{-if|x-x_n|} \quad \begin{matrix} x < x_n \\ x > x_n \end{matrix} \tag{39}$$

$$A = \alpha\beta e^{\frac{\sigma}{M_0}x_n} \tag{40}$$

$$F = f^2 e^{\frac{ifx_n}{M_0}} \tag{41}$$

where a_3 and a_4 are integration constants. It is useful to give the expression of the derivative of p_2 as

$$\hat{p}_{2_x} = if\left(a_3 e^{ifx} - a_4 e^{-ifx} + a_5 \frac{A}{\beta} F e^{-if|x-x_n|}\right) \tag{42}$$

There is no phase shift across the nozzle.

The acoustic pressure in the inlet duct is simply given by

$$\hat{p}_1 = a_1 e^{ifx} + a_2 e^{-ifx} \tag{43}$$

where a_1 and a_2 are integration constants.

The coefficient a_3 can be set to zero to eliminate the left-running "free wave" as was discussed. The remaining integration constants can be determined by the boundary conditions, Eqs. (29) through (33). Since these boundary conditions are homogeneous, the eigenvalue f can be obtained from the condition that the characteristic determinant vanishes.

The eigenvalue problem contains four physical parameters: the convective Mach number M_0, the inlet duct length l, the areal ratio between the duct and the dump R, and an overall interaction parameter A, as defined by Eq. (40). This parameter is non-dimensional and reflects the overall degree of interaction between acoustic oscillations and vorticity dynamics in the system. For example, an unstable shear layer with a large growth rate σ will interact more strongly with acoustic waves. Strictly speaking, A is not independent of the frequency f. However, the present assumption of a constant interaction parameter probably does not affect the real part of the eigenvalue f.

The characteristic condition can be simplified to the following equation:

$$\left(\frac{R+1}{R-1} - \frac{1+M}{1-M}e^{2ifl}\right)(2\Gamma+1) - \left(\frac{2R}{R-1}\right)(1+\Gamma)\left(1+\frac{1+M}{1-M}e^{2ifl}\right) = 0 \tag{44}$$

where R is the areal ratio between the cross section of the dump and the cross section of the inlet pipe, and

$$\Gamma = FAe^{-\sigma l} \tag{45}$$

The frequency is a complex number, and absolute instability is possible when Im (f) < 0. It can be shown that there is a stability criterion for the parameter A below which the system is stable. For large A, it can be shown that the growth rate of the instability behaves as ln A. Figure 16 shows the complex eigenfrequencies for the first two modes for various values of A.

The frequencies of the first two modes computed from this model problem are 190 and 360 Hz, which seems to reflect what has been observed in the numerical simulations, although there are discrepancies in the numerical values. There are quite a number of uncertainties in the model that are still considered as ad hoc assumptions. The convective speed of vortices in the dump is taken as 0.5 of the jet velocity at the dump plane. We used this reduced value, as opposed to the value of 0.6 observed in a free jet, to account for the deceleration of the vortices as they approach the impingement point as was discussed previously. The convection of acoustic waves by the mean flow has been neglected. These factors can certainly affect the computed eigenfrequencies by using the model. Nevertheless, this simple one-dimensional model, using the behavior of the acoustic sources extracted from the numerical simulations, is very helpful in understanding the complex physical processes involved in vortex-acoustic interactions.

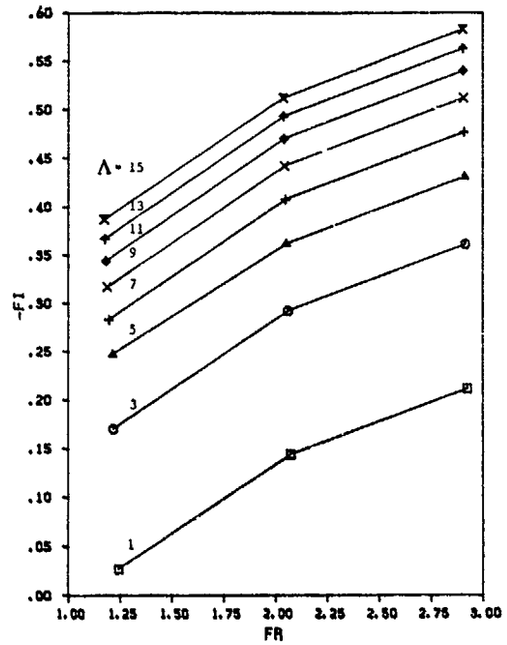


Figure 16. Eigenvalues for the Coupled Mode

8. COMBUSTION MODEL AND SIMULATIONS

To include combustion in the model, we first assume that the thickness of the flame in a large-eddy simulation is only broadened by the subgrid fine-scale turbulence and can be considered as thin in such a simulation. The burning rate in a large-eddy simulation is determined by the propagation of the flame into the fuel stream at a subgrid turbulent flame speed u_T, and the contortion of the flame by the large eddies. The subgrid turbulent flame speed needs to be modeled, while the flame contortion by the large eddies can be directly computed. The model for a subgrid turbulent flame speed can be supplied, for example, by the recent results of Yakhot,[44] who computed the relation between the laminar flame speed u_l, the turbulent flame speed u_T and the turbulent rms velocity u' by a re-normalization group technique. Specifically, he derived the following relation.

$$\frac{u_T}{u_l} = \exp\left|\frac{u'^2}{u_T^2}\right| \tag{46}$$

A progress variable G, with $G = 0$ for the fuel mixture and $G = 1$ for the combustion product, can be defined. The equation governing the progress variable G is given by Kerstein et al.[45] as

$$\frac{\partial G}{\partial t} + \vec{u}\cdot\nabla G = u_T|\nabla G| \tag{47}$$

In this formulation, the turbulent rms velocity must be supplied by the transport equation for the subgrid turbulent kinetic energy equation, i.e., k-equation. This subgrid turbulent kinetic energy equation needs to be derived and modeled. The chemical energy release is then locally related to the flame convolution and the local flame speed. The effects of chemical heat release can be included in the heat of formation in the expression for the internal energy. This model is currently being investigated, and the resulting numerical simulations can be used to study combustion instability. The results of combustion simulations will be reported in the future.

9. SUMMARY AND DISCUSSION

We have investigated pressure oscillations in a ramjet combustor under cold-flow conditions. The main contribution of this investigation is the evidence that both resonant oscillations and coupled-mode oscillations exist in the combustor. The former represent an acoustic free mode excited by vortex activities, and the latter are oscillations in which the vortical disturbances play a primary role in the formation of eigenfunctions. However, the amplitude of these oscillations is small. To understand further

the origin of the large-amplitude pressure oscillations observed in an instability mode in a ramjet combustor, chemical heat release must be included. The interaction among vortical disturbances, acoustic disturbances, entropy disturbances and solid surfaces will be even more complex than in the present case. Both acoustic resonant modes and convective-wave/acoustic-wave coupled modes are potential candidates for combustion instability when heat release is included. Application of the methodology presented in this investigation to cases with heat release is now being attempted.

It is worthwhile to make a few comments on the present numerical simulations. A simulation of the phenomenon of resonant oscillations takes a long computing time for the flow field to evolve into a quasi-stationary state. Even for the present axisymmetric simulation, significant computational time is required to obtain enough data for a meaningful statistical analysis.[13] The results presented here are perhaps the limit of what one can do with state-of-the-art computing capabilities. As discussed in the introduction, our simulations can only be classified as large-eddy simulations. The breakdown of the axisymmetric vortical structures into three-dimensional turbulence cannot be included here. The transfer of spectral energy to high wave numbers by three-dimensional vortex stretching is missing. The resulting dissipation of large vortical structures can only be partially accounted for in the present investigation by the relatively large molecular viscosity and perhaps by the numerical dissipation near the end of the combustor where the grid spacing is large. Extension of the simulations to three-dimensional space requires a computer at least an order of magnitude faster. Even then, a subgrid-scale turbulence model will be required. Subgrid models for compressible flows have just been emerging. These models need to be validated for practical applications.

REFERENCES

1. Chu, B.-T., and Kovasznay, L. S. G., "Nonlinear Interactions in a Viscous Heat-Conducting Compressible Gas," *J. Fluid Mech.*, Vol. 3, 1958, pp. 494-514.

2. Rockwell, D., and Naudascher, E., "Self-Sustained Oscillations of Impinging Free Shear Layers," *Ann. Rev. Fluid Mech.*, Vol. 11, 1979, pp. 67-94.

3. Ohring, S., "Calculations of Self-Excited Impinging Jet Flows," *J. Fluid Mech.*, Vol. 163, 1986, pp. 69-98.

4. Ffowcs Williams, J. E., "Boundary Layer Pressures and the Corcos Model: A Development to Incorporate Low Wave Number Constraints," *J. Fluid Mech.*, Vol. 125, 1982, pp. 9-25.

5. Abouseif, G. E., Keklak, J. A., and Toong, T. Y., "Ramjet Rumble: The Low Frequency Instability Mechanism in Coaxial Dump Combustors," *Combustion Sci. and Tech.*, Vol. 36, 1984, pp. 83-108.

6. Schadow, K. C., Gutmark, E., Parr, T. P., Parr, D. M., and Wilson, K. J., "Large-Scale Structure as a Driver of Combustion Instability," AIAA Paper No. 87-1326, 1987.

7. Sterling, J. D., and Zukoski, E. E., "Longitudinal Mode Combustion Instabilities in a Dump Combustor," AIAA Paper No. 87-0220, 1987.

8. Crocco, L., and Cheng, S.-I., "Theory of Combustion Instability in Liquid Propellant Rocket Motors," AGARDograph No. 8, Butterworths Scientific Publication, 1956.

9. Crocco, L., and Sirignano, W. A., "Behavior of Supercritical Nozzles Under Three-Dimensional Oscillatory Conditions," AGARDograph No. 117, NATO, 1967.

10. Ferziger, J. H., and Leslie, D. C., "Large Eddy Simulation: A Predictive Approach to Turbulent Flow Computation," AIAA Paper No. 79-1471, 1979.

11. Jou, W.-H., and Menon, S., "Simulations of Ramjet Combustor Flow Fields: Part II - Origin of Pressure Oscillations," AIAA Paper No. 87-1422, 1987.

12. Bogar, T. J., and Sajben, M., "The Role of Convective Perturbations in Supercritical Inlet Oscillations," *CPIA Publication No. 412*, Vol. I, 1984, p. 465.

13. Menon, S., and Jou, W.-H., "Simulations of Ramjet Combustor Flow Fields: Part I - Numerical Model, Large-Scale and Mean Motions," AIAA Paper No. 87-1421, 1987.

14. MacCormack, R. W., "The Effect of Viscosity in Hyper-Velocity Impact Cratering," AIAA Paper No. 69-354, 1969.

15. MacCormack, R. W., Rizzi, A. W., and Inouye, M., "Steady Supersonic Flowfields with Embedded Subsonic Regions," *Computational Methods and Problems in Aeronautical Fluid Dynamics*, Hewitt, B. L., et al., eds., Academic Press, 1976.

16. Didden, N., and Ho, C.-M., "Unsteady Separation in a Boundary Layer Produced by an Impinging Jet," *J. Fluid Mech.*, Vol. 160, 1985, pp. 235-256.

17. Gutmark, E., and Ho, C.-M., "Preferred Modes and the Spreading Rates of Jets," *Phys. Fluids*, Vol. 26, 1983, pp. 2932-2938.

18. Ho, C.-M., and Huerre, P., "Perturbed Free Shear Layers," *Ann. Rev. Fluid Mech.*, Vol. 16, 1984, pp. 365-424.

19. Lalufer, J., and Monkewitz, P. A., "On Turbulent Jet Flows: A New Perspective," AIAA Paper No. 80-0962, 1980.

20. Crow, S. C., "Aerodynamic Sound Emission as a Singular Perturbation Problem," *Stud. Appl. Math.*, Vol. 49, 1970, pp. 21-44.

21. Goldstein, M. E., *Aeroacoustics*, NASA SP-346, 1974.

22. Pitz, R. W., and Daily, J. W., "Combustion in a Turbulent Mixing Layer Formed at a Rearward-Facing Step," *AIAA J.*, Vol. 21, 1983, pp. 1565-1570.

23. Eaton, J. K., and Johnston, J. P., "A Review of Research on Subsonic Turbulent Flow Reattachment," *AIAA J.*, Vol. 19, 1981, pp. 1093-1100.

24. Minh, H. H., and Chassaing, P., "Perturbations of Turbulent Pipe Flow," in *Turbulent Shear Flows – I*, Bradbury, L. J. S., et al., eds., Springer-Verlag, New York, 1979.

25. Durst, F., and Tropea, C., "Turbulent Backward-Facing Step Flows in Two-Dimensional Ducts and Channels," Turbulent Shear Flow Conference 3, Davis, CA, 1982.

26. Eaton, J. K., and Johnston, J. P., "An Evaluation of Data for the Backward-Facing Step Flow," 1980/81 AFOSR-HTTM-Stanford Conference on Complex Turbulent Flows, 1980.

27. Gutmark, E., Schadow, K. C., Wilson, K. J., and Parr, D. M., "Small Scale Mixing Enhancement in Acoustically Excited Jets," AIAA Paper No. 86-1885, 1986.

28. Bradshaw, P., and Wong, F. Y. F., "The Reattachment and Relaxation of a Turbulent Shear Layer," *J. Fluid Mech.*, Vol. 52, 1972, pp. 113-135.

29. Arie, M., and Rouse, H., "Experiments on Two-Dimensional Flow over a Normal Wall," *J. Fluid Mech.*, Vol. 1, 1956, pp. 129-141.

30. Hussain, A. K. M. F., "Coherent Structures - Reality and Myth," *Phys. Fluids*, Vol. 26, 1983, pp. 2816-2850.

31. Yates, J. E., "Application of the Bernoulli Enthalpy Concept to the Study of Vortex Noise and Jet Impingement Noise," NASA CR 2987, 1977.

32. Lighthill, M. J., "On Sound Generated Aerodynamically - 1. General Theory," *Proc. Roy. Soc. (London), Series A*, Vol. 211, 1952, pp. 564-587.

33. Ffowcs Williams, J. E., "Hydrodynamic Noise," *Ann. Rev. Fluid Mech.*, Vol. 1, 1969, pp. 197-222.

34. Wills, J. A. B., "Measurement of the Wave Number/Phase Velocity Spectrum of Wall Pressure Beneath a Turbulent Boundary Layer," *J. Fluid Mech.*, Vol. 45, 1970, pp. 65-90.

35. Crighton, D. G., "The Excess Noise Field of Subsonic Jets," *J. Fluid Mech.*, Vol. 56, 1972, pp. 683-694.

36. Culick, F. E. C., and Magiawala, K., "Excitation of Acoustic Modes in a Chamber by Vortex Shedding," *J. Sound and Vibration*, Vol. 64, 1979, pp. 455-457.

37. Ho, C.-M., and Nosseir, N. S., "Dynamics of Impinging Jets: Part I. The Feedback Phenomenon," *J. Fluid Mech.*, Vol. 105, 1981, pp. 119-142.

38. Martin, R. M., Brooks, T. F., and Hoad, D. R., "Reduction of Background Noise Induced by Wind Tunnel Jet Exit Vanes," *AIAA J.*, Vol. 23, 1985, pp. 1631-32.

39. Tam, C. K., and Block, P. J. W., "On the Tones and Pressure Oscillations Induced by Flow over Rectangular Cavities," *J. Fluid Mech.*, Vol. 89, Part 2, 1978, pp. 373-399.

40. Williams, F. A., *Combustion Theory*, Second Edition, Benjamin/Cummings Publishing Company, 1985.

41. Michalke, A., "The Instability of Free Shear Layers: A Survey on the State of the Art," *Prog. in Aerospace Sciences*, Vol. 12, 1972, pp. 213-239.

42. Orszag, S. A., and Crow, S. C., "Instability of a Vortex Sheet Leaving a Semi-infinite Plate," *Stud. Appl. Math.*, Vol. 49, 1970, pp. 167-181.

43. Crighton, D. G., and Leppinton, F. G., "Radiation Properties of the Semi-infinite Vortex Sheet: The Initial Value Problem," *J. Fluid Mech.*, Vol. 64, 1974, pp. 393-414.

44. Yakhot, V., "Propagation Velocity of Premixed Turbulent Flame," submitted to *Combustion Sci. and Tech.*

45. Kerstein, A. R., Ashurst, W. T., and Williams, F. A., "Field Equation for Interface Propagation in an Unsteady Homogeneous Flowfield," *Phy. Rev. Ann.*, Vol. 37, No. 7, 1988, pp. 2728-2731.

ACKNOWLEDGEMENTS

The present work is supported by the Office of Naval Research under Contract No. N00014-84-C-0359. This research would not have been possible without the support from NASA Lewis Research Center for generous computing time on the CRAY-XMP computer, and from the National Aerodynamics Simulator (NAS) at NASA Ames Research Center for high-resolution computations. During the course of the research, comments by Professor F. E. C. Culick of Caltech, Professor C.-M. Ho of the University of Southern California, and Dr. Klaus Schadow of the Naval Weapons Center have been very helpful.

DISCUSSION

A. Laverdant, France

What are your initial conditions, is it zero velocity everywhere in the cavity or is a simplified one dimensional description used ?

Author's Reply :

The flow field was initially set at the stagnation conditions. The flow is started by lowering the exit pressure.

S. Candel, France

Having determined the dilation it is possible to integrate the Poisson equation for the potential and then to get the acoustic pressure from the potential. Did you try to follow this path ?

Author's Reply :

One can certainly integrate the Poisson's equation for velocity potential, subject to certain boundary conditions. This Poisson's equation is a kinematic relation. To obtain the acoustic pressure, the unsteady Bernoull's equation is needed. Although it is an interesting path of research, we have not done so.

S. Candel, France

Are your power spectral densities obtained with the maximum entropy method ? This method provides nice high resolution spectra but it also yields lower level artificial peaks.

Author's Reply :

The power spectral densities were obtained by maximum entropy method. The resulting spectral peaks appear also in the unfiltered spectra as noisy peaks. Therefore, we believe that they are not artificial.

"SIMULATION NUMERIQUE DU FONCTIONNEMENT INSTATIONNAIRE D'UN FOYER A ELARGISSEMENT BRUSQUE"[1]

par

F.GARNIER, B.LABEGORRE, M.SERRANO[2] et A.LAVERDANT

Office National d'Etudes et de Recherches Aérospatiales

92320 Châtillon-sous-Bagneux (FRANCE)

--==ooOoo==--

Les recherches fondamentales peuvent être d'une grande utilité pour la maîtrise des instabilités de combustion haute fréquence des statoréacteurs, notamment par l'identification des mécanismes d'entretien et d'amortissement des instabilités et de leur couplage.

Avec l'avènement des ordinateurs vectoriels et les progrès enregistrés dans les méthodes numériques, la simulation de la combustion instationnaire , biphasique et tridimensionnelle dans les foyers de statoréacteurs devient possible.

Dans cette perspective, l'ONERA a entrepris l'adaptation d'un programme de calcul , KIVA, précédemment développé au Los Alamos National Laboratory pour l'étude des moteurs diésel ; cette adaptation porte en priorité sur l'introduction de conditions de conditions aux limites de type flux entrant et sortant. L'application en est faite sur un foyer à élargissement brusque ("dump combustor"), alimenté par un combustible liquide. Une description détaillée des phénomènes physico-chimiques pris en compte est donnée et les premiers résultats numériques obtenus sont comparés avec les informations provenant de calculs comparables.

"NUMERICAL SIMULATION OF UNSTEADY COMBUSTION IN A DUMP COMBUSTOR"

Basic investigations can be of great interest in the control of high frequency combustion instability in ramjets, in particular by identification of amplifying and damping mechanism of instabilities and of their coupling.

With the advent of vectorized computors and the progress of numerical methods , simulation of unsteady , biphasic and three dimensional combustion is now possible.

In this perspective, ONERA has undertaken the adaptation of a computer code, KIVA, precedently developed by the Los Alamos National Laboratory for diesel engines study; this adaptation is essentially concerned with the introduction of inflow and outflow . The application is made on a dump combustor with liquid fuel injection. A detailed description of physico-chemical mechanism involved is presented and the first numerical results obtained are compared with similar ones.

1-INTRODUCTION

Le fonctionnement des foyers de statoréacteurs est parfois affecté par des instabilités de combustion. Ces mécanismes peuvent avoir des conséquences catastrophiques pour la vie de l'engin [1]. Ils entrainent généralement des vibrations de forte amplitude susceptibles de détruire des équipements, un transfert thermique accru [2], une trajectoire indésirable de l'engin, un risque de pompage de l'entrée d' air. La mise au point des foyers peut être prolongée dans le temps et entrainer une augmentation du coût de développement, voire un ajournement du projet. La démarche employée au cours des années cinquante et soixante, en vue de s'affranchir de ces mécanismes, a généralement consisté à procéder à de nombreux essais où diverses solutions reconnues pour leur efficacité sont testées. Il s'agit de disposer des aubages longitudinaux le long des parois de la chambre [3], de modifier les conditions d'injection [4], de modifier l'écoulement au voisinage d'un accroche-flamme [5]. Au cours des années cinquante, un contrôle acoustique dérivé des techniques d'asservissement a été envisagé pour les fusées à ergols liquides par le Pr. Crocco [6,7], et plus récemment à l'Université de Cambridge [8] ainsi qu'à l'Ecole Centrale de Paris [9]. Ces diverses approches permettent généralement de s'affranchir du problème des instabilités, mais l'idéal reste cependant la prévention dès le stade de l'avant-projet. Cet objectif est à l'origine de nombreuses études à caractère plus fondamental visant l'amélioration des connaissances et la création d'outils prédictifs performants.

Les engins modernes présentent généralement des géométries complexes avec des entrées d'air latérales. Si cette configuration permet de s'affranchir de la présence d'accroche-flamme, elle est à l'origine d'un écoulement tridimensionnel dont l'analyse est particulièrement difficile. Des visualisations hydrodynamiques menées par Hébrard et ses collaborateurs au CERT-DERMES [10] et par Stull et al. à l'AFWAL [11], ont permis de décrire la disposition des recirculations et des jets. Cette démarche qui présente de nombreux aspects intéressants tels que la prédiction des limites pauvres et riches d'extinction, la détermination des paramètres permettant d'améliorer le rendement de combustion ne donne que peut d'indications sur les instabilités. Elle fournit toutefois des informations qualitatives et ne permet pas de prédire l'écoulement réactif rencontré en pratique.

---

[1] Etude financée par la D.R.E.T

[2] Détaché par la D.R.E.T auprès de l'O.N.E.R.A

La complexité des mécanismes tridimensionnels mis en jeu conduit généralement à envisager une géométrie plus simple, du type bidimensionnelle ou à symétrie de révolution, pour l'étude des instabilités de combustion.L 'accrochage de flamme peut être réalisé à l'aide d'un fil catalytique [12], d'une flamme pilote [13], d'un accroche-flamme [14], ou de plusieurs marches [14-21]. Ce dernier type de configuration est le plus souvent retenu et va être le seul cas examiné dans la suite de ce travail.

Des études analytiques sur les instabilités de combustion d'un foyer à élargissement brusque ("dump combustor" dans la littérature anglo-saxonne), ont été envisagées par Culick et ses étudiants au California Institute of Technology [22-25]. Les techniques de résolution employées sont basées sur une méthode de perturbation: l'"averaging" [26]. Les résultats obtenus ne permettent pas une prédiction exacte de la stabilité, mais ils fournissent des indications intéressantes sur la nature des couplages mis en jeu entre l'acoustique et l'entropie, la combustion et l'écoulement moyen, les conditions aux limites.

La majorité des études récentes sur les instabilités de combustion des statoréacteurs font largement appel aux méthodes numériques. Poinsot [21] utilise un schéma aux différences finies pour intégrer les équations d'un modèle simplifié dans le cadre d'une hypothèse de flamme mince. Les résultats obtenus montrent que la prévision des mécanismes d'instabilité, des amplitudes et des phases relatives des différents paramètres de l'écoulement sont satisfaisantes.

Devant la complexité des mécanismes mis en jeu, il est parfois possible d'envisager une démarche numérique simplifiée dans le cadre des hypothèses de linéarisation. La notion d'"écoulement moyen" est alors envisageable et l'acoustique est décrite sous la forme d'une superposition de plusieurs modes acoustiques. La prévision de des deux aspects doit être abordée à l'aide des méthodes numériques. Lilley [27-29] propose une revue des méthodes numériques pour la prédiction d'écoulements stationnaires dans les foyers et étudie l'écoulement avec une composante tangentielle dans un statoréacteur [30]. Une résolution des équations de Navier-Stokes, pour l'étude des recirculations, et des équations de Navier-Stokes paraboliséees en aval des recirculations est effectuées par Brown et Hale [31]. Des prédictions d'écoulements tridimensionnels réactifs et biphasiques dans les foyers de turbomachines ont été effectués à l'Université de Sheffield par Boysan et al. [32]. Les résultats obtenus sont impressionnants et permettent une mise au point plus facile des foyers. Cependant, le temps de calcul requis pour la prédiction d'un problème stationnaire reste généralement supérieur à celui demandé par un problème pseudo-instationnaire.

L'écoulement moyen peut comporter des instabilités à basse fréquence. Une méthode, dite des "tourbillons aléatoires", permet de prédire les écoulements incompressible sans l'utilisation d'un maillage [33,34]. Cette méthode a été adoptée par Giovannini et Karagiannis [35] à l'étude de l'écoulement non réactif dans un moteur alternatif. Cette démarche a nécessité l'introduction d'une compressibilité et a permis de caractériser les grosses structures tourbillonnaires en aval d'une soupape. Cette méthode permet une caractérisation de la turbulence dans des géométries simples. Des travaux récents ont été menés au Massachussets Institute of Technology par Ghoniem et ses collaborateurs pour des cas non réactifs [36-39] et réactifs [40-41]. Les résultats obtenus sont intéressants, mais l'utilisation de la transformation de Schwarz-Christoffel limite l'application de cette technique à des géométries élémentaires.

En résumé, le calcul de l'écoulement moyen, susceptible de comporter des instabilités hydrodynamiques à basse fréquence (quelques Hertz à quelques dizaines de Hertz), fait appel à des méthodes numériques délicates à mettre en œuvre et assez coûteuses en temps calcul. L'analyse de la stabilité nécessite encore la détermination des modes acoustiques de la cavité. Généralement, quand le foyer présente une géométrie proche de celle d'un cylindre,il est supposé que l'influence des perturbations de géométrie et de distribution de célérité du son peuvent être négligées. Cependant , des calculs de modes propres par une méthode d'éléments finis montre que cette hypothèse doit être remise en cause [42]. Si la démarche qui consiste à envisager de séparer l'écoulement moyen et l'acoustique conduit à des résultats intéressants, la précision des résultats est limitée et le coût des calculs est élevé. Cette démarche doit également être abandonnée en raison de l'absence de prise en considération des mécanismes non linéaires de la combustion turbulente.

Devant les limites évoquées précédemment, il a été envisager de simuler directement l'écoulement instationnaire turbulent, réactif et parfois biphasique. Cette démarche vise soit l'étude d'un écoulement moyen, représenté comme la limite asymptotique d'un mécanisme transitoire, soit à l'étude des phénomènes instationnaires. Cette dernière approche a été envisagée à l'ONERA [43-48], à la NASA [49], et à l'Ecole Centrale (CNRS) [18-20, 50, 51]. La simulation directe de l'écoulement comportant des structures tourbillonnaires à grande échelle, l'acoustique et les réactions chimiques, n'a été abordé que récemment au Naval Research Laboratory par l'équipe de Oran et Boris [52]. Les résultats obtenus sont impressionnants. Toutefois, la prise en considération d'un brouillard reste nécessaire et la combustion turbulente n'est pas prise en considération.

Les bases de la modélisation de la combustion d'un brouillard ont été posées par Williams [53,54]. Cette démarche est restée limitée pendant plus d'une décennie à un caractère purement formel. La présence d'ordinateurs puissants capables de prendre en compte les divers mécanismes décrits dans l'équation de Liouville-Boltzmann a conduit Westbrook [55] , en 1977, a une première tentative de résolution, suivi de Gupta et Bracco à l'Université de Princeton [56], pour des moteurs à combustion interne. Au début des années 1980, l'arrivée des super-ordinateurs vectoriels CRAY, a permis de d'aborder la résolution de l'écoulement turbulent, réactif, biphasique dans l'hypothèse d'une symétrie de révolution [58], puis en tridimensionnel dans un moteur à combustion interne [59,60] , au Los Alamos National Laboratory. Une application au cas d'un foyer à élargissement brusque a été effectuée par les concepteurs de KIVA [61]. Elle donne des résultats très réalistes, en particulier pour la forme du brouillard, comparable à celle relevée expérimentalement par Yule et Bolado [62] sur une expérience similaire.

Sous l'égide des services officiels (DRET), ce programme a été implanté sur les ordinateurs CRAY1S, puis CRAY XMP-18 de l'Office. Des tests ont été effectués en vue de vérifier les capacités de KIVA à simuler des mécanismes acoustiques non linéaires (tube à choc). Ensuite, des transformations ont été effectuées dans le programme en vue de permettre la simulation d'écoulements avec des flux entrants et sortants supersoniques et subsoniques. Les premiers résultats obtenus dans le cas d'un écoulement réactif, turbulent, biphasique et instationnaire sont présentés dans cet article.

La modélisation et les équations de base des divers mécanismes physico-chimiques mis en jeu sont présentés au paragraphe 2. Les aspects essentiels des méthodes numériques sont ensuite décrits au paragraphe 3. Cette présentation aborde séparément les phénomènes de champs et les conditions aux limites. Les résultats obtenus sont décrites au paragraphe 4 et discutés au paragraphe 5.

2-EQUATIONS DE BASE

La combustion d'un brouillard en régime instationnaire est décrite par les équations de bilan pour la phase gazeuse (paragraphe A), et par une équation de Liouville-Boltzmann qui permet d'évaluer les termes sources rencontrés dans les équations de bilan (paragraphe B). Les expressions détaillées sortent du cadre du présent article, ce qui conduit à se limiter à un minimum permettant la compréhension de la démarche suivie.

A- Equations de bilan pour la phase gazeuse

Dans tout ce qui suit, il va être supposé que le brouillard reste suffisamment dilué et que le volume déplacé par les gouttes reste négligeable. L'espèce indicée à l'unité est le combustible. Les equations de bilan pour la phase gazeuse sont celles de la densité de l'espèce m, la densité globale, la quantité de mouvement, l'énergie interne, l'énergie cinétique turbulente et l'équation d'état [59,60,63]

$$\frac{\partial \rho_m}{\partial t} + \nabla.(\rho_m \mathbf{u}) = \nabla.\left[\rho D\, \nabla\left(\frac{\rho_m}{\rho}\right)\right] + \dot{\rho}^{c}_{m} + \dot{\rho}_s \delta_{ml} \quad , \tag{1}$$

$$\frac{\partial \rho}{\partial t} + \nabla.(\rho \mathbf{u}) = \dot{\rho}_s \quad , \tag{2}$$

$$\frac{\partial}{\partial t}(\rho \mathbf{u}) + \nabla.(\rho\, \mathbf{u}\mathbf{u}) = -\nabla p + \nabla.\sigma + \mathbf{F}_s \quad , \tag{3}$$

$$\frac{\partial}{\partial t}(\rho I) + \nabla.(\rho I \mathbf{u}) = -p\,\nabla.\mathbf{u} + \sigma : \nabla \mathbf{u} + \nabla.\mathbf{J} + Q_c + Q_s + Q_T \, . \tag{4}$$

$$\frac{\partial}{\partial t}(\rho q) + \nabla.(\rho q \mathbf{u}) = -\frac{2}{3}\rho q\, \nabla.\mathbf{u} + \sigma : \nabla \mathbf{u} + \nabla.(\mu\, \nabla q) - \hat{D}\rho L^{-1} q^{3/2} + \dot{W}_s \quad , \tag{5}$$

$$p = R_g T \sum_m \frac{\rho_m}{\widehat{W}_m} \tag{6}$$

Dans le système ci-dessus, ρ_m est la densité de l'espèce m; $\rho = \sum_m \rho_m$,la densité globale; $\mathbf{u}$, le vecteur vitesse ; D, le coefficient de diffusion supposé constant pour toutes les espèces; $\dot{\rho}^{c}_{m}$, le taux de production de $\rho_m d\hat{u}$ aux réactions chimiques; $\dot{\rho}_s$, est le variation de la densité de l'espèce m= 1 $d\hat{u}$ à l'évaporation ou à la condensation; δ_{ml} désigne le symbole de Kronecker (δ_{ml} =1 si m=l ; sinon=0 si m ≠ l) . $\dot{\rho}^{c}_{m}$ et $\dot{\rho}_s$ vont être exprimés dans ce qui suit. Dans l'équation (3), p est la pression; $\sigma = \mu\,[\,\nabla \mathbf{u} + (\nabla \mathbf{u})^T\,] + (\nabla.\mathbf{u})\mathbf{I}$ est le tenseur des contraintes visqueuses où λ et μ sont les premiers et deuxièmes coefficients de viscosité; $(\,)^T$ et I designent respectivement un tenseur transposé et le tenseur unité; $\mathbf{F}_s$ est la quantité de mouvement par unité de volume et de temps transféré par le brouillard au fluide. Dans (4), I est l'énergie interne du fluide: $I(T) = \sum_m \rho_m / \rho\, I_m(T)$ (sans l'apport d'énergie dû aux réactions chimiques) ; $\mathbf{J} = -K\,\nabla T - \rho D \sum_m h_m \nabla(\rho_m/\rho)$, le flux de chaleur; $\dot{Q}_c$, la chaleur libérée par les réactions chimiques;$\dot{Q}_s$est un terme source associé à l'interaction entre le fluide et le brouillard, tandis que $\dot{Q}_T$ est associé à la turbulence. Dans (5), q désigne l'énergie cinétique turbulente. Les termes du second membre traduisent respectivement la création de turbulence par compression, cisaillement, diffusion de la turbulence, dissipation visqueuse et par le travail des tourbillons sur les gouttelettes. Dans (6), $\widehat{W}_m$ est la masse molaire de l'espèce m.

Dans le système précédent, plusieurs termes sources de la phase gazeuse doivent être explicités : $\dot{\rho}^{c}_{m}$, $\dot{Q}_c$, $\dot{Q}_T$ ainsi que l'expression de la viscosité dynamique μ. Pour un système de réactions chimiques

$$\sum_m a_{mr} \chi_m \rightleftharpoons \sum_m b_{mr} \chi_m \tag{7}$$

où χ_m représente une mole de l'espèce chimique m: a_{mr} et b_{mr} sont les coefficients stoechiométriques entiers pour la $r^{ème}$ réaction chimique, il vient:

$$\dot{\rho}^{c}_{m} = \widehat{W}_m \sum_r (b_{mr} - a_{mr})\, \dot{\omega}_r \, ; \quad \widehat{W}_m \sum_s (b_{ms} - a_{ms})\, \dot{\omega}_s \quad , \tag{8}$$

$$\dot{Q}_c = \sum_r q_r \dot{\omega}_r + \sum_s q_s \dot{\omega}_s \quad . \tag{9}$$

Dans (8) et (9), $\dot{\omega}_r$ et $\dot{\omega}_s$désignent respectivement les taux de production de la $r^{ème}$ réaction de cinétique chimique et de la $s^{ème}$réaction d'équilibre; q_r et q_s sont les chaleurs de réaction négatives au zéro absolu. Le taux de production $\dot{\omega}_r$ est evalué comme suit:

$$\dot{\omega}_r = k_{fr} \prod_m \left(\frac{\rho_m}{\widehat{W}_m}\right)^{a_{mr}} - k_{br} \prod_m \left(\frac{\rho_m}{\widehat{W}_m}\right)^{b_{mr}} \tag{10}$$

k_{fr} et k_{br} sont les coefficients directs et inverse de la réaction r et les exposants a_{mr} et b_{mr} spécifient l'ordre de la réaction (pour une réaction élémentaire $a_{mr} = a_{mr}$ et $b_{mr} = b_{mr}$). k_{fr} et kbr sont exprimés sous la forme d'un loi d'Arrhénius généralisée:

$$k_{fr} = A_{fr} T^{\zeta_{fr}} \exp\left[-\frac{E^{+}_{fr}}{T}\right] \tag{11}$$

$$k_{br} = A_{br} T^{\zeta_{br}} \exp\left[-\frac{E^{-}_{br}}{T}\right] \tag{12}$$

où E_{fr}^{+} et E_{fr}^{-} sont les températures d'activation (en Kelvins). Le taux de progression à l'équilibre $\dot{\omega}_s$ est donné par la condition:

$$\prod_m \left(\frac{\rho_m}{\widehat{W}_m}\right)^{b_{m''}-a_{m''}} = K_c^*(T) = \exp\left(A_s \ln T_A + \frac{B_s}{T_A} + C_s + D_s T_A + E_s T_A^2\right) , \qquad (13)$$

où $K_c^*(T)$ est la constante d'équilibre, écrite en fonction de la concentration pour la $s^{ième}$ espèce et $T_A = T / 1000$.

Dans l'équation (4), $\dot{Q}_T$ qui définit le terme source d'énergie dû à la turbulence prend la forme suivante:

$$\dot{Q}_T = A_0 \left(\hat{D} \rho L^{-1} q^{3/2} - \sigma : \nabla u \right) , \qquad (14)$$

où $A_0 = 0$, dans le cas où l'écoulement est laminaire et $A_0 = 1$, pour un écoulement turbulent. Le coefficient de viscosité dynamique μ est composé de trois termes:

$$\mu = \rho \nu_0 + \mu_{lam} + \mu_t = \rho \nu_0 + A_1 \frac{T^{3/2}}{T + A_2} + A \rho L q^{1/2} , \qquad (15)$$

où ν_0 est une diffusion turbulente uniforme; $A_1 = \mu_{lam}(T_{ref})$ et $A_2 = 110,4$ sont les coefficients de la loi de Sutherland et μ_t correspond à la viscosité turbulente; $A = O(0,05)$, $L = 2\Delta$ pour un maillage régulier où Δ est la taille d'une cellule dans le modèle Sub Grid Scale (S.G.S) [64,65]. Il est intéressant de noter que ce modèle de turbulence est proche de celui de Prandtl-Kolmogorov. Cette transformation peut être réalisée en changeant les valeurs des constantes et l'expression de la longueur L.

Dans le système des équations de bilan, il reste à exprimer les termes sources associés à la phase liquide, qui sont présentés dans le paragraphe suivant.

I -B Equations pour la phase liquide :

Les éléments essentiels de la dynamique de la phase liquide et son interaction avec la phase gazeuse sont prise en compte à travers une fonction de distribution f dérivée de la théorie cinétique des gaz [63,66] :

$$f(x, v, r, T_d, w', t)\, dv\, dr\, dT_d\, dw' \qquad (16)$$

Cette fonction donne le nombre probable de gouttelettes par unité de volume au point x et au temps t, avec des vitesses comprises entre v et v + dv, un rayon appartenant à intervalle [r, r + dr], des températures comprises entre T_d et $T_d + dT_d$, des fluctuations de vitesse turbulente dans intervalle [w', w' + dw']. Cette composante de vitesse turbulente est ajoutée à la vitesse moyenne du gaz dans le calcul de la traînée de la gouttelette et du taux d'évaporation. Il est également supposé que chaque composante de w' obéit à une distribution gaussienne avec une variance 2/3 q. Il est supposé que :

$$f(x, v, r, T_d, w', t) = f^*(x, v, r, T_d, t) \left[\frac{4\pi q}{3}\right]^{1/2} \exp\left[-\frac{3|w'|^2}{4q}\right] , \qquad (17)$$

où f^* est obtenue par intégration sur toutes les valeurs de w'.

La variation de f est obtenue en résolvant l' équation de Liouville-Boltzmann :

$$\frac{\partial f}{\partial t} + \nabla_x \cdot (f v) + \nabla_v \cdot (f F) + \frac{\partial (f R)}{\partial r} + \frac{\partial (f \dot{T}_d)}{\partial T_d} + \nabla_{w'} \cdot (f w') = f_{coll} . \qquad (18)$$

où les quantités F, R, $\dot{T}_d$, w' représentent les variations temporelles, en suivant une gouttelette isolée, de sa vitesse, son rayon, sa température et la fluctuation turbulente de vitesse du gaz.

L'accélération de la gouttelette F est donnée par le produit de la force d'inertie du gaz exercée sur la goutte par un coefficient de traînée, divisé par la masse de la gouttelette:

$$F = \frac{3}{8} \frac{\rho}{\rho_p} \frac{|u + w - v|}{r} (u + w - v) C_D \qquad (19)$$

où ρ_p est la densité du liquide et $C_D = \frac{24}{Re_p}\left(1 + \frac{1}{6} Re_p^{2/3}\right)$ si $Re_p = 2\rho|u + w - v|r / \mu_{air}(\hat{T}) < 1000$ (avec $\hat{T} = T + 2T_d/3$)

$C_D = 0,424$ si $Re_p < 1000$.

Le taux de variation du rayon de la gouttelette R est donné par la corrélation de Frossling [67] :

$$R = -\frac{(\rho D)_{air}(\hat{T})}{2\rho_p r} B_p S_h , \qquad (20)$$

avec $B_p = (Y_1^* - Y_1) / (1 - Y_1^*)$ (nombre de Spalding); $S_h = (2,0 + 0,6 Re_p^{1/2} Sc_p^{1/3}) (\ln(1 + B_p)) / B_p$ (nombre de Sherwood); $S_{cp} = \mu_{air}(\hat{T}) / \rho D_{air}(\hat{T})$ (nombre de Schmidt de la particule); $(\rho D)_{air}$ est la diffusivité du combustible gazeux dans l'air; $Y_1 = \rho_1 / \rho$ et Y_1^* est la fraction massique du combustible gazeux fournit par :

$$Y_1^*(T_d) = \frac{\widehat{W}_1}{\widehat{W}_1 + \widehat{W}_2\left(\frac{p}{p_v(T_d)} - 1\right)} . \qquad (21)$$

Dans (21). $\widehat{W}_0$ est la fraction molaire moyenne de toutes les espèces excepté la première; $p_v(T_d)$ désigne la pression de vapeur saturante à la température ambiante T_∞. Enfin, $(\rho D)_{air}(\hat{T}) = D_1 \hat{T}^{D_2}$, où D_1 et D_2 sont des constantes.

Le taux de variation de la température de la gouttelette est déterminé par le bilan d'énergie :

$$\rho_l \frac{4}{3} \pi r^3 C_l \dot{T}_d - \rho_l 4\pi r^2 \dot{R} L(T_d) = 4\pi r^2 Q_d . \qquad (22)$$

où Cl est la chaleur spécifique du liquide; L (Td), la chaleur latente de vaporisation; Qd , la conduction thermique à la surface de la goutte par unité d'aire. Physiquement, la relation (22) traduit un équilibre entre la chaleur apportée à la goutte qui sert à son chauffage ou fournit l'énergie pour la vaporisation. Qd est donné par la loi de Ranz-Marshall [67] :

$$Q_d = \frac{K_{air}(\hat{T})(T - T_d)}{2r} N_{up} . \qquad (23)$$

avec $N_{up} = (2,0 + 0,6\, R_{up}^{1/2} P_{rp}^{1/3})(\ln(1 + B_p))/B_p$ (nombre de Nusselt); $P_{rp} = \mu_{air}(\hat{T}) C_p(\hat{T}) / K_{air}(T)$,

$K_{air}(\hat{T}) = k_1 \hat{T}^{3/2}/(\hat{T} + K_2)$; où K_1 et K_2 sont des constantes.

Il est également supposé que l'énergie interne du liquide ne dépend que de la température. L'enthalpie du liquide présente quant à elle une faible dépendance vis à vis de la pression : $h_l(T_d) = l_l(T_d) + p/\rho_l$.

La fluctuation de vitesse turbulente du gaz est choisie de façon aléatoire suivant une distribution gaussienne (17) une fois tous les t_{seuil}, avec $t_{seuil} = \min\left(\frac{L}{q^{1/2}}, \frac{L}{|v - u|}\right)$

Le terme source f'_{coll} représente le taux de variation de f dû aux collisions. Il a pour expression :

$$f_{coll} = \frac{1}{2} \iint f^*(x, v, r_1, T_{d1}, t) f^*(x, v, r_2, T_{d2}, t)$$
$$\pi (r_1 + r_2)^2 \left\{ \sigma(v, x, T_d, v_1, r_1, T_{d1}, v_2, r_2, T_{d2}, x, t) \right.$$
$$\left. - \delta(r - r_1)\delta(v - v_1)\delta(T_d - T_{d1}) - \delta(r - r_2)\delta(v - v_2)\delta(T_d - T_{d2}) \right\} \qquad (24)$$
$$dr_1\, dv_1\, dT_{d1}\, dr_2\, dv_2\, dT_{d2}$$

La fonction σ est définie de façon que $\sigma\, d\,v\, dr\, dT_d$ soit le nombre probable de gouttes possédant des vitesses dans l'intervalle [v, v + dv], un rayon appartenant à [r, r + dr], des températures dans [T_d, T_d + dT_d], résultant de la collision d'une goutte possédant les propriétés 1 et une autre les propriétés 2. Deux types de collisions peuvent être rencontrés. Les gouttes peuvent aller vers une coalescence quand un paramètre d'impact b est inférieur à une valeur b_{co} et changer les valeurs de leurs composantes de vitesse tout en gardant les mêmes tailles et températures qu'avant la collision. Le paramètre b_{co} est donné par :

$$b_{co}^2 = (r_1 + r_2)^2 \min(1,0; 2\pi f(\gamma) / We_{12}) ,$$
$$f(\gamma) = \gamma^3 - 2,4\gamma^2 + 2,7\gamma . \qquad (25)$$

où $\gamma = r_2/r_1$ où $r_1 \le r_2$; $We_{12} = \rho_g |v_1 - v_2| r_1 / \sigma(\bar{T}_d)$, où σ est la tension superficielle du liquide. $\bar{T}_d = (r_1^3 T_{d1} + r_{2d}^3)/(r_1^3 + r_2^3)$

La forme adoptée pour σ est la suivante :

$$\sigma = \frac{b_{co}^2}{(r_1 + r_2)^2} \delta\left[r - (r_1^3 + r_2^3)^{1/3}\right] \delta\left[v - \frac{r_1^3 v_1 + r_2^3 v_2}{r_1^3 + r_2^3}\right] \delta\left[T_d - \frac{r_1^3 T_{d1} + r_2^3 T_{d2}}{r_1^3 + r_2^3}\right]$$
$$+ \frac{2}{(r_1 + r_2)} \int_{b_{co}}^{\infty} \left[\delta(r - r_1)\delta(v - v_1)\delta(T_d - T_{d1}) + \delta(r - r_2)\delta(v - v_2)\delta(T_d - T_{d2})\right] b\, db , \qquad (26)$$

où

$$v_1 = \frac{r_1^3 v_1 + r_2^3 v_2 + r_2^3 (v_1 - v_2) \frac{b - b_{co}}{r_1 + r_2 - b_{co}}}{r_1^3 + r_2^3} \qquad (27)$$

et

$$v_2 = \frac{r_1^3 v_1 + r_2^3 v_2 + r_2^3 (v_2 - v_1) \frac{b - b_{cr}}{r_1 + r_2 - b_{cr}}}{r_1^3 + r_2^3} \quad (28)$$

Il est maintenant possible d exprimer les termes sources $\dot{\rho}_s$, F_s, Q_s, W_s :

$$F_s = - \int f \frac{\partial}{\partial t}\left(\frac{4}{3}\pi \rho r^3 \rho_p v\right) dv\, dr\, dT_d\, du = - \int f \rho_p 4\pi r^2 R\, dv\, dr\, dT_d\, du \quad (29)$$

$$Q_s = - \int f \rho_p \left\{ 4\pi r^2 R \left[I_1(T_d) + \frac{1}{2}(v-u)^2 \right] + \frac{4}{3}\pi r^3 \left[C_1 T_d + F.(v-u-u) \right] \right\} dv\, dr\, dT_d\, du \quad (30)$$

$$\dot{\rho}_s = - \int f \frac{\partial}{\partial t}\left(\frac{4}{3}\pi \rho r^3 \rho_p\right) dv\, dr\, dT_d\, du = - \int f \rho_p 4\pi r^2 R\, dv\, dr\, dT_d\, du \quad (31)$$

$$W_s = - \int f \rho \frac{4}{3}\pi r^3 F.u\, dv\, dr\, dT_d\, du \quad (32)$$

Le système des équations de bilan pour la phase gazeuse et les termes de couplage de la phase liquide sont intégrés à l'aide d'un algorithme spécial mis au point à Los Alamos et dont les principales caractéristiques sont données dans ce qui suit

3- METHODES NUMERIQUES [59, 60]

La technique utilisée est du type volume fini. La plupart des grandeurs physiques sont avancées du temps t^n au temps t^{n+1} ($\Delta t^n = t^{n+1} - t^n$) en trois étapes. Dans la phase A, les effets des termes ne prenant pas en compte la pression et la convection sont intégrés. La phase B, encore appelée cycle lagrangien, intègre les termes liés à l'acoustique ainsi que la traînée des gouttelettes. Enfin la phase C, encore appelée remaillage ("rezoning" dans la littérature anglo-saxonne), permet le calcul des flux de masse et de quantité de mouvement.

Dans la discrétisation spatiale, les grandeurs thermodynamiques ou turbulentes sont définies au centre des hexaèdres irréguliers (Figure 1), tandis que les vitesses sont prises aux sommets des cellules (phase A et C), ou égales à la moyenne des vitesses relevées aux quatre sommets d'une face pendant la phase B.

Des cellules de quantité de mouvement sont également définies (Figure 2). Elles sont centrées sur le point i, j, k. Elles possèdent vingt-quatre faces, chacune d'entre elle étant formée d'un quart de la face d'une cellule régulière. Les volumes et les projections des faces suivant une direction donnée sont évaluées à partir des coordonnées des points d'une cellule [59].

Les calculs des intégrales de surface et de volume sont menés avec l'hypothèse que les intégrandes sont uniformes dans les cellules ou sur les faces. Les intégrales de surface sont évaluées en effectuant la somme pour toutes les faces - ou sous-faces -

$$\int F.\, dA = \sum_{\alpha} F_\alpha . A_\alpha \quad (33)$$

Il est également souvent nécessaire de calculer $(\nabla Q)_\alpha . A_\alpha$ sur une face, où Q désigne une grandeur scalaire connue

$$(\nabla Q)_\alpha \; A_\alpha = \left(\frac{Q_b - Q_a}{l_{ab}\, l_{ab}} \right) l_{ab} \; A_\alpha \quad (34)$$

où les point a et b sont les centres des cellules régulières séparés par la face α, l_{ab} est le vecteur qui joint les point a et b.

Les intégrales de surface portant sur la cellule de quantité de mouvement sont converties en intégrales de surface sur les cellules "régulières" à l'aide du Théorème de la divergence

$$\int Q\, dA = Q_{ijk}(A_a + A_b + A_c) = - \frac{1}{8} Q_{ijk}(A_d + A_e + A_f) . \quad (35)$$

où a, b, c sont les trois faces qui appartiennent à la cellule de quantité de mouvement de vecteur normal $A_{ijk}/4$.

La masse de la cellule régulière (i, j, k) est donnée par $M_{ijk} = \rho_{ijk} V_{ijk}$ et la masse de la cellule de quantité de mouvement est égale à

$$M_{ijk} = \frac{1}{8}\left(M_{ijk} + M_{i+1,jk} + M_{i+1,j+1,k} + M_{i,j+1,k} + M_{i,j,k+1} + M_{i+1,j,k+1} + M_{i+1,j+1,k+1} + M_{i,j+1,k+1} \right) \quad (36)$$

3-1 Technique de description des particules :

La technique de résolution est basée sur la méthode de Monte-Carlo. La fonction continue f est approchée par une distribution $\tilde{f}$ de la façon suivante :

$$\tilde{f} = \sum_{p=1}^{N_p} N_p \delta(\mathbf{x}-\mathbf{x}_p)\,\delta(\mathbf{v}-\mathbf{v}_p)\,\delta(r-r_p)\,\delta(T-T_{dp})\,\delta(\mathbf{u}-\mathbf{u}_p) \qquad (37)$$

Chaque particule p est composée de N_p gouttelettes, possédant les mêmes positions $\mathbf{x}_p$, vitesse $\mathbf{v}_p$, rayon r_p, température T_{dp} et soumise à une fluctuation de vitesse turbulente $\mathbf{u}'_p$ Les particules échangent de la masse, de la quantité de mouvement et de l'énergie avec le gaz dans la cellule de calcul où elles se situent (Appendice A dans [59]).

L'échantillonnage à l'injection est aléatoire. Supposons que la distribution f corresponde à la variable aléatoire x ($x_1 \le x \le x_2$.) La fonction de distribution est définie par dN = f (x) dx. Définissons la variable aléatoire $y = \int f(x)\,dx$ (dN = dy) . Ainsi, le nombre de gouttelettes est uniformément distribué par rapport à y .

Dans le cas où $\mathbf{u}'_p$ suit une distribution gaussienne G ($\mathbf{u}'$) :

$$\mathrm{erf}\left(\frac{x}{\sqrt{4q/3}}\right) = 2\int_0^{\mathbf{u}'} G(\mathbf{u}')\,d\mathbf{u} \qquad (38)$$

il faut procéder à l'inversion de la fonction erreur.

Il a été mentionné précédemment que la méthode d'intégration numérique comporte trois phases : A, B, C. Les principales opérations effectuées au cours de chacune d'entre d'elles sont décrites dans ce qui suit.

3-2 Phase A

Au cours de la phase A, les variables dépendantes sont mises à jour en calculant les termes autre que la pression et la convection.

Des masses partielles et totale de chaque cellule sont introduites au cours de la phase A·

$$(M_m)_{ijk} = \int_{V_m} \rho_m\,dV = (\rho_m)_{ijk} V_{ijk} \quad .$$
$$M_{ijk} = \int_{V_m} \rho\,dV = \rho_{ijk} V_{ijk} = \sum_m (M_m)_{ijk} \quad . \qquad (39)$$

où $\rho_m$est supposé constante dans la cellule (i,j,k).

Le calcul de la masse volumique de l'espèce m est effectué en deux temps. Dans une première étape, un "prédicteur" ρ_m est évalué par un schéma explicite pour les faces right (r), left (l), top (t), bottom (b) et une technique implicite pour les faces front (f) et derrière (d). Ce choix est dicté par la très petite dimension des cellules suivant la direction azimutale dans une chambre cylindrique.

Un schéma explicite aurait conduit à un pas de temps très faible. Dans une première, ρ_m est donné par :

$$\frac{(\rho_m)_{ijk} - (\rho_m)^n_{ijk}}{\Delta t} V_{ijk} = \sum_{\alpha = r,l,t,b} (\rho D)^n_\alpha \left[\nabla\left(\frac{\rho_m}{\rho}\right)^n\right]_\alpha \cdot \mathbf{A}^n_\alpha + \sum_{\alpha = f,d} (\rho D)^n_\alpha \left[\nabla\left(\frac{\rho_m}{\rho}\right)^n\right]_\alpha \cdot \mathbf{A}^n_\alpha \qquad (40)$$

Cette équation est linéaire suivant ρ_m et l'aspect implicite n'est présent que dans un direction. Ceci permet d'utiliser une technique directe non itérative pour évaluer ρ_m [59].

Les masses partielles de la cellule (i,j,k) sont ensuite données par:

$$\frac{(M_m)^{\hat{}}_{ijk} - (\rho_m)^n_{ijk} V^n_{ijk}}{\Delta t} = (\dot{\rho}^c_m)^{\hat{}}_{ijk} V^{\hat{}}_{ijk} = (\dot{\rho}_s)^{\hat{}}_{ijk} V^n_{ijk}\,\delta_{ml} \qquad (41)$$

Le terme $\dot{\rho}^c_m$ est défini dans (8) où $\dot{\omega}_r$ et $\dot{\omega}_s$ sont évalués avec les valeurs de la phase A (appendices D et E de [59]); le terme source $\dot{\rho}^{\hat{}}_s$ est donné par (48).

La masse totale de la cellule (sans le brouillard), après la phase A, est donnée par:

$$M^{\hat{}}_{ijk} = \sum_m (M_m)^{\hat{}}_{ijk} = M^n_{ijk} + \Delta t\,(\dot{\rho})^{\hat{}}_{ijk} V^n_{ijk} \quad . \qquad (42)$$

Il est maintenant possible de définir la densité de chaque espèce et la densité globale.

$$(\rho_m)^{\hat{}}_{ijk} = (M_m)^{\hat{}}_{ijk} / V^n_{ijk} \quad .$$
$$\rho^{\hat{}}_{ijk} = \frac{M^{\hat{}}_{ijk}}{V^n_{ijk}} \quad . \qquad (43)$$

Ces densités ne sont pas strictement lagrangiennes car elles font référence aux valeurs des volumes V^n_{ijk} prises à l'itération précédente. Les corrections nécessaires sont effectuées au cours de la phase B.

L'énergie spécifique interne E_{ijk} est aussi évaluée en supposant que cette grandeur est uniforme dans la cellule:

$$E_{ijk} = \int_{V_{ijk}} \rho\, I\, dV = \rho_{ijk} I_{ijk} V_{ijk} = M_{ijk} I_{ijk} \quad . \tag{44}$$

La valeur prise par E_{ijk} au cours de la phase A est donnée par :

$$\frac{E^{A}_{ijk} - E^{n}_{ijk}}{\Delta t} = V^{n}_{ijk} \frac{\Delta t_{ss}}{\Delta t} \sum_{\nu=1}^{N_{ss}} \left[\sigma^{\nu} : \nabla u^{\nu} \right]_{ijk} - \sum_{\alpha} J_{\alpha} . A^{n}_{\alpha}$$
$$+ \left\{ (\dot{Q}_{\epsilon})^{A}_{ijk} + (\dot{Q}_{\omega})^{A}_{ijk} + (\dot{Q}_{T})^{A}_{ijk} \right\} V^{n}_{ijk} \quad . \tag{45}$$

Les termes de dissipation visqueuse σ^{ν} sont évalués par un calcul où chaque sous-cycle ajoute la contribution pour un pas de temps $\Delta t_{ss} = \Delta t / N_{ss}$, où N_{ss} est le nombre de sous-cycles. Le pas de temps est choisi en vue de vérifier un critère de stabilité basé sur l'approximation explicite des termes de contraintes visqueuses dans l'équation de quantité de mouvement.

Les termes de flux de chaleur sont également décrits d'une manière explicite suivant les faces l, r, t, b et implicites suivant f et d :

$$J_{\alpha} . A_{\alpha} = \begin{cases} - K^{n}_{\alpha} (\nabla T^{n})_{\alpha} . A^{n}_{\alpha} - (\rho D)^{n}_{\alpha} \sum_{m} h_{m}(T^{n}_{\alpha}) \left[\nabla \left(\frac{\rho_{m}^{n}}{\rho^{n}} \right) \right]_{\alpha} . A^{n}_{\alpha} \quad . \\ \qquad (\alpha = l, r, t, b) \\ - K^{n}_{\alpha} (\nabla \tilde{T})_{\alpha} . A^{n}_{\alpha} - (\rho D)^{n}_{\alpha} \sum_{m} h_{m}(T^{n}_{\alpha}) \left[\nabla \left(\frac{\tilde{\rho}_{m}}{\rho^{n}} \right) \right]_{\alpha} . A^{n}_{\alpha} \quad . \\ \qquad (\alpha = f, d) \quad . \end{cases} \tag{46}$$

La valeur du prédicteur pour $\tilde{T}^{n+1}_{ijk}$ est obtenue en résolvant l'équation aux différences implicite :

$$M_{ijk} (C_{v})^{n}_{ijk} \frac{\tilde{T}_{ijk} - T^{n}_{ijk}}{\Delta t} = \sum_{\alpha = l,r,t,b} K^{n}_{\alpha} (\nabla \tilde{T})_{\alpha} . A^{n}_{\alpha}$$
$$+ \sum_{\alpha = f,d} K^{n}_{\alpha} (\nabla \tilde{T})_{\alpha} . A^{n}_{\alpha} \tag{47}$$

La quantité $(\dot{Q}_{\epsilon})^{A}_{ijk}$ est donnée par (9) où $\dot{\omega}_{r}$ et $\dot{\omega}_{s}$ sont evaluées en fonction des valeurs prises dans la phase A. Le calcul de $\dot{Q}_{\omega}$ est décrit dans l'appendice A de [59] et $\dot{Q}_{T}$ est décrit dans les lignes suivantes . La valeur de I_{ijk}, dans la phase A, est simplement donnée par :

$$I^{A}_{ijk} = \frac{E^{A}_{ijk}}{M^{A}_{ijk}} \quad . \tag{48}$$

La valeur de la température , dans la phases A, est calculée en inversant $I^{A}_{ijk} = \sum_{m} (\rho_{m} / \rho)\, I^{A}_{m}(T^{A}_{ijk})$, où $\frac{\rho_{m}}{\rho} = \left[\frac{M_{m}}{M} \right]^{A}_{ijk}$.

La pression peut alors être évaluée :

$$p^{A}_{ijk} = R_{g} T^{A}_{ijk} \sum_{m} \frac{(\rho_{m})^{A}_{ijk}}{W_{m}} \tag{49}$$

Le calcul de l'énergie cinétique turbulente est décomposé en trois étapes. Dans un premier temps, l'auto-diffusion de la turbulence est évalué par :

$$M^{n}_{ijk} \frac{\tilde{q}_{ijk} - q^{n}_{ijk}}{\Delta t} = \sum_{\alpha = l,r,t,b} K^{n}_{\alpha} (\nabla q)^{n}_{\alpha} . A^{n}_{\alpha} + \sum_{\alpha = f,d} K^{n}_{\alpha} (\nabla \tilde{q})_{\alpha} . A^{n}_{\alpha} \tag{50}$$

Ensuite, la production des contraintes turbulentes et l'amortissement de la turbulence sont approchés par un calcul de sous-cycles :

$$q^{\nu+1}_{ijk} = q^{\nu}_{ijk} + \frac{\Delta t_{ss}}{\rho^{n}_{ijk}} \left| \sigma^{\nu} : \nabla u \right|^{\nu}_{ijk} - \Delta t_{ss} D L^{-1} (q^{\nu}_{ijk})^{1/2} (q^{\nu+1}_{ijk})^{1/2}$$
$$\nu \in \{ 1, N_{ss} \} \tag{51}$$

Au début du sous-cycle, $\overset{\approx}{q}^{1}_{ijk} = \tilde{q}_{ijk}$. Le terme source $(\dot{Q}_T)^{\Lambda}_{ijk}$ de (45) est évalué par :

$$(\dot{Q}_T)^{\Lambda}_{ijk} = \frac{\Delta t_{vs}}{\Delta t} A_0 \sum_{v=1}^{N_{vs}} \left\{ \widehat{D}\, L^{-1} \rho^{n}_{ijk} q^{v+1}_{ijk} (q^{v}_{ijk})^{1/2} \cdot \left[\sigma^{v} : \nabla u^{v} \right]_{ijk} \right\} \quad . \tag{52}$$

Finalement, l'énergie cinétique turbulente pour la phase A est obtenue par:

$$\frac{M^{\Lambda}_{ijk} q^{\Lambda}_{ijk} - M^{n}_{ijk} \overset{\approx}{q}_{ijk}}{\Delta t} = (\dot{W}_s)^{\Lambda}_{ijk} V^{\Lambda}_{ijk} \quad . \tag{53}$$

où $\overset{\approx}{q}_{ijk} = \overset{\approx}{q}^{N_{vs}+1}_{ijk}$.

Les valeurs des composantes des vitesses dans la phase A sont données par:

$$(M^{\Lambda}_{ijk} + S^{\Lambda}_{ijk}) u^{\Lambda}_{ijk} - \widehat{M}^{n}_{ijk} u^{n}_{ijk} = \Delta t_{vs} \sum_{v=1}^{N_{vs}} \sum_{\alpha} \sigma^{v}_{\alpha} \cdot \widehat{A}_{\alpha} - R^{\Lambda}_{ijk} \quad . \tag{54}$$

où la sommation sur α porte sur les faces des cellules de quantité de mouvement; $\widehat{A_\alpha}$ est la normale à ces faces orientée vers l'extérieur; $\sigma_\alpha{}^v$ est la valeur du tenseur des contraintes dans la cellule où se trouve la face α de la cellule de quantité de mouvement.

L'évaluation du tenseur de quantité de mouvement est basé sur une valeur intermédiaire de la vitesse u^v (appendice F [59]).

La valeur intermédiaire de la vitesse est donnée par:

$$M^{n}_{ijk} (u^{v+1}_{ijk} - u^{v}_{ijk}) = \Delta t_{vs} \sum_{\alpha} \sigma^{v}_{\alpha} \cdot \widehat{A_\alpha} \quad . \tag{55}$$

Les quantités intermédiaires S^{Λ}_{ijk} et R^{Λ}_{ijk} sont associées au couplage implicite du gaz et de la vitesse des particules (Appendice A [59]).

La position des gouttelettes dans la phase A est définie par:

$$x^{\Lambda}_{p} = x^{n}_{p} + \Delta t\, v^{n}_{p} \quad . \tag{56}$$

Dans les phases B et C, les valeurs de x_p, r_p, u_p et Td_p ne sont pas modifiées. Ceci entraine :

$$\begin{aligned} x^{n+1}_{p} &= x^{\Lambda}_{p}; \qquad r^{n+1}_{p} = r^{\Lambda}_{p} \\ (u_p)^{n+1} &= (u_p)^{\Lambda}; \quad T^{n+1}_{\phi} = T^{\Lambda}_{\phi} \end{aligned} \tag{57}$$

3-3 Phase B :

Dans le technique du sous-cycle lagrangien, il est supposé que les sommets se déplacent temporairement à la vitesse locale du fluide. Ce calcul vise le traitement des ondes acoustiques, c'est à dire le gradient de pression dans l'équation de quantité de mouvement, les termes de dilatation dans l'équation de continuité et de l'énergie. Les forces de traînée sur les gouttelettes sont également incluses dans cette phase.

Le pas de temps du sous-cycle δt est un sous-multiple entier de Δt: $\delta t = \Delta t / N_{vs}$. L'indice du sous-cycle est désigné par v ($v \in [1, N_{vs}]$. Dans le calcul lagrangien, une technique du type face centrées est utilisée. Plutôt que d'introduire un systèmes au centre des faces, un facteur proportionnel à l'aire de la face de la cellule est utilisé [60].

Pour chaque face α, la variable utilisée est :

$$(u A)_{\alpha} = u_{\alpha} \cdot A_{\alpha} \quad . \tag{58}$$

Au début de chaque sous-cycle, $(u A)_{\alpha}$ est initialisée par :

$$(u A)_{\alpha} = \frac{1}{4} (u_a + u_b + u_c + u_d) \cdot A_{\alpha} \quad . \tag{59}$$

où a, b, c, d désignent les quatre sommets de la face α. Il est également nécessaire de définir la masse M_α de la cellule, qui est égale à la moyenne des masses de deux cellules adjacentes. De la même façon, une quantité S^{Λ}_{α}, qui prend en compte le couplage entre le gaz et les particules, est introduite pour le centre des faces:

$$S^{\Lambda}_{\alpha} = \left(\frac{S^{\Lambda}_{a} + S^{\Lambda}_{b} + S^{\Lambda}_{c} + S^{\Lambda}_{d}}{M^{\Lambda}_{a} + M^{\Lambda}_{b} + M^{\Lambda}_{c} + M^{\Lambda}_{d}} \right) \cdot M^{\Lambda}_{\alpha} \quad . \tag{60}$$

Les aires de la face A_α sont maintenues constantes au cours du sous-cycle et supposées égales à la valeur au début de la phase B. Le calcul n'est plus strictement lagrangien, mais il le reste cependant pour les termes d'ordre δt .

Les quantités $(u A)_{\alpha}$ sont calculées à partir des pressions en construisant de nouveaux volumes de contrôle de quantité de mouvement centrés sur la face α (Figure 3).

Désignons les faces du nouveau volume de contrôle associé à la face α par l'indice q. La quantité de mouvement $(u A)_{\alpha}$ est calculée à partir de (61):

$$(\widehat{M}^{\Lambda}_{\alpha} + S^{\Lambda}_{\alpha}) \left[(u A)^{v+1}_{\alpha} - (u A)^{v}_{\alpha} \right] = - \delta t \sum_{q} p^{(v)}_{q} \widehat{A}_{q} \cdot A_{\alpha} \quad . \tag{61}$$

qui correspond à l'équation fondamentale de la dynamique. Dans (61), $\widehat{A}_q$ est la normale à la face q orientée vers l'extérieur.

La valeur de p_q pour une face q commune à deux cellules régulières est la moyenne de la pression entre deux cellules adjacentes.

Les variations de volume d'une cellule au cours du sous-cycle sont évaluées comme suit :

$$V_{ijk}^{(\nu+1)} = V_{ijk}^{(\nu)} + \delta t \sum_{\alpha} (\mathbf{u}\mathbf{A})_{\alpha}^{(\nu+1)} \quad . \tag{62}$$

Ceci permet de calculer la pression, l'énergie interne et l'énergie cinétique turbulente :

$$p_{ijk}^{(\nu+1)} = p_{ijk}^{(\nu)} \left[\frac{V_{ijk}^{(\nu)}}{V_{ijk}^{(\nu+1)}} \right]^{\hat{\gamma}_{ijk}} + \delta p_{ijk} \quad , \tag{63}$$

$$I_{ijk}^{(\nu+1)} = I_{ijk}^{(\nu)} \left[\frac{V_{ijk}^{(\nu)}}{V_{ijk}^{(\nu+1)}} \right]^{\hat{\gamma}_{ijk}-1} \quad , \tag{64}$$

$$q_{ijk}^{(\nu+1)} = q_{ijk}^{(\nu)} - \frac{2}{3} q_{ijk}^{(\nu)} \left[\frac{V_{ijk}^{(\nu+1)}}{V_{ijk}^{(\nu)}} - 1 \right] \quad . \tag{65}$$

Dans (63), $\delta p_{ijk} = (\hat{p}_{ijk} - p_{ijk}^{n}) / N_{sub}$, représente les effets de variation de masse et d'énergie interne survenus au cours de la phase A rapportés sur chaque sous-cycle. La phase B étant lagrangienne, les masses des cellules et des sommets ne changent pas:

$$M_{ijk}^{B} = \hat{M}_{ijk} \quad , \quad \widehat{M}_{ijk}^{B} = \widehat{M}_{ijk} \quad , \tag{66}$$

et, par conséquent:

$$(\rho_m)_{ijk}^{B} = (M_m)_{ijk} / V_{ijk}^{B} \quad ; \quad \rho_{ijk}^{B} = \hat{M}_{ijk} / V_{ijk}^{B} \quad . \tag{67}$$

L'initialisation du sous-cycle est réalisée en posant :

$$\begin{aligned} \mathbf{u}_{ijk}^{(0)} &= \hat{\mathbf{u}}_{ijk} \; ; \; I_{ijk}^{(0)} = \hat{I}_{ijk} \; , \\ q_{ijk}^{(0)} &= \hat{q}_{ijk} \; ; \; p_{ijk}^{(0)} = \hat{p}_{ijk} \; ; \; r_{ijk}^{(0)} = r_{ijk}^{n} \; . \end{aligned} \tag{68}$$

Après le calcul du sous-cycle, les vitesses finales des gouttelettes $\mathbf{v}_p^{B} = \mathbf{v}_p^{n+1}$ sont évaluées en utilisant les vitesses dans la phase A.

Dans le cas où la grille est fixe (pas de paroi mobile), l'incrément de volume δV_{α} nécessaire au calcul des flux des quantités prises au centre des cellules est simplement égal à :

$$\delta V_{\alpha} = - \delta t \sum_{\nu=1}^{N_{sub}} (\mathbf{u}\mathbf{A})_{\alpha}^{(\nu)} \quad . \tag{69}$$

3-4 Phase C :

La phase C correspond au remaillage ("rezone phase" dans la littérature anglo-saxonne) au cours duquel le transport convectif associé aux déplacements des sommets pendant la phase B est calculé. Ce transport correspond au mouvement du fluide par rapport au maillage.

La valeur finale de la densité de l'espèce m est donnée par :

$$(M_m)_{ijk}^{n+1} = (M_m)_{ijk}^{n} + \sum_{\alpha} (\rho_m)_{\alpha}^{B} \delta V_{\alpha} \quad , \tag{70}$$

où la sommation porte sur les faces des cellules régulières. La masse finale totale de la cellule est par conséquent égale à :

$$M_{ijk}^{n+1} = M_{ijk}^{B} + \sum_{\alpha} \rho_{\alpha}^{B} \delta V_{\alpha} = \sum_{m} (M_m)_{ijk}^{n+1} \quad . \tag{71}$$

tandis que la masse finale des sommets est obtenue par (36). Il est maintenant possible d'évaluer la densité de l'espèce m et la densité globale :

$$(\rho_m)_{ijk}^{n+1} = (M_m)_{ijk}^{n+1} / V_{ijk}^{n+1} \; ; \; \rho_{ijk}^{n+1} = M_{ijk}^{n+1} / V_{ijk}^{n+1} \tag{72}$$

De la même façon, les valeurs finales de l'énergie interne: l'énergie spécifique interne et l'énergie cinétique turbulente sont données par

$$E_{ijk}^{n+1} = M_{ijk}^{B} I_{ijk}^{B} + \sum_{\alpha} (\rho I)_{\alpha}^{B} \delta V_{\alpha} \quad , \tag{73}$$

$$I_{ijk}^{n+1} = E_{ijk}^{n+1} / M_{ijk}^{n+1} \quad , \tag{74}$$

$$M_{ijk}^{n+1} q_{ijk}^{n+1} = M_{ijk}^{B} q_{ijk}^{B} + \sum_{\alpha} (\rho q)_{\alpha}^{B} \delta V_{\alpha} \tag{75}$$

Les grandeurs $(\rho_m)_{\alpha}^{B}$ dans (70) et $(\rho I)_{\alpha}^{B}$ sont évaluées avec un schéma " partial donor cell ", tandis que $(\rho q)_{\alpha}^{B}$ est calculé avec un schéma " full donor cell " (Appendice H, [59]), afin d'assurer la positivité de q.

La valeur finale de la température est obtenue en inversant $I_{ijk}^{n+1} (T) = \sum_{m} \left(\frac{\rho_m}{\rho} \right) I_m^{n+1} (T_{ijk}^{n+1})$ et en remplaçant ρ_m / ρ par

$(M_m / M)_{ijk}^{n+1}$. Ceci permet de déduire la pression à partir de l'équation d'état:

$$p_{ijk}^{n+1} = R_g T_{ijk}^{n+1} \sum_m (\rho_m)_{ijk}^{n+1} / \widehat{W}_m \quad . \qquad (76)$$

Le transport de la quantité de mouvement est calculé en terme d'incrément de masse à travers les faces de la cellule de quantité de mouvement. Cet accroissement de masse à travers la face α d'une cellule de quantité de mouvement est donné par :

$$\delta\widehat{M}_\alpha = \frac{1}{8}(\rho_o^B \delta V_o - \rho_i^B \delta V_i) \quad , \qquad (77)$$

où les indices "o" et "i" désignent les faces des cellules régulières situées de chaque côté de la face α de la cellule de quantité de mouvement. La face indicée "i" (interne) est celle qui coupe la cellule de quantité de mouvement , tandis que la face "o" ne la coupe pas. Il est commode d'associer $\delta\widehat{M}_\alpha$ avec la face et la cellule de quantité de mouvement en question. Quand la face α est vue depuis une autre cellule de quantité de mouvement qui lui est commune, "o" et "i" sont permutés et le signe de $\delta\widehat{M}_\alpha$ est inversé.

Le flux de quantité de mouvement peut maintenant être calculé par :

$$\widehat{M}_{ijk}^{n+1} w_{ijk}^{n+1} - \widehat{M}_{ijk}^B w_{ijk}^B = \sum_\alpha \delta M_\alpha w_\alpha^B \quad . \qquad (78)$$

où les valeurs de w_α^B sont calculées à partir d'un schéma du type " partial donor cell ". (Appendice H -[59]).

3-5 Description des conditions aux limites:

Dans la version initiale de KIVA, la cavité est fermée. Des modifications ont été apportées à plusieurs sous-programmes en vue d'imposer les vitesses et les flux des différentes variables, en coordonnées eulériennes et lagrangiennes.

La démarche généralement adoptée pour les écoulements non réactifs et monophasique consiste à imposer n-1 grandeurs en entrée(1 extrapolée) et une en sortie (n-1 extrapolées).

Plusieurs techniques peuvent être employées pour l'extrapolation. La méthode des caractéristiques, qui est la plus rigoureuse, est considérée comme la plus précise [70,75]. Des descriptions plus simples sont également utilisées. Il s'agit de conditions de non réflexion ou d'impédance [19,21,72,76,77], des extrapolation de (pente nulle) ou d'ordre un [78-81]. Enfin, il est parfois envisagé, pour un écoulement subsonique, d'imposer toutes les grandeurs en entrées en entrée et de toutes les extrapoler en sortie [78,82]. Cette démarche, bien que mathématiquement inexacte, permet parfois de supprimer des oscillations parasites.

Dans le cas d'écoulements tridimensionnels biphasiques et réactifs, l'utilisation de la technique des caractéristiques n'est plus envisagée en raison de sa complexité. L'extrapolation est effectuée par une technique de pente nulle qui donne de bons résultats (cette remarque est à rapprocher des conclusions de Chu et Sereny [83]).

Dans le plan d'entrée, la vitesse, la densité de chaque espèce, la direction de l'écoulement, l'énergie cinétique turbulente sont imposées. La masse volumique est calculée comme la somme des densités. La pression est extrapolée. La température est évaluée à partir de l'équation d'état. enfin, l'énergie spécifique interne est calculée.

Dans le plan de sortie, la pression est imposée. La densité de chaque espèce est extrapolée. La masse volumique est ensuite calculée comme pour le plan d'entrée. La température est ensuite évaluée à l'aide de l'équation d'état. Les composantes de la vitesse, de l'énergie cinétique turbulente et l'énergie spécifique interne sont extrapolées. Enfin, les particules qui atteignent le plan de sortie ne sont plus prises en compte (bien qu'elles soient représentées sur les tracés).

4- RESULTATS

L'installation considérée est décrite au paragraphe 4-1. Les conditions de fonctionnement sont décrites au paragraphe 4-2. Enfin, les résultats obtenus sont présentés dans la paragraphe 4-3.

4-1 Installation

L'installation est composée d'une entrée d'air et d'une chambre cylindriques présentant une symétrie de révolution. L'entrée d'air a un diamètre de 15 cm et une longueur réduite à 10 cm. La chambre présente un diamètre de 30 cm et une longueur de 40 cm. En aval de l'entrée d'air, le décrochement est brusque. L'injection est effectuée en aval de l'entrée d'air et le long de la paroi verticale de la marche. (Figure 4). Le choix de ce dernier point est retenu en vue d'assurer un bon fonctionnement du réacteur homogène situé en bas de la marche, et par conséquent, une combustion sans soufflage de flamme [10,11]. Le maillage est régulier et composé de mailles de 1 cm.

4-2 Conditions de fonctionnement envisagées

Dans l'entrée d'air, les conditions simulées sont les suivantes. La pression et la température statiques de l'air sont respectivement égales à 6,96 bars et 525 K. La densité de l'air, considéré ici comme composé d'oxygène et d'azote, est de 4,6 Kg/m^3. La vitesse de l'air est de 40 m /sec. Ceci correspond à un débit d'air de 2,83 Kg/sec. Le combustible injecté est de l'iso-octane ($C_8 H_{18}$) dont le rapport de mélange est de 0,0665 (proche du Kérosène : 0,0668). Sa température d'injection est de 293 K. La richesse est égale à l'unité. La masse de combustible injectée est de 9,42 g (pendant 50 ms). Les gouttes présentent un diamètre moyen de Sauter de 24 µm. Elles sont injectées avec une vitesses de 50 m/sec. Les jets conique sont pleins et présentent un demi-angle au sommet de 30°.

L'écoulement dans l'entrée d'air ne comporte pas de mise en vitesse azimutale ("swirl"). Le niveau de turbulence est de 1%.

L'étincelle d'allumage est représentée par un point chaud qui occupe quatre cellules en aval de la marche. La durée de l'apport d'énergie est de 1 ms. Douze espèces chimiques sont considérées ($C_8 H_{18}$, O_2, N_2, CO_2, H, H_2, O, N, OH, CO, NO). Quatre réactionsont retenues pour la cinétique chimique:

$$2\,C_8H_{18} + 25\,O_2 \rightarrow 16\,CO_2 + 18\,H_2O$$
$$O_2 + 2N_2 \rightleftharpoons 2N + 2NO$$
$$2O_2 + N_2 \rightleftharpoons 2O + 2NO$$
$$N_2 + 2\,OH \rightleftharpoons 2H + 2NO$$

Les réactions suivantes sont considérées comme étant à l'équilibre pour une température supérieure à 1500 K [60, 84]:

$$H_2 \rightleftharpoons 2H$$
$$O_2 \rightleftharpoons 2O$$
$$N_2 \rightleftharpoons 2N$$
$$O_2 + H_2 \rightleftharpoons 2\,OH$$
$$O_2 + 2H_2O \rightleftharpoons 4\,OH$$
$$O_2 + 2\,CO \rightleftharpoons 2\,CO_2$$

L'évaporation et la collision des particules sont prises en compte.

4-3 Description des résultats

Les résultats sont présentés suivant l'ordre chronologique.

Après 250 cycles, à t= 2,08724 ms, le brouillard s'étend sur quelques centimètres dans l'entrée d'air et la chambre (Figure 5a). L'écoulement est mis en vitesse dans l'entrée d'air (Figure 5b) et une onde acoustique bidimensionnelle est mise en évidence près du plan de sortie de la chambre (Figure 5c). Enfin, une perturbation d'énergie cinétique turbulente est observée au sommet de la marche (Figure 5d).

Au cycle 500, à t= 4,58724 ms (allumage terminé à 4 ms), les particules injectées au bas de la marche sont transportées par la turbulence, tandis que celles émises dans l'entrée d'air ont dépassé le sommet de la marche (Figure 6a). Le champ de vitesse montre d'une part des perturbations associées à l'injection en aval de la marche et d'autre part la présence d'une onde réfléchie plus en aval dans la chambre (Figure 6b). La présence du point chaud en bas de la marche, associé à l'allumage, est constatée sur la Figure 6c. L'énergie cinétique turbulente, présentée sur la Figure 6d, met en évidence deux zones de fortes amplitudes : le sommet et le bas de la marche. Enfin la concentration d'iso-octane montre l'existence d'un jet cylindrique en sortie de l'entrée d'air qui s'incurve vers le bas de la marche ainsi qu'un jet plus diffus en aval de celle-ci (Figure 6e).

Le cycle 750, à t= 7,08724 ms, montre que le jet de particules émis depuis l'entré d'air s'incurve fortement dans la recirculation tandis que celui qui est injecté depuis la marche diffuse fortement (Figure 7a).L'examen du champ de vitesse, présenté sur la Figure 7b, montre la présence d'une structure tourbillonnaire organisée. La position de sa frontière correspond bien à celle du jet de particules entraînées dans la recirculation. Le champ de pression montre que les ondes acoustiques réfléchies sur le fond arrière de la chambre sont remontées vers l' entrée d'air (Figure 7c). La zone chaude située le long de la marche occupe un volume plus important tandis que le jet de particules, plus froid, enveloppe le point chaud (Figure 7d). L'énergie cinétique turbulente présente une zone d'amplitude élevée d'une superficie accrue par rapport au cycles précédents (Figure 7e).Enfin, laconcentration d'iso-octane, décrite sur la Figure 7f, montre que le combustible est entraîné par le tourbillon.

Au cycle 1000, à t= 9,58706 ms, les particules issues de l'entrée d'air sont entraînées par le tourbillon précédemment. Les particules injectées forment d'abord un jet cylindrique de quelques centimètres qui diffuse ensuite fortement (Figure 8a). Le champ de vitesse montre l'existence d'une structure tourbillonnaire convectée et d'un petit tourbillon contra-rotatif dans le coin inférieur de la marche. De plus, une micro-explosion ("pop corn effect" [60]) est observée près du sommet de la marche (Figure 8b), sur la Figure 8c, des modes acoustiques transverseux sont mis en évidence dans l'entrée d'air et dans la chambre (en particulier le long de la marche). L'examen du champ de température montre que le point chaud en aval de la marche continue de s'étendre, tandis que les jets de particules, plus froid, entourent cette zone (Figure 8d). L'énergie cinétique turbulente met en évidence, d'une part une une zone de forte amplitude dans le sillage de la marche et d'autre part une "zone potentielle" associée au jet (Figure 8e). La concentration d'iso-octane (Figure 8f), met en évidence d'une part une zone présentant des valeurs élevées le long de la marche et d'autre part une zone en forme de champignon pour le combustible issu de l'entrée d'air. L'oxygène, dont la concentration est présentée sur la Figure 8g, s'engouffre à la frontière du tourbillon.

Au cycle 1200, à t= 11,5755 ms, les particules issues de l'entrée d'air sont entraînées plus en aval par la structure tourbillonnaire alors que le jet injecté sur la paroi de la marche s'étend sur quelques centimètres (Figure 9a). Le champ de vitesse, présenté sur la Figure 9b, montre une structure très différente de celles rencontrées précédemment. Le sillage de la marche comporte une zone où les vecteurs vitesse présentent une forme en V. Le phénomène du " pop corn" n'est pas observé. Dans le restant de la cavité, les structures ne sont plus observées. Des perturbations de pression de forte amplitude sont observées au même endroit (Figure 9c). Le champ de température présente un point chaud qui s'étire de plus en plus en aval. Il est entouré par des zones plus froides associées au brouillard (Figure 9d). La configuration du champ d'énergie cinétique turbulente est voisine de celle observée au cycle 1000, toutefois, la zone potentielle s'étend plus vers l'aval (Figure 9e). L'examen des champs de concentrations d'iso-octane (Figure 9f) et d'Oxygène (Figure 9g) est très intéressante. La structure en champignon observée précédemment s'étend plus en aval tandis que la zone de fortes concentrations est encore présente le long de la marche, mais aussi entre le "pied" et le "chapeau" du champignon, ce qui montre l'effet d'engouffrement. Un examen par superposition des courbes de concentration et de température montre que les interfaces correspondent bien.

Au cycle 1400, à t= 13,5486 ms, les particules issues de l'entrée d'air forment un jet cylindrique continu qui s'incurve dans la recirculation vers l'extrémité de la chambre. Le jet injecté le long de la marche reste cylindrique sur quelques centimètres comme sur les planches précédentes (Figure 10a). L'examen du champ de vitesse montre qu'une structure tourbillonnaire est à nouveau présente en aval de la marche. Le phénomène du "pop corn" est encore observé (Figure 10b). Une forte perturbation de pression est observée dans la partie arrière de la chambre ainsi que des modes transverseux (Figure 10c). Le champ de température montre que la zone chaude est plus étendue vers l'aval et que des zones plus froides, associées aux particules, sont observées sur chacun de ses côtés (Figure 10d). L'énergie cinétique turbulente présente une zone de valeurs élevées encore plus étendue vers l'aval et une zone potentielle pour le jet (Figure 10e).Les champs de concentrations pour l'iso-octane (Figure 10f) et l'oxygène (Figure 10g) confirment les résultats décrits au cycle 1200. l'examen par superposition des courbes de contours montre l'engouffrement d'oxygène sous le chapeau du champignon, tandis que l'iso-octane et l'oxygène coexistent en aval de la marche.

Au cycle 1500, à t= 14,0536 ms, le brouillard issu de l'entrée d'air a une configuration comparable à celle des cycles précédents. L'extrémité du tourbillon est près du plan de sortie. Le brouillard injecté le long de la marche pénètre sur quelques centimètres (Figure 11a). L'examen du champ de vitesse montre qu'une structure est à nouveau présente en aval de la marche. La couche cisaillée présente un profil sinueux. L'effet " pop corn" est observé en plusieurs endroits (Figure 11b). Des ondes acoustiques transversales sont mises en évidence dans le jet et vers le plan de sortie (Figure 11c). Le champ de température présente une zone chaude qui s'étend jusqu'à quelques centimètres du plan de sortie (Figure 11d). L'énergie cinétique turbulente présente une configuration comparable à celles précédemment trouvées (Figure 11e). L'examen par superposition des courbes de concentration d'iso-octane (Figure 11f) et d'oxygène (Figure 11g) confirme les remarques effectuées pour les cycles précédents.

Au cycle 1750, à t= 15,3036 ms, le jet de particules issu de l'entrée d'air atteint le plan de sortie de la chambre (les particules tracées sur celui-ci ne sont plus prises en compte dans le calcul). Le jet injecté dans la recirculation mesure toujours la même longueur (Figure 12a). L'examen du champ des vitesses montre qu'une structure tourbillonnaire est à nouveau en formation près du sommet de la marche (Figure 12b). Des ondes de pression acoustique remontent dans l'entrée d'air (figure 12c). La zone de température élevée s'étend maintenant jusqu'au plan de sortie. Elle est toujours encadrée par des zones froides associées aux particules (figure 12d). Le tracé de l'énergie cinétique turbulente montre l'existence d'une couche cisaillée et du cône potentiel du jet issu de l'entrée d'air (Figure 12e). L'examen des courbes de concentration d'iso-octane (figure 12f) et d'oxygène (Figure 12g) montre, là encore, des résultats intéressants. Le "chapeau" du champignon est séparé du "pied" de ce dernier. Une zone comportant de l'iso-octane mélangé à de l'oxygène est observée au fond avant. Le jet d'iso-octane émis depuis l'entrée d'air s'étend jusqu'au plan de sortie et rejoint l'axe de la chambre. Enfin, une poche de combustible, séparée par l'oxygène, du jet émis depuis l'entrée d'air, subsiste près de la "paroi" inférieure de la marche.

Au cycle 2000, à t=16,5471 ms, la configuration du brouillard est identique à celle trouvée au cycle 1750 (Figure 13a). L'examen du champ de vitesse est rendu difficile par les valeurs élevées rencontrées vers le plan de sortie (Figure 13b). Dans l'ensemble des cas, les jet axial est irrotationnel tandis que l'écoulement dans la recirculation montre une structure tourbillonnaire. Une perturbation de pression transversale élevée est observée près du plan de sortie (Figure 13c). Le camp de température a une configuration identique à celle précédemment observée (figure 13d). La présence de fortes perturbations d'énergie cinétique turbulente près du plan de sortie ne permet pas d'interpréter les résultats obtenus pour cette variable (figure 13e). Enfin, les configurations trouvées pour l'iso-octane (Figure 13f) et l'oxygène (figure 13g) sont comparables à celles du cycle 1750. Les positions des zones isolées sont pratiquement comparables à celles du cycle 1750. Les positions des zones isolées sont pratiquement identiques. Ilot de combustible a cependant une surface plus faible.

5- DISCUSSION DES RESULTATS

La mise en vitesse de l'écoulement ainsi que l'allumage engendrent des ondes acoustiques non linéaires dont la configuration est complexe. La diffraction d'une onde acoustique au sommet de la marche produit une structure tourbillonnaire [14 , 85 ,87].

Le brouillard injecté sur le côté de la marche est prémélangé avec l'oxygène. Il permet une stabilisation de la flamme (réacteur homogène). Ceci explique que le jet disparaisse après quelques centimètres. Les particules issues de l'entrée d'air brûlent au contact d'un îlot d'oxygène. Il s'agit d'une flamme de diffusion analogue à celle décrite analytiquement par Karagozian et Manda [88] et numériquement par Laverdant et Candel [89-91]. Des configurations analogues à celles- ci ont été observées à maintes reprises (par exemple [5,12,14-17,21,37,41,46]).expansion des produits de combustion dilate la poche d'oxygène, située entre le pied et le chapeau du champignon, et engendre une poche d'iso-octane contre la paroi.

La zone potentielle du jet, mise en évidence pour l'énergie cinétique turbulente, a une longueur conforme à celle citée dans la littérature (4 à 5 rayons de l'entrée d'air [92]).

Schématiquement, l'écoulement peut être décomposé en deux zones. Il s'agit d'une part du jet issu de l'entrée d'air, qui est irrotationnel (zone potentielle), et d'autre part, de la recirculation tourbillonnaire. L'interface est constituée par une couche de mélange qui présente des instabilités hydrodynamiques.

Le phénomène du " pop corn" est considéré par les concepteurs de KIVA comme étant d'origine numérique [60]. Parmi les moyens d'élimination de ce phénomène, le raffinement de maillage est le plus facilement applicable. Les techniques qui consistent à épaissir artificiellement la zone de flamme par un accroissement des coefficients de diffusion et une diminution des taux de production chimiques [93] ainsi que le remaillage qui suit la zone de flamme sont respectivement mal adapté à l'écoulement (mais très efficace en laminaire) et difficile à mettre en œuvre.

6-CONCLUSION

L'adaptation du programme KIVA, initialement conçu pour les moteurs à combustion interne, a permis de simuler le début du fonctionnement d'un foyer de statoréacteur à élargissement brusque.

Les modifications pour traiter les flux entrant et sortant, initialement absents du programme, donnent des résultats physiquement réalistes. L'utilisation d'une technique de pente nulle, liée aux difficultés que présenterait la mis en œuvre de la méthode des caractéristiques pour un écoulement tridimensionnel, biphasique et réactif , donne de bons résultats.

L'injection du brouillard en aval de la marche conduit à une combustion prémélangée dans la recirculation. Ce fonctionnement, du type réacteur homogène, permet une combustion sans soufflage de flamme. Le combustible injecté dans l'entrée d'air enveloppe le point chaud situé en aval de la marche et brûle avec une flamme de diffusion. La structure est du type champignon, souvent citée dans la littérature

Des instabilités d'origine numériques, liées à la faible définition du maillage dans la zone de flamme, ont été rencontrées précédemment par les concepteurs de KIVA. Un raffinement du maillage devrait permettre de supprimer ces phénomènes parasites.

Les caractéristiques hydrodynamiques de l'écoulement sont également réalistes. Le jet issu de l'entrée d'air est irrotationnel tandis que la recirculation comporte des structures tourbillonnaires. L'interface présente des instabilités hydrodynamiques.

Les travaux ultérieurs vont porter sur l'influence de la définition du maillage. L'influence des parois doit également être prise en considération. Les modèles de combustion turbulente doivent être testés. La présence de structures tourbillonnaires et la combustion dans des tourbillons conduit à envisager un modèle de turbulence du type "Sub Grid Scale" (S.G.S) et le modèle de flamme cohérente développé par Marble et Broadwell [19,94-96].

REFERENCES

[1] BARRERE, M., WILLIAMS, F.A.-"Comparison of Combustion Instabilities Found in Various Types of Combustion Chambers", 12 th Symp. (Int.) on Combustion, pp.169, 181, 1968.

[2] CULICK,F.E.M - "Measurement of Wall Heat Transfer in the Presence of Large- Amplitude Combustion Oscillations", Combustion Science and Technology, Vol.9, pp.49,53, 1974.

[3] CROCCO, L. -"Theoretical Studies on Liquid- Propellant Rocket Instability", 10 th Symp. (Int.) on Combustion, pp.1101,1128, 1965.

[4] BENDOT, J. -Communication au cours de la réunion MWDDEA sue les instabilités des statoréacteurs du 29/11/82 au 3/12/82.

[5] MARBLE,F.E. ,ROGERS, D.E. -"A Mechanism for High Frequency Oscillation in Ramjet Combustor and Afterburners", ARS Journ., June 1956, pp.456, 462.

[6] CROCCO, L., CHENG, S.I. -"Theory of Combustion Instability in Liquid Propellant Rocket Motors", AGARDograph n°8, 1956.

[7] TSIEN, H.S. -"Servostabilization of Combustion in Rocket Motors", Journ. Amer.Rocket Soc., 22, 1952.

[8] HECKL, M.A. -"Active Control of the Noise in a Rijke Tube", Symp. IUTAM, 1985, Lyon, Springer Verlag.

[9] LANG, W., POINSOT, T, CANDEL, S.M. -"Active Control of Combustion Instability", Combustion and Flame, Vol.70,n°3, Déc.1987.

[10] HEBRARD, P., LAVERGNE, G., TOULOUSE, G. -Etude et Modélisation de l'Ecoulement dans un foyer de Statoréacteur à Deux Entrées par le Fond, R.T.S final CERT-DERMES n°1/2116, Fev.1981.

[11] STULL, F.D, CRAIG, R.R ,STREBY, G.D., VANKA, S.P.-"Investigation of Dual Inlet side Dump Combustor Using Liquid Fuel Injection", AIAA Paper n°83- 0420, 1983.

[12] ESCUDIE, D., CHARNAY, G. "Experimental Study of Interaction Between a Premixed Laminar Flame and Coherent Structures", Turbulent Shear Flows Symp. 5th, Springer Verlag, Cornell University, New York, 1985

[13] MOREAU ,P.- "Experimental Determination of Probability Density Functions Within a Turbulent High Velocity Premixed Flame", 18th Symp. (Int.) on Comb, pp.993, 1000,1981.

[14] BARKER, C.L. -"Experiment Concerning the Occuring and Mechanism of High Frequency Combustion Instability", Ph. D. Thesis, California Inst. of Technology, 1958.

[15] MOREAU, P., LABBE, J., DUPOIRIEUX, F., BORGHI, R.-" Experimental and Numerical Study of a Turbulent Recirculation Zone with Combustion", Turbulent Shear Flows Symp. 5th, Springer Verlag, Cornell University, New York, 1985

[16] SMITH, D.A., ZUKOSKI, E.E.- " Combustion Instability Sustained by Unsteady vortex Combustion", AIAA/ SAE / ASEE 21st Joint Propulsion Conf., Monterey, California, 1985.

[17] KELLER, J.O., VANEVELD, L., KORSHELT,D., GHONIEM, A.F.,DAILY, J.W., OPPENHEIM, A.K. "Mechanims of Instabilities in Turbulent Combustion Leading to Flashback", AIAA Jour.20, pp.254, 262, 1982.

[18] GROUSET, D.- Modélisation de l'Ecoulement dans un Foyer de Prémélange ,Thèse de Docteur Ingénieur, Ecole Centrale de Paris, 1980.

[19] DARABIHA, N.-Un Modèle de Flamme Cohérente pour la Combustion Prémélangée- Analyse d'un Foyer Turbulent à élargissement Brusque , Thèse Docteur Ingénieur de l'Ecole Centrale de Paris, 1985.

[20] HOSSEINI, K.M.- Analyse des Zones de Recirculation dans un Foyer Turbulent Prémélangé, Thèse de Docteur Ingénieur, Ecole Centrale de Paris, 1986.

[21] POINSOT, T.-Analyse des Instabilités de Combustion de Foyers Turbulents Prémélangés, Thèse d'Etat de l'Université de Paris Sud, Orsay, 1987

[22] YANG, V., CULICK, F.E.C. "Linear Theory of Pressure Oscillations in Liquid-Fueled Ramjet Engines" AIAA Paper n° 83-0574- 1983.

[24] HUMPHREY, J.W., CULICK, F.E.C. "Pressure Oscillations and Acoustic Entropy Interactions in Ramjet Combustion chambers", AIAA Paper n°87- 1872.

[25] YANG, V., KIM, S.I., CULICK, F.E.C -"Third-Order Nonlinear Acoustic Waves and Triggering of Pressure Oscillations in Combustion Chambers", Part I- Longitudinal Oscillations AIAA Paper n° 87- 1873, 1987.

[26] NAYFEH, A.H. "Perturbation Methods", J.Wiley and Sons, New York, 1973.

[27] LILLEY, D.G. "Flowfield Modeling in Practical Combustors : A Review" , Journ. of Energy, Vol.3, n°4, pp.193,210, July-Aug. 1979.

[28] LILLEY, D.G. " Computer Modeling in Ramjet Combustors", AIAA Journ., Vol.19, n°12, pp.1562,1563, 1980.

[29] LILLEY, D.G. " Prospects for Computer Modeling in Ramjet Combustors" AIAA Paper n°80-1189., 1980.

[30] LILLEY, D.G. , RHODE, D.L., SAMPLE, J.W. -"Prediction of Swirling Reacting Flow in Ramjet Combustors", AIAA Paper n°81- 1485, 1981.

[31] BROWN, E.F., HALE,A.A "Calculation of the flow in a Dump Combustor", AIAA Paper n°85-1309, 1985.

[32] BOYSAN, F., AYERS, W.H., SWITHENBANK, J., PAN, Z. "Three Dimensional Model of spray Combustion in Gas Turbine Combustors ", Journ. of Energy, Vol.6,n°6, pp.368, 375, Nov.-Dec. 1982.

[33] OPPENHEIM, A.K. -"Dynamic Features of Combustion", Phil. Trans. Roy.Soc. London, **A**, 315, pp. 471, 508, 1985.

[34] GIOVANNINI, A., OPPENHEIM, A.K. Analyse de Différents Types d'Ecoulements Internes par la Méthode des Vortex Aléatoires, Journ.de Mécanique Théorique et Appliquée, Vol.6, n°6, pp.771, 787, 1987.

[35] GIOVANNINI, A., KARAGIANNIS, F.- Caractérisation des Grosses Structures Rotationnelles de l'Ecoulement dans le Cylindre du Moteur Alternatif par la Méthode des Vortex Aléatoires, Entropie, n°139, 1988.

[36] GHONIEM, A.F., GAGNON, Y. "Numerical Investigations of Recirculating Flow at Moderate Reynolds Numbers" AIAA Paper n°1986- 0370.

[37] GHONIEM, A.F., NG, K.K " Numerical Study of the Dynamics of a Forced Shear Layer", Phys. of Fluids, 30,(3), pp.706, 721, March.1987.

[38] SETHIAN, J.A., GHONIEM, A.F." Validation Study of Vortex Methods", Journ. of Computational Physics, 74, pp.283, 317, 1988.

[39] NAJM, H.N., GHONIEM, A.F. "Numerical Simulation of the Convective Instability in a Dump ",AIAA Paper,n°87-1874, 1987.

[40] GHONIEM, A.F.,HEIDARINEJAD, G., KRISHNAN, A. "Numerical Simulation of a Reacting Shear Layer Using the Transport Element Method ", AIAA Paper n°87-1718, 1987.

[41] GHONIEM, A.F. "Effect of Large Structures on Turbulent Flame Propagation", Combustion and Flame, 64, pp.321, 336, 1986.

[42] LAVERDANT, A., POINSOT, T., CANDEL, S.M. "Influence of the Mean Temperature Field on the Acoustic Mode Structure in a Dump Combustor", Journ. of Prop. and Power, Vol.2, n°4, pp.311, 316, 1985.

[43] HIRSINGER, F. -Modélisation en Aérothermodynamique Instationnaire", La Recherche Aérospatiale, N° 1979,5, pp.307, 323.

[44] HIRSINGER, F. , TICHTINSKY, H. " Modélisation des Zones de combustion en Régime Instationnaire", 54th Propulsion and Energetics Panel, AGARD, Cologne, 3rd-5th October, 1979.

[45] MAGRE, P. "Semi-Implicit Calculation of the Flow Field in a Duct with the Flame Stabilized by a Step", 6th Int. Symp. on Air Breathing Propulsion, June 6-10, 1983, Paris.

[46] DUPOIRIEUX, F., SCHERRER, D. Méthodes Numériques à Convergence Rapide Utilisées pour le Calcul d'Ecoulements Réactifs, La Recherche Aérospatiale, 1985-5, pp.301, 310.

[47] DUPOIRIEUX, F.- Calcul Numérique d'Ecoulements Turbulents Réactifs et Comparaison avec des Résultats Expérimentaux, La Recherche Aérospatiale, 1986-6, pp. 443, 453.

[48] DUPOIRIEUX, F., DUTOYA, D.- Modèle Numérique pour les Ecoulements Réactifs Axisymétriques avec Vitesse Tangentielle, La Recherche Aérospatiale, 1987, 6, pp.15, 22.

[49] DRUMMOND, J.P. "Numerical Study of a Ramjet Dump Combustor Flow Field", AIAA Paper n°83- 0421.

[50] GROUSET, D., ESPOSITO, E., CANDEL, S.M.- "Model of the Recirculating Flow in a Premixed Combustor", 7th ICOGER, Göttingen, Aug. 20-24, 1979. et Progress in Astronautics and Aeronautics, Combustion in Reactive Systems, Vol.76, AIAA, New York, pp.360, 380, 1981.

[51] CANDEL, S.M., DARABIHA, N., ESPOSITO,E. -" Models for a Turbulent Premixed Dump Combustor", AIAA Paper n°82-1261., 1982.

[52] KAILASANATH, K.,J., GARDNER,J.,BORIS, J.P.,ORAN, E. -"Interactions between Acoustics and Vortex Structures in a Central Dump Combustor, AIAA Paper n° 86-1609, 1986.

[53] WILLIAMS, F.A. -"Progress in Spray -Combustion Analysis " ,8th Symp. (Int.) on Comb, pp. 50,62, 1962.

[54] WILLIAMS, F.A. -"Combustion Theory "- The Fundamental Theory chemically Reacting Flow Systems"-2nd Edition, Benjamin Cummings Pub. Comp., 1985.

[55] KUO, K.K -" Principles of Combustion", Wiley Interscience Publication, J. WILEY and Sons, New York, 1986.

[56] WESTBROOK, C.K. -" Three- Dimensional Numerical Modeling of Liquid Fuel Sprays", 16th Symp. (Int) on Comb., 1977.

[57] GUPTA, H.C., BRACCO, F.V. -" Numerical Applications of Two-Dimensional Unsteady Sprays for Applications to Engines", AIAA Journ., Vol.16, n°10, Oct.1978, pp.1053, 1061.

[58] CLOUTMAN, L.D., DUKOWICZ, J.K., RAMSHAW, J.D., AMSDEN, A.A. -" CONCHAS- SPRAY : A Computer Code for Reactive Flows with Fuel Sprays", Los Alamos National Laboratory Rept., LA-9294, May 1982.

[59] AMSDEN, A.A., RAMSHAW, J.D., O'ROURKE, P.J., DUKOWICZ, J.K. -" KIVA : A Computer Program for Two and Three Dimensional Fluid Flows with Chemical Reactions and Fuel Sprays", Los Alamos National Laboratory Rept., LA- 10245 MS, Feb.1985.

[60] AMSDEN, A.A., RAMSHAW, J.D., CLOUTMAN, L.D., O'ROURKE, P.J. -" Improvements and Extensions to the KIVA Computer Program", Los Alamos National Laboratory , LA-10534, MS, Oct.1985.

[61] O'ROURKE, P.J. -" The KIVA Computer Program for Multidimensional Chemically Reactive Fluid Flows with Fuel Sprays", Numerical Simulation of Combustion Phenomena Proceeding, Sophia - Antipolis, France, 1985.

[62] YULE, A.J., BOLADO, R. -" Fuel Spray Burning Regime and Initial Conditions", Combustion and Flame, 55, pp.1, 12, 1984.

[63] KUENTZMANN, P. Aérothermochimie des Suspensions, Mémoire de Sciences Physiques, Gauthier-Villard, 1973, Paris.

[64] MATHIEU, J., JEANDEL, D., LAUNDER, B.E., REYNOLDS, W.C., RODI, W. - "La Simulation des Modèles de Turbulence et leurs Applications Vol. 1 et 2 CEA-INRIA-EDF Ecole d'Eté et d'analyse Numérique Eyrolles éd., Paris, 1984.

[65] FERZIGER, J.H. -"Large Eddy Simulation : its Role in Turbulence Research " dans Theoretical Approches to Turbulence, Appl.Math. Sci., 58, Dwoyer, D.C., Hussaini, M.Y., Voigt, R.G. éd., Springer Verlag, 1985.

[66] SIVOUKHINE, D. Cours de Physique Générale Tome 2- Thermodynamique et Physique Moléculaire , Edition de Moscou, 1982.

[67] FAETH, G.M. "Evaporation and Combustion of Fuel Sprays", Progress in Energy and combustion Science, Vol.9, pp.1, 76, 1983.

[68] O'ROURKE, P.J. -" Collective Drop Effects in Vaporizing Liquid Sprays", Ph.D. Thesis, Princeton University et Los Alamos National Laboratory Rept., L.A.- 9069-T- Nov.1981.

[69] BORIS,J.P.- "Vectorized Tridiagonal Solvers", Naval Research Laboratory Memo. Rept. 3048, Nov.1976.

[70] MORETTI, G.- " A Physical Approach to the Numerical Treatment of Boundaries in Gas Dynamics", NASA conference Publication 2201 NASA Ames Research Center, Moffet Field , Ca., Oct. 19,20, 1981.

[71] VEUILLOT, J.P., VIVIAND, H.- Méthodes Pseudo- Instationnaires pour le Calcul d'Ecoulements Transsoniques, Publication ONERA n° 1978-4.

[72] CLINE, M.C., WILMOTH, R.G.- " Computation of the Schuttle Solid Booster Nozzle Start - Up Transient Flow", Journ. of Propulsion and Power, Vol.1, n°5, Sept-Oct 1985.

[73] CAMBIER, L., ESCANDE, B., VEUILLOT, J.P. -Calcul d'Ecoulements Internes à Grand Nombre de Reynolds par Résolution Numérique des Equations de Navier- Stokes , La Recherche Aérospatiale, 1986, n°6, pp.415,432.

[74] YEE, H.C., BEAM, R.M., WARMING, R.F. - " Boundary Approximations for Implicit Schemes for One Dimensional Inviscid Equations of Gasdynamics", AIAA Journ. , vol.20, n°9, Sept.1982, pp.1203, 1211.

[75] WALKINGTON, N.J., EVERSMAN, W. - " A Numerical Model of Acoustic Chocking, Part I : Shock Free Solutions", Journ. of Sound and Vibrations, 1983, **90** (4), pp.509,526.

[76] BAYLISS, A., TURKEL, E.- " Outflow Boundary Conditions for Fluid Dynamics", SIAM Journ. Sci. Stat. Comput., Vol.3, n°2, June 1982, pp.250, 259.

[77] HEDSTROM, W.- "Non Reflecting Boundary Conditions for Nonlinear Hyperbolic Systems", Journ. of Comput. Phys., Vol.30, 1979, pp.222, 237.

[78] RAMSHAW, J.D., DUKOWICZ, J.K. -" APACHE : A Generalized- Mesh Eulerian Computer Code for Multicomponent Chemically Reactive Fluid Flow", Los Alamos National Laboratory Rept., n°LA-7427, Jan.1979.

[79] AMSDEN, A.A., RUPPEL, H.M. - " SALE 3D: A Simplified ALE Computer Program for Calculating Three- Dimensional Fluid Flow", Los Alamos National Laboratory Rept., LA-8905, Jan.1982.

[80] SCOTT, J.N., HANKEY, W.L. - " Numerical simulation of Exited Jet Mixing Layers", AIAA Paper n° 87-0016, AIAA 25 th Aerospace Sciences Meeting, Jan. 12-15 th, 1987,Reno, Nev.

[81] BORIS, J.P., ORAN, E.S., FRITTS, M.J., OSWALD, C. -" Time Dependant, Compressible Simulations of Shear Flows: Tests of Outflow Boundary Conditions", N.R.L. Memorandum-Rept. 5249, Dec.12th ,1983.

[82] RUDY, D.H., STRIKWERDA, J.C. - " Boundary conditions for subsonic Compressible Navier-Stokes Calculations", Computers and Fluids, Vol.9, pp.327, 338, 1981.

[83] CHU, C.K., SERENY, A.- " Boundary Conditions in Finite Difference Fluid Dynamic Codes", Journ. of Comput. Phys., Vol.15, pp.476, 491, 1974.

[84] MEINTJES, K., MORGAN,A.P. -" Equilibrium Equations for a Model of Combustion", General Motors Research Laboratories Report GMR- 4361, 1983.

[85] ROTT, N.- " Diffraction of a Shock Wave with Vortex Generation", Journ. of Fluid Mechanics, Vol.1, 1956.

[86] WALDRON, H.F. " An Experimental Study of a Spiral Vortex Formed by Shock-Wave Diffraction", Inst. of Aerophys., UTIA Tech. note n°2, Sept.1954, Univ. of Toronto.

[87] GARNIER, F., LAVERDANT, A.M. - " Etude du Couplage Acoustique Structures Tourbillonnaires. Synthèse Bibliographique, Modélisation analytique Simplifiée et Simulation Numérique du Tourbillon Associé à la Diffraction d'un Choc par un Diaphragme", Rapport Technique ONERA n° 10/3562 EN, 25 Jan. 1988

[88] KARAGOZIAN, A.N., MANDA,, B.V.S. -" Flame Structure and Fuel Consumption in the Field of a Vortex Pair", Comb. Sci. and Tech., Vol.49, pp.185, 200, 1986.

[89] LAVERDANT, A.M., CANDEL, S.M. - " A Numerical Analysis of a Diffusion Flame-Vortex Interaction", ONERA TP n°1987-26, (accepté dans Comb. Sci. and Tech.)

[90] LAVERDANT, A.M., CANDEL, S.M. - "Computation of Diffusion and Premixed Flames Rolled-Up in Vortex Structures", AIAA Paper n°87-1779, 23rd Joint Propulsion Conference , San Diego, Ca.,1987, (accepté dans Journ. of Prop. and Power).

[91] LAVERDANT, A.M., CANDEL, S.M. - Etude de l'Interaction de Flammes de Diffusion et de Prémélange avec un Tourbillon, La Recherche Aérospatiale, n°3, pp.13,28, 1988.

[92]HUGHES, W.F., BRIGHTON, J.A. -Fluid Dynamics, Schaums' Outlines Series, Mac Graw Hill, 1967.

[93] O'ROURKE, P.J., BRACCO, F.V.- " Two Scaling Transformations for the Numerical Computation of Multidimensional Unsteady Laminar Flames", Jour. of Comp. Phys., Vol.33, n°2, pp. 185,203, Nov. 1979.

[94] MARBLE, F.E., BROADWELL, J.E. " The Coherent Flame Model for Turbulent Chemical Reactions", Project Squid Rept., TRW-9-PU, 1977.

[95] DARABIHA, N., GIOVANGLI, V., TROUVE, A., CANDEL,S., ESPOSITO,E.- "Coherent Flame Description of Turbulent Premixed Ducted Flames", Workshop on Turbulent Combustion, July 1987, Rouen.

[96] LACAS, F., VEYNANTE,D. -Quelques Réflexions sur le Modèle de la Flamme Cohérente, Rapport du Lab. EM2C, Sept. 1987.

REMERCIEMENTS

Cette étude a été financée par la D.R.E.T et l'O.N.E.R.A. L'existence du programme KIVA a été porté à la connaissance des auteurs par le Pr.Clavin. Les auteurs souhaitent remercier les concepteurs et le Los Alamos National Laboratory. en particulier le Dr.O'Rourke,pour la transmission gratuite du programme KIVA. Ils souhaitent également remercier les Prs. Borghi (Rouen), Candel (ECP),Marble (CIT),et les Drs. Kuentzmann, Laval, Hirsinger, Errera et Dutoya ,pour des discussions fructueuses. Des informations intéressantes ont également été obtenues auprès des Drs. Poinsot (CNRS -IFP) et Pinchon (IFP), Argueyrolles (RNUR), Gaillard (RVI), Souhaité (PSA), Naji (CORIA-Univ.Rouen), Zellat (Alsthom), Zeller (SACM), Znaty (Bertin), Guillard (INRIA), Lévy (ESI).

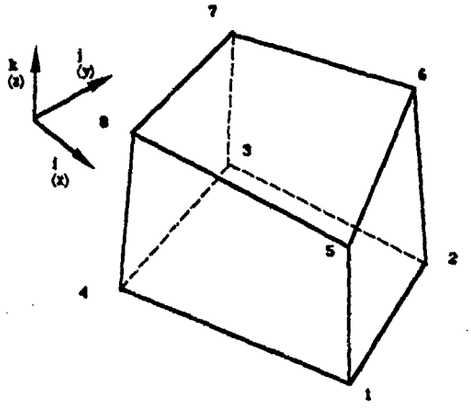


Figure 1 - Cellule d'intégration [59]

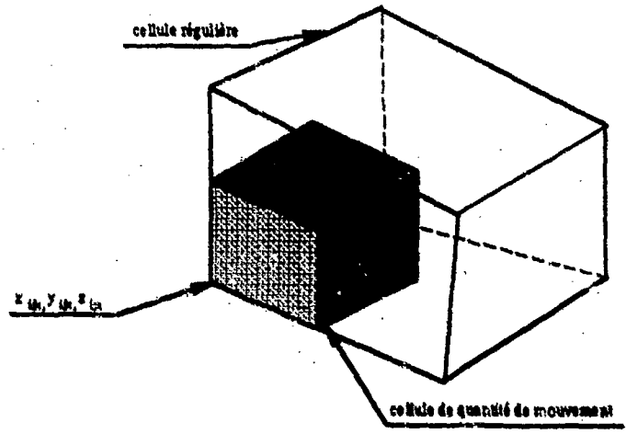


Figure 2- Cellule de quantité de mouvement [59]

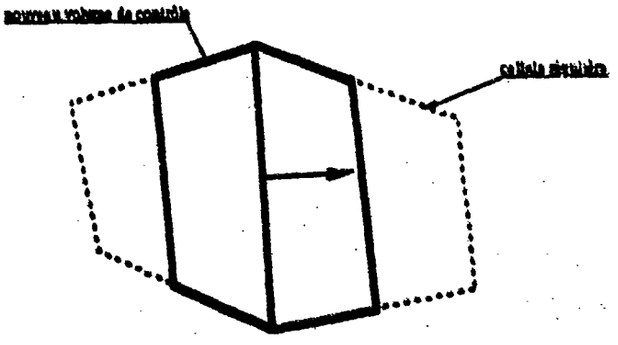


Figure 3- Volume de contrôle utilisé dans la phase B pour le calcul des vitesses normales sur les faces

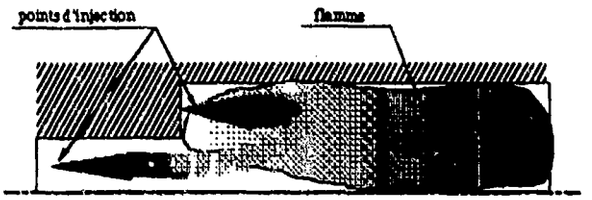


Figure 4 - Schéma du statoréacteur

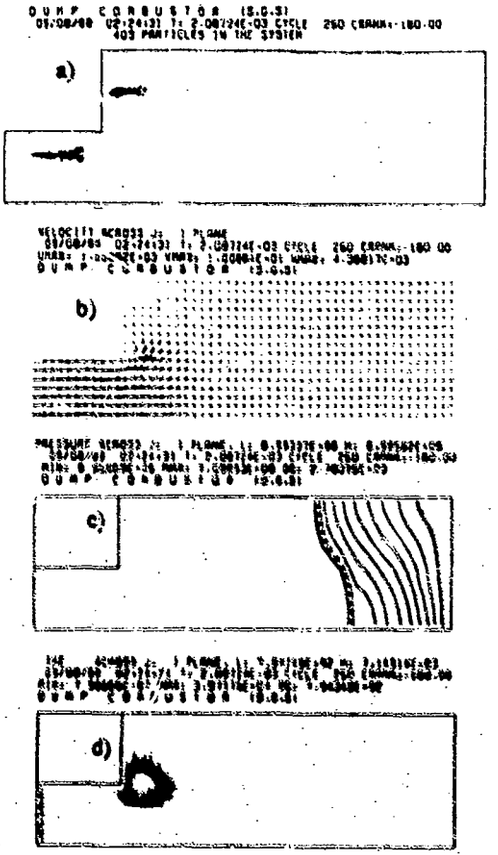


Figure 5: Champs au cycle 250 à t = 2.08724 ms

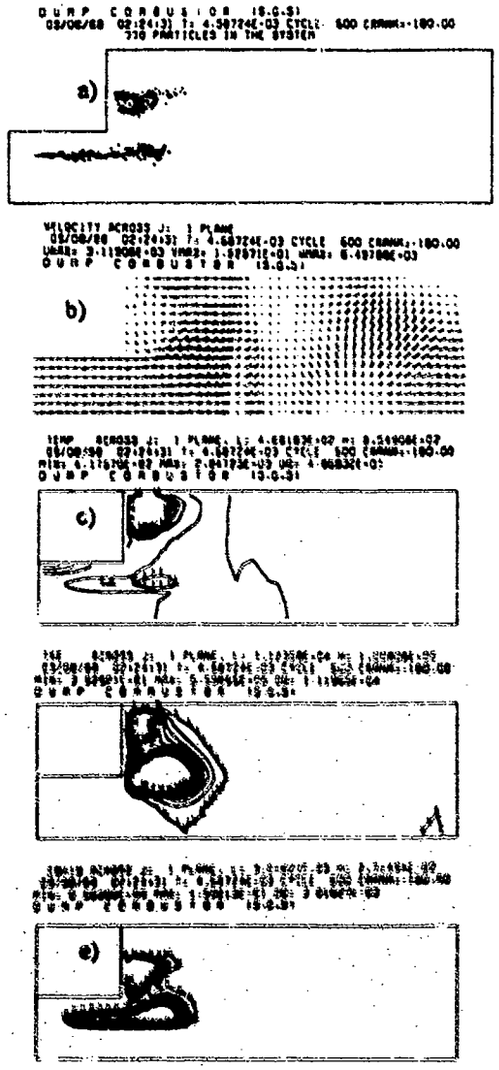


Figure 6. Champs au cycle 500 à t= 4,58724 ms

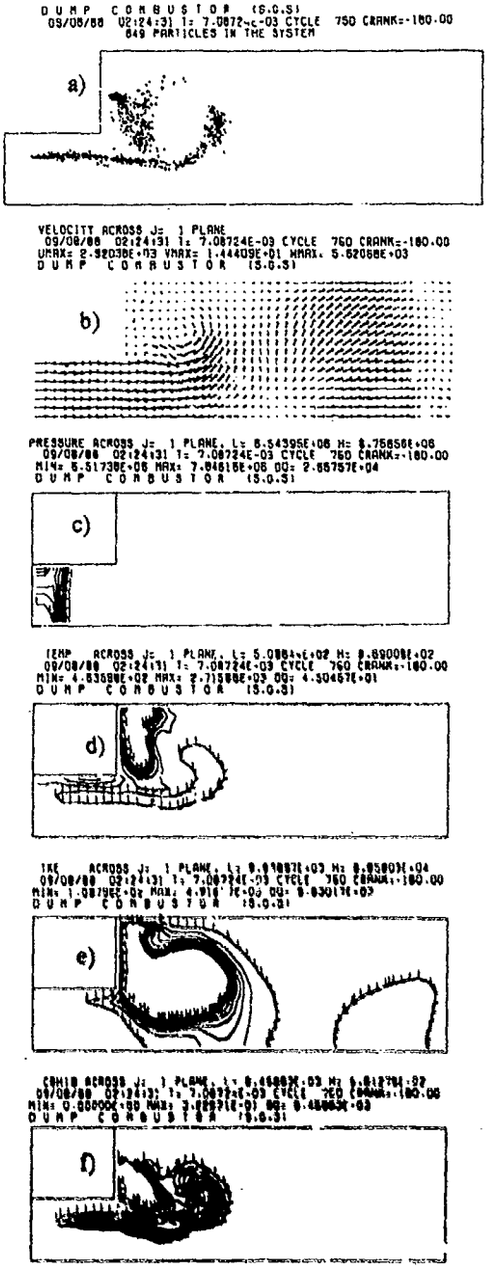


Figure 7- Champs au cycle 750 à t= 7,08724 ms

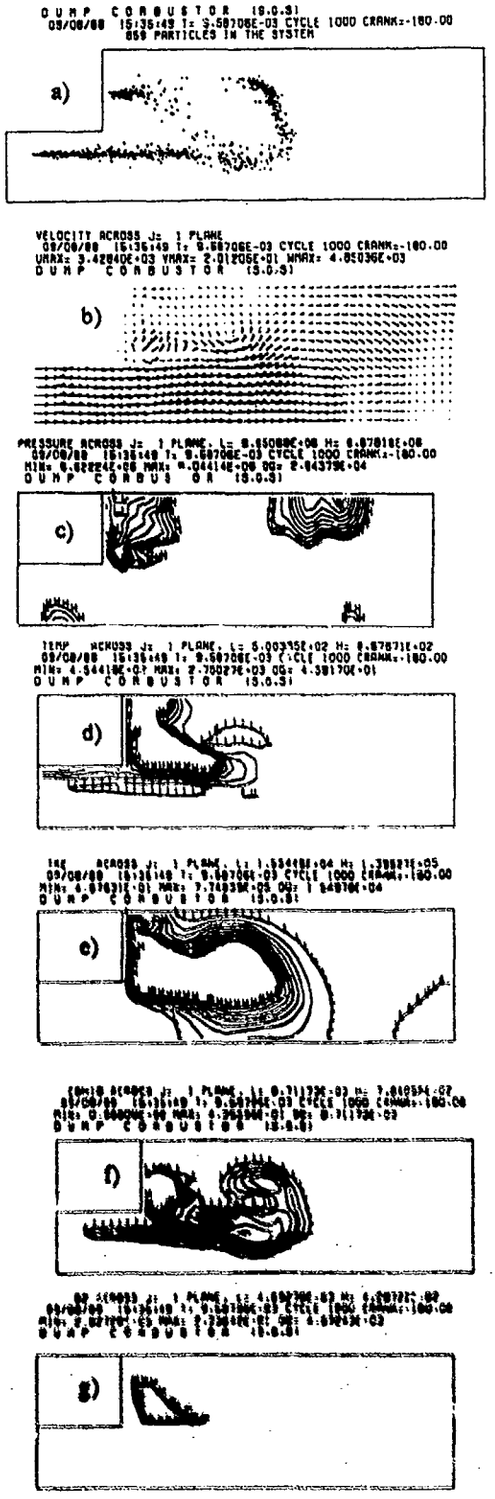


Figure 8- Champs au cycle 1000 à t= 9,58706 ms

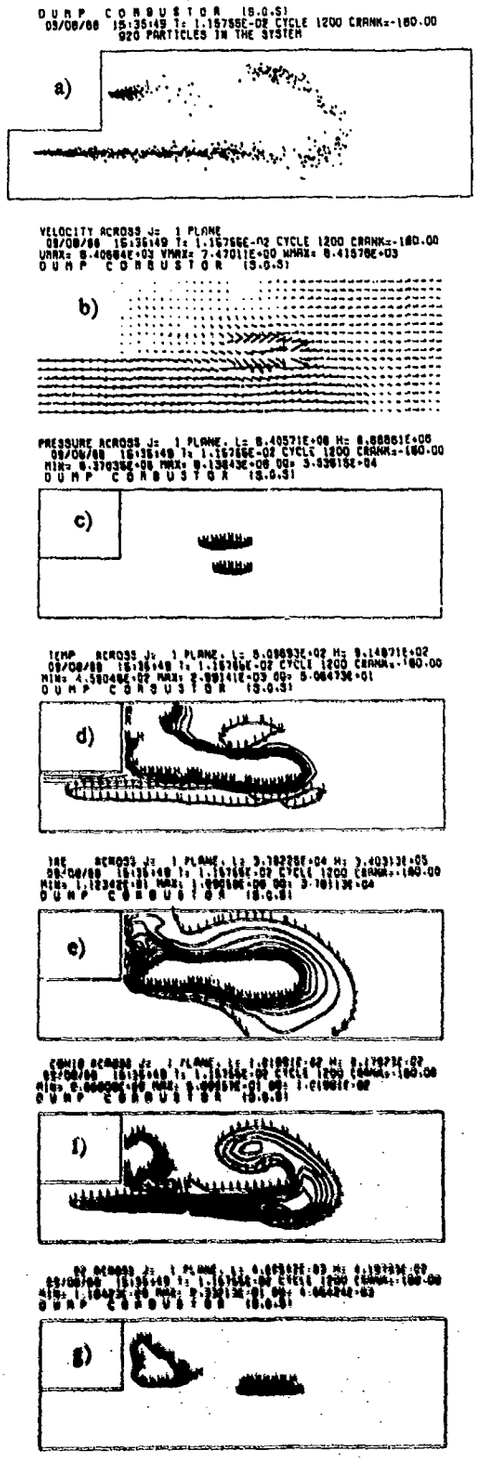


Figure 9- Champs au cycle 1200 à t= 11.5755 ms

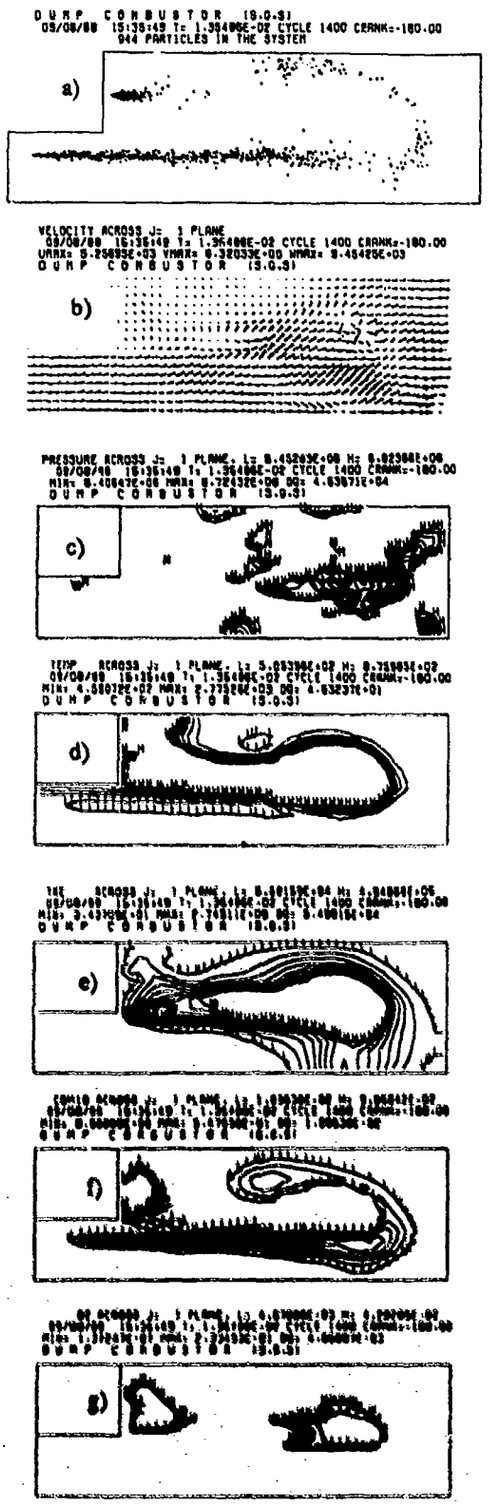


Figure 10- Champs au cycle 1400 à t= 13,5486 ms

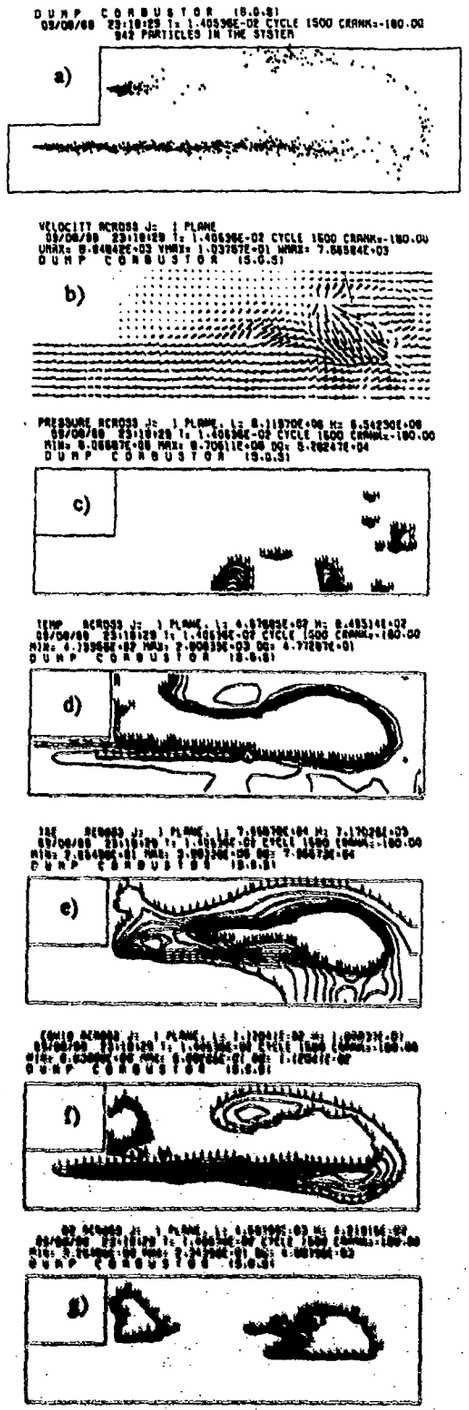


Figure 11- Champs au cycle 1500 à t= 14,0536 ms

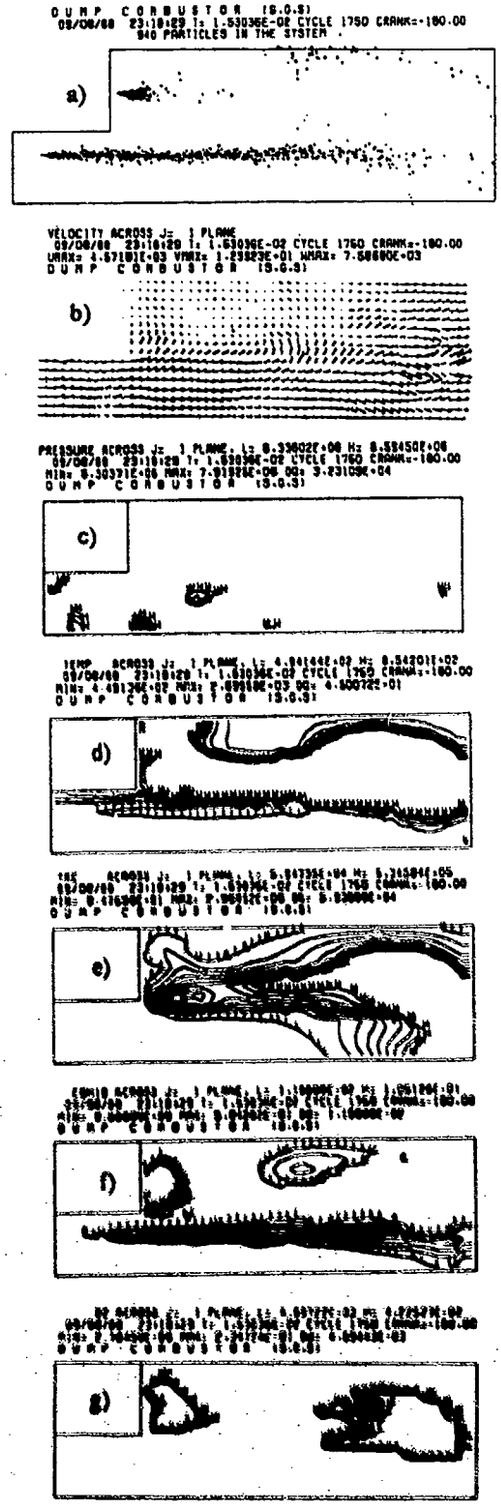


Figure 12- Champs au cycle 1750 à t= 15,3036 ms

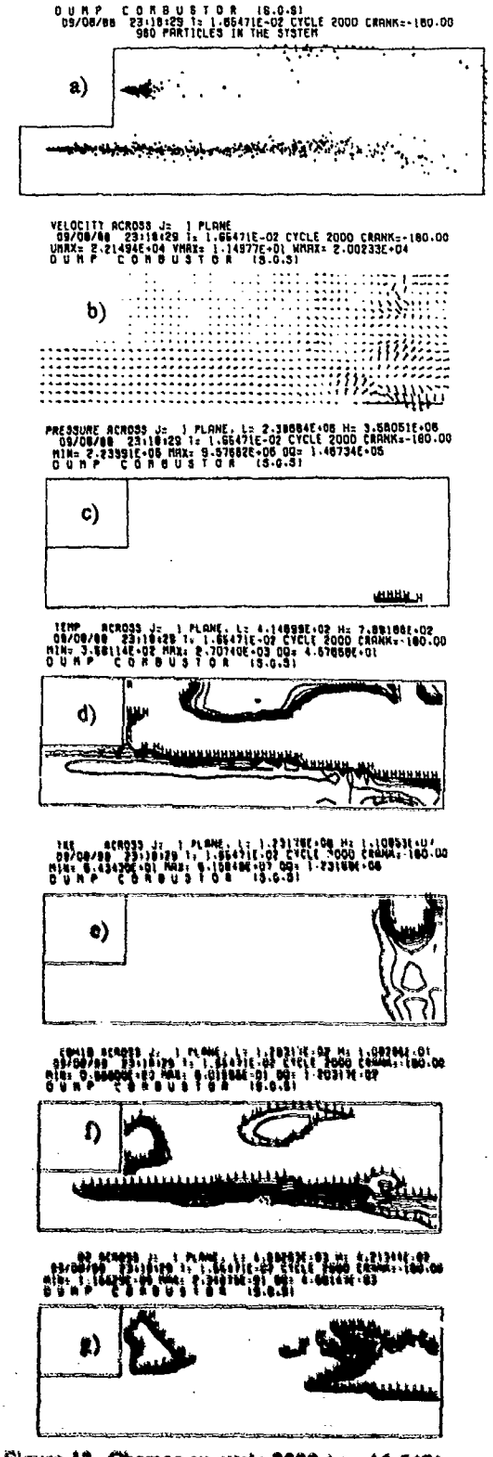


Figure 13- Champs au cycle 2000 à t= 16,5471ms

DISCUSSION

W. H. Jou, US

In your turbulence model for turbulent kinetic energy K, what length scale have you chosen?

Author's Reply:

Dans le modele de turbulence utilisé (Sub Grid Scale), l'évaluation de la viscosité cinématique est basée sur la connaissance de l'énergie cinétique turbulente, qui est évaluée par une équation de lilan, la determination de la densité globale et une échelée de longueur qui est égale à deux fois la taille de la maille.

K. Kailasanath, US

I have two comments:

1) What were your outflow boundary conditions? We find using constant pressure conditions can give erroneous results and it may be more appropriate to use a choked outflow conditions.

2) Have you studied the effects of varying the grid resolution? We find (Journal of Propulsion & Power, Nov-Dec '87) that a coarse grid can give a result which is even qualitatively different from that from a finer grid.

Author's Reply:

Nous avous choisi une condition de sortie subsonique afin de simplifier le traitement dans cette partie de l'éculement. Cette demarche n'inclue pas le traitement de l'avorçage de la trujère. Il est envisagé d'incluse cette forme de condition dans l'areuir.

Les résultats présentés avec un maillage regulier (1 cm x 1 cm) représente des aspects qualitatifs. Le choix de ce maillage a été dicté par la recherche d'une mise au point rapide dans un délai limité. Une étude est actuellement en cours pour déterminer l'influence de la taille des cellules. Ce choix derrait conduire à un meilleur controle le l'effet "pop corn."

VERY-LOW-FREQUENCY OSCILLATIONS IN LIQUID-FUELED RAMJETS

Frederick H. Reardon
Department of Mechanical Engineering
California State University, Sacramento
6000 J Street, Sacramento, California 95819
USA

SUMMARY

Very-low-frequency ("bulk-mode") oscillations have been studied, making use of experimental data gathered at the Air Force Wright Aeronautical Laboratories. This study has considered only those oscillations in which the acoustic resonance characteristics of the combustor were not excited. More than 200 cases of such oscillations in coaxial-dump combustors have been examined. Correlations of oscillation incidence, frequency and amplitude have been made in terms of design and operating parameters, including inlet diameter and length, combustor diameter and length-to-diameter ratio, air inlet temperature and fuel-air ratio. An analytical model has been developed with which the effects of various oscillation driving mechanisms have been examined and compared with the experimental data. Mechanisms considered were: combustion rate fluctuations resulting from fluctuating flow rates of fuel and air, combustion energy release rate variations due to pressure and temperature fluctuations in the flame zone, distortion of the flame zone by vortices shed at the dump plane, generation of an oscillating pressure field by vortex shedding at the dump plane interacting with the exhaust nozzle contraction, and entropy (convective) waves, resulting from fuel/air ratio oscillations, that reflect from the nozzle as pressure waves. Calculations using the analytical model showed agreement with experimental results for nearly 70% of the tests examined. The vortex and entropy wave mechanisms did not substantially improve the model's predictive ability.

INTRODUCTION

Oscillatory operation has been encountered in many liquid-fueled ramjet engines (Ref.1). Although oscillation frequencies have been observed over a very wide range, they tend to fall into three broad ranges, which can be correlated with the acoustic properties of the combustion chamber. "High-frequency" oscillations generally are characterized by frequencies greater than about 1500 hertz; the wave patterns in the combustor are similar to the transverse acoustic modes. "Low-frequency" oscillations typically fall in the 500 to 1500 Hz range and have wave patterns in the combustor resembling longitudinal acoustic modes. "Very-low-frequency" oscillations usually have frequencies below the first longitudinal acoustic mode of the combustion chamber.

This investigation has been concerned with the very-low-frequency type of oscillation, which can be very detrimental to the operation of a ramjet engine, even if the amplitude of oscillation is fairly small, because the pressure excursions, propagating upstream into the diffusor, may cause the inlet shock to be disgorged, drastically reducing the engine thrust and efficiency. In some cases the frequency of very-low-frequency, or "bulk mode", oscillations is close to that of the first longitudinal mode of the combustor. However, because the combustion zone is typically spread over a considerable fraction of the combustor length, the energy release is not in the most effective place to excite the first longitudinal mode.

One objective of this work has been to develop an engineering design tool in the form of a microcomputer-based stability model that is simple to use and easy to interpret. The approach used involves a combustion-time-lag model that was successfully used for very-low-frequency oscillations in liquid propellant rocket engines. Such an approach was suggested by Rogers (Ref. 2), although he did not work out a detailed model. The primary experimental data which provided the foundation for this study were generated by a parametric testing program conducted at the Air Force Wright Aeronautical Laboratories by personnel of the Ramjet Technology Branch. This program has provided the most complete and best-documented ramjet combustion oscillation data available to date.

The first part of this paper will describe the test program and some empirical correlations of the test results. The analytical model will then be presented. Finally, the experimental and theoretical results will be compared.

EXPERIMENTAL PROGRAM AND EMPIRICAL CORRELATIONS

The AFWAL test program consisted of a series of parameter surveys, in which each of the geometrical and operating parameters was varied while the rest were held constant. The apparatus used for these parametric surveys is shown in Figure 1. It has been described in detail by Davis (Ref. 3). The experiments surveyed combustor diameters from 15 to 30 cm (6 to 12 inches), chamber length-to-diameter ratios of 1.5 and 3.0, air inlet diameters from one-half to two-thirds of the combustor diameter, air inlet temperatures from 417 to 694 K (750 to 1250 R), nozzle-to-combustor area ratios from 0.4 to 0.6. On some tests, radial flameholders with 25% or 35% area blockage were installed in the inlet at the dump plane. JP-4 fuel was injected into the air stream

either through orifices in the inlet wall near the dump plane ("wall injection") or centrally in the air stream well upstream of the dump plane, promoting relatively uniform mixing of the fuel and air prior to combustor entry ("uniform injection"). The fuel/air ratio was varied on each test between 0.02 and 0.07.

A simple but straightforward way of examining the experimental data was to determine the fraction of the tests that showed very-low-frequency oscillations. On the basis of such an analysis, some general trends were observed:

(1) Decreasing the air inlet diameter tended to stabilize, that is, reduce the incidence of oscillations.

(2) Adding a flameholder tended to stabilize.

(3) Increasing the air inlet temperature tended to stabilize.

(4) Increasing the combustor L/D tended to stabilize with regard to the very-low-frequency oscillations. Higher frequency, acoustically-coupled oscillations were observed with longer chambers.

(5) The fuel injection location did not have a clear-cut effect on stability, although there were some differences in the patterns of stability.

(6) There was not a clear, general effect of combustor diameter on very-low-frequency oscillations. High frequency oscillations were observed primarily in the largest diameter chambers, as would be expected on the basis of experience with liquid propellant rockets.

Additional data analysis considered the frequency and amplitude of the oscillations. Very-low-frequency oscillations appear to depend on the resonant interaction between the dynamics of the combustion volume, the combustion processes, and the feed systems. Liquid rocket experience has shown that bulk-mode oscillation data can be correlated by the characteristic length (L*) of the combustion chamber and the pressure drop across the injector. To determine whether such parameters would be useful in the ramjet situation, amplitude and frequency data were plotted against L* and the ratio of the dynamic pressure of the inlet jet to the combustion chamber mean pressure. The amplitude data were nondimensionalized by the chamber pressure. A dimensionless frequency was defined by

$$f_{dim} = 2\pi f \theta_c \qquad (1)$$

where f is the oscillation frequency in hertz and θ_c is the mean gas residence time in the combustor. According to theoretical studies[c] of oscillations in liquid-propellant rockets (Ref. 4), the dimensionless frequency should fall in the range from 1 to 6 and should be relatively independent of L*.

Figure 2 shows the dimensionless frequency values observed in the AFWAL parametric testing. It can be seen that they fall in the expected range and show little, if any, dependence on L*. The amplitude data are shown in Figure 3. Although there is considerable scatter in the data, the envelope of the amplitude data clearly decreases with increasing dynamic pressure. Because of the scatter in the amplitude data, detailed correlations with regard to the various design and operational parameters were not possible, although the general trends determined from the incidence rates were generally confirmed.

ANALYTICAL MODEL

Combustion-Time-Lag Model

The analytical model (Ref. 5 - 9) is intended to provide an approximate, global view of the very-low-frequency ramjet oscillation problem. It is based on a linearized small perturbation stability analysis. Although such a model cannot predict the amplitude of the limit-cycle oscillations observed in testing, similar models have proven valuable in the development of stable liquid- and solid-propellant rocket engines. The stability analysis yields a characteristic equation that defines the conditions under which small sinusoidal oscillations will grow or decay.

The major assumptions are: (1) the flow in the air inlet system is compressible and is characterized by longitudinal wave motion during unsteady operation; (2) there is no coupling between the oscillations in the combustion chamber and the acoustic modes of the chamber. The latter assumption is not unreasonable since in many combustors the major energy release zone is located between 25 and 60% of the combustor length, measured from the inlet (dump) plane. Thus, the energy is being introduced in a region that is very inefficient for driving the first longitudinal mode of oscillation. The response of the combustion process to oscillations in chamber conditions is represented by a time lag, t_m, the delay between entry of the reactants into the combustor and the eventual energy release. The time lag is taken to be the sum of a convective part, t_v, which is insensitive to fluctuations in chamber conditions, and a sensitive part, t_c. Although the fuel is supplied to the engine in liquid form, it has been assumed that there is sufficient time available for atomization and vaporization so that the sensitive time lag is essentially a chemical reaction time.

The stability analysis is based on the unsteady energy equation,

$$E_{in} + E_{comb} - E_{out} = dE/dt \tag{2}$$

where E_{in} represents the rate at which energy is convected into the combustor, E_{comb} is the rate at which energy is released by the combustion process, E_{out} is the rate at which energy is convected out through the exhaust nozzle, and E is the energy within the combustor. Each of the energy terms is expressed in term of thermodynamic and fluid dynamic properties. Sinusoidal perturbations superimposed on the mean value are assumed for each property. For example, the combustor chamber pressure is written as

$$p_3(t) = \bar{p}_3 + p_3' \exp(st) \tag{3}$$

where $s = \lambda + i\omega$. The physical interpretation of this formulation is that oscillations of circular frequency ω will grow if the amplification factor λ is positive and will decay if it is negative. The mathematical problem is to find the complex values of s corresponding to a particular engine configuration and test situation.

To simplify the analysis, the distributed combustion zone is replaced by a relatively concentrated flame front, and the three-dimensional flow field is approximated by a one-dimensional one. A simple one-parameter relation between the combustion efficiency e_c (in %) and the combustor length L_3 (measured from the dump plane),

$$e_c = 100\ [1 - (c_t/L_3)] \tag{4}$$

is used to determine the location of an effective, concentrated combustion zone. The value of the parameter c_t was determined from the AFWAL steady-state performance data. Figure 4 compares the calculated and experimental values of combustion efficiency for a typical test condition. The total time lag is calculated by dividing the length from the dump plane to the concentrated combustion zone by the mean velocity of the air/fuel mixture. The location of the combustion zone for this calculation is somewhat arbitrary, and can be used as an adjustable parameter in "calibrating" the theoretical model. Based on liquid-propellant rocket experience, the combustion zone should be taken at a distance corresponding to 25 - 50% combustion efficiency.

Expressing each of the energy quantities in terms of the perturbations of mass flow rates and fluid properties gives a characteristic equation

$$\frac{f_F(G_F, t_v, t_T) + f_A(G_A, t_v, t_T) - n[1-\exp(-st_c)]}{\exp(-st_e) + s\theta_c} + 1 = 0 \tag{5}$$

where G_A and G_F are the admittances of the air and fuel feed systems, respectively, defined by the equations

$$\begin{aligned} m_F'/\bar{m}_F &= -G_F\ p_3'/\bar{p}_3 \\ m_A'/\bar{m}_A &= -G_A\ p_3'/\bar{p}_3 \end{aligned} \tag{6}$$

In Eq. (5), θ_c is the gas residence time in the combustor, n is the "interaction index" that measures the sensitivity of the chemical time lag to pressure and temperature perturbations in the combustion zone, and t_e is the acoustic travel time between the combustion zone and the exhaust nozzle entrance. The first term in the denominator represents an approximate correction for temporal effects that may be significant in long combustors. The functions f_F and f_A include the effects of mass flow rate and fuel/air oscillations on the overall energy release rate; expressions for these functions are given in Ref. 8.

The Nyquist method is used to determine the stability of a given case. Eq. (5) is of the form

$$F(s) + 1 = 0 \tag{7}$$

When the function $F(i\omega)$ is plotted on the complex plane (a typical plot is shown in Figure 5), encirclements of the point (-1,0) indicate instabilities. The frequency at which $F(i\omega)$ crosses the negative real axis while encircling (-1,0) approximates the expected oscillation frequency. The magnitude of $F(i\omega)$ at the crossover point (the so-called "gain") is a measure of the growth rate of the oscillation at that frequency.

In this model, the interaction index n is calculated from an equation given by Crocco and Cheng (Ref. 4). The time lag is determined from equations and data in References 10 - 12. The calculation of the air inlet admittance G_A depends on the boundary condition at the upstream end of the inlet system. The computer model includes three alternative upstream boundary conditions: a large decrease in flow area (corresponding to many connected-pipe test setups), a sonic orifice (used on some of the AFWAL tests), and a specified value of the complex acoustic reflection coefficient at the inlet-diffuser shock. The third boundary condition was included so that the model can be applied to engine testing with supersonic diffusers.

Vortex Shedding Effects

It is well documented that vortices are shed at sudden enlargements, such as the dump plane at which the inlet and combustor meet. Two mechanisms by which these vortices can interact with the combustion process have been identified. Brown and his co-workers (Ref. 13) have proposed that the vortices shed at the dump plane are convected downstream and interact with the convergent part of the exhaust nozzle to generate a pressure oscillation within the combustor. Under the proper conditions, rather large amplitudes can be developed, even without any interaction with the combustion process. Another vortex-shedding mechanism is the direct interaction between the vortices shed at the dump plane and the combustion zone downstream. Marble (Ref. 14) has shown that significant combustion rate perturbations can result from the periodic "rolling up" of the flame zone.

Vortex shedding arises from the inherent instability of the shear layer formed at the dump plane. Shear layers appear to be unstable over wide ranges of conditions. Two classes of flow situations appear to behave differently (Ref. 15). "Impinging" shear layers are those which encounter some kind of physical obstacle downstream. The presence of the obstacle modifies the shear flow such that amplification of small fluctuations may occur. "Nonimpinging" shear layers have no downstream obstructions to feed back flow irregularities that can lead to instability. Rather, any instability of a nonimpinging shear layer is inherent in the flow itself. It is well established that resonant oscillations of impinging shear layers can reach amplitudes of two orders of magnitude greater that those of nonimpinging (or nonresonant) shear layers.

The mechanism that has been incorporated into the stability model to account for the generation of an oscillatory pressure field in the combustor by shear layer instability (based on References 16 - 18) is the following: A pressure oscillation at the dump plane, p_3', results in a velocity oscillation. A vortex is shed, the strength of which is proportional to the velocity oscillation amplitude. The vortex is shed at the instant the velocity reaches its peak. The vortex propagates downstream at about 60% of the velocity of the inlet flow. The vortex strength grows exponentially until a maximum strength is reached or the nozzle is encountered. As the vortex passes through the nozzle, a pressure perturbation is generated that propagates upstream at the sonic velocity relative to the mean flow. If the chamber is shorter than the length required to develop the maximum vortex strength, the pressure perturbation produced by the vortex will be proportional to the original pressure oscillation. If the chamber is longer than the length required to develop the maximum vortex strength, the vortex will tend to dissipate and to lose its coherence. The resulting pressure perturbation will thus be less strong and coherent. Thus, the strength of the resulting pressure perturbation will depend on the Strouhal number and on the chamber length. The phase of the added pressure oscillation will depend on the phase of the velocity perturbation at the dump and on the transport time to the nozzle and back.

This phenomenon is inherently nonlinear. Therefore, all aspects of it cannot be incorporated into a linear theory. Since the combustor length is typically somewhat greater than the distance required to develop the peak vortex strength, it is assumed that the vortex is at its peak strength as it enters the nozzle. The peak vortex strength is a function of the Strouhal number, Sr_m, based on the jet velocity and the momentum thickness of the shear layer at its point of origin, i.e.,

$$Sr_m = f\, t_m/V_j \tag{8}$$

The pressure oscillation resulting from the vortex shedding-nozzle reflection mechanism will be given by

$$p_v' = n_1 p_3' (|V_2'|/\bar{V}_2) M_2 f_1(Sr_m) \exp(-i\omega t_{ve}) \tag{9}$$

where $|V_2'|$ is the magnitude of the inlet velocity perturbation, M_2 is the Mach number of the inlet flow, t_{ve} is the sum of the downstream transport time of the vortex and the upstream propagation time of the pressure wave, and the coefficient n_1 includes the ratio of pressure perturbation to vortex strength resulting from the passage of the vortex through the nozzle as well as the magnitude of the vortex-induced field relative to the combustion noise. The function f_1, which is the ratio of the peak vortex strength to the maximum peak vortex strength and is based on Freymuth's results (Ref. 16), is shown in Figure 6. Since the air and fuel flow rate perturbations are proportional to the combustor pressure perturbation, the effect of the pressure field generated by the vortex shedding can be determined by multiplying the flow perturbations by a correction factor, $1 + p_v'/p_3'$.

For nonimpinging shear layers, there is an apparent streamwise length scale based on the concept of a vortex, traveling downstream at about 60% of the flow velocity, combined with a sound wave propagating upstream (Ref. 15). The phase requirement for instability gives the equation

$$L_v/u_v + L_v/a = m/f \tag{10}$$

where L_v is the apparent length scale, u_v is the vortex propagation speed, a is the speed of sound, and m = 1, 2, . . . Note that if L_v is the distance from the dump to the combustion zone, there is the possibility of instability on the basis of a direct vortex-combustion mechanism.

Schadow (Ref. 19) correlated vortex shedding and rollup frequencies in simulated ramjet combustors with the Strouhal number based on the inlet air jet velocity V_2 and inlet diameter D_2. He found the vortex rollup frequency to be given by

$$Sr_2 = fD_2/V_2 = 0.27 \text{ to } 0.31 \tag{11}$$

Schadow's results have been taken as the basis of the direct vortex-combustion interaction mechanism included in the present stability model. Vortices produced by the natural instability of the shear layer, without interaction with the combustor geometry, form coherent structures (i.e., flowfield perturbations), the strength of which peaks at a frequency corresponding to a Strouhal number (Sr_2) of 0.3. These perturbations, when they reach the combustion zone, result in perturbations of the burning rate. The combustion rate perturbation can then be written as

$$Q' = Q_o'[1 + n_2 f_2(Sr_2)\exp(i\omega t_{vc})] \tag{12}$$

where Q_o' is the combustion rate perturbation in the absence of vortex interaction. In this equation, the function f_2 accounts for the effect of Strouhal number on vortex strength; it reaches a maximum value of unity at $Sr_2 = 0.3$. The function f_2 is shown in Figure 7. The time lag t_{vc} includes both the vortex transport time and the time between the arrival of the vortex at the combustion zone and the enhanced energy release (which has been assumed to be approximately equal to the chemical reaction time lag, t_c). Finally, n_2 is an empirical coefficient that accounts for the magnitude of the flowfield perturbation and the combustion rate response to that perturbation. Based on Marble's analysis (Ref. 14), n_2 should be of the same order of magnitude as the interaction index, n. To include this vortex-combustion mechanism into the analytical model, the second term of Eq. (12) was added to the numerator of the first term of the characteristic equation, Eq. (5).

The effects of the two vortex shedding mechanisms can be seen from calculations of the oscillation frequencies and gains for a typical case. Figure 8 shows the calculated frequency and gain for the vortex-generated pressure field mechanism. It can be seen that increasing n_1 increases the gain over that predicted by the basic combustion time lag model. Moreover, additional modes, at both higher and lower frequencies, are predicted, although the oscillation frequency for any mode is essentially unchanged. Figure 9 gives the calculated results for the same test using the direct vortex-combustion mechanism. Increasing the coefficient n_2 also increases the predicted gain, although the destabilizing effect does not appear to be as strong as for the vortex-pressure mechanism. The oscillation frequency is dependent on the magnitude of n_2, but no additional unstable modes are predicted by this mechanism.

Entropy Wave Effects

The mechanism by which entropy waves can produce self-sustained oscillations can be described as follows (Ref. 20). A pressure disturbance near the dump plane causes perturbations of the fuel and air flows, which are transported with the mean flow to the combustion zone. The alteration of the local fuel/air ratio causes some of the reactants to burn at a temperature different than the mean combustion temperature, resulting in a quantity of products at a different entropy than the mean flow. This "entropy wave" is transported with the flow of combustion products to the nozzle, where it is reflected as a pressure wave.

To investigate the possible role of entropy waves, the sensitive time lag model was modified by augmenting the combustion pressure oscillation felt by the air and fuel feed systems by an oscillation delayed in time and having an amplitude n_{ew} times the original wave. That is,

$$p_{ew}' = p_o'(1 + n_{ew}\exp(-i\omega t_3)) \tag{13}$$

where p_{ew}' is the augmented oscillation and p_o' is the original wave. Since the air and fuel flow rate perturbations are proportional to the combustor pressure perturbation, the effect of the entropy wave is to multiply each of the flow rate perturbations by the factor $(1 + n_{ew}\exp(-i\omega t_3))$. The time delay, t_3, is given by the equation

$$t_3 = L_u/V_u + (L_3 - L_u)/V_b + (L_3 - L_u)'/(a_b - V_b) + L_u/(a_u - V_u) \tag{14}$$

where L_u is the location of the mean combustion zone (from the dump plane), L_3 is the combustor length, V_u and V_b are the mean flow velocities of the unburned reactants and combustion products, and a_u and a_b are the acoustic velocities upstream and downstream of the combustion zone, respectively.

An approximate expression for n_{ew} can be derived by considering the nozzle admittance equation (Ref. 21) for the case of purely longitudinal waves.

$$A_n p'/\bar{p}_3 + \bar{\rho}_n u'/c_p = V_b'/\bar{V}_b \tag{15}$$

where c_p is the isobaric specific heat of the combustion products. Let

$$p' = p_o' + p_e' \tag{16}$$

where p_o' is the isentropic pressure perturbation and p_s' is the pressure perturbation resulting from the entropy wave. Note that p_o' is the combustor pressure perturbation of the basic combustion time lag model and that the nozzle flow condition in the basic model is equivalent to

$$A_n p_o'/\bar{p}_c = v_b'/\bar{v}_b \tag{17}$$

Then, subtracting Eq. (17) from Eq. (16) gives

$$p_s'/\bar{p}_c = -(B_n/A_n)s'/c_p \tag{18}$$

The entropy perturbation can be related to the combustion temperature and combustor pressure perturbations, and thence to the fuel and air flow rate perturbations. The flow rate perturbations are related to the combustor pressure perturbations by tho admittance equations, Eq. (6). Then

$$n_{ew} = (B_n/A_n)(r/T_3)(dT_3/dr)[G_P-G_A-(k-1)/k] \tag{19}$$

where r is the fuel/air ratio. For the frequency range of interest, the calculations of Ref. 21 indicate that the complex nozzle admittance coefficients A_n and B_n are related by the approximate equations

$$\begin{aligned} B_{nr} &= n_3 A_{nr} \\ B_{ni} &= -n_3 A_{ni} \end{aligned} \tag{20}$$

where $0 < n_3 < 1$.

Figure 10 shows theoretical results for a typical test. For values of the coefficient n_3 greater than 0.15, several additional oscillation frequencies appear. Each frequency is nearly independent of n_3, whereas the gain of each mode increases as the value of n_3 is increased. For n_3 between 0 and 0.15 there is a 20% increase in frequency and a curious minimum in the gain curve at $n_3 = 0.1$. It can be seen that the frequency of the dominant mode (i.e., that mode having the greatest gain) for $n_3 > 0.3$ is much lower than that predicted by the sensitive time lag theory without entropy wave effects.

COMPARISON OF THEORY AND EXPERIMENT

Because of the scatter in the experimental amplitude data and the fact that the linearized theory can only predict a growth rate, not a limit-cycle amplitude, the comparison of theory and experiment has been made in terms of the presence of oscillations in the very-low-frequency range. More than 200 tests were analyzed to make this comparison. The comparison was made in two ways: (1) examining the predicted and experimentally observed effects on stability of various design and operational parameters, and (2) noting the agreement between theory and experiment on a test-by-test basis. The design parameters investigated were flameholder blockage, inlet diameter to combustor diameter ratio, combustor length to diameter ratio. The effect of air inlet temperature was also determined. Although the fuel/air ratio was varied on these tests, no attempt was made to include this as a parameter in comparing the calculations with the experimental results. The theoretical predictions were made with the basic combustion-time-lag model and with each of the additional mechanisms added separately to the basic model.

Figure 11 shows the effect of the flameholder blockage on oscillation incidence. The experimental results showed a significant stabilizing effect of increasing the blockage. The theoretical model showed substantially less of a stabilizing effect due to the presence of flameholders. Adding the entropy wave mechanism to the model improved the theoretical prediction slightly, whereas adding the vortex-pressure mechanism made it a bit worse.

Experimentally, increasing the combustor length/diameter ratio was strongly destabilizing, as shown in Figure 12. However, only the direct vortex-combustion mechanism (added to the basic model) showed any destabilizing effect.

Somewhat better results were obtained with the inlet diameter/combustor diameter ratio (Figure 13). All of the theoretical predictions showed good agreement with the destabilizing effect of increasing the ratio observed in the experimental data. Similarly, the effect of the air inlet temperature is seen in Figure 14 to be strongly stabilizing, both by the experimental data and all of the theoretical model calculations.

When the test-by-test results were compared, all of the variations of the analytical model appeared to be equally successful overall. Figure 15 shows a typical result. For the low inlet temperature tests, including the vortex-pressure mechanism gave the best agreement. At the intermediate temperature, the entropy wave mechanism improved the agreement between theory and experiment. However, at the high temperature, the basic model was as good as the model with vortex effects and better than the model with entropy wave effects. Overall, the basic model agreed with experiment on 68% of the tests; adding any of the additional mechanisms reduced the agreement by about 10.

The calculated and observed frequencies are compared in Figure 16. More than 80% of the calculated frequencies fell between 85% and 145% of the corresponding measured values. On the average, the calculated frequency was about 10% larger than that observed. Figure 16 shows that for tests at the lower fuel/air ratios, the analytical model tended to underestimate the frequency, whereas the opposite result was obtained at the highter fuel/air ratios.

CONCLUSIONS

The basic model, which depends primarily on the oscillating feed rates of air and fuel as the driving mechanism for combustion pressure oscillations, gives moderately good agreement with experimental data. Vortex-shedding and entropy wave mechanisms have been shown to increase the tendency of a liquid-fueled ramjet to oscillate, but their inclusion in the analytical model has not led to significantly better agreement with experimental stability behavior. The most serious disagreements between the model's predictions and the experimental results occur for small L/D combustors and for combustors with flameholders at the dump plane. The use of an empirical correlation, rather than an analytical model of the steady state combustion distribution, limits the usefulness of the model in its present form. Another limitation of the model results from the need to guess values of the coefficients used in the formulations of the vortex and entropy wave mechanisms. Further research into these mechanisms is needed.

REFERENCES

1. Waugh, R. C., et al, Ramjet Combustor Instability Investigation: Literature Survey and Preliminary Design Study, Report AFWAL-TR-83-2056, Volume I, United Technologies Chemical Systems, San Jose, California 95150-0015, September, 1983.

2. Rogers, T., Ramjet Inlet/Combustor Pulsations Analysis and Test, NWC TP 6155, Naval Weapons Center, China Lake, CA 93555, October 1980.

3. Davis, D. L., Coaxial Dump Ramjet Combustor Combustion Instabilities, Part I. Parametric Test Data, Aero Propulsion Laboratory, Air Force Wright Aeronautical Laboratories, Wright-Patterson AFB, Ohio 45433, Report AFWAL-TR-81-2047, Part I, July 1981.

4. Crocco, L., and Cheng, S.I., Theory of Combustion Instability in Liquid Propellant Rocket Engines, AGARDograph No. 8, London: Butterworths Scientific Publications, 1956.

5. Reardon, F. H., Investigation of Pressure Oscillations in Ramjet Combustors, California State University, Sacramento, Department of Mechanical Engineering, November, 1980.

6. Reardon, F. H., "Analysis of Very Low Frequency Oscillations in a Ramjet Combustor by Use of a Sensitive Time Lag Model", 18th JANNAF Combustion Meeting, CPIA Publication No. 347, Vol. III, pp. 307-316, October, 1981.

7. Reardon, F. H., Modeling of Combustion Pressure Oscillations in Liquid-Fuel Ramjet Engines, California State University, Sacramento, School of Engineering and Computer Science, February, 1983.

8. Reardon, F. H., "The Sensitive Time Lag Model Applied to Very Low Frequency Oscillations in Side-Dump Liquid-Fueled Ramjet Engines," 20th JANNAF Combustion Meeting, October 1983.

9. Reardon, F. H., "An Examination of Some Possible Mechanisms of Combustion Instability in Liquid-Fuel Ramjets", 22nd JANNAF Combustion Meeting, CPIA Publication No. 432, October, 1985.

10. Toong, T.Y., Combustion Dynamics, New York: McGraw-Hill Book Company, 1983, p. 164ff.

11. Brokaw, R. S., and Gerstein, M., "Correlations of Burning Velocity, Quenching Distances, and Minimum Ignition Energies for Hydrocarbon-Oxygen-Nitrogen Systems," Sixth Symposium (International) on Combustion, New York: Reinhold Publishing Corp., for the Combustion Institute, 1957.

12. Fristrom, R.M., "The Structure of Laminar Flames," Sixth Symposium (International) On Combustion, New York: Reinhold Publishing Corp., for the Combustion Institute, 1957.

13. Brown, R. S., Reardon, F. H., and Hood, T. S., "Combustion Instability Studies in a Small LFRJ Engine", 20th JANNAF Combustion Meeting, October, 1983.

14. Marble, F. E., "Some Comments Concerning Relationships Between Chemical Reactions in Vortex Structures and Unsteady Combustion", ONR/AFOSR Workshop on Mechanisms of Instability in Liquid-Fueled Ramjets, March, 1983.

15. Rockwell, D., "Oscillations of Impinging Shear Layers", AIAA Journal, Vol. 21, No. 5, pp. 645-664, 1983.

16. Freymuth, P., "On Transition in a Separated Laminar Boundary Layer", Journal of Fluid Mechanics, Vol. 25, pp. 683-704, 1966.

17. Aaron, K. M., and Culick, F. E. C., "Coupled Vortex Shedding and Acoustic Resonances in a Duct", 22nd JANNAF Combustion Meeting, CPIA Publication No. 432, October, 1985.

18. Flandro, G. A., and Jacobs, H. R., "Vortex Generated Sound in Cavities", in Aeroacoustics: Jet and Combustion Noise: Duct Acoustics", Nagamatse, H. (Ed.), Vol. 37 of the Progress in Astronautics and Aeronautics Series, AIAA, 1975.

19. Schadow, K. C., Wilson, K. J., and Crump, J. E., "Large-Scale Structure Research in Ramjet-Type Flows", 21st JANNAF Combustion Meeting, October, 1984.

20. Waugh, R. C., and Brown, R. S., "Entropy Wave Instability - Comparison of Data and Analysis," Mechanism in Coaxial Dump Combustors," 21st JANNAF Combustion Meeting, October, 1984.

21. Crocco, L., and Sirignano, W.A., Behavior of Supercritical Nozzles Under Three-Dimensional Oscillatory Conditions, AGARDograph No. 117, Butterworths Publications, Ltd., London, 1967.

ACKNOWLEDGMENT

The work reported herein was supported in part by the United States Air Force under Contract F33615-81-C-2078 through a research agreement with Universal Energy Systems, Dayton, Ohio. Douglas L. Davis was the Technical Monitor for the Ramjet Technology Branch, United States Air Force Wright Aeronautical Laboratories.

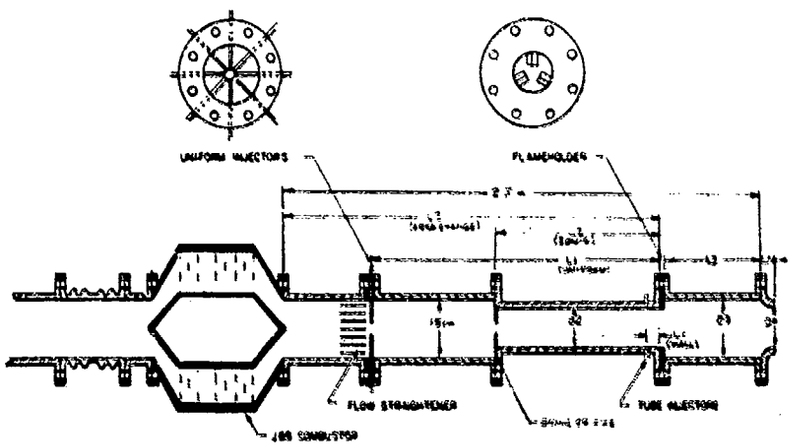


Figure 1. Experimental Apparatus for AFWAL Testing

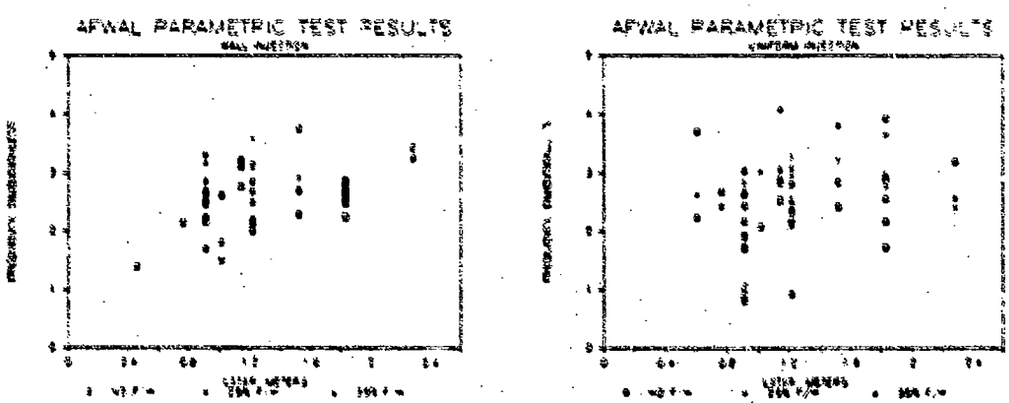
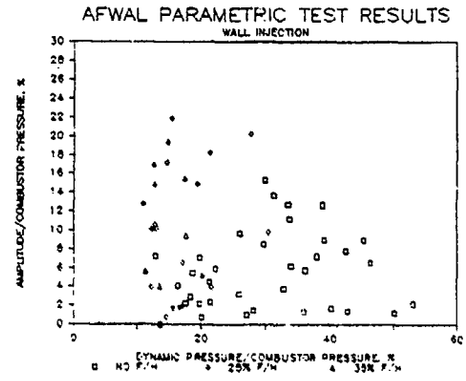


Figure 2. Empirical Correlations of Oscillation Frequency



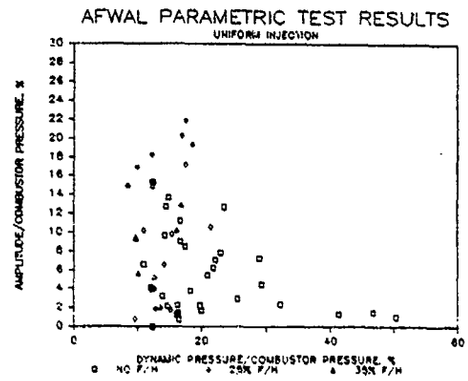


Figure 3. Empirical Correlations of Oscillation Amplitude

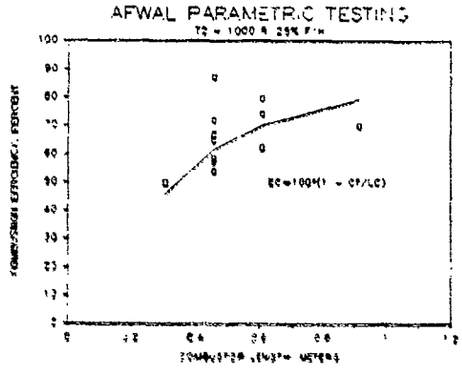


Figure 4. Combustion Distribution

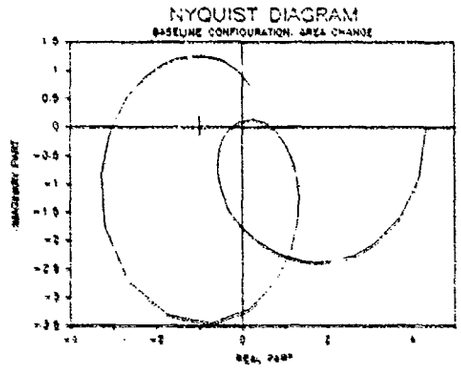


Figure 5. Typical Nyquist Diagram

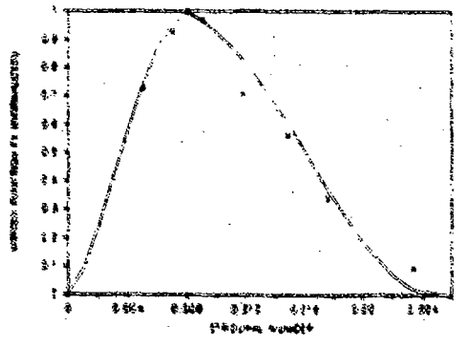


Figure 6. Vortex-Pressure Field Function

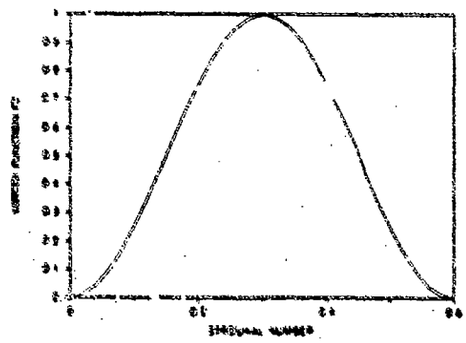


Figure 7. Vortex-Combustion Function

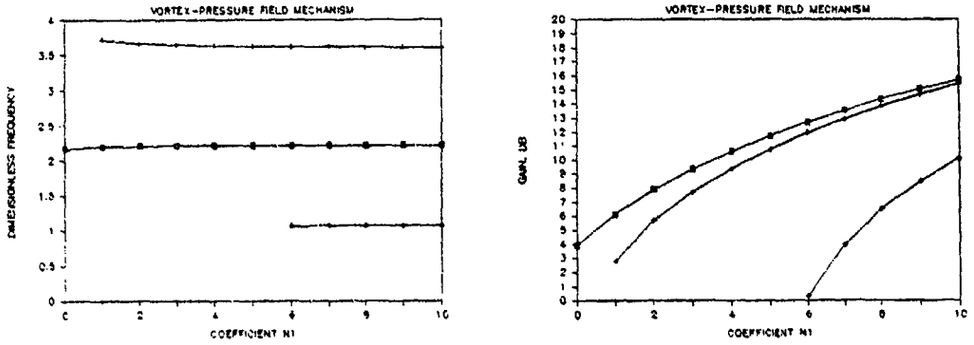


Figure 8. Typical Vortex-Pressure Field Effect on Stability

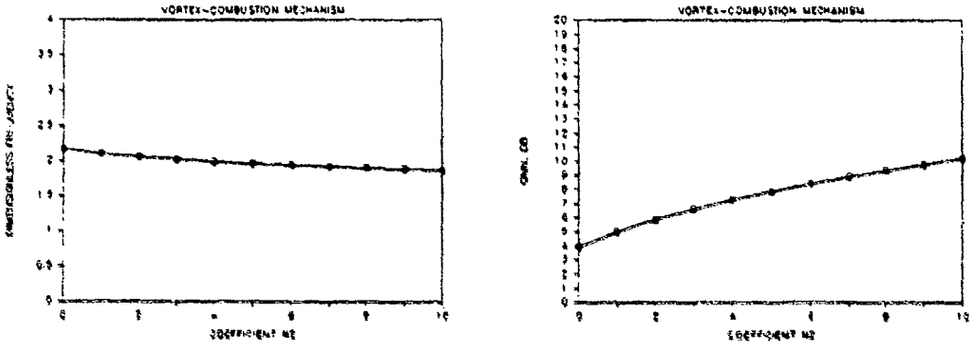


Figure 9. Typical Vortex-Combustion Effect on Stability

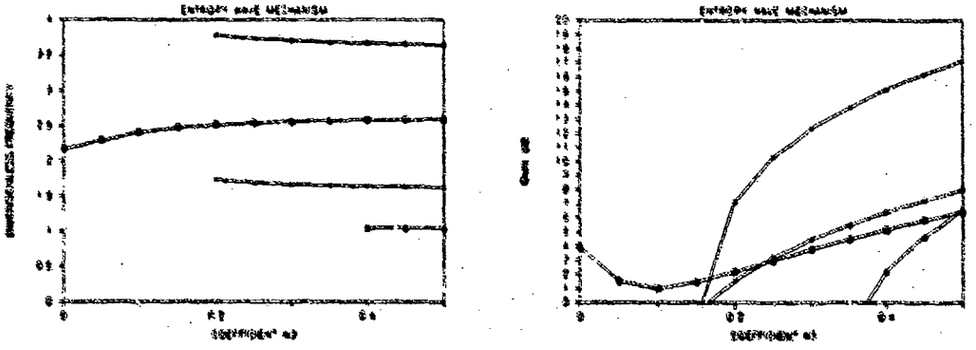


Figure 10. Typical Entropy Wave Effect on Stability

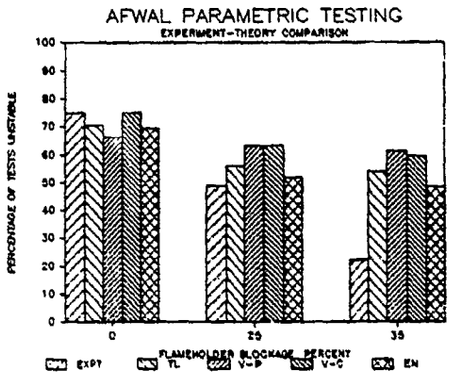


Figure 11. Effect of Flameholder Blockage

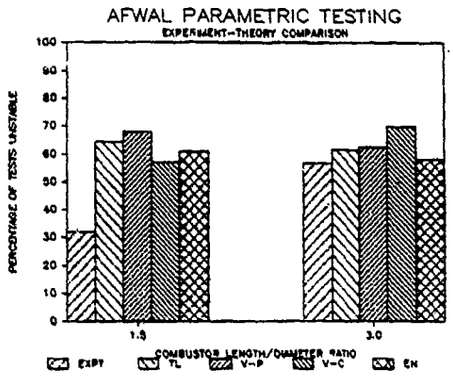


Figure 12. Effect of Combustor L/D

Note: EXPT = Experimental Results, TL = Basic Combustion Time Lag Model, V-P = Vortex-Pressure Mechanism Added, V-C = Vortex-Combustion Mechanism Added, EN = Entropy Wave Mechanism Added

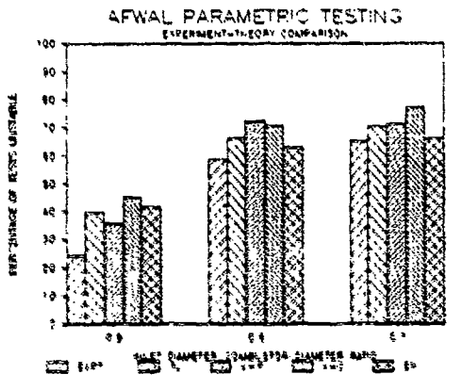


Figure 13. Effect of Inlet/Combustor Diameter Ratio

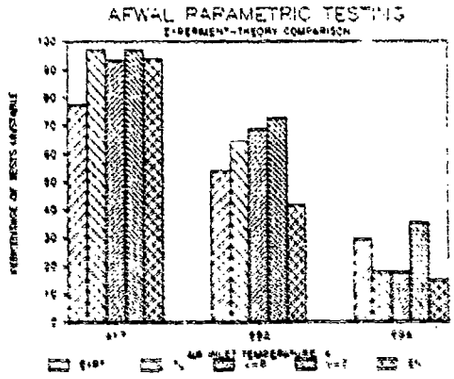


Figure 14. Effect of Air Inlet Temperature

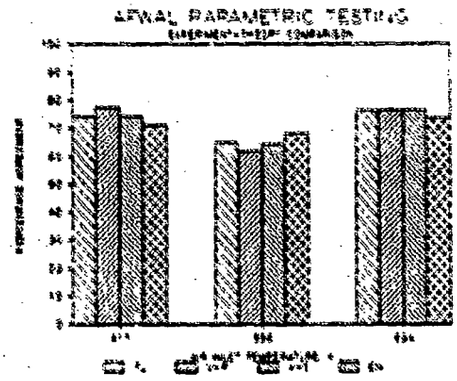


Figure 15. Agreement Between Theory and Experiment

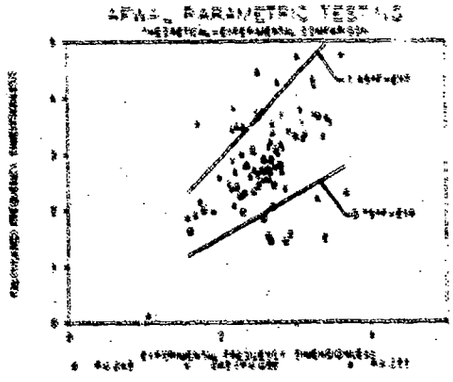


Figure 16. Comparison of Calculated and Experimental Frequencies

DISCUSSION

S. Sivasegaram, UK

Did you investigate the possibility that the observed frequency was related to the longitudinal frequency of the duct, especially of the upstream length, or one of its harmonics?

Author's Reply:

Yes, I did investigate the dependence of the oscillation frequency on the inlet length. I found that the product f L/n (where f is the observed frequency, L is the inlet length, and n = 1, 2, . . .) was approximately constant. As shown by Figure 2 of my paper, the product fL* was also nearly constant, since the combustor gas residence time used to calculate the dimensionless frequency plotted in Figure 2 is proportional to the combustor characteristic length L*. For both of these correlations, the standard deviation was about 20% of the mean. I also found that the product of the observed frequency and the total combustion time lag was approximately constant. There was more scatter in the latter correlation, since the combustion time lag was calculated from the measured combustion efficiency, an assumed axial combustion distribution, and the inlet gas velocity at the dump plane.

These results are in agreement with the concept that the occurrence of very-low-frquency combustion instability depends on the interaction between the dynamics of the propellant feed system, the combustion process, and the combustion chamber (including the exhaust nozzle).

OSCILLATIONS IN NON-AXISYMMETRIC DUMP COMBUSTORS

by

J.H. Whitelaw and S. Sivasegaram
Imperial College of Science & Technology
London SW7 2BX, England.

and

K.C. Schadow and E. Gutmark
Naval Weapons Center
China Lake, California 93555-6001, USA.

ABSTRACT

Instabilities in dump combustors with triangular and round ducts have been investigated with expansion ratio, eccentricity of the dump, equivalence ratio and method of injecting the gaseous fuel as variables, and with and without exit nozzles. The shear flow developing from the vertex of a triangular duct is free from large-scale coherent structures, and the injection of fuel close to the vertices of a triangular upstream duct made the flow less susceptible to periodic heat release and resulted in wider ranges of flammability and stability. This effect is quantified for different arrangements of injection. The effect of eccentricity on flammability and stability characteristics is shown to be unimportant for dump-plane area ratios greater than 2.5 and rough combustion in open-ended ducts gave rise to quarter-wave oscillations while the presence of an exit nozzle caused bulk-mode frequencies to dominate.

NOMENCLATURE

B	:	side of triangular downstream duct
b	:	side of triangular upstream duct
c	:	local velocity of sound
D	:	diameter or equivalent diameter (of downstream duct)
d	:	diameter or equivalent diameter (of upstream duct)
e	:	eccentricity
f	:	frequency
L	:	length of downstream duct
M	:	Mach number = U/c
p	:	pressure, mean wall static pressure
Re	:	Reynolds number = U d/ν
St	:	Strouhal number = f d/U
U	:	mean velocity in duct immediately upstream of the dump plane
X	:	upstream duct length
Y	:	distance of duct axis from vertex of triangular duct
y	:	distance of fuelling hole from vertex of triangular duct
Δp	:	peak to peak amplitude of fluctuating pressure
λ	:	wave length of dominant frequency at ambient conditions
ν	:	kinematic viscosity
ρ	:	density
φ	:	equivalence ratio = (fuel to air ratio)/(fuel to air ratio at stoichiometry)

Subscripts

B	:	bulk mode
E	:	exit
F	:	fuelling location
rms	:	root mean square of fluctuating component
T	:	triangular duct
λ/4	:	quarter-wave
0	:	duct upstream of triangular duct in configuration C

1. INTRODUCTION

Oscillations in premixed flames in axisymmetric dump combustors have been investigated extensively [1-10] and rough combustion in combustors with an unconstricted exit found to be associated with the longitudinal (quarter-wave) frequency of the duct length downstream of the dump plane. The length of the duct upstream of the dump plane did not influence the frequency but could attenuate the oscillations when the quarter-wave frequency of the upstream duct length with an acoustically closed end was the same as the dominant frequency in rough combustion. Methods of suppressing oscillations have also been developed and include the use of quarter-wave tubes and Helmholz resonators attached to the combustor at a location close to a pressure antinode of the longitudinal frequency [9,11,12], the selection of the upstream duct length so as to minimise the amplitude of oscillations [9], the strategic location of an impedance such as an orifice in the upstream duct [9,13,14] and the introduction of oscillations at the same frequency as, but out of phase with, the dominant frequency [15,16]. Crump et al. [6] reported strong pressure fluctuations associated with the longitudinal (half-wave) frequency of the duct length downstream of the dump plane in a combustor with an exit nozzle.

The driving mechanism of instabilities in a dump combustor associated with coherent flow structures has been examined in air and water flows, in diffusion flames and in dump combustors [17-19]. The results show that coherent flow structures are formed by interaction between shear-flow instabilities and acoustic resonance and, where vortices dominated the reacting flow, combustion was confined to the core of the vortices and led to periodic heat release.

Experiments with nozzles of triangular and square section [7, 20-23] have shown that large-scale structures are formed only at the sides, while the regions at the vertices are dominated by small scale turbulence. It has also been shown [24] that combustion developing from the sides of the burner nozzle is associated with vortical structures while that from the corners is fully turbulent and free of coherent structures. These features can be beneficial for non-premixed reacting flows, with the fine-scale mixing at the vertices augmenting molecular mixing and, therefore, the reaction rate. The introduction of fuel into the fine-scale turbulence region at the vertices may also be used to avoid interaction between the flow structures and combustor acoustics. Thus, understanding of the stability characteristics of triangular and other asymmetric ducts may help to extend the operating range of a combustor and the present paper reports measurements of the flammability limits and stability characteristics of non-premixed flames in triangular and round ducts and quantifies the extent to which fuel injection at the vertices of a triangular upstream duct can suppress combustion oscillations in dump combustors with and without an exit nozzle.

The flow configurations and measurement techniques are described briefly in the following section, and the results are presented and discussed in the third section. The final section summarises the main conclusions.

2. FLOW CONFIGURATIONS AND INSTRUMENTATION

The flow configurations are shown in Figure 1 and the important dimensions in Table 1. In configurations A and B, air and fuel were mixed in a swirl register and flowed past a honeycomb to remove the swirl and burned in the downstream section, with the flame stabilised behind the rearward-facing step at the sudden expansion. Alternative fuelling facilities were provided in configuration C for the injection of fuel into a triangular duct immediately upstream of the dump plane either at right angles to the direction of flow or at an angle of 25° to the duct axis at the dump plane or along the direction to the flow. Natural gas (94% CH_4) was the fuel for tests in ducts without an exit nozzle, and bottled propane gas (95% C_3H_8) was used for tests in ducts with an exit nozzle, because the exit constriction necessitated a higher fuel supply pressure. Earlier work [10] has shown that a change in fuel from methane to propane in premixed dump combustors does not affect the stability characteristics or the strength and frequency of combustion oscillations. In configuration D, air flowed past a convergent-divergent nozzle into the upstream duct and ethylene was injected in the direction of the air flow 50 mm upstream of the dump plane.

The flow rates of air and fuel in A, B and C, were obtained with orifice plates and the free-field sound intensity at a location 1.6 m from the duct axis, and in the exit plane of the combustor, and wall static pressure fluctuations were obtained with a Bruel and Kjaer condenser microphone (B&K 4136) and a Kistler pressure transducer (type 6121), respectively, and the output processed in a Spectral Dynamics FFT spectrum analyser (SD 340) to give power spectra. Temperature measurements in the exit plane of the combustor were obtained using 60 mm Pt - 13%Rh/Pt thermocouples and unburnt hydrocarbon using a 1.0 mm internal diameter, 6.0 mm external diameter water-cooled sampling probe and an Analysis Automation FID analyser (model 520 II). Measurements in configuration D comprised air and fuel flow rates and wall static pressure fluctuations obtained with a Kistler pressure transducer (model 202 A1) and processed in a Spectral Dynamics FFT spectrum analyser (SD 372).

3. RESULTS

The results are for a mean air flow rate of approximately 3.0 kg/min, unless otherwise stated, so that the heat release is constant for a given equivalence ratio. The upstream Mach number varied between 0.06 for the 51 mm upstream duct to 0.9 for ducts of 23 mm equivalent diameter. Linear dimensions are nondimensionalised with the mean effective diameter of the downstream duct (D) and Reynolds number is based on the bulk mean velocity and mean effective diameter immediately upstream of the dump plane.

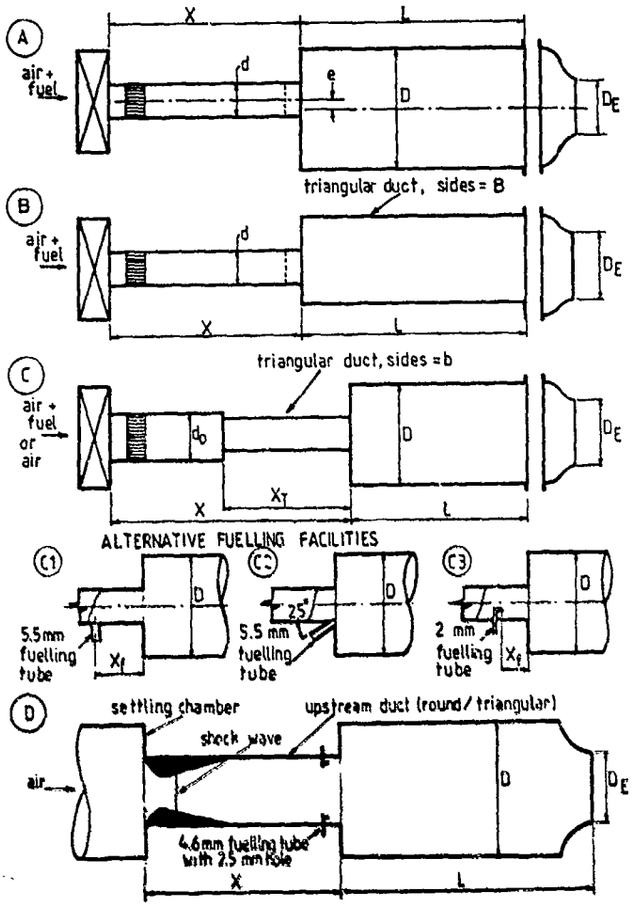


Figure 1. Burner geometries.

3.1 Premixed Flows

Round ducts with eccentric axes

The effect of axial eccentricity was examined for a downstream duct of 80 mm diameter with an unconstricted exit, an upstream duct of 40 mm diameter and eccentricity varying between 0 and 20 mm. The influence of the upstream and downstream duct lengths on flammability and stability limits, and on the radiated sound intensity and dominant frequency, are shown in Figure 2 for an eccentricity of 10 mm and an upstream Reynolds number of 90,000 (M_0 = 0.1). The results are similar to those for the axisymmetric geometry of reference (9) with ducts of similar diameters: rough combustion was observed only for downstream duct lengths greater than 5 D and the stability and flammability limits are almost invariant for duct lengths greater than 7 D. The dominant frequency is associated with the quarter-wave frequency of the downstream duct length, irrespective of the upstream duct length. The sound intensity varies with upstream duct length and is a maximum when the half-wave frequency of the upstream duct length is equal to the dominant frequency and a minimum when the quarter-wave frequency is equal to the dominant frequency. The maximum sound intensity occurs as a result of the three-quarter wave frequency of the entire duct length matching the dominant frequency, and the minimum is due to the suppression of oscillations by the upstream duct length acting like a quarter-wave tube. Discrete frequencies were also observed in smooth combustion and identified as the longitudinal (quarter-wave) frequencies of the downstream duct length and the entire duct length of the combustor or their harmonics. Their amplitudes were small and did not contribute disproportionately to the radiated sound intensity.

The influence of eccentricity on the stability and flammability limits is small except near the maximum value of the eccentricity, e = (D - d)/2, where the flammability range of 0.72 is slightly narrower than the range of 0.8 for the axisymmetric geometry. Also, for a downstream length of 8 D, the onset of rough combustion was at an upstream Reynolds number of 70,000 for the maximum eccentricity compared with a Reynolds number of 60,000 for the axisymmetric geometry. For higher flow rates and

TABLE 1

Main Dimensions of Combustor Geometries

Geometry	D (mm)	B (mm)	d,d_0 (mm)	b (mm)	L/D	x/D	x_T (mm)	x_F (mm)	D_E (mm)
A	80	40			5 -11.5	4 -15			80,53,40,35
B		110	51		4.5-11	4 -7.5			
		110	40		4.5-11	4 -7.5			40,35
		110	23		4.5-11	4 -7.5			
C	51		40	31	3 -12	6 -12	150		51,35
	80		51	41	3 -10	4 -7.5	150		80
	80		40	31	3 -12	4 -7.5	150		80,53,40,35
C1	51		40	31	3 -12	6 -12	150	100	51,35
	80		40	31	3 -12	4 -7.5	150	100	80,53,40,35
C2	80		40	31	3 -12	4 -7.5	150	0	80,40,35
C3	80		40	31	3 -12	4 -7.5	150	30	80,40,35
D	127		63.5		3.4	6		50	76.2

longer downstream duct lengths, the strength and frequency of the oscillations were nearly the same for eccentric and axisymmetric geometries. The differences at shorter downstream duct lengths are probably due to inadequate confinement of the flame in the duct with a large eccentricity.

Triangular downstream duct with round upstream duct

Measurements were obtained with a duct of equilateral triangular cross-section of 110 mm sides (equivalent diameter D = 81 mm) and three values of diameter (23 mm, 40 mm and 51 mm) for the round upstream duct. The downstream duct length was varied between 4.5 D and 11 D with the exit unconstricted and the upstream length between 4 D and 7.5 D. Rough combustion was associated with the quarter-wave frequency of the downstream duct and the respective influences of upstream and downstream duct lengths was similar to those shown in Figure 2. The influence of dump plane area ratio on radiated sound intensity and dominant frequency is shown in Figure 3 for the triangular duct along with that for the 80 mm round duct of reference [9]. It appears that, for dump plane area ratios greater than 2.5, the influence of dump plane area ratio and downstream duct length on the strength and frequency of oscillations is far greater than that of the cross-sectional form of the duct. Discrete frequencies in smooth combustion were similar to those in round ducts and associated with longitudinal quarter-wave frequencies and low amplitudes.

Triangular upstream duct with round downstream duct

Tests were carried out with equilateral triangular upstream ducts of 31 mm and 41 mm sides (equivalent diameters 23 mm and 30 mm, respectively) and round downstream ducts of 51 mm and 80 mm diameter with an unconstricted exit. The dominant frequencies in smooth and rough combustion and the influence of the upstream and downstream duct lengths and the dump plane area ratio on combustion oscillations were, again, similar to those for the axisymmetric geometries of reference [9].

Downstream ducts with a constricted exit

Combustion was smooth throughout the flammability range in the 80 mm combustor of reference [9] with a mean velocity of 35 m/s (M = 0.1) in the 40 mm upstream duct and exit nozzles of 40 mm and 53 mm diameter. The upstream velocity was increased to 100 m/s (M = 0.3) in reference [10] and rough combustion was observed for exit diameters less than 40 mm, but associated with the bulk mode frequency of the combustor and two narrow ranges of equivalence ratios adjoining the flammability limits. Rough combustion associated with the higher, longitudinal (half-wave) frequency occurs within a range of frequencies which is dependent upon the upstream velocity and was not observed because the half-wave frequencies of the downstream ducts of references [9] and [10] were higher than the frequency values associated with the instability. Smooth combustion, however, was associated with the bulk mode and longitudinal frequencies. The acoustic frequency was augmented when it was nearly the same as the shedding frequency of the jet corresponding to a Strouhal number of around 0.3, but did not result in a significant increase in radiated sound intensity.

Tests were carried out with the three asymmetric geometries A, B and C with exit nozzles and the results were similar to those of references [9] and [10], with increase in downstream length and exit constriction resulting in narrower ranges of flammability and stable combustion.

3.2 Fuel Injection into a Triangular Upstream Duct

References [7] and [20-24] demonstrated that large coherent structures exist in the shear layers developing from the sides of a triangular jet, while the flow developing from the corners was dominated by highly turbulent small eddies. It was therefore anticipated that the introduction of fuel into the shear layer developing from the sides would give rise to periodic heat release and favour combustion oscillations and that the introduction of fuel at the corners of the jet would be less susceptible to unstable combustion. Tests carried out in a 127 mm dump combustor with an exit nozzle and a triangular upstream duct showed that fuel injection at the sides of the triangular duct was associated with larger amplitudes of oscillation than with fuel injection at the vertices.

Figure 4 shows the variation of the fluctuating wall static pressure at the dump plane with equivalence ratio in the 127 mm dump combustor with a 76.2 mm exit nozzle (configuration D) for fuel injection at the vertices, and at the midpoint of the 121.2 mm sides of a triangular upstream duct and along the wall of a 63.5 mm round upstream duct with a maximum air flow rate of 1.8 kg/s corresponding to a Reynolds number of 1,000,000. Rough combustion was observed with fuel injection at the sides of the triangular duct and in the round duct, and was associated with the longitudinal half-wave frequency of the downstream duct length. With fuel injection at the vertices of the triangular duct, combustion was smooth across the measured range of equivalence ratios and the amplitude of the fluctuating wall static pressure less than that for the other two methods of fuel injection for all equivalence ratios.

Measurements were carried out in 51 and 80 mm downstream ducts and with a triangular upstream duct of 31 mm sides to examine the influence of the position of the fuelling hole and the direction of fuel injection on combustion oscillations in combustors with and without an exit nozzle and for three methods of fuelling, namely at the vertices, at the sides and at both the sides and the vertices of the triangular duct.

Ducts with a constricted exit

Stability and flammability limits were the same for the 51 and 80 mm ducts and Figure 5 shows their variation, the

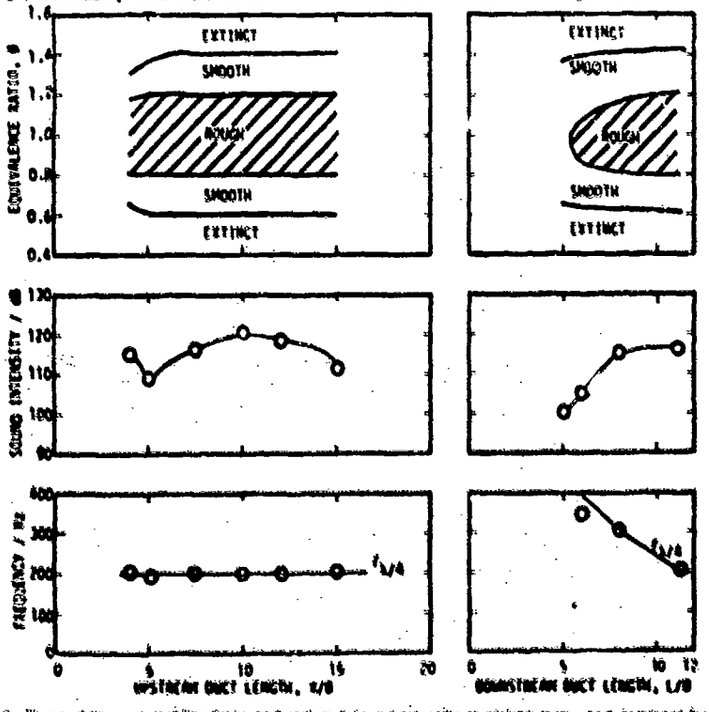


Figure 2. Flammability and stability limits and radiated sound intensity at stoichiometry and dominant frequency.
Geometry A, d = 40 mm, D = 80 mm, δ = 10 mm, D_E = D, Re = 90,000.
(a) Variation with upstream length, L = 11.5 D. (b) Variation with downstream length, X = 0.7L.

radiated sound intensity at stoichiometry and the variation of dominant frequency with downstream length of the 80 mm duct with an exit nozzle of 35 mm diameter and an upstream Reynolds number of 150,000 (M=0.3). The figure allows comparison of results obtained with premixed flows and for the three methods of fuel injection, with the fuel injected normal to the flow direction through 5.5 mm fuelling holes located 100 mm upstream of the dump plane. Rough combustion was observed with all four methods of fuelling and was associated with the bulk mode frequency. Fuel injection at the sides of the triangular duct made the combustor more prone to rough combustion and injection at the vertices limited the rough combustion to equivalence ratios close to the rich extinction limit. These bulk mode oscillations relate to the instability of the flame near extinction and are favoured by an increase in exit constriction and an increase in downstream duct length. The lean flammability limit for fuel injection at the vertices is 0.4 compared with at least 0.6 for the other methods of fuel injection and the rich flammability limit is greater than 1.3 for all

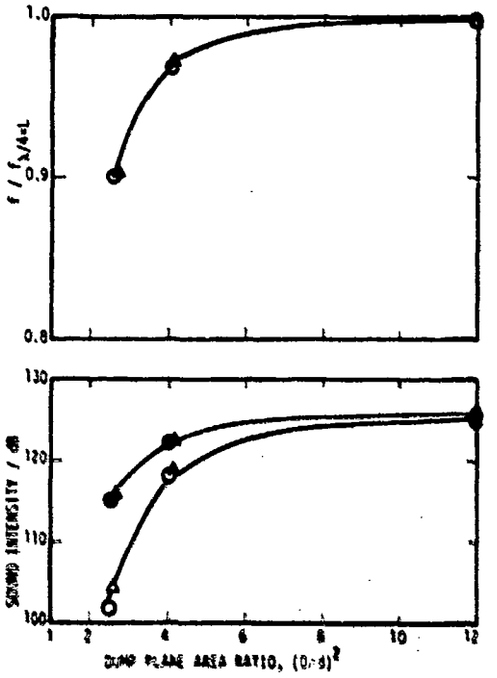


Figure 3. Influence of dump plane area ratio on radiated sound intensity at stoichiometry and dominant frequency.
△, ▲ Geometry D, B = 110 mm (D = 81 mm), L = 11.5 D, D_E = D.
○, ● Round ducts (reference [9]), D = 80 mm, L = 11.5 D, D_E = D.
Re = 90,000.
Open symbols refer to radiated sound intensity with X = 0.3 λ and solid symbols to X = 0.5 λ

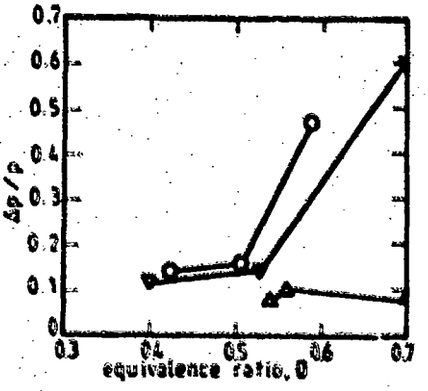


Figure 4. Variation of wall static pressure fluctuation at dump plane with equivalence ratio.
d = 63.5 mm, D = 127 mm, X = 4D, L = 6D, D_E = 76.2 mm, Re = 750,000
△ : triangular duct, injection at vertices, ▽ : triangular duct, injection at sides, ○ : round duct injection at 4 radial locations.

four methods of fuelling and short downstream duct lengths, but decreases to 1.1 for a duct length of 10 D with fuel injection at the sides.

Oscillations associated with bulk mode and longitudinal frequencies were observed in smooth combustion with all four methods of fuelling and oscillations associated with the acoustic frequencies were augmented when the acoustic frequency was nearly the same as the shedding frequency, corresponding to a Strouhal number of around 0.3. The amplitude of the oscillations was about 25% less for fuel injection at the vertices than for other methods of fuelling.

The lower flammability limit obtained with fuel injection at the vertices suggested a region downstream of the dump plane with small scale mixing and a locally high equivalence ratio. To examine the mixing further, radial temperature profiles were measured at the exit plane with an unconstricted downstream duct length of 5 D, which corresponds to the longest downstream duct length for which smooth combustion was possible at the same equivalence ratio for different methods of fuelling. Figure 6 shows temperature profiles, without correction for convection or radiation losses, for the first three methods of fuelling for an equivalence ratio of 0.72 and an upstream Reynolds number of 150,000 (M=0.3). They confirm poorer local mixing for fuel injection at the vertices although the measurements of unburnt hydrocarbon at the exit plane revealed differences of the order of 0.1%.

Fuel injection at the sides of the triangular duct leads to greater heat release in the part of the flow associated with large coherent structures than with premixed flames and the flame was more susceptible to rough combustion, while fuel injected at the vertices entered the part of the flow which was free from large coherent structures and was, therefore, less prone to rough combustion. The influence of air-fuel mixing on flame stability was examined for injection at the vertices in ducts with a constricted exit, by varying the fuelling location and the injection velocity. Injecting fuel 50 mm upstream of the dump plane instead of 100 mm had no effect on the flammability and stability limits. Halving the injection velocity by injecting through two sets of holes located 75 mm and 100 mm upstream of the dump plane, again, made no difference to the flame behaviour. These results were expected since the bulk air velocity was 100 m/s and the mean fuel jet velocities ranged from 5 m/s near lean extinction to 12 m/s at stoichiometry for injection through two sets of holes: the corresponding momentum ratios were correspondingly larger. When the injection velocity was increased by a factor of 13.5, by reducing the diameter of the holes to 1.5 mm, the lean stability limit increased from 0.4 to 0.44, and rough combustion near the rich extinction limit was observed over a slightly wider range of equivalence ratios, for example, between 1.2 and 1.3 compared with between 1.25 and 1.3 for a downstream length of 7 D and an exit nozzle of diameter 0.45 D. The deeper penetration of the fuel jet into the main flow resulted in weaker fuel concentration near the vertex, leading to a higher lean stability limit, and an increase in premixing of air and fuel

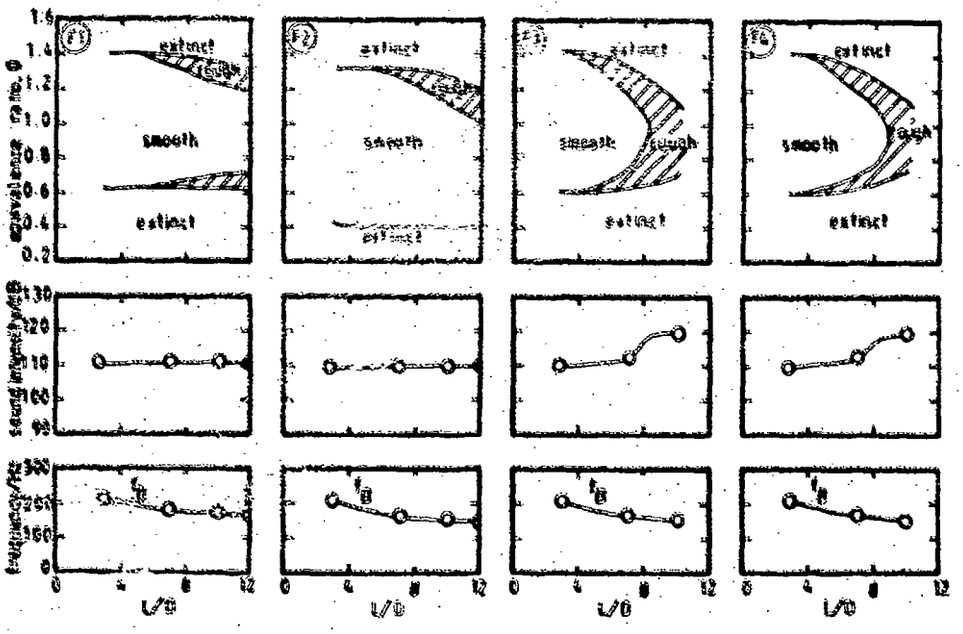


Figure 5. Flammability and stability limits and radiated sound intensity at stoichiometry and dominant frequency.
Geometry C1, b = 31 mm (d = 23 mm), D= 90 mm, ℓ = 7.5 D, D_g = 35 mm, Re = 150,000.
(F1) - premixed flame, (F2) - injection at vertices, (F3) - injection at sides, (F4) - injection at sides and vertices, X_g=100mm.

leading to greater susceptibility to rough combustion.

Injection of fuel at the vertices of the triangular duct and just upstream of the dump plane at a narrow angle to the duct axis ensured that there was little entrainment of fuel into the part of the flow associated with large coherent structures and the flame was, as a result, less susceptible to rough combustion than with injection normal to the axis of the duct. Figure 7 shows the flammability and stability limits for the 80 mm duct with an exit nozzle of 35 mm diameter with downstream duct length as variable for fuel injection at the vertices and at the sides of the triangular opening in the dump plane; other flow conditions are as for Figure 5. The stability characteristics are similar to those in Figure 5 except that rough combustion is observed with downstream lengths greater than 7 D for fuel injection at the vertices, compared with 5 D in Figure 5 and, as expected, is associated with a narrower range of equivalence ratios.

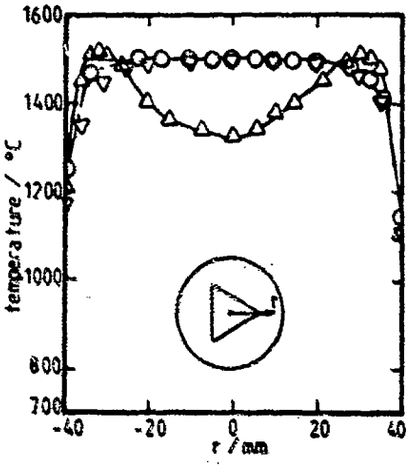


Figure 6. Temperature profiles at exit plane.
Geometry C1, b = 31 mm (d = 43 mm), D = 80 mm, X = 7.5D, L = 5 D, D_E = 0, Re = 150,000, ϕ = 0.72.
△ - injection at vertices, ▽ - injection at sides, ○ - premixed.

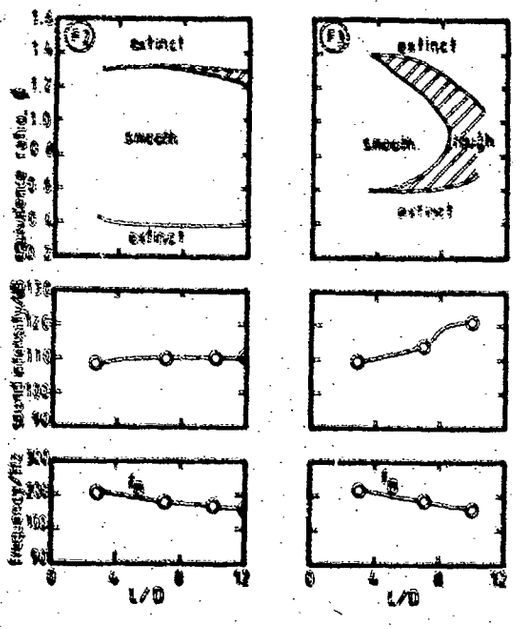


Figure 7. Flammability and stability limits, and radiated sound intensity at stoichiometry and dominant frequency.
Geometry C2, b = 31 mm (d = 43 mm), D = 80 mm, X=7.5 D, D_E =35 mm, Re = 150,000.
(F2) - injection at vertices, (F1) - injection at sides.

Arrangement of fuel injection at the dump plane is not always possible or desirable and fuelling at a location upstream of the dump plane and in the direction of the air flow was examined with the distance of the fuelling hole from the wall as variable. Figure 8 shows the flammability and stability limits for an 80 mm downstream duct of length 7 D with an exit nozzle of 35 mm diameter and with fuel injected near the vertex of the triangular duct and 30mm from the dump plane, other flow conditions are as for Figure 5. The best fuelling location appears to be between 0.3 and 0.5 of the distance between the vertex of the triangle and its centroid. Susceptibility to rough combustion with fuelling near the axis of the duct was anticipated and that with injection very close to the wall appears to be due to the impingement of the fuel jet on the walls adjoining the vertex and the lateral spread of the flow leading to entrainment of fuel into the shear layer emerging from the sides of the triangular jet. The ideal fuelling location for any given geometry will, of course, depend on the dimensions of the fuelling tube and its distance from the dump plane.

Figure 9 shows the flammability and stability limits for an 80 mm duct with a 35 mm exit nozzle with fuel injected in the direction of air flow, 7 mm from the vertices and at a distance of 3 mm from the sides of the triangular duct: other flow conditions are as for Figure 5. The results are similar to those in Figure 7 and confirm that minimising fuel entrainment into the shear layer developing from the side of the triangular jet makes the combustor less susceptible to unstable combustion. Figure 10 shows the variation of the rms wall static pressure 50 mm upstream of the dump plane with equivalence ratio, for a duct length of 6 D and for the two methods of fuelling and flow conditions of Figure 9. In smooth combustion, the fluctuating pressure for fuel

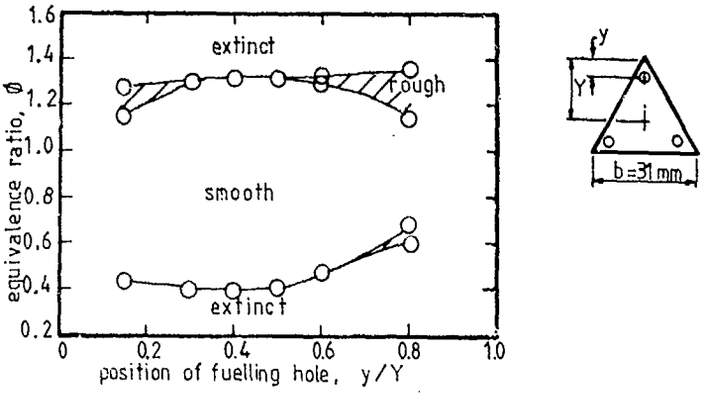


Figure 8. Variation of flammability and stability limits with position of fuelling hole.
Geometry C3, b = 31 mm (d = 23 mm), D = 80 mm, X = 7.5 D, D_E = 35 mm, L = 7 D, Re = 150,000.

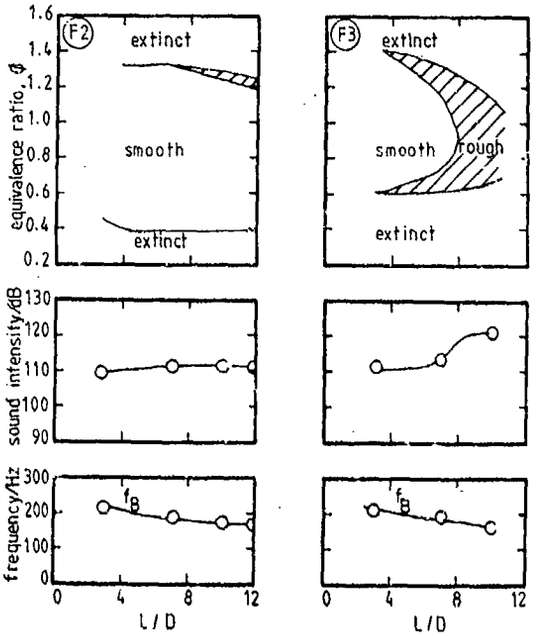


Figure 9. Flammability and stability limits, and radiated sound intensity at stoichiometry and dominant frequency.
Geometry C3, b = 31 mm (d = 23 mm), D = 80 mm, X = 7.5 D, D_E = 35 mm, Re = 150,000.
F2 - injection at 7 mm from vertices; F3 - injection at 3 mm from side

injection near the sides is about 30% higher than for fuel injection near the vertices and rough combustion gives rise to pressure fluctuations at least three times greater than in smooth combustion. These results are similar to those of Figure 4 although the stability limits and the nature of the instabilities are not the same for the respective flows. The results clearly demonstrate that, although injection of fuel at the vertices cannot eliminate rough combustion in long ducts with a constricted exit, the flame is less susceptible to rough combustion, the flammability and stability ranges are wider, and the pressure fluctuations smaller than with other methods of fuelling.

Ducts with an unconstricted exit

Figure 11 shows the variation of lean flammability and stability limits, radiated sound intensity at stoichiometry and the dominant frequency with downstream duct length for the 80 mm duct with an unconstricted exit and an upstream Reynolds number of 150,000 (M=0.3). With fuel injected 30 mm upstream of the dump plane and along the duct axis 7 mm from each of the vertices, the minimum duct length for which rough combustion was observed was 8 D compared with 5 D for other methods of fuelling and

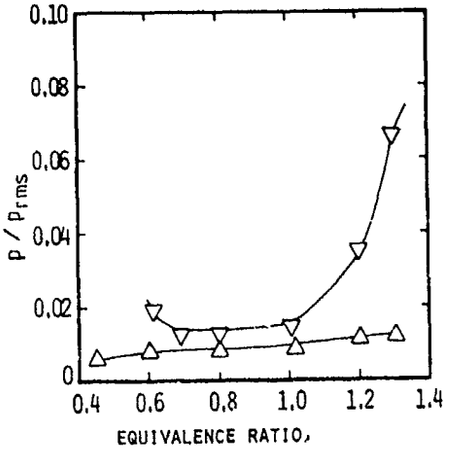


Figure 10. Variation of fluctuating wall static pressure 50 mm upstream of dump plane with equivalence ratio.
Geometry C3, b = 31 mm, (d = 23 mm), D = 80 mm, X = 7.5 D, D_E = 35 mm, L = 7 D, Re = 150,000.
△ - injection at 7 mm from vertices, ▽ - injection at 3 mm from sides.

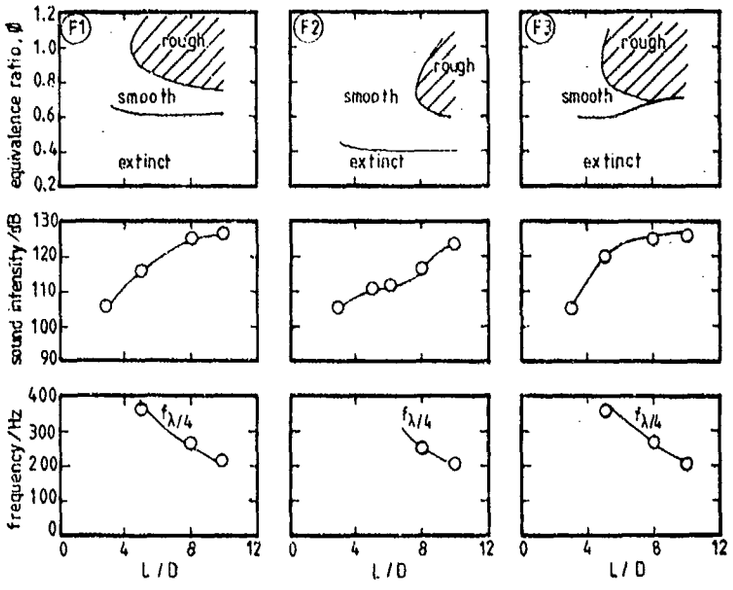


Figure 11. Flammability and stability limits, and radiated sound intensity at stoichiometry and dominant frequency.
Geometry C3, b = 31 mm (d = 25 mm), D = 80 mm, X = 7.5 D, D_E = 80 mm, Re = 150,000.
F1 - premixed flame; F2 - injection at 7 mm from vertices; F3 - injection at 3 mm from sides.

the radiated sound intensity for rough combustion at stoichiometry was, on average, 3 dB less than that for premixed flames and 4 dB less than that with the fuel injected at the sides. The discrete frequencies observed in smooth combustion were small in amplitude and were associated mainly with the quarter-wave frequency of the downstream duct length.

Figure 11 also shows differences in flammability and stability limits for the different methods of fuelling. With injection at the vertices, the lean flammability limit is around 0.4 and the stability limit approaches 0.6 as the duct length is increased beyond 8 D. For premixed flames, the flammability and stability limits are around 0.6 and 0.8, respectively; for ducts longer than 8 D, and with fuel injected at the sides, the flammability limit incrases from 0.6 to 0.7 and smooth combustion is not possible for lengths greater than 8 D.

Fuel injection at the sides, as in ducts with a constricted exit, makes the flame more susceptible to rough combustion than with premixed flows and fuel injection at the vertices makes the flame less susceptible. With increased confinement, however, combustion instability is triggered and the incoherent flow structure along the line of the vertex is no longer preserved so that strong oscillations are sustained by periodic heat release. It is significant, however, that fuel injection at the vertices enables smooth combustion over a wider range of equivalence ratios than with other methods of fuelling.

4. CONCLUSIONS

(1) Fuel injection into the incoherent flow region at the vertices of a triangular upstream duct resulted in a lower value for the lean stability limit than fuel injection at the sides of the triangular duct for combustors with and without an exit nozzle and in a higher value for the rich stability limit for long downstream duct lengths. Fuel injection at the vertices was also associated with a wider range of stability and a lower intensity of radiated sound, and rough combustion in combustors with a constricted exit was limited to a small range of equivalence ratios close to the rich stability limit.

(2) The use of premixed fuel and air was associated with wider ranges of flammability and stability than those for fuel injection at the sides of a triangular upstream duct but narrower than those for injection at the vertices.

(3) Flammability and stability characteristics for eccentric premixed dump combustors with an unconstricted exit and a dump plane area ratio of 2.5 are similar to those for axisymmetric combustors. The effect of eccentricity was important only for large values of eccentricity which led to a 10% reduction of the range of flammability. Rough combustion in the non-axisymmetric geometries was associated with the quarter-wave frequency of the duct downstream of the dump plane and, as in axisymmetric combustors, the dominant frequency decreased slightly with a decrease in dump plane area ratio.

(4) Rough combustion was not observed for downstream duct lengths of up to 12 D when the exit was constricted by nozzles with diameter in the range between 0.7 and 0.8 D. Rough combustion was observed with exit nozzle diameters in the range between 0.45 and 0.75 D and was associated with two ranges of equivalence ratio adjoining the flammability limits and the bulk mode frequency of the combustor.

(5) Oscillations associated with the bulk mode and the longitudinal (half-wave) frequency were observed in smooth combustion in ducts with an exit nozzle and were augmented when the acoustic frequency was close to the vortex shedding frequency.

REFERENCES

[1] Howland, A.H., & Simmonds, W.A. (1953). Combustion inside refactory tubes. 4th Symposium (International) on Combustion, pp. 592-602.

[2] Ross, P.A. (1958). Some observations of flame stabilisation in sudden expansions. Jet Propulsion, 28, pp. 123-125.

[3] Kilham, J.K., Jackson, E.G., & Smith, T.B.J. (1961). An investigation of tunnel burner noise. Institution of Gas Engineers Journal, 1, pp. 251-266.

[4] Kilham, J.K., Jackson, E.G., & Smith, T.B.J. (1965). Oscillatory combustion in tunnel burners. 10th Symposium (International) on Combustion, pp. 1231-1240.

[5] El Banhawy, Y., Melling, A., & Whitelaw, J.H. (1978). Combustion-driven oscillations in a small tube. Combustion and Flame, 33, pp. 281-290.

[6] Crump, J.E., Schadow, K.C., Yang, V., & Cullick, F.E.C. (1986). Longitudinal combustion instabilities in ramjet engines: identification of acoustic modes, Journal of Propulsion and Power, 2, pp. 105-109.

[7] Schadow, K.C., Crump, J.E., Mahan, V.A., Nabity, J.A., Wilson, K.J., & Gutmark, E. (1985). Large-scale coherent structures as drivers of ramjet combustion instabilities, 1985 JANNAF Propulsion Meeting.

[8] Schadow, K.C., Gutmark, E., Parr, T.P., Parr, D.M., & Wilson, K.J. (1986). Passive shear flow control to minimise ramjet combustion instabilities, 23rd JANNAF Combustion Meeting.

[9] Sivasegaram, S., & Whitelaw, J.H. (1987). Oscillations in axisymmetric dump combustors, Combustion Science and Technology, 52, pp. 413-426.

[10] Sivasegaram, S., & Whitelaw, J.H. (1987). Combustion oscillations in dump combustors with a constricted exit, Department of Mechanical Engineering, Imperial College, London, Report FS/87/01. To be published in Proc. I. Mech .E.

[11] Putnam, A.A. (1971). Combustion-Driven Oscillations in Industry, New York: American Elsevier Publishing Company, Inc.

[12] Putnam, A.A., Murphy, M.J., & Locklin, D.W. (1985). Burner technology bulletin: control of combustion noise for small gas burners, Gas Research Institute, Chicago, Topical Report GR1-85/210.

[13] Sivasegaram, S., & Whitelaw, J.H. (1987). Oscillations in confined disk-stabilised flames, Combustion and Flame, 68, pp. 121-129.

[14] Sivasegaram, S., & Whitelaw, J.H. (1987). Suppression of oscillations in confined disk-stabilised flames, Journal of Propulsion and Power, 3, pp. 291-295.

[15] Bloxidge, G.J., Dowling, A.P., Hooper, N., & Langhorne, P.J. (1987). Active control of reheat buzz, AIAA Paper 87-0433.

[16] Lang, W., Poinsot, T., & Candel, S. (1987). Active control of combustion instability, Combustion and Flame, 70, pp. 281-289.

[17] Schadow, K.C., Gutmark, E., Wilson, K.J., Crump, J.E. and Foster, J.B. (1984). Interaction between acoustics and subsonic ducted flow with dump, AIAA Paper 84-0530.

[18] Schadow, K.C., Gutmark, E. and Wilson, K.J. (1987). Characterization of large-scale structures in a forced ducted flow with dump, AIAA Journal, 25, pp.1164-1170.

[19] Schadow, K.C., Gutmark, E., Parr, T.P., Parr, D.M. and Wilson, K.J. (1987). Large-scale coherent structures as drivers of combustion instability, AIAA Paper 87-1326.

[20] Gutmark, E., Schadow, K.C., Parr, D.M., Harris, C.K. and Wilson, K.J. (1985). The mean and turbulent sructure of non-circular jets, AIAA Preprint 85-0543.

[21] Schadow, K.C., Wilson, K.J. and Gutmark, E. (1985). Reduction of flow coherence in forced subsonic jets. AIAA Paper 85-1109.

[22] Gutmark, E., Schadow, K.C., Wilson, K.J. and Parr, D.M. (1986). Small-scale mixing enhancement in acoustically excited jets, AIAA Preprint 86-1885.

[23] Schadow, K.C., Gutmark, E., Parr, D.M., & Wilson K.J. (1988) Selective control of flow coherence in triangular jets, Experiments in Fluids,6, pp.129-135.

[24] Gutmark, E., Schadow, K.C., Parr, T.P., Parr, D.M. and Wilson, K.J. (1987). Non-circular jets in combustion systems,AIAA Paper 87-1379.

ACKNOWLEDGEMENT

Financial support for this work was from the US Office of Naval Research under Grant N00014-84-G-0185 and is gratefully acknowledged.

ACOUSTIC-VORTEX-CHEMICAL INTERACTIONS IN AN IDEALIZED RAMJET

K. Kailasanath, J.H. Gardner, J.P. Boris and E.S. Oran
Laboratory for Computational Physics and Fluid Dynamics
Naval Research Laboratory, Code 4410
Washington, D.C. 20375, U.S.A.

SUMMARY

A potentially important source of large pressure oscillations in combustors is an instability induced by the interactions between large-scale vortex structures, acoustic waves, and chemical energy release. To study these interactions, we have performed time-dependent, compressible numerical simulations of the flow field in an idealized ramjet consisting of an axisymmetric inlet and combustor and a choked nozzle. These simulations have allowed us to isolate the interactions between acoustic waves and large-scale vortex structures and then to study the effects of energy release on the flow field. A number of parameters such as inflow Mach number, inlet and combustor acoustics and energy release rates have been systematically varied in the simulations. A summary of the observations from these various simulations are presented in this paper.

The nonreactive flow calculations show complex interactions among the natural instability frequency of the shear layer at the inlet-combustor junction and the acoustics of both the inlet and the combustor. Vortex shedding usually occurs at the natural instability frequency of the initially laminar shear layer but vortex mergings are affected by the acoustic frequencies of the ramjet. When the frequency of the first longitudinal acoustic mode of the combustor is near the natural instability frequency of the shear layer, then vortex shedding is observed at the acoustic frequency. In many cases the entire flow oscillates at a low frequency which corresponds to that of a quarter-wave mode in the inlet. In these cases, the vortex-merging patterns in the combustor can be explained on the basis of an interaction between the acoustics of the inlet and the combustor.

For the particular reactive flow case discussed in detail in this paper, energy release alters the flow field substantially. In the first cycle after ignition, fluid expansion due to energy release quickly destroys the pattern of vortex mergings observed in the cold flow and a new pattern emerges that is dominated by a large vortex. In subsequent cycles, most of the energy release occurs after vortex mergings have produced this large vortex. Energy release in this large vortex is in phase with the pressure oscillation over a substantial region of the combustor. This results in the observed amplification of the low-frequency oscillations and leads to combustion instability.

INTRODUCTION

In this paper we summarize our work to date on the acoustic-vortex-chemical interactions in an idealized ramjet consisting of an axisymmetric inlet and combustor and a choked nozzle. High-speed flows separate at the inlet-combustor junction and the separated shear layer is usually turbulent. Such transitional shear layers are characterized by large-scale vortical structures. The interactions among these vortical structures can generate acoustic waves. Furthermore, the interactions themselves can be affected by the acoustic waves in the system. Energy release can have a substantial influence on the acoustic-vortex interactions by modifying both the acoustic waves and the flow field in the system. The nonlinear interactions among acoustic waves, large-scale vortex structures and chemical energy release affects the efficient operation of the system and may even result in combustion instability. To study these interactions we are performing two-dimensional, axisymmetric numerical simulations. These simulations allow us to isolate the interactions between acoustic waves and large-scale vortex structures and then to study the effects of energy release on the flow field.

In recent years, numerical simulations have been used to study the flow field in both axisymmetric centerbody [1] and dump combustors [2-5]. In the numerical study of a dump-combustor flow field [2], there was fair agreement between the computed quantities such as mean axial velocity profiles and experimental data. However, these computations predicted a steady solution with a large recirculation zone. Simulations of a centerbody combustor [1] showed an oscillating flow field with periodic vortex shedding. Neither of these simulations considered the effects of an exit nozzle or acoustic waves on the flow field in the combustor. More recent simulations have considered the effects of exit nozzles and the acoustics of the inlet and combustor [3-5].

Our work can be broadly divided into three categories. In the first, the effects of varying the acoustics while keeping the flow parameters fixed (inflow velocity of 50 m/s) was investigated [3,5,6]. The acoustics of the ramjet was varied by separately varying the length of the inlet and the combustor [6]. These simulations indicate a strong coupling between the acoustics of the ramjet, both the inlet and the combustor, and the flow field. In all cases, a low frequency oscillation is observed. Pressure oscillations in the inlet indicates that the quarter-wave acoustic mode of the inlet is the origin of this low frequency. Changing the length of the inlet or the sonic velocity in the inlet appropriately changes the observed low frequency. Simulations also show that acoustic forcing at the first longitudinal acoustic mode of the combustor induces vortex-rollup near the entrance to the combustor at the forcing frequency when the forcing frequency is close to the natural shedding frequency of the shear layer. It was also found that the merging pattern of the vortices in the combustor is influenced by the length of the combustor. These merging patterns have been explained on the basis of an interaction between the vortex-rollup frequency and frequency of the quarter-wave mode in the inlet [6].

In the second set of simulations, the effects of varying the flow parameters on vortex shedding and merging has been studied [7]. When the flow velocity is increased, the natural instability frequencies of the shear layer also increases while the acoustic frequencies remain essentially the same. Vortex shedding and initial vortex-mergings occur at the natural shear layer instability frequency and its subharmonics if these frequencies are significantly different from the dominant acoustic frequencies of the system. Subsequent vortex-mergings are influenced by the longitudinal acoustic-mode frequencies. The presence of many significant frequencies results in less organized and more complex merging patterns. We have identified a number of different interactions of acoustic modes with the vortex mergings which explain these complex merging patterns. These interactions can be used as a means of controlling the formation of large scale structures by inducing many possible less well organized coherent structures.

Finally, the effects of chemical reactions on the flow field was investigated [8]. The first case studied was that of a pre-mixed, lean hydrogen-oxygen-nitrogen mixture flowing into the combustor at 200 m/s. In this case, energy release alters the flow field in the combustor substantially. Energy release quickly destroys the pattern of vortex mergings observed in the cold flow and a new pattern emerges that is dominated by a large vortex. However, the low frequency oscillation observed in the cold flow persists and its amplitude increases substantially when there is energy release. In the simulations investigated so far this mode has again been identified with the quarter wave mode of the inlet. The coupling between the energy release and the pressure fluctuations in the combustor has been studied in detail. Energy release is in phase with the pressure oscillations over a substantial portion of the combustor and this results in amplification of the pressure fluctuations and eventually leads to combustion instability. There are regions in the combustor where the oscillations are damped. This suggests that combustion instability may be controllable by increasing the regions where the energy

release and pressure are out of phase. Several approaches to controlling the combustion instability as well as additional parametric studies of the effects of chemistry are currently being persued.

In this paper, we first briefly discuss the numerical model and then present examples from the three categories of simulations discussed above. Low-frequency oscillations such as those described here, which depend on the acoustics of the inlet have been observed in experiments in dump combustors with a constricted exit [9].

THE NUMERICAL MODEL

The numerical model solves the compressible, time-dependent, conservation equations for mass, momentum and energy in a two-dimensional axisymmetric geometry. The fluid dynamics and chemistry terms in the conservation equations are solved separately and coupled using timestep splitting [10]. The algorithm used for fluid dynamic convection is Flux-Corrected Transport (FCT) [11], a conservative, monotonic algorithm with fourth-order phase accuracy. FCT algorithms can be constructed as a weighted average of a low-order and a high-order finite-difference scheme. During a convective transport timestep, FCT first modifies the linear properties of the high-order algorithm by adding diffusion. This prevents dispersive ripples from arising and ensures that all conserved quantities remain monotonic and positive. Then FCT subtracts out the added diffusion in regions away from discontinuities. Thus it maintains a high order of accuracy while enforcing positivity and monotonicity. With various initial and boundary conditions, this algorithm has been used previously to solve a wide variety of problems in both supersonic reacting flows [12-14] and subsonic turbulent shear flows [5,15,16].

The calculations presented below are inviscid, that is, no explicit term representing physical viscosity has been included in the model. Also, no artificial viscosity is needed to stabilize the algorithm. There is a residual numerical diffusion present which effectively behaves like a viscosity term for short-wavelength modes on the order of the zone size. Unlike most numerical methods, however, the damping of the short-wavelength modes is nonlinear. Thus the effects of this residual viscosity diminish very quickly for the long wavelength modes. In the problem considered in this paper, we are primarily interested in the interaction of the acoustic modes with large-scale vortex structures, which is essentially an inviscid interaction.

The large number of species and reactions involved make it computationally impractical to include a detailed chemical reaction rate scheme in a complex multidimensional fluid dynamic problem such as the one discussed here. A detailed reaction rate scheme even for a 'simple' fuel such as hydrogen in air involves 9 species and about 50 reactions [17]. Therefore we have modelled the combustion of premixed hydrogen-air mixture using a simplified two-step parametric model. The first step is an induction step during which there is no energy release. The second step models the energy release process and starts only after the induction time has elapsed. During the induction step, the reactions taking place are modelled by

$$fuel + oxidiser + diluents \leftrightarrow radicals \tag{1}$$

and during the energy release step,

$$fuel + oxidiser + radicals + diluents \leftrightarrow products. \tag{2}$$

In an actual combustion system both steps occur simultaneously after the first step has been initiated. However, during the induction step, the change in the concentrations and the amount of energy released are small enough that they can be neglected in a simplified model. Thus the temperature and pressure may be assumed to be constant during the induction period. This simplification enables us to use the chemical induction time data which are usually available at constant temperatures and pressures for mixtures of specified stoichiometry. The induction time data may be obtained from experiments or from calculations using detailed elementary reaction mechanisms[17]. We have used a table of induction times which were obtained by integrating a detailed set of reaction rates. These induction times have been compared to experimental data where available and found to be in good agreement [17]. Currently, the energy releasing reactions are assumed to take place at a constant rate. The emphasis in this paper is on the qualitative effects of energy release on the flow field and the coupling between the energy released and the pressure field in the combustor. Future calculations will include varying the energy release times and the amount of energy release to gain a qualitative understanding of the effects of these parameters on the flow field in the combustor.

GEOMETRY AND BOUNDARY CONDITIONS

A schematic of the idealized central-dump combustor used in the simulations is shown in Fig. 1. A cylindrical jet with a prescribed mean velocity (50-200 m/s for the simulations described here) flows through an inlet of diameter, D into a cylindrical combustion chamber (dump combustor) of larger diameter. The dump combustor acts as an acoustic cavity and its length has been varied to change the frequency of the first longitudinal mode. An annular exit nozzle at the end of the chamber is modelled to produce choked flow.

The initial thrust of the modelling was to develop appropriate inflow and outflow boundary conditions [3, 18]. The choked outflow conditions force the flow to become sonic at the throat of the exit nozzle. At solid walls the normal flux is set to zero and the pressure is extrapolated to the normal stagnation condition. At the inflow, the pressure is allowed to fluctuate, but the mass flow rate and the inflow velocity are specified. These conditions allow the acoustic waves to reflect without amplification or damping at the inflow. These inflow boundary conditions could be modified to partially damp the acoustic waves originating downstream. More detailed discussions and tests of the boundary conditions have been presented in earlier papers [5, 18].

The computational cell spacing was held fixed in time. Fine zones were used near the entrance to the combustor (the dump plane) in both the radial and axial directions. In both directions the cell sizes gradually increased away from the dump plane. The effects of numerical resolution were checked by comparing calculations with 20× 50, 40 × 100 and 80 × 200 cells. These grids were generated by either doubling or halving the cell sizes used in the 40 × 100 cell calculations. The 20× 50 grid was too coarse to resolve the vortex shedding and merging resolved by the other two grids. With the finer 80× 200 grid, smaller structures and higher frequencies can be resolved than with the coarser (40× 100) grid. However, it was found that the 40 × 100 grid was adequate to resolve the major frequencies and all the large-scale structures observed in the cold flow [5, 18]. In order to improve the resolution of the flame front, a 60 × 120 grid is used in most of the calculations reported here. The smallest cell size in this grid is comparable to those in the 80 × 200 grid. The smallest cell size in the radial direction is 0.0529 cm and in the axial direction is 0.3069 cm. A typical timestep in the reactive flow calculations is 0.144 μs and takes 0.25 s of CPU time on the NRL CRAY X-MP/24 computer.

RESULTS AND DISCUSSION

The numerical simulations predict values of the density, momentum, and energy for each of the computational cells as a function of time. From this information we can selectively generate the various physical diagnostics. The analysis presented below uses three diagnostics extensively: the local time-dependent velocity and pressure fluctuations at various locations in the flow field, the

time-dependent energy release at various stations in the combustor, and instantaneous flow visualization at selected times. For flow visualization, we use streamlines and temperature contours. Streamlines of the instantaneous flow field are a useful visual diagnostic for studying the structure of the flow. They also allow correlation and tracking of the coherent vortex structures and their merging patterns.

ACOUSTIC-VORTEX INTERACTIONS

In the cold flow calculations discussed below, a portion of the rear wall of the dump combustor acts as an acoustic source, simulating a planar loudspeaker. The forcing amplitude is 0.5% of the initial chamber pressure and the frequency is that of the first longitudinal acoustic mode of the dump chamber.

Case 1: Basic Configuration—a Combustor of length 5.8 D

The physical dimensions of the inlet and combustor used in the first set of calculations are given in Fig. 1. In addition, the exit consists of an annular ring at 0.64 D (from the axis of the combustor) with an area of 7.99 cm^2. The mass inflow rate is 0.38 kg/s with a mean velocity of 50 m/s. The initial chamber pressure is 186 kPa. These conditions were chosen to match those in the experiments of Schadow et al. [19]. In this case the forcing frequency is 450 Hz. This corresponds to the first longitudinal acoustic mode of the combustor and is also in the range of the most amplified frequencies near the dump plane [19]. This case has been discussed extensively in earlier papers [3,5] and is summarized below.

Evidence that forcing in the range of the locally most amplified frequency produces highly periodic and coherent vortex structures can be seen from studying streamlines describing the instantaneous flowfield. Figure 2 shows the streamlines within the dump chamber at a sequence of times. The various frames in this figure are instantaneous "snapshots" of the flowfield taken 1.093 ms apart. This corresponds to 1000 timesteps in the calculation. In each frame, the dump plane is at the left and the exit plane is at the right. The paths of the various vortices are also indicated in the figure. In the first frame (timestep 31000) we see a vortex structure near the dump plane. In the second frame (timestep 32000), this structure has grown and moved downstream. In the third frame (timestep 33000), not only has this structure moved further downstream, but a new structure has formed near the dump plane. This process continues with a new vortex structure appearing near the dump plane at intervals of 2000 timesteps, at timesteps 33000, 35000, 37000, 39000, 41000 and 43000. This corresponds to a frequency of 458 Hz, which is close to the forcing frequency of 450 Hz. The small disagreement of 8 Hz is an artifact of showing the flowfield snapshots at intervals of 1000 timesteps rather than 1017 timesteps.

Figure 2 also shows that the two structures, that were first seen near the dump plane at timesteps 31000 and 33000, have merged (paired) at about 2.4 D by timestep 37000. As this large, merged structure moves downstream, another vortex, first seen near the dump plane at timestep 35000, merges with it. This new merging occurs by timestep 43000 at about 4.8 D. The structures which appeared near the dump plane at timesteps 37000 and 39000 merge together at about 2.4 D by timestep 43000. That is, at either 2.4 D or 4.8 D, a merging is observed only at about every 6000 timesteps which corresponds to a frequency of about 150 Hz. Since new vortices appear near the dump plane every 2000 timesteps, we note that two successively generated vortices do not always merge with each other.

The time evolution of the flowfield described above can be correlated with the fourier analysis of the pressure and velocity fluctuations observed at various axial locations in the combustor. In Fig. 3 we show the fourier analysis of the velocity fluctuations at the six axial locations, 0.1, 1.05, 2.03, 3.03, 4.07 and 5.14 D . All the locations are at the level of the step, a constant radial distance of 0.5 D from the axis of the combustor. At 0.1 D, the dominant frequency is 450 Hz. This is at least partly due to the velocity fluctuations associated with the forcing frequency of 450 Hz. Some of it may also be due to velocity fluctuations associated with the vortex roll-up seen in Fig. 2. The amplitude at 450 Hz increases significantly as we go downstream to 1.03 D. This corresponds to the passage frequency of the vortices first seen near the dump plane. We also see some amplitude at 150 Hz. The amplitude at 150 Hz increases further by 2.03 D and that at 450 Hz decreases. This is because of the vortex mergings which have begun to occur. By 3.03 D, the vortex merging is complete and the 450 Hz is no longer significant. This is consistent with the flowfield visualization in Fig. 2 which shows vortex mergings near 2.4 D at a frequency of about 150 Hz.

At 2.03 and 3.03 D, there is a new feature in the spectrum: there is significant amplitude at 300 Hz. As discussed earlier, two successively generated vortices do not always merge with each other at 2.4 D. Therefore, between 2.03 and 3.03 D, we see both vortex mergings and a smaller vortex passing by that eventually merges with the larger one. This smaller vortex passes by once between successive mergings. Since successive mergings occur with a frequency of 150 Hz, we see velocity fluctuations at the higher frequency of 300 Hz. At 4.07 D, the dominant frequency is 150 Hz corresponding to the passage of the vortex that was formed by merging between 2.03 and 3.03 D. At 5.14 D, the dominant frequency is 150 Hz because of the mergings which take place near 4.8 D at that frequency. Furthermore, we no longer see a significant amplitude at 300 Hz because only one type of large merged vortex passes by 5.14 D. The fourier analysis of the pressure fluctuations corroborates the observations made based on the velocity fluctuations and the flowfield visualization [5].

Low frequency Oscillations

Figure 2 shows that the entire flow undergoes a complete cycle in approximately 6000 timesteps. For example, at timesteps 33,000 and 39,000 a large-scale structure has partially exited through the nozzle. At these times, we also see similar flow structures of about the same sizes at about the same positions in the chamber. This similarity exists between any two frames which are 6000 timesteps apart. The frequency corresponding to this cycle is about 150 Hz. This frequency is one third of the forcing frequency or the first vortex merging frequency near the dump plane.

There are many possible mechanisms that can generate such a low frequency oscillation. One such mechanism is the interaction between the vortices convecting downstream and the exit nozzle or wall of the combustor. Another possibility is that the low frequency is an acoustic mode associated with the inlet. These two mechanisms are examined below in some detail.

The interaction between vortices and a surface of impingement as a source of low frequency oscillations has received considerable attention in the past [20-22]. The basic mechanism has been examined in detail by Ho and Nosseir [20] in their study of the dynamics of a jet impinging on a flat plate. The low frequency oscillation they observed depended on the convective speed of the vortices, the speed of upstream-propagating waves, and the distance between the jet nozzle and the plate. To examine the similarity between the two phenomena, calculations similar to the simulations discussed above were performed for dump chambers of different lengths. This is equivalent to changing the distance between the jet nozzle and the plate in the Ho and Nosseir experiment. However, we found [6] that the frequency of the oscillations were essentially independent of the length of the combustor. Therefore the interaction between the vortices and the end wall of the combustor does not seem to play an important role in determining the low frequency.

As mentioned above, the acoustics of the inlet may be a source of the low frequency. The inlet is essentially a long pipe with

flow coming in from one end and flowing out into the combustor at the other end. The inflow boundary conditions specified in the numerical model allow complete reflection of the pressure waves that reach the upstream end of the inlet. If the downstream end of the inlet behaves like an open end, the dominant acoustic mode of the inlet would be the quarter wave mode. Since the length of the inlet is 8.8 D, the frequency of this mode corresponding to the physical conditions in the simulation discussed above is about 148 Hz, which is close to the observed frequency of 150 Hz.

In order to study the acoustic modes of the ramjet in greater detail, the fourier analysis of the pressure fluctuations at various locations in the inlet were studied. The dominant frequency near the upstream end of the inlet (−7.4 D) was 150 Hz, but there was also some fluctuation at 450 Hz. Closer to the combustor, the amplitude of the 150 Hz mode decreased and that of the 450 Hz mode increased. If the downstream end of the inlet behaved like an ideal open end, the amplitude at 150 Hz should decrease as we move towards it and reach zero at the dump plane. There was a very small amplitude near the dump plane (−0.7 D) perhaps due to the interaction with the 450 Hz mode. The spatial distribution of the fluctuating pressure within the inlet and the combustor indicates that the mode in the inlet is not a pure quarter wave mode.

In order to further confirm that the acoustics of the inlet does indeed determine the low frequency, the length of the inlet was decreased to 7.2 D. The low frequency oscillations appropriately shifted to 174 Hz.

Case 2: Calculations with a Longer Combustor

Although the acoustics of the inlet determines the low frequency oscillation, simulations of ramjets with different combustor lengths provide valuable information on the flow field in the combustors. Here we discuss one case, in which the length of the dump chamber was increased to 8.6 D. All the other dimensions were the same as those described earlier. The forcing frequency was decreased to 300 Hz because the length was increased.

The instantaneous flow field (Fig. 4) within the combustor at a sequence of timesteps shows a new large-scale structure appearing near the dump plane at intervals of three thousand timesteps, that is, at timesteps 40000, 43000, 46000, 49000 and 52000. This corresponds to a frequency of about 300 Hz, which is the same as the forcing frequency. Our first conclusion, therefore, from changing the length of the combustor is that the first vortex merging frequency near the dump plane changes to match the first longitudinal mode of the combustor.

Figure 4 shows that two successively generated vortices merge with each other at about 3.5 D. No further mergings occur as the vortices convect downstream and exit through the nozzle. This is in contrast to Case 1 in which a further merging with a single vortex occured before the pair could exit. The frequency corresponding to the vortex mergings is about 150 Hz since it occurs at approximately every 6000 timesteps. The lowest dominant frequencies observed in Cases 1 and 2 are both about 150 Hz. *The low frequency does not change when the length of the combustor is increased.* Instead, the merging pattern has changed to accomodate the low frequency of 150 Hz. From this we conclude that the shear layer at the step responds to the acoustics of both the dump chamber and the inlet.

Further confirmation that the merging pattern in the combustion chamber changes to accomodate the low frequency associated with the inlet was obtained by changing the length of the combustion chamber to 7.2 D. In this case the forcing frequency corresponding to the longitudinal mode of the combustor was 338 Hz. The merging pattern was quite complicated, involving features of Cases 1 and 2 discussed above. The lowest dominant frequency observed was 143 Hz. This case is discussed in greater detail elsewhere[6,23].

EFFECTS OF INFLOW MACH NUMBER

Case 3: Inflow Mach Number 0.31

The physical dimensions of the inlet and combustor used in the simulations are the same as those given in Fig. 1. In addition, for Case 3, the exit consists of an annular ring at 0.625 D (from the axis of the combustor) with an area of 14.89 cm^2. The mass inflow rate is 0.78 kg/s with a mean velocity of 100 m/s. The initial chamber pressure is 188 kPa.

Vortex Shedding and Merging near the Combustor Step

A series of snapshots of the flow field at a constant interval of 0.376 ms, every 1000 timesteps, is shown in Fig. 5. New vortices appear near the combustor step in the first, third, fifth and seventh frames. That is, vortex shedding occurs approximately every 2000 timesteps. This corresponds to a frequency of about 1330 Hz. The paths of the vortices have also been drawn in Fig. 5. They show that the vortex shed at timestep 125,000 merges with the one shed at timestep 123,000 around timestep 127,000. The merging location is within two diameters off the step in the combustor. The previous timestep at which such a merging occurred is 123,000. Therefore the approximate merging frequency at this location is 665 Hz. Figure 5 also shows the two processes by which vortices grow: entrainment of the surrounding fluid and vortex merging. The vortex shed at timestep 123,000 grows by entraining the surrounding fluid before another vortex merges with it.

It is difficult to determine the vortex shedding and merging frequencies precisely from streamlines such as in Fig. 5 where the flow field is depicted only every 0.376 ms (at a frequency of 2660 Hz). The fourier analyses of velocity fluctuations at two locations close to the step in the combustor are shown in Fig. 6. At 0.57 D from the dump plane, there is only one dominant frequency, 1330 Hz. This is the passage frequency of vortices at this location. It also corresponds to the vortex-shedding frequency of the shear layer at the combustor step because vortex mergings are not observed to take place before this location. At 1.63 D, the significant frequency is 690 Hz, the first subharmonic of the vortex-shedding frequency. This is the passage frequency of the larger vortex formed by the first merging of vortices which occurs before this location in the combustor. Therefore, based on the fourier analysis of the velocity fluctuations and the flow-field visualization, we conclude that vortex shedding occurs with a frequency of about 1330 Hz and these vortices merge within 2 D to a frequency of about 690 Hz.

For a configuration such as the one discussed in this paper, it is difficult to define a characteristic thickness for the shear layer at the combustor step because of the large recirculation zone. The momentum thickness is highly dependent on the velocity cut-off chosen. Because viscosity is not explicitly included in these simulations, the smallest scale in these calculations is the grid spacing in the transverse direction at the combustor step. However, a necessary condition for the shear layer to be unstable is an inflection point in the velocity profile. In order to resolve an inflection point, at least two computational cells are required. Therefore we take the width of two cells as a characteristic dimension for the shear-layer thickness. In this simulation, this thickness is 0.106 cm. Using this thickness and a frequency of 1330 Hz, we obtain a Strouhal number of 0.015. An initially laminar shear layer has been observed experimentally [24] to roll up at $St_\theta = 0.012$. The theoretical value [25] is 0.017. Considering the uncertainty in the determination of the shear layer thickness in our simulations, the value of 0.015 for the Strouhal number suggests that the frequency 1330 Hz is the natural instability frequency of the shear layer in the simulations.

Vortex mergings occur not only near the combustor step at a frequency of about 690 Hz, but also further downstream in the combustor. The time intervals between successive vortex mergings are not all the same, suggesting that vortex mergings are not

occuring with an unique frequency. Furthermore, the location where vortex merging takes place is also observed to change suggesting that the vortex-merging patterns is also changing. The frequencies observed most often are close to the passage frequency following the first vortex-merging (690 Hz) and beat frequencies between this and the quarter wave mode frequency of the inlet (150 Hz). Vortex-mergings are also occuring sometimes at 442 Hz and 295 Hz. These frequencies are close to the first longitudinal mode frequency of the combustor (450 Hz) and a beat frequency between the inlet and combustor frequencies (300 Hz).

In summary, vortex mergings in most of the combustor are not observed to take place at any particular dominant frequency but at frequencies resulting from the interaction between the vortex shedding frequency and its subharmonics and the dominant acoustic frequencies of the system.

REACTIVE FLOW SIMULATIONS

The first reactive-flow case studied was that of a pre-mixed, lean hydrogen-oxygen-nitrogen mixture flowing into the combustor at 200 m/s. The calculations were carried out to 160,000 timesteps without considering the effects of chemical reactions. Below we first briefly discuss these "cold-flow simulations" and then present results of the reactive flow simulations.

Case 4: Inflow Velocity 200 m/s

The vortex dynamics very near the step in the combustor for this case is very similar to that observed in case 3. Vortex shedding is observed to take place at the natural instability frequency of the shear layer. Within one diameter of the inlet-combustor junction, vortex-pairing occurs at the first sub-harmonic of the shedding frequency. The fourier analysis of the velocity fluctuations at different locations in the combustor show the presence of multiple frequencies. These frequencies include the quarter-wave mode frequency of the inlet and beat frequencies between the inlet and combustor acoustics as well as sub-harmonics of the shear-layer instability frequencies. In spite of these complexities, the flow field is approximately periodic at the quarter-wave mode frequency of the inlet.

Effects of Energy Release.

The mixture was ignited at timestep 160000 by assuming that the induction time has elapsed for a pocket of the gaseous mixture near the step. This causes the mixture to begin releasing its energy. The instantaneous flow fields in the combustor are shown at a sequence of timesteps in Fig. 7 using two different visualizations, contours of constant temperature and streamlines. Although timestep 160000 is before any energy release has occured, there are temperature fluctuations due to the compressibility of the flow. At step 165000, energy release has caused a reaction front (flamefront) distinguished by the location of the high-temperature contours and the darkened lines caused by closely spaced contours. The presence of a vortex near the step at this time is seen in Fig. 7b and the entrainement of the cold gases by it can be seen in Fig. 7a. With time, the shear layer roll-up causes the reaction front to curve downwards and engulf the cold mixture which subsequently burns. As the reaction front moves downstream, a new vortex forms near the step between timesteps 175000 and 180000. This mixes the burnt gases with the incoming fuel-air mixture and acts as an ignition source. Except for the first time at step 160000, it was not necessary to provide an external ignition source. The relation between the flamefronts and the vortices in the subsequent frames can be established by comparing the two figures. Comparing the flow fields at steps 160000 and 185000, one can see how rapidly energy release alters the features of the cold flow.

Another interesting observation from Fig. 7a is the presence of an unburned gas pocket at step 185000. This pocket of material has been cut off by the interaction of two flamefronts, seen at step 180000. The pocket subsequently burns up and its remnants can be seen in the center of the forward most (closer to the exit) structure in step 190000. By step 195000, the flamefronts have reached the rear wall of the combustor and the burnt material has begun to exit.

Streamlines and temperature contours depicting the flow field in the combustor at a subsequent sequence of timesteps are shown in Figs. 8a and b. The presence of large-scale vortex structures in the reactive flow case is evident from these figures. The flow fields at steps 200000 and 225000 and those at 205000 and 230000 are similar to each other, suggesting that the reactive flow field undergoes a cycle of roughly 25000 timesteps or 3.463 ms. This corresponds to a frequency of 288 Hz, which is close to the low frequency of about 250-280 Hz observed in the cold-flow simulations.

The pressure and velocity fluctuation spectra at all locations are dominated by this low frequency of 288 Hz. A large-scale vortex rollup also occurs at this frequency as can be seen by comparing steps 200000 and 225000 in Fig. 8b. However, vortex shedding does occur more frequently as seen in steps 205000 and 215000. These small vortices merge quickly to the larger vortex generated periodically at 288 Hz resulting in a still larger vortex which dominates the entire flow field. As discussed below, energy release in this large vortex is crucial in sustaining the low frequency oscillation.

Unsteady Energy Release.

Figures 7 and 8 indicate that combustion is associated with vortices in the flow field. This can result in both temporal and spatial variations in the energy released. Figure 9 shows the energy released as a function of time and space. The energy released is always minimal near the entrance to the combustor. Also, initially there is no energy release in portions of the combustor because the ignited vortex has not yet reached these locations. Locations of strong energy release move in space because the energy release is taking place in burning vortices which are being convected. Note that the temporal nonuniformity in energy release is different at different locations. One approach to summarizing the information in this figure and determining the spatial distribution of energy release is to consider the time-averaged energy release at various locations in the combustor. Taking the time-average of the energy released over one cycle of the oscillation (determined from the flow visualisation in Figs. 7 and 8) showed that most of the energy is released in the second half of the combustor, that is, the half closest to the exit nozzle. Figures 7, 8 and 9 give a picture of the temporal and spatial distribution of energy release and suggest that events occuring in the second half of this combustor between 42.7 and 44.1 ms (during one cycle) are important in assessing the global effects of energy release on the flow field.

Unsteady Pressure Fluctuations.

One of the important reasons for simulating the flow fields in ramjets is to evaluate the coupling between the energy released and the pressure oscillations. Figure 10 shows the pressure fluctuations at a particular location (3.04 D from the inlet-combustor junction). There are approximately three cycles of large pressure oscillations. During the cycle of interest to us, the pressure is rising at 42 ms, attains a maximum between 42.7 and 43.5 ms, and then decreases to a minimum at about 45 ms. The fourier analysis of this data and similar data at six different locations in the combustor show that the large-amplitude oscillations are at about 280 Hz. The cause of these large pressure oscillations is the strong coupling between the pressure and the unsteady energy release.

Rayleigh's Criterion

A criterion first proposed by Lord Rayleigh [26] is a convenient method for evaluating the interaction between the energy released and the pressure waves in the system. Rayleigh's criterion states that pressure oscillations will be amplified if the energy release is

in phase with the pressure and will be diminished if they are out of phase. The frequency will be affected if the energy release occurs at a quarter period before or after the maximum pressure. In a complex flow field such as that in the combustor discussed here, the unsteady energy release and the pressure fluctuations do not have simple waveforms and hence the phase relation between the two can vary from one location to another. In this context, Rayleigh's criterion implies that the instability is *locally amplified* if the unsteady energy release $e_r'(x,t)$ and pressure fluctuation $p'(x,t)$ are in phase. More generally, if we define

$$D(x) = \frac{1}{T}\int_T e_r'(x,t)p'(x,t)dt \tag{3}$$

where T refers to the period under consideration. Local amplification (or driving) occurs if $D(x)$ is positive and local attenuation (or damping) occurs if $D(x)$ is negative.

In principle, we can evaluate $D(x)$ at all locations in the combustor if we know e_r' and p' at all locations through out the cycle. Because of the large amount of data required, it is impractical to evaluate this criterion at all locations (or volume elements) in the combustor. Therefore, we discretized the combustor into a series of axial stations and evaluated the criterion at these stations. A station is defined as a slice through the combustor and has the thickness of an axial computational cell. The drawback with this approach is that all radial variations in the energy released are averaged out. The pressure fluctuations used are those calculated at half the radius of the combustor because the radial variations in the pressure are not significant in this problem which is dominated by longitudinal oscillations. The integrand in the above equation evaluated at a number of stations showed that the oscillations locations were damped at some stations while being amplified at other locations. The experiments of Hegde et al. [27] have shown similar results.

The total effect over the whole combustor can be determined by evaluating the criterion at various axial stations in the combustor and integrating it over the whole combustor. Figure 11 indicates that there is damping at axial locations up to about 2.3 D over the cycle considered. Locations between 3 and 4.5 D are strongly driving the oscillations. Similar results have been obtained over other cycles of oscillations indicating that the ramjet is operating in an unstable mode for the conditions considered in this simulation.

SUMMARY AND CONCLUSIONS

In this paper we have presented the highlights of our numerical investigations of the acoustic-vortex-chemical interactions in an idealized ramjet. These simulations have allowed us to isolate the interactions between acoustic waves and large-scale vortex structures and then to study the effects of energy release on the flow field. Our simulations can be broadly divided into three categories.

First, the effects of varying the acoustics while keeping the flow parameters fixed (inflow velocity of 50 m/s) was investigated. The acoustics of the ramjet was varied by seperately varying the length of the inlet and the combustor. These simulations indicate a strong coupling between the acoustics of the ramjet, both the inlet and the combustor, and the flow field. In all cases, a low frequency oscillation is observed. Pressure oscillations in the inlet indicates that the quarter-wave acoustic mode of the inlet is the origin of this low frequency. Changing the length of the inlet or the sonic velocity in the inlet appropriately changes the observed low frequency. Simulations also show that acoustic forcing at the first longitudinal acoustic mode of the combustor induces vortex-rollup near the entrance to the combustor at the forcing frequency when the forcing frequency is close to the natural shedding frequency of the shear layer. It was also found that the merging pattern of the vortices in the combustor is influenced by the length of the combustor.

These merging patterns have been explained on the basis of an interaction between the vortex-rollup frequency and frequency of the quarter-wave mode in the inlet.

In the second set of simulations, the effects of varying the flow parameters on vortex shedding and merging has been studied When the flow velocity is increased, the natural instability frequencies of the shear layer also increases while the acoustic frequencies remain essentially the same. Vortex shedding and initial vortex-mergings occur at the natural shear layer instability frequency and its subharmonics if these frequencies are significantly different from the dominant acoustic frequencies of the system. Subsequent vortex-mergings are influenced by the longitudinal acoustic-mode frequencies. The presence of many significant frequencies results in less organized and more complex merging patterns. We have identified a number of different interactions of acoustic modes with the vortex mergings which explain these complex merging patterns. These interactions can be used as a means of controlling the formation of large scale structures by inducing many possible less well organized coherent structures.

Finally, the effects of chemical reactions on the flow field was investigated. The first case studied was that of a pre-mixed, lean hydrogen-oxygen-nitrogen mixture flowing into the combustor at 200 m/s. In this case, energy release alters the flow field in the combustor substantially. Energy release quickly destroys the pattern of vortex mergings observed in the cold flow and a new pattern emerges that is dominated by a large vortex. However, the low frequency oscillation observed in the cold flow persists and its amplitude increases substantially when there is energy release. In the simulations investigated so far this mode has again been identified with the quarter wave mode of the inlet. The coupling between the energy release and the pressure fluctuations in the combustor has been studied in detail. Energy release in the second half of the combustor (the half nearer to the exit nozzle) is in phase with the pressure oscillations over a substantial period and this results in amplification of the pressure fluctuations and eventually leads to combustion instability. There are regions in the combustor where the oscillations are damped. This suggests that combustion instability may be controllable by increasing the regions where the energy release and pressure are out of phase. Several approaches to controlling the combustion instability as well as additional parametric studies of the effects of chemistry are currently being persued.

REFERENCES

1. Scott, J.N., and Hankey, W.L., "Numerical Simulation of Cold Flow in an Axisymmetric Centerbody Combustor," *AIAA Journal*, Vol. 23, May 1985, pp. 641-649.
2. Drummond, J.P., "Numerical Study of a Ramjet Dump Combustor Flowfield," *AIAA Journal*, Vol. 23, Apr. 1985, pp. 604-611.
3. Kailasanath, K., Gardner, J.H., Boris, J.P. and Oran, E.S., "Acoustic-Vortex Interactions in an Idealized Ramjet Combustor," *Proceedings of the 22nd JANNAF Combustion Meeting, Pasadena, CA*, CPIA publication 432, Vol. I, Oct. 1985, pp. 311-320.
4. Jou, W.H. and Menon, S., "Large Eddy Simulations of Flow in a Ramjet Combustor," *Proceedings of the 22nd JANNAF Combustion Meeting, Pasadena, CA*, CPIA publication 432, Vol. I, Oct. 1985, pp. 331-339.
5. Kailasanath, K., Gardner, J., Boris, J. and Oran, E., "Interactions Between Acoustics and Vortex Structures in a Central Dump Combustor," AIAA paper 86-1609, also see *J. Prop. Power*, Vol. 3, Nov-Dec. 1987, pp. 525-533.
6. Kailasanath, K., Gardner, J.H., Boris, J.P., and Oran, E.S., "Acoustic-Vortex Interactions and Low Frequency Oscillations in Axisymmetric Combustors," AIAA paper 87-0165, AIAA 25th Aerospace Sciences Meeting, Reno, Jan. 1987 (also to appear in *J. Prop.Power.*, 1988).

7. Kailasanath, K., Gardner, J.H., Oran, E.S., and Boris, J.P. "Numerical Simulations of High-Speed Flows in an Axisymmetric Ramjet," AIAA paper 88-0339, AIAA 26th Aerospace Sciences Meeting, Reno, Jan. 1988, AIAA, Washington, D.C.

8. Kailasanath, K., Gardner, J.H., Oran, E.S. and Boris, J.P., "Numerical Simulations of the Reactive Flow Field in an Axisymmetric Combustor," AIAA paper 87-1423, AIAA 19th Fluid Dynamics, Plasma Dynamics and Lasers Conference, Honolulu, HA, June 1987, AIAA, Washington, D.C.

9. Sivasegaram, S. and Whitelaw, J.H.,"Oscillations in Axisymmetric Dump Combustors," *Combust. Sci. and Tech.* 52, pp. 413-426.

10. Oran, E.S. and Boris, J.P.,"Detailed Modelling of Combustion Systems," *Prog. Energy Combustion Sci.* 7, 1.

11. Boris, J.P. and Book, D.L., "Solution of Continuity Equations by the Method of Flux-Corrected Transport," *Methods of Computational Physics*, Academic Press, New York, 1976, Vol. 16, Chap. 11, pp. 85-129.

12. Oran, E.S., Young, T.R. and Boris, J.P., "Application of Time-Dependent Numerical Methods to the Description of Reactive Shocks," *Seventeenth Symposium (International) on Combustion*, The Combustion Institute, Pittsburgh, 1979, pp. 43-54.

13. Kailasanath, K., Oran, E.S., Boris, J.P. and Young, T.R., "A Computational Method for Determining Detonation Cell Size," AIAA paper No. 85-0236, AIAA 23rd Aerospace Sciences Meeting, Reno, NV, Jan. 1985, AIAA, Washington, D.C.

14. Guirguis, R.H., Grinstein, F.F., Young, T.R., Oran, E.S., Kailasanath, K., and Boris, J.P., "Mixing Enhancement in Supersonic Shear Layers," AIAA paper 87-0373, AIAA 25th Aerospace Sciences Meeting, Reno, NV, Jan. 1987, AIAA, Washington, D.C.

15. Boris, J.P., Oran, E.S., Gardner, J.H., Grinstein, F.F., and Oswald, C.E. "Direct Simulations of Spatially Evolving Compressible Turbulence--Techniques and Results," *Ninth International Conference on Numerical Methods in Fluid Dynamics*, pp. 98-102. Springer-Verlag, 1985.

16. Grinstein, F.F., Oran, E.S. and Boris, J.P., "Direct Simulation of Asymmetric Mixing in Planar Shear Flows," *J. Fluid Mech.*, Vol. 165, 1986, pp. 201-220.

17. Burks, T.L., and Oran, E.S., "A Computational Study of the Chemical Kinetics of Hydrogen Combustion," NRL Memorandum Report 4446, Naval Research Laboratory, Washington, D.C., 1981.

18. Kailasanath, K., Gardner, J.H., Boris, J.P. and Oran, E.S., "Numerical Simulations of the Flowfield in a Central-Dump Ramjet Combustor--I. Tests of the Model and Effects of Forcing," NRL Memorandum Report 5832, Naval Research Laboratory, Washington, D.C., 1986.

19. Schadow, K.C., Wilson, K.J., Crump, J.E., Foster, J.H. and Gutmark, E., "Interaction Between Acoustics and Subsonic Ducted Flow with Dump," AIAA paper No. 84-0530, presented at the AIAA 22nd Aerospace Sciences Meeting, January 1984

20. Ho, C.M., and Nosseir, N.S., "Dynamics of an Impinging Jet. Part 1. The Feedback Phenomenon," *J. Fluid Mech.*, Vol. 105, 1981, pp. 119-142

21. Flandro, G.A., "Vortex Driving Mechanism in Oscillatory Rocket Flows," *J. Prop. Power*, Vol. 2, 1986, pp. 206-214.

22. Abdelwahed, G.E., Keklak, J.A., and Tsang, T.Y., "Ramjet Rumble:The Low-Frequency Instability Mechanism in Coaxial Dump Combustors," *Combust. Sci. Tech.*, Vol. 36, 1984, pp. 83-105.

23. Kailasanath, K., Gardner, J.H., Boris, J.P. and Oran, E.S., "Numerical Simulations of the Flowfield in Central Dump Ramjet Combustors--II. Effects of Inlet and Combustor Acoustics," NRL Memorandum Report 6214, Naval Research Laboratory, Washington, D.C., 1988.

24. Hussain, K.B.M.Q., and Hussain, A.K.M.F., "Vortex Pairing in a Circular Jet Under Controlled Excitation. Part 1. General Jet Response," *J. Fluid Mech.* Vol. 101, 1980, pp. 111-119.

25. Michalke, A., "On Spatially Growing Disturbances in an Inviscid Shear Layer," *J. Fluid Mech.* Vol. 23, 1965, pp. 521-544

26. Rayleigh, J.W.S., "The Explanation of Certain Acoustical Phenomena," *Nature*, Vol. 18, 1878, p. 319 also see *Theory of Sound*, Vol. II, pp. 224-235, Dover, New York, 1945

27. Hegde, U.G., Reuter, D., Daniel, B.R. and Zinn, B.T., "Flame Driving of Longitudinal Instabilities in Dump Type Ramjet Combustors," *Combust. Sci. and Tech.*, Vol. 55, 1987, pp. 125-138.

ACKNOWLEDGEMENTS

This work was sponsored by the Office of Naval Research and the Naval Air Systems Command. The support and encouragement from Dale Hutchins at NAVAIR, Robert J. Hansen and James Fein at ONR and Douglas Davis at AFWAL is acknowledged. The computational support from the Numerical Aerodynamic Simulation facility at NASA-Ames is also gratefully acknowledged.

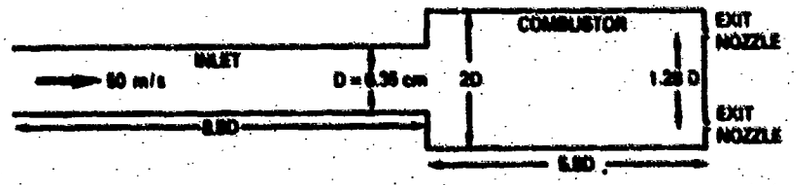


Figure 1. Basic configuration of the idealized axisymmetric ramjet combustor.

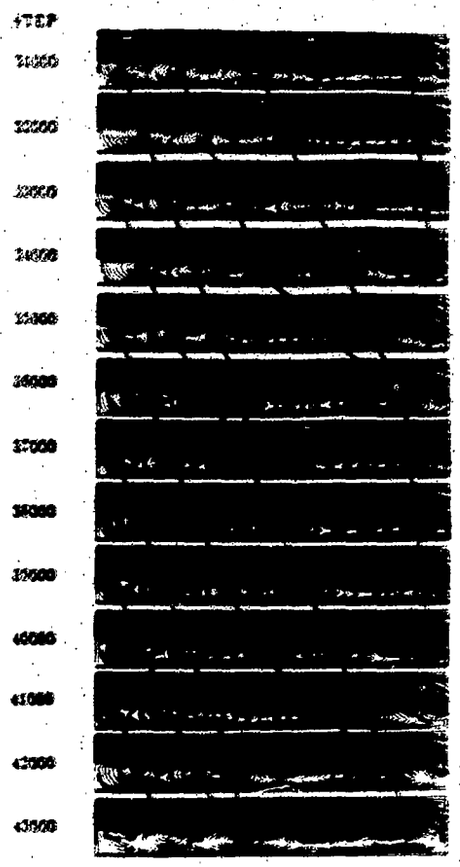


Figure 2. Streamlines showing the instantaneous flow field at a sequence of timesteps for Case 1. The time interval between any two successive frames is 1.002E-03.

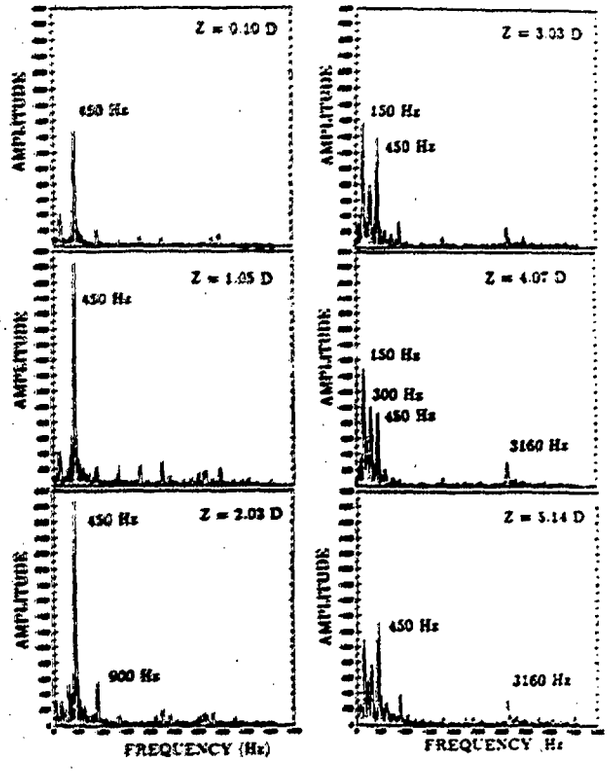


Figure 3. Frequency spectra of velocity fluctuations in the shear layer at a series of axial locations for Case 1.

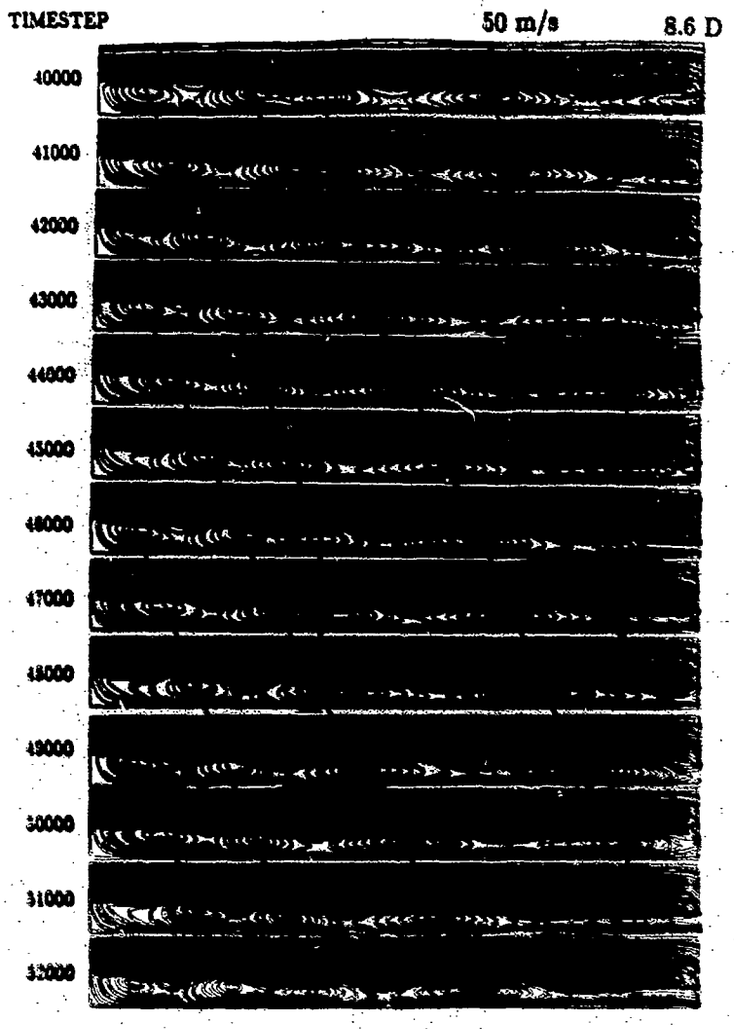


Figure 4. Streamlines showing the instantaneous flow field at a sequence of timesteps for Case 2. The length of the combustor is 8.6 D.

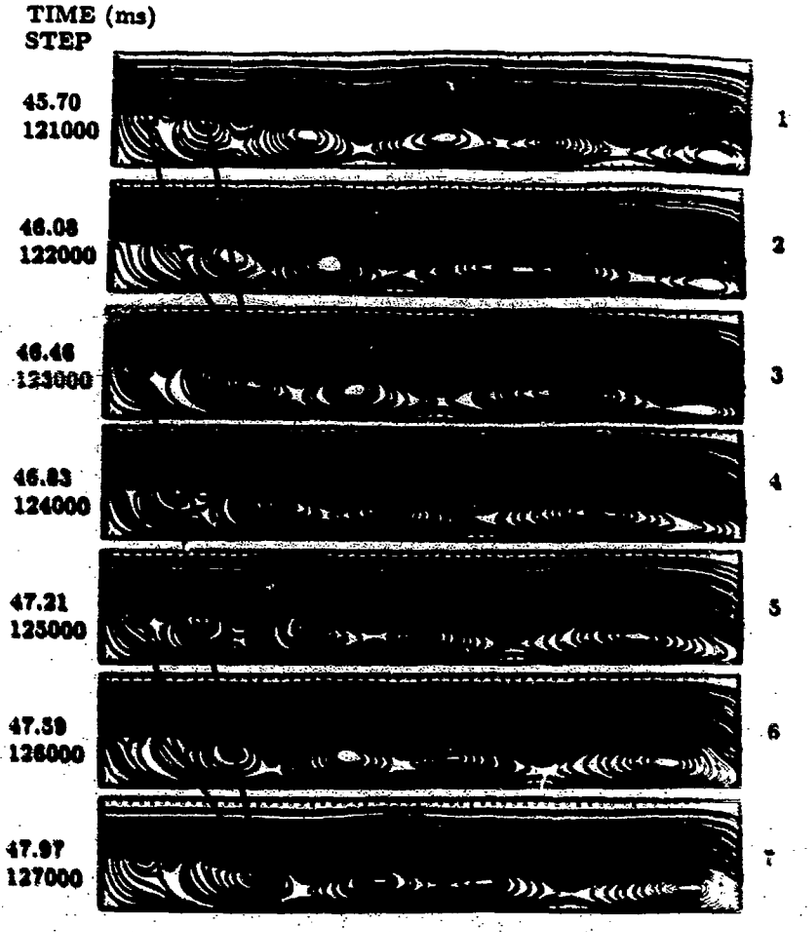


Figure 5. Sequence of instantaneous streamlines showing vortex shedding and merging near the step in the combustor for Case 3. The inflow velocity is 100m/s (M=0.31).

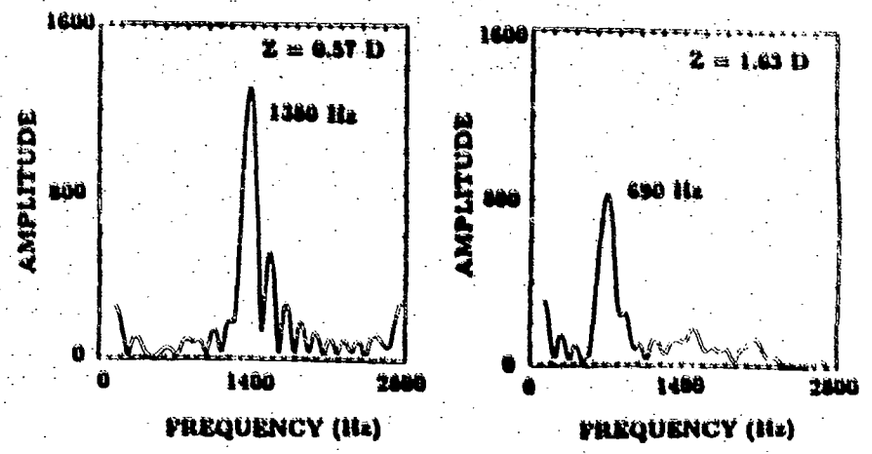


Figure 6. Frequency spectra of velocity fluctuations in the shear layer at two locations near the step in the combustor for Case 3.

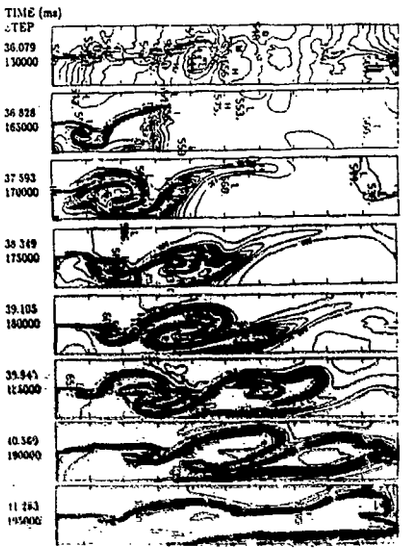


Figure 7a. Temperature contours showing the instantaneous flow field at a sequence of timesteps in the early stages of the reactive flow case. The mixture is ignited at the end of timestep 160000.

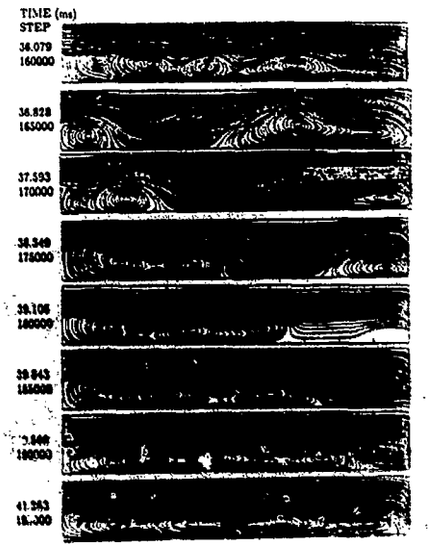


Figure 7b. Streamlines corresponding to the temperature contours in Figure 7a.

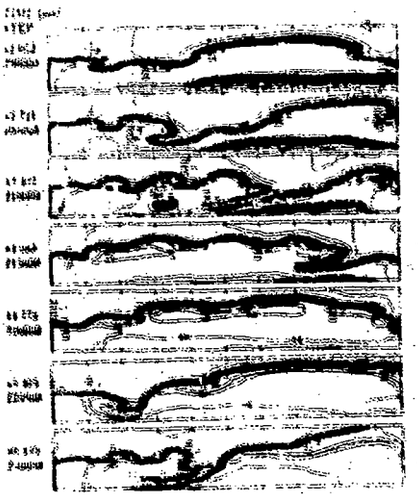


Figure 8a. Temperature contours showing the instantaneous flow field at a sequence of timesteps in the later stages of the reactive flow case.

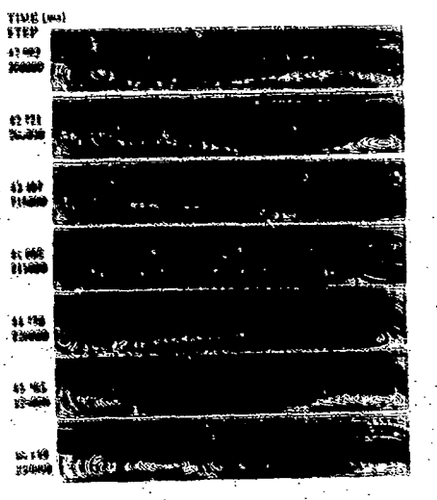


Figure 8b. Streamlines corresponding to the temperature contours in Figure 8a.

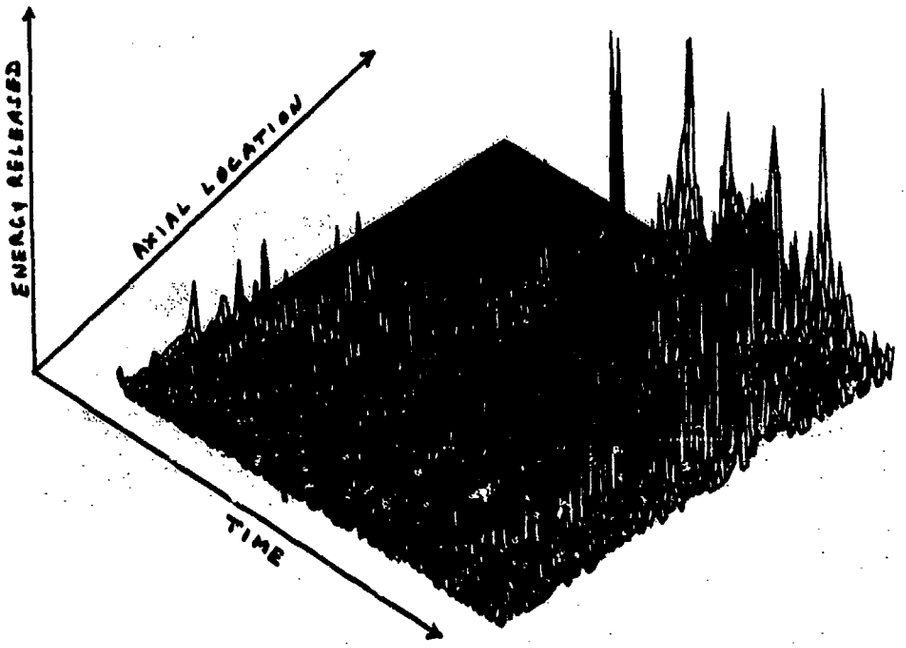


Figure 9. Temporal variation of instantaneous energy release at various axial stations in the combustor.

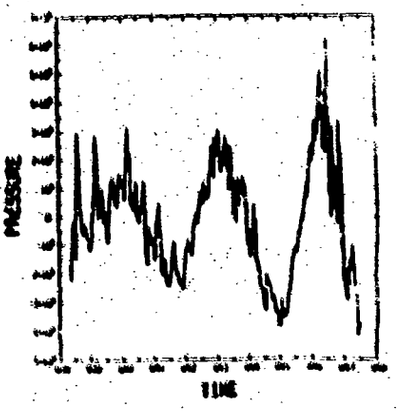


Figure 10. Time evolution of instantaneous pressure fluctuations at a particular location (3.04 D) in the combustor.

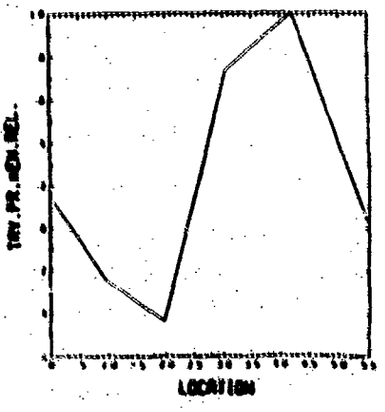


Figure 11. Time-averaged value of the integral expressing Rayleigh's criterion at a series of axial stations in the combustor.

DISCUSSION

C. M. Coats, GB

Does your simulation incorporate sub-grid-scale diffusion? I would also comment that it is far from ideal to use a global reaction-rate expression for such a highly strained flow in which local extinction is almost certain to occur.

Author's Reply:

Originally our plan was first to do large scale eddy simulation like Dr. Jou described, and then do as many sub-grid scales as possible. However, we have not yet introduced sub-grid models.

I agree with your comment. We are not happy with our two-step global mechanism. Unfortunately, even with that simple model, the costs are extremely high and we cannot afford to improve the approximation. Perhaps with the next generation of computers we shall be able to do better.

COMBUSTION-DRIVEN OSCILLATION IN LARGE COMBUSTION SYSTEMS FOR POWER GENERATION

by

G. BENELLI*, V. COSSALTER**, G. DE MICHELE*
* Thermal and Nuclear Research Center - ENEL -
Via A. Pisano 120, 56100 Pisa - Italy
** Institute of Applied Mechanics - Padua University
Via Venezia 1, 35131 Padova - Italy

SUMMARY

Intense pressure oscillations reaching peak values of about 1200 Pa in the 50÷100 Hz range occurred in the combustion chamber of a 480 t/h steam generator, fed with gas or oil and gas together.

Through experimental analysis it was possible to identify the acoustic modes of the furnace excited by combustion and to assess the effect on instability of certain characteristic parameters of the burner.

Furthermore, a finite-element mathematical model was devised for modal analysis of the combustion chamber; the numerical results were in close agreement with the experimental data.

The analysis carried out showed what modifications needed to be made to the geometry of the burners in order to reduce the self-excited vibrations to acceptable limits.

1. INTRODUCTION

In special conditions, in a generic combustion system, even one ten-thousandth of the thermochemical energy released by combustion may be enough to cause instability phenomena. Thus, permanent pressure oscillations may occur in the combustion chamber ranging from a few 10s of Pa to ±50% of the absolute pressure present in the said chamber in normal conditions.

In the case of industrial combustors, normally characterized by low-velocity flows, the stability criterion that can be applied is the one defined by Lord Rayleigh as long ago as 1878: "If heat is periodically added to, and taken from, a mass of gas oscillating, for example, in a cylinder bounded by a piston, the effect produced will depend upon the phase of the oscillation at which the transfer of heat takes place". Rayleigh's criterion can be expressed as follows:

$$\int_V \oint Q' p' \, dt \, dV$$

in which Q' and p are the instantaneous fluctuations of the heat released and of the pressure inside the flame volume V, respectively [1].

In the literature, the forms of instability arising from the interaction between the pressure field and heat release are classified in [2,3,4]:

- instability of the combustion chamber, involving all the phenomena situated in the chamber;
- system instability involving, essentially, interactions between the processes inside the combustion chamber and those occurring in at least one other component of the plant such as the inlet duct (air and fuel) and/or the exhaust duct of the combusted gases;
- intrinsic kinds of instability depending on chemical kinetics, and not on the kind of combustion chamber.

This last type of instability may take different forms since such phenomena are specific to the reactants and are independent of the properties of the chamber; they may depend, for instance, on combustion kinetics.

The system oscillations are generally characterized by a lower frequency than the acoustic oscillations. Low frequency instabilities in liquid-propellant rocket motors are examples of coupling between combustion phenomena, the propellant feed system and also the structure of the vehicle by means of the thrust fluctuations that arise from pressure fluctuations in the chamber.

Finally, the instability of the combustion chamber is perhaps the most common and is due to the generation and propagation of acoustic waves. This kind of instability is, in its turn, subdivided into three categories according to the mechanism involved:

- acoustic instability, concerning the effect of the propagation of acoustic waves inside the chamber;
- shock instability, characterized by the propagation of pressure waves inside the chamber, with a very steep front, from a certain point of view, these waves are similar to those caused by explosion;
- fluid dynamic instability, which is associated with the onset of special flow conditions.

Acoustic instability concerns acoustic oscillatory modes in the combustion chamber, the frequency of which are determined by the geometry of the chamber, by the impedance of the terminations and by the sound velocity in the gas contained in the chamber.

One of the greatest difficulties arising when instability occurs is the identification of the mechanism of interaction between the combustion process and the oscillatory phenomenon, capable of generating a fluctuating heat flow which is in phase with the pressure. There are a number of possible mechanisms of self-excited vibrations, which may even be present at one and the same time.

These may be due to [3,5,6]:

- the feeding system for the fuel and the air flow sensitive to the pressure field inside the combustion chamber and such as to supply a fluctuating flow with a frequency equal to that of the pressure field and in phase with it;
- fluctuations of the so-called combustion delay which, by being reduced in the interaction between the flame and the acoustic wave, causes a positive fluctuation in the release of heat with the possibility of supporting self-induced vibration;
- fluctuations in the front area of flames following interactions with pressure waves which, as in the case of pre-mixed flows, are linked to fluctuation in the quantity of heat released;
- fluctuations in the flame-front, such as in pre-mixed flows where they undergo area variation and collide with a pressure wave; consequently there are variations in the quantity of heat released and, with suitable delay times, the fluctuation of the flame can support oscillations;
- vortex shedding present in the combustion zone, giving rise to oscillating flows capable of modulating the mixing and of exciting acoustic modes with frequencies near those of the frequency of the shedding of vortex pairs; in such a case this may set up phenomena of synchronization of the shedding frequency of the vortices that are not strictly in agreement with Strouhal's equation.
- combustion roar whose frequency spectrum is continuous and which can cause the acoustic modes to vibrate in the combustion chamber.

The present paper describes both the theoretical and the experimental approach concerning a case of instability which occurred in the combustion chamber of a gas-fed 480t/h steam generator, producing intense vibrations such as to prevent full use of the chamber itself.

The combustion chamber, 7.5x7.4x19 m in size, was fed by 9 frontal axial-type burners, for burning oil, gas and a mixture of both. When burning oils no significant vibrations occurred throughout the entire working range, whereas, in certain conditions, the burning of gas and the oil-gas mixture produced intense oscillations in pressure, reaching peak values of 1200 Pa in the 50÷100 Hz field.

An experimental survey was carried out on the plant with a view to identifying the kind of instability involved and the support mechanisms of the self-excited oscillations. The pressure and the acceleration of the structures were measured at various points of the combustion chamber and in various kinds of set up.

Furthermore, a numerical model was devised based on the finite elements, making it possible to calculate the natural frequencies and the vibration modes, as well as to assess the effect of the smoke-duct upon the damping of the individual modes. Numerical and experimental analyses suggested modifications in the geometry of the burners which made it possible to keep the vibrations within acceptable limits.

2. CASE DESCRIPTION AND MEASUREMENT APPARATUS

As mentioned in the Introduction to this paper, the vibratory phenomena observable in a steam generator can be characterized, from the point of view of time, as random processes and as deterministic processes of an almost periodical nature.

Oscillations connected with "combustion roar" or those connected with wakes caused by flame stabilizers are random processes, whereas oscillatory phenomena connected with the geometry of the combustion system and that, in the last resort, are those which characterize instability, are deterministic-type processes.

While, in the case of deterministic processes, we can resort to definitions based on explicit mathematical functions of time, in the case of random processes we resort to the assessment of probability density functions, to self-correlation functions and to power spectrums [7]. Should it be desiderable to set up delay, amplitude and phase relations between the signs, we can resort to cross-analysis techniques; in this way, for example, the cross-correlation function and the frequency-response of the system can be established.

Definition of the transfer function implies that the system possesses the following requisites: time-invariance, limited response to limited inputs and linearity and that the response-function to impulse $h(\tau)$ is equal to 0 when $\tau<0$. The hypothetical existence of linearity is probably the condition that is most often not fulfilled in pratical applications. However, such a condition can be checked by means of the definition of the coherence function which establishes the degree of linear relation, on a scale from 0 to 1, between the frequential components of the two signals.

In the practical analysis of a random process of infinite duration, we must necessarily resort to the assessment of the spectrum of a segment, thereby obtaining an approximate evaluation of the power spectrum; however, thanks to a concept attributed to Bartlett [8], the variance of the evaluation can be reduced by obtained the average of various independent evaluations. The equations of the main functions mentioned above can be found in the Appendix.

Concerning the solution of the practical problem of vibrations described above, the generator was fitted with instruments, as shown in Fig. 1, whereas Fig. 2 shows the geometric features of the burner, the injection heads with the relevant outflow angle of the gas. Finally, Fig. 3 shows the layout of the measurement system.

The oscillations in pressure were recorded by means of a type 412 Kistler piezoelectric pressure transducer with a Kistler 500i amplifier. The pressure in the combustion chamber was recorded by means of the same pressure transducers mounted on probes with linear response in the 0÷400 Hz field.

The accelerations were recorded by means of type 4370 B&K piezoelectric accelerometers and type 2635 B&K amplifiers. The measurement lines of the pressure oscillations were calibrated in order to make a comparison with the microphone recording system.

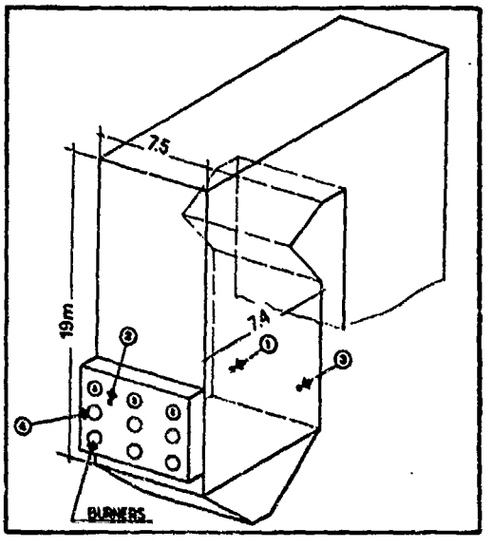


Fig.1 Boiler and measurement points.

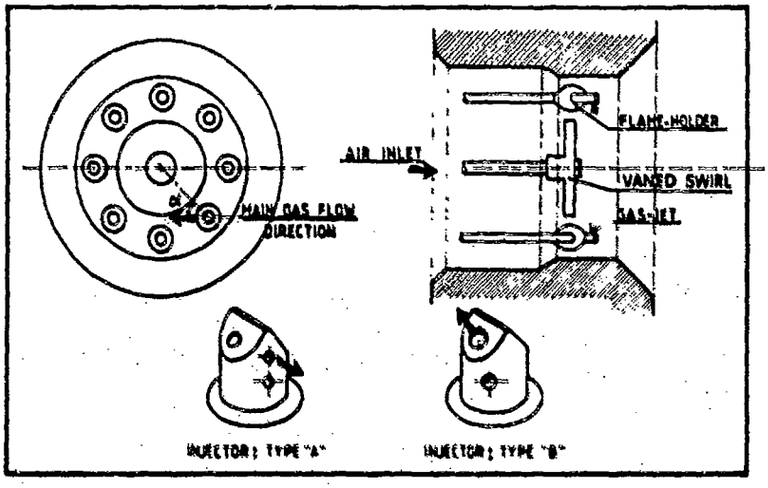


Fig.2 Burner geometry.

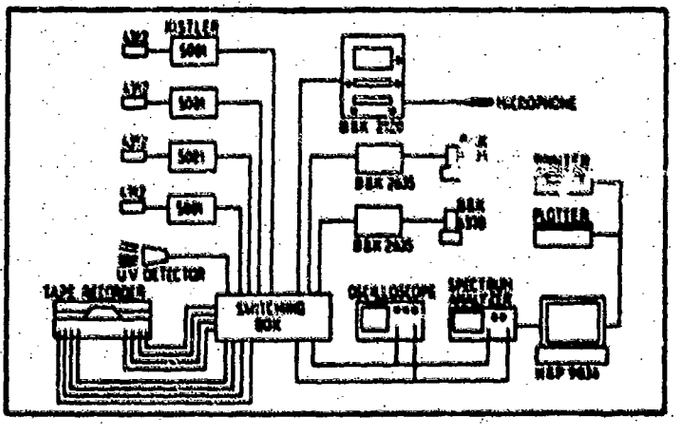


Fig.3 Measurement apparatus.

The ultraviolet emission of the flame was recorded with a probe constructed for the purpose and described in [9].

The signal relevant to the measurements taken for each test were recorded on tape and analyzed in couples with the 3582A Hewlett&Packard spectrum analyzer.

The amplitude spectrum for each signal was evaluated in real time as an average of 128 independent measurements so as to obtain an estimate within the ±0.7 dB interval around the true value at a confidence level of 90%; moreover, the phase values, corresponding to the frequential components with the most significant amplitude spectrums and coherence values higher than 0.95 has been determined.

The amplitude spectrum was evaluated by using the "flat" window of the spectrum analyzer in such a way as to obtain the maximum accuracy of amplitude.

3. NUMERICAL MODEL

Assuming the gas is perfect, compressible, non-viscous, non-conductible, with no external forces per volume unit, with uniform stationary motion in the domain being considered, the equation of the propagation of waves proves to be[6]:

$$\frac{\partial^2 p'}{\partial t^2} - \bar{c}^2 \nabla^2 p' = \bar{p}(\gamma - 1) G \frac{\partial p'}{\partial t}$$

where ρ= density, p= pressure, $\bar{c}^2 = \gamma \bar{p} / \bar{\rho}$ = propagation velocity and G is the complex number representing both the spatial link of heat release in the flame volume and the local delay in the fluctuations of heat in relation to pressure (the apex indicates the perturbed motion, the overlining indicates the stationary motion).

The regime solution , separating the spatial part from the time part, is of the following kind:

$$p' = p'_0(x, y, z) e^{s t} = p'_0(x, y, z) e^{\omega_r t} e^{i \omega_i t}$$

If we introduce this into the propagation equation, we obtain the equation of frequencies in the presence of internal generation of heat:

$$\nabla^2 p'_0 + k^2 p'_0 + \alpha p'_0 = 0 \qquad \text{where:} \quad k^2 = -s^2 / \bar{c}^2 \qquad \alpha = \frac{s \bar{\rho}(\gamma - 1) G(x, y, z, s)}{\bar{c}^2}$$

The solution supplies the complex eigenvalues $s_n = \omega_r + i\omega_i$, the imaginary part represents natural frequency and the real part the damping coefficient $\omega_r<0$ or the amplification coefficient $\omega_r>0$.

Instability occurs for values of $\omega_r>0$, the degree of instability is defined by the logarithmic decrease $\delta = 2\pi\omega_r / \omega_i$.

The spatial part of the solution $p'_{0_n}(x, y, z)$ represents the autovector or the acoustic mode of vibrating associated to pulsation ω_n.

The solution to the equation of the frequencies must be sought in compliance with the surrounding conditions. The boundary of the integration domain can be subdivided according to the conditions imposed:

$$\Gamma_1: \quad p'_0(x, y, z) = 0 \qquad \Gamma_2: \quad \frac{\partial p'_0(x, y, z)}{\partial n} = 0 \qquad \Gamma_3: \quad \frac{\partial p'_0(x, y, z)}{\partial n} = \frac{-s\bar{\rho}}{Z(x, y, z, s)} p'_0(x, y, z)$$

The third condition establishes a link between the velocity at a given point on the boundary and the pressure at the same point. This hypothesis proves to be an over-simplifications in as far as no relation is established between nearby points on the boundary.

The solution of the equation of the frequencies can be carried out in an approximate manner. The domain of integration can be subdivided into a certain number of subdomains Ω^e ; following the procedure described in [10], we obtain:

$$\sum_{e=1}^{n} \left\{ s^2 M^e_{k,e} + s B^e(s)_{k,e} - C^e(s)_{k,e} + K^e_{k,e} \right\} u^e_e = Q_e^{in} + Q_e^{ex} \qquad k = 1, n$$

since we have:

the stiffness matrix

$$K^e_{i,j} = \int_{\Omega^e} \left[\frac{\partial \psi_i^e}{\partial x} \frac{\partial \psi_j^e}{\partial x} + \frac{\partial \psi_i^e}{\partial y} \frac{\partial \psi_j^e}{\partial y} + \frac{\partial \psi_i^e}{\partial z} \frac{\partial \psi_j^e}{\partial z} \right] d\Omega$$

the mass matrix

$$M^e_{i,j} = \int_{\Omega^e} \frac{1}{\bar{c}^2} \psi_i^e \psi_j^e d\Omega^e$$

the self-excitement matrix

$$C^e(s)_{i,j} = \int_{\Omega^e} \frac{\bar{\rho}(\gamma - 1) G(x, y, z, s)}{\bar{c}^2} \psi_i^e \psi_j^e d\Omega$$

the impedance matrix

$$B^e(s)_{i,j} = \int_{\Gamma_3^e} \frac{\bar{\rho}}{Z(x, y, z, s)} \psi_i^e \psi_j^e d\Gamma^e$$

the flow exchanged with other elements

$$Q_i^{in} = \int_{\Gamma_2^e} \frac{\partial p'}{\partial n} \psi_i^e d\Gamma^e$$

the outward flow:

$$Q_i^{ex} = \int_{\Gamma_1^e} \frac{\partial p'}{\partial n} \psi_i^e d\Gamma^e$$

Putting everything together for the entire domain, we get:

$$s^2 [M^e](u) + s[B^e(s) - C^e(s)](u) + [K^e](u) = \{Q^{ex}\}$$

where the terms with the apex G represent the matrices relevant to the entire domain.

Once this operation in completed, we obtain the following eigenvalue problem:

$$[s^2[M] + s[B-C] + [K]]\{u\} = 0$$

The problem is expressed in the generalized form with the transformation: $\{w\} = s\{u\}$

$$(\omega_i - i\omega_r)\begin{bmatrix} [0] & -i[M] \\ i[M] & i[B-C] \end{bmatrix}\begin{Bmatrix} w \\ u \end{Bmatrix} + \begin{bmatrix} [M] & [0] \\ [0] & [K] \end{bmatrix}\begin{Bmatrix} w \\ u \end{Bmatrix} = \begin{Bmatrix} 0 \end{Bmatrix}$$

It should be observed that, if functions Z and G are considered to be dependant on s, then the matrix also proves to be a function of s. Such a problem is efficiently solved from a numerical point of view with a solution technique taken from the "Sub-space Iteration" method. The numerical solution makes it possible to determine the vibration modes in the combustion chamber and the actual frequencies both partly real and partly imaginary.

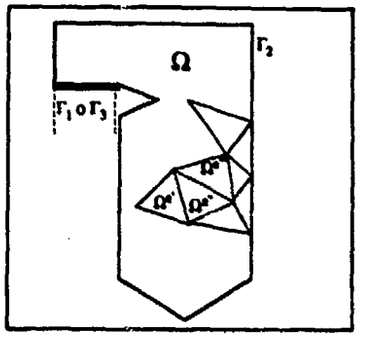


Fig.4 Layout of the domain.

4. NUMERICAL RESULTS

The layout of the combustion chamber has been given in the form of a two-dimensional model, with 325 triangular elements and 193 nodes, representing the orthogonal section on the burners wall. The walls of the chamber are represented as being ideal, that is perfectly reflecting and infinitely rigid. The exhaust duct is the most sensitive point of the layout since there is no such things as a perfect opening or closure.

The first simulations were carried out with a view to studying the influence of the non-uniform temperature field on the vibration modes. It must be noted that, in view of the hypotheses stated when obtaining the propagation equation, the speed of propagation cannot vary greatly in space; indeed, the propagation equation was obtained by disregarding the terms containing the spatial derivatives of the stationary terms.

The temperature field used is shown in Fig. 5.

The boundary conditions assumed to represent the exhaust duct affect the values of the natural frequencies and the relevant vibration modes, to a certain extent.

In order to assess its effect upon the vibration modes, the smoke duct was simulated both with a perfect opening and with a perfect closure. The numerical results are given in Table 1.

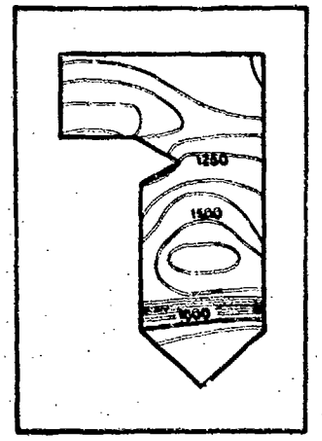


Fig.5 Temperature field.

The fundamental frequency proves to be equal to 7.8 Hz in the case of ideal opening and 16.2 Hz in the case of perfect closure. These are the borderline values between which the real value must be found. Indeed, experimental tests gave a value of 10÷13 Hz, according to the thermal load.

The table also contains the values obtained by representing the surrounding part, relevant to the exhaust duct, with an impedance value such as to simulate an intermediate condition in relation to the ideal conditions of perfect opening and closure.

The experimental values given for comparison refer to measurements taken with conditions of the thermal load of the generator varying from about 25% to 100%.

Figure 6 represents the vibration modes of the combustion chamber with the layout of the smoke duct as a perfectly open-wall, whereas Figure 7 contains the vibration modes obtained assuming the smoke duct with a perfectly closed wall.

The position of the antinods and the nodal lines makes it possible to foresee which modes can be most easily self-excited by the release of heat.

TABLE N°1 NATURAL FREQUENCIES.

N° MODE	EXPERIMENTAL VALUES	NUMERICAL VALUES		
		REPRESENTATION OF THE GAS-PATH		
		OPEN	CLOSED	IMPEDANCE
1	10.0÷13.0	7.80	8.8	9.76
2	15.1÷17.2	23.6	16.2	13.3
3	46.3÷50.0	41.5	31.8	38.4
4	48.2÷51.8	48.4	44.5	44.3
5	52.0÷57.6	51.4	54.3	54.3
6	58.1÷59.5	64.8	61.3	61.3
7	61.1÷69.6	68.4	69.3	64.3
8	78.3÷79.2	74.1	73.2	73.8
9	77.0÷87.2	82.1	88.2	81.3
10	83.6÷96.8	97.2	83.5	82.8

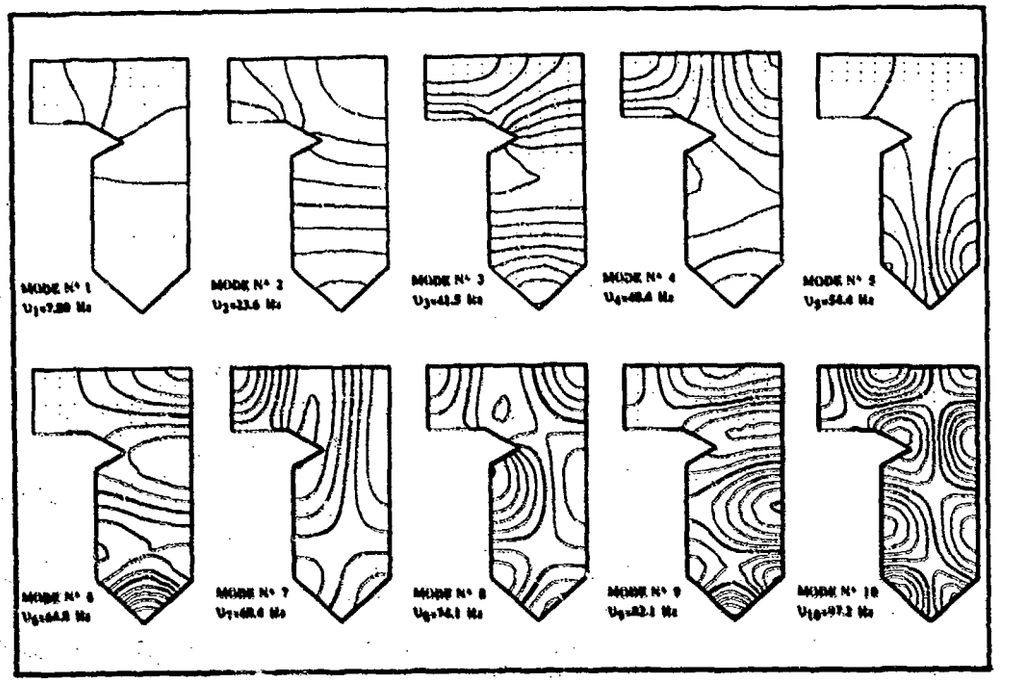


Fig.6 The first 10 vibration modes of the combustion chamber.
The gas-gaze is assumed to be perfectly open.

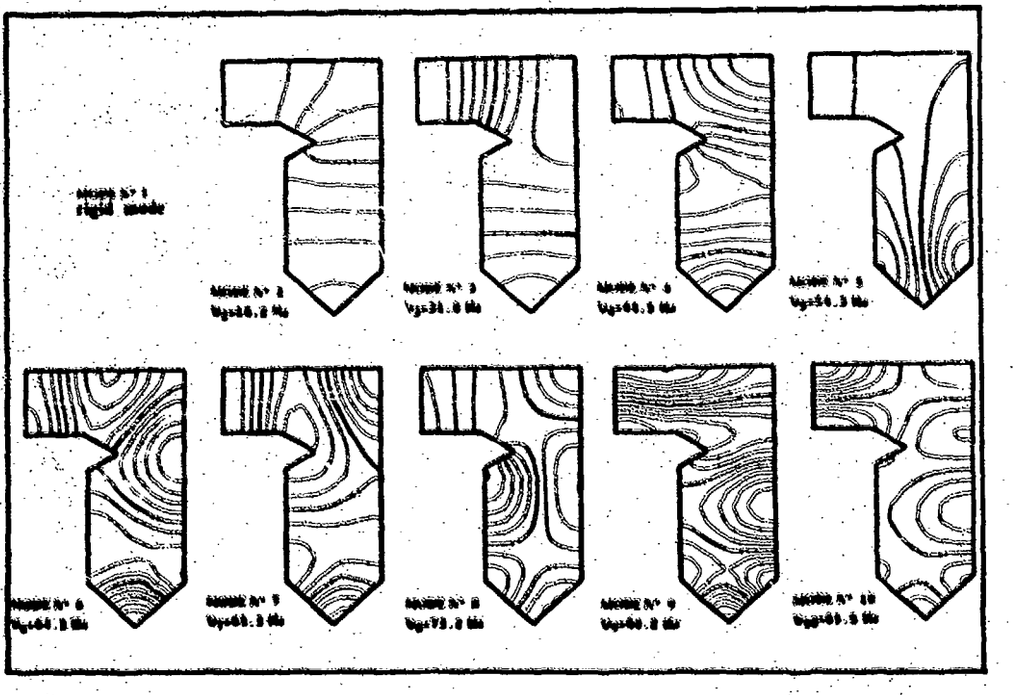


Fig.7 The first 10 vibration modes of the combustion chamber.
The gas-gaze is assumed to be perfectly closed.

According to Rayleigh's principle, the mechanism of self-excitement reaches maximum efficiency when two circumstances occur at the same time:

- maximum self-excitement due to the flow of heat, in phase with the pressure, located at an antinode;
- minimum energy loss.

Of the various dispersion mechanisms present (absorption by the walls, turbulence, presence of tube bundles, absorption of energy by the exhaust duct with subsequent irradiation by the chimney), the main one is considered to be that of the transfer of energy to the exhaust duct. Therefore, the minimum loss of energy occurs when a nodal line is near to the piece of boundary relevant to the exhaust duct.

The modes with antinodes roughly located near the burners are 5th, 6th, 7th and 8th, when closure is "ideal", while both conditions exist in the case of 5th and 8th.

In the last analysis, the exhaust duct has little effect on the values of the natural frequencies but plays an important part in the damping of the various vibration modes.

This proved to be so even numerically. A simulation was carried out with a view to evaluating its influence, by assuming the duct has very little damping effect (the real part of the impedence consists in the adsorption or transfer of energy).

Comparison of the values of the logarithmic decrements of the individual modes made it possible to approximately assess the damping effect of the exhaust duct on the individual modes of the combustion chamber. This comparison can be found in Table 2.

This comparison indicates that the 5th mode is virtually unaffected by the exhaust duct and, of all the modes higher than the 5th, the 8th is the least damped.

These, then, are the modes most likely to undergo high-amplitude oscillation, in the case of self-excitement.

TABLE N°2 LOGARITHMIC DECREMENT.

N° MODE	$\frac{\delta_i}{\delta_{max}}$ %
2	100
3	58
4	10
5	1
6	83
7	71
8	20
9	83

5. EXPERIMENTAL RESULTS AND DISCUSSION

The first series of tests, carried out with the plant in its original layout and with gas combustion alone, showed, in accordance with the numerical results, that the fifth and eighth vibration modes tended to be amplified as the load conditions increased. This sometimes happened simultaneously and sometimes separately. In all cases, use of the plant became impossible.

Figure 8 shows the amplitude spectrums of pressure measured at number 1 measurement point situated in front of the burners.

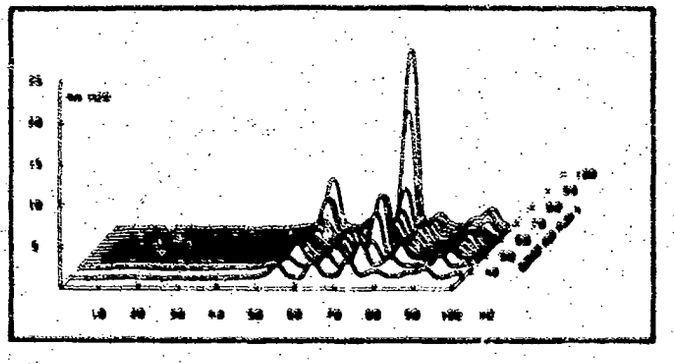


Fig.8 Amplitude spectrum of pressure in the combustion chamber.
Plant layout: 6 gas burners with type A injectors. α=67°, θ=1.

As can be seen, the noise in the combustion chamber reaches its maximum when the air supply is around 40% of the maximum per burner. In this situation, the oscillations in pressure grew bigger with small variations in the layout of the plant. Once this instability zone was passed through, the noise in the combustion chamber decreased and combustion became stable.

Subsequently, with an increase in the air supply, the noise in the combustion chamber grew again and combustion with air supplies above 67% became extremely instable.

When fuel oil alone was used, recordings made by means of quick filming show the flame tended to be somewhat instable, especially at low loads, but with subsequent moderate oscillations in pressure inside the combustion chamber.

Certain modifications to the burners described in (9), the carrowing of the flues in particular, considerably improved the stability of the fuel-oil flames but did not significantly improve the situation during combustion with gas or a mixture of oil and gas.

In order to check that the working was not due to flame instability, flame stabilizers of different shapes were tested without significantly improving the phenomena of the plant.

However, tests carried out by varying the components of the gaseous mixture and its composition (the percentage of hydrogen varied during the tests from 25% to 50%) showed that the flame was not intrinsically instable.

Acceleration and pressure were measured at various points of the plant with a view to checking whether there were any possible combinations of the combustion chamber with other elements of the plant (fan, wind box, convective zone, gas feed-line, gas-pass).

Analysis showed that the eighth vibration mode of the combustion chamber excited (though only slightly) an acoustic mode of the wind box with roughly the same frequency.

An investigation was also carried out into the sensitivity of the phenomenon with variations in the excess of oxygen; Fig. 9 shows that the vibratory phenomenon decreases, as excess oxygen decreases, without, however, disappearing.

Figure 10 shows the behaviour of the natural frequencies with variations in the thermic load; the frequency values are seen to increase with the increase in the thermic load, depending on the average temperature. The same figure also contains the frequencies of the vortices shed from the gas and oil flame stabilizers, calculated on the basis of Strouhal's relation, assuming a value of the Strouhal number equal to 0.20. We see that, for thermic loads below 50%, the frequencies of the vortex wake produced by the gas-flame stabilizers may involve modes 5,6,7 and 8, according to the load.

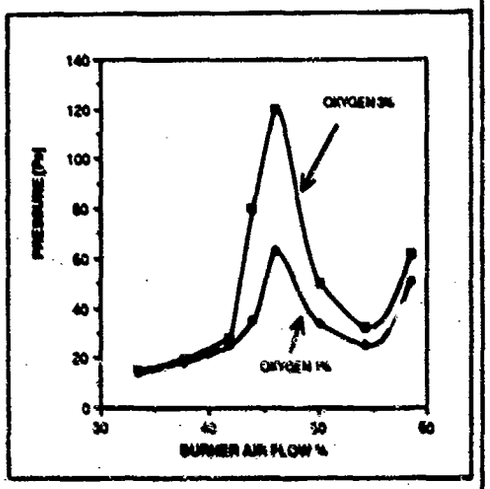


Fig.9 Amplitude of the oscillations of the 75 Hz component with load and excess oxygen variations.
Plant layout: 6 gas burners with type A injectors: α=180°.

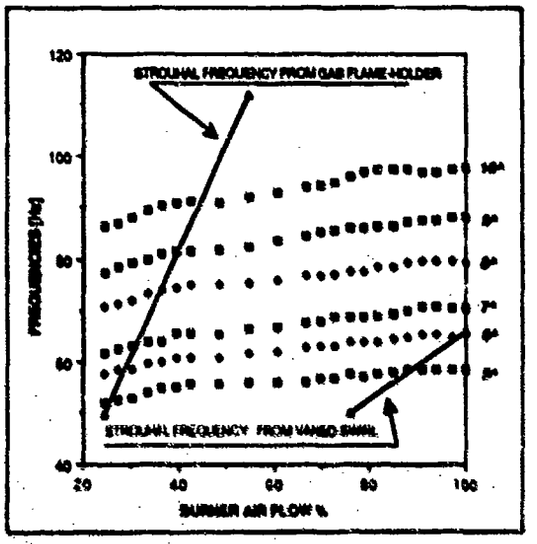


Fig.10 Frequencies of the oscillations with load variations.

It was not possible to measure the frequency of the vortices with the instruments available; it was therefore not possible to examine how the phenomenon of the cause of the vortex wake was affected by the oscillations in the pressure field.

Lock-in phenomena of the vortex shedding frequency may reasonably be assumed to occur, that is, the vortices within a certain velocity field shed with equal frequency to those in the pressure field, which violates Strouhal's relation.

In order not to modify the geometry of the burners, we decided to alter the dynamics of the release of heat by changing the mixture of air and gas.

Fig. 11 contains a summary of the results of such tests: the parts with a dashed line indicate combustion with oscillations in pressure in the boiler greater than 50 Pa and characterize working zones assumed to be instable; the white areas, showing working zones assumed to be stable, indicate combustion with oscillations in pressure lower than 50 Pa. It should be noted that, for angles of around 0°, the stability area reaches maximum values of the air flow and therefore values of maximum power. Indeed, in such a layout, the spectrum of the combustion noise recorded in the furnace is substantially changed compared to the previous situation (fig. 12).

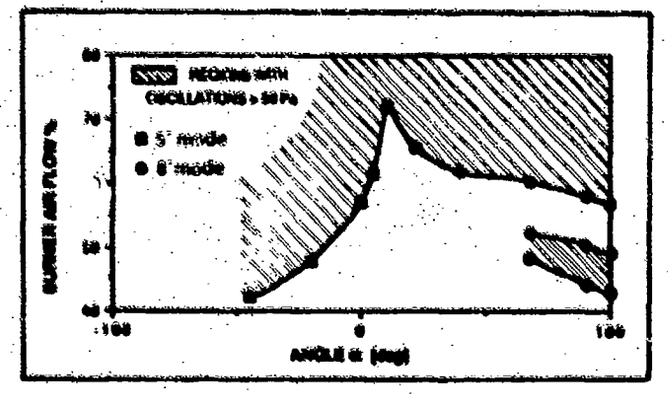


Fig.11 Effect of the rotation angle of the injectors on the vibration amplitudes of the fifth and eight modes.
Plant layout: 6 gas burners with A-type injectors.

With the injectors at an angle of about 10°, the gas was directed towards the centre of the flue. This area was relatively poor in air and rich in partly-combusted gases, and was not influenced by the effects of the vortex shedding flame stabilizers.

Combustion was slower and less noisy. The flames were longer and the difference in position of the area where energy was released in the combustion chamber meant that the excitement is predominantly of the 5th and not the 8th mode.

The instability area, encountered when the flow was at 48% of the maximum, disappears, the burners reached 80% of their maximum load, the flames became much longer and the phenomenon proved to be less sensitive to O_2.

With injectors at angles of between 30°÷100°, instable areas were obtained for flows above 60%.

With such outlet angles, the gas was directed towards the edge of the flue of the burner where, when it was mixed well with the air, it quickly burnt with considerable variations in volume. The flames were still very short and noisy and the release of energy is concentrated in the area where the amplitude of the stationary pressure wave was at its maximum.

In accordance with the results of these tests, type-B injectors were used, with sections of the gas outlet increased by 1/3 and with outlets at an angle of 8°, so as to direct most of the gas towards the axis of the burners.

By reducing the speed of the outlet of the gas, it was possible to be bring the burners to their full load, with stability, in a large field of excess O_2.

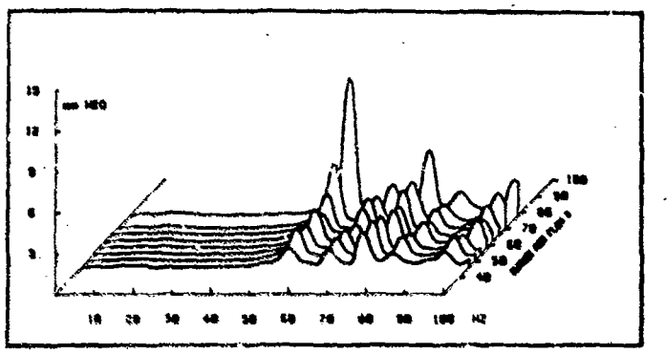


Fig.12 Pressure spectrum in the combustion chamber. Plant layout: 6 gas burners with type A injectors. α=10°. O_2=3%.

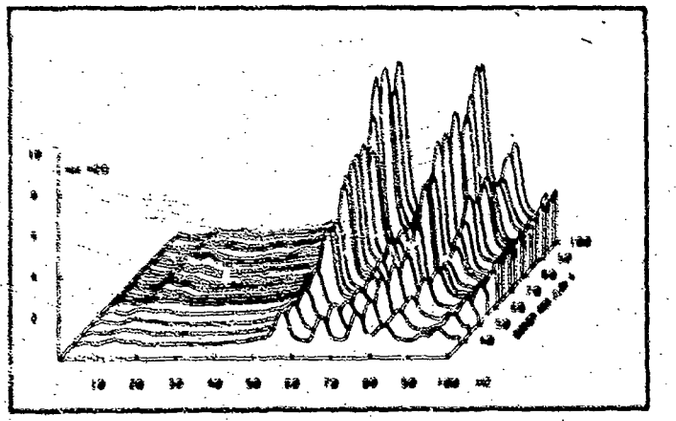


Fig.13 Pressure spectrum in the combustion chamber. Plant layout: 9 gas burners with type B injectors. α=8°. O_2=1÷3%.

The spectrums and the data relevant to such a situation, considered to be a perfectly normal operative situation, are shown in figure 13.

The experimental results reported here show that the phenomenon of self-excitement caused by the oscillating thermal flow is still present, even though it may take a very different form, greatly depending on the angle of injection of the gaseous fuel.

The generation process of the self-excited oscillations differs according to air flow.

In the case of air-flows below 60%, the frequencies of the vortex wake that shed from the injectors may give rise to lock-in phenomena of the 5th, 6th, 7th and above all 8th vibration mode.

For intermediate flows, the phenomenon seems due to coupling between combustion chamber and wind-box. Pressure fluctuations in the wind-box produce flows with oscillating components that prove to be able to sustain oscillations.

In the case of high flows, and therefore for high thermal loads, the eighth mode proves to be less excited. The fifth, on the other hand, remains both because it is less damped and because the frequency of the vortex wake that is shed away from the oil flame stabilizer is close to that of the fifth vibration mode, in the case of maximum flows.

6. CONCLUSIONS

The present paper describes an instability phenomenon that occurred in a steam generator. Numerical analysis made it possible to identify the vibration modes that are most easily self-excited by interaction with the combustion process.

Signal analysis techniques proved to be an effective approach to the practical problem in hand, notwithstanding the complexity of the typically multiburner system.

Instabilities of an acoustic nature were shown to exist and the process of mixing air and fuel was shown to affect the emission of noise.

A different layout of the burner made it possible to solve the problems of the plant.

7. REFERENCES

[1] Rayleigh J.W.S. "The explanation of certain acoustical phenomena", Nature, 18, Vol. II, p. 226 I878; also "The Theory of Sound", Dover, New York, 1945

[2] Barrère M., Williams F. A., "Comparison of Combustion Instabilities Found in Various Types of Combustion Chambers" 12th Symposium (Int.) on Combustion, The Combustion Inst.,1969, pp.169-181

[3] Putnam A. A. , "Combustion Driven Oscillations in Industry" Elsevier P.C., New York, 1971

[4] Thring M. W., "Combustion Oscillations in Industrial Combustion Chambers". 12th Symposium (Int.) on Combustion, The Combustion Inst.,1969,PP.163-169

[5] Crocco L., Cheng S.I.,"Theory of Combustion Instability in Liquid Propellant Rocket Motors" Agardograph n^8, Butterworths, 1956

[6] Zinn B. T. "Pulsating Combustion" Advanced Combustion Methods edited by Felix J. Weinberg, 1986

[7] Papoulis A. "Probability, random variables, and stochastic processes", Mc GraW-Hill Book Company , New York 1965.

[8] Oppenheim A. W., Schafer R. W. "Digital Signal Processing" Prentice Hall, Ing. Engle-Wood 1975

[9] Ligasacchi S., Nencini F., De Michele G. "Internal Report ENEL-DSR-CRTN: T10-06/81, T10-02/82.

[10] Reddy J. N., "Applied Functional Analysis and Variational Methods in Engineering", Mc GraW-Hill Book Company , 1986.

8. APPENDIX

The function of autocorrelation R_{XX} (t) for a random process $f_X(t)$ at an average of nought is:

$$R_{xx}(\tau) = \lim_{T\to\infty} \frac{1}{T} \int_{-T/2}^{T/2} f_x(t) f_x(t+\tau) dt \qquad (A.1)$$

while the Fourier trasform of A.1 constitutes the power spectrum:

$$F_{xx}(\omega) = F[R_{xx}(\tau)] \qquad (A.2)$$

The crossed power spectrum $F_{yx}(\omega)$ for two functions $f_X(t)$ and $f_Y(t)$ is defined by the Fourier Transform of their function of cross-correlation:

$$F_{xy}(\omega) = F\left[\lim_{T\to\infty} \int_{-T/2}^{T/2} f_x(t) f_y(t+\tau) dt\right] \qquad (A.3)$$

The ratio between (A.3) and (A.2) constitutes the frequency response of the system.

The extent of the degree of linearity between two functions $f_X(t)$ and $f_Y(t)$ can be determined by means of the coherence function obtainable as a relation between the square of the cross-spectrum and the product of the power spectrums.

$$\gamma^2_{xy}(\omega) = \frac{\left|F_{xy}(\omega)\right|^2}{F_{xx}(\omega) F_{yy}(\omega)} \qquad (A.4)$$

DISCUSSION

A.Laverdant, Fr

In your calculation, you have introduced an impedance. How is this quantity evaluated? Is it by a theory, numerical method, or experiments?

Author's Reply

The impedance plays its role of course as a boundary condition. So we have introduced the following expression in our numerical model:

$$B^e(s)_{ij} = \int_{\Gamma_i} \frac{\rho}{Z(x, y, z, s)} \Psi_i^e \Psi_j^e d\Gamma$$

derived from:

$$-\int_{\Gamma_i} \frac{\partial u^e}{\partial n} V^e d\Gamma = -\int_{\Gamma} - \frac{\rho \tilde{\rho}}{Z(x, y, z, s)} n^e V^e d\Gamma$$

LeBlond, Fr

Could you describe the experimental device related with ultra-violet measurements to detect and measure the amplitude of combustion instabilities?

Author's Reply

The detector for U.V. is necessary for revealing hydrogen and methane flames because those gases don't give sufficient emission at visible wavelengths. So we used a commercial probe equipped with a special lens for detecting the flames.

REPORT DOCUMENTATION PAGE

1. Recipient's Reference	2. Originator's Reference	3. Further Reference	4. Security Classification of Document
	AGARD-CP-450	ISBN 92-835-0503-4	UNCLASSIFIED

5. Originator	Advisory Group for Aerospace Research and Development North Atlantic Treaty Organization 7 rue Ancelle, 92200 Neuilly sur Seine, France
6. Title	COMBUSTION INSTABILITIES IN LIQUID-FUELLED PROPULSION SYSTEMS
7. Presented at	the Propulsion and Energetics Panel 72nd B Specialists' Meeting, held in Bath, United Kingdom, 6—7 October 1988.

8. Author(s)/Editor(s)	9. Date
Various	April 1989
10. Author's/Editor's Address	**11. Pages**
Various	310

12. Distribution Statement This document is distributed in accordance with AGARD policies and regulations, which are outlined on the Outside Back Covers of all AGARD publications.

13. Keywords/Descriptors

Afterburners	Oscillations
Buzz	Propulsion systems
Combustion	Ramjet
Instability of Combustion	Rocket
Liquid-fueled propulsion	Turbine engine
Modelling of combustion	

14. Abstract

The Conference Proceedings contain 16 papers presented at the Propulsion and Energetics Panel 72nd-B Specialists' Meeting on 'Combustion Instabilities in Liquid-Fuelled Propulsion Systems' which was held 6 – 7 October 1988 in Bath, UK.

The Specialists' Meeting was arranged in the following sessions: Keynote/Overview (1); Turbine Engine Development Experience (3); Rocket and Ramjet Development Experience (4); Theoretical Modelling and Experimental Methods and Results (8). The Technical Evaluation Report is included at the beginning of the Proceedings. Questions and answers of the discussions follow each paper.

While recent Symposia of the Propulsion and Energetics Panel (in Fall 1983 and in Fall 1987) dealt with stabilized combustion, this Specialists' Meeting served as a forum for specialized experts to discuss their experience with combustion instabilities and oscillations occurring in liquid-fuelled engines, i.e. gas turbines, ramjets and rockets. A better fundamental understanding was required in order to achieve further improvements in engine design, and the impact on future design was outlined.

AGARD Conference Proceedings No.450 Advisory Group for Aerospace Research and Development, NATO COMBUSTION INSTABILITIES IN LIQUID-FUELLED PROPULSION SYSTEMS Published April 1989 310 pages The Conference Proceedings contain 16 papers presented at the Propulsion and Energetics Panel 72nd-*B* Specialists' Meeting on 'Combustion Instabilities in Liquid-Fuelled Propulsion Systems' which was held 6—7 October 1988 in Bath, UK. The Specialists' Meeting was arranged in the following sessions Keynote/Overview (1); Turbine Engine P.T.O.	AGARD-CP-450 Afterburners Buzz Combustion Instability of combustion Liquid-fueled propulsion Modelling of combustors Oscillations Propulsion systems Ramjet Rocket Turbine engine	AGARD Conference Proceedings No.450 Advisory Group for Aerospace Research and Development, NATO COMBUSTION INSTABILITIES IN LIQUID-FUELLED PROPULSION SYSTEMS Published April 1989 310 pages The Conference Proceedings contain 16 papers presented at the Propulsion and Energetics Panel 72nd-*B* Specialists' Meeting on 'Combustion Instabilities in Liquid-Fuelled Propulsion Systems' which was held 6—7 October 1988 in Bath, UK. The Specialists' Meeting was arranged in the following sessions Keynote/Overview (1); Turbine Engine P.T.O.	AGARD-CP-450 Afterburners Buzz Combustion Instability of combustion Liquid-fueled propulsion Modelling of combustors Oscillations Propulsion systems Ramjet Rocket Turbine engine
AGARD Conference Proceedings No.450 Advisory Group for Aerospace Research and Development, NATO COMBUSTION INSTABILITIES IN LIQUID-FUELLED PROPULSION SYSTEMS Published April 1989 310 pages The Conference Proceedings contain 16 papers presented at the Propulsion and Energetics Panel 72nd-*B* Specialists' Meeting on 'Combustion Instabilities in Liquid-Fuelled Propulsion Systems' which was held 6—7 October 1988 in Bath, UK. The Specialists' Meeting was arranged in the following sessions Keynote/Overview (1); Turbine Engine P.T.O.	AGARD-CP-450 Afterburners Buzz Combustion Instability of combustion Liquid-fueled propulsion Modelling of combustors Oscillations Propulsion systems Ramjet Rocket Turbine engine	AGARD Conference Proceedings No.450 Advisory Group for Aerospace Research and Development, NATO COMBUSTION INSTABILITIES IN LIQUID-FUELLED PROPULSION SYSTEMS Published April 1989 310 pages The Conference Proceedings contain 16 papers presented at the Propulsion and Energetics Panel 72nd-*B* Specialists' Meeting on 'Combustion Instabilities in Liquid-Fuelled Propulsion Systems' which was held 6—7 October 1988 in Bath, UK. The Specialists' Meeting was arranged in the following sessions Keynote/Overview (1); Turbine Engine P.T.O.	AGARD-CP-450 Afterburners Buzz Combustion Instability of combustion Liquid-fueled propulsion Modelling of combustors Oscillations Propulsion systems Ramjet Rocket Turbine engine

Development Experience (3); Rocket and Ramjet Development Experience (4); Theoretical Modelling and Experimental Methods and Results (8). The Technical Evaluation Report is included at the beginning of the Proceedings. Questions and answers of the discussions follow each paper.

While recent Symposia of the Propulsion and Energetics Panel (in Fall 1983 and in Fall 1987) dealt with stabilized combustion, this Specialists' Meeting served as a forum for specialized experts to discuss their experience with combustion instabilities and oscillations occurring in liquid-fuelled engines, i.e. gas turbine engines, ramjets and rockets. A better fundamental understanding was required in order to achieve further improvements in engine design, and the impact on future design was outlined.

ISBN 92-835-0503-4

Development Experience (3); Rocket and Ramjet Development Experience (4); Theoretical Modelling and Experimental Methods and Results (8). The Technical Evaluation Report is included at the beginning of the Proceedings. Questions and answers of the discussions follow each paper.

While recent Symposia of the Propulsion and Energetics Panel (in Fall 1983 and in Fall 1987) dealt with stabilized combustion, this Specialists' Meeting served as a forum for specialized experts to discuss their experience with combustion instabilities and oscillations occurring in liquid-fuelled engines, i.e. gas turbine engines, ramjets and rockets. A better fundamental understanding was required in order to achieve further improvements in engine design, and the impact on future design was outlined.

ISBN 92-835-0503-4

Development Experience (3); Rocket and Ramjet Development Experience (4); Theoretical Modelling and Experimental Methods and Results (8). The Technical Evaluation Report is included at the beginning of the Proceedings. Questions and answers of the discussions follow each paper.

While recent Symposia of the Propulsion and Energetics Panel (in Fall 1983 and in Fall 1987) dealt with stabilized combustion, this Specialists' Meeting served as a forum for specialized experts to discuss their experience with combustion instabilities and oscillations occurring in liquid-fuelled engines, i.e. gas turbine engines, ramjets and rockets. A better fundamental understanding was required in order to achieve further improvements in engine design, and the impact on future design was outlined.

ISBN 92-835-0503-4

AGARD
NATO OTAN
7 rue Ancelle · 92200 NEUILLY-SUR-SEINE
FRANCE
Telephone (1)47.38.57.00 · Telex 610 176

DISTRIBUTION OF UNCLASSIFIED AGARD PUBLICATIONS

AGARD does NOT hold stocks of AGARD publications at the above address for general distribution. Initial distribution of AGARD publications is made to AGARD Member Nations through the following National Distribution Centres. Further copies are sometimes available from these Centres, but if not may be purchased in Microfiche or Photocopy form from the Purchase Agencies listed below.

NATIONAL DISTRIBUTION CENTRES

BELGIUM
Coordonnateur AGARD – VSL
Etat-Major de la Force Aérienne
Quartier Reine Elisabeth
Rue d'Evere, 1140 Bruxelles

CANADA
Director Scientific Information Services
Dept of National Defence
Ottawa, Ontario K1A 0K2

DENMARK
Danish Defence [illegible]
Ved Idraetsp
2100 Copenl

FRANCE
O.N.E.R.A. (I
29 Avenue de
92320 Châtil

GERMANY
Fachinformat
Physik, Mathe
Karlsruhe
D-7514 Eggen

GREECE
Hellenic Air F
Aircraft Supps
Department of
Holargos, Ath

ICELAND
Director of Av
c/o Flugrad
Reyjavik

ITALY
Aeronautica Militare
Ufficio del Delegato Nazionale all'AGARD
3 Piazzale Adenauer
00144 Roma/EUR

LUXEMBOURG
See Belgium

NETHERLANDS
Netherlands Delegation to AGARD
National Aerospace Laboratory, NLR
P.O. Box 126
2600 AC Delft

NORWAY
Norwegian Defence Research Establishment
Attn: Biblioteket

Postage and Fees Paid
National Aeronautics and
Space Administration
NASA-451

Official Business
Penalty for Private Use $300

NASA
National Aeronautics and
Space Administration
Washington, D.C.
20546

SPECIAL FOURTH CLASS MAIL
BOOK

L1 001 AGARDCP450896614300267 2D
DEPT OF DEFENSE
DEFENSE TECHNICAL INFORMATION CENTER
DTIC-FDAC
CAMERON STATION BLDG 5
ALEXANDRIA VA 223046145

Glasgow G2 8EX

UNITED STATES
National Aeronautics and Space Administration (NASA)
Langley Research Center
M/S 180
Hampton, Virginia 23665

THE UNITED STATES NATIONAL DISTRIBUTION CENTRE (NASA) DOES NOT HOLD STOCKS OF AGARD PUBLICATIONS, AND APPLICATIONS FOR COPIES SHOULD BE MADE DIRECT TO THE NATIONAL TECHNICAL INFORMATION SERVICE (NTIS) AT THE ADDRESS BELOW.

PURCHASE AGENCIES

National Technical
Information Service (NTIS)
5285 Port Royal Road
Springfield
Virginia 22161, USA

ESA/Information Retrieval Service
European Space Agency
10, rue Mario Nikis
75015 Paris, France

The British Library
Document Supply Centre
Boston Spa, Wetherby
West Yorkshire LS23 7BQ
England

Requests for microfiche or photocopies of AGARD documents should include the AGARD serial number, title, author or editor, and publication date. Requests to NTIS should include the NASA accession report number. Full bibliographical references and abstracts of AGARD publications are given in the following journals:

Scientific and Technical Aerospace Reports (STAR)
published by NASA Scientific and Technical
Information Branch
NASA Headquarters (NIT-40)
Washington D.C. 20546, USA

Government Reports Announcements (GRA)
published by the National Technical
Information Services, Springfield
Virginia 22161, USA

Printed by Specialised Printing Services Limited
40 Chigwell Lane, Loughton, Essex IG10 3TZ

ISBN 92-835-0503-4

Best Available Copy